Aerogels synthesised from Canola seed meal protein: Processing-structure-property relationships

Sarah Elizabeth FitzPatrick

A thesis submitted in partial fulfilment of the requirements for the Degree of Doctor of Philosophy in Mechanical Engineering in the University of Canterbury

April 2021

Dedicated to Octávio Vahia de Abreu Teixeira, for determination to pursue dreams.

Contents

Acknowledgements

I would like to express my infinite gratitude to Assoc. Prof. Mark Staiger for the exceptional guidance and support he provided during my doctorate. I attribute my growth as a researcher to the consistently high standards Mark encourages and exemplifies in his own research. The clear direction that Mark provided for all the quandaries I encountered throughout my thesis has helped me to hone my own decision-making skills. I also thank Mark for the teaching opportunities he granted me throughout my studies, and the encouragement to publish and present my work. I feel privileged to have been mentored in so many aspects of my development as a researcher while under his wing.

I am extremely grateful to Dr. Santanu Deb-Choudhury for his exemplary supervision of this thesis too. Santanu's approachability and exceptional wisdom in all things relating to proteins (especially collagen), research, commercial applications, and his general passion for science, have allowed me to fast-track my own learning in these areas while thoroughly enjoying the journey.

Furthermore, this research would not have been possible without the generous stipend & funding, co-ordination, and research resources provided by The Biopolymer Network Limited (NZ). My gratitude, in particular, to Mr. Steve Ranford for his role in co-ordinating and overseeing this project and his infinite optimism for CSM protein aerogels. Thanks also to Dr. Kate Parker, for her role on my supervisory team and her continued praise and encouragement of my work. I am also grateful for all the advice and ideas offered by the wider BPN team, especially Sarah Heine and Dr. Ben Schon.

Throughout the course of my project, I visited and worked in numerous laboratories throughout New Zealand, and I am eternally grateful to the staff in those labs who facilitated my use of numerous expensive machines and offered helpful tips and ideas. Specific mention is made to many staff from these labs below, though I also acknowledge the wider network of contacts at these institutions who have also inspired and assisted my work and career.

AgResearch (Lincoln)

A huge thank you to the Proteins and Metabolites Team (previously 'Proteins and Biomaterials') at AgResearch Lincoln for hosting me throughout this project. Every person on the team has helped and supported me in some way with my thesis and I cannot trust myself to remember all the ways in which you have all helped. Thank you to all the scientists, technical staff, and students on the team.

I must specifically mention Dr. Duane Harland for his many enthusiastic and exciting contributions to my thesis. I think it is fair to say that I adopted Duane as an 'invisible' supervisor on this project, and I would like to take this opportunity to formally thank him for trusting me with many a precious instrument and also apologise again for breaking one of his beloved desiccators. They don't make them quite like they used to.

I would also like to thank Mr. Paul Middlewood (now Fibre and Bioproduct Team) for his help with almost everything in the chemistry lab, particularly the canola seed meal extractions, his humour-filled conversations across the lab benches and also for letting me constantly steal his callipers. Also, thanks to Dr. Sonya Scott (also now Fibre and Bioproduct Team) for her enthusiastic help with mulling over many technical queries and odd results.

I am also very grateful to Mrs. Erin Lee for help with numerous biochemical protocols, especially sample preparation for LC-MS/MS experiments, the amino acid analyses, and SDS-PAGE experiments. Further thanks to Dr. Marina Richena (for help with microscopy and cryofracture), Dr. Stephen Haines (for help with bioactivity prediction and GFC analysis), Dr. Jeff Plowman (for help

with electrophoresis protocols), and to Mrs. Ancy Thomas, Dr. Jess Gathercole and Dr. Evelyne Maes (for help with LC-MS/MS protocols and analyses).

Finally, I thank my fellow PhD students at AgResearch for their help, companionship, and patience (especially over the heat pump). Their cheerful companionship, especially those with whom I have shared an office over the years, has made my daily grind in the labs and office a delight.

The University of Canterbury (UC)

To the staff and postgraduate students of the Department of Mechanical Engineering for providing further guidance, resources, and companionship. Especially to Mr. Kevin Stobbs for his help with all my technical enquiries, to Mr. Shaun Mucalo for help with SEM imaging, and to Alice Young for her help and companionship with teaching roles.

Thanks to Dr. Tim Huber and Prof. Conan Fee of the UC School of Product Design. Tim, for his enthusiasm and ideas provided during my mid-term examination and Conan, also for his enthusiasm regarding the project.

I am also very grateful to Mr. Michael Sandridge of the Department of Chemical and Process Engineering, for his patient (and always jovial) assistance with many enquiries regarding the operation of the Gemini (gas porosimetry) over many, many weeks.

My sincere thanks also to Dr. Ren Dobson and Dr. Sarah Kessens from the UC School of Biological Sciences for their help with my UV-CD experiments.

Thank you to Mr. Samir Shah, Dr. Meeta Patel, Miss Rosalee Collins-Gargan, and Dr. Marie-Joo Le Guen for their friendly assistance with my experiments at Scion (New Zealand Forest Research Institute Limited).

Additionally, I am very grateful to Andrew McNaughton of the Otago Micro and Nanoscale Imaging Centre at Otago University (New Zealand) for kindly analysing my aerogel sample on the µ-CT and helping with image analysis.

Finally, I would like to thank all my family and friends for their support throughout my studies.

Fionnuala, for her amazing friendship during this long journey to acquire a doctorate. I found it incredibly important to have someone to share the PhD journey with from the inside, and Fionnuala has been my sounding-board and listening-ear for most of my PhD. I wish her all the best for her own thesis.

Infinite thanks to my parents, John and Leanne, for always going above and beyond to support my education from childhood to now. Particular thanks to my Mum for generously giving her time to babysit so that I may complete this thesis. I am continuously humbled by her generosity. Without her, this work would never have been summarised on paper and would remain forever in the dusty archives of my computer, my doctorate on (seemingly indefinite) hold.

I also thank my partner Octávio, for assuming all parenting duties on all his weekends, also so that I may finish writing my thesis. I dedicate this thesis to Octávio, for providing me with the initial inspiration and encouragement to apply for a PhD programme.

Abstract

Novel bioaerogels produced *via* the gelation of protein extracts from canola seed meal (CSM) are described for the first time, adding to the scant collection of aerogels that are derived from plant-based biotechnology. Aerogels are incredibly valuable and versatile advanced materials with unique uses in aerospace, construction, laboratory science, medicine, pharmaceuticals, environmental clean-up, high-energy physics, sporting equipment, and clothing. Bioaerogels are modernising this field by addressing questions of sustainability and eco-friendliness and further broadening application potential in industries such as food, medicine, and biosciences. Proteins are one of the least researched precursor materials for bioaerogel production, yet they are often untapped sources of biomass and can provide unique biochemical attributes. Canola seed meal protein is a lower-value co-product of the food industry that can be upcycled for materials production and possesses chemistry amenable to aerogel manufacture. The central aim of this thesis was to use canola protein as a precursor polymer for developing aerogels. The resulting novel protein aerogels had their morphologies and properties characterised for comparison with other bioaerogels. Biochemical analyses examined whether the canola protein possesses bioactivity for unique application potential and permitted an understanding of the chemistry responsible for gelation. Finally, elucidating the relationship between processing parameters, aerogel morphologies, and aerogel properties revealed the tailorability of these aerogels to specific target applications.

The CSM protein aerogels were successfully synthesised by manipulating aqueous chemical parameters of the protein solution to form gels, and subsequently drying the gels using freeze drying or supercritical carbon dioxide drying. Gelation success and gel properties were dependent in the first instance on protein concentration and solution pH. Substantial gel viscosities (up to 80,000 mPa.s) were achieved when CSM protein gels (10 *wt%*) were manipulated to an optimum pH (8.0 ± 0.2) and/or strengthened with heating (to 95 °C), $CaCl_2$ (20 mmol/L) or fibrous biomolecules (chitin and collagen). $CaCl_2$ and pH limits proved essential tools for the development of supercritically dried aerogels, while freeze dried gels were possible from a broader range of CSM protein solutions. The CSM protein aerogels were comprised of a particulate-based gel network formed after denatured

canola proteins were driven to gelation by the formation of hydrophobic and electrostatic interactions. The resulting freeze dried gels (or cryogels) demonstrated an average density of 0.13 g/cm^3 and competitive density-specific mechanical properties (specific compressive strengths up to 4.5 kPa/(kg/m^3), specific compressive moduli up to 0.15 MPa/(kg/m^3)). Supercritically dried CSM protein aerogels experienced a slight increase in density (0.2 g/cm^3) with a corresponding shift in pore size distribution that permitted a mesoporous (Barrett-Joyner-Hallett) pore volume of 0.5 cm^3/g and a Brunauer-Emmett-Teller specific surface area of 113 m^2/g.

Gelation of canola protein extracts using pH, $CaCl_2$, and heating has shown how these bioaerogels are manufacturable and tailorable using environmentally friendly chemical techniques. Thus, ensuring the final aerogel products are likely environmentally safe, biocompatible, and potentially bioactive. Tailorable pore sizes and gel morphologies were identified after variations to protein concentration, solution pH, and drying methods. Variations to morphological features consequently influenced aerogel properties such as strength-to-weight ratios and specific surface areas. Owing to fundamental structural differences, supercritically dried and freeze dried gels (‘aerogels’ and ‘cryogels’, respectively) demonstrated distinct property differences, therefore possessing different application potentials. Additionally, unique biochemical potential, optical features, and controllable degradation rates suggest this novel system of bioaerogels has potential uses in food, cosmetic, and biopharmaceutical applications.

List of Figures

List of Tables

Chapter 1

1. Introduction

The present thesis aims to develop and characterise a novel protein-based aerogel using protein extracted from canola seed meal. The thesis contributes new knowledge concerning canola protein gelation, protein-based materials science, and processing-structure-property relationships in bio-based aerogels. Chapter 1 provides an introduction into aerogel science and includes a brief history of the aerogel.

1.1. Aerogels

Aerogels are an exciting advancement in materials science where highly porous (up to 99.9 % air) and super-low density (as low as 1 kg/m^3) solid matrices can be created from a range of inorganic, metallic and organic substances [1, 2]. The resulting aerogel structures have very high strength-to-weight and surface-area-to-volume ratios, and as a consequence of their porosity are excellent thermal, acoustic, and electric insulators [3, 4]. Aerogels can also be highly absorbent and in some cases highly transparent [5]. Applications for aerogels and aerogel-like materials are numerous (see **Table 1.1**). Current production and research of aerogels is focused on applications in space exploration [6], construction [7], electronics [8], medicine [9], wastewater treatment [10], and food technology [11].

Table 1.1*: List of applications where aerogels are used or proposed, along with the relevant aerogel properties*

Application	**Property**	**Citation**
Insulation in buildings, aircraft, and vehicles.	Thermal insulation, lightweight, refractive index,	[4, 12, 13]
Cherenkov counters (high energy physics research) & optics	Refractive index, porosity, hydrophobicity (chemical modification ability)	[4, 12-14]
Hypervelocity particle entrapment (space exploration), energy absorber, spacecraft insulation, thermoelectrics,	Elastic and lightweight, large pore volume, thermally insulating,	[7, 12]
Energetic materials (explosives, propellants, pyrotechnics)	Particle size, surface area	[15]

Chemical sensors	Low density/high porosity, surface area, tailorable chemistry, optical properties	[7, 16, 17]
Catalysis, and sorbers	Chemical (O2 – generation), surface area	[12, 13]
Filtration/Purification/water treatment	Absorbency, surface area, variable chemistry	[7, 17]
Thickening agent (rocket fuel)	Porosity, absorbency	[13]
Insecticide (*via* dissection)	Absorbency, chemical	[13]
Nuclear waste containment, cryogenic fluid (liquid He) containment	Chemical durability, low thermal expansion, thermal shock resistance, openly porous,	[18]
Acoustics (impedance matchers in transducers, speakers, range finders)	Low sound speed, acoustic insulation	[4, 12]
Electronics (dielectrics, spacers, capacitors)	Dielectric constant and strength, surface area	[4, 12]
High-voltage insulators	Electrical insulation	[12]
Foundry applications	Thermal insulation,	[19]
Biomaterials/pharmaceuticals (cardiovascular implantable devices, tissue engineering scaffolds, drug delivery vehicles, wound care dressings)	Porosity, absorbency (surface area), biocompatibility, biodegradability, light-weight, mechanical properties (flexible + strong aerogels)	[17, 20]
Cosmetics + personal care (toothpaste, facial creams)		[21, 22]
Food	Absorbency / digestibility	[17, 23]
Clothing + sports equipment	Insulation / lightweight	[24]

Aerogels possess high levels of porosity due to the occurrence of two different phases in the material: solid and gas. As the name aerogel suggests, the gas is generally air while the solid can be a variety of polymeric compounds. Materials that contain two phases are known as colloids and those that contain gas dispersed in a solid are known as solid foams (**Figure 1.1**). A common example of a solid foam is expanded polystyrene. Aerogels have been defined by the International Union of Pure and Applied Chemistry (IUPAC) as 'gel(s) comprised of a microporous solid in which the dispersed phase is a gas' [25]. Describing the gels as 'microporous'[1] implies a major portion of the porosity is found to have pores with a diameter of 2 nm or less. Other pore sizes present in aerogels include mesopores (2-50

[1] The convention in aerogel research of naming 'micro'-, 'meso'-, and 'macro'-pores is determined by property-relevant nanometre limits and does not reflect the SI units of measurement for each material (*i.e.* nanometre sized pores can be 'micropores' or 'mesopores' while micrometre sized pores are 'macropores').

nm) and macropores (> 50 nm) [26]. Generally, aerogels have pore sizes ranging from 1 nm to 1 µm and particle sizes typically in the range of 1 to 100 nm [27, 28].

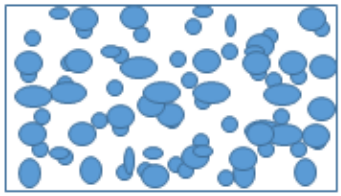

Continuous phase \ Dispersed Phase	Gas	Liquid	Solid
Gas	None	Liquid Aerosols (clouds)	Solid Aerosols (smoke)
Liquid	Foam (shaving cream)	Emulsion (milk)	Sol (paint, blood)
Solid	**Solid Foam (Aerogels)**	Gel (jelly)	Solid Sol (stained glass)

Figure 1.1: *Types of colloids*

1.2. History of aerogels

The aerogel was first described by Samuel Kistler in 1931 with his pioneering half-page letter in Nature entitled: “Coherent expanded aerogels and jellies” [29]. The origin of the term ‘aerogel’ also originates from Kistler’s publications in 1931 and 1932 where he described them as gels in which a gas has replaced the liquid (without collapse or shrinking of the solid). Many excellent reviews in the field revisit Kistler’s work, sometimes adding other useful descriptors such as typical values of porosity. Pierre’s ‘*History of Aerogels*’ which is the opening Chapter of ‘*The Aerogels Handbook*’ adds that porosity is typically ‘of the order of 90 %’ [30]. This gives some additional clarity as to what separates an aerogel from other classes of solid foams. However, Pierre adds that using specific values to define this class of materials will always find exceptions and concludes that it is still ‘more realistic to define these materials with reference to the initial idea of Kistler, simply as gels in which the liquid has been replaced by air, with very moderate shrinkage of the solid network’. Hüsing and Schubert also discuss the definition of an aerogel in their 1998 review, where they consider the merits of two slightly different definitions. The first, defines aerogels as dried versions of gels where a specific processing method, the supercritical drying process, has been employed to remove the liquid. The second, does not mandate the use of the supercritical drying process, and simply defines them as gels where the pore liquid has been replaced with air, although it stipulates that the structure of the network shall be largely maintained [31]. Overall, the authors conclude that materials considered for review in their work shall be broadly defined by the second definition but that they would not exclude gels that only fall into the first category.

Although Kistler’s definition does not specifically mandate which methodology must be used to dry a gel without shrinkage, his paper is built on the discovery of completing this task using supercritical fluids. In his 1931 Letter to Nature, Kistler proposed the idea of using supercritical fluids to transform the liquid in a gel into a gas while avoiding the capillary forces that cause most gels to collapse upon drying. Supercritical heating involves heating the liquid beyond the critical point by maintaining the pressure above the vapour pressure. Beyond the critical point, a substance has no distinct liquid-gas phase boundary and no surface tension exists, meaning it can then be evaporated without the

consequence of gel collapse [27]. Achieving this often requires the exchange of the solvent in the gel network to a solvent that was more amenable to the process of supercritical evaporation.

The thinking behind this technique was quite radical, since it was not certain that gels were independent of the type of liquid filling the pores in the material. Kistler ends his introduction with the observation: "...such facts as those above, and others, have led me to the conviction that when once formed, a jelly is in general independent of the fluid filling its meshes, and this fluid might just as well be a gas as a liquid. The fact that all coherent jellies are filled with a liquid is accidental and of little significance" [32]. Upon testing this idea, he subsequently discovered that he was correct, and that many gels could be converted to aerogels using his supercritical fluid drying technique which preserved the solid component of the gel. In 1932 he published "Coherent expanded aerogels" which elaborated on this discovery by describing the production and properties of aerogels he had successfully produced with this method. "Coherent expanded aerogels" covered many types of gels including: silica, alumina, tungstic oxide, iron oxide, stannic oxide, nickel tartrate, cellulose, nitrocellulose, gelatine, agar, egg albumin, and an attempt using rubber [32]. These successful aerogel experiments led Kistler to conclude that the ability to produce an aerogel using this technique was a general property of all gels.

Since Kistler's publication, many other aerogel types have been added to his impressive variety by aerogel researchers. These include examples of transition, lanthanide and actinide metal oxides, organic polymers (resorcinol-formaldehyde, phenol-formaldehyde, polyacrylates, polystyrenes, polyurethanes, and epoxies), carbon (graphene) and biological polymers (polysaccharides and proteins) [33-42]. The variability in the elements and compounds used to make aerogels is an important reason why they are such useful materials with such varied applications. Chemical properties specific to the precursor molecules can be harnessed in combination with the porosity-dependant properties of the aerogel structure. Aerogels can therefore be tailored for specific practical applications. An example of this combined effect is the use of aerogels in energetic materials. Such materials rely on the highly exothermic combustion of metals as well as the rapid kinetics offered by the aerogel structure having a high surface area and small particle size [15].

The silica aerogel is the archetypical aerogel, and the aerogel of choice for many researchers. The renewal of interest in Kistler's work in 1962 led to the development of the modern 'sol-gel' method for producing silica aerogels. Stanislas Teichner's group of the University of Lyons (France) were endeavouring to make a porous solid for storage of rocket fuel when they pursued a new, faster method for producing Kistler's 'water glass' silica gels. The water-glass method Kistler had employed relied on a long process of saturating a mixture of sodium silicate (water glass) and hydrochloric acid with methanol. For Teichner's student in 1962, this process was too time-consuming for his purposes and so the group developed a faster alternative by using an organosilane: tetramethoxysilane (TMOS) [4]. TMOS was dissolved in methanol and then reacted by an excess of water with an acid or base catalyst, satisfying the overall reaction:

$$Si(OCH_3)_4 + H_2O \rightarrow SiO_2 + 4\,CH_3OH$$

Modern productions of silica aerogels still use organosilanes but now replace the TMOS with the safer tetraethylorthosilicate (TEOS) and use caron dioxide (CO_2) instead of methanol as the supercritical fluid. Both changes lead to safer processing. Silica aerogels are inert but can also be chemically modified, allowing for both hydrophobic and hygroscopic aerogels to be made from the same basic silica structure. Silica is also biocompatible thus making it appropriate for medical applications. The main drawback of silica-based aerogels is the brittle nature of the mechanical properties and the subsequent difficulties in machining commercial aerogel products made from silica [43].

Issues with the mechanical properties of silica were overcome in the development of organic aerogels in the late 1980s by Rick Pekala's group at the Lawrence Livermore National Laboratory (California, U.S.A.) [44]. Organic aerogels also proved to have superior insulative properties [44] to silica aerogels, and upon pyrolysis, very high surface areas [45]. These aerogels were mainly made from resorcinol and formaldehyde or from melamine and formaldehyde and were also developed into the first carbon aerogels by pyrolysis. Organic aerogels from oil-derived phenolic resins (and their carbon derivatives) continue to achieve phenomenal surface areas and small pore sizes today but remain reliant on the fossil fuel-derived precursors and many are toxic. It is these short-comings which are

addressed in the next generation of organic aerogels: the bio-based organic aerogels. Bio-based precursors had been possibilities for aerogel manufacture since Kistler's work but were mostly overlooked until experiencing a resurgence in the 2000s [11]. In addition to the oil-based organic polymers, bio-based polymers may also provide improved mechanical properties over silica-based aerogels [46] as well as providing more sustainable and environmentally friendly products to the aerogel market. Bio-based aerogels and the motivations for their production is addressed in **Chapter 2.**

The first attempts to commercialise aerogels were initiated by Kistler himself and sold by the Monsanto Company under the tradename Santocel [4]. Santocel was a silica aerogel powder used to thicken paint, make-up, and napalm, and as a cigarette filter and for insulation in freezers. Today, aerogels can be found in many products, most of them utilising the insulative properties of aerogels. Cabot Corporation (Boston, U.S.A.) are manufacturers of aerogels for building insulation and daylighting, industrial and piping insulation, coatings and paints, clothing insulation, and skin & beauty products. Aspen Aerogels® (Northborough, U.S.A.) also manufacture aerogel products for insulation as do BASF (Ludwigshafen, Germany) who are manufacturing a mechanically durable organic aerogel. Aerogel Technologies™ (Boston, U.S.A.) sell a range of aerogel products including organic aerogels which broaden the properties and machinability of aerogel products. Another more recent manufacturer is Aerogelex (Hamburg, Germany) whose products include biopolymer aerogels for applications in cosmetics and life sciences.

Chapter 2

2. Literature Review

Chapter 2 begins with the manufacture, structure, properties, and applications of aerogels generally, followed by a focus on bio-based aerogels (*aka* bioaerogels), and protein-based aerogels. The third Section of Chapter 2 reviews the current knowledge of canola seed meal and its protein extracts. The motivation for using canola protein as the principal bio-based material in the present work is established by examining the gelation behaviour and chemistry of the proteins in canola seed meal. In the final Section of Chapter 2 the summary will demonstrate how these general motivations for researching bioaerogels and canola protein are brought together in central aim of the current thesis.

2.1. Aerogels

2.1.1. Manufacture

Fabrication of an aerogel begins with a solid-liquid colloidal system known as a sol. In a sol, the solid phase is dispersed as particles within the liquid medium (sometimes referred to as a solvent although the solid phase is not solvated but is rather suspended particles). These particles are usually composed of polymeric molecules resulting from reaction of the precursor monomeric molecule/s. However, in the case of some bioaerogels the particles may be aggregates of pre-existing polymeric molecules associated mostly or solely through secondary bonding (discussed in **Section 2.2**). Particle sizes can range from a few nm to a few microns in diameter though typical microporous aerogels will have particle sizes of a few nm [31].

A sol can be converted to a gel state if these sol-state particles continue to polymerize, aggregate, physically entangle, or crosslink, to form long-range connections resulting in a continuous, rigid network (**Figure 2.1**). Gelation is defined as the point of network formation (chemical or physical

polymer network which spans the entire system) and is accompanied by the viscosity tending to infinity [25]. The macroscopic material appears to transform from liquid to solid and the point of gelation is sometimes determined by an inversion test if more accurate methods such as rheology are not available. Gels can result from more than one type of molecular process, although most commonly gelation is a result of homogenous crosslinking throughout the material. Long-range order produced from such crosslinking reactions is reminiscent of a thermoset plastic, however in the case of a gel, the network contains pores which retain the solvent. The resulting material has the physical appearance of a semi-solid.

This continuous solid matrix could result in encapsulated pockets of the liquid, inverting the continuous and discontinuous phases with one another. However, in sol-gel structures the liquid phase remains mostly continuous, resulting in a series of channels which will ultimately become the open porous network of an aerogel. A significant degree of closed porosity in the structure can limit many aerogel properties and applications as well as presenting difficulties for techniques designed to measure aerogel porosity. The key structural change that occurs during the sol to gel process is the polymerisation or network formation of the solid particles, resulting in an increased independence of this solid network from the liquid.

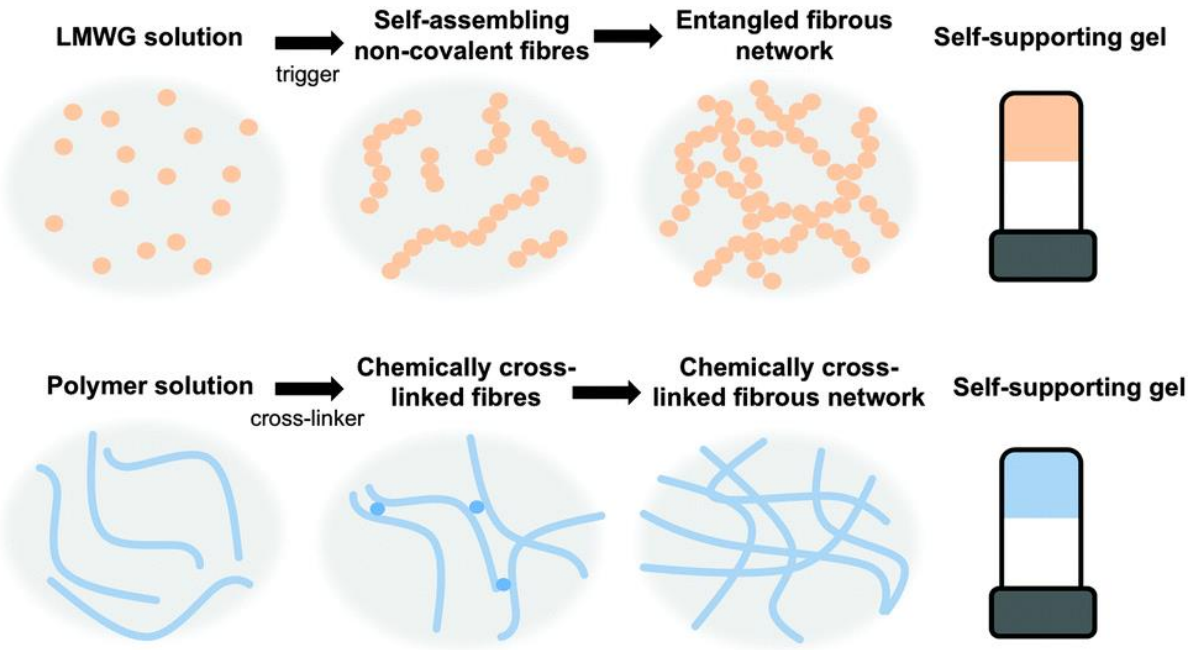

***Figure 2.1**: Examples of gelation from sol to gel reliant on entanglement (top) or chemical bonds (bottom). Reprinted from reference [47]: Draper, E.R. and D.J. Adams, Photoresponsive gelators. Chemical Communications, 2016. 52(53): p. 8196-8206. Copyright 2016, Royal Society of Chemistry*

When network formation is complete, the average length of the polymeric chains in the gel is greater than 1 µm and pore sizes are typically less than 1 µm. Gel networks can also have various morphologies (**Figure 2.2**) including both ordered and disordered structures, and polymeric or particle-based aggregated networks [28].

The next stage of aerogel manufacture after gelation is the drying stage. The goal of the drying stage is to replace the liquid in the gel with a gas (ultimately air), without causing collapse of the solid network or significantly changing the porosity. Importantly, Kistler discovered that drying can occur independently of the solid material because the liquid and solid behave as separate phases in the gel. Researchers and manufacturers have the freedom to select various precursor molecules due to this independence, where the liquid can be subsequently dried mostly without concern that chemical properties of the solid material will change or interfere with this process. Drying is commonly achieved in many aerogels using Kistler's method of supercritical heating and subsequent evaporation of the supercritical fluid.

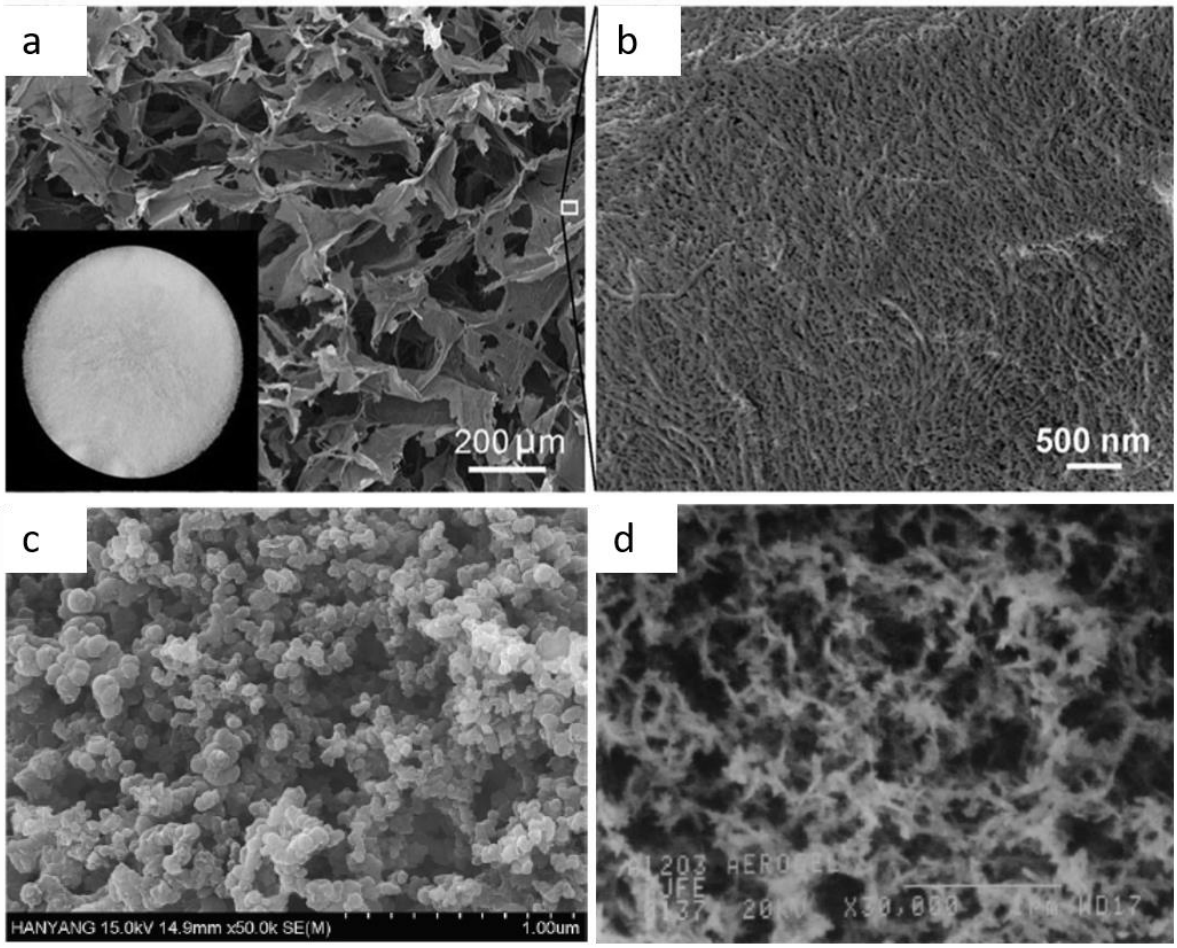

Figure 2.2*: Examples of aerogel morphologies from cellulose-collagen aerogel* ***(a-b)****, silica aerogel* ***(c)****, and alumina aerogel* ***(d)****. Adapted and reprinted from:* ***(a-b)*** *[48] Lu, T., et al., Composite aerogels based on dialdehyde nanocellulose and collagen for potential applications as wound dressing and tissue engineering scaffold. Composites Science and Technology, 2014. 94: p. 132-138, Copyright Elsevier* ***(c)*** *[49] H. Zhang, C. Hong and Y. Qiao, Synthesis, Structural and Thermal Properties of Nano-porous SiO2-based Aerogels N2 in Advances in Nanocomposites - Synthesis, Characterization and Industrial Applications, B. Reddy, Editor. 2011, InTech. p. 39 – 60, Copyright IntechOpen.* ***(d)*** *[50] Poco, J.F., et al., Synthesis of high porosity, monolithic alumina aerogels. Journal of Non-Crystalline Solids, 2001. 285(1): p. 57-63, Copyright Elsevier*

Although Kistler tried a few choices of solvents and mostly used alcohol to achieve supercritical evaporation, modern aerogel researchers and manufacturers prefer to use carbon dioxide as it is safer and requires lower temperatures and pressures to reach the critical point [39]. Gels are prepared in more practical solvents such as ethanol or water since carbon dioxide is only liquid when pressurised. Carrying out the supercritical fluid extraction first requires a solvent exchange process (or series of solvent exchanges) to replace the formulation solvent with an intermediate solvent which is then miscible with liquid carbon dioxide (CO_2). Ethanol is miscible both with water and carbon dioxide thus is often used as the intermediate solvent for these solvent exchange steps (**Figure 2.3**). A

graduated process of solvent exchange is required in many cases to reduce shrinkage or porosity changes which can occur in weaker gels with sudden drastic changes of solvent chemistry. The gels are referred to as alcogels when the liquid filling the pores is an alcohol such as ethanol. When a gel is immersed in 100% ethanol and all water is removed it may be introduced to an autoclave chamber in preparation for mixing with liquid CO_2. Solvent exchange with liquid CO_2 occurs under the appropriate pressures necessary to maintain the CO_2 in liquid form.

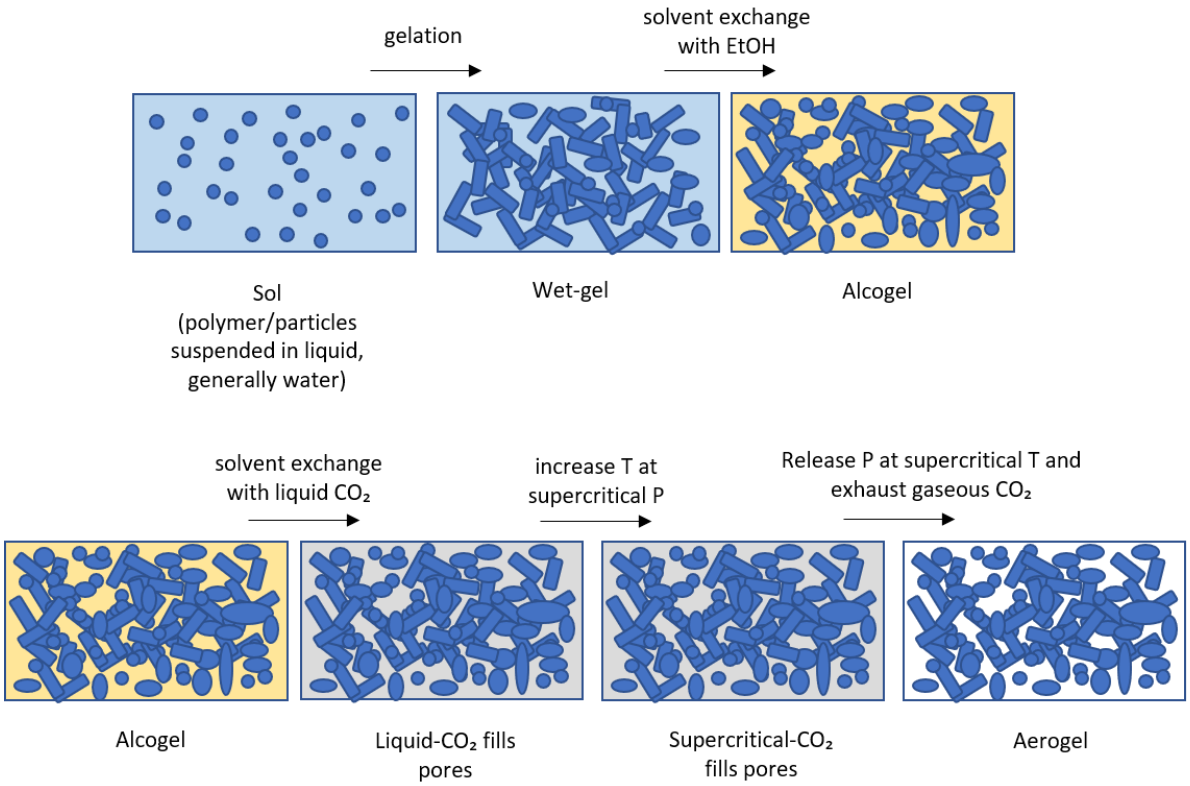

***Figure 2.3**: Sol conversion to an aerogel using supercritical carbon dioxide*

The most basic of systems required for the supercritical fluid drying process is composed of an autoclave chamber (with pressure and temperature control) connected to a source of liquid carbon dioxide. It should have an exhaust system for removal of the alcohol (or alternate solvent) and at later stages, the CO_2 gas. The alcogel is sealed in the chamber with sufficient ethanol to cover the sample and the entire system is cooled to the temperature of the liquid CO_2. Solvent exchange is then carried out, sometimes for extended time periods, as liquid carbon dioxide is introduced to the sample and dilutes the ethanol from the gel. The ethanol is gradually removed from the system *via* continued

flushing with fresh CO_2. Once ready for the supercritical stage, the chamber and sample are filled with fresh liquid CO_2, the chamber is sealed, and the system heated under pressure to supercritical levels. Appropriate pressure control must be used to maintain the system in the liquid phase until heated to supercritical temperatures. Once supercritical conditions are achieved, the carbon dioxide can then be vented from the gel (converting the supercritical fluid to a gas) without inducing capillary forces which cause the gel to collapse. The system achieves this by bleeding the chamber through controlled release of the pressure while heating to maintain the temperature above the critical temperature (**Figure 2.4**). Venting of the CO_2 results in gaseous CO_2 leaving the system and being replaced with air, which eventually fills all the pores in the gel, resulting in an aerogel.

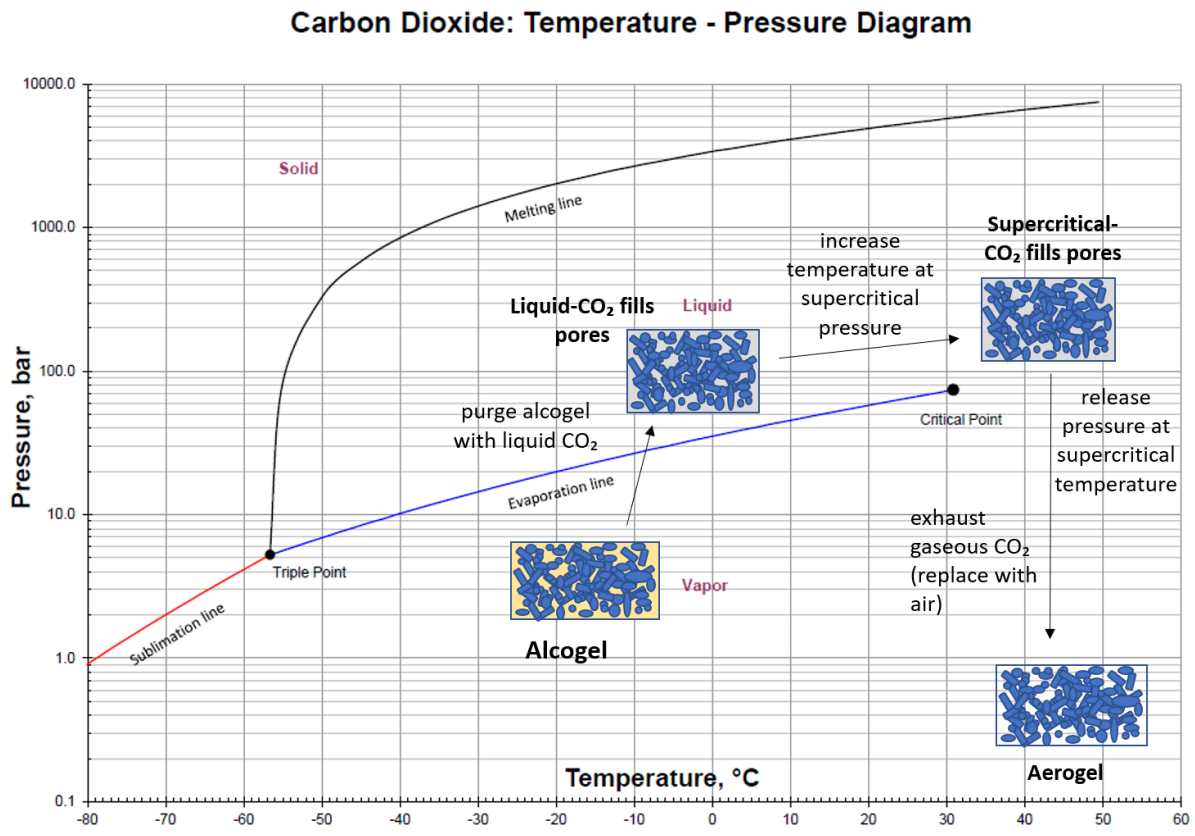

***Figure 2.4**: Temperature-Pressure diagram of CO_2 with sublimation, melting and evaporation lines (Image Copyright: ChemicaLogic Corporation, 1999). Overlain diagrams demonstrate supercritical drying process of an aerogel with respect to the temperature and pressure of CO_2*

This process allows the gel structure to be preserved due to the elimination of a density difference between the liquid and gas. A supercritical fluid has no surface tension since there is no liquid-gas phase boundary. Evaporation of the supercritical fluid from the pores in the gel occurs without the gel

experiencing capillary forces on its pore walls which would normally occur when surface tension is present in the liquid phase (**Figure 2.5**). In the absence of capillary forces, a dried gel will avoid shrinkage and collapse of porosity.

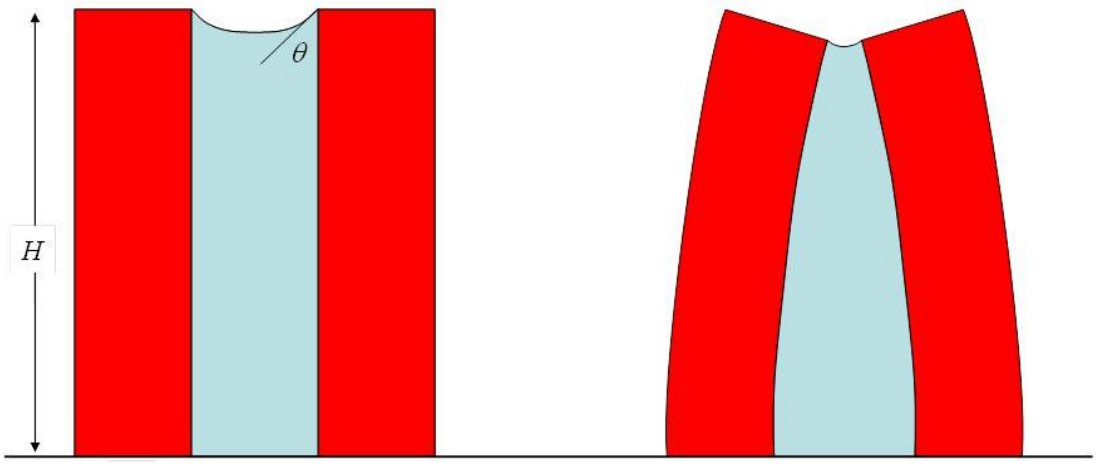

Figure 2.5*: Capillary forces caused by solvent surface tension pulls pore walls inwards and causes the collapse of pore structures during evaporation (Image Source: [51] Mack, C., Fundamental principles of optical lithography: the science of microfabrication, 2008, Copyright John Wiley & Sons)*

Technological advances in the field have explored alternate drying methods that have eliminated the need for supercritical temperatures and pressures. These alternate drying methods include freeze drying (lyophilisation) and in some cases ambient (pressure) drying [52]. Ambient drying is generally associated with a significant loss of porosity due to gel collapse. However, some researchers acknowledge the need to investigate ambient drying technologies further in order for successful large-scale commercialisation of aerogels to proceed [53]. Such advancements are already being commercially employed, for example, the aerogel manufacturer Aerogel Technologies® produced the world's largest aerogel panel using a new technique the company says is performed at ambient conditions [54]. Ambient drying of gels was first achieved by chemically modifying the surfaces of the silica aerogel to become more hydrophobic and thus create low-energy and therefore low surface-tension-promoting surfaces [55]. The gels can then undergo evaporation of the solvent in ambient conditions and resist shrinkage. The alternative to producing a low-energy gel surface through solid modification is to use a low-surface tension solvent such as *tert*-butanol. Such solvents can undergo

evaporation in ambient conditions with minimal capillary forces and thus creating minimal shrinkage of the gel.

Another alternative to supercritical drying is the use of lyophilisation or freeze drying. Freeze drying requires the gels to be first frozen and then the water (or solvent) can be removed from the pores by sublimation at low pressures and ambient or near ambient temperatures. The ice (in the case of an aquagel) is converted directly to vapour without passing through the liquid phase, thereby avoiding capillary forces that would collapse the gel network [56] (**Figure 2.6**). The major drawback of this drying technique is the disruption of the wet-gel network by unconstrained crystal growth of the solidifying solvent (especially problematic in aquagels). Avoiding unconstrained crystal growth requires fine control over crystal nucleation by introducing other solvents such as *tert*-butanol to form a eutectic mixture [57] .

Dried structures resembling aerogels that are produced *via* freeze drying are often termed cryogels and are generally not considered true aerogels. This exclusion is based on the IUPAC requirement for pore sizes in an aerogel to be predominantly microporous and mesoporous. Freeze dried structures produced from wet-gel aerogel precursors undergo microstructural changes due to the freezing process, driven by the growth of ice crystals in the gel. As the liquid in the pores of the gel freezes, the solvent crystals expand and exert stresses on the surrounding gel matrix, often resulting in a rearrangement of the solid material. Commonly they form into lamellae or layers, aligned with the growth of ice crystals. However, according to some definitions, cryogels can be useful alternatives to 'true aerogels' when resulting properties, particularly pores, approach or meet typical aerogel properties. This technique also alleviates the commercial costs associated with using supercritical fluid drying (though ambient drying remains the easiest and most cost-effective option). The use of solvents with low expansion coefficients coupled with strongly crosslinked gels can allow cryogels to achieve, or even exceed, the properties typically seen in supercritically dried aerogels, as demonstrated by the high surface areas ($> 2500\ m^2\ g^{-1}$) of freeze dried organic aerogels [58]. Additionally, if anisotropic properties and/or macroporous structures are desired, such as is the case

for applications as cell scaffolds in tissue engineering, the use of the freeze drying technique may even be preferable to the supercritical drying method.

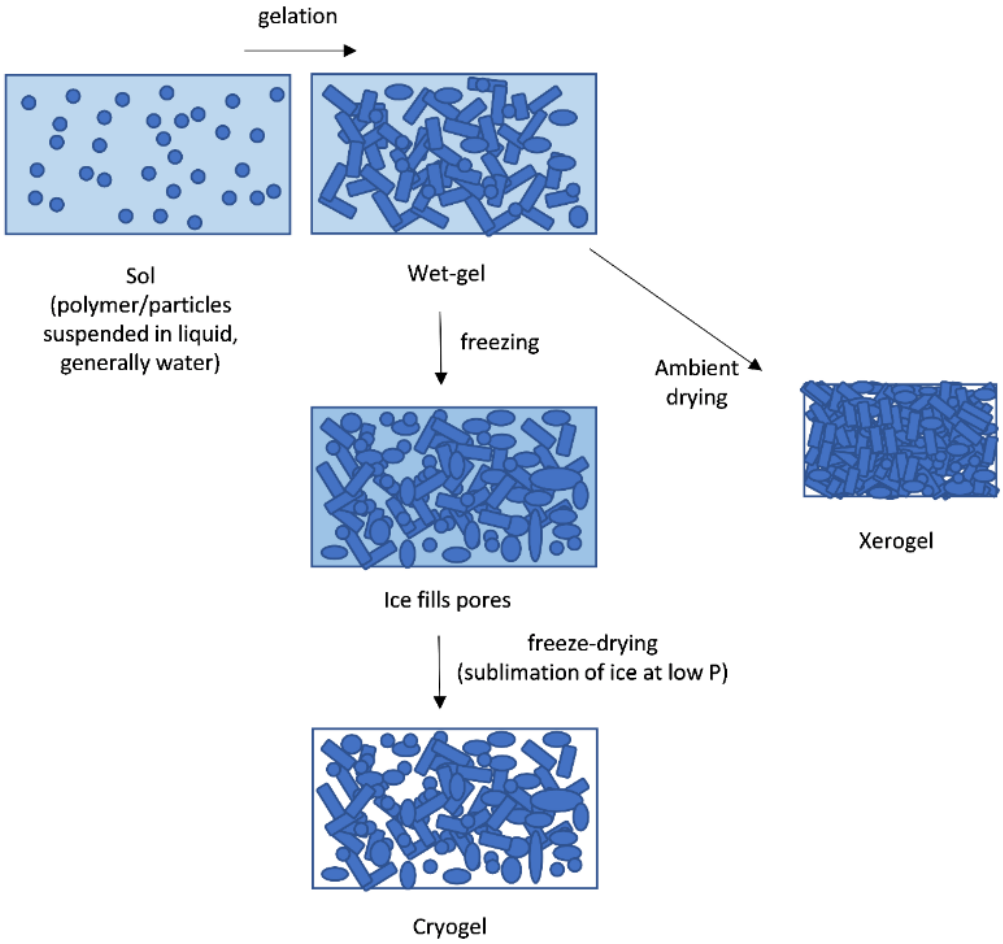

***Figure 2.6**: Process of transforming a sol to a cryogel or xerogel.*

Moving forward from Kistler's success with the initial aerogels, research can now be focussed on manipulating and fine-tuning this sol-to-gel-to-aerogel process. Understanding of the physical effects of the drying stage and of the chemistry during gelation is increasingly becoming outdated for some aerogels as an increasing variety of precursors are used in aerogel research. Elucidating the connections between the processing stages and the resulting aerogel properties of new aerogel types will provide critical information for future aerogel manufacturers looking to adapt their aerogels to designated applications.

2.1.2. Morphology

The study of the morphology of aerogels encompasses macroscopic and microscopic studies of both the particles/matrix (solid component) and the pores. Morphological data provides important explanations for certain aerogel properties. Microstructure studies can also explain how macroscopic physical changes in the aerogels result from the preceding processing methods. Understanding of the morphology allows for subsequent predictions about aerogel performance in certain applications, often prior to measuring these application-specific properties. Morphology is assessed with a variety of techniques including visual assessment/photography, microscopy (light and electron), X-ray imaging, porosimetry, pycnometry, and gas physisorption. **Section 2.2.3.3** describes some of these techniques in detail with respect to protein-based aerogels and the relevant experimental procedures for those used in this thesis can be found in **Chapter 4**.

The archetypical aerogel is that of the silica aerogel with its distinctive spherical particulate microstructure and meso-scale range pores (5 – 100 nm) (see **Figure 2.2c**). The structure is amorphous and typically > 90 % porous, and specific surface areas are high, typically 250 – 800 m^2/g [59]. Other inorganic aerogels include: alumina, zirconia, titania and further examples of metal oxides, these aerogels are also highly porous and achieve similar specific surface areas as silica aerogels [27] though with distinct microstructures that are dendritic-like rather than spherical (see **Figure 2.2d**).

The morphology of organic aerogels (resorcinol-formaldehyde, phenol-formaldehyde, polyacrylates, polystyrenes, polyurethanes, and epoxies) can differ in particle size and shape due to the difference in molecular structure and gelation mechanisms of each precursor. Perhaps the most popular organic aerogels are the resorcinol-formaldehyde (RF) examples (**Figure 2.7**) that may have fibrous, 'polymeric' appearances, 'colloidal' or 'string-of-pearl' appearances, and range in particle sizes depending on the type of catalyst used (base or acid) and ratio of resorcinol to catalyst. Consequently, the typical specific surface area values for base-catalysed and acid-catalysed RF aerogels are 800 m^2/g and 300 m^2/g, respectively [60]. RF aerogels are most known for their superior insulative properties (typical thermal conductivity of 0.012 W/m.K) over silica aerogels (0.016 W/m.K) due to small particle and pore sizes, as well as being stiffer and stronger than silica aerogels [60]. RF aerogels are

also commonly carbonized (**Figure 2.7**) to slightly shrink the aerogels, reducing particle sizes and increasing surface areas. The increased pore volumes and surface areas can even be achieved without changing the basic structure [61].

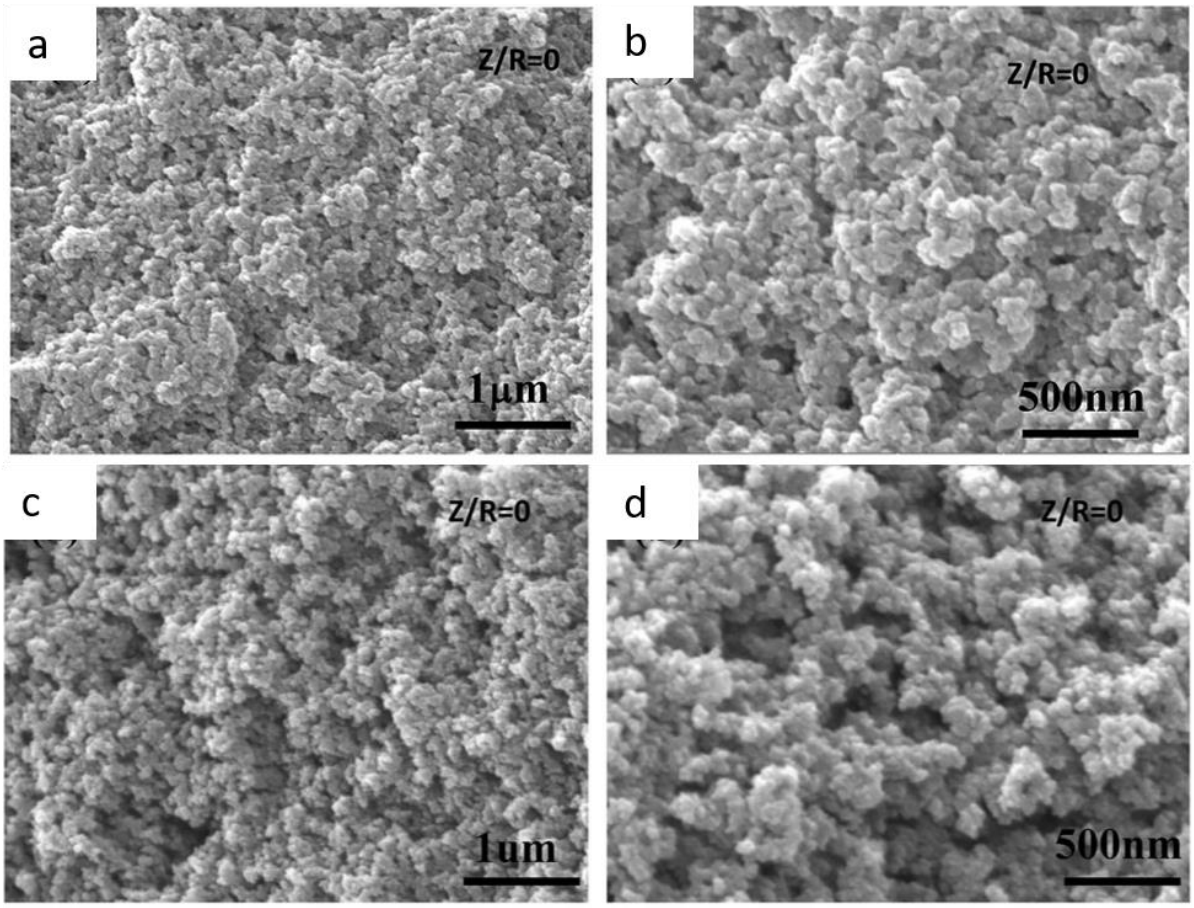

Figure 2.7*: Resorcinol-formaldehyde aerogel microstructure* ***(a-b)*** *and corresponding carbonised aerogel* ***(c-d)****. Adapted from images in reference [62]: Zhang, H., et al., Controlling the microstructure of resorcinol-furfural aerogels and derived carbon aerogels: Via the salt templating approach. RSC Advances, 2019. 9: p. 5967-5977, Copyright 2019, The Royal Society of Chemistry*

Many organic precursors (*e.g.* epoxies) can also be used in conjunction with metals to create a variety of aerogel architectures and consequently create mixed properties such as high surface area aerogels with reduced stiffness [63]. Organic aerogels also include the category of bioaerogels, which are the subject of **Section 2.2**. Bioaerogels differ from the above listed organic examples not only by origin of the precursor molecules but also because they are predominantly made from polymeric precursors rather than monomers which are polymerised during gelation. In discussing the types and forms of biopolymeric aerogels and their production, **Section 2.2** highlights another factor that influences the morphology of an aerogel: the choice of drying method. The drying stage is highly influential on the

final aerogel morphology. RF gels demonstrate this difference in RF aerogels dried using ambient drying, freeze drying (with *tert*-butanol as solvent) or supercritical CO_2 drying. The specific surface areas of these aerogels range from < 900 m^2/g (ambient dried) to > 2500 m^2/g (freeze dried) attributed to differences in particle diameters (100 nm diameter in ambient drying, 30 nm in freeze drying) which subsequently influence pore sizes [58]. The exact effect on morphology of freeze drying versus supercritical CO_2 drying also depends on the aerogel type and amenable solvents.

Understanding how processing conditions influence the morphology of aerogels brings an understanding of how those conditions affect the aerogel properties. The choice of precursor molecule/s, gelation mechanism, drying method, and post-drying processing (*e.g.* carbonisation) can all independently influence the resulting morphologies of the aerogels, sometimes to quite large extents. Investigating morphological variance alongside aerogel properties reveals the link between structure and function. Consequently, the morphology of the aerogels is a crucial factor when producing aerogels with improved and desirable properties for specific applications.

2.1.3. Properties and Applications

The extensive list of aerogel applications introduced in **Table 1.1** are made possible by the properties of the aerogel which can be adapted and enhanced for certain commercial settings. Many of these applications are directly reliant on the impressive aerogel property of ultra-high specific surface areas which occur alongside high pore volumes. The properties are direct consequences of porosity. Although high surface areas are also found in bulk materials composed of small particles such as powders, the porosity of aerogels allows them to be handled and manufactured like monolithic solids rather than liquid-like, free-flowing particles. A free-standing monolith with high surface area can be used for the applications in **Table 1.1** much more readily than powders.

The few morphological features responsible for the properties of aerogels are pore structures (size, interconnectivity, shape) and matrix structures (particle/fibre size, connectivity, orientation,) with some properties also a result of the chemistry of the precursor material. Aerogels are known for: low-

densities, high specific surface areas (600 - 1000 m^2/g [2]), high specific strengths (0.6 - 2.2 MPa/(kg/m^3) [64]), and low thermal conductivities (0.016 W/m.K [60]). These properties are generally found in all (mesoporous) aerogel types though specific aerogel types tend to be known for one or two of these properties. For example, silica aerogels are renowned as thermal insulators but are generally considered to have relatively poor mechanical properties.

Additionally, certain aerogel types exhibit complementary properties that make them further suitable for the principal application. For example, silica aerogels have high transparency due to a refractive index close to 1, making them excellent materials for high-energy particle capture (Cerenkov counters) [14] and insulative panels for daylighting [65]. Another property which complements typical aerogel properties is a high strength-to-weight ratio, resulting from the extremely low densities of aerogels. For example, the combination of low mass, low thermal conductivity, and high compressive strength makes aerogels a preferred choice for thermal insulation panels in aircraft and spacecraft [66]. The high strength-to-weight ratio means the payload for the aircraft can be lowered without compromising the function of the structural material in question.

Silica aerogels have hydrophilic behaviour due to silanol groups on the surface but can also be readily prepared as hydrophobic materials using silicon precursors containing non-polar chemical groups (*e.g.* $RSi(OR')_3$) or treated with a non-polar reactant after aerogel drying. Selective hydrophobicity/hydrophilicity makes silica aerogels useful in fluid separation applications such as oil-spill clean-up and similar environmental remediation applications [67]. Silica aerogels are also useful for entrapment or encapsulation of other molecules which serve to functionalise the aerogels (see **Section 2.2.3.5**). Advances in aerogel manufacture through use of organosilicons have resulted in super-flexible aerogels with much improved elasticity and low values of Young's modulus, reminiscent of rubber and polymer-like materials [68]. Inorganic aerogels such as Fe (III) oxide aerogels can be used as energetic materials in applications such as explosives, propellants, and pyrotechnics. A specific reduction/oxidation reaction known as a thermite reaction can be engineered into metal oxide aerogels through homogeneous gel preparation of the reactive metal and metal oxide components [15]. The resulting aerogel facilitates rapid (explosive) combustion due to porosity and

high surface areas. A similar capacity to homogeneously incorporate reactive molecules through an aerogel structure allows inorganic and carbon aerogels to be used as catalytic platforms and chemical sensors [16]. Biocompatible aerogels, namely silica and bio-based aerogels, find unique application in medicine and pharmaceutical applications such as in implant devices, tissue engineering and drug delivery [20, 21]. The unique advantages of bioaerogels are further discussed in **Section 2.2**.

The myriad of applications for these amazing materials is an exciting prospect for aerogel researchers. Aerogels offer exciting potential in yet undiscovered applications due to the infancy of aerogel commercialisation. Known properties of aerogels, such as high-surface areas, may yet be used in novel ways in new industries. Additionally, the development of novel aerogel types, forms and processes also offers promise in developing novel aerogel properties or combinations of properties, which could also be used in entirely new applications and markets.

2.2. Biopolymers and bioaerogels

Materials science now sees burgeoning interest in the development of sustainable and recyclable or biodegradable products. Sustainability and biodegradability concerns around aerogels, their precursors, and the processes used to produce them, remain largely unaddressed by most aerogel research. Aerogels remain largely high-cost and purpose-built for expensive applications with long durations (years). Aerogels have historically been produced from non-sustainable and/or non-biodegradable resources due to the exceedingly impressive properties of inorganic and synthetic organic aerogels (see **Section 2.1**). However, there has been recent interest in using biopolymers as precursors for aerogel materials [69]. Much of the motivation for developing bioaerogels is the promise of new applications. These new applications are likely to be due to the unique properties of bioaerogels, such as combined biocompatibility and biodegradability, in applications such as medicine and food.

2.2.1. Biopolymeric materials

The use of biopolymers for materials applications is a recent and growing shift towards sustainable, carbon neutral and biodegradable materials [70]. Biopolymers are polymeric molecules produced by living organisms of which the most ubiquitous and well-known are polynucleotides (*e.g.* deoxyribonucleic acid (DNA)), polysaccharides (*e.g.* cellulose), and polypeptides (*e.g.* proteins such as casein). Biopolymers are strong candidates for the manufacture of environment-friendly products, due to the sustainable nature of their production as well as inherent biodegradability and biocompatibility [71]. If processing techniques retain the biodegradability and biocompatibility of the original biopolymer, materials produced from polysaccharides and/or proteins are generally regarded as sustainable, compostable, and non-toxic. Many biopolymers have already become well-researched alternatives to petroleum-based polymers in materials, such as cellulose [72]. While this review of the aerogel literature highlights only naturally occurring polymers from biomass (such as polysaccharides

and proteins), there is also potential for biodegradable polymers synthesized from biomass (*e.g.* poly(lactic acid) (PLA)) to be used in future bioaerogel research.

Bioaerogels have existed since Kistler's publications describing aerogels for the first time (refer to **Section 1.2)**. Bioaerogels are candidates for uniquely biological applications such as cell scaffolding and drug delivery due to biocompatibility and biodegradability [20]. Bioaerogels are also cited as preferable to inorganic and synthetic organic aerogels in some applications for their inherent biodegradability [73]. For example, biocompatible aerogels with specific porosities are effective cell scaffolds in tissue engineering applications [17]. Other bio-specific applications where biopolymers offer an advantage due to digestibility include drug delivery [74] and food science [75]. Bioaerogels are demonstrating potential in further fields of application such as environmental remediation [76] and the use of sustainable precursors is also a strong driver in this field [11]. Bioaerogels based on polysaccharides are a popular choice due to the natural abundance of the raw materials and the ability to use both raw material (polymeric) and the molecular (monomeric) feedstocks in the production of the aerogels [11]. Bioaerogels based on proteins are possibly the least-known of all aerogel types but are an emerging field of research.

2.2.2. Polysaccharide versus protein aerogels

Much of the research within biopolymer-based aerogels focusses on polysaccharide-based gels (almost 90 % of bioaerogel examples), while protein-based aerogels make up < 8% of the literature (with composite or hybrid aerogels as well as polyphenols (*e.g.* lignin) also contributing to bioaerogel research) [11]. Polysaccharide aerogels are usually cellulose, chitosan, alginate, starch, or pectin, where cellulose is used in almost 50 % of all polysaccharide aerogels. Other examples of polysaccharide aerogels include carrageenan, agar, xanthan, guar and pullulan [11].

Biopolymer aerogel research is in part motivated by the presence of functional chemical groups on many of these molecules. Most aerogel researchers work with materials that have known chemical structures and, in many cases, preestablished chemical methods of gelation. For example, the

polymerisation process in silica gels depends on the simultaneous hydrolysis of the silanol (≡ *Si-O-H*) groups and the condensation of water, resulting in a network of siloxane bridges (≡ *Si-O-Si* ≡) [59]. Commonly used polysaccharide precursors for bioaerogels also have well-understood gelation chemistries, often employing pH changes, divalent cations, or cross-linking *via* functionalised chemical groups and added crosslinkers [11]. Cellulose can form a gel with the use of calcium thiocyanate ($Ca(SCN)_2$) as a salt-hydrate melt that dissolves the strands of cellulose into a colloidal system [77]. Alginate also interacts with divalent or multivalent cations to form gels [78]. In both cases the cation coordinates to carboxyl and hydroxyl groups on the polysaccharides, a functional group plentiful to polysaccharides. Chitosan (a derivative of chitin) can form chemically crosslinked gels as well as reversible ones from pH-controlled solutions [79]. Chitosan is popular as a precursor due to the presence of the amine group which can be functionalised with a range of electrophiles [78]. Understanding of the chemical processes during the gelation helps to guide aerogel researchers in developing new preparation methods and improved properties in these aerogels.

Polysaccharide aerogels are often composed of fibrillar networks, contrasting the particle-based, 'string-of-pearl' structures seen in silica aerogels. Densities, pore sizes and specific surface areas of polysaccharide aerogels are more varied than inorganic and RF counterparts and are often dependant on the drying method [11]. For example, *Zhao et al.* report a variety of (mostly web-like) morphologies produced from different types of biopolymers and various production methods (**Figure 2.8**) [11].

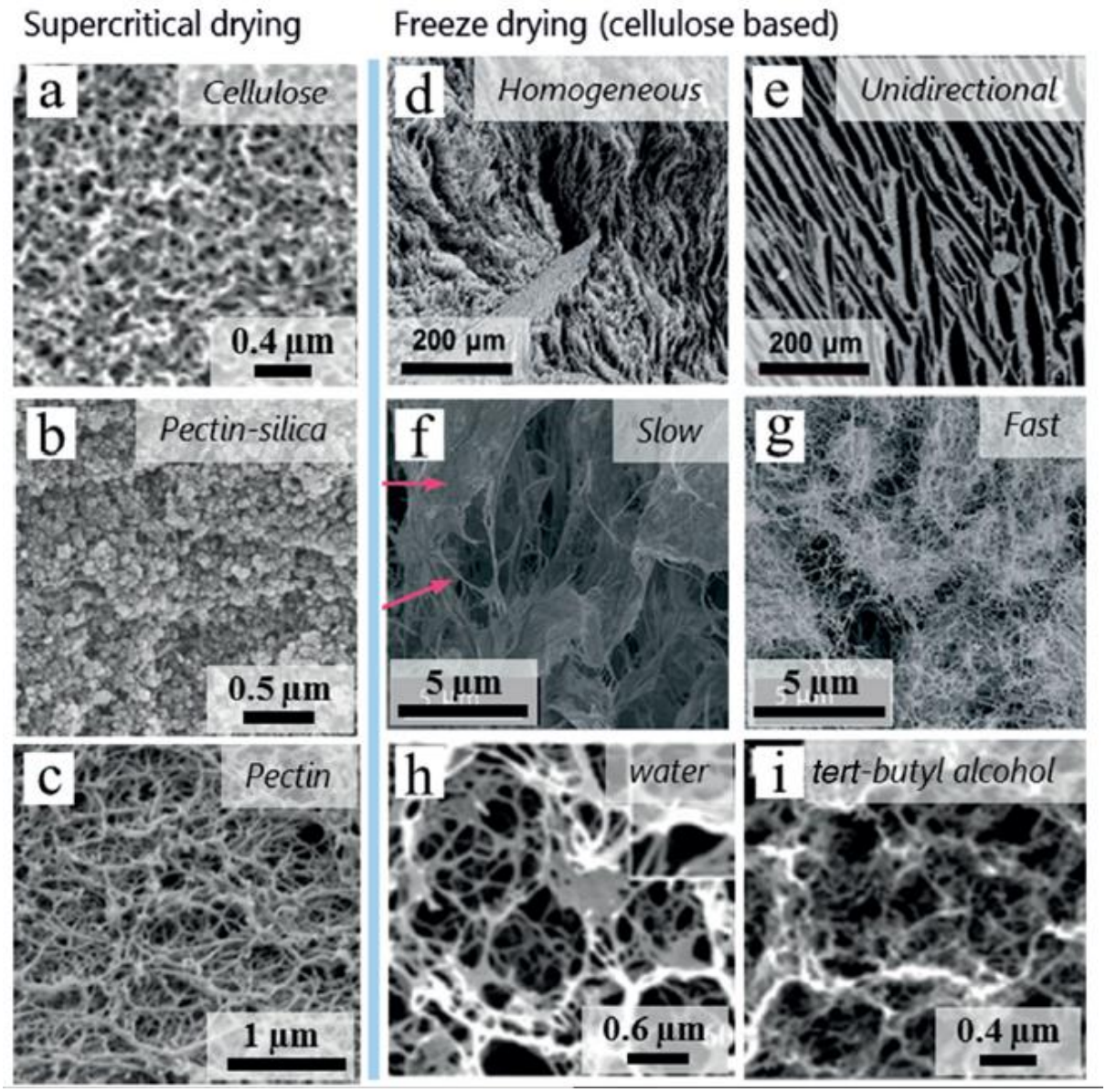

Figure 2.8: *Examples of bioaerogel microstructures. Aerogels are either supercritically dried* ***(a-c)*** *or freeze dried* ***(d-i)*** *and composed of cellulose* ***(a, d-i),*** *pectin-silica (hybrid)* ***(b)****, or pectin* ***(c)****. Freeze dried cellulose aerogels demonstrate a variety of microstructures due to various drying conditions (homogenous* ***(d)****, unidirectional* ***(e)****, slow* ***(f)****, fast* ***(g)****) and different solvents (water* ***(h)****, tert-butyl alcohol* ***(i)****). Image adapted from Zhao, S., et al. (2018). Angewandte Chemie International Edition, 57(26), 7580-7608 [11]*

The advantages of polysaccharide aerogels include: (i) chemical functional groups that allow for aerogels with application-specific chemistries; and (ii) improved flexibility that improve mechanical performance in composite aerogels (such as silica-cellulose aerogels for insulation). Polysaccharide fibres are also used to strengthen various composite aerogels while maintaining traditional aerogel properties such as low thermal conductivity (< 20 mW/m.K). However, the thermal conductivity of

biopolymer aerogels is generally higher than pure silica counterparts, therefore the low thermal conductivities of composite aerogels are attributed to the silica component [11]. A disadvantage of pure polysaccharide-based aerogels in commercial applications (*e.g.* as insulation) is their inherent hydrophilicity. Water absorption and water damage can exclude these materials from being commercially practical and jeopardises the long-term stability of any commercial polysaccharide product that has not been sufficiently hydrophobized.

The functionalisation of polysaccharide aerogels allows them to be used for oil-water separation, reversible gas sorption, and metal-ion or dye sorption, in applications such as bio-sensors, catalysis, environmental remediation, and filtration systems [11]. The most well-known areas of application in polysaccharide aerogels are possibly as drug and nutrient delivery systems in medicine and food due to both chemical functionalisation potential and biocompatibility/biodegradability [80, 81].

Protein-based aerogels, first seen in Kistler's work with gelatine, have only very recently seen a resurgence and are still very rarely seen in aerogel laboratories. However, within this limited cohort of protein-based or protein-encapsulated aerogels, proteins have been shown to provide exciting functionality to aerogels, including enzymatic function [82, 83], improved drug release [84] and other unique protein-specific bioactivities [85]. In contrast with other aerogel precursors, proteins have less well-characterised gelation methods and chemistries. Proteins have a selection of functional groups that undergo a range of chemical bonding types such as salt bridging, hydrogen bonding, covalent bonding and hydrophobic secondary interactions [86]. These interactions form part of the native protein structure and function. The exact type and locations of bonds that occur when a protein undergoes gelation is relatively more complex due to the wider variety of chemical interactions when compared to that of other aerogels (*e.g.* silica and polysaccharide). The precise gelation mechanism/s of proteins can be difficult to describe due to this abundance of varied chemical interactions, large molecular weights, and complex molecular conformations.

Proteins have attracted less attention than polysaccharides as bioaerogel precursors. Consequently, there is a distinct lack of data about protein aerogels available, especially in some areas such as mechanical performance. However, the potential use of proteins as a precursor material for

bioaerogels is of interest due to the (i) abundance of biomass-derived proteins available globally [87], (ii) gel-forming characteristics of proteins, and (iii) chemical functionality of proteins. Proteins obtained as co-products from food processing are particularly promising sources of raw feedstocks for bio-based materials [88]. Certain polysaccharides are chosen for their functional surface groups (*e.g.* amino groups on chitosan) [89]. However, the presence of functional groups in amino acids (*e.g.* thiol, hydroxy, amine, amide and carboxy groups) suggests that proteins may have extended chemical functionality over their polysaccharide counterparts (refer **Section 2.2.3**). Indeed, enzymes have been preserved during formation of aerogels, and the resulting aerogels retained the functionality of those enzymes [90]. Functionalising protein aerogels with inorganic particles has also been demonstrated and paves the way for possible applications in bio-catalysis and bio-detection [91]. Similar to polysaccharide aerogels, protein-based aerogels are also candidates for drug or nutrient delivery and are of particular interest as tissue scaffolding materials due to macroporous morphologies [92]. The inherent gelation capacity of certain proteins [93] facilitates processing of aerogels by removing the need for added crosslinkers. Despite these promising attributes, there are limited examples of protein-based aerogels in the literature, with the bulk of these derived from animal sources (*e.g.* egg protein [94], milk protein [95], silk [96], and collagen [48, 97]). Reports on the use of plant-derived proteins in aerogels in the literature are scarce and mostly limited to soy protein [98], chosen for its availability as a renewable resource [99].

Section 2.2.3 explores the literature around protein-based aerogels in further detail.

2.2.3. Protein-based aerogels: Precursors, processing, morphology, and properties

As part of the literature review for this thesis, a book Chapter (Fitzpatrick, S.E., *et al*, *Chapter 6 Protein-based Aerogels: Processing and Morphology*, in *Biobased Aerogels: Polysaccharide and Protein-based Materials*. 2018, The Royal Society of Chemistry. p. 67-102. [87]) was published by the Royal Society of Chemistry. This book Chapter contains a comprehensive review of the

processing methods and resulting aerogel morphologies from protein-based aerogels published in the literature prior to March 2017. Modified text from this review is presented in **Sections 2.2.3.1** to **2.2.3.6**.

2.2.3.1. Protein-based Aerogels – An Overview

Since the time of Kistler, research studies have been largely focussed on exploring the synthesis and properties of aerogels based on inorganic compounds. In contrast, organic-based aerogels including those based on natural compounds (bioaerogels) received very little attention until the late 1980s and early 1990s [41, 52, 100]. The precursor materials used in the synthesis of bioaerogels have been mainly based on various polysaccharides (*e.g.* cellulose) or proteins. Protein-based aerogels are a relatively new trend in the aerogel field, although the idea was also first explored by Kistler, using ovalbumin (egg white) and collagen (gelatine) proteins [101]. General interest in naturally sourced materials has increased dramatically in recent years, leading to a retracing of the steps made by Kistler in the earliest studies of bio-based aerogels. The supercritical drying technique has been used by researchers developing specific protein-based gels, as has the more recent technique of freeze drying. For example, the first protein-based aerogels were reported by Kaplan *et al.* in 2004-2005 using the freeze drying technique. Kaplan and co-workers produced silk fibroin protein-based aerogels in order to expand the application of biopolymer implant materials based on silk fibroin hydrogels [42, 102].

Proteins of both animal and plant origin have been used for aerogel production including ovalbumin (egg white protein) [32, 103-105], collagen (and gelatine) [32, 48, 101], silk fibroin (SF) [42, 92, 102, 106-110], wheat gluten [111], soy protein isolates (SPI) [98, 99, 112-115], corn zein [116, 117], and milk proteins (whey protein isolates (WPI) [91, 118-120] and casein [121]). The above proteins have been selected for their inherent fibrous/gel forming properties (collagen, gluten, silk fibroin, ovalbumin) and/or availability (gluten, whey, and soy protein isolates). The exploration of protein-based bioaerogels is largely motivated by the development of aerogels with characteristics of biodegradability and/or biocompatibility. The biodegradability of these materials could be considered

obvious, although some researchers are endeavouring to measure the biodegradability of bioaerogels in practice [73]. Many researchers have targeted naturally-occurring proteins due to their abundance and biodegradability [98, 103]. The biocompatibility and low toxicity of many proteins is also a consequence of their natural origins that may be coupled with benign processing routes. Biocompatibility has already been established for many of these proteins in the areas of medical and food research where the toxicity of the wet-gel precursors has been extensively studied [48, 122].

A main application of protein aerogels is tissue engineering, specifically the development of cell-culture scaffolds for supporting the growth of various tissues (see **Table 2.1**) [42, 48, 92, 102, 106, 123]. Drug delivery is a further medical application that is receiving great attention in the field of organic aerogels where biocompatibility is also a requirement [107, 109, 119, 120, 124]. The biodegradation of the materials is important for medical applications where there is a requirement for the material to be eventually absorbed by physiological systems. The remainder of the protein aerogel field sees applications in the laboratory (*e.g.* biomolecular catalysis and separation platforms [91]), environmental clean-up (*e.g.* waste-water treatment [113]) and industrial applications as bio-friendly versions of their silica and synthetic counterparts, for which the biodegradability, permeability and/or chemical specificity of the aerogel are important properties [98, 99, 108, 111, 118].

Since this current research began (since 2017), protein-based aerogel research has been focussed on using the supercritical drying technique (

Table 2.2). These later publications remain focussed on existing (animal) protein types (egg protein, silk fibroin, milk proteins, and collagen), further developing the potential of protein aerogels in the fields of nutrient and drug delivery, tissue engineering, catalysis and metal absorbents, and water-oil filtration. Supercritical CO_2 drying is a popular drying method due to the competitive porosity and surface area measurements that it permits. To this day, the gelation methods largely remain free of chemical crosslinkers, relying on aqueous chemistry or physical approaches to achieve these competitive protein aerogel examples (

Table 2.2).

Properties such as strength and bioactivity are largely dependent on the choice of protein precursor and the subsequent gelation methods. Contrastingly, the surface areas and porosities of protein aerogels are largely dependent on the drying method. Protein aerogels are generally nominated for applications in drug/micronutrient encapsulation or tissue engineering due to their existing presence in the food industry (egg and milk proteins) and medical industry (collagen). For such applications, the porosity and surface areas are the most relevant properties after biocompatibility and digestibility. 'Non-bio' applications of protein aerogels are rarely suggested and investigations into aerogel properties for 'non-bio' applications (*e.g.* mechanical performance and thermal conductivity) remain scarce, with just a handful of investigations reporting the compressive strengths (0.05 MPa [125] to 14 MPa [126]) and compressive moduli (up to 18 MPa [127]) of protein aerogels.

.

***Table 2.1**: Comparison of processing methods and applications across protein-based aerogels in the literature from 2004 - 2017 (organised by protein type).*

Protein	Other	Protein %	Gelation method	Drying method	Application	Year	Reference
Whey proteins	-	20	pH / heat	SC-CO_2	Medical - Drug delivery	2012	[95]
	-	20	pH / heat	Freeze drying			
	-	10 - 25	heat / salt	Freeze drying	Industry - Insulation	2013	[127]
	alginate	7.5 - 12.5	heat / salt	Freeze drying			
	-	-	Heat / salt / acid	Freeze drying	Medical - Drug delivery	2016	[120]
	cellulose	-	Heat / salt / acid	Freeze drying			
	-	1 - 3.5	Salt	SC-CO_2	Laboratory - catalysis / biodetection	2016	[91]
Silk fibroin (SF)	-	10 - 17	alcohol / salt / base	Freeze drying	Medical - Tissue engineering	2004	[42]
	-	4 - 10	salt	Freeze drying	Medical - Tissue engineering	2005	[102]
	-	6 - 12	heat	Freeze drying	Medical - Tissue engineering	2006	[123]
	clay	0.05 - 5	-	Freeze drying	Industry - not specified	2008	[125]
	-	5	salt	Freeze drying	Medical - Tissue engineering	2012	[110]
	-	4	heat / acid	SC-CO_2	Medical - Drug delivery	2014	[128]
	-	4 - 13	acid	SC-CO_2	Medical	2014	[129]
	graphene	7 - 8	base	Freeze drying then carbonisation	Industry - Capacitors	2014	[130]
	-	2 - 6	acid / salt	SC-CO_2	Medical - Tissue engineering	2015	[92]
	-	2 - 6	acid / salt	Freeze drying			
	-	10 - 15	salt / alcohol	SC-CO_2	Medical - Tissue engineering	2016	[96]
Soy proteins	clay	0.05 - 5		Freeze drying	Industry - not specified	2008	[125]
	-	25	chemical / heat	SC-CO_2	Industry - Insulation	2012	[98]
	cellulose	4 - 8	heat	Freeze drying	Industry - Fluid absorbents	2013	[131]
	graphene	-	heat	Freeze drying	Environment - Water treatment	2015	[132]
	graphene	-	acid	Freeze drying	Environment - Water treatment	2015	[113]
	-	-	chemical	Freeze drying	Industry - Insulation	2016	[114]
	graphene	-	acid	Freeze drying	Environment - Water treatment	2016	[115]
Ovalbumin	-	1.5	heat (directly carbonised)	SC-CO_2	Environment - CO_2 absorption + Laboratory - catalysis/separation	2011	[104]
	-	10	pH / heat	SC-CO_2	Food – microencapsulation	2015	[94]
	cellulose	11	acid then heat (directly carbonised)	Freeze drying	Environment - Water treatment	2015	[133]
Gluten	-	11 – 17	glycerol and heat	Freeze drying	Industry - general absorbents + Medical/Cosmetics – drug delivery	2010	[111]
	cellulose	11 - 14	heat	Freeze drying			
Zein	agar	3 - 6	heat	Freeze drying	Industry - not specified	2012	[134]
	silica	-	chemical / heat / gas	SC-CO_2	Industry – thermoplastics	2014	[135]
Collagen	cellulose	-	chemical	Freeze drying	Medical - Wound dressing /Tissue engineering	2014	[48]

	alginate	3	gas	SC-CO_2	Industry - Insulation Medical - Tissue engineering	2015	[136]

***Table 2.2**: Summary of protein-based aerogels and their properties that were published after 2017.*

Protein	Other	Gelation method	Drying method	Morphology	Properties	Application	Year	Reference
Silk Fibroin (SF)	Pd, Pt, Au	Physical crosslinking *via* solvent exchange	SC-CO_2	Network of 500 nm particles in 'string of pearl' larger fibres. Mesoporous, SA = 72 – 268 $m^2 g^{-1}$	Templates for noble metal nanoparticle growth	Energy storage	2019	[137]
	Polymethyl-silsesquioxane (PMSQ)	Acid catalysis of SF	SC-CO_2	Macroporous network of strands with micro- and *mesoporous* sub-structure, ρ = 0.08 – 0.23 g cm^{-3},	Compressive strength up to 14 MPa and high compressibility, hydrophobic and thermally insulating.	Oil separation, fire retardant,	2018	[126]
Egg and milk proteins	-	pH, heat, enzymatic crosslinking	SC-CO_2	Mesoporous, ρ = 0.29 g cm^{-3}, SA = 210 - 420 $m^2 g^{-1}$	pH-dependency of rheological and mechanical properties, high surface areas	Microencapsulation in food, cosmetics, or pharmaceuticals	2018	[75]
	-	pH, heat, enzymatic and salt ion crosslinking	SC-CO_2	Mesoporous, ρ = 0.18 – 0,43 g cm^{-3}, SA = 48 - 354 $m^2 g^{-1}$	High surface areas, capable of loading with fish oil and antioxidants	Microencapsulation in food	2019	[138]
Egg protein	-	Heat and pH	SC-CO_2	mesoporous, ρ = 1.31 – 1.56 g cm^{-3}, SA = 65 - 252 $m^2 g^{-1}$	High surface areas, readily gelled, food-grade structures.	Carriers of active substances	2019	[139]
Collagen/gelatine	Poly(lactic-co-glycolic) acid, glass fibres	Heat, physical crosslinking using electrospinning	Freeze drying	Fibrous, macroporous network composed of 100 nm wide fibres.	Bioactivity and mechanical stability, bone regeneration studies	Tissue engineering: bone regeneration	2018	[140]

Currently, there is a similar level of research activity associated with pure and hybrid protein aerogels. A hybrid gel consists of two or more constituents that make up the solid network [118]. Note that aerogels that include the use of crosslinking molecules for bridging protein molecules in their synthesis are not categorised here as hybrid protein aerogels. Consequently, only those materials that are able to inherently form a gel network (*e.g.* silica, clay, carbohydrates, *etc.*) are categorised as hybrid protein aerogels, where additives are not required for the gel network formation [141]. Hybrid protein aerogels have been produced for each of the protein types already used in aerogel research (ovalbumin, collagen, silk fibroin, gluten, soy protein, corn zein and whey protein), often alongside aerogels of each of the pure constituents for comparison. A wide range of applications from tissue engineering to absorbent materials to capacitors have all spurred on the development of hybrid bioaerogels due to their customisable physiochemical properties.

2.2.3.2. Processing and fabrication of protein-based aerogels

The synthesis of an aerogel begins with a sol – a stable colloidal suspension of solid particles in a continuous liquid medium. The protein is the solid phase in the sol of a protein-based aerogel; or in the case of a hybrid protein aerogel, the solid phase may consist of both proteins and polymers. Gelation of the sol creates a continuous network of the solid particles that are suspended in the liquid medium (**Figure 2.9**). Subsequently, evaporation of the liquid medium by drying allows an aerogel to be formed as gas (normally air) replaces the liquid medium that surrounds the gel network.

Sol-gel processing

In protein chemistry, the route to a sol involves manipulation of certain conditions to make the protein less soluble in aqueous solution – a transformation that is termed protein aggregation. Proteins are dissolved in an aqueous solution at a pH and salt concentration near to physiological concentrations to mimic biological conditions. Such biomimetic approaches support natural (or native) protein conformation and activity that is useful for studies and applications of normal protein conformation and function. Generally, the formation of an aerogel does not require the protein to maintain its native

conformation and in fact more facile aerogel formation is often possible using alternative conformations induced prior to gelation [91].

Proteins with an alternative (or non-native) conformation are described as being denatured. A sol may be obtained from a protein solution by precipitating the protein as stable aggregates that remain suspended in the liquid. Precipitation of the protein is achieved by disrupting the chemical interactions that stabilise the conformation of a protein molecule in water. The destabilised protein will exhibit different chemical moieties at the protein surface that tends to lead to protein aggregation. The newly exposed and/or activated chemical groups subsequently create new chemical interactions within the protein and with other protein molecules. Such interactions could be hydrogen bonding between polar groups (-OH, -SH, $-NH_2$), salt bridges between charged groups ($-COO^-$, $-NH_3^+$) or hydrophobic interactions of non-polar groups ($-CH_3$, aromatic groups); although, in general, it is the hydrophobic residues that drive protein aggregation since this reduces their interaction with the surrounding water [142]. The hydrophobic residues would normally be buried within a native protein conformation, away from the water molecules in which the protein is solvated. Once the native conformation is disrupted and hydrophobic residues are exposed, these denatured proteins develop hydrophobic interactions with neighbouring protein molecules to exclude water, leading to aggregation of the protein. The aggregated solid protein needs to be stable in the solvent, otherwise a solid mass of precipitate will form and separate completely from the water, rather than progressing to the hard gel stage.

Prevention of complete precipitation in part relies on the protein and solution conditions. However, complete precipitation can also be prevented by agitating the sol and/or rapidly progressing to the gelation stage. The aggregated protein will remain dispersed throughout the solvent if a delicate balance between attraction and repulsion of the aggregates can be maintained. Spontaneous gelation will occur without the need for further gelation induction if crosslinking and associative forces are more dominant than any electrostatic repulsion [143].

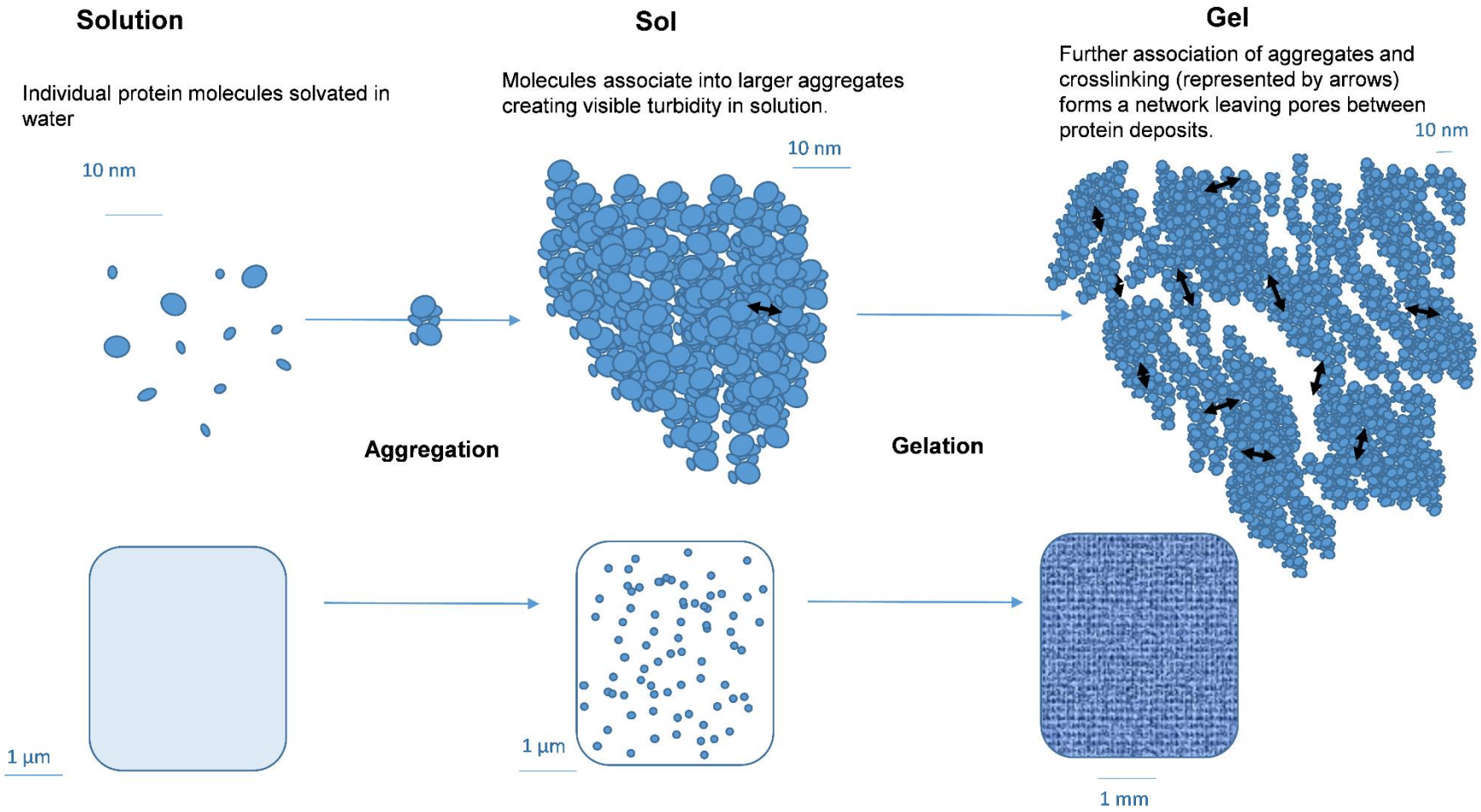

***Figure 2.9**: Representation of molecular and visible changes in a protein solution transforming to a hydrogel*

The formation of a gel (in this case a hydrogel) from the aggregation stage is essentially a continuation of the same chemical driving forces. Gelation is partly due to the same protein-protein chemical interactions as those described above and partly due to irreversible chemical crosslinking (*e.g.* disulphide bridge formation) [143, 144]. Disulphide crosslinks are covalent chemical bonds, formed between thiol (-SH) groups on amino acids. The formation of irreversible chemical crosslinks marks the permanent transition from the sol to gel and can be between any functional groups on the protein able to form covalent bonds (*e.g.* $–NH^{3+}$, -S-, $-COO^{-}$, *etc.*). The importance of crosslinking was illustrated by Chen *et al.* who conducted comparative studies of whey protein isolate (WPI) aerogels using salt and heat. It was observed that combining a denaturation step (heat) with a crosslinking inducer (salt) significantly improved the mechanical properties of the aerogel when compared to those only treated with heat. The increased crosslinking due to the salt not only improved the network strength but did so without affecting the density [118].

The gel network formation is controlled by both the rate of the crosslinking reaction and amount of net charge on the aggregates. Charged groups on proteins (*e.g.* $-COO^{-}$, $-NH_3^{+}$, $-S^{-}$) endow the overall molecule (and aggregate) with a positive or negative charge depending on the pH of the solution. Electrostatic repulsion between aggregates will slow the association of protein with greater charge on the aggregates. However, the electrostatic repulsion must be overcome by hydrophobic interactions to form a gel network, with the gel network then being stabilised by crosslinking. The morphology and physical characteristics of a gel are a result of the balance between the attractive and repulsive forces within the protein network and the overall degree of chemical interaction [142].

The protein concentration also influences the formation of the gel. The continuous gel structure cannot be formed below a certain concentration (critical concentration) since a certain amount of protein entanglement or cross-over is required to sustain the solid network [142]. Consequently, the higher the protein concentration, the less need there is for strong driving forces to induce aggregation prior to crosslinking.

The chemistry of protein gelation can be categorised as intrinsic or extrinsic [142]. The type of protein will dictate the intrinsic properties such as the amino acid residue composition, while the molecular

weight of the protein determines the likelihood of spontaneous gel formation. Additionally, there are 5 extrinsic factors (or solution properties) that can be manipulated to increase the likelihood of gelation: protein concentration, pH, temperature, pressure, and ionic strength/type of ion in solution [86]. Techniques aimed at manipulating the above properties are the focus of the sol-gel chemistry in the early stages of protein aerogel processing.

Denaturation or aggregation techniques are chemically simple, being induced by either a pH change, salt addition or increase in temperature. The technique often depends on the natural tendency of the protein (or polymer) to gel. For example, Selmer *et al.* heated an ovalbumin solution to simultaneously denature and induce crosslinking in the protein, producing a hydrogel in a one-step process [103]. This is effectively identical to the process of cooking an egg, producing a white gelatinous substance that is irreversibly changed from the viscous semi-transparent raw egg white. These two stages can be combined into a single denaturation and gelation step since aggregation and gelation involve similar chemistry and one is essentially an extension of the other.

Manipulation of the extrinsic properties (pH change, salt concentration, heat, *etc.*) is the most accessible method of inducing gel formation, although gel formation may also be induced by additives. For example, aldehydes can be used to react with protein to form covalent bonds that help to solidify the gel network [48, 98]. Other additives can be used to replace water as the solvent in the solution (*e.g.* methanol [42]) so as to disrupt normal protein-water interactions. High pressure (200-500 MPa) can also be used to induce hydrophobic interactions and disulphide bonds between protein molecules, while enzymes are able to catalyse the crosslinking of specific amino acids [143]. While high pressure and enzymatic techniques are utilised in protein sol-gel chemistry, these methods have not yet been applied to the protein gels used to synthesise aerogels.

pH-, salt-, heat- and additive-induced gels are discussed in detail below, using examples from the literature on protein-based aerogels. It is also possible to employ a combination of techniques to induce gel formation (*e.g.* pH change, salt or crosslinking agent in combination with heat, see **Table 2.1**).

Heat-induced gelation

Dissolving protein precursors in an aqueous solution and inducing gelation through heating is the simplest and most common method used to produce protein hydrogels. A variety of protein types have been gelled by this method including the previously described 'cooking' of the ovalbumin protein by Selmer *et al.* [103]. Increasing the temperature of a protein encourages dehydration and unfolding of the protein conformation by destabilising the chemical interactions and exposing residues within the protein core. The exposed residues are generally hydrophobic and will contribute to protein aggregation as the denatured protein seeks to re-stabilise its conformation within the aqueous solution. Examples of proteins where straightforward heat-induced gelation has been used include whey proteins [118-120], ovalbumin [103-105], zein [116], gluten [111], and soy proteins [99, 112, 115]. Moreover, the rate of protein aggregation, and hydrophobicity and size of the protein may influence the homogeneity of the gel (*e.g.* homogenous transparent gel *cf.* turbid coagulum-type gel). A gel may not form if the molecular weight and concentration of the protein are below critical levels [142].

In some proteins, the heating step can separate denaturation from the gelation step. For example, a common gelation technique with whey proteins is known as the cold-set gel procedure. The protein is first denatured *via* heating and then cooled, remaining soluble due to repulsive charges on protein molecules. Aggregation (and subsequent gel formation) is then induced by the addition of a salt. Separating these two steps is useful for studying the effects of denaturation, aggregate size, and crosslinking on the final aerogel morphology and properties [145, 146]. However, the fast and simple single-step heating could be a preferable gelation option for the industrial up-scaling of the process.

pH-induced Gelation

Varying the pH away from the isoelectric point (pI) of the protein induces a non-native protein conformation by altering the quantity and type of charged ions on the protein. Carboxylic acid (R-COOH $\rightleftharpoons$ R-COO^-) and amine (R-NH_2 $\rightleftharpoons$ R-NH_3^+) groups become protonated or deprotonated as the solution pH changes. Changing the protonation state of these chemical groups affects internal electrostatic interactions of the protein and its solubility. Charged groups on the protein interact with

each other (*via* ionic bonding) and with water. If the location or type of a charge on the individual protein molecule is changed (due to pH) these intramolecular protein bonds and the protein interaction with water can be disrupted, resulting in a denatured protein. In addition to intramolecular effects, the pH change can also affect the intermolecular interactions of the protein molecule with other protein molecules. The ratio of the charges (negative and positive) results in an overall molecular charge for each individual molecule. This charge helps to determine the amount of attraction that a single protein molecule will have to the neighbouring protein molecule in solution. A high degree of overall charge in one direction (*i.e.* highly negative or highly positive) will increase repulsion between individual protein molecules and counter-intuitively slow aggregation. Thus, an extreme change in pH value from the protein pI will denature protein molecules but resist aggregation through high electrostatic repulsion of molecules. To induce aggregation in this state, the charges need to be shielded by the addition of a counter ion from a salt which will neutralise the charges and allow protein molecules to aggregate.

Most frequently, a simple hydrochloric acid or sodium hydroxide adjustment for pH manipulation is performed prior to other processing steps being employed (*e.g.* heating) [103, 105, 119]. Alternatively, pressurised CO_2 gas is usually used to manipulate the pH in the gelation of silk fibroin (SF) protein [92, 106, 107, 144]. Glucono-δ-lactone is another acid used to modify pH of protein solutions and is common in sol-gel food chemistry of whey proteins [142]. Ahmadi *et al.* report the use of glucono-δ-lactone alongside heat and salt to induce gelation of a whey protein solution in the production of aerogels [120].

Salt-induced gelation

Salt additions (in excess of physiological concentrations) result in aggregation and gelation *via* an increase of ions in the solution. The ions (usually Na^+, Ca^{2+} and Cl^-) are electrostatically attracted to charged moieties ($-COO^-$, $-S^-$ and $-NH_3^+$) on the protein thereby creating a shielding effect. The salt ions effectively prevent the charges on the proteins from interacting with water *via* hydrogen bonding. Inner hydrophobic residues are then exposed and contribute towards protein-protein interaction that drives aggregation. In addition, the electrostatic repulsive forces between protein molecules are

decreased due to the ion shielding effect. Consequently, the protein molecules tend to aggregate, and a gel is formed (**Figure 2.10**). Salt-induced gelation is most used in whey protein isolate (WPI) gels where NaCl and $CaCl_2$ are known to be gelation agents of whey proteins. WPI will gel directly upon addition of $CaCl_2$ or NaCl to the solution, without the need for prior heat denaturation [142]. Salt can be used to induce aggregation and gelation of already denatured (but still soluble) whey proteins in such solutions. In this technique, the protein is first denatured (but not aggregated) using controlled heating, subsequently salt is added for the gelation step. This gelation technique is termed cold-set gelation since salt-induced gel formation is carried out at ambient temperatures [146].

The power of electrostatic forces within the protein dispersions (or sol) has been demonstrated by an incorporation of charged metal particles (*e.g.* gold) [91]. The gold nanoparticles nucleate on the surface of the denatured protein providing an electrostatic charge on the protein molecule. Following addition of salt as the gelation agent, the Au-Au repulsion is greatly reduced allowing the denatured protein to gel instantly [91].

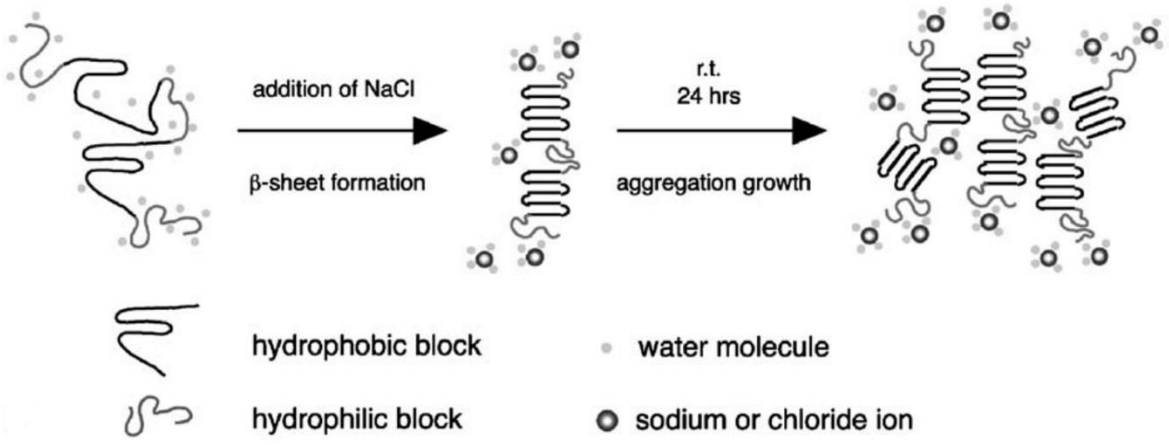

Figure 2.10*: Schematic of mechanistic basis for the structural changes occurring during salt-induced protein aggregation. Reprinted from Biomaterials, 26, U.-J. Kim, J. Park, H. J. Kim, M. Wada and D. L. Kaplan, Three-dimensional aqueous-derived biomaterial scaffolds from silk fibroin, 2775-2785, Copyright 2005*

Salt-induced gelation has also been shown to occur with silk fibroin (SF) proteins. A salt leaching method was employed where salt granules are used as porogens – a technique that is adapted from the production of porous scaffolds for use in tissue engineering [42, 102]. The porogen acts as a physical mould, allowing the protein to precipitate in the spaces around it to create a scaffold. The use of a salt

porogen effectively saturates the aqueous solution with dissolved ions and initiates the salt-induced gelation described above. An investigation of the structural changes induced by the salt porogens concludes that salt-induced dehydration exposes hydrophobic residues, initiating β-sheet formation in the secondary structure – a type of protein conformational change [102]. The salt is then removed by a leaching process with water followed by a solvent exchange with alcohol which is eventually evaporated, leaving behind the porous structure. The resulting porous structure can be further dried using freeze drying to ensure that all solvent is removed from the resulting aerogel.

Chemical additives

A less commonly used technique to achieve gelation is that of introducing other molecules to the solution that induce gelation *via* solvent removal or chemical crosslinking. Chemical crosslinking between protein molecules drives aggregation and stabilises the network within the hydrogel. Although covalent crosslinking occurs naturally in some proteins, the degree and rate of crosslinking may be increased by chemical additives. Crosslinking can be induced by adding a reactive molecule, such as an aldehyde, that forms covalent bonds with reactive groups on protein amino acids [114]. An example of this technique is the synthesis of a collagen-cellulose hybrid aerogel by prior oxidation of the cellulose fibres to create dialdehyde functionality on the glucose molecules of the cellulose chain. The dialdehyde-functionalised cellulose reacts with amine groups on the collagen protein, thereby crosslinking the two biopolymers [48]. Thus, the gelation of the collagen and cellulose is spontaneously driven by a crosslinking reaction of the aldehyde groups on the cellulose and amines of the protein. A crosslinking agent that forms covalent bonds with two protein functional groups can be utilised to achieve gelation in non-hybrid cases (*i.e.* where only the protein contributes towards the gel network structure). Repetition of the protein + crosslinking agent reaction results in two new covalent bonds which allow the crosslinking molecule to act like a bridge between two points on the protein molecule or molecules. An example of this bridging mechanism is observed for soy protein, formaldehyde and tannin aerogels as reported by Amaral-Labat *et al.* (**Figure 2.11**) [98]. Formaldehyde reacts with both the tannin and protein molecules and can undergo two reduction

reactions, allowing the formation of -CH_2- bridges between molecules. Thus, a complex network of protein-protein, protein-tannin and tannin-tannin crosslinks are formed to create the gel.

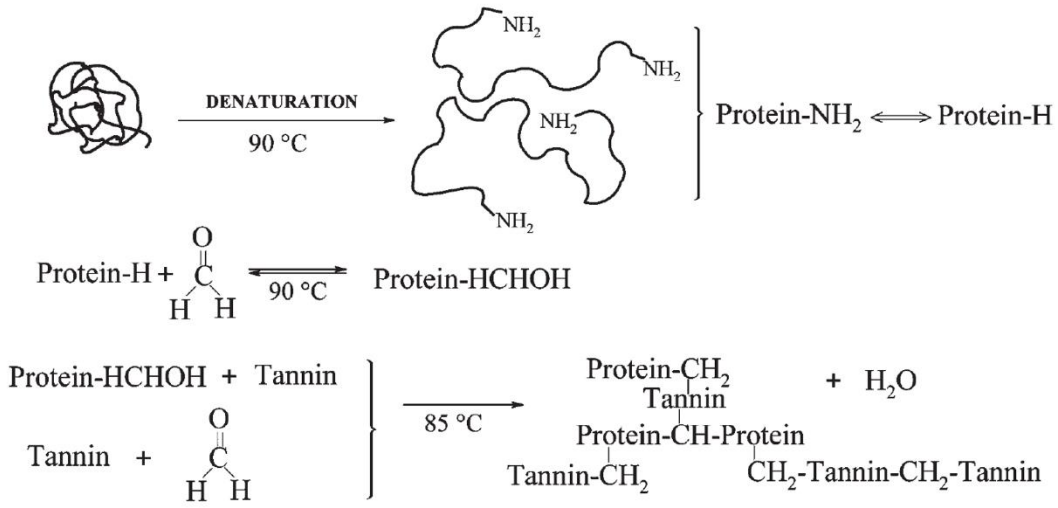

Figure 2.11*: Supposed crosslinking reactions of soy protein, tannin and formaldehyde. Reprinted from Amaral-Labat, et al. (2012). Green Chemistry, 14(11), 3099-3106 [98]*

Chemical crosslinking techniques take advantage of the existing chemistry within the proteins. The logical next step is to attempt an even wider range of chemically-induced crosslinking or other chemical interactions between protein aggregates by exploiting the chemistry of existing amino acid residues on the protein. Although this is slightly more complicated than a simple heat or pH induced gelation, this kind of chemical manipulation during the formation of the gel networks could be the key to tailoring the resulting aerogel properties such as elastic modulus, strength, density, and homogeneity.

The importance of these covalent crosslinks has been demonstrated in ovalbumin wet-gels by Van Kleef *et al.* where the resulting mechanical properties of the hydrogel are attributed directly to the number of thiol groups in the protein network [143]. Although these studies were completed on the hydrogel rather than the corresponding aerogel, this work provides clear evidence that covalent crosslinking (*e.g.* disulphide bonds) in a protein network is an important molecular feature in describing the processing-structure-property paradigm of protein-based gels.

Molecules that interfere with protein solvation, specifically a dehydration agent, may also induce gelation. For example, the use of alcohol to dehydrate the protein and encourage aggregation has been applied to the processing of protein aerogels [42]. Alcohol-induced gelation is similar in its mechanisms to that of heat-induced gelation. Alcohol destabilises the native protein conformation by reducing protein-solvent interactions due to the alcohol being significantly less polar than water. Alcohol dehydrates the protein molecules, and with a lower solubility of proteins in alcohol compared to water, the proteins are forced to aggregate. β-sheet structures form due to water removal during the aggregation. β-sheets are a secondary protein structure where the backbone of the protein takes on a pleated conformation. β-sheets may be part of normal protein structure or induced in a protein because other backbone geometries have been destabilised. The chemistry of protein folding is complicated, but it is necessary to note here that the β-sheet structure often stabilises hydrophobic amino acid residues that are exposed in denatured protein prior to the aggregation. It is the formation of non-native β-sheet structures that causes globular proteins in the neuronal tissue to denature and adopt the dangerous plaque-forming fibrous conformations, known as amyloid fibres, in those suffering from Alzheimer's disease. This mechanism of protein denaturation has been exploited by Nystrom *et al.* to produce extremely low density aerogels from β-lactoglobulin, a normally globular whey protein [91].

Therefore, it is clear that various parameters related to the protein solution and subsequent processing methods may affect the formation of a protein-based gel network (**Figure 2.12**). The network is composed of crosslinked protein aggregates that are in turn composed of denatured protein molecules. The gel network can range from a loosely connected agglomeration of large aggregates (where conditions favour large globular protein aggregation) to a tightly crosslinked network of smaller, fibrous aggregates separated by smaller spacing. The aggregation and gelation factors are influenced by the protein type, protein concentration, heat, pH, salt, and presence of crosslinking molecules.

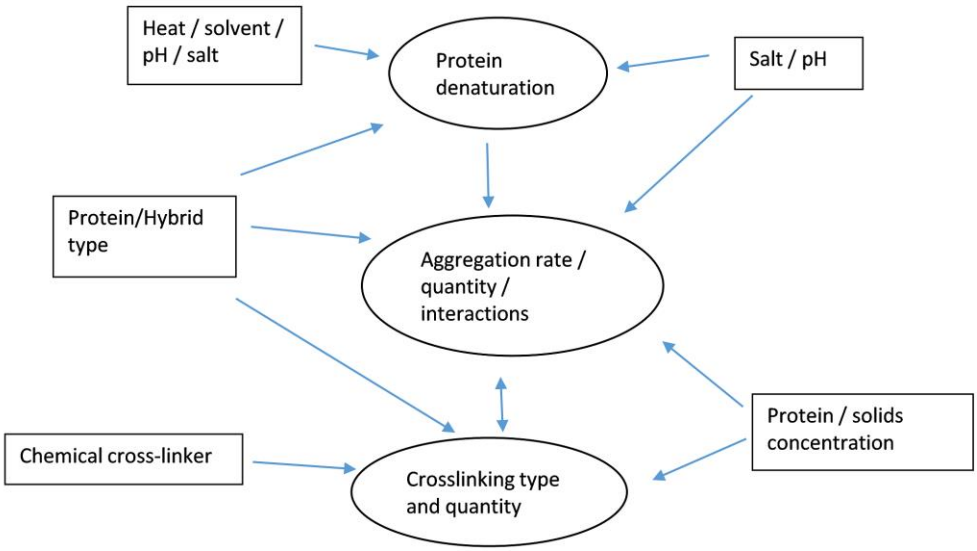

***Figure 2.12**: Schematic showing the effect of variables in a protein solution on the gelation process*

Gel-aerogel processing

Gels prepared in aqueous solution require conversion to a dry state such that air is dispersed throughout the solid gel network (see **Section 2.1**). Freeze drying involves the freezing and subsequent sublimation of the solvent (*e.g.* water) at low pressure. Supercritical carbon dioxide (SC-CO_2) drying involves replacing the liquid in the gel with supercritically-heated and compressed CO_2 that is then evaporated by reducing the pressure. As seen in sol-gel processing, the choice of solvent for protein solutions is always water but a solvent that may be dissolved in SC-CO_2 is required for this process. Therefore, water is solvent-exchanged with ethanol, or a similar non-polar solvent, that is more soluble in the SC-CO_2 and can be flushed out and replaced with the SC-CO_2.

Interestingly, the selection of the drying technique in the production of protein-based aerogels has not been discussed in the short history of these materials (drying techniques are listed in **Table 2.1**). Thus, there is no apparent preference of one technique over the other as a function of the protein or application. At these early stages in the protein aerogel field, researchers may be non-selective about drying techniques or may even experiment with both [92, 119] due to a lack of compelling evidence for the selection of one technique over the other. Cost, accessibility, ease of use, environmental

impact and effect on resulting aerogel properties will all be factors taken into consideration when a drying technique is selected. The exact effects of the drying process on aerogel properties may have high importance for the future of aerogel processing beyond the laboratory. Researchers may simply opt for the cheapest or most accessible option. Basic morphological and other physical properties such as strength, are not always reported in the literature with novel protein aerogels. The various applications of these gels mean that researchers are interested in investigating very different properties of the aerogels making it harder to collate information and draw basic conclusions regarding the processing-property relationships of protein-based aerogels. Nevertheless, **Sections 2.2.3.3** and **2.2.3.4** will investigate what relationships there may be between drying technique (among other processing differences) and the resulting aerogel morphologies and properties.

2.2.3.3. Morphology of aerogels

The morphological structure of aerogels is characterised in terms of the quantity, shape, size, and connectivity of its pores. A detailed knowledge of the pore structure is central to understanding the performance of an aerogel in a specific application. Low density and high porosity are two of the defining features of all aerogels. Density and porosity are interrelated such that lower density aerogels will generally have greater percentage porosity and total pore volume. Density is measured with straightforward laboratory assessments and can be used to calculate the quantity of air, or percentage of porosity, that the aerogel contains. Highly accurate mass and dimension measurements are taken of the entire aerogel to determine the bulk density of the intact aerogel structure. Measurements of the solid component in the aerogel can be taken by grinding it down and measuring the volume of the powdered aerogel in a pycnometer. A pycnometer is a device that detects the volume of a solid sample through displacement of a gas, usually helium. The sample is introduced into a pressurised chamber and the pressure change of the gas held in the chamber is used to calculate the volume that the sample occupies (pressure and volume are related by the ideal gas law). Combining this measurement with the mass of the sample, the skeletal density of the solid component can be calculated. Bulk and skeletal density can then be used to calculate the porosity. Dividing the bulk

density by the skeletal density gives the fraction of the aerogel volume that is due to the solid phase. Subtracting this value from 1 then yields the fraction of the aerogel that is air, thus indicating the porosity [98]. Alternatively, the total volume of the pores (measured in cm^3/g) can be calculated by subtracting the volume of the skeletal structure (solids) from the bulk volume.

Porosity can be further elucidated by measurements using nitrogen adsorption-desorption techniques. Nitrogen gas (or any appropriate gas) can be introduced in a controlled manner to a chamber containing the sample. The gas will adsorb on the surface of the material and upon subsequent release at increasing temperatures, will result in a measurable increase in gas pressure. An isotherm which tracks these pressure changes can be plotted and using appropriate mathematical tools the volume of gas adsorbed on the material surface can be calculated. This technology allows the specific surface area (measured in meters squared per gram of aerogel structure) of the aerogel to be calculated from the quantity of gas (nitrogen) absorbed on the surface. The most popular analysis used to calculate the surface area from nitrogen adsorption-desorption information is based on the Brunauer–Emmett–Teller (BET) equation [147]. Other theories used to analyse the nitrogen adsorption-desorption information include the Dubinin-Radushkevich method for determining micropore volume [148] and the Barret-Joyner-Halenda (BJH) method for determining pore size distribution [149]. Pore size and shape can also be crudely assessed using microscopy such as Scanning electron microscopy (SEM) which can be useful when nitrogen absorption-desorption approaches cannot accurately assess the pore size of interest [119].

The International Union of Pure and Applied Chemistry (IUPAC) defines pore sizes in three categories: < 2 nanometres (nm) pores are ‘microporous’, 2 -50 nm pores are mesoporous and > 50 nm are macroporous [74]. Limitations of the BET equation come into effect when samples exhibit a wide range of pore sizes. If adsorption is limited to a single layer of gas molecules (termed monolayer adsorption) then the results are best converted to surface area data using a different model, the Langmuir equation [150]. However, if the adsorption occurring is of more than one layer of gas molecules (termed multilayer adsorption) then results are best interpreted using the Brunauer–Emmett–Teller (BET) equation [151]. Other adsorption phenomenon such as pore filling (gas

molecules completely fill micropores) and capillary condensation (gas molecules condensing to liquid in pore corners) further complicate analysis and require other modifications to these models (*e.g.* Dubinin-Radushkevich method). Complications in analysis occur when these types of adsorption happen simultaneously in the sample. Generally, this can be prevented in flat surface adsorption by controlling the vapour pressure; lower pressures are not conducive to multilayer adsorption and thus the Langmuir model can be used. The BET model is most appropriate where multilayer and condensation adsorption is assumed in the porous material [150]. However, neither of the above models is an accurate analysis of the resulting isotherms when these two types of adsorption occur simultaneously, requiring a choice to be made as to which model represents most of the adsorption. Thus, BET data reflects only surface area in the mesoporous range.

The morphology of macropores can extend well into the micrometre (μm) scale and can be very different to that of the smaller mesopores and micropores that are restricted to the nanometre (nm) scale. Different morphologies based on these ranges can emerge when the aerogel structure contains sheet-like solid scaffolds [48, 112, 113]. These sheets or walls can be deposited in layers or web-like structures with micron-sized slits or spherical macropores between walls. Upon closer inspection these walls or sheets can also contain mesopores and micropores within the wall structure itself (**Figure 2.13**). One drawback of the nitrogen adsorption-desorption BET technology is its inaccuracy when determining surface areas of matrices with larger macropores (>100 nm) [119]. Thus, the pore size distribution should be discussed alongside surface area measurements where possible. The reported surface area values should therefore be considered an indication of the surface area of the mesoporous and microporous range than of the total surface area of the aerogel skeleton.

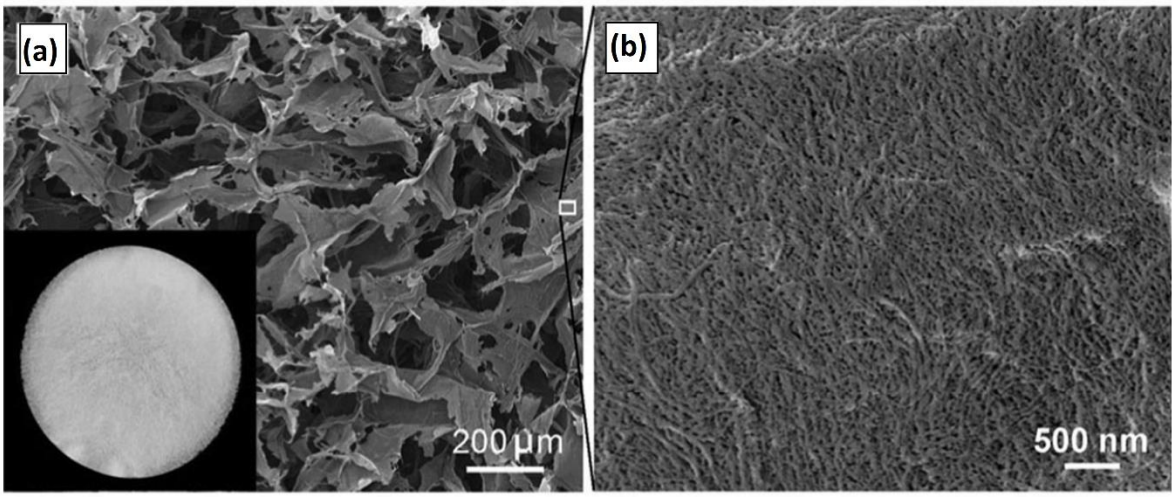

Figure 2.13*: Macroscopic (inset) and microscopic scanning electron micrographs of a hybrid collagen-cellulose aerogel. Macropores (> 200 µm) are observed between scaffold walls (a), while nanometre-sized mesopores are observed within the wall of the scaffold at higher magnification (b). Reprinted from Composites Science and Technology, 94, T. Lu, Q. Li, W. Chen and H. Yu, Composite aerogels based on dialdehyde nanocellulose and collagen for potential applications as wound dressing and tissue engineering scaffold, 132-138, Copyright 204 [48]*

Another technique used for measuring porosity is Mercury Intrusion Porosimetry (MIP) where mercury is forced into the evacuated sample while the intrusion pressure and quantity of mercury introduced are recorded. The pore sizes and volumes can be calculated from the intrusion since a specific pressure of mercury will correspond with intrusion into a specific pore size. Measuring the amount of mercury introduced at a known pressure, allows calculation of the pore volume at a particular pore size [152]. Increasing the pressure will introduce an additional mercury quantity from which the same calculation of pore volume can be made but for a slightly smaller pore size, and so on. However, the friability of many aerogel structures makes them unsuitable for MIP due to the high pressures necessary for intrusion of the mercury.

The methods used to measure density and porosity demonstrate that they are intimately linked, and thus basic density measurements can be used to crudely assess porosity. The typical density of a silica aerogel is ~ 0.1 g/cm^3, although this may range from 0.001 to 0.9 g/cm^3 [2, 153]. The average protein aerogel density reported is ~ 0.2 g/cm^3, while the porosity averages ~ 92 % [42, 91, 92, 102-104, 106, 107, 109-111, 118-120, 123]. Although 0.2 g/cm^3 is slightly heavier than the typical densities of other aerogels, in general the protein aerogels exhibit densities, porosities and even mechanical properties that rival those of the non-protein aerogels. Notably, early protein aerogels have been reported with

densities as low as 0.03 g/cm^3 [42]. Since these early reports, lower density protein aerogels have only been achieved by amyloid fibril aerogels, having a phenomenally low density of 0.003 g/cm^3 [91].

The summary of morphology information given in **Table 2.3** attempts to place protein aerogels and their hybrids in context with other aerogel types from the literature [154-161]. It should be noted that the variety of protein types, gelation methods, drying methods and hybrid material types can have a profound influence on aerogel morphologies and properties. This very wide scope of variables means that average protein aerogel morphologies and properties are less useful for a comparison with the more widely studied silica and other organic aerogel fields. However, dissecting the resulting morphological information with respect to these processing variables will reveal more specific relationships between certain protein aerogel processes and the resulting morphologies and properties.

***Table 2.3**: A comparison of morphological data from different aerogel types*

Aerogel type	Density (g/cm³)	% porosity	SA (m²/g)	Pore size distribution	Average mesopore diameter (nm)	References
Silica	0.003 - 0.5	90 - 99.8	500 -1200	mostly mesoporous	20 - 40	[2, 13, 155, 159]
Synthetic organic	0.02 - 0.2	> 80	400 -1200	mostly lower mesoporous range	3 - 20	[2, 154, 156-158, 160]
Carbonised	0.001-0.5	99.9	600 - 800	micro and low mesopore range	7 - 20	[157, 162]
Polysaccharide	0.008-0.46	52 - 99	30 - 850	mesoporous/macroporous	2- 11	[153, 161, 163]
Proteins	0.003 - 0.5	75 - 99.9	0.12 - 478	mesoporous/macroporous	2- 30	[42, 91, 92, 94, 95, 98, 102, 104, 111, 114, 120, 123, 127-129]
Hybrid proteins	0.02 - 0.12	90 - 95	1.72 - 451	mesoporous/macroporous	3- 40	[48, 111, 113, 115, 120, 125, 127, 130-136]

Composition

The type and amount of protein is the first stage in controlling protein aerogel morphology. A clear trend in increasing density and a decrease in porosity with increasing protein concentration can be seen across all protein types. However, the effect on density becomes less pronounced beyond a certain protein concentration and is independent of protein type and gelation methods [91, 102, 111, 118, 123]. Protein (or total solids) concentration has an immediate effect on the rate of protein solution aggregation and the rate of gel network formation. More aggregates contribute more solids to the scaffold of the aerogel resulting in denser network formation. SEM micrographs can demonstrate the decrease in pore sizes with increasing aerogel density (**Figure 2.14**). Interestingly, an increase in protein concentration also result in a marked increase in the Brunauer–Emmett–Teller (BET) surface area [92]. It might be expected that aerogels with reduced porosity should have correspondingly lower surface areas as reduced pore numbers result in reduced scaffold walls. However, higher density structures formed at higher protein concentrations demonstrate the opposite trend. The effect is related to the decrease in average pore size that is seen with increased concentrations and densities. A larger pore will have reduced surface area when compared to many smaller pores of equivalent volume. Even if the combined pore volume of these smaller pores is less than the single larger pore, surface area can still be higher. Moreover, BET surface area measurements are usually biased toward the mesoporous range (see above) and thus a reduction in pore size will result in greater number of pores detectable by the technique, even where overall porosity has reduced.

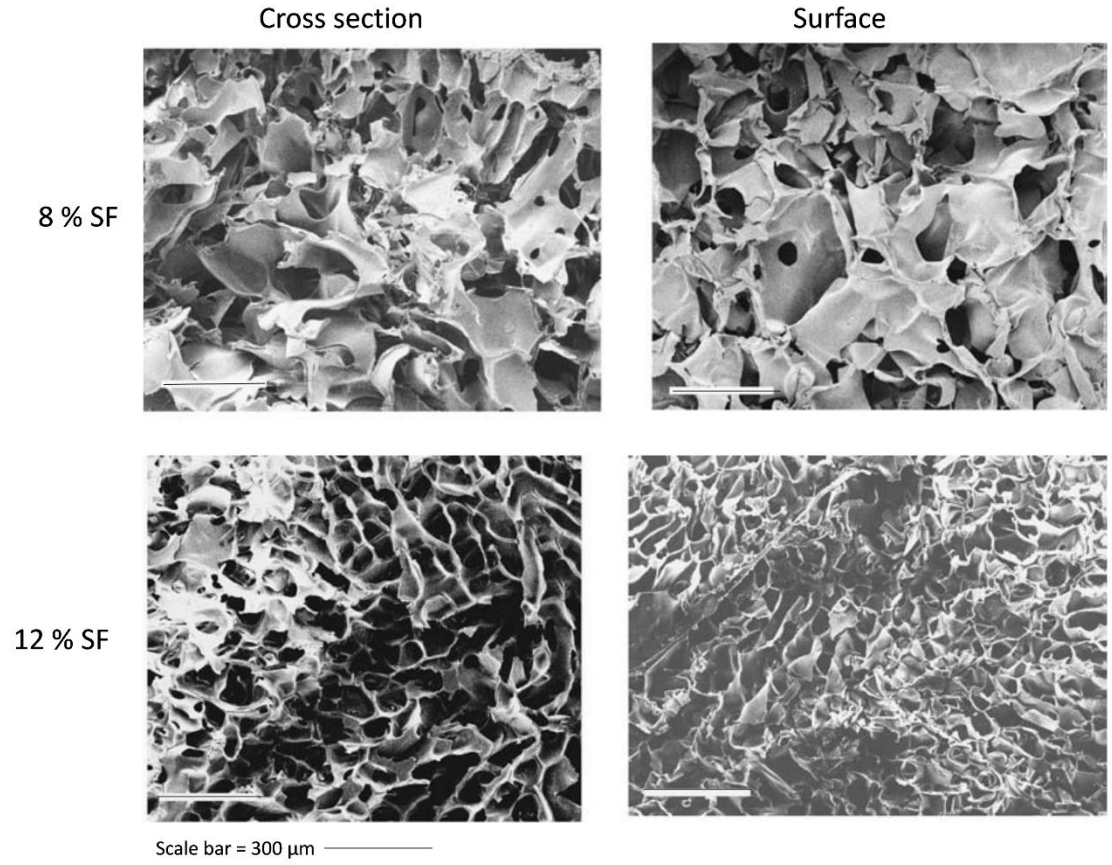

Figure 2.14*: Scanning electron micrographs of the cross-sectional (left) and surface (right) morphologies of silk fibroin (SF) aerogels prepared from an 8 wt% protein solution (top) and 12 wt% protein solution (bottom). Reproduced from Journal of Materials Science: Materials in Medicine, Preparation of 3-D regenerated fibroin scaffolds with freeze drying method and freeze drying/foaming technique, 17, 2006, 1353, Q. Lv, Copyright Springer Science + Business Media, LLC 2006*

The type of protein chosen to form the aerogel also dictates the nature of the gel network and ultimately the aerogel morphology. Certain proteins are chosen based on their structural and chemical compositions with known influences on resulting gel viscosities, strengths, and functionalities. This aerogel morphological dependency on protein type can be clearly seen when average structures from the various protein types are compared; silk fibroin tends to produce largely macroporous structures of lower densities while whey and soy proteins tend to be denser yet more mesoporous (**Table 2.4**).

***Table 2.4**: A comparison of drying method and reported morphological data from protein aerogels*

Protein	Drying method	Density g/cm³	% porosity	Pore volume cm³/g	Pore distribution			Average mesopore width	SA m²/g (<100nm pore size range)	Year	Reference
					Micro	Meso	Macro				
Whey proteins (WP)	SC-CO_2	0.30-0.43	-	1.34-1.72	mesoporous and macroporous			12 - 27 nm	14-447	2012	[95]
	Freeze drying	0.23-0.30	-	-	macroporous			-	< 5	2012	[95]
	Freeze drying	0.11-0.26	-	-	-			-	-	2013	[127]
	Freeze drying	0.13	-	0.0061	mostly meso and micro			-	2.08	2016	[120]
β-lactoglobulin amyloid (WP)	SC-CO_2	0.003-0.03	98-99.9	2.7	-	10%	mostly macro	-	325	2016	[91]
Silk fibroin	Freeze drying	0.03 -0.12	87-99	-	macroporous - 15 - 155µm			-	-	2004	[42]
	Freeze drying	-	85-96	-	mostly large macropores			-	-	2005	[102]
	Freeze drying	0.09 - 0.20	75 - 97	-	large macropores up to 150µm - 1000 fold greater than mesopores			-	-	2006	[122]
	Freeze drying	-	-	-	macroporous (~ 400µm)			-	-	2012	[110]
	Freeze drying	-	-	0.04-0.05	Shift towards both macroporous and microporous ends of spectrum from SC-CO_2 results			3 nm	45-59	2015	[92]
	SC-CO_2	0.058	-	-	none	mostly mesopores	up to 130 nm	20 nm	424	2014	[128]
	SC-CO_2	-	-	-	mostly mesoporous			-	-	2014	[129]
	SC-CO_2	-	-	1.6-1.8	mostly mesoporous			17 nm	260-308	2015	[92]
	SC-CO_2	-	88-93	-	macroporous			-	-	2016	[96]
Soy proteins	SC-CO_2	0.19-0.25	84-88	3.31-4.67	3-4%	40-50%	40-60%	30-40 nm	384-478	2012	[98]
	Freeze drying	-	-	0.001-0.009	smallest	>50%	>micro	8 - 40 nm	0.12 - 4.49	2016	[114]
Ovalbumin	SC-CO_2	0.07	95 -97 %	0.38-0.7	8 - 24 %	85 - 92 %	-	-	247-476	2011	[104]
	SC-CO_2	0.22-0.47	-	0.2-2.4	mesoporous and macroporous			-	16-380	2015	[94]
Gluten	Freeze drying	0.08-0.20	49 - 93 %	-	mostly macro (30 - 73µm)			-	-	2010	[111]

An obvious exception is that of Nyström *et al.* who produced a phenomenally light 0.003 g/cm³ protein aerogel from a whey protein using the unique amyloid fibril induction as discussed earlier. The amyloid fibril structures were induced conformations of β-lactoglobulin, a normally globular (non-amyloid) protein which is one of the two main proteins found in whey. Whey protein aerogels reach their lowest density of 0.06 g/cm³ in the hybrid alginate-whey aerogels of Chen *et al.* [118], but are usually around 0.1 – 0.2 g/cm³. Thus, the fibrillar nature of the amyloid version is thought to contribute towards the incredible gelling ability in these aerogels – a distinct advantage of using a protein whose fibrous aggregates can maintain a less dense network. Nyström's β-lactalbumin amyloid aerogels surpass even the lightest polysaccharide aerogels that have a density of 0.008 g/cm³ [163]. This incredible achievement highlights the manipulation of the protein structure as a key advancement and provides researchers with a tantalising prospect for future aerogel research.

Methods of production

Once the protein type is selected, the density and porosity can be further influenced by the method of aerogel production. This can be categorised into two key stages, namely: gel network formation and drying. At the gel network stage, the amount and type of protein, solubility conditions and additional crosslinking additives will affect the protein denaturation, aggregation, and crosslinking. Thus, it is expected that these variables will influence the porosity and density of the resulting gel network. The second stage of the process that involves drying can also have a significant effect on the resulting porosity and density as the solvent is removed from this gel network and replaced with air.

Factors that influence the gel network during the gelation process are the next important variables after protein type to be considered as they control how the protein will aggregate and gel. These gelation techniques depend intimately on the type of protein being gelled. As discussed, pH changes, ionic strength adjustments and heat-induced denaturation involve destabilisation of existing protein chemical bonds and interactions. Some proteins can be gelled at acidic pH values [120], while others at basic or neutral pH values [103, 108] depending on the protein isoelectric point (pI). The effect of pH is best seen when compared against the pI of the protein as this indicates how much charge each protein molecule carries and therefore how fast aggregation (and gel formation) can result. A lower

density is observed, surface area of the aerogel structure is reduced and the size of the protein aggregates is increased when the pH is close to the pI of the protein (**Figure 2.15**). These effects can be described by considering how the rate of protein aggregation and subsequent network crosslinking are altered with changes in protein electrostatic charge and the level of denaturation. At pH values close to the pI of the protein there is little to no repulsion between protein molecules once they are denatured by other means (*e.g.* heat) and thus aggregation (driven by hydrophobic interactions) is fast, creating large globular aggregates of protein before gelation and any crosslinking sets in. As a result, the gel network is comprised of very large aggregates which subsequently create larger pores and less dense aerogels due to limited crosslinking. At pH values far from the pI of the protein, aggregation is slower due to ionic charges on protein molecules resulting in smaller aggregates where protein denaturation has had more time to allow for unfolding of proteins [103]. These aggregates contain more exposed reactive groups and can then crosslink to a greater extent, forming a more filamentous network before aggregate size is increased excessively [119]. Thus, the resulting gels are denser and more homogenous, and the pore size is shifted to a more microporous and/or mesoporous range.

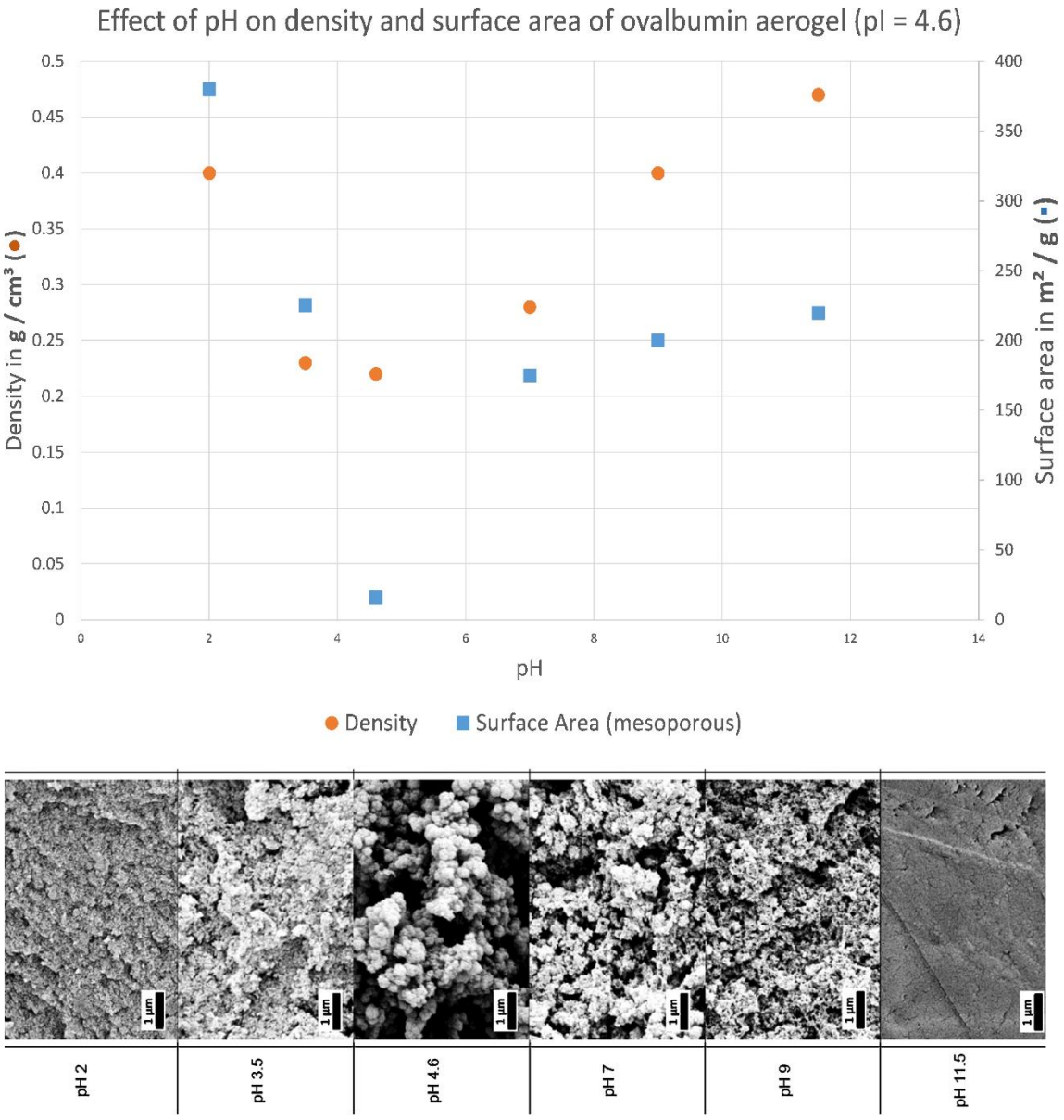

***Figure 2.15**: (Top) Plot of ovalbumin aerogel densities and BET surface areas with varying pH. (Bottom) SEM images of ovalbumin aerogels showing aggregate size increase as pH approaches the pI (4.6) of the protein. Both the data for the plot and the SEM images are obtained from Selmer, I., et al. (2015). Journal of Supercritical Fluids, 106(Aerogels: Synthesis and Applications), 42-49 [94]*

In a similar manner, the use of salt in the protein gelation procedure can affect the morphologies of the gels. The best examples of this are whey protein aerogels that are gelled using pH, salt, or heat methods. The cold-set gelation method involves the use of both salt and heat, allowing a similar control over the aggregation and gelation rates observed with pH change methods. The addition of salt decreases the surface charge in proteins, thereby increasing aggregation. This is similar to the control of the aggregation rate seen in pH manipulation [103]. It is also possible to denature the protein with

heat prior to the salt treatment. After heat-treatment, gelation can be induced when salt is added. Salt ions shield charge on protein molecules, reducing repulsion between like-charged molecules which might otherwise prevent gelation of a denatured protein. The resulting gel network may also contain ionic crosslinking due to the salt ions binding to negatively charged amino acid residues. Salt-crosslinked protein gel networks can be stronger and more mesoporous in structure due to these crosslinks (**Figure 2.16)** [118, 120].

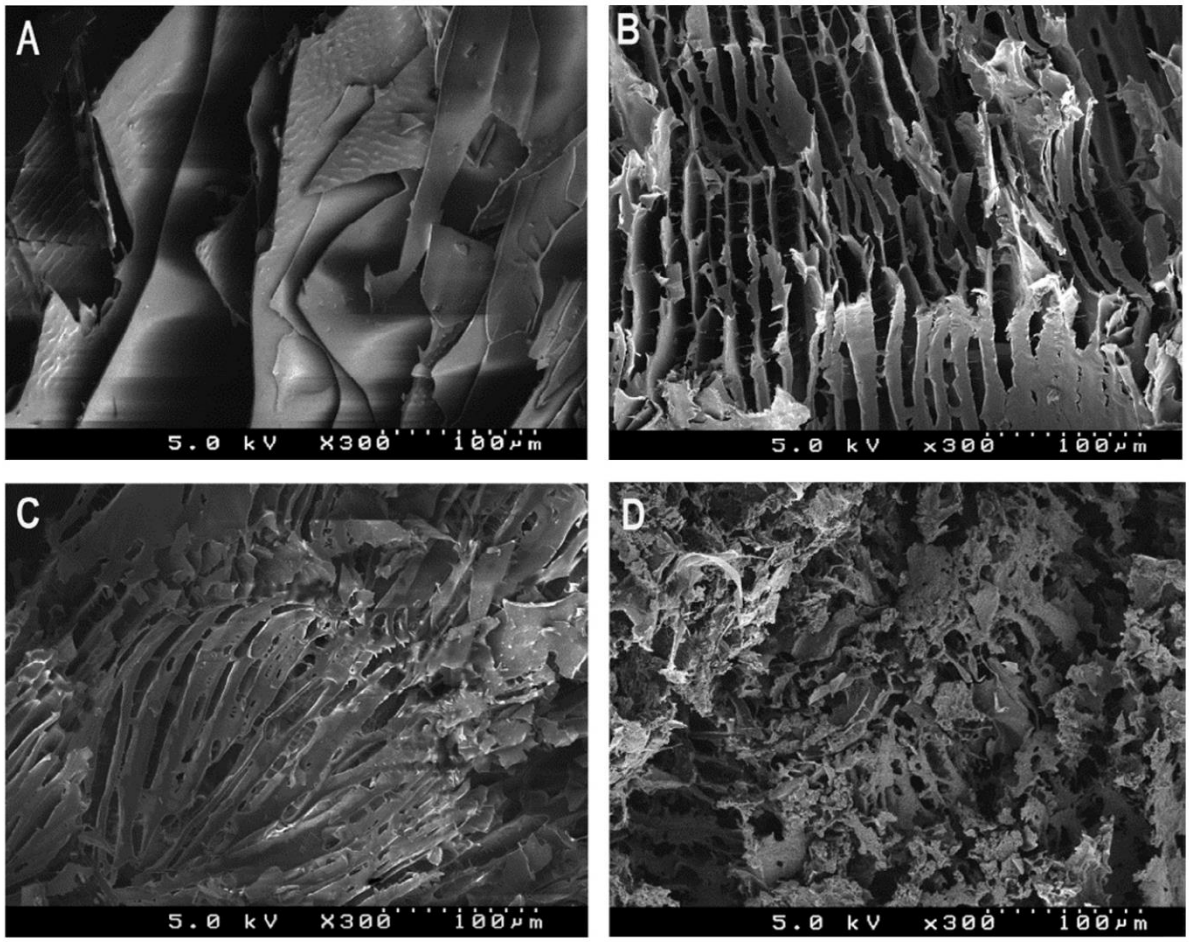

Figure 2.16*: SEM micrographs of whey protein isolate (WPI) aerogels. Micrograph B (WPI denatured by salt and heat treatment) demonstrates the effect of dual gelation method over simple heat treatment (micrograph A). Micrographs C (WPI and alginate) and D (WPI, alginate and clay) demonstrate the effect of hybridisation with other polymers. Reprinted from European Polymer Journal, 49, H.-B. Chen, Y.-Z. Wang and D. A. Schiraldi, Foam-like materials based on whey protein isolate, 3387-3391, Copyright 2013 [127]*

Chemical crosslinks also influence the gel network homogeneity and average pore size. The crosslinks, such as the $-CH_2-$ bridges that form between amine groups in the formaldehyde crosslinking reaction, create extensive networks. The resulting aerogels have less distinguishable

aggregates but are more homogeneous with reduced pore sizes (**Figure 2.17**) and increased BET surface areas [114].

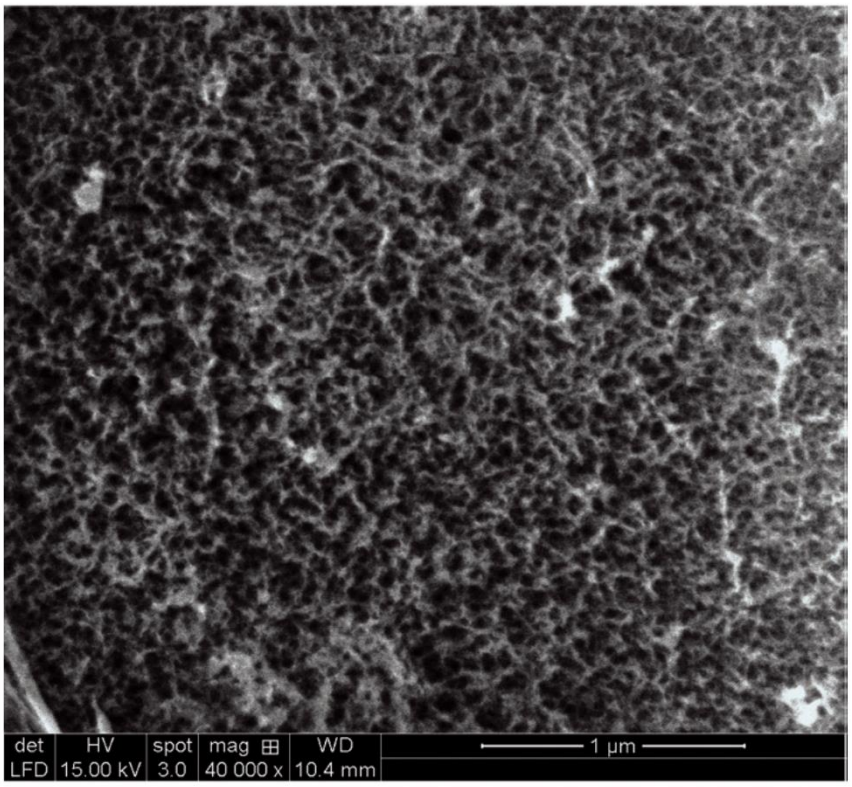

Figure 2.17*: SEM micrograph of soy protein-based aerogel with tannin and formaldehyde crosslinking. SEM image adapted from Amaral-Labat et al. (2012). Green Chemistry, 14(11), 3099-3106 [98]*

Following the gelation stage, the morphology of aerogels can be further influenced by the drying process. During SC-CO_2 drying, gels are expected to experience the least amount of surface tension within the pores and therefore less prone to collapse of the internal structure [164]. Consequently, the aerogels are expected to have the best-preserved gel network structures in the final dry scaffold. Freeze drying techniques are expected to involve a small amount of structural breakdown as the solvent undergoes freezing before it is sublimed at low pressures. Interestingly, the freeze drying technique tends to produce aerogels with lower densities and higher porosities than those produced by SC-CO_2 drying [119]. The average density of protein aerogels obtained by SC-CO_2 drying is 0.19 g/cm^3 [98, 103, 104, 107, 111, 118] while that *via* freeze drying is 0.12 g/cm^3 [42, 48, 98, 110, 115, 117-120, 123]. This surprising combination of results has been elucidated by Betz *et al.* who conclude that the use of freeze drying produces a shift in pore size towards a more macroporous structure (pore

diameters > 50 nm) where surface area and pore volume readings are harder to determine by BET N_2 adsorption-desorption. Larger ice crystals form as the freezing stage of the process is extended such that growth of the ice porogens increase the pore size over that initially present [114]. Thus, aerogels obtained by freeze drying have lower densities and lower BET surface areas due to the larger pore sizes created *via* large ice-crystal formation [119]. Differences in density and pore size caused by these drying techniques can be observed macroscopically (**Figure 2.18**) and at higher magnifications using SEM (see **Figure 2.8**) [92].

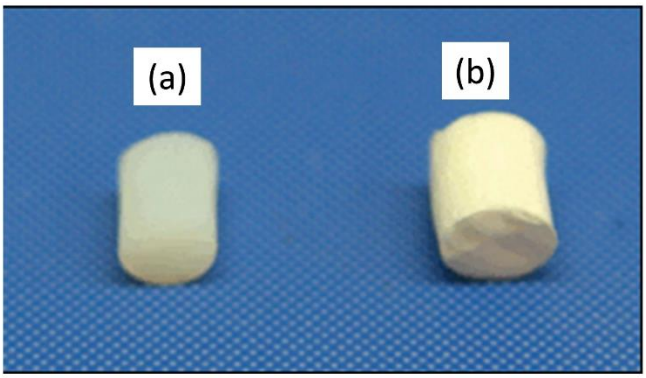

Figure 2.18*: Whey protein aerogels prepared by supercritical carbon dioxide drying (a) and by freeze drying (b). Adapted from The Journal of Supercritical Fluids, 72, M. Betz, C.A. García-González, R.P. Subrahmanyam, I. Smirnova and U. Kulozik, Preparation of novel whey protein-based aerogels as drug carriers for life science applications, 111-119, Copyright 2012, reprinted with permission from Elsevier*

Hybrid protein-based aerogels

Hybrid protein-based aerogel production is driven by the idea of improving or tailoring the resulting properties of the aerogel. In general, proteins are not fibrous in nature like most carbohydrates, which limits their mechanical properties in the wet-gels and aerogels. A comparison of protein gels and their hybrids demonstrates a preference for globular (non-fibrous) proteins such as those found in whey and soy isolates, zein and gluten to be supplemented with other non-proteinaceous constituents. Often these second constituents are polysaccharides, which in addition to being biodegradable and biocompatible, can also provide additional strength and absorbency to the aerogels, due to a more fibrous nature. The naturally fibrous (silk fibroin) or induced fibrous proteins (amyloid fibrils of β-lactoglobulin) tend to be used in hybrids less often, although this may also be due to the intended

application of the aerogel. The obvious exception to this apparent trend is collagen (gelatine) which, with the exception of Kistler's work, has only been produced in hybrids thus far but is naturally fibrous [48, 124, 165-167].

In general, the densities and porosities of hybrid protein aerogels are more desirable when compared to that of their pure protein counterparts (**Table 2.5**). The densities are significantly reduced to an average value of ~ 0.08 g/cm^3 [48, 99, 108, 111, 112, 115, 117, 118, 120, 141, 167]. In the literature, hybrid aerogels are most based on the combinations of polysaccharide-protein and clay-protein, having average densities of 0.076 and 0.085 g/cm^3, respectively.

Chen *et al.* demonstrated that the density of a whey protein isolate (WPI) aerogel (0.165 g/cm^3) reduces as the whey protein is mixed with first alginate (0.098 g/cm^3) and then with both clay and alginate (0.082 g/cm^3). However, these hybrid densities are still higher than the corresponding alginate aerogel density (0.047 g/cm^3). Interestingly, the incorporation of alginate and clay appear to reduce the pore size which should result in increased density (**Figure 2.16**). However, Chen *et al.* observe that the alginate hybrids appear to have thinner layered structures when compared to the pure whey protein aerogels that explains the reduced pore size and density [118].

Various other hybrid combinations of proteins and polysaccharides reveal that incorporation of polysaccharides generally leads to reduced densities and pore size shifts towards mesoporosity as compared to the 100 % protein aerogels. However, some studies show that the average gel density of protein aerogels is unaffected by the addition of polysaccharides, although they may improve other properties such as the homogeneity and strength of the gels [111].

***Table 2.5**: Summary of morphological data and important findings of hybrid protein aerogels*

Protein	Hybrid type	Density g/cm³	Pore volume cm³/g	Pore distribution			Average mesopore diameter	SA m²/g (limited to mesopore range)	Findings	Reference
				Micro	Meso	Macro				
Whey protein	alginate	0.06 - 0.1	-		-		-	-		[127]
	cellulose	0.11-0.16	0.0025 - 0.0078		micro and mesoporous		-	1.72-3.04	Nano-crystalline cellulose increases pore size while micro-crystalline cellulose reduces it	[162]
Silk Fibroin	graphene	-	-		Between graphene sheets - macroporous Within graphene sheets - 1 - 160 nm pores		11 nm	180.7	Higher silk to graphene ratio results in denser structures	[130]
	clay	0.08 - 0.12	-		-		-	-		[125]
Soy Protein	clay	0.06 - 0.1	-		-		-	-		[125]
	cellulose	0.111-0.115	-		macroporous		-	1.9	Increasing soy content decreases porosity and surface area	[131]
	graphene	-	0.02 - 0.6		large number of ~2 nm		3-5 nm	30 - 156	graphene has slit shaped small pores between layers (with macropores)	[132]
	graphene	-	0.843	14%	85%	1%	10	30 - 119		[113]
Ovalbumin	cellulose	-	0.18		mostly mesoporous with 34% microporous volume		-	38		[133]
Gluten	cellulose	0.08-0.20	-		mostly macro (30 - 73µm) - pore size reduces as density increases		-	-		[111]
Zein	agar	0.03 - 0.04	-		mostly macroporous but significant mesopore presence		43 nm	451	Addition of protein to agar reduced pore size, increasing SA	[134]
	silica	-	-		macroporous		-	-		[135]
Collagen	cellulose	0.02 -0.03	-		-		-	-	Highly absorbent	[48]
	alginate	0.043	3.24		-		-	208	Collagen increases pore size, reducing SA and pore volume compared to alginate alone	[136]

2.2.3.4. Processing-property relationships

Looking beyond morphology, it is possible to draw correlations between processing techniques and other properties. Properties such as strength and absorbency can be influenced by the morphology of the aerogels, which is in turn influenced by processing as previously discussed. The morphology of the aerogel and the properties it may influence are ultimately connected to the intended application of the aerogel. In silica aerogel technology, high porosity, smaller pore sizes and lower densities are preferable where the aerogels are used in thermal insulation [2, 168]. Targeted morphologies that are specified by the application are also a focus of protein aerogel development.

In industry, materials must have higher mechanical and insulating properties while processing must be achieved in a cost-effective manner. A technical challenge for aerogel insulating materials is the combination of both low density and small pore size that is useful for increasing the thermal insulating properties of the material [98]. Thus, many protein aerogels being targeted at general industry material applications tend to use hybrids due to the combined effect of protein and polysaccharide in increasing the strength, and reducing density and pore size, while remaining economically viable. Mechanical properties are useful measurements for industrial based applications such as packaging and construction but are also important for medical applications such as tissue culture. A useful comparison for bio-aerogel mechanical performance are the compressive moduli of silica aerogels which range from 50 – 400 kPa and are current competitors in medical applications of aerogels [159, 160]. Protein aerogels demonstrate compressive moduli ranging from 19 kPa [92] to 18.2 MPa [118] and with an average of 2.5 MPa [42, 92, 102, 118] they can offer a competitive edge over silica aerogels. However, polysaccharides are by comparison a much better mechanically performing aerogel option and thus the polysaccharide-protein hybrid aerogels offer the best compromise between strength, biodegradability, and biocompatibility.

Whey protein aerogels produced by the cold-set gelation method (combination of heat denaturation and salt gelation) have significantly improved mechanical properties, with compressive moduli up to 20 times higher than those prepared by a simple heat gelation process of equivalent density [118]. This effect is undoubtedly due to the crosslinking and protein association in the gel network and could

become a useful insight for future protein aerogel research into tailored mechanical properties. Mechanical properties are improved in hybrid protein aerogels with an average compressive modulus of 3320 kPa (calculated using all reported compressive moduli from references [99, 118, 141]. Protein aerogels are in general not this strong without a corresponding loss in density. The work of Arboleda *et al.* looks extensively at how the cellulose content of soy protein-cellulose hybrid aerogels affects the mechanical properties of the gels. Not only does the addition of the nano-fibrillar cellulose markedly improve the compressive modulus of the soy aerogel, but interestingly the effect is not linear. The improved compressive modulus can be seen at just a 1:5 ratio of cellulose to soy protein. Aerogels with just a 1:3 ratio of cellulose to soy protein demonstrate equivalent strength to pure nano-fibrillar cellulose gels. Arboleda *et al.* conclude that the inclusion of the cheaper soy protein in these cellulose aerogels "endows the system with interesting chemical features while maintaining a high compression modulus" [99]. Clearly the hybrid has advantages over both types of parent aerogels. Such studies are a useful indication of how cheaper protein products such as soy can be incorporated into the stronger polysaccharide aerogels for viable industrial applications.

Tissue engineering applications are at the centre of silk fibroin (SF) aerogel research as silk is already a popular material for *in vivo* studies and medical applications. The unusual amino acid composition and subsequent secondary protein structure makes it less vulnerable to degradation *in vitro* and *in vivo* and its natural fibrous structure and mechanical strength make it ideal as a scaffold [144]. Additionally, in medical applications larger aerogel pores are more suitable for supporting cell growth in tissue cultures as cell size approach micrometre scales rather than nanometre scales [92]. Thus, the silk fibroin aerogel field is suited for salt leaching, CO_2 acidification and freeze drying techniques that lead to the larger pore sizes required for cell culture scaffolds.

In laboratory technology, high pore volume and surface areas at the nanometre scale indicate increased efficiency of aerogels as absorbents and filters [74]. Absorbency is crucial for applications in drug delivery, waste-water treatments and bio-sensor applications [169]. Thus, many aerogels intended as absorbent materials in medical or laboratory applications have processes optimised for more homogenous gels with reduced pore sizes and larger surface areas.

2.2.3.5. Protein Encapsulation

Proteins are also used in silica aerogel technology in a hybrid-like structure resulting in biologically functional encapsulated proteins. This technology, although not strictly 'bio' in its origin due to the use of silica aerogels, can be considered a type of hybrid material with proteins as one component. Essentially a silica aerogel matrix is impregnated with protein (more specifically, an enzyme) which is immobilised inside the pores of the structure, rather than being a structural element of the gel network itself. The purpose of this protein encapsulation is to create a bio-catalytic or bio-specific filtration scaffold – a material which can detect certain molecules in liquid or air. Extending this concept out of the laboratory allows these bio-catalytic scaffolds to be used in applications such as forensics and waste-water treatment in addition to laboratory assays. Enzyme catalysis and bio-detection offer an unparalleled level of chemical specificity which is exploited in these types of applications and aerogels can help them become more practical.

Enzymes are utilized in laboratories for a myriad of catalytic identification and isolation assays of biological fluids. These assays are usually conducted in solution, in a single vessel. Immobilizing enzymes on a solid scaffold such as an aerogel adds utility and practicability to these techniques. They key to immobilising an enzyme on a surface is being able to fix the enzyme without disturbing its biological functionality. Rather than a chemical immobilization, encapsulation within the pores of an aerogel physically restrains the enzyme (**Figure 2.19**), allowing it to retain its normal chemical function. Furthermore, the open porous nature of the aerogel allows the testing fluid to permeate the structure and filter through the enzyme laden matrix, resulting in a chemically selective (*via* the enzyme) filtration, catalysis, or bio-detection of that fluid. In fact, the very first report of enzyme encapsulation in aerogels indicates that the matrix can even protect the immobilised enzyme from external degradation by factors such as heat [170]. Since this first report, research in this area has included various processing and solvent techniques [90], application in biodiesel processing [171], and the ability of these aerogel-enzymes to be bioactive in air [83, 85, 172, 173]. Although this technology produces aerogels with a different structural matrix to the protein aerogels discussed thus far, the processing techniques are remarkably similar in a practical sense. Preparing the gel is

performed using the same two-phase process of gelation and drying. The enzyme is simply added at the wet-gel stage prior to drying. The technique allows the enzyme to permeate the silica gel network and once dry remains immobilised within the pores of the silica matrix.

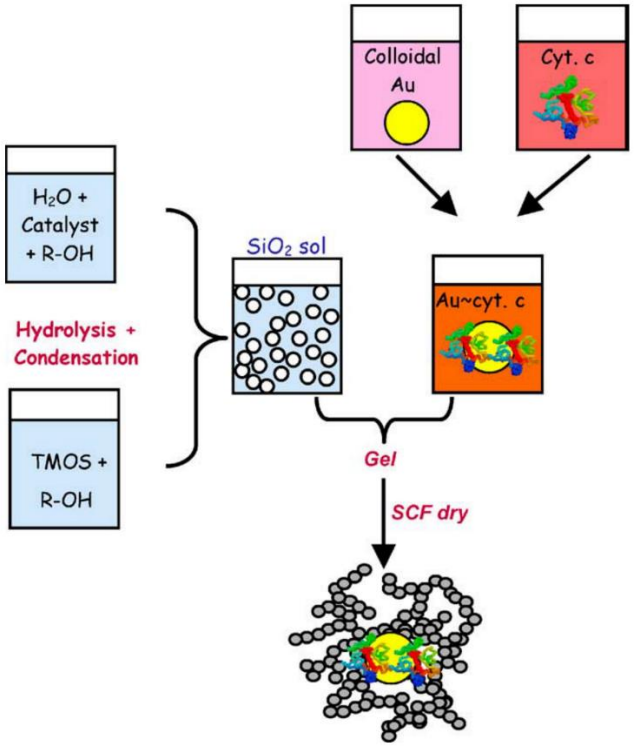

Figure 2.19*: Schematic of the process used to encapsulate a cytochrome c protein within a silica aerogel. Reprinted from Journal of Non-Crystalline Solids, 350, J. M. Wallace, R. M. Stroud, J. J. Pietron, J. W. Long and D. R. Rolison, The effect of particle size and protein content on nanoparticle-gold-nucleated cytochrome c superstructures encapsulated in silica nanoarchitectures, 31-38, Copyright 2004 [173]*

The incredible feature of this technology is its ability to retain the chemical functionality of the enzyme after the drying phase. Maury *et.al.* were able to demonstrate that encapsulation within an aerogel matrix can even enhance enzyme performance and the storage stability of the enzyme [174]. Manipulation of the aerogel properties such as pore size has also allowed this type of bio-incorporated aerogel technology to extend to bacterial cells. Bacterial cells have sizes on the micrometre scale rather than nanometre (as for proteins) and so encapsulation requires a macroporous aerogel structure. Power *et al.* demonstrated this novel concept by encapsulating bacterial cells in a silica aerogel and using it to detect the presence of a virus in air [169]. This work demonstrates the huge potential of aerogels and their unique properties within the field of bio-detection and bio-sensors.

2.2.3.6. Protein aerogels: a summary

Protein aerogels can produce equivalent morphological features to other aerogels. The most exciting prospect is the vast chemical potential of protein molecules and the unique chemical and biochemical specificity they may offer, both during processing and as the resulting aerogel. Protein aerogels can obtain densities rivalling those of the silica and synthetic carbon aerogels and generate variety in pore size. The inherent biocompatibility and biodegradability of proteins can be retained throughout aerogel processing which can rely solely on simple aqueous chemistry and freeze drying techniques. In addition, proteins obtained as a by-product from industry, specifically from the food processing industry, can be a relatively cheap and an accessible source of biopolymers for aerogels. The morphology and strength can be improved by protein choice, process parameters and hybridisation with polysaccharides and clay. Manipulation of process parameters is generally chemically simple (pH or salt concentration changes) and most improvements in morphology are achieved using the cheaper and easier freeze drying technique rather than supercritical CO_2 drying. The catalytic potential of proteins has been exploited by encapsulating enzymes in aerogel matrices, a unique use of proteins in aerogel technology.

Less desirable qualities of the protein aerogels are generally higher densities and lower porosities along with relatively weaker mechanical properties when compared to polysaccharide-based bioaerogels. However, protein-based bioaerogels already offer improved chemical functionality, cost, and control of morphologies. The scope of the research in this field is large and promising and much more specific research is needed to further elucidate the connections between process and morphology. A greater understanding of these connections will lead to better customisation of the protein aerogels to applications. The increasing focus on this field should produce further process improvements and help achieve similar standards in density, strength, and porosity as the polysaccharide-based aerogels.

2.2.4. Protein aerogel potential

Proteins are slowly becoming more well-known within the field of aerogel research and in the wider field of bio-based materials. The identification of new protein sources for aerogel production increases the scope for aerogels with unique biochemistries and unique application potentials. Promising properties of protein aerogels have been highlighted (see **Section 2.2.3.6**), however, there is a need for further research, particularly in new protein sources as aerogel precursors. The combining of other molecules with proteins into single aerogel structures (highlighted in **Sections 2.2.3.3** and **2.2.3.5**) demonstrates the most likely route for commercialisation of protein-based aerogels. In these examples the traditional properties of aerogels such as mesoporosity, high surface areas, and high strength-to-weight ratios are provided by other constituents while the proteins provide cheaply sourced biomass with unique bioactivities such as enzymatic catalysis. Such properties are neatly complemented by the biodegradability, biocompatibility, and sustainability that protein aerogels share with polysaccharide aerogels. Protein aerogels also provide routes for aerogel processing to be reliant only on 'green' chemistry due to inherent gelation mechanisms and controls with basic aqueous chemistry.

2.3. Canola seed meal protein

Novel aerogels from polymers previously unknown in aerogel research can certainly be produced from proteinaceous precursors. Moreover, proteins make a good choice for bringing unique biochemical activities to aerogels as outlined in **Section 2.2.3**. The small list of protein precursors that have been researched thus far can be expanded to include other protein types that have yet to be trialled as precursors for bio-based materials or aerogels. **Sections 2.3.1** to **2.3.4** provide background on one such proteinaceous precursor; canola protein extract, that is obtained from *Brassica napus* seeds and is nominated (see **Chapter 3**) as a target precursor for novel bioaerogels in this thesis.

2.3.1. Canola: crop, market, and seed meal.

Canola is the term usually given to the oil obtained from certain cultivars of three distinct brassica crop species. The cultivars that are considered canola crops are grown as oilseed crops (rather than for foliage, roots, or flowers like related *Brassica* crops). The species from which these cultivars are derived all belong to the *Brassica* genus in the *Brassicaceae* family of plants, known more commonly as brassicas or members of the mustard/cabbage family. The most common reference to 'canola' comes from the brassica crop rape (or rapeseed) which is the species *Brassica napus*. This species is predominantly an oilseed crop although one subspecies of *B. napus* is the swede (a root vegetable). The second type of canola comes from the species *Brassica rapa,* which includes a variety of subspecies vegetables such as bok choy, turnips, and field mustard. It is one of these subspecies specifically bred as an oilseed crop that is also a type of canola – *B. rapa* subspecies *oleifera* (also known by the synonym *Brassica campestris)*. The third species used in the canola industry is *Brassica juncea* which is a mustard plant that includes varieties known as 'Chinese mustard' 'mustard greens' and 'leaf mustard'. There is one subspecies also grown for oilseed and it is *B. juncea* subspecies *juncea.* The subspecies or cultivars highlighted in these three species of brassicas are termed canola because they have been specifically bred to produce an oil with low (< 2 %) erucic acid content and low levels of glucosinolates (< 30 µmoles per gram oil-free dry seed matter) [175]. The name 'canola'

originates from the words ‘Canada’ (the location of the breeding development) and ‘oil’ (or in some citations ‘oil, low acid’). Thus, the term canola most appropriately describes any brassica oilseed crop which has been bred for the specified low erucic acid and glucosinolate contents. The original oil obtained from *B. napus* had unacceptably high levels of erucic acid, which has been associated with cardiac toxicity [176], and so the low acid content varieties were developed. Nowadays the term canola is used to refer to either the oil or the brassica cultivars that are ‘double low’ in both glucosinolates and erucic acid [175].

***Table 2.6**: Three of the eighteen species in the Brassicaceae (family) Brassica genus showing relationship between plants termed 'canola' and 'rapeseed'*

Species	***Brassica juncea***			***Brassica napus***		***Brassica rapa***					+15 more including *B. Oleracea*
Common name/s for species	Mustard greens, leaf mustard, Chinese mustard, Indian mustard			**Rape/rapeseed**							
Subspecies or variety	***juncea***	*tatsai*	*japonica, crispifolia, interifolia*	***napus***	*rapifera*	*chinensis*	*rapa*	*pekinensis*	***Oleifera***	+ 5 more subspecies	*B. Oleracea* includes the subspecies kale, cabbage, broccoli, cauliflower, *etc.*
Common name/s for subspecies	***canola***	Zha cai	Mizuna, juk gai choy, takana	**Argentine canola, canola, colza, oilseed rape, rape, swede rape**	Swede (among others)	Bok choy	Turnip	Napa cabbage	**Canola (*B. campestris) or* field mustard**		

The term ‘rape’ or ‘rapeseed’ refers to oilseed cultivars specifically from the species *B. napus* while ‘canola’ describes the oil (and plant) from any brassica oilseed crop that is deemed low (less than 2%) in erucic acid (**Table 2.6**). ‘Canola’ is therefore not synonymous with ‘rapeseed’, but the terms can be used interchangeably with reference to *B. napus napus.* A further complication to the terminology is the fact that these terms are not used consistently throughout the globe. In the USA and Canada, the term rapeseed is only used to describe *B. napus* varieties that are high acid (*i.e.* not bred to be edible) making rapeseed and canola mutually exclusive terms. In other countries (Australasia, and parts of Europe) some low acid and low glucosinolate varieties of rapeseed are still referred to as rapeseed, despite being edible varieties and thus satisfying the definition for the term ‘canola’. As mentioned, the ‘double low’ cultivars of rapeseed crops (*i.e.* canola) have reduced levels of erucic acid and glucosinolate through selective breeding programs, but the protein biochemistry largely remains undifferentiated and can be considered as interchangeable with rapeseed protein [177]. Global oilseed markets differentiate between rapeseed (as non-edible, for biodiesel) and canola (edible). This thesis refers to the plant, meal, and protein extracts as ‘canola’ unless it is specifically relevant to identify the *B. napus* species.

Global trends show that the production of canola is increasing. Canola is currently the world’s second largest oilseed crop [178, 179]. In 2010 the USDA reported that rapeseed/canola oil was 13.7 % of the world’s oilseed production [180] surpassed by only the soya bean, which make up over 60 % of the oilseed market and far outstrips the production of any other oilseed crop [181]. World production of canola has increased 6 fold since 1980 with the average oil production reaching 20 - 30 million metric tons in the last decade [178]. Most of the world’s canola is produced in Europe, North America, Australia, and Asia, although there are countries in every continent that contribute to the canola market.

The main product of the canola crop is the oil obtained from the seed through crushing or extraction. The seed meal (or meat, abbreviated CSM) is a co-product of the oil extraction process and accounts for the remainder of the seed material which is about 60 % of the seed mass [182]. The market for the

crop is determined by the oil, and the meal is sold as a low-value co-product for livestock feed (horses, pigs, chickens, cattle) and for aquaculture. The canola seed meal (CSM) derives its value as a protein supplement having a well-balanced amino acid profile [177, 178]. The canola crop generates on average 10 -14 million metric tons of plant protein per annum (over the last decade) with the tonnage of oil being roughly twice that [178]. The major drawback of canola meal is the glucosinolate content which makes the meal less palatable, although improvement of modern cultivars continues to address the erucic acid and glucosinolate content of the seed. Although the meal can be sold as a high-protein feed supplement for livestock, research has also highlighted the potential of canola seed protein to be sold for human consumption. Such research is considered highly relevant to the food industry as global trends for protein supply shift from meat based sources to plant based sources [183]. The increasing demand for canola oil and this increased interest in the meal and its protein suggests a bright future for the already lucrative canola crop.

2.3.2. Canola seed meal extract: principal proteins and extraction

The canola seed meal can contain up to 48 % protein [184], although is typically 36 – 40 % protein dry weight [178], with the remaining material being carbohydrate (as indigestible fibre, starch, sugars, totalling about 55 %), residual fats (4.4 %), and an ash (mineral) content (8 %) [185]. This puts the total protein content of the seeds at 17 – 26 % [182], which is less than the protein content of soybean (37 %), but is nevertheless a comparable value with many other oilseed crops (*e.g.* safflower, mustard, sesame, sunflower) [180]. The precise protein content varies each year, dependent on the crop season, with the percentage for the latest 5 years being 19.6 - 23.5 % in the seeds and 37 - 41.4 % in the meal [178]. CSM as a stock feed in agriculture does not require further processing. However, research into applications for human consumption reveal the need for specific extraction techniques to eliminate unpalatable and anti-nutritional molecules. The high value protein can be extracted from the carbohydrates and other small-molecule contaminants (phytates, phenolics, glucosinolates, tannins) and from any residual oil. Protein extractions aim to maximise the total amount of protein that can be obtained (yield) and the final percentage of protein that the product contains (purity).

The extractable protein mass is mainly storage proteins (80 %) which are used by the cell as reserves of amino acids and ions. The remainder of the CSM proteins are structural proteins, and like many oilseeds, the main structural proteins identified are oil body proteins. These serve to stabilise the cell organelles that store the lipids in the seed [180]. The storage proteins are the most studied components of the CSM and are present in two types; a small albumin protein of 12 – 16 kilodaltons (kDa) called napin, and a much larger globulin protein called cruciferin that is 300 – 350 kDa in size [178]. The albumin and globulin families of proteins are distinguished by their solubility in certain solutions according to Osborne fraction nomenclature [177]. The albumins are extracted as a water soluble fraction while the globulins are the salt soluble fraction. Other nomenclature that is found in the literature includes reference to sedimentation coefficients in Svedberg units (S) for these proteins. Under Svedberg unit terminology the napin and cruciferin proteins are referred to as the 2S and 12S CSM proteins respectively, however there can also be a significant 7S fraction present which is attributed to cruciferin (a dissociated subunit) [186]. These two storage proteins make up a combined 80 % of the total protein content of CSM with napin contributing 20 % (although it ranges from 13 to 46 % of the total protein [187]) and cruciferin around 60 %. One study of certain European cultivars suggests that cruciferin and napin are present in a ratio of 0.6 : 2.0 though with variation across genotypes [188]. The structure of cruciferin and napin proteins has been elucidated by Tandang-Silvas *et al.* [189] and Rico *et al.* [190], respectively (**Figure 2.20**).

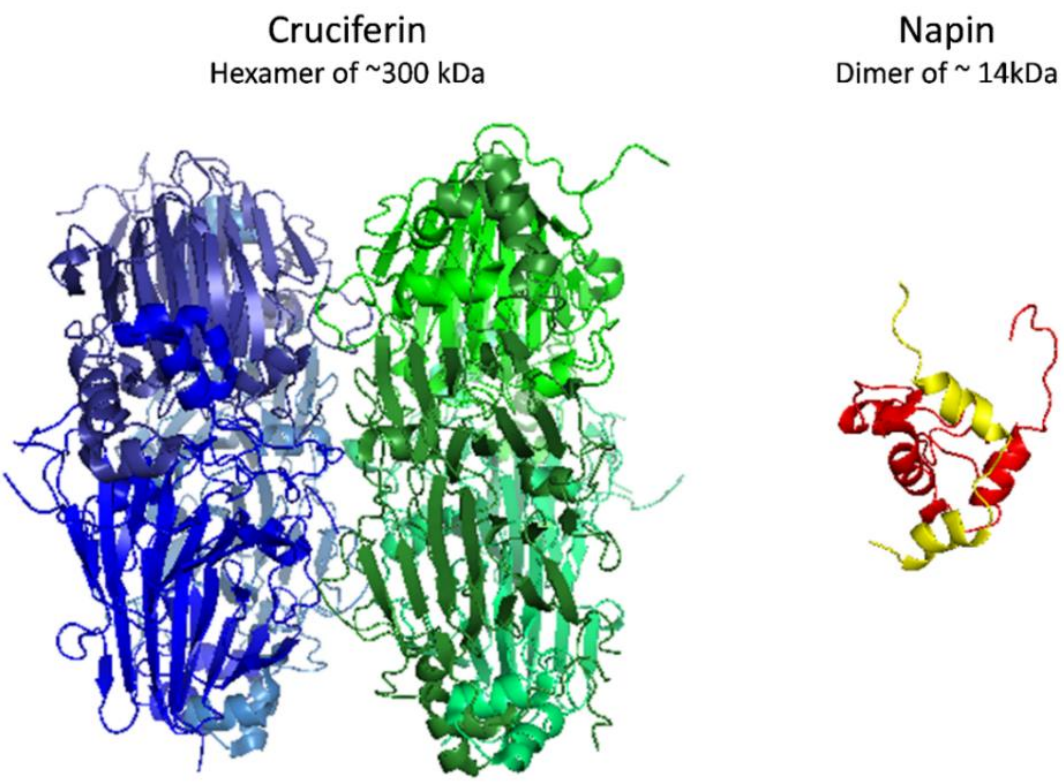

Figure 2.20*: Solved crystal structures of the cruciferin and napin proteins where protein secondary structures are represented as arrows (β-sheets), coils (α-helices), and string (random coils). Structures sourced from the RCSB Protein Data Bank: Cruciferin: PDB ID: 3KGL, [189] Tandang-Silvas, M.R.G., et al., Conservation and divergence on plant seed 11S globulins based on crystal structures. Biochimica et Biophysica Acta (BBA) - Proteins and Proteomics, 2010. 1804(7): p. 1432-1442. Napin: PDB ID: 1PNB, [190] Rico, M., et al., 1H NMR Assignment and Global Fold of Napin BnIb, a Representative 2S Albumin Seed Protein. Biochemistry, 1996. 35(49): p. 15672-15682*

The cruciferin molecule has 6 subunits arranged as two large trimers which are held together predominantly by non-covalent bonding such as hydrophobic and electrostatic interactions, and hydrogen bonding. The monomeric subunits of the cruciferin have been identified as CRU1, CRU2, CRU3, CRU4, CRUA and are each composed of 2 polypeptide chains. The first is approximately 40 kDa (254 - 296 amino acids in length) and the other about 20 kDa (189 - 191 amino acids in length) and they are linked by disulphide bonding (**Figure 2.21**) [178].

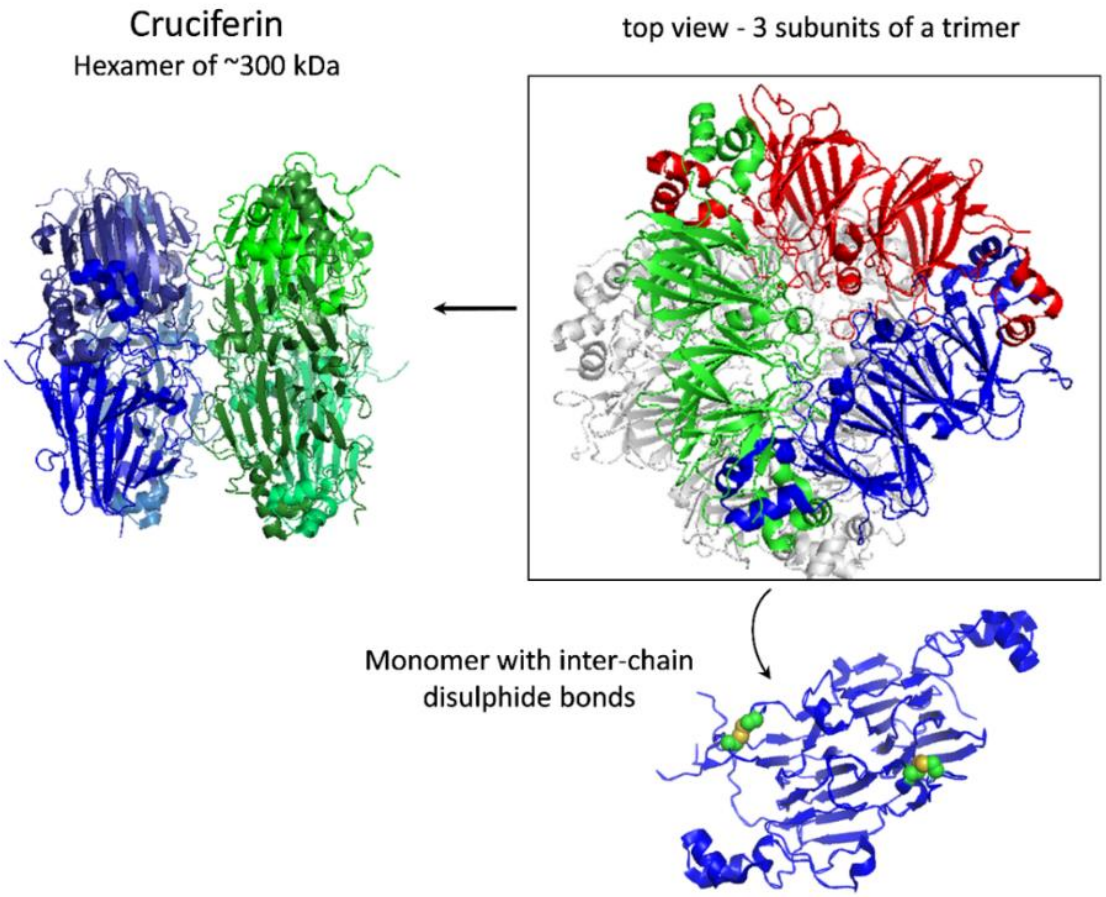

Figure 2.21*: The detail in the cruciferin subunits where disulphide linkages are shown in green and yellow spheres. Structure sourced from the RCSB Protein Data Bank: PDB ID: 3KGL, [189] Tandang-Silvas, M.R.G., et al., Conservation and divergence on plant seed 11S globulins based on crystal structures. Biochimica et Biophysica Acta (BBA) - Proteins and Proteomics, 2010. 1804(7): p. 1432-1442*

The napin molecule is comprised of two polypeptide chains, the smaller being only 4 kDa in size and linked to the larger 9 kDa chain through two disulphide bonds. The larger chain is further stabilised by an additional two intra-chain disulphide bonds between cysteine residues (**Figure 2.22**) [178].

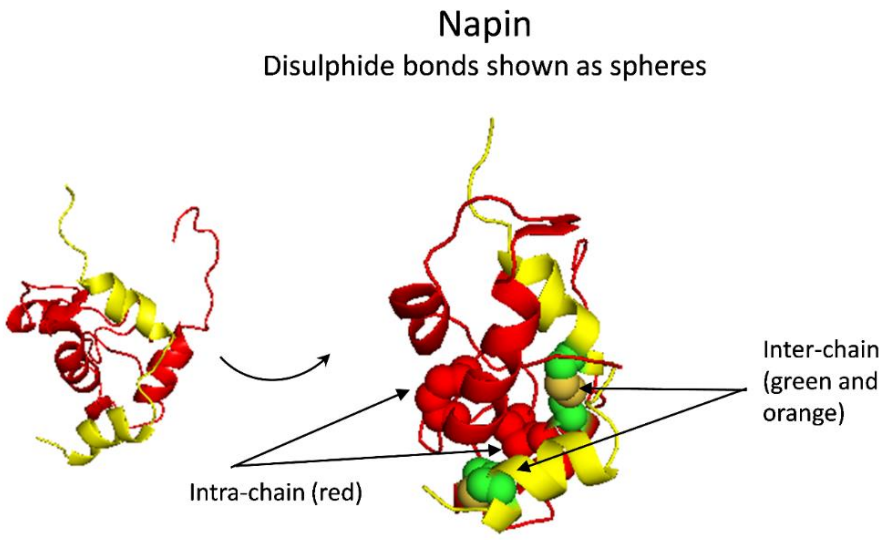

Figure 2.22*: The detail in the napin subunits where disulphide linkages are shown as spheres. Structure sourced from the RCSB Protein Data Bank: PDB ID: 1PNB, [190] Rico, M., et al., 1H NMR Assignment and Global Fold of Napin BnIb, a Representative 2S Albumin Seed Protein. Biochemistry, 1996. 35(49): p. 15672-15682*

The other notable protein component of the CSM is an oil body protein called 'oleosin'. Oleosin makes up 2 – 8 % of the total protein content and is between 15 and 26 kDa in size [191]. Other oil body proteins in canola seed are steroleosins (39 or 41 kDa) and caleosins (27 kDa) [178]. Minor proteins present in the CSM extracts include thionins, trypsin inhibitors, and lipid transfer proteins which are other structural and functional cell proteins.

The categorising of certain molecular weight components in CSM extracts as either cruciferin or napin can pose a challenge when dissociation of cruciferin subunits is considered. The identification of the protein components by separation techniques such as polyacrylamide gel electrophoresis (PAGE) and gel filtration chromatography (GFC) allows for the canola proteins to be separated and identified by molecular weight. Molecular weights of subunits and multimers are also identified in the resulting bands and peaks from these techniques. Generally, the sodium dodecyl sulphate (SDS)-PAGE bands corresponding to 14 kDa and 59 kDa probably represent napin and cruciferin, respectively [177, 192]. Commonly, bands of around 27 – 28 kDa are present and are attributed as a dimer of napin [192]. Napin is also the likely source of a band of approximately 9.5 kDa that appears under reducing conditions. This band is probably the larger polypeptide that makes up the napin

protein, as the disulphide linkages binding it to the 4 kDa subunit are disrupted in reducing conditions such as in the presence of dithiothreitol (DTT) [177, 192]. The molecular weight profile for cruciferin is more complicated but studies agree that a band of around 50 – 60 kDa is probably the cruciferin monomer, which, when reduced appears as a band at 30.5 kDa [177] or at 20 kDa - 22 kDa [192]. The hexamer can be seen as a range of molecular weights from approximately 300 to 360 kDa [178, 192].

Most extracts used for research and sold for consumption contain both the cruciferin and napin proteins alongside smaller amounts of the other proteins such as oleosin. The ratio of these two major proteins varies across extract types since extraction chemistry can be manipulated to preferentially isolation one of the proteins over the other. There are identifiable trends between the extraction technique, extract composition, and certain extract properties such as solubility [177]. CSM protein extraction techniques aim to isolate the proteinaceous component of the meal from the residual oils, the carbohydrates, and the small metabolites. Ideally the protein is solubilised (selectively) in a solution from which the non-proteinaceous material, being insoluble, can be removed *via* filtration or centrifugation. In practise this extraction process has varying degrees of success in terms of yield and purity. An extract with a very high level of purity (contains at least 90% protein) is called an isolate [193].

There are also some commercially available protein isolates (or extracts) which are sold as protein supplements for human consumption. These products are Puratein® and Supertein™ (Burcon NutraScience), Vitalexx® and Isolexx® (Teutexx Proteins) and the Can Pro IP (Can Pro Ingredients Ltd.) [178, 180, 194]. There are patents for certain extraction processes used to produce these protein extracts or isolates [193, 195-197]. These methods use two principal steps: first selectively solubilising the protein fraction of the meal and then isolating that protein from the solvent. Variations to the aqueous chemistry such as pH levels, salt concentrations, and temperatures are used to develop the differing extraction methods and optimise the concentrations of specific proteins and small molecules. The extraction methods fall broadly into two categories: the ‘alkali method’ and the ‘PMM (protein micellar mass) method’.

As the name implies, the alkali method is a pH dependant solubilising technique while the PMM method is dependent on salt-assisted solubilisation of the protein. An initial solubilisation of the protein in an aqueous solution is followed by separation of the solvent from the non-soluble material by centrifugation or filtration. For the alkali method this is achieved by manipulating the pH of an aqueous solution to high (> 9) values because at this range both the cruciferin and napin are soluble. The alkali method relies on this high pH followed by a subsequent reduction in pH (values range from 3.5 to 6) to precipitate the dissolved protein (isoelectric precipitation) which can then be isolated by centrifugation and freeze dried to a powder. In addition to the isoelectronic precipitate (termed PPI for precipitate protein isolate), the protein that remains soluble at the low pH value can also be recovered by ultrafiltration of this supernatant and freeze drying. This fraction is termed the soluble protein isolate (SPI).

The protein micellar method (PMM) also relies on solubilising of the protein and subsequent concentration from the solvent but uses a calcium or sodium salt solution (at neutral pH) rather than using an alkaline pH to solubilise the protein. This is followed by an ultrafiltration or dialysis step where the protein is concentrated and precipitated by reducing the ionic strength to near zero. The ultrafiltration uses a membrane that retains the larger molecular weight species (*i.e.* the proteins) in the system while separating the solvent and any small molecules into the permeate. The ultrafiltration step allows the volume of the protein solution be reduced, retaining all the protein while a large amount of the solution is filtered out to waste, thus removing a significant quantity of the salt, especially when volume is replenished with water. The retentate of this dialysis contains the bulk of the salt-soluble canola protein, thought to be largely cruciferin due to its salt-soluble nature. Replacement of the lost fluid with water causes a subsequent reduction in ionic strength and allows the volume of solution to remain manageable. The low ionic strength conditions combined with low temperatures results in protein micellar formation (a sticky precipitate) which is then collected using centrifugation and freeze drying. The precipitate obtained in this way from the PMM-salt extraction contains between 60 and 98 % 7S protein (cruciferin) while the precipitated fraction from the alkali-acid method is 60 – 95 % 2S protein (generally interpreted as the napin protein although can also be

subunits of cruciferin if it has been denatured) [191]. These two techniques are summarised in **Figure 2.23**.

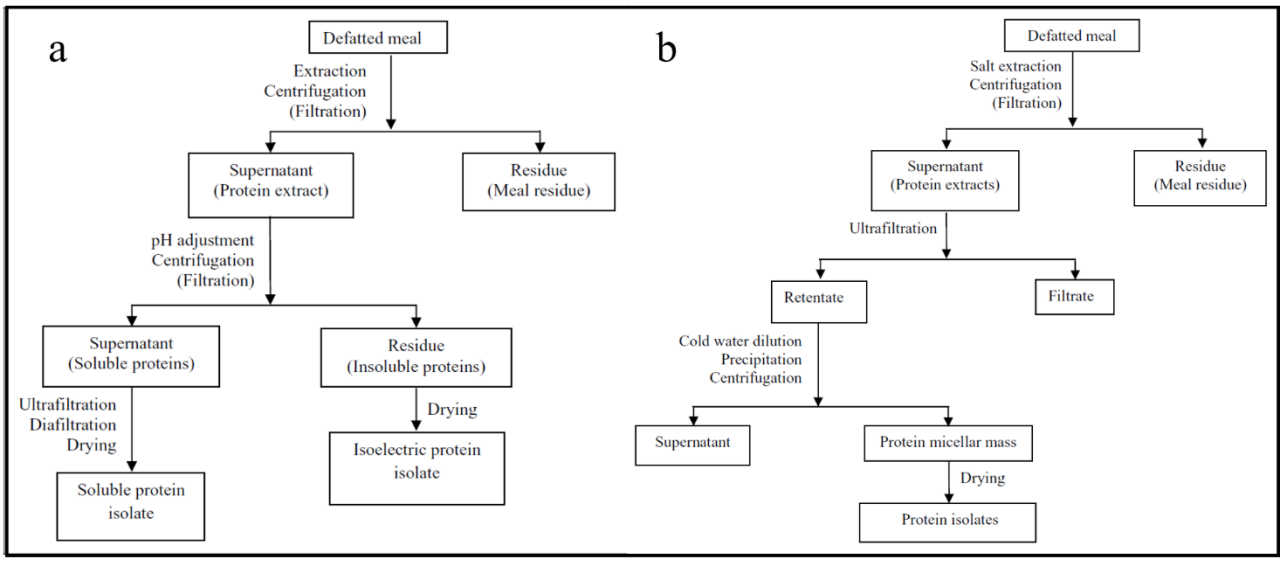

Figure 2.23: *Schematic representation of the* ***(a)*** *alkali-acid and* ***(b)*** *salt-PMM extraction techniques for recovery of protein from canola seed meal. Adapted from Figures 1 & 3 of Tan, et al. (2011). Journal of food science, 76(1), R16-R28 [177]*

An ammonium sulphate precipitation of the soluble protein has also been used to extract CSM protein (Wu & Muir, 2008 [192]). An initial dissolution of the protein is achieved in a phosphate/NaCl buffer allowing for separation from the non-proteinaceous solids. The dissolved protein is then precipitated using ammonium sulphate to 85 % saturation at low temperature [192].

Typically the extractions have a poor yield (30 %) [191] especially if collection of only one fraction is carried out at the second separation stage (*e.g.* insoluble fraction). However, yield can be significantly improved if multiple fractions are combined. For example, the second separation stage of the 'alkali-acid' extraction involves precipitation of the protein where the precipitate is around 37 % of the total protein in CSM [184]. The remaining protein (up to 32 % of total protein [184]) remains soluble at this acidic pH, meaning final protein yield can be increased beyond 60 % if the supernatant fraction is also recovered. However, separating these fractions may be useful for certain applications, since they contain different ratios of cruciferin, napin and other proteins. Indeed, it is this separate isolation of cruciferin and napin that serves as the main difference between Burcon NutraScience's Supertein™ and Puratein® products. The Supertein™ product is marketed as comprised principally of albumin

proteins, which corresponds to a napin-rich isolate, while the Puratein® product is mostly globulins (cruciferin) [178]. This difference allows the company to market these two products as having slightly different properties. Extraction of canola protein for use as a human foodstuff is an ongoing focus of canola research and is likely to see the expansion of such products as Supertein™ and Puratein® in the future.

2.3.3. Canola protein gelation

Assessing the quality of protein extracts for use in food means investigating properties of the extracts such as their solubility, nutritive value, water absorption capacity, and their ability to form gels. It is the gel-forming ability of proteins which is of relevance to researching aerogels. Protein gels are important for food quality, nutrient and bioactive delivery systems, and even the possible development of edible packaging in the food industry [198]. Commonly used protein gels in food science include those from soybean and other legume & oilseed crops [86]. Soy protein is a component in many processed foods, particularly where a proteinaceous component is required for its texture and gelling ability [86]. The possibility of canola protein in place of soy in products where allergies, availability or price make canola a more favourable option would further increase the value of the canola crop and meal. Studying the gelation properties (among others) of the canola protein meal and its extracts has been a focus of canola research [199, 200]. **Section 2.2.3.2** provides an outline of protein gelation mechanisms and influencing factors known from researching protein-based aerogels. The specifics of canola protein gelation are now considered.

The gelation of many proteins is not as well understood as the gelation mechanisms that occur in polysaccharides such as alginate and chitosan (see **Section 2.2.2**). Despite the complexity, a general mechanism for protein gelation is understood as the partial denaturation and aggregation of protein molecules, followed by a network formation driven by a mixture of covalent and secondary bonding [86]. Typically, this denaturation is achieved by raising the temperature that exposes buried residues (usually hydrophobic) to the surface of the denatured protein. The molecules then aggregate partially

and can develop particulate-based or fibrous networks [201]. Various intrinsic properties such as the specific quantities of amino acid residues on the protein molecules, and external factors such as the solution pH and ionic strength, determine the nature of the final structure [198].

Current knowledge of canola protein gelation generally attributes the gelation phenomenon to cruciferin. It is well established that cruciferin forms a heat-set gel under alkaline conditions [202] and that napin forms only weak gels [199]. Gill and Tung are probably responsible for the first demonstration of the gelling ability of the 12S rapeseed protein and established the dependency of the gelation on high pH and ionic strength [203]. Studies on the gelation of the canola protein extracts, reveal that even stronger gels (higher shear modulus) are produced when they are made from only purified cruciferin rather than the general isolate [204]. Carrying out gelation of a canola protein dispersion first requires the dispersion of an appropriate protein concentration to be adjusted to the correct pH value. The dispersion may then be gelled by raising the temperature. A further stage of addition of salt may be carried out in some studies once the heated dispersion is cooled, also known as the cold-gelation method (see **Section 2.2.3.2**). Therefore, the three external factors that are generally specified are the gelling temperature, pH, and wt% of protein in the dispersion. The canola or rapeseed protein isolate (and the cruciferin that is purified from it) has a thermally-induced gelation point at around 70 °C (69 °C [204] - 72 °C [205]) and the gelation is also dependant on the prior adjustment of the suspension to an alkaline pH (pH 9.0 [204] - 9.5 [205]).

Canola protein gels are shear thinning, thermally irreversible, and not able to be disrupted by 8M urea (hydrogen-bonding disruptive) unless also heated to temperatures approaching 100 °C [203]. Ageing gel samples at cooler temperatures may also increase viscosity [203] and has been attributed to hydrogen-bonding that strengthens the gel, after initial gelation takes place [200]. However, gels exposed to hydrogen-bond disruptors and thiol reducing agents did not demonstrate reductions in gel integrity [203]. Hence, it is unlikely that hydrogen-bonding is a critical factor in the formation of CSM protein gels but may play a role in post-gelation curing. It is also likely that if disulphide bonding is present in CSM protein gels, it likely does not influence the rheological properties of the gel [198, 203]. Canola gels containing NaCl had increased viscosities [203] suggesting a possible role

for cations in the gelation mechanism. An investigation to remove free ε-amino groups of lysine (through reductive alkylation) inhibited the CSM protein gelation; although, the likely reason was inhibition of another functional group essential for gelation in preference to the lysine ε-amino groups [203].

Kim *et al.* [198] provide recent studies of canola protein gelation that demonstrate canola protein gels are inhibited by high concentrations of urea. Kim *et al.* attribute this to the disruption of hydrophobic interactions in the gel, resulting in less protein-protein aggregation (critical for gel network formation). Recent studies confirm that CSM protein (cruciferin) gelation is stabilised initially by hydrophobic interactions then hydrogen bonding and with some contribution from disulphide bridging [198].

2.3.4. Canola protein: other properties

Canola protein is considered a promising source of dietary protein for a growing global population. It is especially promising in a market where the consumer has an ever-increasing focus on plant protein sources [194]. Current research is very much focussed on addressing limitations of the CSM protein nutritional profile. While the CSM protein may have a balanced amino acid profile and have a high protein efficiency ratio (PER) it also contains an excess of molecules which have negative effects on nutritional value or palatability of the meal [177]. The common challenge of food researchers is to develop extraction techniques that minimise the amounts of these anti-nutritional compounds found in the final product. The review of *Tan et al.* discusses the quantities and impacts of these molecules, namely phenolic acid esters, glucosinolates, phytic acid, and tannic acid. They conclude that while certain extraction methods can reduce the quantities of these molecules, that research in the area is still required: "a new processing method for the (canola) protein isolates must establish a clear pathway for their incorporation into human foods without significant effects on sensory and nutritional qualities" [177].

In their 2016 review of canola protein functionality, Wanasundara *et al.* noted that canola proteins have shown promising results in pharmaceutical and health related applications. The potential therapeutic benefits come from bioactive peptide sequences embedded in the proteins of CSM extracts. A bioactive molecule is any molecule that can affect a living cell, tissue, or organism. Many proteins and smaller peptides are known to possess bioactivity (or multiple bioactivities). These include peptides with anti-amnestic, antihypertensive, antithrombotic, antioxidative, and anorectic effects [178]. A complete summary of bioactive peptides that have been derived from canola protein was presented in Table 3 of their paper (**Figure 2.24**) and mostly highlights work where canola proteins were hydrolysed using enzymes to release these bioactive peptide sequences.

Bioactivity	Study details	Reference
Angiotensin I-converting enzyme (ACE) inhibiting, *in vitro* and *in vivo*	• Peptides having IY, RIY, VW and VWIS sequences with ACE inhibiting activity was generated from enzyme-assisted hydrolysis of rapeseed meal.	Marczak *et al.*, 2003
	• Sequences of VSV and FL from ACE inhibitory protein hydolysate from canola meal.	Wu and Muir, 2008
	• Rapeseed protein hydrolysed with Alcalase generated RIY peptide has high potency as an antihypertensive component in spontaneously hypertensive rat models.	Pedroche *et al.*, 2004
	• The potential of generating ACEI peptides from Hydrolysis of *B. napus* proteins (alkali extracted and acid precipitated) with endoprotease.	Yoshie-Stark *et al.*, 2006
Antioxidative	• Ethanol soluble peptides of rapeseed meal protein hydrolysates possessed antioxidant activities as indicated by reducing power, hydroxyl and DPPH radical scavenging activity and ferrous-induced phosphotidyl choline oxidation inhibition, and antithrombotic activity.	Zhang *et al.*, 2008
Antifungal	• Napins recovered from commercial canola showed strong activity in suppressing growth of *Fusarium langsethiae*.	Noi *et al.*, 2012
Affecting food intake	• Oral feeding of RIY peptide of canola hydrolysate exhibited anorexic effects on fasting ddY male mice and the same peptide was capable of blocking cholecystokinin-1 (CCK1) receptor antagonist lorglumide and decrease of gastric emptying rate by blocking lorglumide.	Marczak *et al.*, 2003
Affecting blood sugar	• Canola protein isolates exerted preventive effects on the early onset of insulin resistance in rats fed with high saturated fat and sucrose diets.	Mariotti *et al.*, 2008
Affecting cell growth	• Rapeseed protein hydrolysate with mostly <1 kDa molecules enhanced the growth of insect cell Sf9 line in serum-free media more effectively than bovine lactalbumin hydrolysate without affecting the general metabolism of the cells.	Deparis *et al.*, 2003
	• Rapeseed protein hydrolysates containing peptides of 0.5 to 5 kDa enhanced CHO C5 cell line growth rate.	Farges-Haddani *et al.*, 2006
	• Canola meal hydrolysate from Alcalase showed anti-inflammatory anti-wrinkle activity by inhibiting myleperoxidase and elastase activity.	Rivera *et al.*, 2016
Antiviral	• Alcalase-assisted hydrolysis of canola protein generated peptides capable of inhibiting human immunodeficiency virus (HIV) protease.	Yust *et al.*, 2004

Figure 2.24: *Summary of reported bioactivities found in peptides derived from canola protein as published in Wanasundara, J. P., et al. (2016). Canola/rapeseed protein-functionality and nutrition. OCL, 23(4), D407 [178]*

Wanasundara *et al.* also describe research in the canola protein field which address non-food and non-therapeutic applications [178]. This research includes examples of canola protein in: films [206, 207], hydrogels [179, 208], surfactants and foaming agents [209, 210], adhesives [211], and plastics [212, 213].

2.4. Literature review: summary

This review demonstrates the incredibly versatility and value of aerogels and how scientific understanding of aerogel manufacture processes can provide commercially valuable information for aerogel commercialisation (**Section 2.1**). Bioaerogels are highlighted as a promising way to address questions of sustainability and eco-friendliness in the field and are shown to open further application potential of these materials in industries such as food, medicine and biosciences (**Section 2.2**). Novel precursors, such as yet-untested biopolymers, have the chemical potential to further broaden the versatility of aerogels.

Protein-based aerogels are particularly good candidates for introducing chemical functionality to bioaerogels and are currently underrepresented in research (**Section 2.2.3**). There is a clear opportunity to untap the potential of novel protein sources for bioaerogel production, particularly where bioactivity or enzyme functionality is desired for bioscience applications. Protein gelation mechanisms are inherently more complex that other, more well-known, aerogel precursors, requiring many more studies for elucidation.

Proteins extracted from canola (*Brassica napus*) seed meal (CSM) could be used to produce a new range of bioaerogels due to their abundance as a co-product of canola oil (refer **Section 2.3.1**) and tendency for gelation (refer **Section 2.3.3**). Cruciferin is known to be a major protein constituent of *Brassica napus* seed meal extracts (refer **Section 2.3.2**) and is also known to contribute towards gelation in canola protein isolates. Canola protein also has demonstrated potential in the food industry, as a source of medicinal bioactivity, and is also amenable to plastic and film processing in other, non-food and non-medicinal, applications (refer **Section 2.3.4**).

Studies on the possible manipulation of canola gelation and subsequent processing into dried materials (aerogels) could also contribute knowledge to related canola protein research such as canola protein hydrogels, films, and plastics. The study of canola protein gelation with specific focus on subsequent aerogel properties is absent from the literature for the simple reason that canola gels have never been converted to aerogel structures. The development of a canola protein aerogel and the

subsequent characterisation of aerogel structure and properties would increase knowledge about protein aerogels and their potential, contributing to both canola protein research and bioaerogel research.

Chapter 3

3. Thesis outline

Chapters 1 & 2 give an overview of aerogel research, including aerogel properties and commercial potential and highlight the advantages of bio-based aerogels and specifically protein-based aerogels. A review of canola seed meal (CSM) protein and its potential for use in materials science was also included. The use of canola protein as a precursor polymer for developing aerogel structures is the central proposal of this thesis. As highlighted in **Section 2.4**, aerogels have never been produced from CSM protein, but if they were developed, could contribute to research knowledge about both aerogels and canola protein materials.

3.1. Thesis motivation and aims

The primary aim of this research is to develop and characterise a novel bioaerogel formed from canola protein. There are several hypotheses associated with this aim that are explored in the following Sections.

3.1.1. Aerogels can be made from canola protein

The motivation for developing an aerogel from a novel biopolymeric source emerges from Kistler's concept that any gel can theoretically be processed into an aerogel. Novel precursor molecules (including biopolymers) trialled in aerogel technology often produce unique variations in aerogel chemistry, morphology, and properties as compared to existing aerogel precursors (see **Chapter 2**). Therefore, substantial research scope (and application potential) exists for the exploration of a novel polymer source for making aerogels. This thesis focuses on a novel bioaerogel, produced from a bio-sourced polymer, due to interest in sustainable and eco-friendly (*e.g.* biodegradable) aerogels. Bioaerogels also generate the possibility of new applications in biosciences, where novel functionality

can be developed from novel bio-precursors (see **Chapter 2**). Further focus on protein-based aerogels shows these aerogel types are currently underrepresented in research yet offer unique processing and biochemical potential (refer **Section 2.2.3**). Some evidence suggests an advantage of using the supercritical drying technique over freeze drying, for producing bioaerogels with higher specific surface areas and smaller (more desirable) pore sizes. Thus, there is a motivation in this thesis to develop a novel bioaerogel with the use of both drying techniques and to analyse the resulting aerogels for a comparison of properties.

Canola meal protein has been identified as a candidate for the development of novel bioaerogels due to its: gelling ability, bio-based nature, commercial availability, and pre-established potential in food, biosciences, and sustainable materials (refer **Section 2.3**). Canola meal protein is a co-product of the food industry (canola oil production) and carries the potential to increase canola crop value if used in high-value industries such as those associated with existing aerogel applications.

This thesis hypothesises that aerogels from canola protein will be viable, since canola protein gels have been readily prepared for other purposes and since aerogel production processes (supercritical drying and freeze drying) are theoretically applicable to all gels.

3.1.2. Canola protein aerogels will be comparable to other protein-based aerogels

Characterising and comparing the structure and properties of canola protein aerogels with other aerogels is an essential research goal for this thesis since canola protein aerogels are intended for the same or similar applications as existing protein-based and bioaerogels. Providing a comparison to other bioaerogels gives an initial appraisal of the value of canola protein-based aerogels.

Canola protein has been used for development of other bio-based materials (see **Section 2.3.4**) suggesting canola protein can be a viable ‘greener’ alternative to existing polymers in such fields as hydrogels, films, and plastics. However, protein-based aerogels are generally less robust and have less

desirable porosities than existing types of aerogels. Protein-based aerogels do not generally out-perform their polysaccharide counterparts in properties such as specific surface area measurements, pore volumes and mechanical performance (refer **Section 2.2.3**). Current benchmarks in such properties are set by polysaccharide aerogels intended for applications in tissue engineering, drug delivery and filtration, and these benchmarks are a challenging target for protein aerogels. However, they are attainable in some cases (refer **Section 2.2.3**) and are yet to be measured in many protein aerogels. Given that protein aerogels are understudied, the conclusion that protein aerogels generally do not compete with polysaccharides in this field is still an uncertain one. It is additionally difficult to develop an expectation of a plant-based protein as examples are even scarcer than animal-based protein sources. Thus, the measuring and characterising of the morphologies and properties of the canola protein aerogels for such a comparison is of high importance to this thesis, but also more generally to protein aerogel research.

This thesis hypothesises that canola protein aerogels will have lower specific surface area measurements, pore volumes and mechanical performance as compared to other bioaerogels, but that they will be comparable to other protein-based examples. It is proposed that processing methodology for canola protein aerogels will require amendments and improvements but leading to a range of canola protein aerogel specimens with varying levels of competitiveness against other bioaerogels. Some evidence indicates that hybridised bioaerogels can be counted amongst the best examples of bioaerogels (refer to **Section 2.2.3**) and so hybridisation of CSM-based aerogels with other biopolymers requires further investigation.

3.1.3. The canola protein will undergo pH- and temperature-dependant gelation

Understanding gelation mechanisms can assist with the manufacture of tailorable aerogels. However, the gelation mechanisms of protein gels are often difficult to elucidate (refer **2.2.2** & **2.3.3**). Canola protein gelation is known to be influenced by pH and temperature. However, these studies include varying forms of the protein (*e.g.* meal, extract (and its various types), isolated protein *e.g.* cruciferin)

and a broad range of chosen pH values and temperatures. Therefore, the applicability of these studies to the current thesis requires confirmation with results from similar investigations on the canola protein extract used in this project.

Investigations that determine whether aqueous parameters, namely pH and temperature, influence the resulting viscosity, stiffness and behaviour of the gels will be carried out. The specific effects of each parameter on these gel properties, on protein structure, and on protein charge, will be reported. Resulting data will be combined with literature knowledge to determine the most plausible type of protein-protein interaction occurring during gel formation of the CSM proteins studied in this thesis.

This thesis hypothesises that aqueous chemical techniques (such as pH and temperature control) can be used to manipulate the gelation success of the protein. Such evidence would also show how canola aerogels can be tailored for applications using only green-chemistry principles. The potential for such aqueous parameters to produce tailorable canola aerogels is promising, given the use of these techniques in existing studies on canola protein and the use of similar methods in other protein aerogels.

3.1.4. Canola protein possesses unique biochemical attributes that can be harnessed in aerogel structures for relevant applications

The presence of bioactive molecules in proteins prompts research into their use in various medical, pharmaceutical, cosmetic, and food applications (refer **Section 2.2.4**). Directed studies that specifically look for canola protein bioactivity relevant to materials applications (*e.g.* anti-microbial properties) are yet to be reported. Additionally, the retention of bioactivity following the processing of the protein into new formats (*e.g.* aerogels) cannot be assumed from studies on the raw extract and require investigation. Since canola protein aerogels are a new format of canola protein material, their bioactive potential will be screened in this thesis to address these questions around the type and amount of bioactivity present and whether it is influenced by protein processing.

This thesis hypothesises that bioactive molecules relevant to materials applications, will be identified in the canola protein extract, but that aerogel processing is likely to reduce the quantity or quality of any such bioactivity. It is expected that chemical changes during processing or a reduction in the availability of molecules (as they are 'locked' into the matrix structure of the aerogel) will limit the detection of bioactive peptides in canola protein aerogels.

3.1.5. Processing parameters that affect gelation also influence aerogel morphology and properties.

Investigating the influence of certain parameters on the gelling ability of the canola protein will be useful for understanding the gelation mechanism (refer **Section 2.2.3**). However, it cannot be assumed that such influences (*e.g.* specific pH values lead to highest gel stiffness) are translatable to the aerogel structures or that these same parameters will be the determining factor in subsequent aerogel properties. It is known that the drying stage of the aerogel process can have a crucial influence on the aerogel morphology and subsequent properties, regardless of variations at earlier stages of the process such as during gelation (refer **Section 2.1.2**). Hence, a crucial part of the aerogel characterisation in this thesis is to investigate the effect of processing parameters on the aerogel properties themselves. This information will complement investigations into the effect of processing parameters on gelling ability (refer **Section 3.1.3**.) and assist with the comparison of canola aerogels to other aerogel types (refer **Section 3.1.2**).

This thesis hypothesises that gelation parameters that influence wet-gel stiffness and strength will also influence the corresponding aerogels in a similar manner. An extension of this hypothesis is that these effects will be explained by parallel studies on the protein molecular state (*e.g.* charge, conformation, chemistry) in the precursor solutions.

3.2. Thesis layout

3.2.1. Chapters 1 & 2

Chapters 1 and 2 present a broad introduction and history of the aerogel (**Chapter 1**) followed by an extensive literature review (**Chapter 2**) evaluating research on bioaerogels, protein-based bioaerogels, and canola seed meal protein. The purpose of **Chapter 2** is to detail the current knowledge, and deficiencies in that knowledge, of bio-based aerogels according to the published literature. **Chapter 2** will identify the open research questions that then form the specific objectives of the thesis.

3.2.2. Chapter 3

The purpose of the current Chapter is to provide the reader with a clear link between research needs identified in the literature review and the subsequent studies undertaken in this thesis. The motivation and direction for each Chapter and investigation will be linked to one or more aspects of the overarching goal: to develop and understand aerogel structures made from CSM protein.

3.2.3. Chapter 4

Chapter 4 describes the general materials and experimental protocols for the techniques in the subsequent results Chapters. Certain techniques that have been used across multiple experiments and adapted differently each time are described more generally in **Section 4.1**. Any experiment-specific deviations are found in the relevant results Chapters (**Chapters 5, 6,** & **7**) under dedicated experimental procedure sections. **Chapter 4** continues with the remaining experimental procedures explained in three dedicated Sections for each of the results Chapters. Thus, the experimental procedures are documented in a loose chronology reflecting the workflow of the project.

3.2.4. Chapter 5: ‘Canola seed meal protein and its potential use in novel materials’

Chapter 5 focuses on the study of the precursor polymer: the canola protein extract (see **Section 5.1**). It provides an overview of how the protein is extracted from raw meal (**Section 5.3**), the content of that protein extract (**Section 5.3**), and the reasons why that extract is amenable to bio-based materials and bioaerogel production (**Section**s **5.4** & **5.5**).

An appropriate precursor material that is identifiably canola protein, is required to address the thesis objective of developing canola protein aerogels. Canola protein is not available for commercial purchase through biochemical laboratory suppliers, and those products that can be obtained on the market are scarce (see **Section 2.3.2**). Chapter 5 describes the process used to obtain canola protein for this thesis and investigates the effectiveness of that extraction process (**Section 5.3.1**).

The assessment of the resulting extract for batch consistency and protein content is carried out to firstly justify the use of the extraction technique for CSM aerogel preparation. An analysis of the amino acid content of the extract is performed using appropriate chemical derivatisation and high-performance liquid chromatography (HPLC) to determine extract purity (**Section 5.3.2**). Amino acid analysis also provides nutritive information which can help determine application potential of the extract and aerogels. This is useful information for comparison with other bioaerogels (objective in **3.1.2**) and determining biochemical potential (objective in **Section 3.1.4**). Separation of the proteinaceous components of the extract is also carried out (**Section 5.3.3**) to compare batch consistency and to identify the various proteinaceous components (since the seed meal contains a mixture of protein types (see **Section 2.3.2**)). Gel Filtration Chromatography (GFC) is performed to assess how these constituents may change at various points in extraction. Sodium dodecyl sulphate – polyacrylamide gel electrophoresis (SDS-PAGE) is carried out on all batches of protein extract to compare the molecular weights of constituent proteins, assessing batch consistency. Results from these techniques ensure that all subsequent aerogels produced from the extract are made from a consistent source of canola protein.

Protein identification using molecular weight information alone can be difficult in canola protein research (see **Section 2.3.2**). Identification of the protein constituents in the extract provides information for understanding the gelation (objectives outlined in **Sections 3.1.3** & **3.1.5**), and understanding some aerogel properties (*e.g.* for bioactivity - proposed for investigation in **Section 3.1.4**). Knowing the exact sequences of proteins in the extract allows existing knowledge on those proteins to be cross-referenced with confidence when discussing the findings in this thesis. Identification of the protein constituents in the extract will be carried out using tandem mass spectrometry (**Section 5.3.4**). Mass spectrometry can identify amino acid sequences derived from protein components in the extract. The identification of peptides in the extract allows for accurate identification of those proteins and this information is mapped to the various molecular weight components identified in SDS-PAGE.

Determining if the canola extract is appropriate to produce viable and useful aerogel products is also explored in this Chapter. The potential for bioactivity in the canola protein extract and subsequent aerogel structures has previously been discussed and will be the primary result that addresses the objective outlined in **Section 3.1.4**. The canola protein and canola aerogels will be screened for known bioactive peptides using mass spectrometry and *in silico* database screening of identified peptides (**Section 5.4**). Though the development of canola aerogels is first described in **Chapter 6**, it is relevant to include bioactivity analysis of the canola aerogels alongside the canola extract in **Section 5.4**, addressing the objective around whether the bioactivity profile may change with aerogel processing.

Canola protein is a judicious choice as an aerogel precursor material due to its propensity for gelation (see **Section 2.3.3**). The objectives in **Section 3.1.3** propose to confirm this gelation propensity and determine how and why certain gelation parameters may influence it. Additionally, the objectives in **Section 3.1.5** extend this question to include the effects of such parameters on aerogels too. Both objectives will be primarily addressed by experiments in **Chapter 6**; however, information regarding how aqueous parameters (*e.g.* pH and temperature) influence canola protein molecules (the basic building blocks of subsequent gels and aerogels) will be required to address these objectives fully

(**Section 5.5**). Circular dichroism (CD) spectroscopy is used to analyse the effect of various aqueous conditions on the secondary structure of canola protein molecules (**Section 5.5.1**). These same aqueous conditions are subsequently investigated for their influence on gel properties (in **Chapter 6**, see **Section 6.3**), allowing possible links between molecular structure and gelation success to be drawn. Polyacrylamide gel electrophoresis on protein samples not subject to denaturation (native-PAGE) are used to analyse the electrostatic charge on canola protein molecules (**Section 5.5.2**). The study of how protein electrostatic charge can change under certain aqueous conditions may also inform about gelation propensity and subsequent aerogel properties.

3.2.5. Chapter 6: 'Novel bioaerogels derived from canola seed meal protein'

Chapter 6 will describe the first example of a canola protein aerogel (see **Section 6.2**), produced from the CSM protein extract in **Chapter 5**. The processes of gelling the CSM extract and drying the gels are described, alongside structural and property studies on those gels and aerogels.

The development of canola protein aerogels is the core aim of this thesis (see **Section 3.1**) and is directly addressed in **Section 6.2** (with later developments described in **Section 7.4**). The experimental methods required to manufacture these novel aerogels are presented (**Section 6.2**) and morphological data about the resulting structures (including densities) confirming typical aerogel structure is provided in **Section 6.4**. Further investigations in **Section 6.5** characterise the aerogel properties and allow for a comparison with other aerogel studies, addressing the objective outline in **Section 3.1.2.**

The thesis objective of determining how and why processing parameters (*e.g.* pH and temperature) influence gelation success (see **Section 3.1.3**) and aerogel properties (see **Section 3.1.5**) is addressed using information collected on the wet-gels described in Chapter 6. Rheological studies of the canola protein suspensions and gels are carried out using viscometry and rheometry (**Section 6.3**). Gel properties such as stiffness and viscosity can be used to quantify gelation success. This information can be linked to data about protein molecular behaviour (see **Section 3.2.4**) and aerogel properties.

The data obtained also reveals details about viscoelastic behaviour of gels and allows inferences about gel structure, useful for accessing the relationship between processes, morphologies, and properties.

Morphological data collected from density measurements (**Section 6.4.1**), X-ray tomography (**Section 6.4.2**), and scanning electron microscopy (**Section 6.4.2**) provide information about the general structure of the aerogels, confirming the development of a novel canola protein aerogel (objective in Section **3.1.1**). Porosity measurements from X-ray tomograms and scanning electron micrographs also provide quantitative information for comparing the structure of canola protein aerogels with other bioaerogels (objective **3.1.2**). Finally, morphological information can be used to link the effects of processing changes to structural changes in the aerogels, and eventually to differences in properties. This critical connection between processing and properties is required for addressing the objective outlined in **Section 3.1.5**.

Subsequently, the mechanical (**Section 6.5.1**), thermal (**Section 6.5.2**) and solubility properties (**Section 6.5.3**) of the aerogels are examined. The mechanical testing of the aerogels provides comparative data for investigating the effect of processing conditions on mechanical performance (objective **3.1.5**), while contributing to protein aerogel research for which mechanical properties are scarcely reported. An investigation of the mechanical performance of these materials helps to identify potential applications of canola protein aerogels, and allows comparisons with other non-proteinaceous aerogels (see objective outlined in **Section 3.1.2**).

Section 6.5 also investigates the possible differences in thermal stability and intermolecular bonding between the unprocessed canola protein extract and the aerogels (*via* differential scanning calorimetry (DSC) and thermogravimetric analysis (TGA) (**Section 6.5.2**). This information is useful for assessing gelation success (helping to address objectives outlined in **3.1.5**) and potential applications of the aerogels. Finally, a brief description of the water solubility of the aerogels is included to assess the possibility of unique applications in active molecule release (**Section 6.5.3**).

3.2.6. Chapter 7: 'Improved canola protein aerogels: techniques for tailoring aerogel properties'

Chapter 7 investigates possible morphological and mechanical improvements to the canola aerogels from **Chapter 6** using further variations to the gel processing. Specifically, the influences of additional components to the canola gels are investigated, in the form of Ca^{2+} ions (**Section 7.4**) and other biopolymers such as casein, collagen, hydrolysed collagen (gelatine), and chitin (**Section 7.3**). The work attempts to understand how these changes in formulation may change the (a) strength-to-weight ratio and (b) specific surface area and porosity of canola protein aerogels. The further development and modification of the canola protein aerogels allows a broadening of potential applications and comparisons to other bioaerogels (objectives outlined in **Section 3.1.2**).

The manufacture of hybrid canola wet-gels is described in Section **4.4.1**, however the development of the Ca^{2+}-gelled canola wet-gels is described in **Section 7.4.1** due to the novelty of the subsequent CSM protein aerogels that the Ca^{2+}-gelation enables. The effects of incorporating additional biopolymers into the canola protein aerogels are presented using morphological data (**Section 7.3.1**) and mechanical data (**Section 7.3.2**). These investigations provide information that not only addresses the competitiveness of canola protein aerogels, but also reveals further knowledge about the links between processing, structure, and properties.

Aerogels produced using freeze drying are not considered true aerogels according to some definitions (refer **Chapter 1** and **Section 2.1**). Thus, the primary aim of the thesis (outlined in **Section 3.1**), to develop canola aerogels, remains incomplete without investigations into the supercritical carbon dioxide (SC-CO_2) drying technique. The development of supercritically dried canola aerogels *via* Ca^{2+}-canola gels is presented in **Section 7.4.2**.

Investigations into the effect of the Ca^{2+} on gel stiffness were also carried out using rheometric analysis (**Section 7.4.1**), complementing observations on Ca^{2+} and its influence on gelation propensity (made in **Section 5.5**). Further investigations into the effect of Ca^{2+} on the mechanical properties of the aerogel (**Section 7.4.4**) help to describe the link between Ca^{2+}, gel structure, and aerogel

properties. Moreover, it is found that the use of Ca^{2+} to assist gelation is a novel approach in canola extracts. Consequently, the rheometric data on Ca^{2+}-canola gels provides insights into further applications of canola protein gels.

Finally, the supercritical drying method is known to increase the pore volume and specific surface area and reduce pore size of the resulting aerogels when compared to those from freeze drying (refer **Section 2.1**). The use of gas physisorption and BET analysis to compare the porosity of supercritically dried and freeze dried aerogels is combined with scanning electron microscopy (SEM) studies to analyse the possible influence of drying technique on aerogel structure (**Section 7.4.3**). Investigating the porosities and specific surface areas of these variants provides additional evidence for the development of novel canola protein aerogels (objective outlined in **Section 3.1.1**) and for comparing these aerogels to other types (objective **3.1.2**).

3.2.7. Chapters 8 & 9

A dedicated discussion (**Chapter 8**) coherently connecting the outcomes of individual experiments across multiple Sections and Chapters is provided after the results Chapters (5 – 7). **Chapter 8** assesses the success of the thesis investigations outlined here in **Section 3.1**, and provides both qualitative and quantitative summaries of the results for each thesis aim. The concluding Chapter (**9**) summarises the thesis findings and assesses the expected impact of this research in relevant fields including both bioaerogel research and canola protein research. Pathways for future research that may strengthen, complement, or stem from these findings are also outlined in **Chapter 9**.

Chapter 4

4. Experimental procedures

4.1. General techniques used across multiple Chapters

4.1.1. Polyacrylamide gel electrophoresis (PAGE)

Background

Polyacrylamide gel electrophoresis (PAGE) is a common biochemical technique that separates macromolecules (specifically proteins and nucleic acids) for identification and/or further analyses. The macromolecules are separated by using a gel matrix and applying an electric field to the gel. The macromolecules are drawn through the matrix due to the polarity in the electric field and their electric charge, but their diffusion is simultaneously hindered by the gel matrix. The rate at which the molecules migrate through the gel is dependent on the molecular weight, strength of attraction to the charged end, and extent of hindrance by the gel matrix. This translates to a dependency on the molecular weight, electrostatic charge, length, and shape of the molecule. The result is a staggered positioning of the molecules within the gel due to the unique combinations of weight, charge, length, and shape.

Sodium dodecyl sulphate (SDS) is a denaturing chemical that interferes with the native molecular structure (*i.e.* secondary, tertiary, and quaternary structure) of a protein such that the molecule unfolds to a single long chain of peptides (or nucleic acids). SDS also binds to the protein molecules to make them negatively charged and thus eliminating their own native electrostatic charges. When the denatured, negatively charged molecules are subject to electrophoresis, their rate of migration in the gel is influenced only by their length and molecular weight. The weight-to-length ratio of proteins is consistent since they are composed of the same amino acid building blocks, and thus proteins undergoing SDS-PAGE experience a migration rate dependant only on their molecular weight. If a standard sample of molecules of known molecular weights is run simultaneously, the exact molecular weights of sample molecules can

be determined. Native-PAGE refers to the use of PAGE on biomacromolecules that are not pre-treated with the SDS denaturing agent and thus maintain their native shapes and charges. Native-PAGE can be used to analyse the native conformations and/or charges of proteins in addition to molecular weight.

Materials

Methanol (99.9 %) was obtained from Thermo Fisher Scientific (New Zealand). Tris(hydroxymethyl)aminomethane (Tris), dithiothreitol (DTT), urea, sodium dodecyl sulphate (SDS), acetic acid, ethanol (absolute), ammonium sulphate, and phosphoric acid, were obtained from Merck (New Zealand). Bromophenol blue and glycerol were obtained from Bio-strategy (New Zealand). SDS concentrate buffer (0.25 M Tris, 1.92 M glycine, 1 % SDS), 4-20 % Criterion™ TGX™ precast gel, Coomassie blue stain G250, and Precision Plus Protein™ Standards were obtained from Bio-Rad (New Zealand). All solutions were prepared using reverse osmosis (RO) water (resistivity 18 MΩ) from a Milli-Q water purification system.

Protocol for SDS-PAGE

The canola protein extract was analysed by SDS-PAGE using a 4-20 % Criterion™ TGX™ precast PA-gel (Bio-Rad) and a 0.025 M tris, 0.192 M glycine, 0.1 % w/v SDS buffer (Bio-Rad). Protein extract samples were solubilised in electrophoresis buffer (6 M urea, 0.062 M Tris, 6 % DTT, 10 % glycerol, 0.001 % bromophenol blue, 2 % SDS, pH 6.8) at a concentration of 6.67 mg mL^{-1} and heated in boiling water for 4 mins. The electrophoresis tank was prepared with 10 × diluted SDS buffer (final concentration 0.025 M Tris, 0.192 M glycine, 0.1 % w/v SDS, pH 8.3) and the PA-gel. 5 µL of denatured extract samples were then loaded onto the gel alongside a Precision Plus Protein™ Standards (Bio-Rad) molecular weight marker. Electrophoresis was carried out at 200 V, 0.08 A, 15 W for 45 mins. The gel was then immersed in a fixing reagent (10 % acetic acid, 40 % water, 50 % ethanol) for 30 mins then stained using Coomaisse Brilliant Blue G-250 solution (16.6 % w/v ammonium sulphate, 0.166 % w/v

Coomaisse Brilliant Blue G-250, 16.6 % v/v phosphoric acid, 33.3 % v/v methanol) overnight and finally de-stained using RO water and lint-free tissues.

Protocol for native-PAGE

Canola protein extract was prepared as a 20 mg/mL solution (1 gram in 50 mL) and then adjusted to the prescribed pH value using 2 M NaOH where the varying pH values were: 6.0, 8.0 and 10.0. The resulting pH adjusted solutions/dispersions were then aliquoted into 3 equal volumes (per pH value) where one aliquot was subjected to a 10 min submersion in a water bath held at 95 °C and then allowed to cool to room temperature. A prescribed volume of 1 M $CaCl_2$ solution was added to the second aliquot such that the final $CaCl_2$ concentration was 20 mmol/L. The third aliquot was tested without further heat- or Ca^{2+}-treatment.

Native-PAGE sample buffers were prepared (9 M urea, 0.0938 M Tris, 7.5 % glycerol, 0.0015 % bromophenol blue) and titrated to appropriate pH values for each sample set (6.0, 8.0 or 10.0). Each of the 9 samples (3 pH values x 3 treatments) was mixed with the appropriate sample buffer (same pH) at a ratio of 200 µl buffer to 100 µl sample to give a final protein concentration of 6.7 mg/mL. Electrophoresis tanks were prepared with three precast PA-gels (separate gel and tank per pH value) and approximately 1 L of running buffer (0.025 M Tris, 0.192 M glycine) adjusted to the appropriate pH (6.0, 8.0 or 10.0). Sample aliquots of 5, 10, and 20 µL were then loaded onto the gel, using one set (same pH value) of three samples (pH only, heat-treated, or Ca^{2+}-treated) per gel (arranged as in **Figure 4.1**). 2 drops of bromophenol blue were added to each well for visual monitoring of progress during electrophoresis.

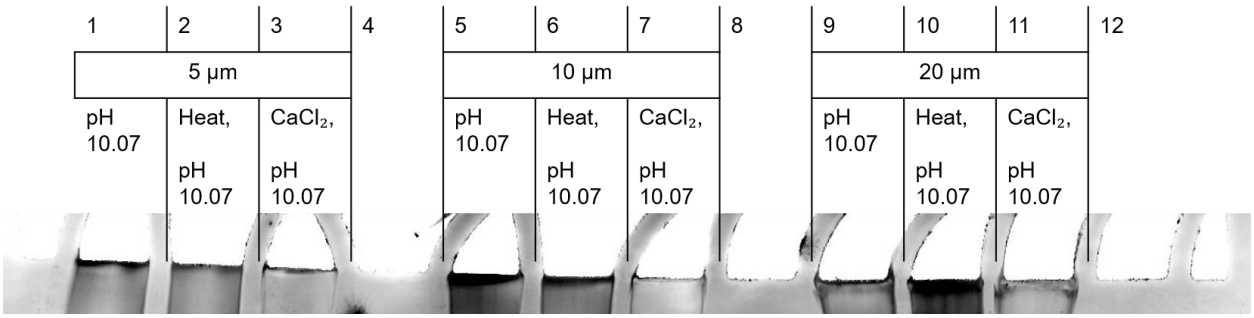

Figure 4.1: *Example of sample loading pattern on polyacrylamide gel for native-PAGE analysis. 9 wells from the available 12 (labelled 1-12) were loaded with either 5, 10, or 20 µL of sample from a set of three samples with the same pH value*

Electrophoresis was carried out at 200 V, 0.08 A, 15 W until visible bands of bromophenol blue reach bottom of gel (38 – 52 mins according to pH value). Gels were then immersed in a fixing reagent (10 % acetic acid, 40 % water, 50 % ethanol) for 30 mins then stained using Coomaisse Brilliant Blue G-250 solution (16.6 % w/v ammonium sulphate, 0.166 % w/v Coomaisse Brilliant Blue G-250, 16.6 % v/v phosphoric acid, 33.3 % v/v methanol) overnight and finally de-stained using RO water and lint-free tissues.

Analysis

Coomassie Brilliant Blue G250 stained gels were scanned using a Typhoon FLA 9500 scanner (GE Healthcare) in fluorescent mode at 635 nm, with a power setting of 600 V and resolution set to a pixel size of 25 µm. The fluorescence attributed to each protein band (peak volume) was quantified using Image Quant TL software (GE Healthcare) by integrating fluorescence intensity plots. Quantity of fluorescence for protein bands was recorded in arbitrary units, allowing for comparative assessments. During native-PAGE analysis, less distinct protein bands were quantified by adjusting the boundaries of the integral to include the entire smear rather than only including the peak of the fluorescence at the

leading edge (**Figure 4.2**).

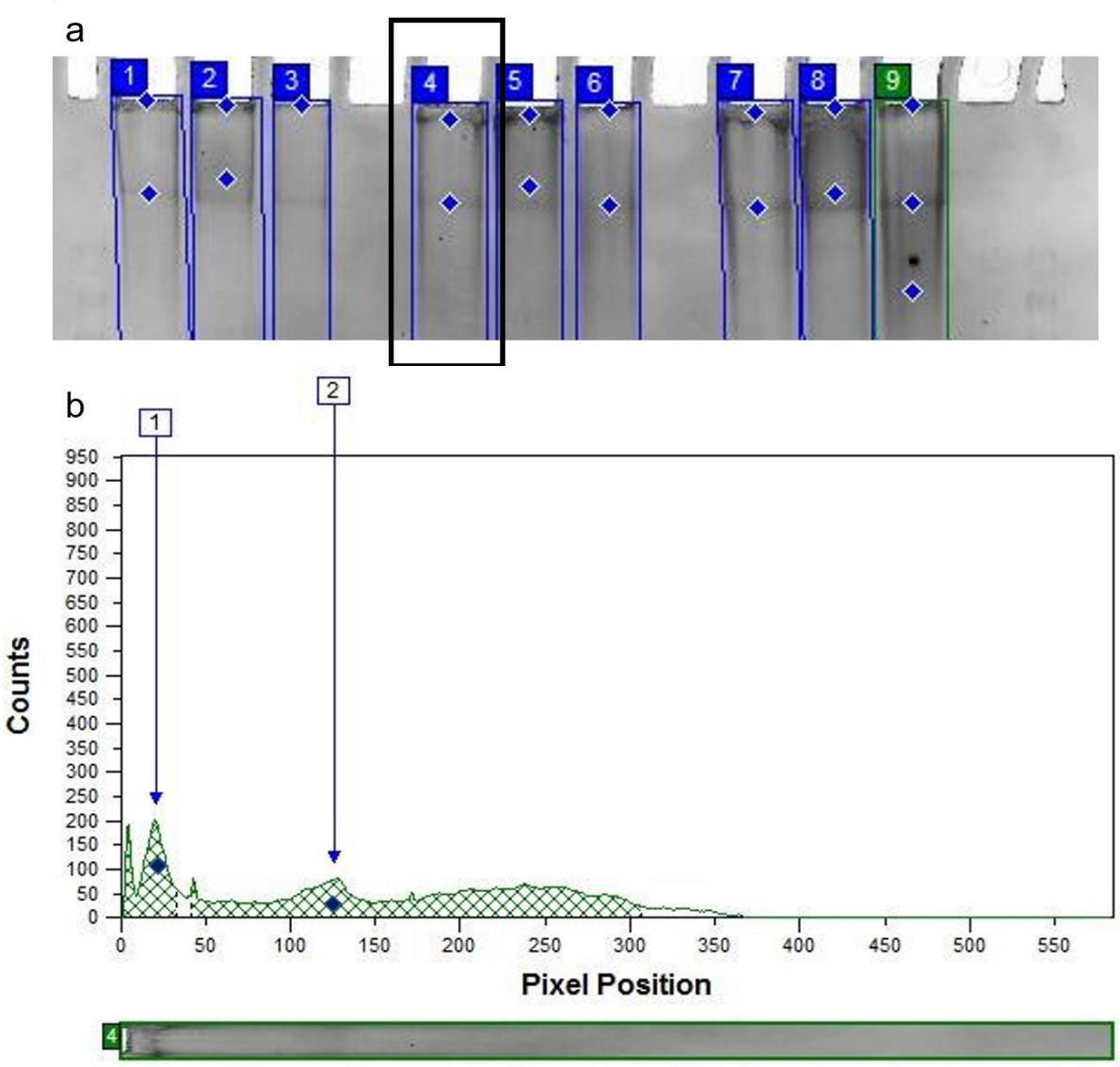

Figure 4.2: *Example of band selection and integration boundaries for quantifying total fluorescence in protein bands generated from native-PAGE analysis*

4.1.2. Viscometry

Protocol

The viscosity of the prepared CSM protein gels was measured using a Brookfield DV-II+ Pro Viscometer equipped with Brookfield spindles V72, V73, RV4, RV5, RV6, & RV7 for initial trialling and with V73 for later measurements. Spindle speed (and corresponding shear rate) was adjusted and viscometric data was recorded using Brookfield Rheocalc32 software. The viscosity and the % torque were recorded for each sample at a prescribed speed (5 - 200 rpm) 30 seconds after establishing a new speed. All measurements were conducted at 25 °C.

4.1.3. Rheometry of gels

Background

The viscosity and other rheological properties of wet-gels can be measured using viscometers (see **Section 4.1.2**) but these instruments are limited by their unidirectional shear force and can also have limited programmability. The Brookfield DV-II+ Pro has unidirectional rotation and requires operator intervention to progress through a series of rotational velocities, making the data collection process laborious and time-consuming. The shear rate was predetermined for each test and thixotropic properties were ignored during viscometer measurements. A response to shear rate was determined through multiple runs, each with different shear rates corresponding to single data points. However, this is a painstakingly slow method of collecting data sets and limits the amount of useful data that can be collected before the sample concentration is influenced by evaporation. A viscometer is useful for quick comparisons of viscosity taken on samples destined for aerogel production, while rheometric analyses (see below) were conducted on purposely formulated gels which were later discarded.

The collection of fast, accurate, and detailed rheological data is achieved by use of a rheometer using oscillatory strains. A gel (or viscous fluid) can also be analysed in smaller quantities (as little as 0.6 mL) while collecting a wider range of data (*e.g.* storage and loss moduli, loss factor, shear strain and stress, complex shear modulus, and viscosity). The main advantage of a rheometer is the possibility of oscillatory strain, allowing for rapid investigation of viscoelastic properties. Additionally, rheological data can be collected at a much faster rate and the rheometer can be programmed to 'sweep' through a variety of shear strains, frequencies, and temperatures. These sweeps measure multiple data points for a variety of rheological properties from oscillatory strains at each stage of the sweep.

Protocol - Rheoplus/32 V3.61

Initial strain amplitude sweep experiments were conducted on two CSM protein solutions (10 wt%, pH 11.5 ± 0.2) using a Rheoplus/32 V3.61 (Anton-Paar) rheometer to establish methodology and to investigate the effects of ageing (1 day versus 18 days). The samples were tested using a CP50-1 cone geometry (with a Peltier plate base protected with a corrosive resistant disposable pan) and approximately 0.7 mL volume of sample, trimmed to match the gap (0.102 mm) upon lowering of the geometry. The samples were subjected to a strain amplitude sweep from 0.01 to 100 % strain at a frequency of 10 rad/s (1.59 Hz) at 20 °C with a total of 6 repeats per sample.

Protocol - MCR 302

Further rheological testing was conducted on a range of CSM protein solutions and gels using a MCR 302 (Anton-Paar) rheometer equipped with a Viscotherm VT2 water cooling system and a CP50-1 cone geometry (with a Peltier plate base). Samples were measured in aliquots of approximately 0.6 mL which were trimmed to match the gap of 0.102 mm after the cone geometry was lowered. Initially, three samples (varying pH) were subject to a fixed-strain (0.1 %), fixed-frequency (1 Hz) measurement for 20 minutes at room temperature with viscosity and storage modulus monitored. Each sample was measured twice with one of the two repeats receiving 2-3 drops (approximately 20 – 40 µL) of low viscosity mineral oil

(p15(H) paraffinic hydrogenated white oil) to the edge of the trimmed sample. The oil was used for all aliquots tested in subsequent strain amplitude sweep and frequency sweep experiments to protect from evaporation during testing.

A range of CSM protein solutions and gels were then each subject to strain amplitude sweep and frequency sweep measurements. Each sample was tested in triplicate (using a fresh aliquot for each repeat) for both the strain amplitude and frequency sweeps. Strain amplitude sweep experiments were conducted at a frequency of 1 Hz from 0.005 % to 399 % strain, collecting a total of 25 data points. Frequency-sweep experiments were conducted at a strain of 0.1 % from 50 Hz to 0.075 Hz, collecting a total of 20 data points. All measurements were conducted at 22°C.

Data Analysis

Storage moduli, loss moduli, and loss factors for strain sweep experiments were plotted against % strain and analysed for a linear viscoelastic (LVE) region. The average complex viscosity ($|\mu|$ in Pa.s), storage modulus (G' in Pa), loss modulus (G'' in Pa) and loss factor ($\tan\delta$) were calculated for each run using all measurements from within a strain range of $0.1\ \% \leq \varepsilon \leq 1\ \%$ (corresponding with the LVE). Additionally, the critical strain ($\%\ \varepsilon_{crit}$) for each run was determined as the strain at which $G'' > G'$ ($\tan\delta \geq 1$). Results were further refined by calculating the average $|\mu|$, G^*, G', G'', $\tan\delta$, and $\%\ \varepsilon_{crit}$ for each sample from all repeat runs ($n = 3$ or 6) and reporting alongside the standard deviation. Storage moduli, loss moduli, and loss factors for frequency sweep experiments were plotted against frequency and analysed for shear thinning behaviour. The slope of the log G'-log f plot was calculated for $0.1\ \text{Hz} \leq f \leq 1\ \text{Hz}$ in each frequency sweep experiment.

4.1.4. Preparation of aerogels using freeze drying

Background

A total of 244 monolithic cryogel specimens were prepared throughout this work, each requiring between 2 and 5 days on a manifold freeze dryer to complete the drying process. Gels were prepared in batches according to prescribed gelation parameters of various investigations conducted over multiple years. However, freeze drying operation remained consistent across the production of multiple batches of cryogels and is therefore described as a stand-alone procedure.

Materials

15 mL (15.0 mm Ø (internal)) and 30 mL (30.0 mm Ø (internal)) Falcon™ Conical Centrifuge Tubes and Parafilm™ laboratory film were sourced from Thermo Fisher Scientific (New Zealand). Polyethylene (PE) block rectangular moulds (10 x 40 x 10 mm) and stainless-steel tube moulds (cylindrical (10.0 mm internal Ø x 40 mm) and rectangular (10 x 40 x 10 mm)) were designed and manufactured in-house.

Protocol

CSM protein dispersions and gels were transferred to a chosen vessel, selected for preparation of the most appropriate aerogel specimen dimensions for subsequent intended testing. Falcon™ Tubes were filled to between one and two thirds of the volume, open top PE moulds were filled to surface, steel tube moulds were filled to two-thirds of the volume. Open ends of tubes and moulds were then covered with Parafilm™ film and pierced with a pin to leave small holes in the film. Prepared tubes and moulds were stored at -80 °C for 6 – 72 hours, though generally 12 hours, prior to freeze drying. Freeze drying was carried out in a Dura-Dry MP manifold dryer (FTS Systems) at 30 to 50 mTorr and room temperature until specimens were dry and could be removed from vessels by inverting tubes (**Figure 4.3**).

Figure 4.3: *CSM protein aerogels in the process of freeze drying in the Dura-Dry MP manifold dryer*

4.1.5. Density measurements

Protocol

The bulk density of the aerogels was determined from measurements of the volume and mass. Vernier callipers (± 0.01 mm) were used to measure the average (n = 3) diameter (⌀) (from which radius (*r*) is calculated as half the diameter) and height (*h*) of cylindrical specimens. The average (n = 3) length (*l*), width (*w*) and height (*h*) of rectangular prism specimens were also measured with the callipers. A microbalance was used to weigh the aerogel specimens (Mettler Toledo AB204, ± 0.001 g). Bulk density was calculated according to the equation:

$$\rho = \frac{m}{V} \quad (1)$$

where the volume (V) of the cylindrical specimens is calculated as:

$$V = \pi r^2 h \tag{2}$$

and V of rectangular prism specimens is calculated as:

$$V = lwh \tag{3}$$

Bulk densities are recorded in units of grams per centimetre (g/cm^3) or grams per litre (g/L) as appropriate for comparison with other aerogel studies. Shrinkage values for aerogels were determined using measured bulk densities and hypothetical densities calculated from mass fractions as follows:

$$\%\ shrinkage = 100 \times \left(1 - \left({}^{w_{CSM}}/_{\rho_{bulk}}\right)\right) \tag{4}$$

Where the mass fraction (w_{CSM}) is represented as a fraction (*e.g.* 0.075) rather than percentage (*e.g.* 7.5 wt%) and the bulk density (ρ_{bulk}) is measured in g/cm^3.

4.1.6. Scanning electron microscopy (SEM)

Materials

Double sided carbon tape (ProSciTech) was sourced from Electron Microscopy Sciences (Australia). Surgical scalpel blades (Swann-Morton No.10) were sourced from Lab Supply (New Zealand). Liquid nitrogen was sourced from BOC (New Zealand).

Protocol

Aerogel specimens were carefully prepared for electron microscopy by cutting with blades (at ambient or liquid nitrogen temperature) or cryo-fracturing (at liquid nitrogen temperature) and were then adhered to a microscopy stub with double sided carbon tape. Specimens were sputter-coated with gold to a thickness

of 100 Å (DSR1 Desk Sputter Coater (Nanostructured Coatings Co.) prior to secondary electron imaging. The microstructure of the aerogels was characterised using a Hitachi TM3030 Plus scanning electron microscope (SEM) (magnifications < 2000 ×) and a JEOL JSM 7000F SEM (magnifications > 2000 ×). Specimens were imaged using an accelerating voltage of 15 kV (JSM 7000F) or 5 kV (JSM-IT300). Microstructural features were quantified by image analysis using Fiji Image J image processing software [214].

4.1.7. Static compression testing

Protocol

Aerogels were carefully prepared for compression testing by cutting each aerogel into replicate specimens (2 – 4 as permitted by size) cross-sectionally, using microscopy blades. Specimens were cut to 15 - 20 mm in height (determined by original sample length) while retaining a diameter of 11 – 13 mm. Cut specimens were subject to density measurements according to the protocol described in **Section 4.1.5**, including obtaining dimension measurements for subsequent stress and strain calculations.

The CSM aerogels were tested in compression mode using a universal electro-mechanical testing system (Model 4204, Instron, Norwood USA) equipped with either a 10 N (1kg) or 100 N load cell (10kg) (load range set to 50 % when using the 100 N load cell). Preloads of up to 100 mN (10 g) were applied, and then specimens were subject to a set rate of negative extension (compression) of 1 mm/min. Extension (in mm) and force (in Kg force) were measured and recorded at a data acquisition rate of 10 Hz using an in-house (AgResearch Ltd.) designed data logging software (‘Instron Data Logger_11’) developed using the LabView platform (National Instruments). Testing was stopped after achieving permanent deformation (evident by change in shape and/or the appearance of cracks and slips) or after reaching 90 % compression.

Data analysis

Compressive stress-strain plots were determined from the load-displacement data. Extension (Δh) and load (F) were converted to engineering strain (ε) and engineering stress (σ) by the following equations:

$$\sigma = \frac{F}{A_0} \tag{5}$$

$$\varepsilon = \frac{h_f - h_0}{h_0} \qquad where\ \ h_f - h_0 = \Delta h \tag{6}$$

The force recorded from the Instron is measured in Kg force but is converted to units of Newtons for the stress calculation. Cross-sectional area of the sample (A_o) is measured in m² and is perpendicular to the direction of compression, with variations depending on the sample shape as follows:

$$A_{cylindrical} = \pi . r^2 \tag{7}$$

$$A_{rectangular} = b . h \tag{8}$$

Additionally, crosshead position is recorded in mm with respect to the sample height with extension and force being negative values for compressive mode. Stress-strain plots were thereby produced by transforming the recorded data using the following amended equations for stress (σ):

$$\sigma_{Rectangular} = -(\frac{F\ x\ 9.80665}{b\ x\ h}) \tag{9}$$

$$\sigma_{Cylindrical} = -(\frac{F\ x\ 9.80665}{\pi\ x\ r^2}) \tag{10}$$

where *F* is recorded in Kgf and *b*, *h*, and *r*, are the base and height or radius of the samples, measured in metres. Strain was calculated using Equation (6) and multiplying by - 1.

Resulting stress values are plotted against strain for each specimen and analysed for yield stress (stress at the onset of the non-linear region), compressive elastic modulus (slope of the linear region), and elastic limit (strain at yield). These analyses were achieved by first fitting a linear regression model to the linear region of the curve such that a minimum coefficient of determination (R^2) of 0.99 was achieved (**Figure 4.4**). The elastic modulus was calculated as the slope of this linear regression model. The yield (or collapse) strength & elastic limit were identified using the last data point from the truncated data set used to generate the linear model.

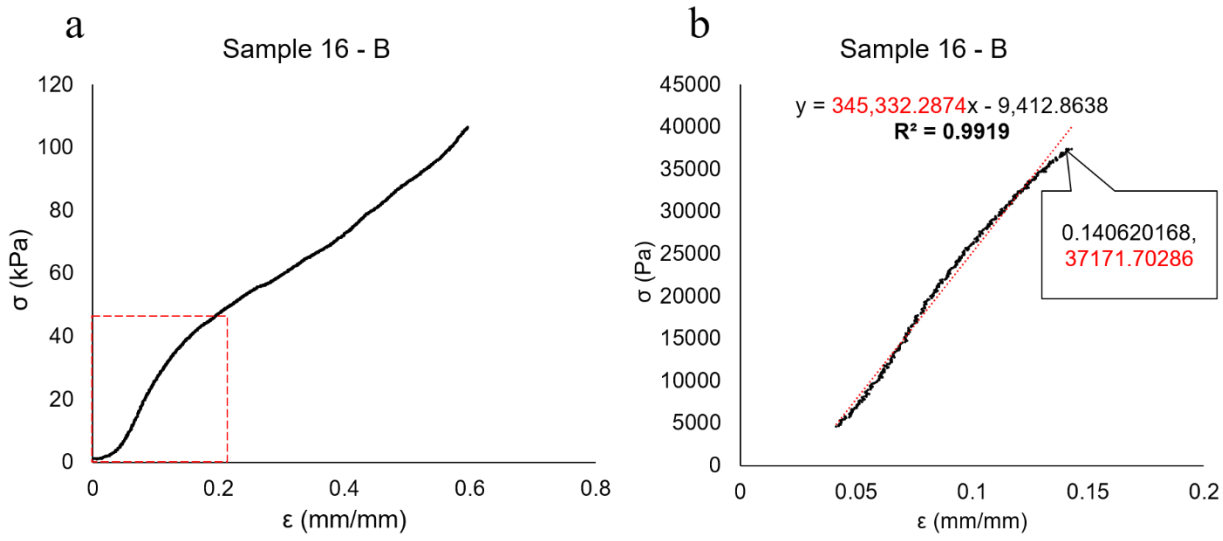

Figure 4.4 (a) *Example stress-strain plot from compressive testing of a CSM protein aerogel with* ***(b)*** *the linear regression model fitted to the plot demonstrating a minimum coefficient of determination (R^2) of 0.99. The elastic modulus and yield stress are identified in red*

Some curves possessed a 'toe region' at the initiation of the test which was initially attributed to sample surfaces bedding into compression platens (specimen cutting was highly challenging due to the delicate and brittle nature of samples and some samples were not perfectly parallel). However, later analyses may indicate that initial non-linear regions could be a phenomenon of the aerogels (see Section **6.5.1.1**). Nevertheless, since the elastic moduli were calculated for comparative purposes only, these initial non-linear regions (or 'toe regions') were excluded when calculating elastic moduli to achieve consistent comparisons of the linear regions ($R^2 > 0.99$). Toe regions did not affect the yield stress measurements

but complicated the assessment of elastic limits (see **Section 6.5.1.1**). The use of crosshead displacement measurements in the data collection can be less accurate than non-contact methods of strain detection (*e.g.* by video). However, crosshead displacement was determined to be the most practical measure of strain in the current research and sufficient for comparative purposes of the resulting moduli data. The average and standard deviation (n = 2 – 10 (experiment specific)) of the elastic modulus (E), yield strength (σ_y), and elastic limit (% ε_y) of the aerogels were determined.

4.2. Experimental procedures for deriving and characterising protein (Chapter 5)

Chapter 5 examines the chemical nature of the canola protein extract obtained from industrially sourced *Brassica napus* rapeseed (canola) seed meal. Canola seed meal protein was first extracted from raw meal in batches, dried, and then was stored at – 80 °C until used for experiments. Biochemical analyses conducted on the extract included amino acid analysis, separation and identification of proteins, bioactive peptide profiling, and circular dichroism spectroscopy. These biochemical techniques are commonly employed in the study of proteins and are used according to generic protocols, though some adjustments are made for application to canola protein extract.

4.2.1. Canola protein extraction

Materials

Canola seed meal (CSM) was sourced from *Brassica napus* seed following a chemical-free cold press to extract the canola oil (Pure Oil NZ Limited, Rolleston, New Zealand). N-hexane, sodium hydroxide (NaOH) pellets (98.5-100 %), and hydrochloric acid (36.5-38 %) were obtained from Thermo Fisher Scientific (New Zealand). Tris(hydroxymethane)aminomethane (≥ 99.8 %), sodium chloride (≥ 99.0 %), and filter paper (hardened, ashless, Grade 540 (8 µm) (Whatman®) & glass microfibre GF/C, 1822 090 (1.2 µm) (Whatman®)) were sourced from Sigma Aldrich (now Merck) New Zealand. A 10 kDa molecular weight cut-off (MWCO) membrane (ST-2B-1812F (Synder® Filtration)) for ultrafiltration and membrane housing (MA06) were purchased from Smart Membrane Solutions Ltd. (New Zealand). All the solutions were prepared, and precipitates washed, using reverse osmosis (RO) water (resistivity 18 MΩ) from a Milli-Q water purification system.

Protocol – Alkali-acid method

Canola proteins were extracted from CSM using an alkali-acid extraction method adapted from Klockeman *et al.* [185]. Firstly, 200 - 250 g of CSM was rinsed in 400 - 500 mL of hexane (immersed with agitation for at least 20 minutes, followed by sieving off the meal and drying until all excess solvent is removed) to remove residual oil. After drying, 200 g of the CSM was suspended in 2 L of a 0.4 % NaOH solution (at 10 % w/v ratio) and agitated for at least 1 hour. The solubilised protein was separated from the insoluble fraction by decanting and centrifugation at 18520 × g for 30 mins. Cloudy supernatant was further clarified by vacuum filtering through 8.0 µm, or 1.2 µm (pore size) Whatman® filter paper. The protein extract was then precipitated by the addition of 2 M HCl until a pH of 3.5 was attained. Following agitation for a further 30 minutes, the precipitate was then isolated using one or two rounds of centrifugation at 18520 × g with a washing step (using 2L Milli-Q water) between centrifugation rounds. Once isolated, the washed precipitate was frozen at -80 °C overnight prior to freeze drying on a Dura-Dry MP manifold dryer (FTS Systems) at 30 to 50 mTorr and room temperature until a dry powder was obtained. Throughout the thesis the alkali-acid extraction technique was used eleven times following the same general protocol outlined above. However, some variations (see **Table 4.1**) were used for the preparation of certain batches as the method was undergoing refinement to strike a practical balance between extraction yield and total processing time.

Table 4.1: *Variations to the alkali-acid extraction method for batches*

Batch number	Ratio of meal to buffer (w/w % meal)	Solubilisation pH	Solubilisation time (mins)	Sieved/filtered following 1st centrifugation	Precipitation pH	Precipitation time and temperature	Wash steps	Other comment
1	1 to 9.1 (9.9 %)	not recorded	90	sieved then 8.0 - µm filter paper	3.5	45 mins (25 °C)	2	supernatant stored overnight in fridge prior to acid addition
2	1 to 9.1 (9.9 %)	not recorded	85	sieved then 8.0 - µm filter paper	3.5	52 mins (25 °C)	1	
5	1 to 10 (9.1 %)	not recorded	180	sieved then 1.2- µm filter paper	3.6	120 mins (25 °C)	1	supernatant stored overnight in fridge prior to acid addition
6	1 to 10 (9.1 %)	10.04	100	sieved then 8.0 - µm filter paper	3.5	55 mins (25 °C)	1	supernatant stored overnight in fridge prior to acid addition
7	1 to 10 (9.1 %)	10.50	120	sieved then 8.0- µm filter paper	3.5	310 mins (4 °C)	1	Material loss during alkali solubilisation due to equipment failure
8	1 to 10 (9.1 %)	11.03	360	sieved	3.5	18 hours (4 °C)	1	
9	1 to 19.6 (4.9 %)	not recorded	180	sieved	4.0	360 mins (4 °C)	1	
11	1 to 9.9 (9.2 %)	11.18	90	sieved	3.5	18 hours (4 °C)	1	
12	1 to 10 (9.1 %)	11.26	150	no	3.6	18 hours (4 °C)	1	Sodium azide (0.02 %) added to supernatant as preservative while stored 3 days at 4 °C, prior to acid precipitation.
13	1 to 11.4 (8.0 %)	not recorded	120	no	3.5	18 hours (4 °C)	1	

Protocol – Protein Micellar Method (PMM)

Canola proteins were extracted from CSM using a protein micellar extraction method adapted from Kim *et al.* [200]. Firstly, 200 g of CSM was rinsed in 500 mL of hexane (immersed with agitation for at least 20 minutes, followed by sieving off the meal and drying until all excess solvent is removed) to remove residual oil. After drying, the CSM was suspended in 2 L of 0.05 M Tris / 0.1 M NaCl buffer (thus 10 % w/v ratio) that was pH adjusted to 7.0 using 2 M HCl and agitated for at least 1 hour. The pH was regularly checked and readjusted to pH 7.0 during solubilisation. The solubilised protein was separated from the insoluble fraction by decanting and centrifugation at 3000 × g for 60 mins (at 25 °C). The supernatant was further clarified by vacuum filtering through 1.2 µm (pore size) Whatman® filter paper and stored at 4 °C prior to ultrafiltration. The ultrafiltration system (10 kDa MWCO membrane (ST-2B-1812F (Synder® Filtration), membrane housing) was assembled and attached to a peristaltic pump with clean rubber tubing and inlet and outlet pressure gauges (**Figure 4.5**).

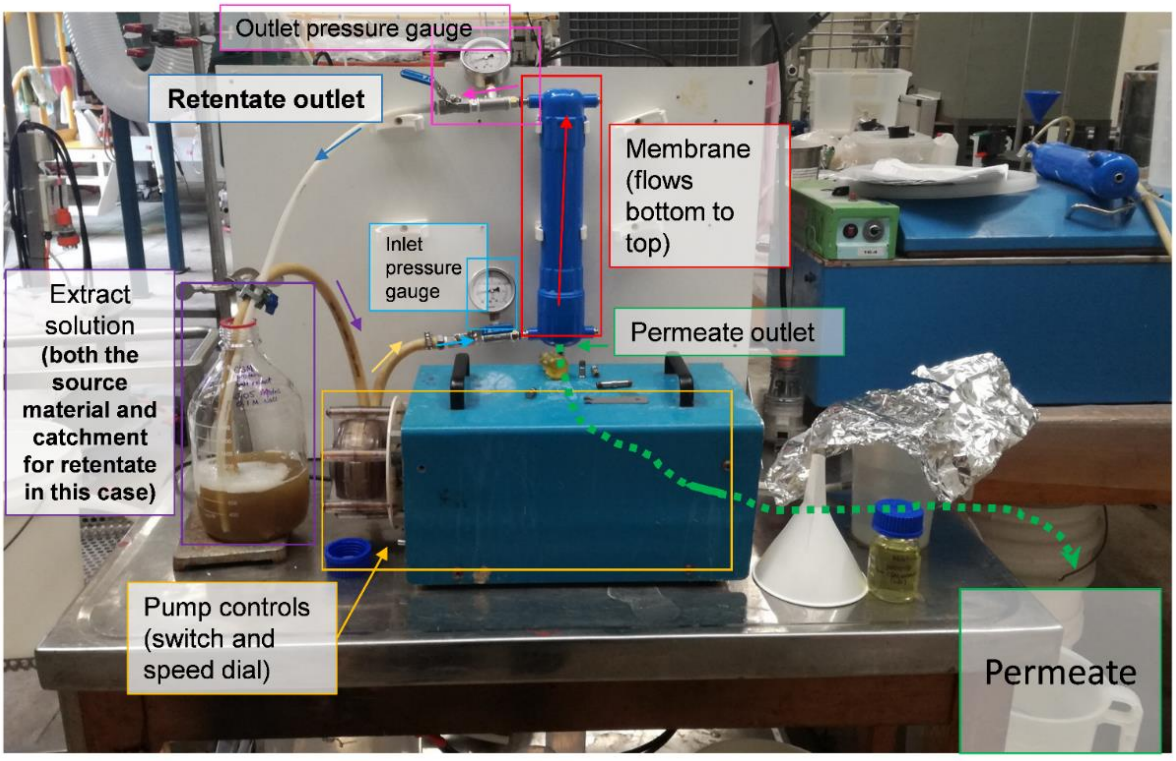

***Figure 4.5**: Equipment assembly for ultrafiltration of CSM solubilised protein using the ST-2B-1812F (Synder® Filtration) membrane*

The solubilised CSM (retentate) was then ultrafiltered at 7 - 10 psi (inlet pressure) until the volume was reduced to approximately 700 mL, discarding the permeate. Two equivalents (1.4 L) of RO water were then added to the retentate (total volume 2.1 L), before again being concentrated by filtration, to 850 mL. A third cycle of filtration was then carried out by first adding another 700 mL of RO water and then reducing the volume to 700 mL, at which point the system was reversed to drain the product. The membrane was then flushed with 500 mL of RO water at 0 psi for 10 minutes (circulating), before this was also drained and added to the product. The final 1.2 L of product contained 1.16 times the concentration of the original solubilised protein but with one tenth the ionic strength as final concentrations of Tris and NaCl were 0.005 M and 0.011 M, respectively. The obtained product was then stored at 4 °C overnight to allow for protein micelles to form and these were then isolated by centrifugation at 15500 × g for 30 minutes (at 6 °C). Once isolated, the precipitate was frozen at -80 °C overnight prior to freeze drying on a Dura-Dry MP manifold dryer (FTS Systems) at 30 to 50 mTorr and room temperature for 5 days.

4.2.2. Amino Acid Analysis

Materials

Amino acid standard H was sourced from Thermo Scientific (Rockford USA). AccQ-Fluor reagent and AccQ-Taq eluent were sourced from Waters Corporation (Milford, USA). Acetonitrile (LC-MS grade) was sourced from Thermo Fisher Scientific (New Zealand). Performic acid was made by mixing formic acid with hydrogen peroxide where the formic acid was sourced from Ajax Finechem Pvt. Ltd, NSW, Australia, and the hydrogen peroxide was sourced from Thermo Fisher Scientific (Australia). Hydrochloric acid was sourced from Sigma-Aldrich (USA).

Protocol

Accurately weighed (to an accuracy of 0.0001 g) CSM protein extract samples (approximately 10 mg) were transferred to glass hydrolysing tubes alongside an analysis standard. Samples were subject to acid hydrolysis using HCl vapour at 110 °C for 24 h followed by derivatisation with AccQ-Tag reagent according to methods described by S.A. Cohen in *Methods in molecular biology*, 2003. **211**: p. 143-154 [215]. Amino acid analysis was performed using an Ultimate 3000 HPLC system (Dionex). 5 µl of the derivatised samples was injected onto a Thermo Accucore XL C18 column (4.6mm i.d. × 250 mm, 4 µm particles) protected with a C18 guard column. The separation was performed at 37 °C using a flow rate of 1.0 mL/min using a gradient from 1.5 - 16.5 % mobile phase B over 52 min. Mobile phase A was AccQ-Tag eluent A, and mobile phase B was 100 % acetonitrile. An excitation wavelength of 250 nm and emission wavelength of 395 nm were used for the quantitative analysis using a fluorescence detector (Dionex Ultimate FLD 3000).

Performic acid oxidation was performed on all the samples for the quantitative assessment of total cysteine. The formation of crosslinked amino acids (lanthionine and lysinoalanine) was also analysed. The level of tryptophan could not be determined by this method because the indole ring of this amino acid is highly sensitive to the acidic conditions. Three full technical repeats for each sample were carried out for this analysis.

4.2.3. Gel Filtration Chromatography

Background

Gel-filtration chromatography (GFC) (also known as Size-exclusion Chromatography (SEC)) is a separation technique that uses a gel matrix to hinder molecular movement in a flowing, aqueous medium. Smaller molecules are hindered to a higher degree, thus eluted molecules appear in descending order by size, though elution is also influenced by other factors such as molecular shape and hydrophobicity. GFC

is used to directly compare the proteins found in the two canola extract types used in this thesis: 'alkali-acid' and 'salt-PMM' CSM protein extracts.

Materials

Sodium chloride (analytical reagent grade) (Thermo Fisher brand), ammonium bicarbonate (> 99.5 %) (BDH Chemicals), sodium azide (> 99.0 %) (BDH Chemicals), potassium dihydrogen orthophosphate (> 99.5 %) (BDH Chemicals), sodium hydrogen orthophosphate (analytical reagent grade) (Univar), sodium hydroxide (NaOH) pellets (98.5-100 %), and hydrochloric acid (36.5-38 %) were sourced from Thermo Fisher Scientific (New Zealand). The Superose® 12 10/300 GL prepacked column (GE Healthcare Life Sciences, now Cytiva) was obtained from Sigma-Aldrich (New Zealand).

Protocol

Gel filtration chromatography was performed on a HPLC system (Knauer, Berlin, Germany) equipped with an A 3800 auto sampler and a S 2600 photodiode array detector. Two litres of filtered and degassed buffer (0.05 M ammonium bicarbonate / 0.3 M NaCl) was prepared with a final pH of 7.84. A further 2 L of filtered and degassed 0.1 % sodium azide (NaN_3) solution was also prepared and both buffers were assembled on the HPLC system (line A corresponding to the NaN_3 solution and line B to the NH_4HCO_3 buffer). 20 mg of the CSM protein extracts were each dissolved in 2.0 mL of 0.05 M potassium phosphate / 0.3 M NaCl buffer (1 % w/v) at pH 12 (adjusted using 2 M NaOH) to facilitate solubility of the extract, and then pH adjusted to pH 7.7 using 1 M HCl. Liquid samples (see

Table *4.2*) were obtained as 2.0 mL aliquots at various stages of canola protein extraction and subsequently pH adjusted as appropriate for GFC analysis.

Table 4.2: *Summary of sample information for CSM extract samples prepared for GFC analysis*

Sample name (run number/s)	Extraction method (batch number)	Sample type	Sample description
Extract 1 (170526_1436)	Alkali-acid (1)	Precipitated product	Isoelectric protein precipitate (alkali-soluble, acid-insoluble proteins)
Extract 3 (170526_1617)	Salt-PMM (3)	Precipitated product	PMM precipitate (salt-soluble, insoluble in low ionic strength)
Sample 1 (170721_1155 and 170722_0235)	Salt-PMM (4)	Soluble product	Supernatant prior to ultrafiltration (all salt-soluble proteins)
Sample 2 (170721_1327 and 170722_0034)	Salt-PMM (4)	Soluble product	Ultrafiltration retentate (> 10 kDa salt soluble proteins)
Sample 3 (170721_1458 and 170721_2233)	Salt-PMM (4)	Soluble waste	Ultrafiltration permeate (< 10 kDa salt soluble peptides)
Sample 4 (170721_1629)	Alkali-acid (5)	Soluble product	Supernatant prior to acid precipitation (all alkali-soluble proteins)
Sample 5 (170721_1830)	Alkali-acid (5)	Soluble waste	Supernatant after acid precipitation (alkali and acid soluble proteins)
Sample 6 (170721_2032)	Salt-PMM (4)	Soluble waste	Supernatant from retentate after the PMM precipitation (salt-soluble, also soluble in low ionic strength)

The solubilised samples were injected (10 μL) onto a Superose® 12 10/300 GL prepacked column (GE Healthcare) with a separation range of 1000 Da to 300 000 Da. Elution was performed at a flow rate of 0.5 mL/min with the 0.05 M ammonium bicarbonate / 0.3 M NaCl buffer (pH 7.84) as the mobile phase. The column eluate was monitored at 230, 260, and 280 nm.

4.2.4. Tandem mass spectrometry (LC-MS/MS)

Background

Mass spectrometry (MS) is a common technique in chemical and biochemical labs for the study of chemical composition. A sample matrix (which can be a complex mix of compounds) can be identified by spectra of ions detected as a function of their mass-to-charge ratio. Sample molecules are first ionised, each with a unique mass and charge. These ions are identified by accelerating them in an electric or magnetic field and measuring the type and amount of deflection (which is a function of a mass-to-charge ratio). They can then be identified by comparison with theoretical molecular mass-to-charge ratios of atoms and molecules to identify the original molecule. Tandem mass spectrometry (LC-MS/MS) uses this process to identify protein molecules in a sample by employing multiple rounds of MS. High-performance liquid chromatography (HPLC) may first be used to separate peptides from many others, followed by an initial round of MS that breaks the protein into smaller fragments. A repeated round of MS can isolate one peptide ion, fragment this into even smaller peptide fragments that will allow for chemical identification, ultimately permitting identification of the original protein. A series of ion-pairs is produced which can be arranged in an overlapping sequence to represent the parent analyte. Furthermore, a single sample of protein can be digested (*via* enzymatic or other hydrolysis) to produce a mixture of oligopeptides which are of sufficiently small mass to be identified by LC-MS/MS. Consequently, a compilation of the resulting oligopeptides can allow for the identification of the parent protein due to sequence specificity by comparing with amino acid sequences from protein databases. LC-MS/MS is used in this thesis to identify the proteins present in the canola seed meal extracts, by first isolating molecular weight bands from SDS-PAGE gels (refer to **Section 4.1.1**) and then employing LC-MS/MS.

Materials

Ammonium bicarbonate (≥ 99.0 %), tris(2-carboxyethyl)phosphine (TCEP) (≥ 98.0 %), iodoacetamide (≥ 99.0 %), acetonitrile (LC-MS grade), formic acid (LC-MS grade), and methanol (LC-MS grade) were

obtained from Merck (New Zealand). Modified Trypsin (Sequencing Grade, Porcine) (Promega) and Trypsin Resuspension Dilution Buffer (Promega) were obtained from In vitro Technologies (New Zealand). Optima LCMS-grade water was purchased from Thermo Fisher Scientific (New Zealand). Empore™ C18 disks were from Sulpelco (Bellefonte, PA, USA).

Protocol – Sample preparation

SDS-PAGE analysis was performed on 5 batches of CSM extract (protocol described in **Section 4.1.1**) and the resulting protein bands were analysed by liquid chromatography-tandem mass spectrometry (LC-MS/MS). The selected gel bands (**Figure4.6**) were excised from the SDS-PAGE gel using a surgical scalpel blade (Swann-Morton No.10). and deposited into 0.5 mL Eppendorf Safe-Lock Microcentrifuge Tubes, numbered 1 – 14 in order of decreasing molecular weight (**Table 4.3**).

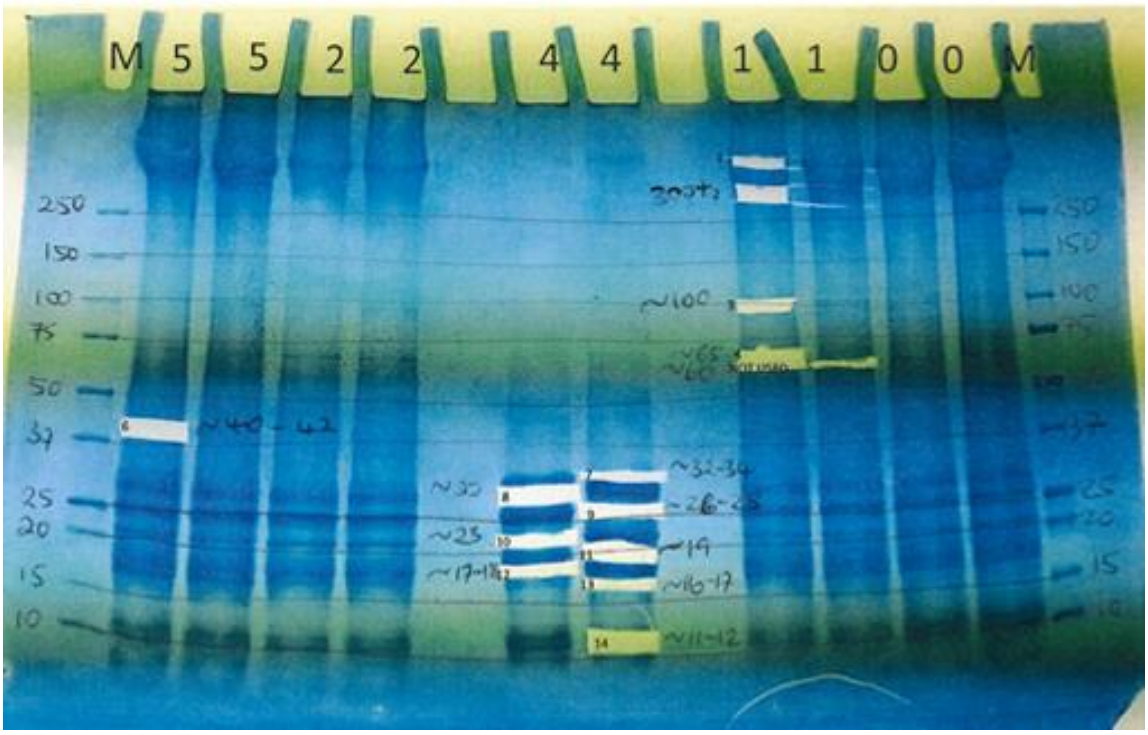

Figure4.6*: Gel bands from an SDS-PAGE analysis of CSM extracts that were excised for LC-MS/MS analysis*

The excised bands were de-stained in 200 mM ammonium bicarbonate in 50 % acetonitrile for one hour at 37 °C. The de-staining solution was then removed, and the de-stained gels bands were then reduced

with 50 mM tris(2-carboxyethyl)phosphine in 100 mM ammonium bicarbonate followed by alkylation using 150 mM iodoacetamide in 100 mM ammonium bicarbonate. The gels bands were then subjected to trypsin digestion at 37°C for 18 hours. Empore™ disks were then used for peptide purification [216] and the peptides analysed using LC-MS/MS.

Table 4.3: *Molecular weight bands isolated from SDS-PAGE gel for LC-MS/MS analysis*

Sample	**Mw (kDa)**	**Sample**	**Mw (kDa)**
1	350	8	30
2	300	9	26 -28
3	90 – 100	10	22 -23
4	65 - 70	11	18 -20
5	60 - 65	12	17-18
6	40 - 45	13	16-17
7	32	14	11-12

Protocol - LC-MS/MS analysis

The peptide extracts were resuspended in 100 µL of 0.1 % formic acid, and Nanoflow LC-MS/MS was performed on a UltiMate 3000 RSLC nano UHPLC (Thermo Fisher Scientific Waltham, MA, USA) coupled to an Impact HD Q-TOF mass spectrometer equipped with a CaptiveSpray ion source (Bruker Daltonik, Bremen, Germany). Samples were loaded at 5 µL min-1 onto on a trap column (5 mm × 300 µm ID, 5 µm, C18 PepMap100, Thermo Fisher Scientific), which was then switched in-line with an analytical column (ProntoSIL, C18AQ, 100 µm ID x 15 cm, 3 µm, 200 Å; nanoLCMS Solutions). Elution was performed at 800 nl min-1, using a linear gradient for solvent B (98% acetonitrile, 0.1% formic acid) as follows: 0 – 20 % in 6 minutes followed by 20 – 55 % in the subsequent 22 minutes, 55 – 96 % in a further 1 minute, held at 96 % for the next 4 minutes, followed by 96 – 3 % in a further one minute and then held at 3 % for the remainder of the run (5 mins). Solvent A was LCMS-grade water with 0.1 % formic acid. The column oven temperature was maintained at 50 °C. Automated information dependent

acquisition (IDA) was performed for each MS spectrum (m/z 350-1500) which was followed by MS/MS spectra of the top 10 precursor ions.

Data analysis

After each LC-MS/MS run, the peak list data was extracted using DataAnalysis v4.2 (Bruker) followed by protein identification using ProteinScape v3.1 (Bruker). Peak lists were queried against *Viridiplantae* sequences in the SwissProt database (release date: 27th of May 2014) using the Mascot search engine (v2.2.06, Matrix Science) maintained on an in-house server. The following Mascot search parameters were used: 'semiTrypsin' as the proteolytic enzyme with one missed cleavage permitted; 5.0 ppm peptide error tolerance for MS and 0.3 Da for MS/MS. Search results were compiled and analysed using the ProteinExtractor function in ProteinScape. Peptide acceptance threshold of 20 and protein acceptance threshold of 80 with at least one peptide with a score higher than the identity threshold determined by the search engine was required for protein identification and results assessed as true matches were used for further analysis.

4.2.5. Bioactive peptide profiling

Background

Canola protein extracts and aerogels (refer to **Section 5.2**) for gel and aerogel processing methods, respectively) were analysed for known bioactive peptides using LC-MS/MS identification and subsequent *in silico* bioactivity screening against online databases. Identified peptide sequences were screened against a database of known bioactive peptides using an in-house (AgResearch Ltd.) devised algorithm developed using the Microsoft Excel platform and online databases of bioactive molecules. The algorithm identifies both identical matches and similarities, such as partial matches and cryptides, between the databases and the sample peptide sequences.

Materials

Ammonium bicarbonate (≥ 99.0 %), tris(2-carboxyethyl)phosphine (TCEP) (≥ 98.0 %), iodoacetamide (IAM) (≥ 99.0 %), acetonitrile (LC-MS grade), formic acid (LC-MS grade), methanol (LC-MS grade), chloroform, were obtained from Merck (New Zealand). Modified Trypsin (Sequencing Grade, Porcine) (Promega) and Trypsin Resuspension Dilution Buffer (Promega) were obtained from *In vitro* Technologies (New Zealand). 3 kDa dialysis filter (Microcon, Ultracel YM-3) was sourced from Millipore (Bedford, USA). Empore™ C18 disks were from Sulpelco (Bellefonte, PA, USA). Optima LCMS-grade water was purchased from Thermo Fisher Scientific (New Zealand) and double distilled water was provided by in-house distillation.

Protocol – Preparation of enzyme-digested samples

Approximately 10 mg of canola protein aerogel specimens "A13" (prepared from 'alkali-acid' extract, at 10 wt%, pH 10.55, & 25 °C) and "A15" (prepared from 'salt-PMM' extract, at 10 wt%, pH 10.55, & 25 °C) was measured accurately (A13 = 10.8 mg, A15 = 10.3 mg) and dissolved in 0.5 mL of 50 mM ammonium bicarbonate. Samples were then vortexed and sonicated to facilitate dissolution before being subject to centrifugation at 14,000 × g to remove undissolved solids from the samples.

A 20µl aliquot of supernatant from sample A15 was added to 980 µl of RO water (1:50 dilution) and the resulting diluted sample analysed for protein concentration using IR-based protein quantitation system (Merck KGaA, Darmstadt, Germany) (resulting protein concentration = 0.445 mg/mL, therefore undiluted sample = 22 mg/mL). Aliquots of the aerogel solutions (11.4 µL) were taken and added to 88.6 µL of 50 mM ammonium bicarbonate to achieve a final concentration of 250 µg / 100 µL of protein (2.5 mg/mL). The required amount of enzyme (trypsin) for subsequent digestion was calculated using this concentration. Two additional samples were prepared by solubilising CSM protein extract from batches 4 (salt-PMM) ("E4") and 5 (alkali-acid) ("E5") at 2.5 mg/mL in 50 mM ammonium bicarbonate.

400 µL of methanol was added to a 100 µL aliquot of each sample (A13, A15, E4, E5) and vortexed for 5 mins. 100 µL of chloroform was then added to each and the samples were vortexed for a further 5 mins. 300 µL water was then added to each, followed by a further 5 min vortex and then centrifugation for 1 min at 14,000 × g. The top aqueous layer is then removed by careful pipetting to leave the protein concentrated on top of the organic layer. A further 400 µL of methanol was added to each sample, followed by another 5 min vortex and 2 min centrifugation at 14,000 × g. Methanol was then removed by pipetting without disturbing the protein pellet and pellets were subsequently dried in a fume hood and then stored at -20º until next use.

The protein pellets were thawed and resuspended in 100 µL of 50 mM ammonium bicarbonate with vortexing for 1 h in preparation for enzymatic digestion with trypsin. 20 µL of 50 mM TCEP was added to each and samples were then vortexed for 30 seconds before being incubated for 45 mins at 56 ºC. Following incubation, the samples were removed and allowed to cool to room temperature. 20 µL of IAM solution (29 mg IAM in 1074 µL of 100 mM ammonium bicarbonate, kept in dark) was then added to each sample for alkylation. Samples were vortexed in the dark at room temperature for 30 mins. Following alkylation, 5 µL of trypsin stock solution (20 µg of trypsin enzyme in 20 µL of trypsin buffer) was added to each sample, followed by 14 µL (10 % of total volume) of ACN to each. Samples were incubated at 37 ºC for 19 h and 15 min and then concentrated by evaporation using a CentriVap vacuum centrifuge (Labconco, Kansas City, MI, USA) until dry. Dried samples were reconstituted with 100 µL of 0.1 % formic acid with vortexing and sonication (3 min) until dissolved. Samples were then centrifuged for 10 min at 10,000 x g after which the supernatant was transferred to a fresh Eppendorf® tube. Empore™ disks were then used for peptide purification [216] and the peptides analysed using LC-MS/MS.

Protocol – Preparation of non-digested (filtered) samples

10 mg of the same aerogel specimens used for the enzymatic digest (A13 & A15) were dissolved in 1000 µL of double distilled H_2O then filtered through a 3 kDa molecular weight cut off (MWCO) filter by

centrifugation at 8980 × g. 10 mg each of the same extract batches (E4 & E5) were also hydrated in 1000 µL of double distilled H_2O for 5 h with vortexing followed by filtration through a 3 kDa MWCO filter at 8980 × g. 100µl of filtrate from each sample was transferred to an Eppendorf® tube and then dried at 40 ºC using a CentriVap vacuum centrifuge (Labconco, Kansas City, MI, USA). Dried samples were stored overnight at - 20 ºC until reconstitution in 100 µL of 0.1 % formic acid for LC-MS/MS analysis.

Protocol – LC-MS/MS

All samples were analysed on an Ultimate 3000 UPLC system (Thermo Scientific) coupled to an Impact II UHR QTOF mass spectrometer *via* a CaptiveSpray source equipped with a nanoBooster device (Bruker Daltonik, Bremen, Germany). 1 µg of each sample was loaded on a C18 PepMap100 nano-Trap column (300 µm ID × 5 mm, 5 micron, 100 Å) (Thermo Scientific) at a flow rate of 3 µL/min. The trap column was then switched in line with the analytical ProntoSIL C18AQ column (100 µm ID × 150 mm, 3 micron, 200 Å). The reverse phase elution gradient was from 2% to 20% to 45% B over 30 minutes, totalling 49 minutes at a flow rate of 600 nL/min. Solvent A was LCMS-grade water with 0.1% formic acid; solvent B was LCMS-grade acetonitrile with 0.1% formic acid. Data were acquired *via* data-dependent acquisition with the following settings: a full scan MS spectrum, with a mass range of 150–2200 m/z, was followed by a maximum of 10 collision-induced dissociation tandem mass spectra (350–1,500 m/z) at a sampling rate of 2 Hz for MS scans and 1–20 Hz for MS/MS (depending on precursor intensity). Precursors with charges 1+ to 5+ were preferred for further fragmentation.

Data Analysis - Peptide sequence identification from MS/MS spectra

After the LC-MS/MS run, the Mascot script for Analyst QS 1.1 (Matrix Science, London, UK) was used to extract peak lists from the data. The peak lists were searched against the SwissProt database (20140227; 545,388 sequences) using an in-house Mascot server (Mascot v2.5.1, Matrix Science). Enzyme specificity was set to semi-trypsin for the enzyme digested samples and no enzymes were chosen for the non-digested samples. Taxonomy was restricted to *Viridiplantae*, in the search criteria.

Methionine oxidation and deamidation of asparagine and glutamine were set as variable modifications. Two missed cleavages were allowed, and the error tolerance was 0.15 Da for LC ESI-MS and 0.3 Da for LC ESI-MS/MS respectively. ProteinScape 4.0.3 315 (Bruker) was used to store peak list data and result analysis. Acceptance thresholds for peptide and protein scores were set at 25 and 80, respectively. Each protein identification was required to have at least one peptide with a Mascot score greater than the Mascot Identity Score at a Significance Threshold of $p < 0.05$. Peptides with scores ≤15 or lengths below five residues were all rejected. A peptide decoy database (reverse sequences) search was performed for each search. Protein lists were compiled using the Protein Extractor function and only those results assessed as true matches were used for further analysis.

Data Analysis – In-silico prediction of bioactivity

Bioactivity profiling using custom VBA macros in Microsoft Excel (Version 16.0.13801.20266) was conducted, seeking to match peptide sequences obtained from the CSM protein extract and aerogel samples with bioactive peptides from a database containing 69,326 peptide entries. The database was compiled from the AHTPDB, AMPer, APD2, BIOPEP, EROP, MBPDB, MilkAMP, NeuroPep, PeptideDB and SATPdb databases alongside additional entries from the scientific literature.

4.2.6. Circular dichroism (CD) spectroscopy

Background

UV-CD spectroscopy can be used to detect changes in protein secondary conformation that may be induced by changing aqueous conditions (pH, ionic strength *etc.*) like those used to gel canola proteins in this thesis. The technique of circular dichroism (CD) spectroscopy involves the transmission of circularly polarised light and the subsequent detection of changes in that polarisation caused by molecular chirality in samples. Left circularly polarised (LCP) and right circularly polarised (RCP) light are absorbed to different extents by chiral samples and provide a difference in circularly polarised light absorbance, or

circular dichroism (ΔA). ΔA can be converted to a value of molar ellipticity ([θ]) through the molar extinction coefficient (ε), molar concentration of the sample (c) and the optical path length of the CD spectrophotometer (l) according to Beer's law [217]. The greater the degree of circular dichroism (ΔA) the greater the ellipticity (θ). CD spectroscopy can be applied to proteins and peptides because they are optically chiral molecules, owing to the distinct conformational features of their secondary structures: α-helices and β-sheets. Chirality refers to the specific geometry of a molecule that means it is non-superimposable on its mirror image; it has no mirror plane, centre of inversion or rotational-reflection axis. Amino acids themselves are chiral molecules (except glycine) but it is the strong contribution of asymmetrical secondary structures that allow for the study of chiral optical activity in proteins.

In addition to chirality, proteins also possess optically active molecular electronic transitions in certain chemical moieties. These transitions allow for the detection of proteins using spectroscopy, which is used in many biochemical techniques (such as chromatography). The optically active transitions in proteins which occur in peptide bonds and amino acid side chains provide spectral features in the UV region between 140 and 225 nm. Molecular electronic transitions of amide groups ($n \rightarrow \pi^*$ and $\pi \rightarrow \pi^*$) dominate the far ultraviolet regions of protein spectra. These transitions are influenced by the polypeptide backbone geometries and are therefore used to measure differences in secondary structure [218]. The effect of secondary structure on chirality and on these transitions is used in the combined technique of UV - CD spectroscopy. Typical CD data reports ellipticity (θ) in millidegrees (m° or mdeg) which allows for the conversion to molar ellipticity ([θ]), typically measured in deg.cm^2/dmol, using the concentration of protein in g/L, the average molecular weight of the amino acids in g/mol, and the path length of the light (width of cuvette) in cm (Equation (11)).

$$[\theta] = {}^{\theta . M_r}/_{10. l. c} \tag{11}$$

Various methods exist for the deconvolution of UV-CD spectral data obtained from proteins. Results describing the helical secondary features are most reliable. Thus, the deconvolution of CD data generally describes the proportions of α-helix and β-sheet structures represented in the spectra. Typical spectral features identified from UV-CD spectral data feature negative and positive intensities at the wavelengths shown in **Table 4.4**.

Table 4.4: *Typical features of UV-CD spectral data obtained from protein secondary structures*

Secondary structure	**Negative bands**	**Positive bands**
α-helix	222 nm, 208 nm, (strong)	190 nm
β-sheet	210 - 220 nm (1/3 the strength of α-helix)	195 - 200 nm
Random coil	195 – 200 nm (strong)	

Additional differences in the peaks caused by secondary protein features include greater variance and lower intensity of β-sheet negative peaks found at higher wavelengths (approximately one third the intensity of an α-helix negative peak) [218]. Proteins also contain residual secondary structures which are not classified as any of helices, sheets or turns, and these are often called ‘random coil’ or ‘other’. These structures have a wide range of angles and are simply categorised together as non-helix/sheet structures. The proportion of α-helix, β-sheet, β-turns and random coil secondary structures in the protein sample can be obtained from deconvolution of CD data. Reference databases containing existing protein CD spectra and associated secondary structure information (from X-ray crystallography) are required for the deconvolution of new protein CD spectra. These databases are used by downloadable software and online deconvolution services to produce reports on protein secondary structure. Deconvoluted CD spectral data (along with the root-mean-square deviation (RMSD) and normalised root-mean-square deviation (NRMSD)) from various algorithms are obtained from the DICHROWEB server, an online service used in this thesis.

Protein CD data is dependent on extrinsic factors such as the temperature, concentration, and chemical environment of the samples, since molecular conformation (and therefore chirality) also depends on these same factors. Consequently, CD data can be used to determine the degree of denaturation in a protein. UV-CD analysis of CSM protein extracts aims to investigate the structural effects of gelation parameters on the protein which may be implicated in the gelation mechanism. Varying aqueous treatments were applied to CSM protein extract solutions to mimic gelation conditions as closely as possible while retaining the lower protein concentrations required for UV-CD analysis.

Materials

Sodium hydroxide (NaOH) pellets (98.5 – 100 %), calcium chloride ($CaCl_2$) (anhydrous, ≥ 93.0 %), and hydrochloric acid (36.5 – 38.0 %) were obtained from Sigma Aldrich (now Merck) New Zealand. All solutions were prepared using reverse osmosis (RO) water (resistivity 18 MΩ) from a Milli-Q water purification system.

Protocol

CSM extract samples were solubilised in Milli-Q water at concentrations of 0.1 mg/mL, 0.05 mg/mL, or 0.01 mg/mL. Solutions were then pH adjusted to a prescribed pH (see **Table 5.10**) using sodium hydroxide (1 M) and hydrochloric acid (1 M). $CaCl_2$ was added to selected protein solutions to final concentrations of 0.2 mM or 20 mM. The UV-CD spectra of the protein solutions were measured using a Jasco 815 CD spectropolarimeter under constant flow of nitrogen gas in 1 mm path length quartz cuvettes. The spectra recorded were from 190 nm to 380 nm. Each protein solution was measured in the CD spectropolarimeter in triplicate measurements (three cuvette preparations (n = 3)). The recorded spectrum of each cuvette preparation was produced from an average of 3 scans. Final data was produced by subsequently subtracting the corresponding blank (water with appropriate pH adjustment and $CaCl_2$ preparation) from the averaged spectrum of each sample.

Data Analysis

Resulting molar ellipticity ([θ]) was then plotted against wavelength (λ) for each sample. Calculation of secondary structure fractions from the molar ellipticity data was achieved by deconvolution of the spectra using the DICHROWEB online deconvolution service [218-220] with the CDSSTR secondary structure determination algorithm [221-223] and the reference database set '7' [223, 224]. Results were reported as calculated fractions of α-helix, β-sheet, β-turn, and unordered secondary structures present in the proteins under each set of aqueous conditions.

4.3. Experimental procedures for developing and characterising gels and aerogels (Chapter 6)

Chapter 6 of this thesis focusses on the first development and characterisation of aerogels from CSM protein. The aerogels produced and characterised in Chapter 6 are all cryogels; they are produced by freeze drying. The specific methodology for preparation of freeze dried aerogels is described in **Section 4.1** since it has been also used in **Chapter 7**. However, methods unique to Chapter 6 include the development of pH-controlled canola gels, and the characterisation of canola cryogels by X-ray microtomography (μ-CT), Differential scanning calorimetry (DSC), and thermogravimetric analysis (TGA). Other methods pertaining to Chapter 6 are described in the Chapter itself (the solubility of CSM protein cryogels in aqueous solutions in **Section 6.5.3**) or in **Section 4.1** since the following methods are also used in Chapter 7: scanning electron microscopy, viscometry, rheometry, density measurements, and static compressive testing.

4.3.1. Preparation of canola protein gels using pH control

Owing to its importance in addressing the central aim of this thesis, the methodology for developing the first canola seed meal (CSM) protein gels through pH manipulation is described in full in **Section 6.2.1**. Upon completion of gel formulation, samples were then subject to freeze drying according to protocols described in **Section 4.1.4**.

4.3.2. X-ray microtomography (μ-CT)

Protocol

The structure of the canola aerogel was imaged using a SkyScan 1172 micro-computed tomography scanner (Bruker-microCT, Kontich, Belgium) at 34 kV and 210 μA producing 2400 images at 15.18 μm resolution.

Data Analysis

Reconstruction procedures (NRecon version 1.6.10.2 software, Bruker-microCT) produced axial cross-sections and a 3-dimensional (3D) reconstruction of the specimen. Pore volume measurements were computed using the 3D analysis function in the CT Analyser software (V. 1.8.1.4, Bruker-microCT, Kontich, Belgium).

4.3.3. Differential scanning calorimetry (DSC)

Protocol

Approximately 3 - 6 mg of selected aerogel and CSM extract samples were accurately weighed and then loaded into TZero™ standard aluminium pans. Samples were then analysed on a Discovery DSC (TA Instruments) where thermograms were recorded while heating from – 60 °C to 225 °C (most samples) or from room temperature (≈ 25 °C) to 200 °C (earlier samples) at 10 °C/min. Modulated DSC (MDSC) experiments were conducted with a heating rate of 3 °C/min from – 50 °C to 225 °C, a modulation amplitude of 1 °C, and period of 60 s. Heat-cool-heat cycles were recorded for selected samples with all heating rates and cooling rate also at 10 °C/min, cycling between - 60 °C and 225 °C. All thermograms were recorded under a nitrogen flow of 10 mL/min and samples were measured in triplicate.

Data analysis was performed using TRIOS (v5.0.0.44616) software (TA Instruments).

4.3.4. Thermogravimetric analysis (TGA)

Protocol

Thermogravimetric analysis (TGA) was performed using a Discovery TGA (TA Instruments) and loading approximately 8 mg of selected aerogel and CSM extract samples (accurately weighed) on high temperature platinum pans. Samples were then heated from room temperature (≈ 25 °C) to 600 °C at a rate of 10 °C/min and under a nitrogen flow of 10 mL/min.

Data Analysis

Data analysis was performed using TRIOS (v5.0.0.44616) software (TA Instruments). The largest weight loss step was identified in a temperature range of 150 °C < T < 250 °C and used as a measure of thermal stability by calculating the temperature at the highest degradation rate (peak in the derivative curve *d(% weight)/d(T)*).

4.4. Experimental procedures for improved aerogels and their characterisation (Chapter 7)

Chapter 7 of the thesis is focussed on increasing the mesoporosity and the mechanical strength of canola aerogels. Consequently, the techniques specific to Chapter 7 are the preparation of reinforced gels, dynamic mechanical analysis (DMA) of cryogels, the preparation of supercritically dried aerogels, and gas porosimetry of aerogels. Additional characterisation techniques that are also used in earlier Chapters include: Sodium dodecyl sulphate polyacrylamide gel electrophoresis (SDS-PAGE), Scanning electron microscopy (SEM), viscometry, rheometry, density measurements, and static compressive testing, and these are all described in **Section 4.1**.

4.4.1. Preparation of canola protein hybrid gels

Materials

Canola seed meal (CSM) was sourced from the *Brassica napus* plant from Pure Oil NZ Limited (Rolleston, New Zealand) and protein was extracted according to protocols outline in **Section 4.2.1**. Sodium hydroxide pellets (98.5-100 %), and hydrochloric acid (36.5-38 %) were obtained from Thermo Fisher Scientific (New Zealand). Chitin (extracted from the gladii of *Nototodarus sloanii*) was sourced from Plant and Food Research Limited (New Zealand). Collagen (Type I, bovine Achilles tendon) and gelatine (Type B, from bovine skin) were purchased from Sigma Aldrich (now Merck) New Zealand. Liquid nitrogen was sourced from BOC (New Zealand). All solutions were prepared using reverse osmosis (RO) water (resistivity 18 MΩ) from a Milli-Q water purification system.

Protocol

Chitin fibre and collagen fibre were each subject to cryomilling at - 196 °C (using liquid nitrogen) in a SPEX Certiprep 6750 Freezer/Mill, where fine powders were produced following 3x 60-second rounds of milling with 3-minute cooling periods between rounds. The dried canola extract powder and the powdered biopolymer (cryoground chitin, cryoground collagen, or gelatine) were then dispersed in Milli-Q water to a final concentration of 10 wt% total solids (unless otherwise stipulated). The pH of these dispersions was adjusted to within the range of 8.4 – 8.7 (unless otherwise stipulated) using 2 M NaOH and 2 M HCl solutions. Following adjustment of the pH, the dispersions were mixed until homogenous with CSM protein-gelatine suspensions also gently heated (to approximately 60 °C) during mixing to facilitate dissolution of gelatine. pH measurements were checked and readjusted as necessary. Selected CSM protein-gelatine gels were then transferred to quartz vials for UVB treatment using a Luzchem UV chamber (LZC4-14, Luzchem, Ontario, Canada) equipped with UVB narrow bandwidth lamps (spectral distribution 281 – 315 nm, dose 35.337 W/m^2 (Luzchem LZC-UVB)). UVB irradiation was performed for 30 minutes. All hybrid gels (irradiated and non-irradiated) were then frozen at – 80 °C and freeze dried according to protocols outlined in **Section 4.1.4**.

4.4.2. Dynamic mechanical analysis (DMA)

Protocol – Sample Preparation

Aerogels were prepared for static and dynamic compression testing by cutting each aerogel into replicate specimens (4-5 as permitted by size) cross-sectionally, using microscopy blades (Swann-Morton No.10). Specimens were cut to approximately 6 mm in height (determined by original sample length to permit repeats) while retaining a diameter of approximately 12 mm. Cut specimens were subject to density measurements according to the protocol described in **Section 4.1.5**.

Protocol – Static testing

The CSM aerogels were tested in static mode using a DMA Q800 V21.3 (TA Instruments) fitted with compression platens. Specimens were preloaded with a force of 10 mN (1 g) and then subject to a set compression rate of 0.4 N/min, 1.0 N/min, or 4.0 N/min to a maximum force of 18.0 N (load cell limit), or until failure. All tests were conducted at 25 °C. Automated data collection (2 s / point) included automatic calculation and recording of stress and strain values, allowing for the subsequent generation of stress-strain plots.

Data Analysis – Static Testing

Stress-strain plots were generated from each sample data set and analysed for yield stress (where samples reach yield prior to load cell limit) and compressive elastic modulus (slope of the linear region). Some curves possessed a 'toe region' like earlier compressive testing conducted on the Instron universal electro-mechanical testing system. Moduli were calculated using only the linear region of curves, excluding the "toe regions" where present.

Protocol – Dynamic Testing

The CSM aerogels were also analysed in dynamic compressive mode, firstly using a strain amplitude sweep to establish the linear viscoelastic (LVE) region for subsequent dynamic testing. Specimens were preloaded with a force of 10 mN (1 g) and then subject to strain sweeps up to 0.8 % ε at 1 Hz. Storage modulus was plotted as a function of strain amplitude (**Figure 4.7**) establishing a strain of 0.2 % as within the LVR and thus appropriate for further dynamic testing at 1 Hz.

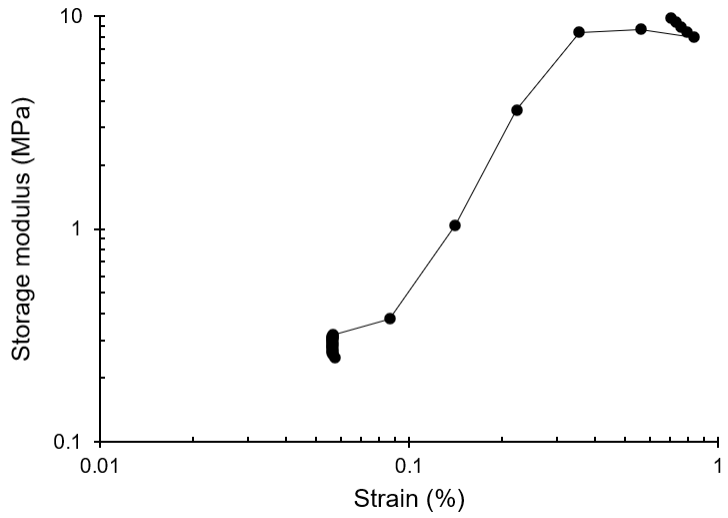

Figure 4.7: *Example plot of storage modulus as a function of strain amplitude from a strain amplitude sweep experiment on a CSM protein aerogel*

Fresh specimens of each aerogel sample were then subject to a temperature sweep with dynamic compressive testing at a strain amplitude of 0.2 % and a frequency of 1 Hz. Temperature sweeps were from 25 °C to 80 °C at a prescribed heating rate (3 - 6 °C/min, specified for each sample result) and each sample was tested in duplicate or triplicate (fresh specimens per each run). Automated data collection (2 s / point) included automatic calculation and recording of the storage moduli (E'), loss moduli (E''), and loss factors (tan δ) for each temperature sweep.

4.4.3. Preparation of canola protein gels using $CaCl_2$

Methodology for developing CSM protein gels using $CaCl_2$ as a gelation agent is described in **Section 7.4.1** due to the importance of this protocol in developing supercritically dried aerogels. Experimental materials and further method details are also outlined below. Upon completion of gel formulation, samples were subject to either freeze drying (according to protocols described in **Section 4.1.4**) or solvent exchange processing followed by supercritical drying (see **Section 7.4.2**).

Materials

Canola seed meal (CSM) was sourced from the *Brassica napus* plant from Pure Oil NZ Limited (Rolleston, New Zealand) and protein was extracted according to protocols outline in **Section 4.2.1**. Sodium hydroxide pellets (98.5-100 %), and hydrochloric acid (36.5-38 %) were obtained from Thermo Fisher Scientific (New Zealand). Calcium chloride ($CaCl_2$) (anhydrous, ≥ 93.0 %), was sourced from Sigma Aldrich (now Merck) New Zealand. All solutions were prepared using reverse osmosis (RO) water (resistivity 18 MΩ) from a Milli-Q water purification system.

Protocol

The dried extract powder was dispersed in Milli-Q water to a final concentration of 10 wt% and adjusted to a pH of either 8.0 ± 0.2 or 10.0 ± 0.2 using 2 M NaOH and 2 M HCl solutions. Control samples were set aside following pH adjustment while the remaining gel formulations were separated into thirds for subsequent heat- and Ca^{2+}-treatments. Two equivalents of gel at each pH value were transferred to sealed Schott Duran® bottles and heat treated in a water bath at 95 °C for 30 minutes. Aliquots of 1 M $CaCl_2$ were added to the non-heated samples such that the final concentration of $CaCl_2$ was 20 mmol/L. $CaCl_2$ was also added to a final concentration of 20 mmol/L to one of the heated samples for both pH values. Gels were well mixed and pH measurements were regularly checked and readjusted as necessary throughout formulation.

4.4.4. Preparation of aerogels using supercritical carbon dioxide (SC-CO_2) drying

The development of supercritically dried CSM protein aerogels was enabled by the prior production of CSM protein-Ca^{2+} gels (described in **Section 7.4.1**). A selection of these CSM protein-Ca^{2+} wet-gels were used in a solvent exchange process and subsequent SC-CO_2 drying process to develop supercritically dried CSM protein aerogels. The methodologies used for solvent exchange and SC-CO_2 drying are both described in **Section 7.4.2** owing to their importance in addressing the aims of this thesis. Experimental materials and some additional method details are presented below.

Materials

Absolute ethanol (analytical grade, stored under N_2 atmosphere) was sourced from Fisher Scientific (New Zealand) and 96 % ethanol (food grade) was purchased from Southern Grain Spirits NZ Ltd. Liquid carbon dioxide (high-grade dry) was sourced from BOC (New Zealand).

Protocol

Following production of CSM protein-Ca^{2+} gels, the samples were poured into 5 mm diameter syringes with the needle end cut open to a flat surface. The cut ends of the syringes were sealed with Parafilm™ and refrigerated for 12 hours, standing in an upright position, to facilitate further hardening of the gels. Gels were then plunged as a single cylindrical monolith into a bath of ethanol (96 % EtOH) and left for at least 24 hours. Gels which retained monolithic form (see **Section 7.4.2**) were subsequently transferred to a vial of absolute ethanol (stored under N_2 atmosphere) for further solvent exchange processing according to the process described in **Section 7.4.2**.

4.4.5. Nitrogen gas porosimetry

Background

N_2 gas porosimetry (or physisorption analysis) is typically used to measure the porosity of nano-scale porous systems. An adsorption-desorption isotherm is generated when nitrogen (or other non-reactive) gas is progressively introduced to a completely degassed sample in an evacuated chamber near the condensation temperature of the gas. This measures the molar quantity (n) of gas (or the volume V_a) adsorbed and then desorbed by a clean, solid surface as a function of the gas pressure (P). Porosity facilitates the adsorption of gases and makes corresponding desorption processes more difficult, thus altering the isotherm shape in comparison to a non-porous surface. The adsorption data is collected over a series of relative pressures (actual pressure divided by saturation pressure), beginning at very low

pressures (< 0.01 P/P_0) up to $P/P_0 = 1$. Adsorbed quantities are then measured again over a series of descending partial pressures (a desorption process) as the sample is evacuated, once more, to low pressure. The adsorption-desorption data often shows a hysteresis loop due to the difference in mechanism between gas evaporation, and condensation in pores (Type IV curve, **Figure 4.8**).

Various models can be applied to the isotherm data to calculate values of interest such as the specific surface area of the material (*e.g.* BET model). These models are usually designed to analyse isotherms optimised for mesoporous materials. At lower pressures, large pores (macropores) behave like flat surfaces and different models (*e.g.* Langmuir monolayer adsorption model) are used for the analysis [3]. A difficulty is in measuring the pore volume of an aerogel containing a large range of pore sizes since there is no 'one-size-fits-all' model for analysing gas adsorption-desorption isotherms. The models used to analyse N_2 adsorption-desorption are designed to ignore the volumes of gas adsorbed in pore sizes beyond a chosen limit (*e.g.* 30 nm for the Barrett, Joyner, Halenda (BJH) model [4]) as they are optimised for specific types of porosity (*e.g.* 2 – 50 nm sized pores).

There are six characteristic shapes of adsorption-desorption isotherms (**Figure 4.8**). Type I is indicative of micro-porosity (pores < 2 nm) and is of interest in aerogel research. Type II is indicative of a non-porous material or one with very large pores (micrometre scale). Type III and Type V are produced in conditions where the adsorptive molecules have greater affinity for one another than for the solid, and therefore not suited to surface area or pore analysis. Type IV is the most observed curve in aerogel analyses, representing materials with a mostly mesoporous (2 – 50 nm sized pores) structure or a combination of meso- and micro-porosity. Type VI is a rare curve generated from a non-porous solid with an almost completely uniform surface.

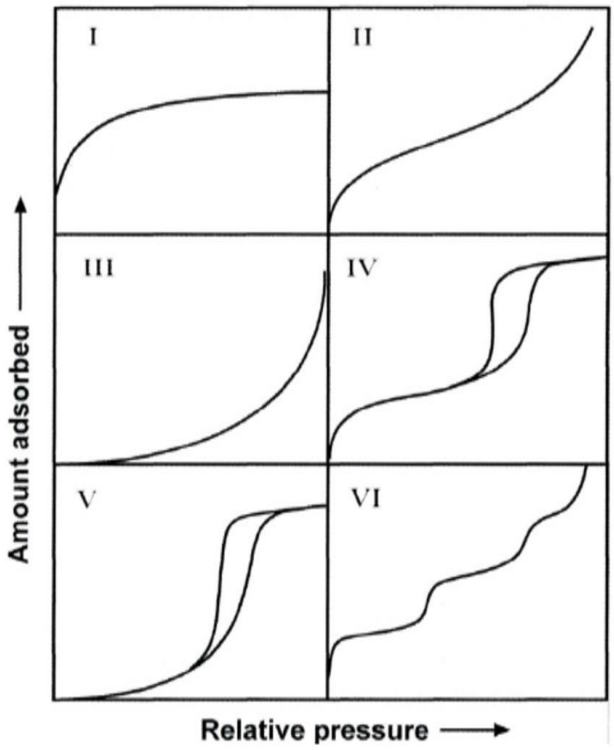

Figure 4.8: *Example gas adsorption-desorption curves generated from gas sorption porosimetry measurements. Image adapted from Alothman, Z.A., Materials, 2012.* ***5****(12): p. 2874-2902 ([225])*

The appropriacy of a curve to a model can be tested by accessing the correlation coefficient of the applied models. For example, a plot of P/V_a versus P is linear if the Langmuir model applies, where P is the pressure and V_a is the volume of gas adsorbed. BET theory states that:

12

$$\frac{P}{V_a(P_0 - P)} = \left(\frac{1}{V_m}\right)\left(\frac{P}{P_0}\right)$$

where P is pressure, V_a is the volume of gas adsorbed, P_0 is the saturation pressure, and V_m is the adsorbed gas volume for a monolayer. Therefore, a plot of $P/[V_a (P_0 - P)]$ vs. P/P_0 is linear if the BET theory applies. Pore volumes are calculated by first creating normalisations for the monolayer capacity, allowing only the V_a due to porosity to be calculated. Additionally, other equations have been developed and

adapted to provide relationships between pore size and P/P_0, allowing isotherm data to be related to further porosity information such as pore size distribution [226].

Protein cryogels generally comprise of macropores, and for the most part, they score low on pore volume analysis (*e.g.* 0.009 cm^3/g [5] in protein aerogel literature and 0.0014 cm^3/g (CSM aerogels from this project)) in gas physisorption experiments. Comparatively, other aerogels can achieve significantly higher specific pore volumes (> 3 cm^3/g) [6]. Protein aerogels with more mesoporous structures (pore sizes < 50 nm) can achieve a higher specific pore volume since the gas physisorption is most effective in assessing this type of porosity. N_2 physisorption experiments are therefore used to analyse CSM protein cryogels and aerogels with subsequent data analysis using both the Langmuir and BET models for specific surface area calculations, and a BJH analysis of pore volumes.

Protocol

Nitrogen gas (N_2) adsorption-desorption experiments were carried out using a Gemini VI 2385C automated N_2 physisorption analyser (Micromeritics, Norcross, GA, USA) equipped with a VacPrep™ 061 degassing unit (Micromeritics, Norcross, GA, USA). Accurately weighed CSM protein aerogel samples were prepared for degassing in Gemini sample tubes (Micromeritics, Norcross, GA, USA). The supercritically dried canola aerogel was successfully degassed for 6 days at 25 °C and < 5 mT, while the freeze dried CSM protein cryogel was initially degassed for 6 days at 25°C, measured, and then returned to the degassing unit for a further 24 hours at 50 °C (< 5 mT). Degassed samples were accurately weighed then measured on the N_2 physisorption analyser with an initial evacuation rate of 10 mmHg for 50 minutes. Data was collected over a series of partial pressures (P/P_0) from 0.050022730 to 0.986165874 with 19 measurements for the adsorption curve and 12 measurements for the desorption curve.

Data analysis

Resulting pressure measurements were used to calculate total surface area, based on the Langmuir model, using Gemini v.2.01 software. The mesopore surface area was calculated using the Brunauer-Emmett-

Teller (BET) model while mesopore volume was calculated using the Barrett, Joyner, Halenda (BJH) model.

Chapter 5

5. Canola seed meal protein and its potential use in novel materials

5.1. Introduction

Canola protein extract obtained from canola meal (itself a co-product of the canola oil industry) is a promising precursor for aerogels and related materials due to its availability [227] and predisposition to gelation [191] (refer **Section 2.3**). Popular bio-derived polymers such as cellulose, chitin and collagen are commercially available from a variety of chemical suppliers. However, canola protein isolates are not widely available for commercial purchase (refer **Section 2.3**). The recovery of canola seed meal (CSM) protein from raw canola seed meal is described in the current Chapter. The canola meal is sourced from a local canola oil producer (see **Section 4.2.1**), taken from the processing line after the seed had been cold pressed for oil extraction. The canola seeds processed were from the *Brassica napus* species and grown on Australian and New Zealand arable farms. Following extraction, the canola seed meal (CSM) protein, more accurately described as CSM extract, is studied for its protein content, biochemical features, and gelation propensity. These studies provide information about extract quality, content, and amenability to aerogel processing.

5.2. Experimental methods

The experimental materials and procedures for the techniques in Chapter 5 can be found in Sections 4.1 & 4.2 and are summarised in **Table 5.1**.

Table 5.1: *Summary of experimental techniques from Chapter 5 and the corresponding sections of Chapter 4 describing the experimental procedures*

Section (Chapter 5)	Technique	Section of Chapter 4 pertaining to this technique
5.3.1.	Canola protein extraction	4.2.1.
5.3.2.	Amino acid analysis	4.2.2.
5.3.3.	SDS-Polyacrylamide Gel Electrophoresis	4.1.1.
5.3.3.	Gel Filtration Chromatography	4.2.3.
5.3.4.	Tandem Mass Spectrometry (LC-MS/MS)	4.2.4.
5.4.	Bioactive peptide profiling	4.2.5.
5.5.1.	Circular dichroism spectroscopy	4.2.6.
5.5.2.	Native-Polyacrylamide Gel Electrophoresis	4.1.1.

5.3. Canola protein extraction and constituents of resulting extract

Production of CSM protein aerogels necessarily begins with extraction of the precursor protein from the raw canola seed meal. Extraction of the proteinaceous component of canola seed meal generally results in a mix of protein types, where the predominant proteins are two seed storage proteins known as napin and cruciferin (refer **Section 2.3.2**). Extraction of protein from the canola seed meal is a semi-selective method that relies on the solubility of certain proteins under specific aqueous conditions such as high pH. Documented in this Section are the resulting yields of various batches (varying extraction methodology and various repeat extractions) of CSM protein extract followed by the identification of specific protein molecules within these extracts. Characterisation of the proteinaceous components in the extract provides key information about extraction reproducibility and aids in understanding of gelation chemistry and application potential (*e.g.* the assessment of nutritive value).

5.3.1. Extraction

The extraction processes used to isolate canola protein from pressed seed meal have been adapted from Klockeman *et al.* [185] and Kim *et al.* [200] (see **Section 4.2.1**). The purpose of the extraction was to obtain sufficient quantities and purities of canola protein for subsequent development of CSM protein gels and aerogels. While some attention is given to extraction variability and efficiency, the optimisation of the extraction process remained largely out of scope for the current work. The potential for improvement of the extraction process is later discussed in Section 8.2.

CSM protein extraction was performed on CSM a total of thirteen times, where both the ‘alkali-acid’ and ‘salt-PMM’ extraction methods where initially investigated and then after the fourth batch, a single method (‘alkali-acid’ method adapted from Klockeman *et al.*) was chosen for the latter nine batches. The protein micellar method (‘Salt-PMM’, adapted from Kim *et al.*) was trialled twice and allowed for investigations into possible biochemical differences between the two extract types. In practise the extraction of protein from CSM has varying degrees of success in terms of yield (% of

total CSM protein obtained by mass with respect to the meal). The average yield (per measure of dry meal) of the protein extraction using the alkali-acid and salt-PMM processes were 15.0 % and 1.6 %, respectively (**Figure 5.1**). These averages were generated from a total of eleven extractions using the alkali-acid method and two extractions using the salt-PMM method (see **Table 4.1** for summary of extraction conditions). Assuming the dry meal has a protein content of 40 % [178], these yields equate to 37.4 % and 4.0 % of the total available protein. Recovering 37.4 % of the total protein is consistent with use of the alkali-acid extraction technique in other studies, where 30 % of total protein is typically extracted [191]. The salt-PMM extraction process typically recovers 10 % of the total protein in the dry meal [200], indicating that the technique was not as effective as expected, in this study (at only 4.0 % protein recovery).

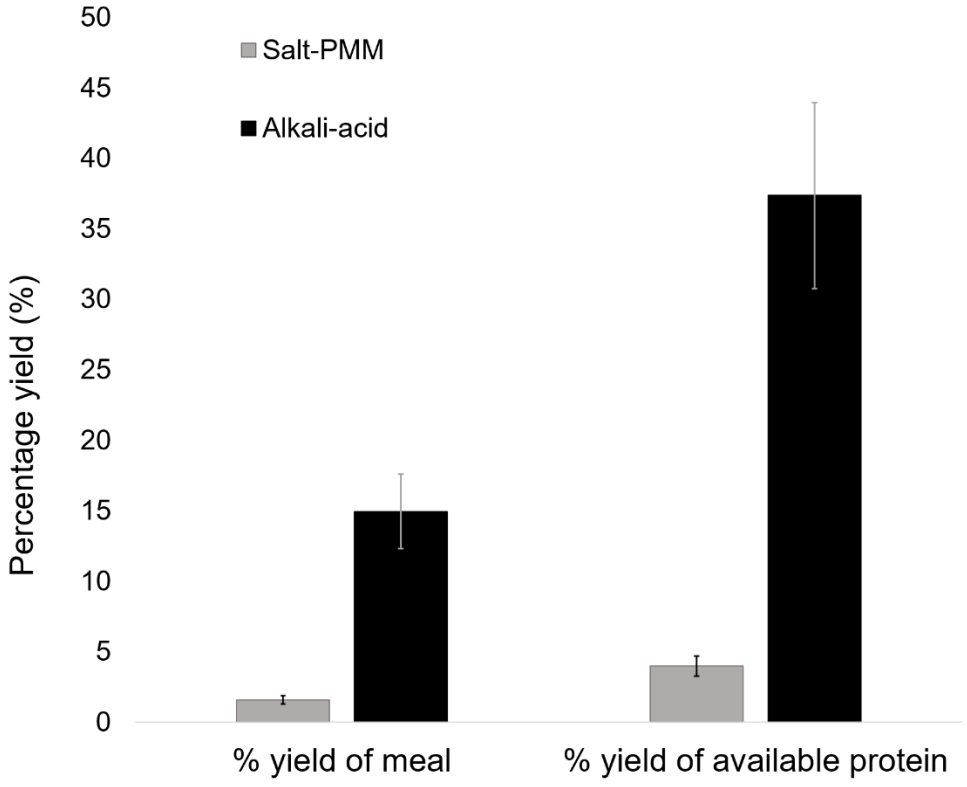

Figure 5.1: *Average protein extraction yields from the two extraction methods used in this thesis. Error bars represent standard deviation of the batches*

The salt-PMM method gave much lower yields than the alkali-acid technique but also lower yields than expected, based on other studies (*e.g.* 9.8 % per measure of dry meal [200]). It is likely that the salt-PMM method requires further optimisation. For example, the solubilisation time of the meal in the Tris / NaCl buffer was limited to less than 2 hours based on similar extraction protocols in the literature; extending the solubilisation time could be investigated for effects on the percentage of protein recovered. Other parameters that could be optimised include the dilution factor used during ultrafiltration, and the precipitation time and temperature. Due to a minimum of 3 days being required for the salt-PMM extraction, such optimisations were not investigated. The alkali-acid technique offers a shorter preparation time (1 day) and simpler resourcing (no need for expensive membrane or pump system) with much improved yields.

Variance in extract yield between extract batches that used the same extraction methodology demonstrates that optimisation is possible through varying certain extraction parameters. Certain batches produced with the alkali-acid method were prepared with slight modifications to the general protocol, such as the inclusion of extra filtration step and the varying of the meal to buffer ratio, stirring time, and precipitation time (see **Table 4.1** in **Section 4.2.1**). Some of these factors may be responsible for the variations in yields seen across batches produced using this method. For example, batches 9, 12 and 13 produced three of the highest yields among the alkali-acid extracts (**Table 5.2**) and were also the batches with the lowest w/v ratio of meal to solubilisation buffer during the alkali solubilisation step (4.9, 8.0 and 8.1 % w/v, respectively, while all other batches were 9.1 – 9.9 % w/v). This indicates that saturation of the protein in the solubilisation buffer may affect the efficiency of extractions where the meal to buffer ratios exceed 1:10 (9.1 wt%.). These same batches were also subject to longer precipitation times at 4 °C (see **Table 4.1** in **Section 4.2.1**). Therefore, extraction conditions (*e.g.* precipitation times and temperatures) may also be implicated in yield variances and provide another avenue for future optimisation of the extraction method.

Table 5.2: *Protein extraction yields from batches of CSM protein produced in this thesis*

Batch number	Extraction method	Meal used (grams)	Yield of extract (grams)	% yield of meal[1]	% yield of available protein[2]
1	Alkali-acid	219	25.7	11.7	29.3
2	Alkali-acid	220	32.4	14.7	36.9
3	Salt-PMM	228	4.1	1.8	4.5
4	Salt-PMM	200	2.8	1.4	3.5
5	Alkali-acid	200	29.2	14.6	36.5
6	Alkali-acid	140	23.6	16.9	42.2
7	Alkali-acid	200	22.1	11.1	27.6
8	Alkali-acid	187	28.0	15.0	37.4
9	Alkali-acid	97	15.9	16.4	41.0
11	Alkali-acid	201	25.6	12.8	31.9
12	Alkali-acid	140	23.4	16.7	41.8
13	Alkali-acid	176	34.7	19.8	49.4

[1] % yield of meal = (dry mass of extract / dry mass of defatted meal) x 100

[2] % yield of protein = ((dry mass extract / (0.4 x dry mass defatted meal) x 100) since typical percentage of protein in seed meal is 40 % [178]

5.3.2. Amino acid analysis

Analysis of amino acids present in the protein extract can provide information about the total protein content of the extract as well as useful information about the nutritional value of the CSM proteins. Three aliquots of CSM extract from batch 13 ('alkali-acid' extract) were subject to amino acid analysis. The samples were hydrolysed with 6 N HCl, derivatised with an AccQ-Flour™ reagent kit (to allow for detection by fluorescence) and constituent amino acids then separated, identified, and quantified using reverse phase – high performance liquid chromatography (RP-HPLC). An additional three aliquots of the same extract were also analysed but were first subject to an oxidising treatment for total cysteine analysis. These oxidised samples provided the quantitative measure of cysteine residues in the extract by detection as cystic acid. The resulting amino acid quantities are reported in **Table 5.3** in mg per 100 mg of dry meal and also as mole and mass percentages of the total amino acid (protein) content detected. The extract is also compared to the amino acid profile of other protein sources including other CSM protein alkali extracts from Tzeng *et al.* [228] and Alashi *et al.* [229].

Table 5.3: *Amino acid composition of CSM protein extract (from this study and others), soy protein isolate (SPI) (from other study), and casein (from other study), detected in mg of each amino acid per 100 mg of dry extract. Mass of each amino acid is also presented as a percentage of the total mass of amino acids detected. The amino acid composition of the CSM protein extract in this work is also presented as mole percentages of the total detectable amino acids (tryptophan content was not determined).*

		% by moles	**mg / 100 mg dry extract**					**% by mass**				
			CSM alkali extract			SPI	casein	CSM alkali extract			SPI	casein
		This work		Tzeng *et al.* [228]	Alashi *et al.* [229]	Tan *et al.* [177]	Tan *et al.* [177]	This work	Tzeng *et al.*	Alashi *et al.*	Tan *et al.*	Tan *et al.*
Essential	Histidine	2.49%	1.7	3.17	3.6	2.81	2.7	3.01%	3.17%	3.62%	2.97%	3.26%
	Isoleucine	4.03%	2.34	5.18	4.3	4.35	4.9	4.14%	5.18%	4.33%	4.60%	5.91%
	Leucine	8.17%	4.73	9.26	7.9	6.79	8.4	8.37%	9.26%	7.95%	7.18%	10.13%
	Lysine	4.71%	3.03	5.62	5.4	5.23	7.1	5.36%	5.62%	5.43%	5.53%	8.56%
	Methionine	2.13%	1.4	2.6	1.9	0.92	2.6	2.48%	2.60%	1.91%	0.97%	3.13%
	Phenylalanine	3.72%	2.71	5.13	5	5.14	4.5	4.80%	5.13%	5.03%	5.44%	5.43%
	Threonine	6.00%	3.15	5.3	5.2	3.98	3.7	5.58%	5.30%	5.23%	4.21%	4.46%
	Tryptophan	nd	nd	nd	0.9	nd	nd	nd	nd	0.91%	nd	nd
	Valine	5.70%	2.94	5.85	5.8	4.28	6	5.21%	5.85%	5.84%	4.53%	7.23%
Conditionally essential	Tyrosine	2.95%	2.36	3.93	3.9	3.61	5.5	4.18%	3.93%	3.92%	3.82%	6.63%
	Cysteine	2.33%	1.74	0.39	0.7	0.05	0.04	3.08%	0.39%	0.70%	0.05%	0.05%
	Arginine	5.58%	4.28	7.66	7.9	7.35	3.3	7.58%	7.66%	7.95%	7.77%	3.98%
	Glycine	10.10%	3.34	5.05	5.7	3.74	1.6	5.91%	5.05%	5.73%	3.96%	1.93%
	Proline	5.89%	2.99	4.32	5.7	5.13	nd	5.29%	4.32%	5.73%	5.43%	nd
	Glutamic acid & Glutamine	13.02%	8.44	17.27	15.7	20.67	19	14.94%	17.27%	15.79%	21.86%	22.91%
Non-essential	Alanine	7.52%	2.95	5.14	4.8	3.72	2.7	5.22%	5.14%	4.83%	3.93%	3.26%
	Aspartic acid & Asparagine	9.20%	5.39	9.41	9.7	11.47	6.3	9.54%	9.41%	9.76%	12.13%	7.60%
	Serine	6.47%	2.99	4.74	5.3	5.32	4.6	5.29%	4.74%	5.33%	5.63%	5.55%
Total			**56.48**	**100.02**	**99.4**	**94.56**	**82.94**					

.

The amino acid analysis revealed that extract 13 contained between 54 and 60 mg of (detectable) amino acids per 100 mg of extract. This suggests an average protein content of 56.48 % in the extract, a lower purity than expected for the precipitated protein. A broad range of purities is reported for the alkali extract (70 – 90 % [177]) though nothing lower than 60 %. The low purity of this extract suggests there may be a significant ash, and/or salt content from the seed meal present. The quantities of residual carbohydrates and oil are also unknown (not tested in this study) and may have contributed toward low purity of the extract. CSM also contains small molecules such as phenols and phytates that may have persisted in the extract.

The effect of the lower overall quantity of amino acids per 100 mg of extract can be seen when the results are compared to other studies (**Table 5.3**). Extract 13 reveals lower levels of all amino acids when compared to the studies from Tzeng *et al.* [228] and Alashi *et al.* [229], except for cysteine (1.7 mg per 100 mg of extract compared to 0.4 and 0.7 for the Tzeng *et al.* and Alashi *et al.* studies, respectively). A comparison where the non-proteinaceous mass is ignored and amino acids are reported as mass percentages of the total amino acid content (**Table 5.3**, last five columns) shows comparable amino acid composition between the CSM extract of this study and those from others. However, the cysteine level is still higher (3 % of amino acids by mass while in other studies it remains at 0.4 % and 0.7 %). One explanation for this difference could be the use of the oxidisation treatment used for total cysteine estimation, which was not used in the Tzeng *et al.* study. However, the Alashi *et al.* study also used performic acid oxidation treatment to determine cysteine and methionine content and reported only 0.7 % cysteine. A report of rapeseed protein cysteine content from Ohlson and Anjou, *1979* [230] is considered to have found high sulphur-containing amino acids [177] where cysteine and methionine contents were 2.7 % and 2.4 %, respectively. A result of 3.0 % cysteine can therefore be considered high but is comparable to the Ohlson and Anjou study and may reflect species or cultivar differences in the *Brassica* genus (*Brassica napus*, *Brassica juncea*, and *Brassica campestris*).

A comparison of canola protein amino acid profiles with other protein sources was provided in the 2011 review by Tan *et al.* [177]. They conclude that CSM protein is a good source of histidine,

glutamine, and arginine, and provides nutritive advantages over one or both of soy protein and casein for the following amino acid components: methionine and cysteine (combined content), threonine, histidine, and arginine. They also determine that the CSM protein could be less lipidemic and less atherogenic than casein based on the lysine to arginine ratio, and that the protein efficiency ratio of CSM protein (2.64) exceeds that of soybean meal (2.19) [177]. The amino acid analysis of those same residues in this study are largely consistent with the summaries by Tan *et al.* and support the conclusions in their review that the CSM protein extract is a balanced source of essential amino acids and compares favourably with soy protein in amino acid requirements for human consumption [177].

5.3.3. Protein separation

Protein separation is required for analyses of the protein profile of the CSM extract, identifying the number and type of peptide constituents in the canola extract. Separating the components also allows for relatively quick comparisons of protein profiles across various extracts to check for batch consistency. Furthermore, mass spectrometry analyses for identification of the proteins (see Section 5.3.4) is achieved only after the isolation of purified components of the protein extract. Two common techniques are Gel Filtration Chromatography (GFC) and Polyacrylamide Gel Electrophoresis (PAGE) (refer to **Sections 4.2.3** and **4.1.1** for experimental procedures). GFC is used here to analyse the number of different proteins and polypeptides present in the canola extract, including during various preliminary stages and in waste products of the extraction processes. GFC also provides information about the relative sizes of these protein constituents as well as identifying lost yield. Sodium dodecyl sulphate (SDS)-PAGE is then used to measure the molecular weight of the dominant protein constituents in the final extract products. These results can be compared to literature to assist with preliminary protein identification, later confirmed by a mass spectrometry study (see **Section 5.3.4**).

The GFC technique was used to track the changing protein profile during the extraction techniques. Samples analysed by GFC (refer **Table 4.2**) included the final precipitated extract products from both

techniques, three pre-product samples taken at earlier processing stages in the extraction, and three samples from waste products (see **Figure 5.2**). The samples collected from the alkali-acid extraction process included: 'extract 1' (final product), 'sample 4' (pre-product), and 'sample 5' (waste). Those from the salt-PMM extraction process were: 'extract 3' (final product), 'samples 1 & 2' (pre-products), and 'samples 3 & 6' (waste).

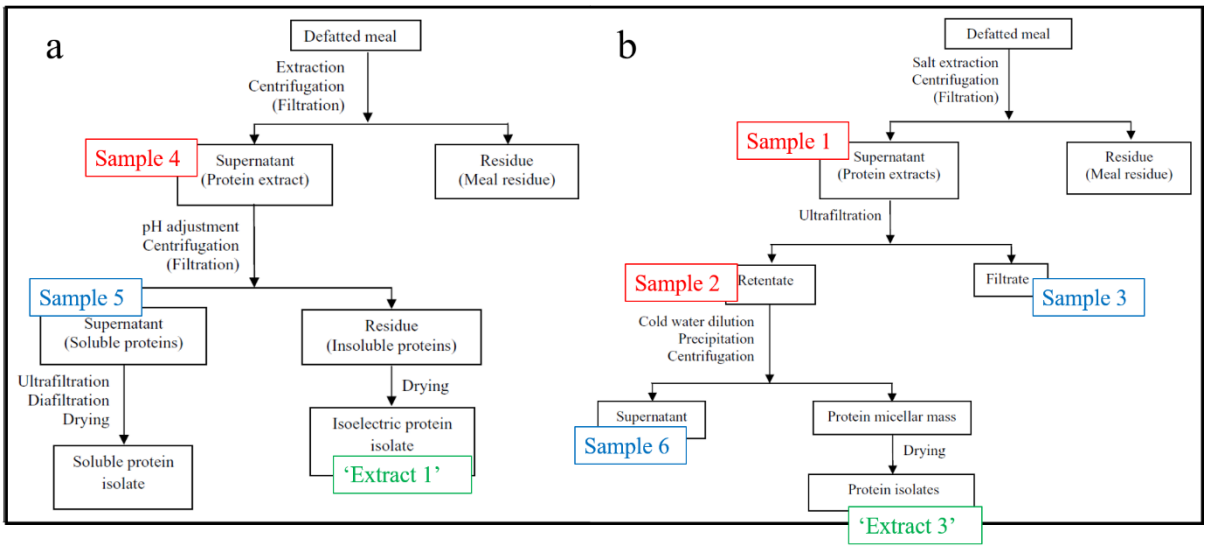

Figure 5.2: *Summary of liquid samples and solid extracts from the* ***(a)*** *alkali-acid and* ***(b)*** *salt-PMM extraction processes of canola protein that were analysed by Gel Filtration Chromatography (GFC). Pre-product samples (liquids) in red, waste samples (liquids) in blue, and extract samples (solid precipitates) in green (extract numbers refer to batches 1 and 3)*

An attempt to calibrate the chromatograms obtained from the GFC process using molecular weight standards was unsuccessful due to poor resolution obtained from the standard sample. Chromatograms were therefore used to provide comparative information about protein molecular weights using elution times with absorbance peak areas. The total amount of protein content in each sample was determined by the total area of all absorbance peaks at 214 nm. This comparison was made only between the liquid samples (prior to precipitation). Extract samples had differing levels of solubility in the GFC buffer, thus the total re-dissolved (in GFC buffer) protein was not reflective of all protein in the extract.

Sample 5, a supernatant representing acid-soluble protein, was collected after removal of the Extract 1 product (see **Figure 5.2**). Sample 5 was compared to the Sample 4 (**Figure 5.3**) since all proteins from Sample 5 were necessarily present in Sample 4 (see **Figure 5.2**). Sample 5 measured 48 % of the total

absorbance of sample 4, thus indicating that approximately 52 % of the solubilised protein in the alkali extraction was recovered in the final extract ('extract 1', **Figure 5.3**). Since the alkali-acid technique recovered on average 38 % of the total available protein in the meal (see **Section 5.3.1**) this result indicates that some of the CSM protein remained insoluble at the first stage of the process and was lost in the discarded insoluble material.

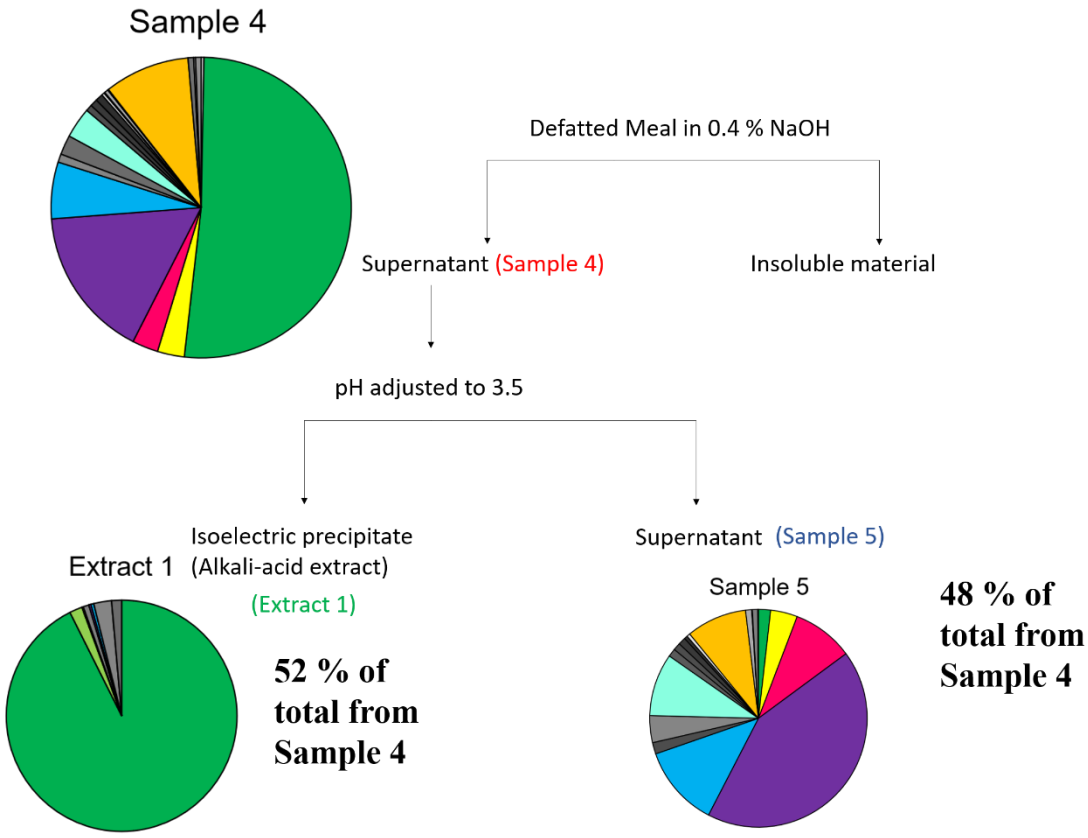

***Figure 5.3**: Proportions of protein constituents in the CSM protein extract at various stages during the alkali-acid extraction process as determined by GFC. Elution times increasing (molecule size decreasing) in a clockwise direction for each pie chart starting at the 12 o'clock position. Colours correspond to same elution times (molecular size) across all samples. Pie chart size represents total protein amount with respect to sample from previous processing stage*

Sample 3, the permeate (waste product) from the ultrafiltration stage in the salt-PMM extraction process, represented 20 % of the total protein detected in the original supernatant (sample 1) (**Figure 5.4**). A further 20 % of the remaining 80 % (16 % of the protein in sample 1) remained soluble in the retentate after PMM precipitation and was also lost during this process. This indicates that 64 % of the salt-soluble protein is collected as the salt-PMM extract (extract 3) but fails to explain the average yield of 4.0 % of the available protein for this extraction process. The salt buffer must therefore fail to

solubilise a substantial amount of the meal protein and, like the alkali-acid process, this protein is lost in the insoluble material obtained from the first centrifugation.

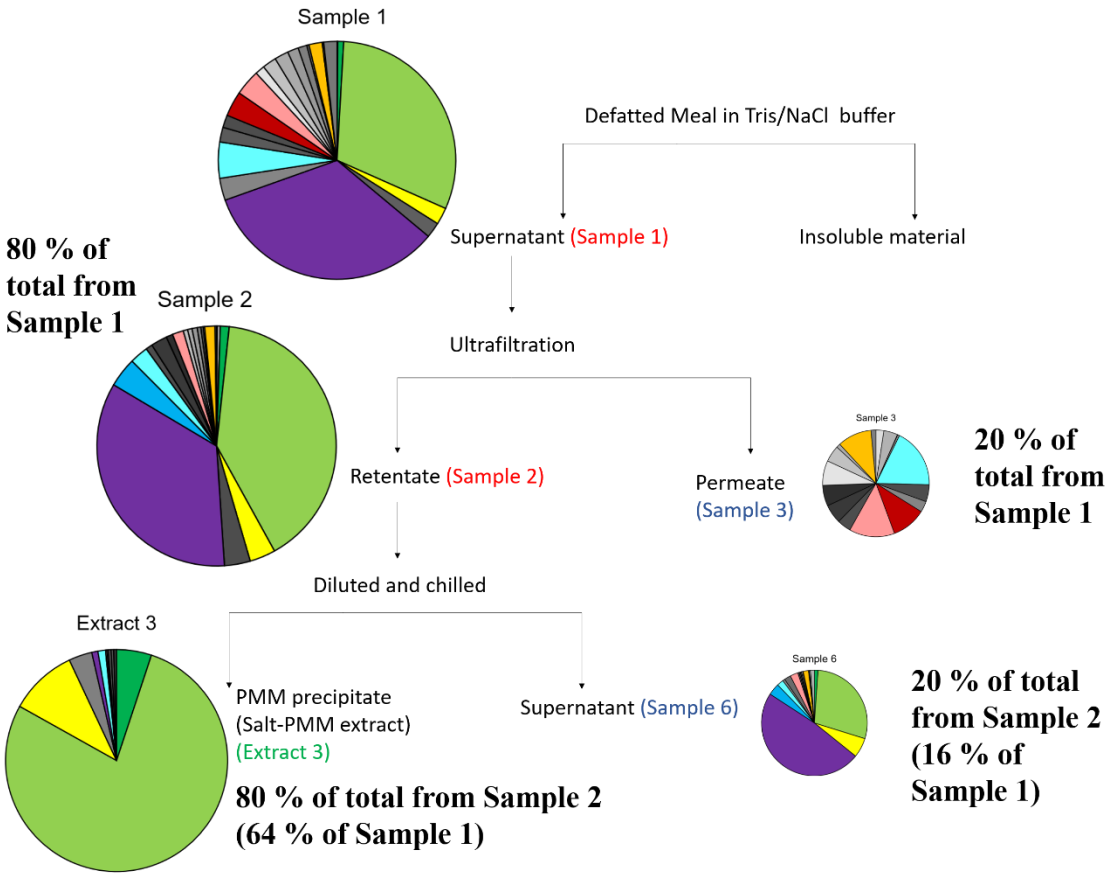

Figure 5.4: *Proportions of protein constituents in the CSM protein extract at various stages during the salt-PMM extraction process as determined by GFC. Elution times increasing (molecule size decreasing) in a clockwise direction for each pie chart starting at the 12 o'clock position. Colours correspond to same elution times (molecular size) across all samples. Pie chart size represents total protein amount with respect to sample from previous processing stage*

The GFC technique also reveals how various proteins within the meal may be selectively extracted using the two techniques. Elution times (listed alongside corresponding pie charts and identified by separate colours in **Figure 5.5** & **Figure 5.6**) demonstrate how various eluents are separated during the gel filtration chromatography process. Each peak (elution time) therefore represents a unique protein type, subunit, or multimer, separated by unique molecular weights and hydrophilicities. It can be seen that the major protein product in each of the two extraction processes is likely a different protein type since elution times are different (10.3 minutes for Extract 1 vs. 14.4 mins for Extract 3) (**Figure 5.5**).

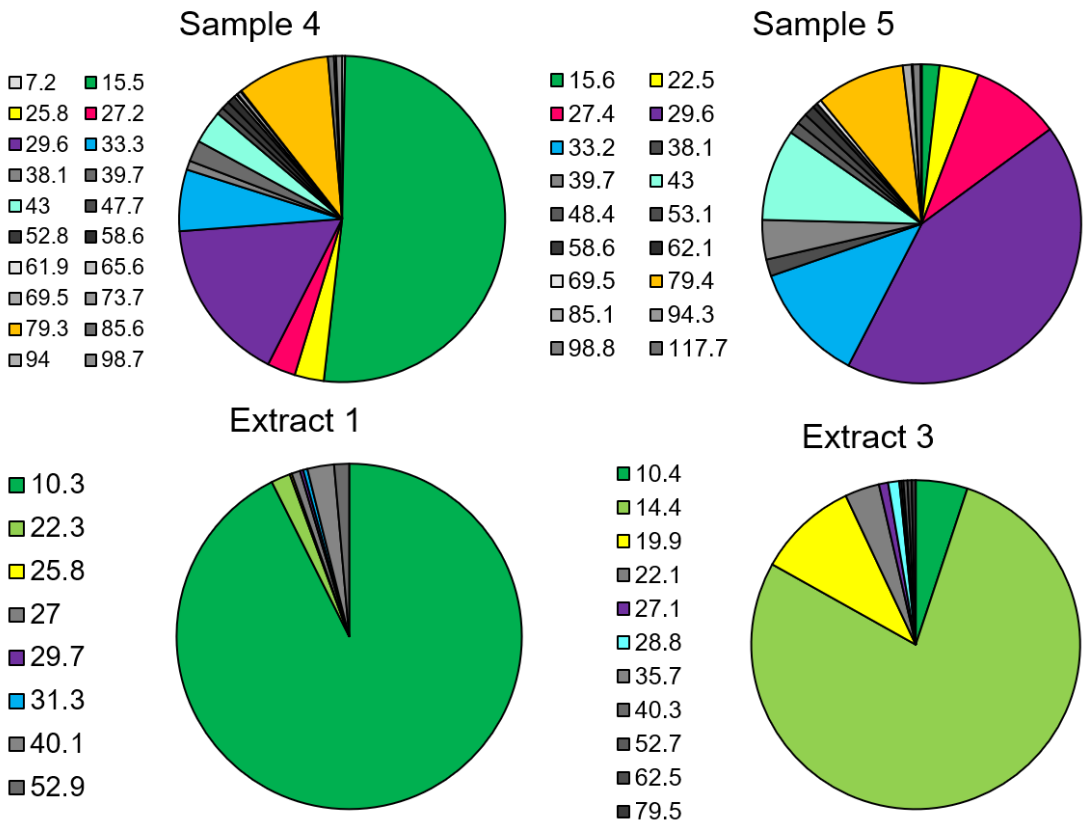

Figure 5.5: *Proportions of various proteins in GFC samples. Each absorbance peak (protein) is identified by elution time in minutes (colour coded alongside charts). Elution times increasing (molecule size decreasing) in a clockwise direction for each pie chart starting at the 12 o'clock position. Absorbance was at 214 nm. Samples 4, 5 and extract 1 are from the alkali-acid extraction process, extract 3 is the salt-PMM product*

It should be noted that extract 3 was run at a slightly faster elution rate (0.75 mL min^{-1}) due to being the first sample run. The flow rate was lowered for subsequent runs (0.5 mL min^{-1}, Samples 1 – 6 and Extract 1) to avoid damaging high pressures in the system. Thus, all later samples were analysed using a consistent flow rate but Extract 3 elution times should be slightly shorter. Future work with GFC analysis of CSM protein extracts should incorporate collection of eluted fractions and identification by LC-MS/MS to confirm the identity of various eluents (see **Section 9.2.1**).

However, elution times are indicative of molecular weight and hydrophilicity so can be used to draw some conclusions about the differing protein profiles in the samples. The alkali-acid extraction process appears to concentrate the larger molecular weight proteins in the final extract while the protein content lost in the acid-soluble fraction (Sample 5) is mostly composed of either small and/or hydrophobic proteins (**Figure 5.5**).

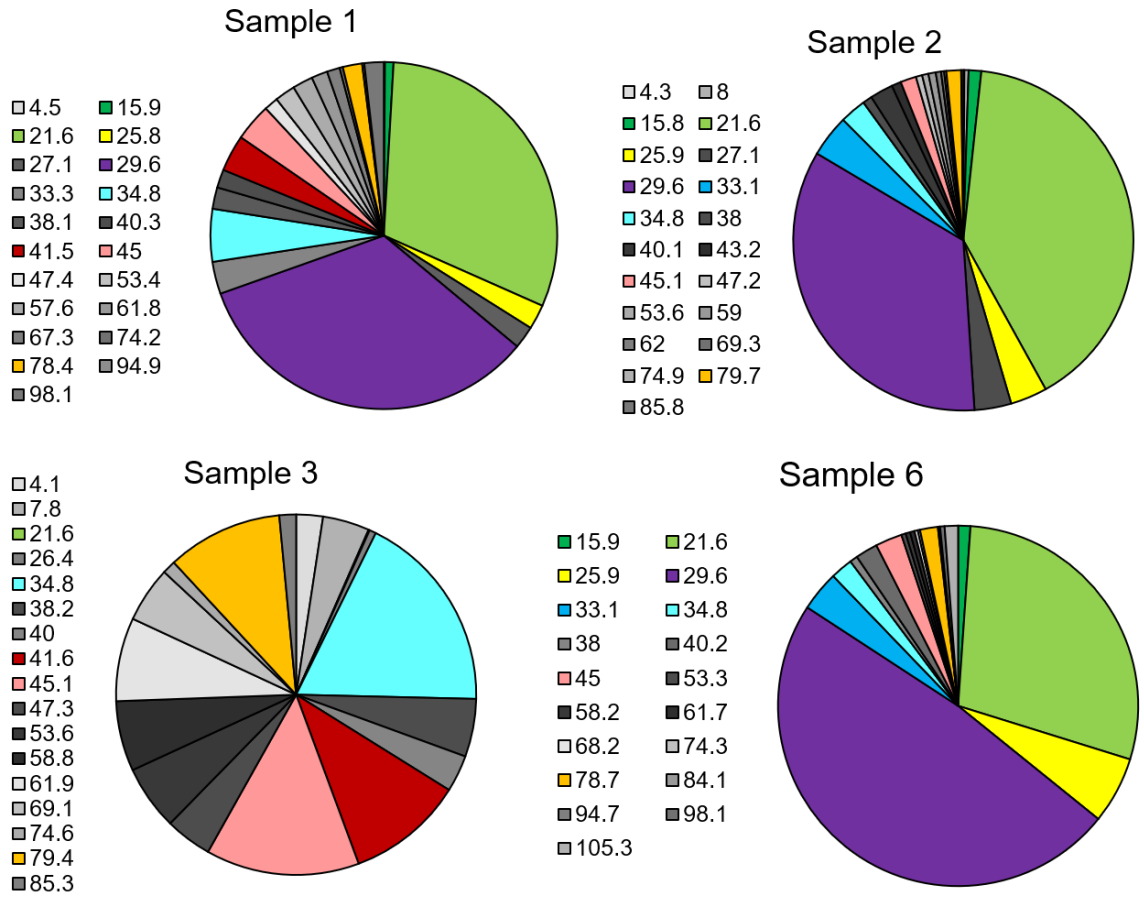

Figure 5.6: *Proportions of various proteins in GFC samples. Each absorbance peak (protein) is identified by elution time in minutes (listed in legends on pie charts). Elution times increasing (molecule size decreasing) in a clockwise direction for each pie chart starting at the 12 o'clock position. Absorbance was at 214 nm. Samples 1-3 and 6 are from the salt-PMM extraction process*

GFC results from the salt-PMM extraction process likely demonstrate the successful separation of the larger and smaller constituents at the ultrafiltration step. The salt-soluble proteins detected prior to the ultrafiltration (Sample 1) are separated as the smaller molecules are removed in the permeate (Sample 3) along with a large amount of the salt content, leaving the larger protein constituents (and most of the protein yield) in the retentate (Sample 2) (**Figure 5.6**). The final precipitation stage seems to further concentrate the larger constituents (Extract 3, **Figure 5.5**) while a proportion of all the retentate proteins is left in the supernatant (Sample 6, **Figure 5.6**) after recovery of Extract 3.

Analysis of the molecular weight profiles of the two extract products was then carried out using SDS-PAGE. This technique was used to compare the batch consistencies of the CSM protein extracts (batches 1-2, 5-9 (alkali-acid precipitate) and batches 3-4 (salt-PMM precipitate) (**Figure 5.7**). SDS-

PAGE gels were also used for isolation of individual proteins and polypeptides for later identification with tandem mass spectrometry (see **Section 5.3.4**).

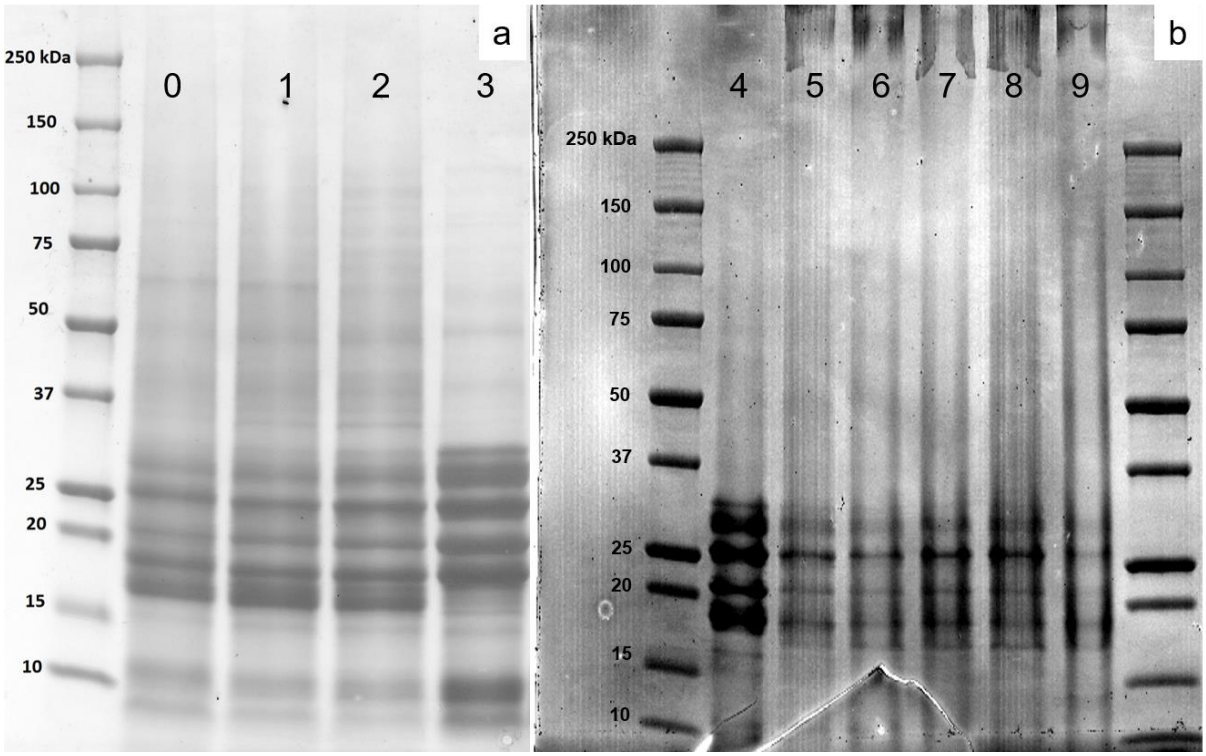

Figure 5.7: *Gels resulting from SDS-PAGE analysis of CSM protein extract, batches 0 - 3 (a) and 4 - 9 (b) where batch numbers are annotated at the top of the corresponding lane. Molecular weight standards from 10 – 250 kDa are annotated adjacent to the corresponding protein band.*

Figure 5.7 shows the SDS-PAGE results of the CSM meal extracts used in this study. The batch consistency across the various alkali-acid extracts was excellent (extracts 0 – 2, 5 – 9) as was the batch consistency with the two salt-PMM extracts (3 & 4). The major bands present in both extracts were: 28, 24, 20, 17, 15, 9 & 6 kDa (**Figure 5.8** & **Figure 5.9**) while a major band present only in some of the alkali-acid extracts was found at 320 – 350 kDa (**Figure 5.10**). Additional bands observed in the extracts were found at 61, 34, 29, & 16 kDa (**Figure 5.8**). The main difference between the salt-PMM extract and in the alkali-acid extract is the different intensities of these protein bands. For example, the bands found at 9 kDa and 6 kDa are present at 1.3 × and 1.4 × higher intensity in the salt-PMM extract (batch 3) than in the alkali-acid extracts (batches 0 - 2), while the 15 kDa band is 3.2 x higher intensity in the alkali-acid extracts (**Figure 5.8**). However, the semi-quantitative comparisons of densitometric scans are only indicative of protein concentration. Furthermore, the variable solubilities

of the two extracts in the SDS-PAGE sample buffer limits the accuracy of initial concentrations in the SDS-PAGE sample buffer.

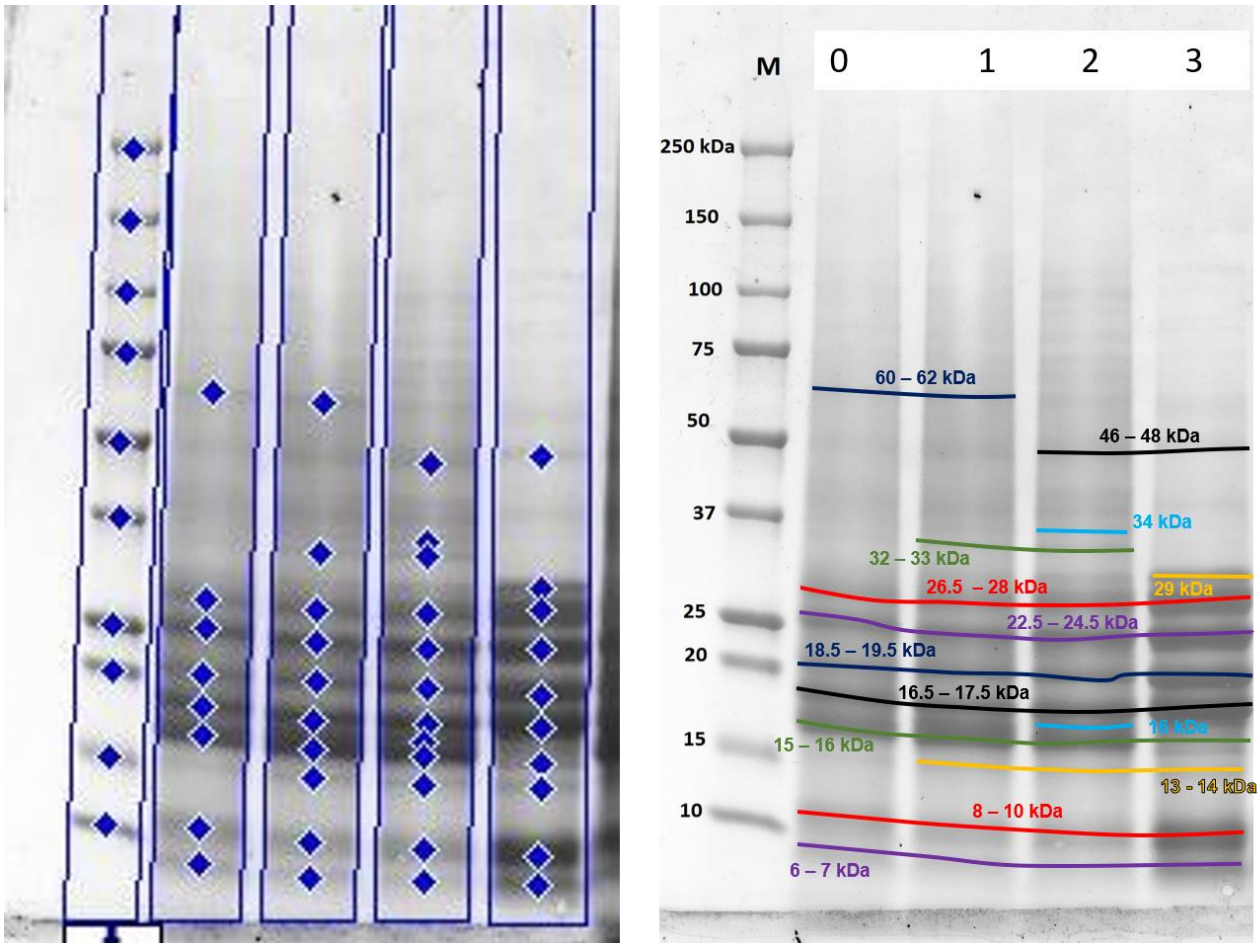

Figure 5.8: *Identification of molecular weight values of major protein bands from CSM protein in extracts 0 – 3 as determined by SDS-PAGE analysis*

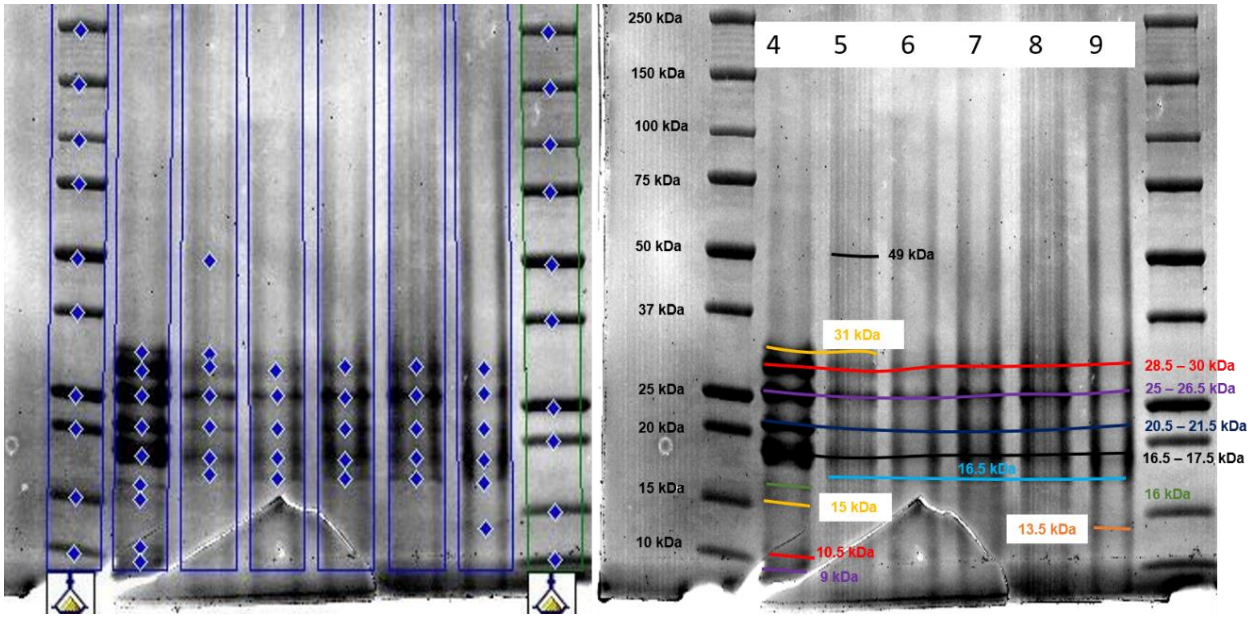

Figure 5.9: *Identification of molecular weight values of major protein bands from CSM protein in extracts 4 - 9 as determined by SDS-PAGE analysis*

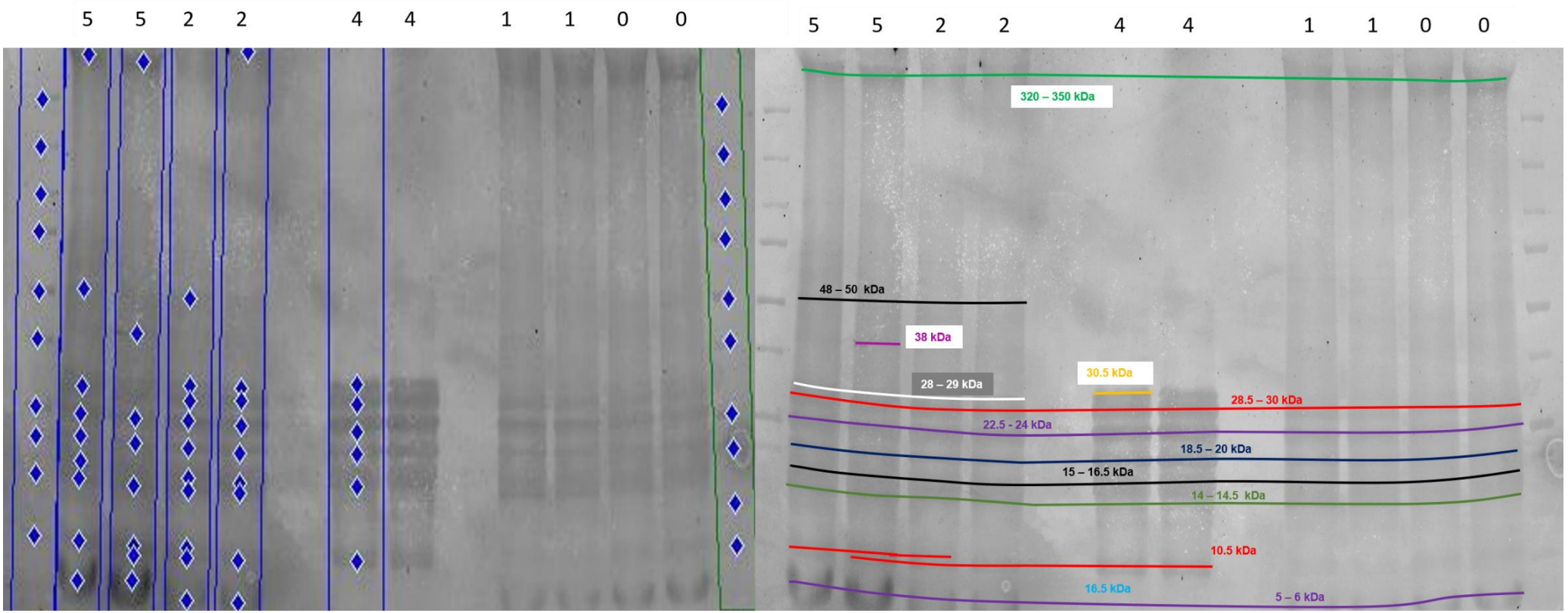

Figure 5.10: *Identification of molecular weight values of major protein bands from CSM protein in extracts 2, 4 & 5 as determined by SDS-PAGE analysis*

A comparison with other studies of CSM proteins suggests that the larger molecular weight bands are mostly due to cruciferin (or polypeptides originating from cruciferin) and that lower molecular weights (those below 16 kDa) are likely due to the napin protein (**Table 5.4**). The band identified in the alkali-acid extract at 320 – 350 kDa is probably the hexamer structure of cruciferin, given that native cruciferin is 300 - 350 kDa (refer **Section 2.3.2**), while the native structure of napin (generally found at 14 kDa) likely corresponds to the band at 15 kDa.

Table 5.4: *Comparison of molecular weights identified from SDS-PAGE bands in this study and others*

Molecular weight (kDa) this study	**Probable identification (based on other study)**	**Molecular weight (kDa) other study**	**Reference**
320 – 350	Cruciferin – hexamer	300 - 310	[191]
		300	[231]
61	Cruciferin – monomer	50	[192]
34	Cruciferin – reducible subunit	44	[192]
29	Cruciferin – reducible subunit	29.5	[192]
28	Napin – dimer	27.5	[192]
24	Cruciferin – non-reducible subunit	22	[192]
20	Cruciferin – non-reducible subunit	20	[192]
17	Oleosin	15 – 26	[191]
16			
15	Napin - monomer	14	[192]
		12.5 – 14.5	[191]
9	Napin – subunit	9	[192]
		9.5	[232]
6	Napin – subunit	4	[232]

Attempts to correlate these results to earlier GFC data are difficult due to the denaturing conditions used in SDS-PAGE. It is unlikely that protein bands identified in SDS-PAGE always have a direct correlation to individual peaks eluted in GFC since sample preparation for SDS-PAGE is designed to denature and reduce proteins into constituent polypeptides. The GFC technique is likely to preserve proteins as multimers, native structures, and even aggregates. While it is plausible that the larger protein bands identified in SDS-PAGE (*e.g.* the cruciferin band at 320 – 350 kDa) may correlate to protein fractions eluted during GFC (*e.g.* the major constituent in Extract 1, eluted at 10.4 minutes), it is not possible to say with certainty without a successful molecular weight reference on the GFC results and collection and identification of the eluent fractions.

5.3.4. Tandem Mass Spectrometry (LC-MS/MS)

Mass spectrometry permits the unambiguous identification of proteins by the unique array of molecular masses generated after ionisation and fragmentation. Identifying the exact amino acid sequences of the canola proteins aids in understanding of the gelation chemistry and more generally about the chemical nature of the resulting gels and aerogels. The identification of the protein components from molecular weight alone relies on the availability of previous studies for comparison. Accurate identification of individual protein components in CSM can be carried out using tandem mass spectrometry (LC-MS/MS) to identify the constituent amino acid sequences and subsequently derive the identity of the original protein molecule. Identification of the protein molecules may be achieved through first separating them (using SDS-PAGE, refer **Section 4.1.1**), then partially breaking them down into smaller peptides (using enzymatic digestion), further separating those peptides from each other (using liquid chromatography (LC)) and then identifying amino acids sequences in those peptides using tandem MS. Peptides are subsequently analysed by their mass-to-charge ratios (see **Section 4.2.4**) . Parent proteins can then be identified by comparison with database information of known protein sequences.

The samples used for LC-MS analysis in this thesis originated from the SDS-PAGE gel obtained after analysing extracts 0 – 2, 4 & 5 (**Figure 5.10**). A total of 14 bands were identified and excised for an enzymatic digest and subsequent LC-MS-MS analysis (**Figure 5.11**).

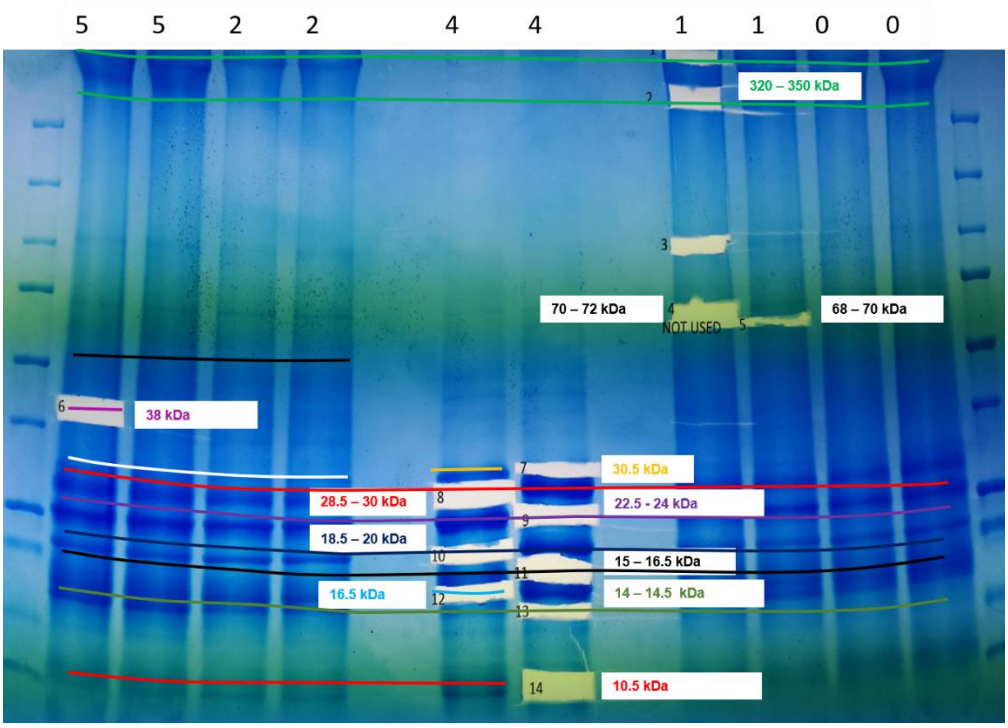

Figure 5.11: *Excised gel bands 1 – 14 from SDS-PAGE gel (extracts 0 -2, 4 &5) annotated with corresponding molecular weights.*

Samples 1 – 6 corresponded to protein bands from the alkali-acid extract while samples 7 – 14 were from the salt-PMM extract (**Table 5.5**). However, bands 7 – 14 were also found in the alkali extracts while band 6 was also faintly present in the salt-PMM extract.

Table 5.5: *Molecular weight of protein bands analysed in LC-MS*

Alkali-acid extract		Salt-PMM extract	
Sample number	**M_w (kDa)**	**Sample number**	**M_w (kDa)**
1	350	7	30.5
2	320	8	28 – 30
3	100	9	23 – 24
4	72	10	18 – 20
5	68	11	15 – 17
6	38	12	16 – 16.5
		13	14 – 15
		14	9 – 10.5

Proteins isolated from *B. napus* can be checked for peptide sequence matches against Viridiplantae sequences from the proteomic database SwissProt. The proteins identified in the samples are summarised in **Table 5.6** while the full list of amino acid sequences and corresponding proteins can be found **Table A.1** (in Appendix).

The LC-MS/MS results identify almost all the polypeptides as being from cruciferin (CRU1, CRU2, CRU3, CRU4, CRUA, highlighted in bold in **Table 5.6**), one of the two main seed storage proteins found in canola seed meal (refer **Section 2.3.2**). The other storage protein, napin (2SS3), was identified in just one band (sample 14 with a molecular weight of 9 – 10.5 kDa). Oleosin (OLES2), an oil-body protein typical of oil seeds [233] was also identified (in samples 1 & 2) while EF1A1 (elongation factor 1) and DEF4 (defensin-like protein) were also observed. These latter two proteins are common eukaryotic proteins which are used by the organism for protein synthesis (translational elongation) [234] and defence against pathogens, respectively [235].

Table 5.6: *Proteins identified in CSM protein extracts identified by LC-MS/MS analysis*

Sample	M_W (kDa)	Identified proteins	Sample	M_W (kDa)	Identified proteins
1	350	**CRUA**	9	23 – 24	**CRU4**
		EF1A1			**CRU3**
		OLES2			**CRU2**
		CRU4			**CRU4**
2	320	**CRU4**			**CRU1**
		OLES2			**CRU2**
		EF1A1	10	18 – 20	**CRU3 (BRANA)**
3	100	**CRU4**			**CRU3 (ARATH)**
4	72	(no peptides identified)			**CRU4**
5	68	**CRU4**			**CRUA**
		CRUA	11	15 – 17	**CRU4**
6	38	**CRUA**			**CRUA**
		CRU3			**CRU3**
		CRU4			**CRU2**
7	30.5	**CRU3**	12	16 – 16.5	**CRU4 (BRANA)**
		CRUA			**CRUA**
		CRU4			**CRU3**
8	28 – 30	**CRU3**			**CRU2**
		CRU1			**CRU4 (ARATH)**
		CRU3	13	14 – 15	**CRU4**
		CRU2			**CRUA**
		CRU4			**CRU3**
			14	9 – 10.5	**CRU4**
					CRU3
					CRU1
					2SS3
					DEF4

The absence of napin from most of these protein bands, particularly the lower molecular weight bands, is surprising given that literature suggests the alkali method should favour the extraction of

albumin proteins (napin) over globulins (cruciferin). Cruciferin is generally preferentially extracted using the salt-PMM method [191]. However, no difference is seen in the identified proteins between these two extracts in this study (almost all bands, regardless of extract type, are exclusively composed of cruciferin). An explanation could be found in the different solubilities of the proteins as preferential extraction of cruciferin or napin has been achieved by recovering soluble and precipitated fractions separately (see **Figure 2.23**). The higher solubility of albumins over globulins means that cruciferin tends to be predominant in precipitated fractions while napin remains soluble. In this project the fractions collected from both methods are precipitated and the remaining supernatant is discarded. GFC analysis has revealed up to 36 % of the protein initially solubilised can be lost in the discarded supernatants providing a possible explanation for why identified protein was largely cruciferin. Another explanation is that various cultivars and crops of the canola seed can contain variable quantities of these proteins, and it is plausible that the seed meal used in this project contains predominantly cruciferin. The absence of significant quantities of napin is a promising result for subsequent aerogel research since cruciferin is the major contributor to the gelation properties of CSM extracts. The possible loss of the napin content was not investigated any further, given that the CSM extracts obtained could be successfully formed into gels and aerogels (described in **Chapter 6**).

5.4. Biochemical potential of canola protein extract

The bioactive potential of canola protein isolates was briefly explored in **Section 2.3.4**. Known anti-hypertensive [236, 237], antioxidative [238], and nutritional properties [239], are examples of biochemical features that could be harnessed to provide additional function to aerogels for potential nutraceutical applications. These studies demonstrate the potential of the CSM extract to contain bioactive peptides for wider applications. Investigations into whether such bioactivity is retained after aerogel processing could provide information about the relevance of canola protein bioactivity in a canola protein aerogel or similar material. In the current Section, canola proteins obtained from both the extracts (described in **Section 5.3.1**) and the aerogels (described in **Chapter 6**) of this thesis, are screened for possible bioactivity using an *in silico* technique.

Bioactive peptides can fall into three categories: exact matches, partial matches, and cryptides. An exact match is where the sample sequence is identical to that of a known bioactive with no missing residues and no additional residues. A partial match is where the sample sequence is shorter than the sequence of the known bioactive, but it matches with a section of the complete bioactive sequence. Finally, a cryptide is where the sample sequence is longer than the bioactive sequence because it contains additional residues on one or both ends of the bioactive sequence identified within it. The bioactive sequence is hidden or encrypted in the larger molecule and so it is called a cryptide. One example of peptide bioactivity is angiotensin-converting-enzyme (ACE) inhibitory effect, which is useful for treating hypertension. Other bioactivities detected in peptides can include enzyme inhibition (*e.g.* ACE inhibition), neuronal signalling, immune responses, antioxidants, anti-microbial, and anti-viral effects.

The search for unique properties of the CSM aerogels has included an assessment of the bioactive potential of CSM extract and aerogels. The approach taken for bioactive searching was to use LC-MS analysis and identify peptides obtained from the CSM proteins (refer **Section 4.2.5**). Once identified, the sequences of these peptides were screened against a database of known bioactive molecules to look for matches. The study consisted of 8 distinct samples which were subject to varying degrees of processing prior to analysis with LC-MS. These processing conditions are summarised in **Table 5.7**.

The first attempt to generate bioactive peptides from the samples involved the LC-MS/MS analysis of a 3 kDa filtrate obtained from extracts 2 and 4 ('SEF-Extrn 2' and 'SEF-Extrn 4', **Table 5.7**). This approach searches for small endogenous peptides in the extracts, likely generated from larger proteins. However, no peptides were identified in these samples after LC-MS/MS analysis. This result indicated that the 3 kDa molecular weight cut-off (MWCO) filter had removed all peptides from the samples, meaning no smaller peptides (less than approximately 30 amino acid residues long) were detected. This is problematic for detection of bioactive peptides since most are small (less than 7 amino acid residues) and require liberation from the much larger protein molecules in order to function [240].

Table 5.7: *Summary of sample preparation conditions for CSM extract and aerogel samples analysed for bioactive peptides*

Sample name as in MS data	Extract No.	Extract Type	Extract or aerogel (sample #)	Trypsin or 3kDa filtrate?
SEF-Extrn 2	2	Alkali-acid	Extract only	Filtrate
SEF-Extrn 4	4	Salt-PMM	Extract only	Filtrate
Aerogel – A	**1**	**Alkali-acid**	**Aerogel # 13**	**Trypsin digest**
Aerogel – S	**3**	**Salt-PMM**	**Aerogel # 15**	**Trypsin digest**
Aerogel – S – Ultrafiltrate	3	Salt-PMM	Aerogel # 15	Filtrate
CSM – Ext 4	**4**	**Salt-PMM**	**Extract only**	**Trypsin digest**
Aerogel – A – Ultrafiltrate	**1**	**Alkali-acid**	**Aerogel # 13**	**Filtrate**
CSM – Ext 5	**5**	**Alkali-acid**	**Extract only**	**Trypsin digest**

Therefore, the use of an enzyme (porcine trypsin) was introduced to partially digest samples prior to LC-MS/MS analysis, generating smaller peptides that could be detected and potentially carry bioactivity. The LC-MS/MS result for the subsequent 6 samples in **Table 5.7** identified peptide sequences in all the samples digested with trypsin and also in the 3 kDa MWCO filtrate from the dissolved aerogel sample prepared with extract 1 (boldened samples in **Table 5.7**). The total number of qualifying peptides (those which meet LC-MS/MS data quality thresholds) from each of these samples was between 32 and 172 (**Figure 5.12**), with the trypsin digestion clearly facilitating the production of these peptides. Interestingly, aerogel processing also appears to increase the overall number of small peptides available in the samples after trypsin digest. Higher numbers of unique

peptide sequences obtained from the aerogel samples suggests that the gelation process (refer **Chapter 6**) may have increased the potential for the CSM extracts to produce bioactive peptides. This is a promising result for aerogel bioactive functionality. Breakdown of proteins during the aerogel processing may produce smaller peptide products that facilitate gel production. Subsequent release of these smaller peptides during dissolution and enzymatic digestion results in a wider variety of small peptides found in the aerogel samples. However, quantitative LC-MS/MS studies on the total number of peptides would need to be carried out to determine if the overall number (regardless of sequence) of small peptides is higher in extract or aerogel samples. The results presented here describe only the number of unique sequences identified, but do not provide information about the abundance of each of those peptides in the samples.

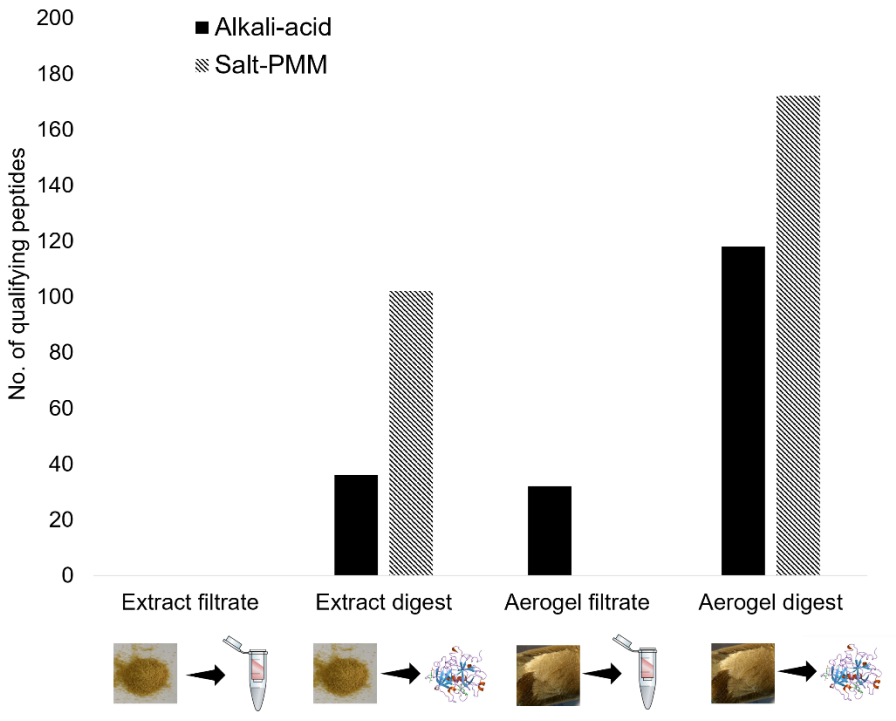

Figure 5.12: *Number of qualifying peptides identified in extract and aerogel samples by LC-MS/MS analysis, following filtering with a 3 kDa Molecular weight cut-off filter or enzymatic digestion with porcine trypsin*

The detection of 32 peptide sequences from the 3 kDa MWCO filtrate obtained from one of the aerogel samples is a very promising result given that earlier attempts to detect small endogenous

peptides in the extracts were unsuccessful. This result again suggests that the aerogel processing (when using the alkali-acid extract) has facilitated the breakdown of larger proteins into small peptides, which are then detectable upon dissolution of the aerogel structure in water. The corresponding extract did not demonstrate any endogenous peptides after a filtration at 3 kDa MWCO. The lack of peptide sequences in the 3 kDa filtrate from the salt-PMM aerogel sample is interesting, since aerogels are prepared using the same methods regardless of the extract type (see **Chapter 6**). This result suggests that it may be the combination of both the harsh extraction conditions (extreme pH values) in the alkali-acid extraction and the subsequent aerogel processing conditions that are necessary for production of small peptides. The peptide sequences were subsequently screened for matches to known bioactive peptides using the databases described in **Section 4.2.5**. The search results found no exact matches of bioactive peptides, however, there was one partially matching sequence (see **Section 5.4.2**) and there were numerous cryptides identified (**Section 5.4.1**).

5.4.1. CSM protein cryptides

The CSM extracts and aerogels have shown a promising tally of cryptides. An example cryptide is a sequence such as 'ADA' that has known bioactivity and was found within a longer peptide sequence from the CSM protein samples: 'MADAVGYAGQK'. Some cryptide sequences are found in more than one longer sequence, for example 'FQ' was identified in 28 sequences from the samples. In the canola extracts there are up to 288 unique cryptides identified in a single sample (the salt-PMM extract, trypsin digest), where those cryptides occur in the 102 qualifying peptides of that sample up to 2314 times (**Figure 5.13**). The presence of cryptides is more prominent in the salt-PMM extract and aerogel derived from it, however the aerogel prepared from the alkali-acid extract demonstrated the presence of cryptides without the need to first digest with the trypsin enzyme. Cryptides identified from this aerogel structure without the assistance of an enzyme demonstrate the plausibility of added functionality in aerogels from potential bioactive peptides.

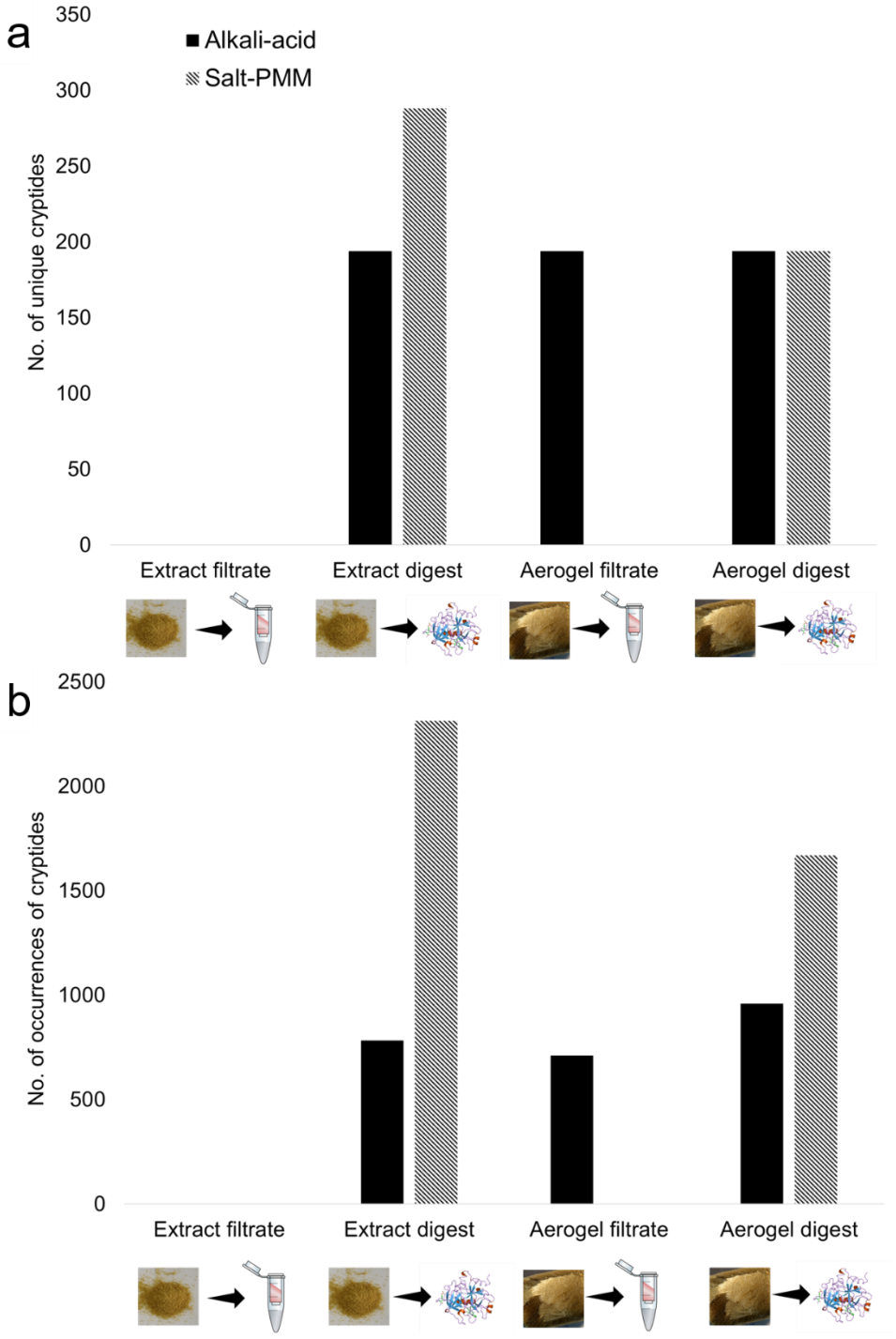

Figure 5.13: *Number of cryptides detected* ***(a)*** *and the number of occurrences of these sequences* ***(b)*** *in the CSM extract and aerogel peptides*

The canola extract and aerogel samples returned a total of 9 different bioactivities including physiological and antimicrobial bioactivities (**Table 5.8**). The sample with the highest tally of cryptides was the aerogel produced from the alkali-acid extract and subsequently digested with trypsin (522 database 'hits'). Multiple bioactivities can be associated with a single cryptide molecule, for

example, an identified cryptide (such as ‘AA’) could be counted twice in the total number of bioactivity database ‘hits’ if it carried both antihypertensive and antimicrobial properties. Therefore, the tally of bioactivity is not a quantitative measure of those activities but rather an indication of how much bioactive potential each sample possesses. The CSM protein extracts and aerogels possess a variety of cryptides having potentially physiological effects (*e.g.* antihypertensive and anti-diabetic) alongside antimicrobial bioactivities. These bioactivities can both provide added functionality to a CSM protein aerogel and alongside others identified, such as antifungal activity, are generally applicable to applications in personal care products, food, medicine, and veterinary science. These areas are possible avenues of application for canola protein aerogels and related materials.

It can be concluded that some cryptides, can be found in the CSM extract aerogels. However, this bioactivity may not be immediately accessible in many applications of the aerogel structures since it is found in the form of cryptides and require additional treatment for the bioactive sequences to be released (*e.g.* targeted enzymatic cleavage of the peptides). The most promising result from this study was the revelation that some endogenous cryptides can be identified from a CSM protein aerogel without the need for initial enzymatic digestion. The canola protein aerogels are degradable in aqueous environments and therefore able to release molecules from the protein matrix, and as demonstrated in these results, some of these molecules carry bioactive potential.

Table 5.8: *Types of bioactivities and their occurrence in CSM extract and aerogels in the form of cryptides*

Bioactivity	**Alkali-acid extract, trypsin**	**Salt-PMM extract, trypsin**	**Alkali-acid aerogel, 3kDa filtrate**	**Alkali-acid aerogel, trypsin**	**Salt-PMM aerogel, trypsin**	**Total:**
antihypertensive (ACE inhibitor)	118	176	130	212	206	**842**
anti-diabetic (dipeptidyl peptidase-4 inhibitor)	114	167	127	197	188	**793**
Antimicrobial, antibacterial	16	22	18	27	27	**110**
antioxidative	7	16	5	25	20	**73**
antiviral	10	14	12	18	17	**71**
antiparasitic	11	12	11	14	14	**62**
antifungal	7	8	8	9	9	**41**
neuropeptide	5	9	4	11	11	**40**
anticancer	6	8	7	9	10	**40**
Total:	**294**	**432**	**322**	**522**	**502**	

Further analysis of this bioactivity would involve quantification of each peptide as an amount per mole or per gram of CSM protein. Harnessing the bioactive potential of CSM protein extracts and aerogels requires further chemical analysis for quantification, controlled chemical/enzymatic release experiments, and subsequent *in vitro* or *in vivo* testing for verification and quantitation of the bioactivity. Should the CSM protein aerogels be utilised in an application where these bioactivities are relevant, the salt-PMM extraction method may be the preferable type of extract to use due to its larger range of potential bioactive molecules. Certain bioactivities may lead to unique applications for the canola protein structures where this bioactivity can be combined with aerogel properties like large surface area, to meet the requirements of an application.

5.4.2. Partial bioactivity matches

One partial match was found in the bioactivity prediction analysis. The sequence for the partial match identified (AGLQFPVGR) is the incomplete sequence to 8 longer sequences with known bioactivities (antimicrobial, antifungal, etc., see **Table 5.9**) and demonstrated potential as a drug delivery vehicle (also included as an 'activity' in **Table 5.9**). Despite being identified in one of the aerogel samples, a partial match of this nature is not a promising discovery for application potential since partial matches cannot be reliably predicted to retain the bioactivity of the longer (active) peptide. Partially matched oligopeptides, such as the sequence 'AGLQFPVGR', would need to be tested for such bioactivity *in vitro* and *in vivo*. The peptide found is partially matched to a total of 8 larger peptides that have antimicrobial, antiviral, anticancer, and antifungal bioactivities, while some are also toxins (**Table 5.9**). The sequence is just 9 residues long which is significantly shorter than most of the bioactive sequences with which it is a partial match (13 to 51 residues) and with each missing residue the chance of disrupting the bioactivity increases. However, the type of bioactivities identified in these partial matches are applicable to current aerogel industries such as medicine and cosmetics, therefore this result could impact the applicability of CSM protein aerogels.

Table 5.9: *List of bioactive peptides to which the sequence AGLQFPVGR, identified in an aerogel sample prepared from extract 1, is a partial match.*

Sequence	Activity	Database	Accession	Length
TRSSRAGLQFPVGRVHRLLRK	Antimicrobial, antibacterial	AMPer	H2A_BUFBG (2)	21
		BIOPEP	5524	
		EROP	E02712	
		SATPdb	satpdb18145	
	anticancer	SATPdb	satpdb13924	
	antifungal	SATPdb	satpdb18145	
	antiviral			
AGLQFPVGRIGRLLRK	antibacterial	SATPdb	satpdb14051	16
	antifungal			
RAGLQFPVGRLLRRLLRRLLR	antibacterial	SATPdb	satpdb19931	21
	anticancer			
	drug delivery vehicle			
	toxin			
RAGLQFPVGRLLRRLLR	drug delivery vehicle	SATPdb	satpdb15223	17
	toxin			
RAGLQFPVGRLLR	drug delivery vehicle	SATPdb	satpdb12691	13
	toxin			
AGRGKQGGKVRAKAKTRSSRAGLQFPVGRVHRLLRKGNY	Antimicrobial, antibacterial	AMPer	H2A_BUFBG (1)	39
		BIOPEP	5523	
		EROP	E02711	
		SATPdb	satpdb14077	
	antifungal			
SGRGKTGGKARAKAKTRSSRAGLQFPVGRVHRLLRKGNYAHRVGAGAPVYL	Antimicrobial, antibacterial	AMPer	H2A_HIPHI (1)	51
		APD2	AP00489	
		SATPdb	satpdb11761	
SGRGKQGGKARAKAKTRSSRAGLQFPVGRVHRLLRKG	drug delivery vehicle	SATPdb	satpdb10708	37

5.5. Protein structure and propensity for gelation

Canola seed meal protein is known for its propensity to form gels (refer **Section 2.3.3**), providing one of the key motivations for its nomination as an aerogel precursor in this thesis (see **Chapter 3**). Conditions that support the gelation of canola proteins have been explored to some degree in the literature, although the exact nature of the underlying biochemical and structural changes occurring under these conditions remain elusive (refer **Section 2.3.3**). Connections between gelation conditions, protein structure, and protein charge can assist in describing the likely gelation mechanism of canola protein with various aqueous conditions. The specific details of how various aqueous conditions influence the structure and the charge of the canola protein molecules are investigated in this Section, with a focus on the required conditions to develop canola protein gels and aerogels as demonstrated in later Chapters.

5.5.1. Protein secondary structure

Circular dichroism (CD) is a spectroscopic technique that uses UV light to probe the structure of solvated molecules. In proteins, these investigations reveal information about conformation (shape), particularly the conformations of single sections of the peptide chain (protein secondary structure). Studying the conformations in the canola protein provides information about native versus denatured states, which subsequently indicate the liklihood of gelation. Generally, native conformations must be partially or completely unfolded (denatured) before alternate (gel-producing) conformations can be formed. UV-CD spectroscopy was carried out to establish (i) if the denaturation of the canola proteins was correlated to propensity for gelation, and (ii) a basic understanding of how pH and Ca^{2+} may influence the protein structure. UV-CD spectroscopy measures the difference in circularly polarised light (circular dichroism (ΔA)) absorbed from a chiral molecule, such as a peptide or protein. Circular dichroism is expressed as ellipticity (θ) (see **Figure 5.14**) and can be used to interpret the secondary structure of the peptide or protein.

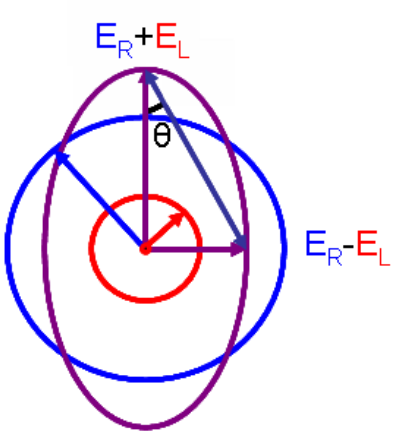

Figure 5.14: *Elliptical polarized light (purple) is composed of unequal contributions of right (blue) and left (red) circular polarized light. The angle theta (θ) represents the ellipticity value of a measurement, usually reported in millidegrees (m°)*

Typical UV-CD spectral data for protein secondary structures (**Figure 5.15**) can be used to identify the contribution of α-helix, β-sheet, and random coil conformations in a sample protein structure (see **Table 4.4**) [241].

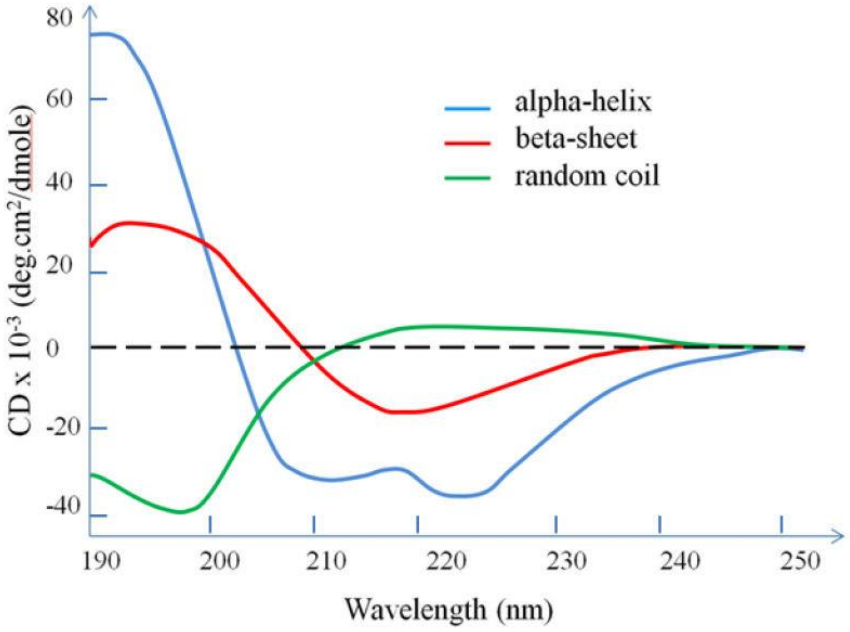

Figure 5.15: *UV-CD spectral data for pure alpha-helix, beta-sheet and random coil structures. Image obtained from: Wei, Y., A. Thyparambil, and R. Latour, Protein Helical Structure Determination Using CD Spectroscopy for Solutions with Strong Background Absorbance from 190-230 nm. Biochimica et biophysica Acta, 2014. 1844 [242]*

Ellipticity measurements from CD spectroscopy were collected for dissolved CSM extract where samples had a range of pH values (pH 3.4 – 11.0), protein concentrations (0.01 mg/mL (0.001 wt%) to 0.1 mg/mL (0.01 wt%)), and $CaCl_2$ concentrations (20 and 0.2 mM) (**Table 5.10**). The samples analysed in this study were exploratory, and measurements collected were representative of conditions later used for CSM gelation and aerogel manufacture, although protein concentrations required for gelation are much higher. Furthermore, the trial nature of this investigation meant limited reference samples (pH-adjusted water with no protein) were collected and in some instances the reference sample pH values did not match those of the corresponding protein samples (*e.g.* the samples containing $CaCl_2$). Further CD studies would be required to establish clear correlations between solution conditions and secondary structural changes in the canola protein samples but such studies are outside the scope of this project. However, the preliminary data presented in this Section provides an indication about possible links between solution conditions and protein secondary structure.

Table 5.10: *Samples of CSM protein extract analysed by CD spectroscopy*

Sample	pH	Protein concentration (mg/mL)	$CaCl_2$ concentration (mM)	Reference sample
1	3.4	0.1	-	pH 3.55
2	7.5	0.1	-	pH 7.4
3	10.8	0.1	-	pH 10.8
4	10.5	0.1	0.2	pH 6.4, $CaCl_2$ 0.2 mM
5	4.3	0.05	-	pH 3.55
6	8.1	0.05	-	pH 7.7
7	11.7	0.05	-	pH 11.0
8	9.5	0.05	20	pH 6.9, $CaCl_2$ 20 mM
9	8.3	0.01	-	pH 7.7

Plots of the measured ellipticity against wavelength (**Figure 5.16** & **Figure 5.17**) reveal a strong negative band at 210-220 nm for all samples, with some samples (samples 2 – 4 & 6) displaying two separate bands within this range at around 210 and 220 nm. The samples also show a positive band in the 190 – 200 nm range though this band is much harder to discern accurately due to a reduction in data quality at lower wavelengths. These findings are consistent with other CD studies on canola protein isolate, where a positive band is found near 190 nm and a negative band near 208 nm [243]. The ideal concentration of CSM extract for these studies is between 0.01 and 0.05 mg/mL. At higher concentrations (0.1 mg/mL) high photon absorbance occurs resulting in little light transmission to the

detector. High tension (HT) voltage associated with automatically amplifying the photon signals can be used to monitor this effect. Data cannot be considered reliable in samples where high tension (HT) voltages exceed 700 V, indicating insufficient photons reached the detector to provide a valid CD signal [218]. The CSM extract samples tested here were all affected by this limitation with the exception of samples 5 (**Figure 5.16e**) & 9 (**Figure 5.17c**), which can be seen with clearer signals at low wavelengths.

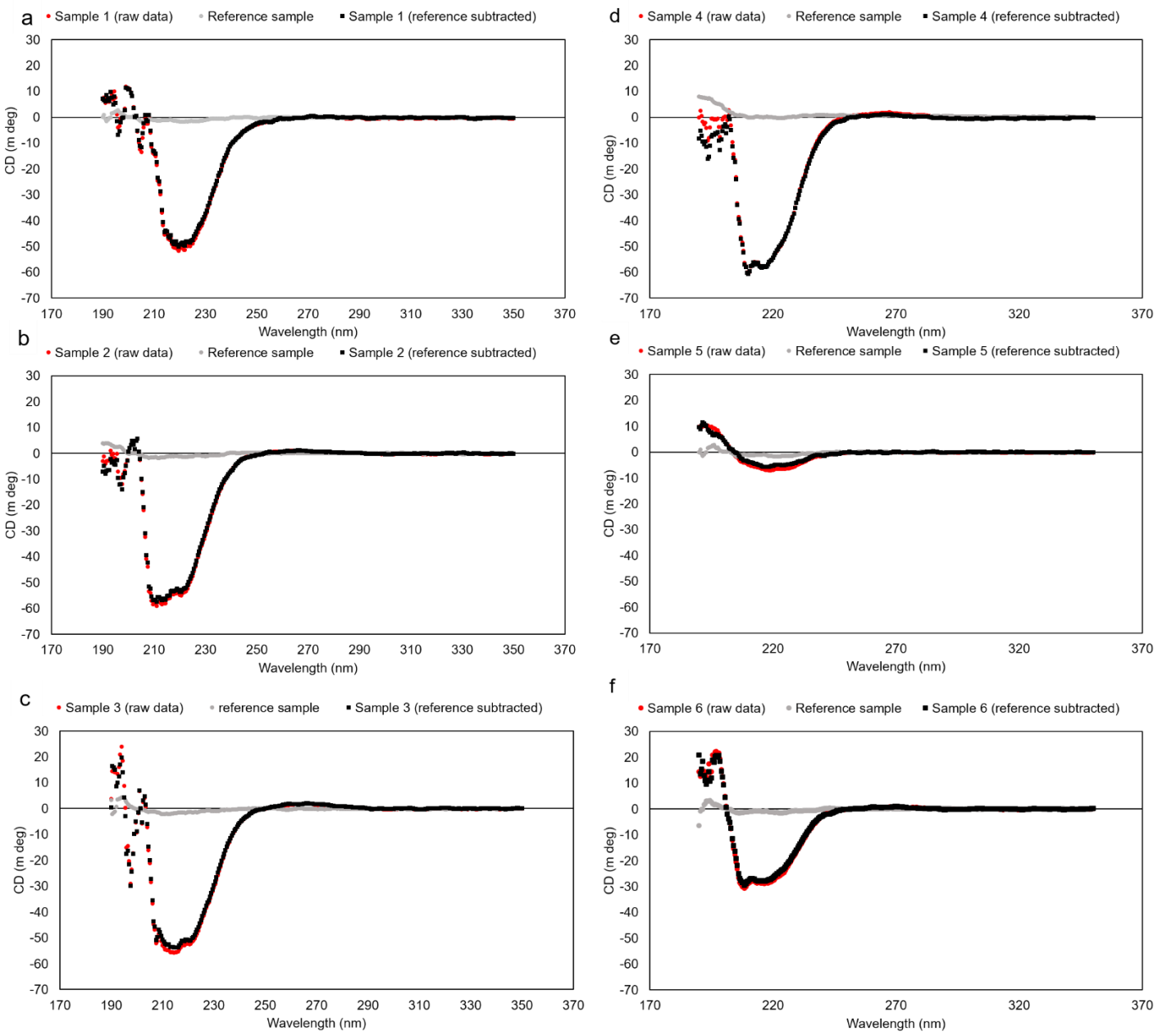

Figure 5.16: *CD (ellipticity) data obtained from CSM extract samples at 0.1 mg/mL* ***(a-c)****, 0.05 mg/mL* ***(e-f)*** *and 0.5 mg/mL* ***(d)****, with varying pH values (refer to* ***Table 5.10****) and a sample with 0.2 mM* $CaCl_2$ ***(d)***

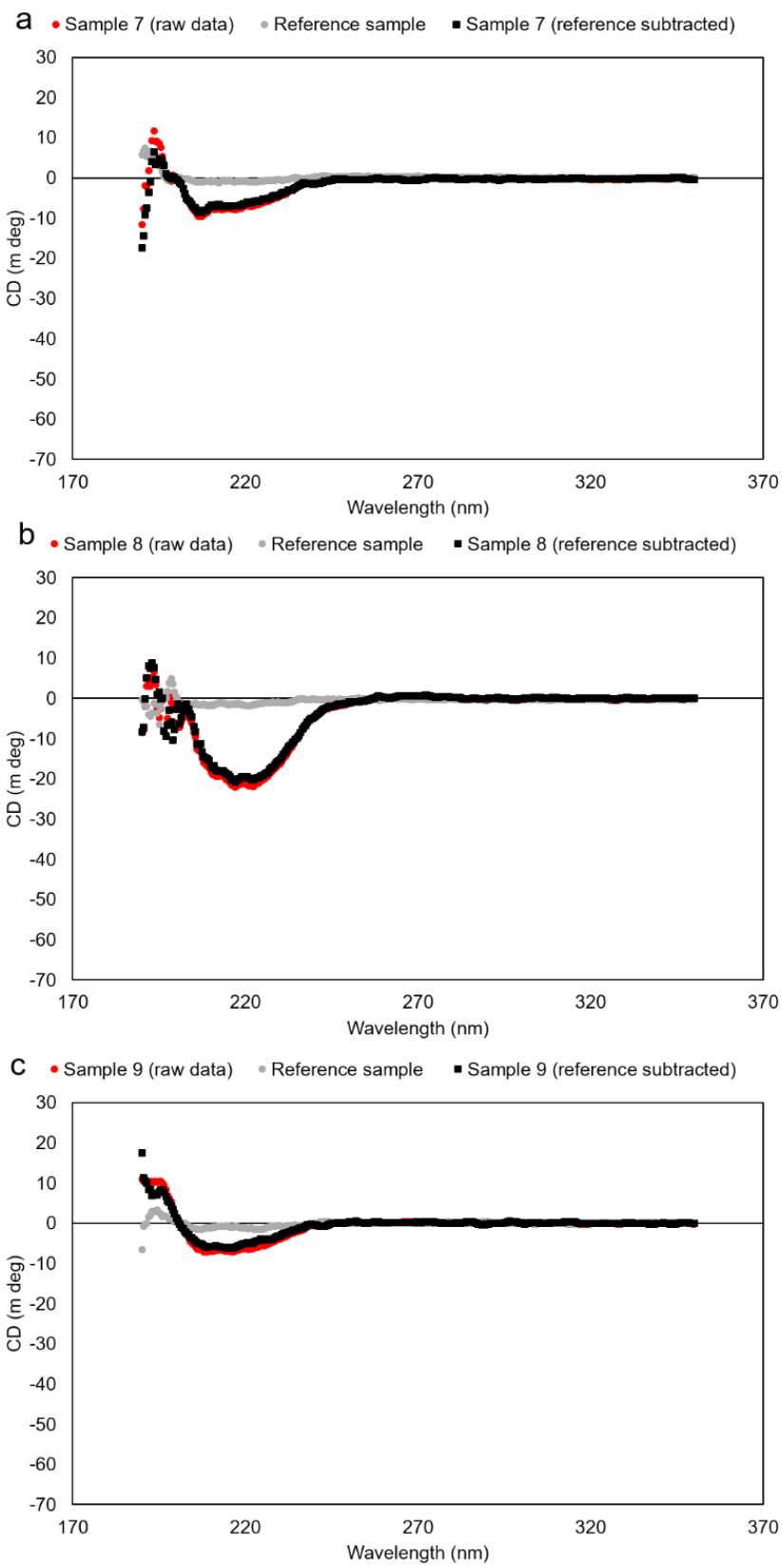

Figure 5.17: *CD (ellipticity) data obtained from CSM extract samples at 0.05 mg/mL* ***(a-b)*** *and 0.01 mg/mL* ***(c)****, with varying pH values (refer to* ***Table 5.10****) and one sample with 20 mM* $CaCl_2$ ***(b)***

The CD data in **Figure 5.16** & **Figure 5.17** report the ellipticity (θ) in millidegrees (*mdeg*) but can be converted to molar ellipticity (*[θ]*), (measured in *deg.cm^2/dmol*) using the known concentrations of protein (extract) in *g/L*, the average molecular weight of the amino acids in *g/mol* (113 Da), and the path length of the light (width of cuvette) in *cm* (0.1 cm) according to the equation:

$$[\theta] = {}^{\theta . M_r}/_{10 . l . c}$$

This was carried out for samples 1 – 9 using the DICHROWEB server (see **Section 4.2.6**) followed by data deconvolution to extract secondary structure information from the molar ellipticity values (**Table 5.11**).

Table 5.11: *The contribution of α-helices, β-sheets, β-turns, and unordered (random coil) secondary structures to the molar ellipticity of CSM extract samples as compared to the native CSM protein and a heat-denatured CSM protein from reference [243].*

Sample	α-helix	β-sheet	β-turn	Unordered
1	52 %	20 %	8 %	20 %
2	53 %	25 %	7 %	16 %
3	51 %	28 %	5%	16 %
4	52 %	27 %	6 %	16 %
5	36 %	24 %	20 %	21 %
6	60 %	16 %	6 %	18 %
7	59 %	18 %	7 %	16 %
8	53 %	21 %	7 %	19 %
9	44 %	31 %	7 %	17 %
Native CSM protein (pH 7) [243]	43.6 ± 0.3 %	10.3 ± 0.1 %	15.5 ± 0.2 %	22.6 ± 0.2 %
Heated CSM protein (100 °C, pH 7) [243]	19.0 ± 0.3 %	33.2 ± 0.3 %	18.9 ± 0.3 %	28.3 ± 0.3 %

The conversion to molar ellipticity (*[θ]*) allows for a direct comparison of the various pH conditions between samples 1 – 9 by eliminating the differences in protein concentration (**Figure 5.18**). Comparisons of the secondary structures across various pH values reveal fluctuating contributions depending on the pH of the sample. Measurements of the secondary structures in native and heat-denatured CSM protein from other studies reveal how the secondary structure might be expected to change between native and denatured forms (compare purple and green symbols in **Figure 5.19**) [243]. The secondary structures present in the native protein listed by descending order of percentage are: α-helix (43.6 %), unordered (22.6 %), β-turn (15.5 %), & β-sheet (10.3 %). In the denatured protein this order becomes: β-sheet (33.2 %), unordered (28.3 %), α-helix (19.0 %), β-turn (18.9 %). Interestingly,

while small increases in unordered (+ 5.7 %) and β-turn (+ 3.4 %) structures occur upon denaturation, the largest changes are a drop in α-helix content (- 24.6 %) and an increase in β-sheet content (+ 22.9 %). Therefore, it is the change in α-helix and β-sheet contents which are tracked across CSM protein solutions at varying pH values to attempt to assess effects of pH on the protein denaturation state.

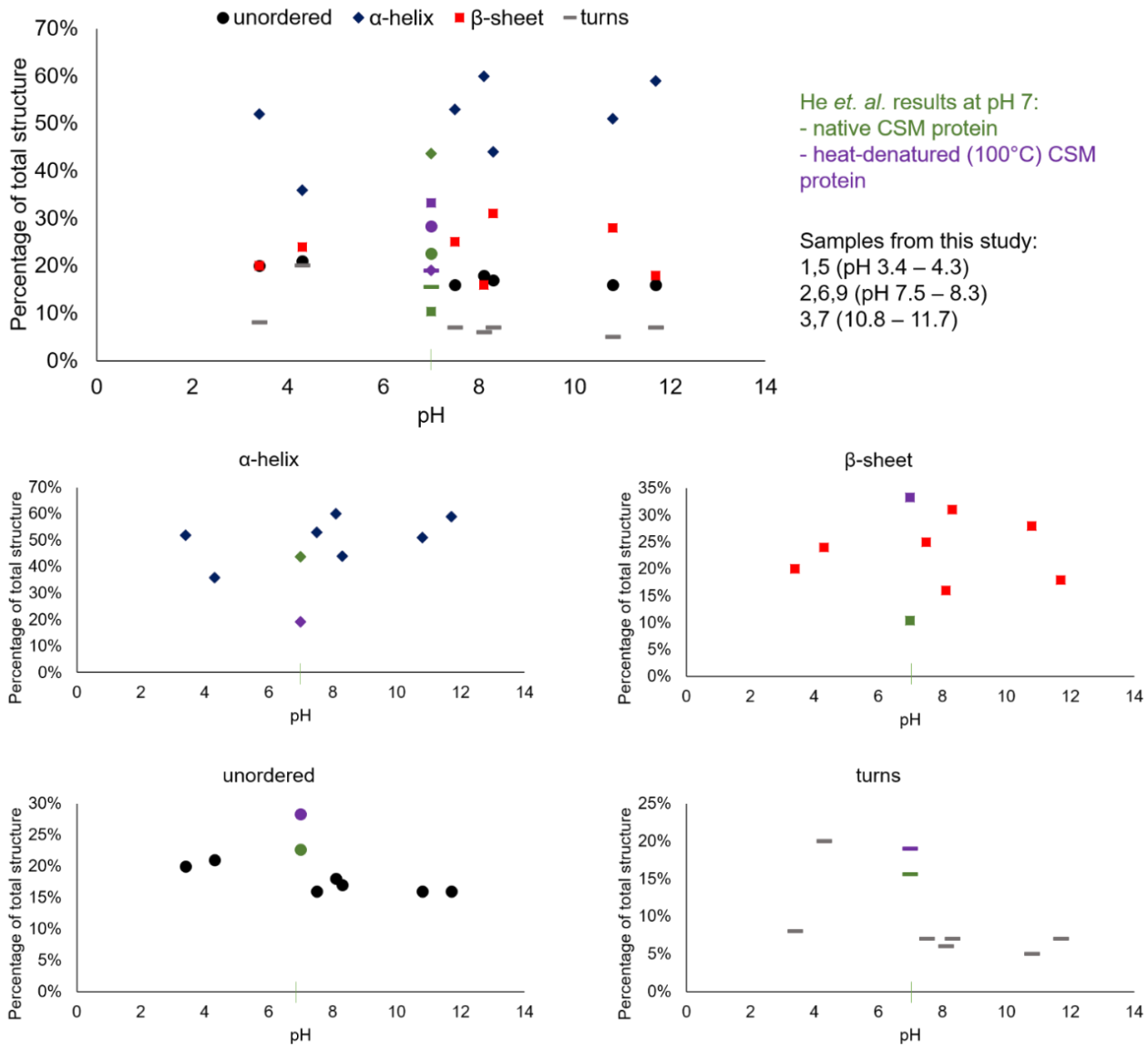

Figure 5.18: *Percentages of α-helices, β-sheets, β-turns, and unordered (random coil) secondary structures in CSM protein samples from pH 3.4 to 11.7. A comparison to literature results from reference [243] is shown at pH 7 where the native CSM protein is represented in green and the heat-denatured CSM protein is represented in purple*

Measurements of protein secondary structure in CSM protein solutions from this study are difficult to compare with the results from He *et al.* While the α-helix and unordered contents remain mostly similar to the native CSM protein in other studies, the β-sheet contents are intermediate between the

two states (**Figure 5.19**). No clear pH-dependent trends are evident except for a subtle drop in unordered structure with increasing pH values. However, even at low pH values (near the isoelectric point) no CSM protein solution in this study demonstrated a percentage of unordered structure approaching 30% nor an α-helix content as low as the 19.0 % as seen in the heat-denatured sample from He *et al.*. The sample prepared at pH 4.3 demonstrated the greatest departure from native conformations with the lowest α-helix content (36 %) and a high β-turn content (20 %). The impact of pH on protein secondary structure and denaturation state is probably minimal compared to other conditions, such as heat, which have shown more dramatic influences on secondary structure.

In addition to pH, the effect of salt ions on the CD of CSM extract was briefly investigated by comparing samples 4 and 8 (containing $CaCl_2$) to samples 9 and 3 (similar alkalinity, no $CaCl_2$) to investigate the effect of Ca^{2+} ions (**Figure 5.19**). Small changes were observed with a concentration of 20 mM $CaCl_2$, β-sheet content dropped slightly while unordered structures increased a small amount. These changes, however slight, may indicate an effect of divalent cations on the secondary structure of the protein that should be investigated further. One explanation for this effect is that Ca^{2+} ions may interfere with regular structures such as the β-sheets, promoting the slight unfolding of the protein *via* ionic interactions with negatively charged residues such as glutamic acid and aspartic acid. This effect could be heightened when the protein is first exposed to alkaline pH values.

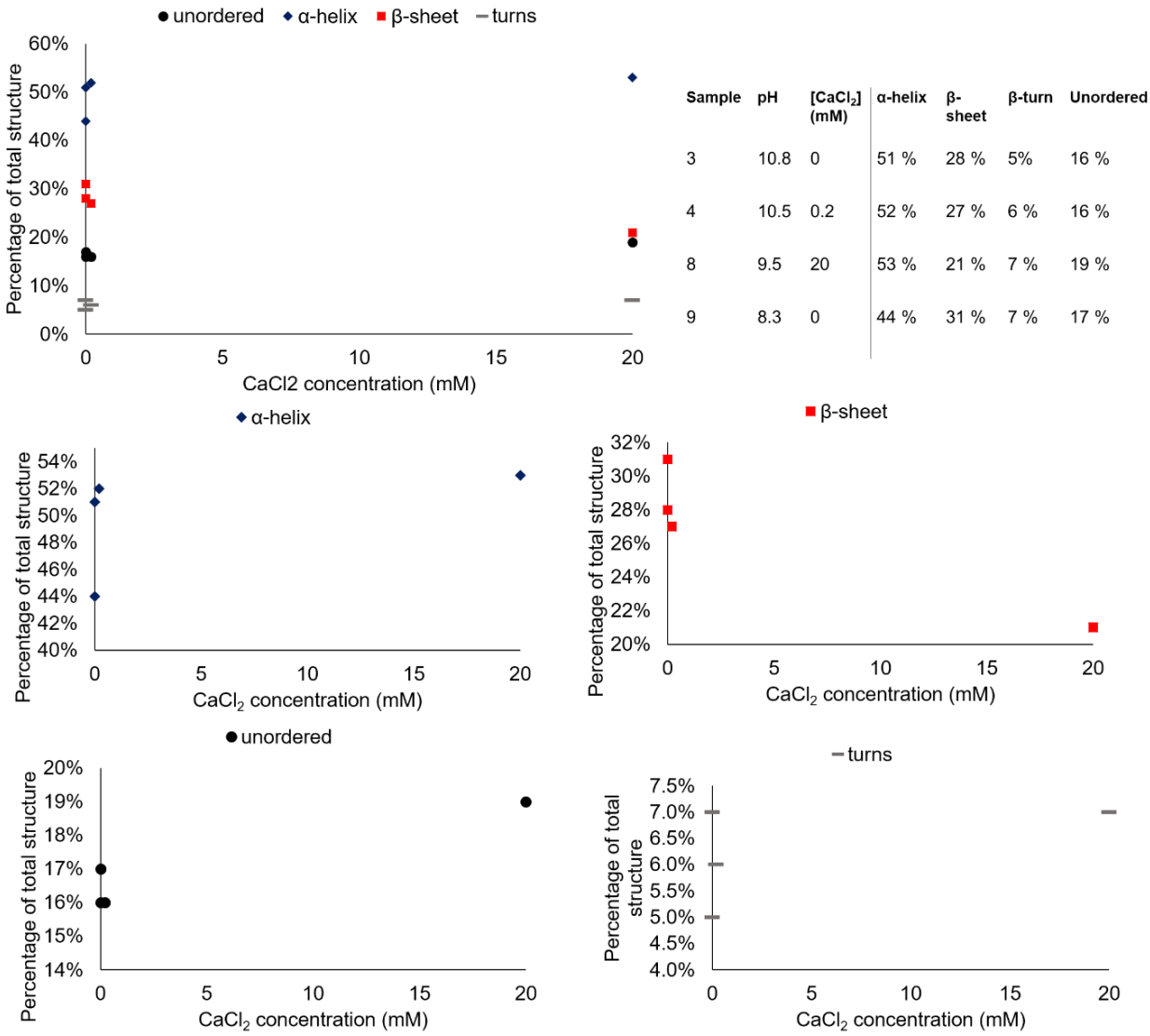

Sample	pH	[$CaCl_2$] (mM)	α-helix	β-sheet	β-turn	Unordered
3	10.8	0	51 %	28 %	5%	16 %
4	10.5	0.2	52 %	27 %	6 %	16 %
8	9.5	20	53 %	21 %	7 %	19 %
9	8.3	0	44 %	31 %	7 %	17 %

Figure 5.19: *Percentages of α-helices, β-sheets, β-turns, and unordered (random coil) secondary structures in CSM protein samples with a [$CaCl_2$] of 0.0, 0.2, or 20 mM*

5.5.2. Protein charge

Proteins are chemically complex macromolecules which contain a certain quantity of electrostatically charged moieties along their peptide chain. These charges collectively endow the protein molecule with an overall electrostatic charge, influencing its properties in solution, most notably solubility. Charge will also influence the interaction of proteins with other molecules in solution and influences the gelation process in proteins (refer **Section 2.2.3.2**). The charge is influenced by the pH of the solution, where the isoelectric point of a protein (or mix of proteins) is the pH value at which the protein (or collective proteins) carries an overall charge of zero (though amino acids within the protein may carry a mix of opposing charges that sum to zero charge). The effect of solution pH on the overall charge of the CSM protein extract is investigated in this Section using native polyacrylamide gel electrophoresis (native-PAGE). Understanding of the overall molecular charge on the canola proteins over a range of gelling and non-gelling pH values, aids a chemical description of the gelation mechanism.

SDS-PAGE is a protein separation technique (previously introduced in **Section 5.3.3**) that is usually used to separate proteins according to their molecular weight. Electrophoresis requires that the subject molecules carry an electric charge, and this is usually achieved in proteins by binding a negatively charged detergent (*e.g.* sodium dodecyl sulphate (SDS)) to the denatured protein along the entire length of the molecule. The binding of SDS to the protein endows it with an overall negative charge. The electrophoresis is then run by applying a negative to positive electromagnetic field (EMF) on the samples, and the denatured protein molecules coated in SDS, migrate towards the anode (positive pole) at migration rates dependant on their size (or molecular weight). Native-PAGE however, can be used to investigate the intrinsic (native) charge and shape of a protein by removing the denaturing (heating) stage of the sample prep and not using the negatively charged detergent (SDS). Under these non-denaturing conditions, the technique relies on the intrinsic electrostatic charge of the molecules for mobility across the EMF. Protein structure will also influence mobility in native-PAGE gels.

The samples prepared for native-PAGE analysis in this study had a final concentration of 6.67 mg of extract per mL of sample buffer. They were prepared from CSM extract batch 11, at pH 6, 8 or 10 and

with replicates subject to heat-treatments or 20 mM of $CaCl_2$ to imitate conditions used to gel the protein in later studies (summarised in **Table 5.12**). Each set of samples with the same pH were run in one gel and with a running buffer prepared at the appropriate pH. The gels were loaded with each sample in triplicate (*e.g.* lanes 1, 5, 9 for the un-heated, $CaCl_2$-free samples) using a range of sample volumes (*e.g.* 5, 10, 20 µL for the pH 10 samples) to ensure a protein band of appropriate intensity could be detected in the gel result.

Table 5.12: *Sample preparation conditions for native-PAGE analysis of CSM protein extract*

pH protein solution	Heat	$CaCl_2$	pH sample buffer	Gel	pH running buffer	Quantity loaded (µL)	Lanes
10.07	-	-					1, 5, 9
10.07	10 mins, 95°C	-	10.01	1	10.02	5, 10, 20	2, 6, 10
10.07	-	20 mM					3, 7, 11
7.99	-	-					1, 5, 9
8.14	10 mins, 95°C	-	7.96	2	7.98	10, 20, 30	2, 6, 10
7.90	-	20 mM					3, 7, 11
6.06	-	-					1, 5, 9
6.05	11 mins, 95°C	-	5.97	3	6.00	10, 20, 30	2, 6, 10
5.89	-	20 mM					3, 7, 11

Due to the non-denaturing conditions, the resulting gels show smears of protein content rather than discreet bands of set molecular weight seen in SDS-PAGE. The position of the leading edge of the smear and intensity of the smear provide information about the overall charge on the proteins. Each CSM protein sample may present different protein conformations and electrostatic charges due to the influence of different solution pH values, prior heat treatments, and the presence of Ca^{2+}. These factors therefore influence the migration rates during native-PAGE resulting in variations to band position and intensities. Samples subject to heating undergo unfolding of the protein structure, changing the conformation and exposing different amino acid residues to the surrounding solution. A comparison of the heat-treated samples across varying pH values allows for a crude evaluation of how heating may influence protein charge and shape in the gels later produced for aerogel manufacture. However, these conditions also influence the solubility of the protein. This limits the accuracy of quantitative comparisons of the protein bands. The actual concentration of dissolved protein content

in the pH 6 samples is expected to be less than 6.67 mg/mL due to the limited solubility of the extract at acidic pH values. However, insoluble protein which has precipitated as large aggregates may remain as a concentrated band at the top of the lane due to the impeding size and lack/reduction of electrostatic charge.

Resulting gels from the native-PAGE analysis demonstrate strong protein smears in the pH 10 samples, less intense but still visible smears in the pH 8 samples, and no clear smears but some precipitate at top of gel in the pH 6 samples (**Figure 5.20**).

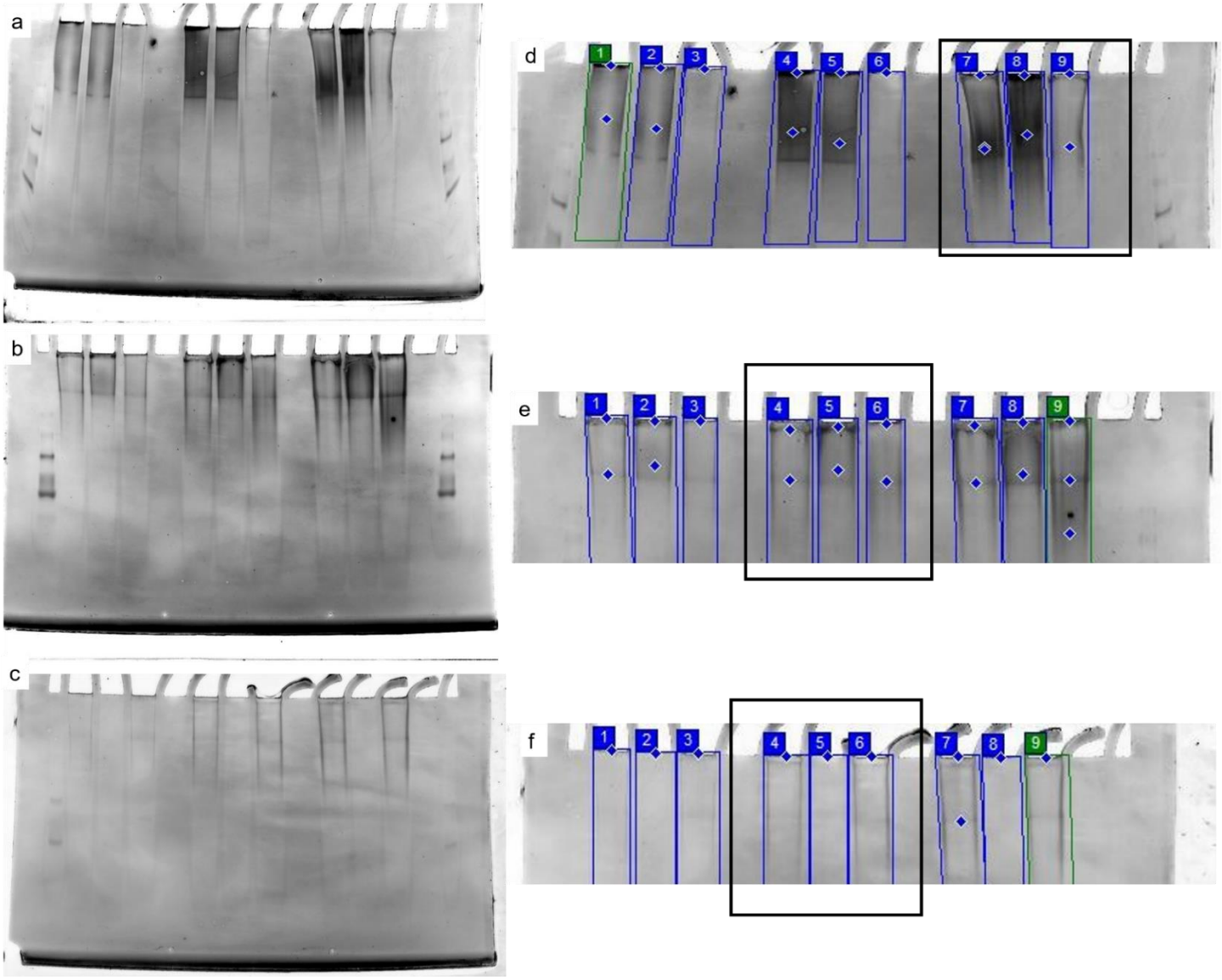

Figure 5.20: *Native-PAGE gels* ***(a-c)*** *overlain with lane and band markers* ***(d-f)*** *for analysis. Gel 1 at pH 10* ***(a & d)****, gel 2 at pH 8* ***(b & e)****, and gel 3 at pH 6* ***(c & f)***

The EMF on the native-PAGE is negative to positive, therefore proteins which carry an overall positive or zero charge, will not migrate to the anode and will remain at the top of the gel. The conditions for most of the samples were alkaline and therefore encourage negatively charged groups on the proteins (*e.g.* the anion glutamate is favoured in neutral to alkaline conditions over the protonated glutamic acid or the zwitterionic form). The results seen in **Figure 5.20** reflect this with a significant loss in negative charge occurring from pH 8 to pH 6. The position in mm of the leading edge of the main 'band' or smear is identified and the relative quantity of protein in the smears is calculated using image analysis software: ImageQuant (see **Section 4.1.1**). A smaller band of protein appears at the top of the gel lanes in many of the samples (position < 2 mm from top) showing that some of the protein content was unable to migrate in the native-PAGE, due to lack of negative charge and/or size (*e.g.* aggregation to large particles).

A comparison of the position and intensity of these two protein bands from the nine samples clarifies the effect of the pre-treatments and pH on the protein charge (**Figure 5.21**). While native PAGE is not generally used as a quantitative measure of protein (*e.g.* the quantity of protein solubilised at each set of conditions is not known, molecular weights cannot be determined),some comparative information may be gleaned from the relative amounts of migrated protein as determined by image analysis of total fluorescence in each 'smear'.

The main protein band (or smear) is of higher intensity and travelled further towards the anode in the pH 10 samples. A reduction in quantity and migration distance is seen at pH 8, while no protein migrates at pH 6 (protein detected down the sides of each lane in **Figure 5.20** is ignored as it has not migrated through the polyacrylamide gel). These results indicate the CSM extract protein begins to lose its negative charge around pH 8 and is neutral or positively charged once a pH of 6 is reached. These results are complemented by the observation that insolubility and protein aggregation begin from pH 7 as the pH is dropped and is a significant problem at pH 6 and below. Neutrally charged and/or misfolded protein molecules are more easily aggregated (provided driving forces such as exposed hydrophobic residues are present). Aggregation of like-charged molecules is not favoured as they repel one another. The intensity of the non-migrated protein band near the top of the lanes is

highest in the pH 8 samples, suggesting that the protein at this pH was still soluble (and therefore present in the aliquot loaded on the gel) but had a much reduced or absent negative charge. The pH 6 samples display some non-migrated protein (at top of lanes) though it is less than at other pH values, likely due to the difficulty in solubilising the extract at this pH (less protein loaded onto gel).

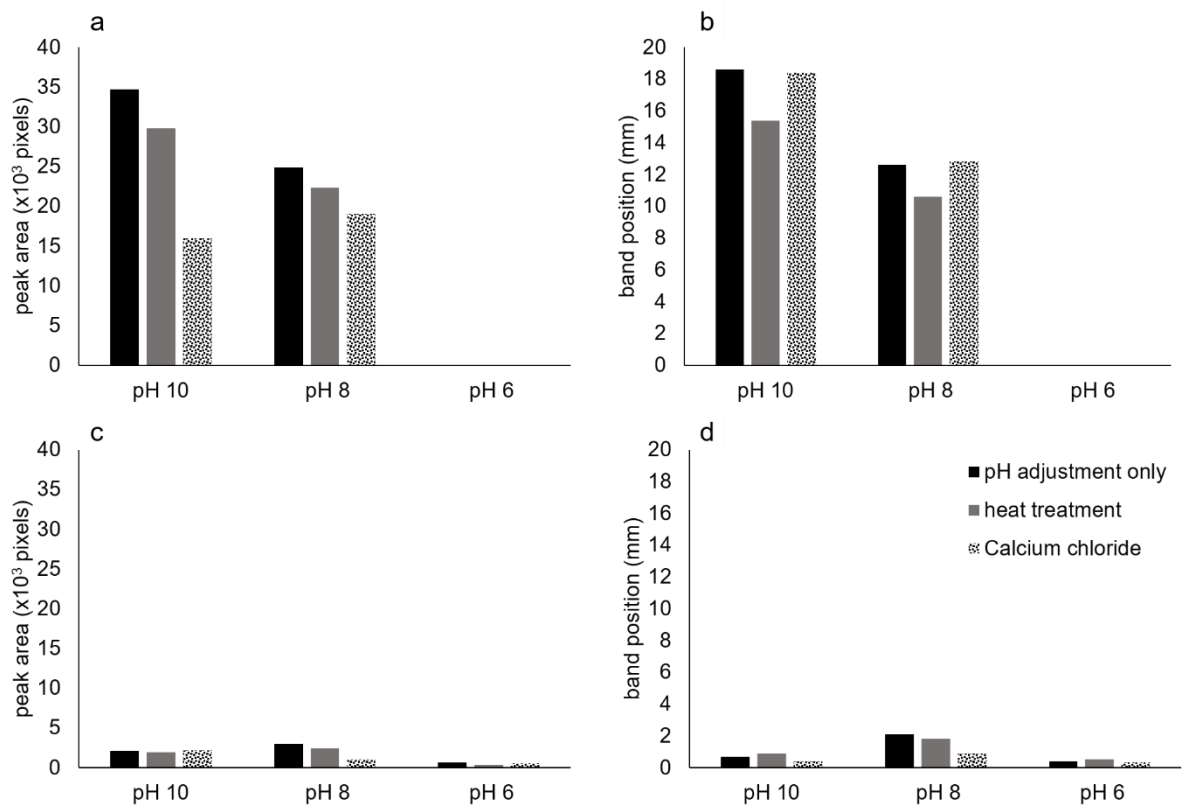

Figure 5.21: *A comparison of CSM protein migration in native-PAGE across varying pH values. The major band* ***(a-b)*** *and the non-migrated protein* ***(c-d)*** *are analysed for intensity* ***(a & c)*** *and position down the* ***gel (b & d)***

Heating of the protein, regardless of pH, reduced the intensity of the protein bands and reduced the migrated distance. This is an indication that the protein has changed in conformation and/or charge following the heat treatment, likely due to the exposure of hydrophobic residues during partial or complete denaturation of the structure. Denaturing conditions and exposure of hydrophobic residues generally facilitates protein aggregation and gelation (see **Section 2.2.3.2**). The change in conformation afforded by the heat-denaturation of a protein often is the likely explanation for the reduction in migration distance seen in the heated samples. Aggregated molecules present a larger surface for migration through the polyacrylamide gel and are inhibited more during the PAGE, with respect to molecules of similar charge but smaller size.

Finally, the exposure to 20 mM of Ca^{2+} is expected to reduce the overall negative charge on the CSM protein as the negatively charged groups are engaged in ionic bonding with Ca^{2+}. This effect is seen in the major protein band at both pH 10 and 8 as the quantity of migrated protein is decreased in the Ca^{2+} samples. The distance these bands migrate appears unchanged and probably indicates that the entire population of protein molecules in the samples was not saturated with Ca^{2+} at the concentration used.

The investigation into the effect of Ca^{2+} suggests a promising set of conditions for subsequent investigations into CSM protein gelation, as the native-PAGE results indicate Ca^{2+} ions have indeed bound to the protein. Ca^{2+} ions could therefore be implicated in inter-molecular ionic bridging for facilitated gelation in CSM protein. The effect of a reduced overall negative charge at alkaline pH values in both the heated and Ca^{2+} samples also suggests promising conditions for gelation. A controlled level of protein aggregation is required for particle-based gelation while partial solubility (CSM protein solubilises in alkaline pH) must still be maintained to prevent complete precipitation. The combination of alkaline pH values with some denaturation, charge shielding, or intermolecular ionic bonding, creates these conditions necessary for a particle-based gelation of CSM protein.

5.6. Summary

The investigations of this Chapter demonstrate that canola protein is an extractable material from an accessible co-product (canola seed meal) of the oilseed industry. Extraction can be done using pH solubilisation methods ('alkali-acid' extraction) or salt buffer and ultrafiltration methods ('salt-PMM' extraction) but is faster, cheaper, and higher yielding when the alkali-acid extraction technique is used. The resulting extract has lower purity compared to other studies, however both yield and purity may be improved with optimisation of the extraction protocol.

The amino acid profile of the extract, like other canola and rapeseed protein products, has promising nutritional potential, comparable to soy and milk proteins. The extract contains a variety of polypeptides or proteins which can be selectively concentrated and retained at various stages during the extraction process. Most of these varyingly sized polypeptides are revealed to be different multimers or subunits of the *B. napus* cruciferin protein, with minor contribution from napin and oleosin. The molecular weight range of most of these contributing polypeptides is between 10 and 30 kDa, though cruciferin multimers are present at up to 300 kDa (native hexamer structure) and larger aggregates of the protein are likely present in the precipitated extract.

The CSM extracts, and aerogels prepared from them, contain a variety of potential bioactive peptides in the form of cryptides. The detection of medically relevant and anti-pathogenic bioactive potential in the canola protein extracts and aerogels reveals they could be well-placed for unique bio-applicability in fields such as medicine, veterinary science, cosmetics, and food. Further investigation, such as quantification of *in silico* results, *in vitro*, and *in vivo* studies, would reveal the extent of these unique properties.

Finally, the CSM protein extract demonstrates changes in protein secondary structure and protein charge with simple modifications to the aqueous chemical environment of CSM protein solutions. The use of pH, heat, and calcium salts to manipulate solution conditions produces changes in the overall protein charge and secondary structure conformations of the protein. Some of these changes appear

conducive to macroscopic structural changes such as gelation of a protein solution and suggest that CSM protein-based gels could be achievable and tailorable using these processing parameters.

Chapter 6

6. Novel bioaerogels derived from Canola seed meal protein

6.1. Introduction

Aerogels are unique materials with intriguing and useful properties as reviewed in **Chapters 1 & 2**. The development of new types and forms of aerogels is focussed on improving the properties or efficiency of production of existing aerogels for commercialisation. However, there is also a burgeoning interest in new aerogels based on biopolymers, particularly if they can be made to be sustainable and environmentally-friendly (refer **Section 2.2**). Additionally, novel bio-based aerogels have also allowed for aerogel uses in new industries, such as in regenerative medicine as tools for tissue engineering, or in food products as colon-targeting delivery systems [244]. The biopolymeric-based aerogels have different morphologies, properties, and uses to those of their inorganic counterparts, with the added possibility of creating sustainable and biodegradable aerogels. Furthermore, the prospect of discovering new uses for novel aerogels through harnessing of unique chemical properties provides additional reasoning for the use of proteins and polypeptides in aerogel manufacture. Polypeptides and proteins contain varied chemical moieties and have been shown to preserve their biological functions for example, enzymatic action, despite being incorporated into a dry aerogel structure (refer **Section 2.2.3**).

The above motivations lead to the studies in this Chapter where the previously investigated canola protein extract is used as a basis for creating a range of aerogels (specifically cryogels). Canola protein is a compelling choice for novel aerogel structures (studied in **Chapter 5**) as: (i) it is easily extracted from an accessible co-product of a thriving oilseed industry; (ii) it has demonstrable propensity towards gelation using simple aqueous chemistry; and (iii) the subsequent aerogel will contain bioactive potential that could render medicinal, nutritional and/or anti-pathogenic qualities to the material. This Chapter describes the discovery that canola protein can be manipulated into aerogel-like structures using pH-controlled gelation and a freeze drying method. Some highlights of

this Chapter have been published in the journal article: “Fitzpatrick, S.E., *et al*, Novel protein-based bioaerogels derived from canola seed meal. Journal of Materials Science, 2020. 55(11): p. 4848-4863. [245]”. Additional investigations included in this Chapter are further compressive testing experiments, rheological studies of the gel precursors, brief thermal analyses of the aerogels, and a basic description of degradation behaviour of the aerogels in aqueous media. The development of the canola protein aerogels is complemented with studies into the effects of various pH and temperature controls on the resulting aerogel morphologies and properties, and with comparisons to other bioaerogels.

6.2. Experimental methods

The experimental materials and procedures for the techniques in this Chapter can be found in **Sections 4.1** & **4.3**, and are summarised in **Table 6.1**.

Table 6.1: *Summary of experimental techniques from Chapter 6 and the corresponding sections of Chapter 4 describing the experimental procedures*

Section (Chapter 6)	Technique	Section of Chapter 4 pertaining to this technique
6.3.1	Viscometric analysis	4.1.2
6.3.2	Rheometric analysis	4.1.3
6.4.1	Bulk density and shrinkage measurements	4.1.5
6.4.2	Scanning electron microscopy (SEM)	4.1.6
6.4.2	X-Ray microtomography (μ-CT)	4.3.2
6.5.1	Static compression testing	4.1.7
6.5.2.1	Differential scanning calorimetry (DSC)	4.3.3
6.5.2.2	Thermogravimetric analysis (TGA)	4.3.4

Additionally, the experimental method used to develop the first canola protein aerogels is described in the current Chapter due to the novelty of the development of canola protein aerogels. CSM protein gels were prepared using primarily a pH-controlled gelation method to produce a basic canola protein gel from which other processing variations could be introduced (see **Section 6.2.1)**. These variations are later studied for their potential to tailor the canola protein aerogels. Finally, freeze drying is used to produce aerogel structures from the canola gels (see **Section 6.2.2**).

6.2.1. Canola protein wet-gels

Materials

Canola seed meal (CSM) extract was produced according to the methods previously described in **Section 4.2.1** and the results presented in **Section 5.3.1**. Sodium hydroxide pellets (98.5 - 100 %), and hydrochloric acid (36.5 - 38 %) were obtained from Thermo Fisher Scientific (New Zealand). All solutions were prepared using reverse osmosis (RO) water (resistivity 18 MΩ) from a Milli-Q water purification system.

Protocol

The dried extract powder was dispersed in Milli-Q water to a final concentration of 10 wt% (unless otherwise stipulated) and adjusted to a pH value between the ranges of 6.0 and 12.0 using 2 M NaOH or 2 M HCl solutions. The aqueous protein dispersions were then mixed until homogenous and the final pH checked. Following adjustment, a selection of dispersions was also heat treated in a water bath at a temperature of 60, 70, 80, 90 or 95 °C for durations of 10, 30, 60, or 120 mins. This was achieved by transferring the stirred and pH-adjusted suspensions to a sealed Schott Duran® bottle and immersing in the water bath. Selected dispersions were also sonicated for 5 mins to remove air bubbles. The gels or dispersions were then transferred to an appropriate vessel for aerogel preparation or rheological analysis.

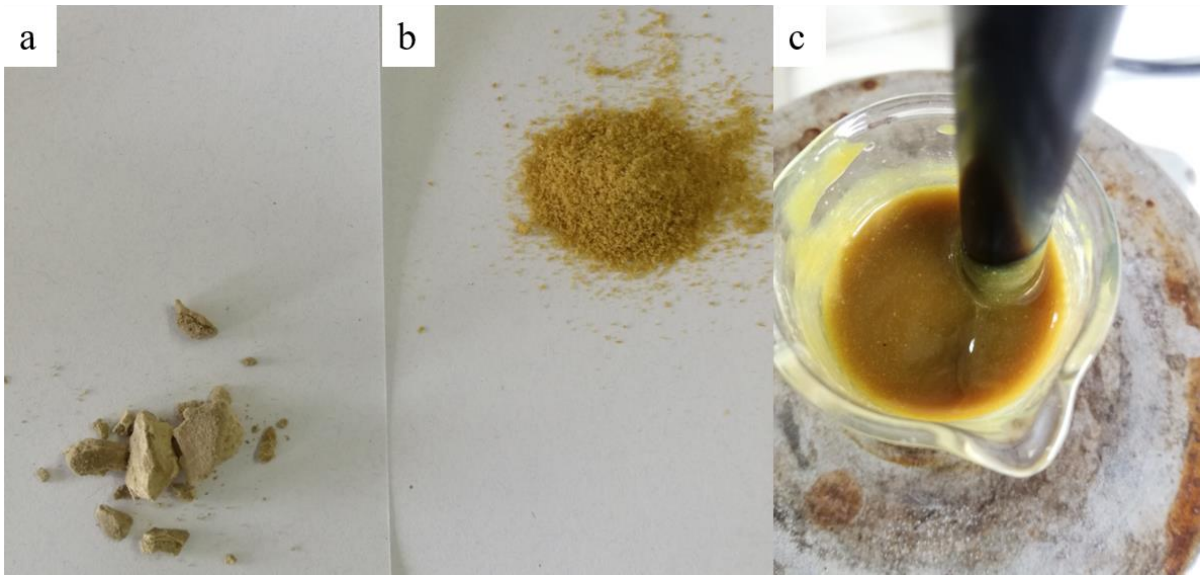

Figure 6.1: *CSM protein extract from the (a) PMM and (b) alkali-acid extraction methods; and (c) CSM protein suspended in water (10 wt%) during pH adjustment*

6.2.2. Canola protein aerogels

Upon completion of gel formulation, samples were then subject to freeze drying according to protocols described in **Section 4.1.4**. Briefly, the gels were transferred to an appropriate drying vessel and the open ends of vessels were covered with Parafilm™ film and pierced with a pin to leave small holes to allow the vacuum to permeate the sample during freeze drying. Prepared samples were stored at - 80 °C prior to freeze drying carried out on a Dura-Dry MP manifold dryer (FTS Systems) at 30 to 50 mTorr and room temperature.

6.3. Viscometry and rheometry of canola protein gels

Viscometric and rheometric analyses of the CSM protein gels allow for a quantitative comparison of gelation success across various gel preparations. Comparisons include measurements of gel stiffness, viscosity, and elasticity, which can also help to elucidate the molecular details of the gel network Observations during gel preparation revealed that the pH of the formulation was critical to the formation of stable gels and subsequent aerogels. Wet-gels prepared at a pH around 8 at ambient temperatures formed the most viscous wet-gels and gelled more rapidly than other pH values. In general, gels that were prepared with a pH of 8 to 8.5 did not flow upon inversion of the gel after 10 – 20 minutes post-pH adjustment (**Figure 6.2**). The suspension became darker in colour, less opaque, and flowed upon inversion at a pH > 9. Low pH values (pH = 3 – 6) resulted in incomplete solubilisation of the CSM extract powder and no gels were formed, but rather lumpy, precipitates suspended in the water. Interestingly, the CSM extract appeared to solubilise again at a lower pH values (pH = 2) and formed a viable aerogel after freeze drying. The pH-dependant gelation properties were investigated using viscometric and rheometric techniques.

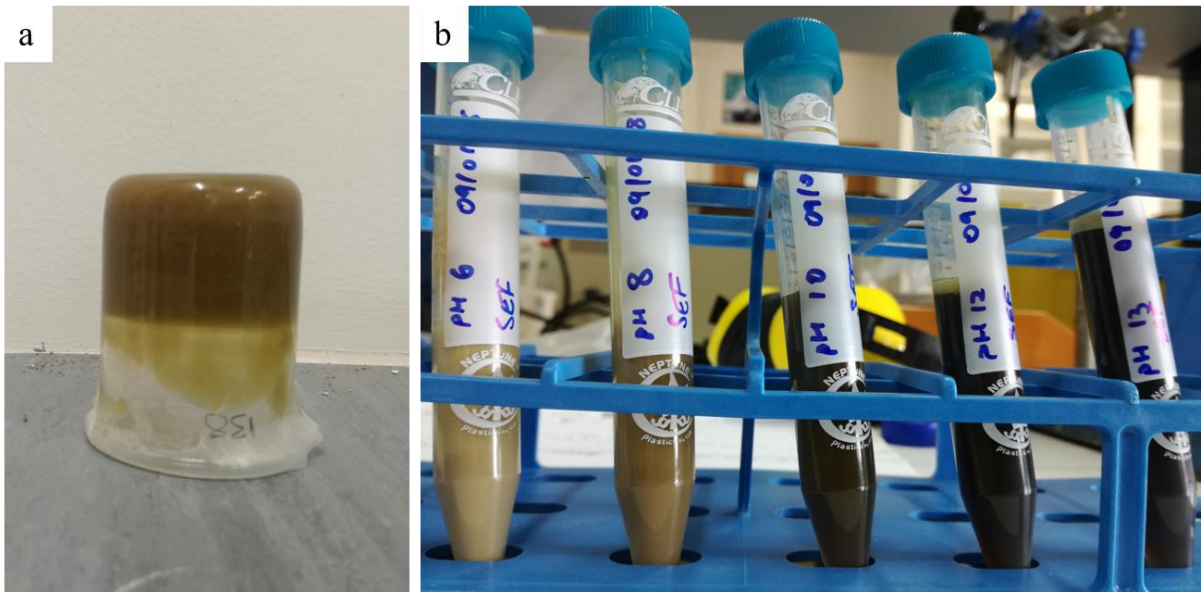

Figure 6.2: (a) *CSM protein gel prepared at pH 8.49 with beaker inverted.* ***(b)*** *CSM protein gels and suspensions prepared across a pH range of 6 to 13*

Viscometric analyses allowed for the measurement of the gel viscosities and the influence of changing shear rate (speed) on the viscosities. Viscosity and shear thinning behaviour could be compared between various gel formulations to reveal how pH and temperature treatments influenced the gels. A Brookfield DV-II+ Pro (Brookfield, MA, U.S.A) viscometer was used to collect brief viscometric measurements of canola gel formulations during the processing of the gels, prior to freezing in preparation for freeze dried production of aerogels. The viscometric data was collected across different formulations, where pH and heating conditions were varied. The viscometric data also provided a useful starting point for designing experiments on an oscillatory rheometer to follow.

Although the viscosity is measured relatively quickly using a viscometer during gel formulation, further rheometric data such as instantaneous measurements of shear moduli (including the storage and loss components) can be collected on an oscillatory rheometer. The rheometer can probe the shear stress in response to an applied shear strain and provide real-time measurements of the moduli. This allows the experiment to be run while variations are made to other parameters such as the shear strain amplitude, shear rate (frequency) or temperature. Strain sweep experiments were conducted to establish the critical strain level of the gel, above which there is a departure from linear viscoelastic behaviour. Thus, the strain amplitude dependence of the moduli was measured within the linear viscoelastic range (LVR). LVR is defined as the region in which the stress within the gel varies linearly with applied strain. Generally, the structure of the network within the gel is disrupted at strains beyond this linear range so rheometric analysis are generally conducted within the LVR [246]. The loss factor (tanδ) is the ratio of the loss modulus (G'') to the storage modulus (G') and provides information about the particle interactions in the gel or fluid. A tanδ less than 1 indicates a strong interaction between particles that leads to a more elastic (or solid-like) behaviour of the gel. In contrast, a high tanδ suggests that the particles are largely un-associated and flow is quite unrestricted (low G′) [247]. Rheometric measurements can be used to compare viscosities and gel stiffness (complex shear modulus (G*)) within the stable linear region of strain amplitudes after being identified in the strain sweep data. Beyond a simple viscosity comparison, the nature of the gel network can be further elucidated with a frequency sweep, also using a strain amplitude within the

LVR. The elastic modulus (G′) is independent of frequency in a solid elastic-like material but can be frequency-dependent when the material is more fluid-like (*i.e.* viscoelastic).

Initial rheometric data was collected on two samples (where gel ageing time was varied) using a Rheoplus/32 V3.61 (Anton-Paar, Graz, Austria) oscillatory rheometer to investigate the practicality of using the rheometer to study the canola wet-gels. Certain pH values (> 9) produce canola wet-gels with visibly reduced viscosities (see **Section 6.2**) and it was anticipated that these low viscosities may cause problems in gaining useful rheological measurements of the samples. Following this trial and method development, a set of refined rheometric data were collected on canola wet-gel samples across a range of gelation conditions using an MCR 302 oscillatory rheometer (Anton-Paar, Graz, Austria).

6.3.1. Viscometry

Owing to accessibility, viscometry measurements were conducted on CSM protein gel samples during formulation (prior to aerogel production) to provide fast 'on-the-spot' comparisons of gelation success *via* measuring gel viscosities. Samples investigated for viscosity were prepared at 10 wt% CSM protein at a pH value of either 8.0 ± 0.2 (three samples) or 10.0 ± 0.2 (a further three samples). One sample from each pH preparation was then subject to a heat treatment at 95 °C for 30 minutes, before being separated into two further samples for either transfer to 4 °C, or addition of $CaCl_2$. Viscosity measurements were collected on the heat-treated samples prior to these further treatments with refrigeration or salt addition. The remaining two samples at each pH value were measured for viscosity before addition of $CaCl_2$ was carried out on one sample at each pH value (pH 8 and 10). All gels were re-tested for viscosity following the final treatments with $CaCl_2$ or refrigeration. A summary of these treatments is found in **Table 6.2**.

Viscometric measurements are collected as single data points at each rotational speed (where sample volume, spindle geometry, and container size are set). Initial recordings were taken using a variation of spindle geometries coupled with various container sizes in order to determine optimal set-up of the equipment and gel sample volumes. Comparative data is therefore limited to measurements taken with

identical spindle geometries. Spindle geometries trialled included vanes (V 72 & 73) and discs (RV 4-7) of varying sizes (**Figure 6.3**). The larger spindle geometries (V 72, RV 4, RV 5) were problematic where the sample volume was insufficient to completely cover the spindle, while smaller geometries (V 73 and RV 7) would give torque readings (%) that were lower than the recommended minimum for optimal accuracy. The mid-range geometry RV 6 could be covered with the sample but operated too close to the edge of the vessel, causing turbulence that interferes with the measurements. These problems could have been resolved with larger sample sizes and vessels. The data was eventually collected using a V 73 geometry due to the limited amounts of CSM protein, although torque levels were below the recommended on the less viscous samples at a pH of 10. Therefore, the absolute values of viscosity may not be accurate, although the measurements still enabled a comparative analysis between the samples.

Table 6.2: *CSM protein gel samples measured on viscometer*

pH	Gelation Temperature (°C)	Time at temperature (mins)		[$CaCl_2$] (mM)	Storage temperature pre-test (°C)	Storage time (hrs)		Corresponding aerogel sample number/s
10.12	25	-	Viscosity measured	-	-	-		124
7.99	25	-	Viscosity measured	-	-	-		125
8.22	95	30	Cooled to RT and viscosity measured	20	25	-	Viscosity measured	126
				-	4	18	Viscosity measured	130
9.95	95	30	Cooled to RT and viscosity measured	20	25	-	Viscosity measured	127
				-	4	18	Viscosity measured	131
8.15	25	-	Viscosity measured	20	25	-	Viscosity measured	128
10.17	25	-	Viscosity measured	20	25	-	Viscosity measured	129

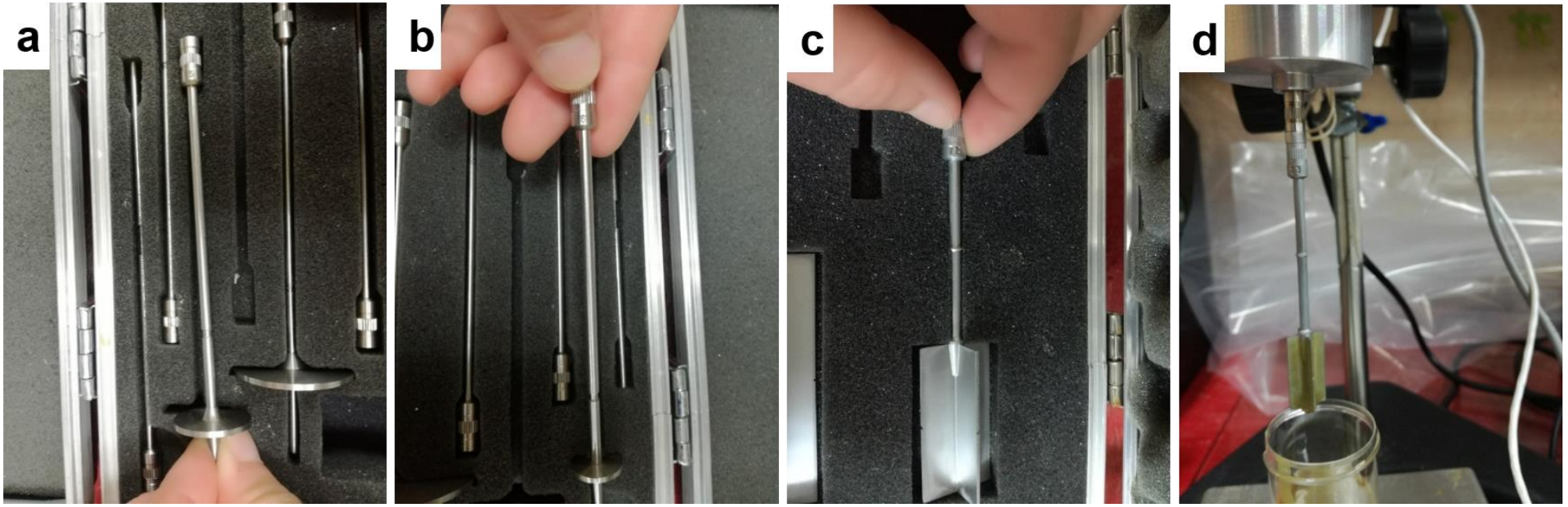

Figure 6.3: *Various geometries trialled for use on the viscometer with CSM protein gels including (a) disc RV 5, (b) disc RV 6, (c) vane V 72 and (d) vane V 73. V 73 was chosen for the CSM protein gel measurements*

The clearest observation confirmed by the viscometry experiments was that a pH of around 8 formed more viscous gels than those at pH 10. The viscosities measured in pH 8 gels were two orders of magnitude greater than at pH 10 (**Figure 6.4**).

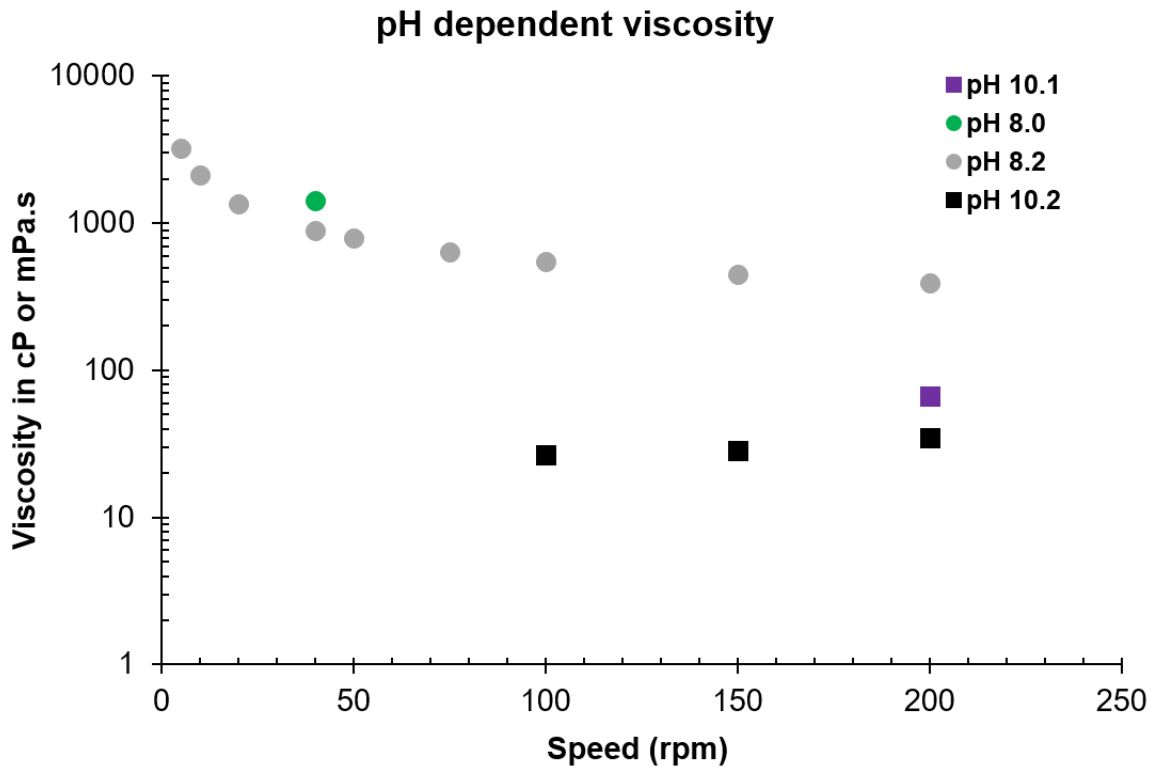

Figure 6.4: *Viscosity as a function of the spindle speed and pH for the CSM protein gels. No data on statistical variance is available since replicate viscosity measurements were not conducted*

Shear thinning behaviour was observed in the pH 8 gels but could not be confirmed in the pH 10 suspensions. Shear thinning has been previously observed to occur in canola protein gels [203]. A single measurement taken at pH 8.0 demonstrates a slightly higher viscosity than the sample at pH 8.2, suggesting that refined pH investigations (with replicates) are necessary to establish the exact pH value for the highest viscosity. pH values above 9 were generally detrimental to the gel structure, with more fluid-like behaviour being exhibited.

CSM protein gels were also subjected to a heat treatment after the pH adjustment (pH 8) by immersion in a water bath at 95 °C for 30 minutes and then cooled to room temperature prior to

viscometric analysis. The effect of the heat treatment was a visible increase in the viscosity of the CSM protein gels, both during heating and further upon cooling. The viscosity of the heat-treated gel was 8 times greater than the non-heated gel at higher shear rates and up to 12-fold greater at the lowest shear rate (**Figure 6.5**).

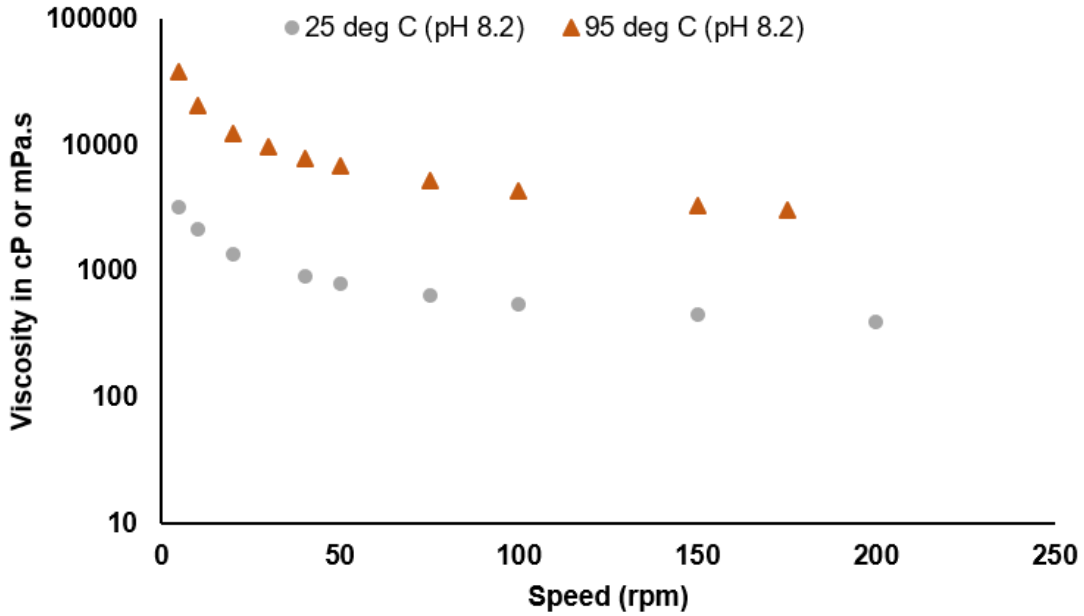

Figure 6.5: *Viscosity of the CSM protein gels at pH 8 as a function of the spindle speed and heat treatment. All viscosities were measured at room temperature. No data on statistical variance is available since replicate viscosity measurements were not conducted*

An increase of 1.8- to 2.8-fold in viscosity with heating was also detected in the gels at pH 10. However, the viscosities of all of the gels at pH 10 remained below 110 mPa.s, at least 3.5 times less viscous than the non-heated pH 8 gels (**Figure 6.6**). The measured viscosity in the pH 10 formulations were close to the minimum level of accurate detection by the viscometer, with torque dropping below 3 % at speeds under 100 rpm. Measurements where torque < 3 % lead to an overestimation of viscosity.

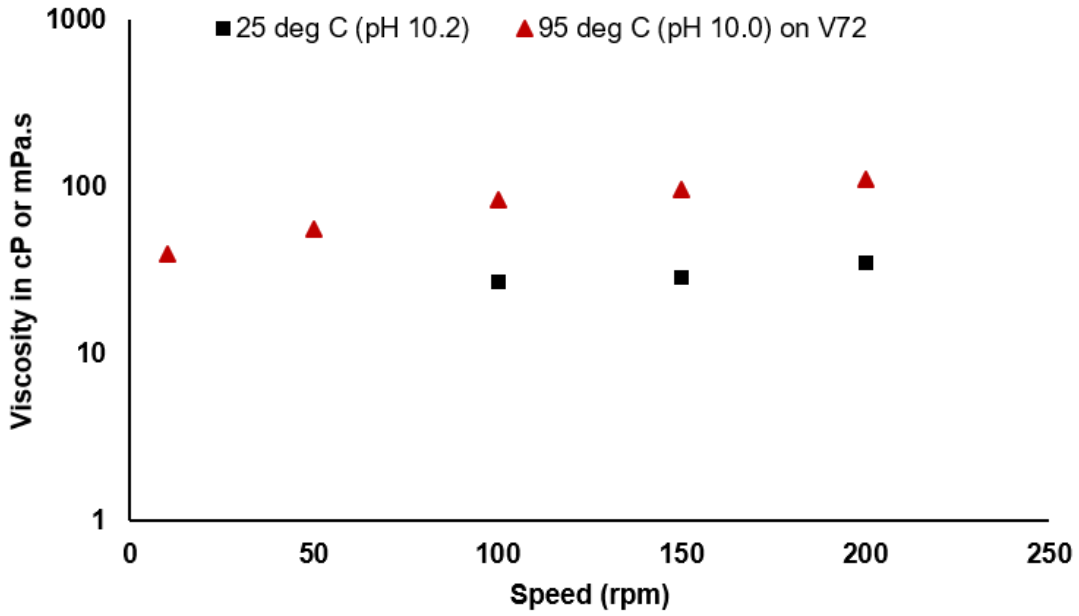

Figure 6.6: *Viscosity of the CSM protein gels at pH 10 as a function of the spindle speed and heat treatment. All viscosities were measured at room temperature. No data on statistical variance is available since replicate viscosity measurements were not conducted*

The effect of cooling on the heated gels was briefly investigated in viscometry measurements of refrigerated samples after these had been subject to the earlier heat treatment (**Figure 6.7**). Canola protein gels have previously demonstrated stiffening upon cooling from 98 °C to 20 °C [199] so it was expected that cooling from 25 °C to 4 °C could change viscosity further. Refrigerated heat-treated samples at pH 8 demonstrated a slight increase in gel viscosity (1.8 fold) as compared to the heat-treated samples that were not refrigerated. However, a similar increase could not be confirmed in pH 10 formulations with small differences at low viscosities fluctuating between increases and decreases dependant on shear rate. Since the viscosity investigations were carried out with one sample per series there is no statistical information available to indicate how these fluctuations may or may not be significant. Viscosity measurements were time-consuming as compared to subsequent rheometric analyses. Further investigations into the effect of cooling on gel viscosity were not conducted but remain an avenue for future rheometric studies with refined samples and repeated testing.

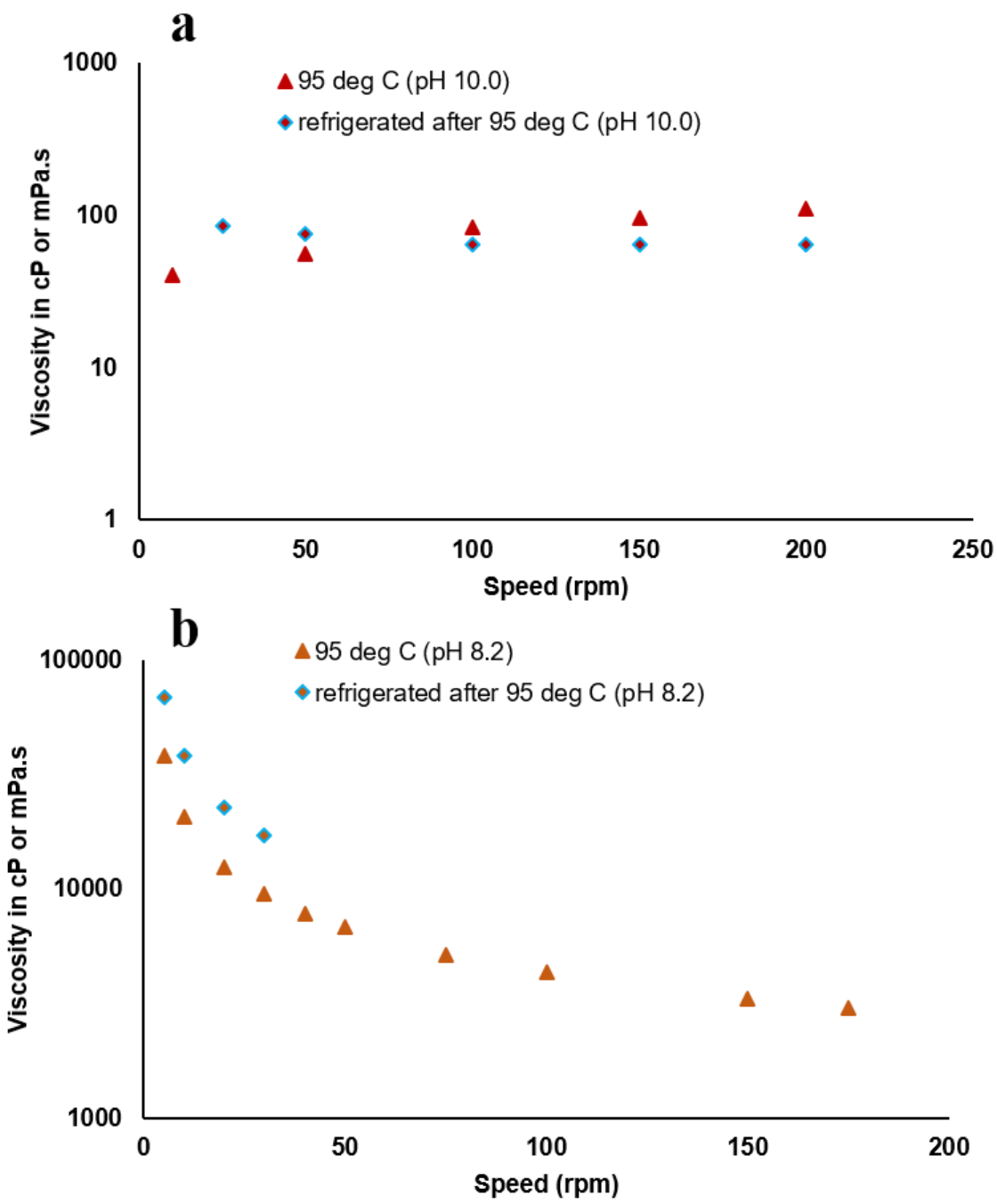

Figure 6.7: *Viscosity of the CSM protein gels at* ***(a)*** *pH 10 and* ***(b)*** *pH 8.2 as a function of the spindle speed and cooling treatment. All viscosities were measured at room temperature. No data on statistical variance is available since replicate viscosity measurements were not conducted*

6.3.2. Rheometry

Using rheometry, the CSM gels could be analysed for both gelation success (*via* basic comparisons of gel stiffness) and information that can help elucidate molecular details about the gel networks (such as the elasticity, stiffness, and shear thinning behaviour). Rheometric analysis of CSM protein gels and suspensions requires care and precision with sample loading and evaporation protection. Initial rheometric analyses conducted on a Rheoplus/32 V3.61 (Anton-Paar) oscillatory rheometer determined that the CP50-1 cone and plate geometry was the optimal geometry for ease of use with CSM protein gels and suspensions. Low viscosity suspensions at high pH values were more easily confined in the CP50-1 due to the small gap (0.102 mm). Further method investigations on an MCR 302 (Anton-Paar) showed that evaporation from the sample over time altered the measured viscosities and storage moduli (**Figure 6.8**). The addition of 2 drops (approximately 20 – 40 µL) of low viscosity mineral oil (p15(H) paraffinic hydrogenated white oil) to the edges of the trimmed sample after loading of the cone geometry were beneficial in preventing this evaporation of the water from a sample and stabilising the measurements taken over a 20 minute period at 22 °C. The oil tends to reduce the complex viscosity and storage moduli in the samples, seen as a decrease of 15 % at pH 8 (**Figure 6.8c**) and a decrease of 30 % at pH 10 (**Figure 6.8b**). However, at pH 6 the oil resulted in an increase of 250 % in the complex viscosity (**Figure 6.8c**) while samples without oil were stable across the 20 minute time sweep. Since the effect of the oil is documented in these recordings and the purpose of the rheometry was a comparative analysis across various gel formations, the use of the oil was determined necessary for the remainder of rheometric testing, including at pH 6 for a consistent methodology.

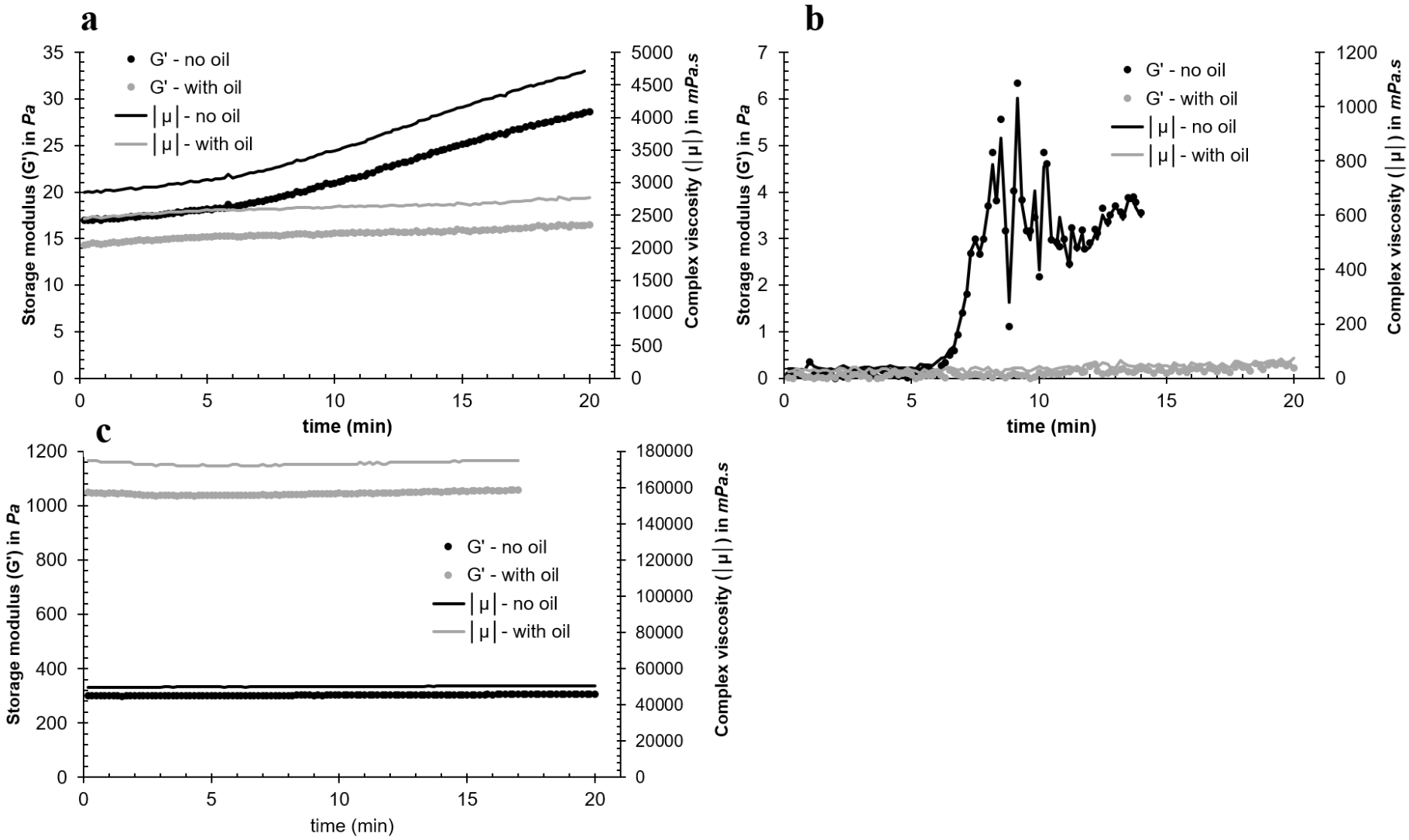

Figure 6.8: *Storage moduli and viscosities of CSM protein gels measured on an MCR 302 oscillatory rheometer at 0.1 % strain amplitude and 1 Hz for 20 minutes. Samples were prepared at pH 8 (a), pH 10 (b), and pH 6 (c) and loaded to the rheometer both with and without a protective layer of mineral oil*

Two samples with varied ageing times were briefly investigated for differences in viscoelastic behaviour during a strain amplitude sweep. The strain amplitude sweep of a viscoelastic gel is designed to probe the sample for the linear viscoelastic (LVE) range marked by a stable region of moduli measurements which ends with a crossover point of the storage and loss moduli, marking the critical strain. Measurements of a sample at pH 11.3 – 11.7 (low viscosity suspension) revealed some samples of very low viscosity do not display any solid-like nature ($G' > G''$) at the strain amplitudes tested and measurements are unstable where the moduli are below 1 Pa. Such behaviour was found in the 1-day-old pH 11.7 sample, while the pH 11.34 sample was aged sufficiently (18 days) to demonstrate a stable LVR in the strain amplitude sweep and provide some indication of a stable storage modulus (G' averaging 4 Pa) and critical strain (11 – 41 %) (

Figure *6.9*). However, there was significant variance across 6 replicates of the 18-day-old sample such that the standard deviation in the viscosities and moduli ranged from 23 to 64 % of the values recorded. Alongside the large variance in critical strain (11 – 41 %), this result showed the limitations of measuring samples with such low viscosities, even when a stable LVR is identified.

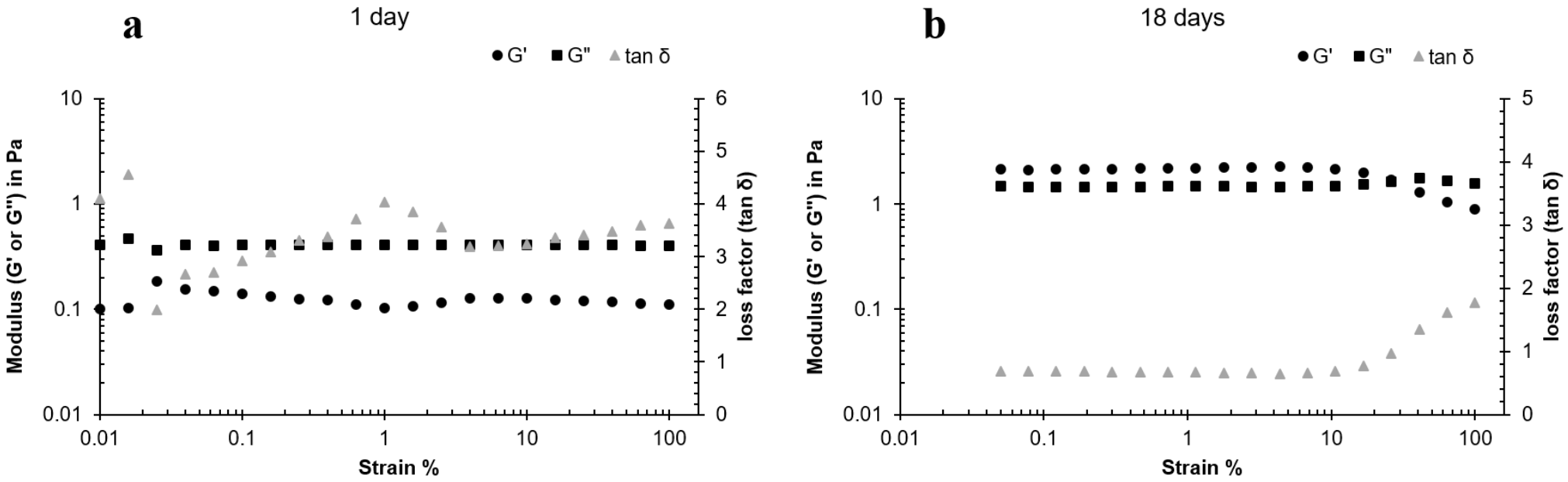

Figure 6.9: *Strain sweep at 10 rad/s (1.6 Hz) from 0.01 to 100 % strain amplitude on CSM protein suspensions at 10* wt% *and pH of approximately 11.5 after (a) 1 day of ageing (pH 11.67) and (b) 18 days of ageing (pH 11.34). One example plot is shown for each ageing variant from a set of 6 repeats*

The average storage moduli of the pH 11.5 samples tested in **Figure 6.9** are 0.39 Pa ± 0.48 Pa and 4.0 ± 2.5 Pa for the 1-day old sample and the 18-day old sample, respectively, where the error is the standard deviation of the 6 replicates. Such large standard deviations (123 % and 64 %) indicate the broad range of contributing values and undermine the reliability of the measurement. However, these measurements can provide an indication of the general range of values to be expected from these formulations.

Subsequent testing of gels prepared at other pH values revealed measurements of moduli and viscosity that were greater and therefore more stable, and problems with unstable data collection were limited to some pH 10 suspensions only (**Figure 6.10**). The data from **Figure 6.9** demonstrated that ageing the suspension can cause transition from a suspension ($\tan\delta < 1$ at all strain amplitudes tested) to a gel ($\tan\delta > 1$) for high pH formulations (pH > 10) and could be a used as a methodological variation to influence wet-gel strength and possibly aerogel properties. This finding is strengthened by literature evidence that canola protein gels experience increased viscosity with ageing [200, 203].

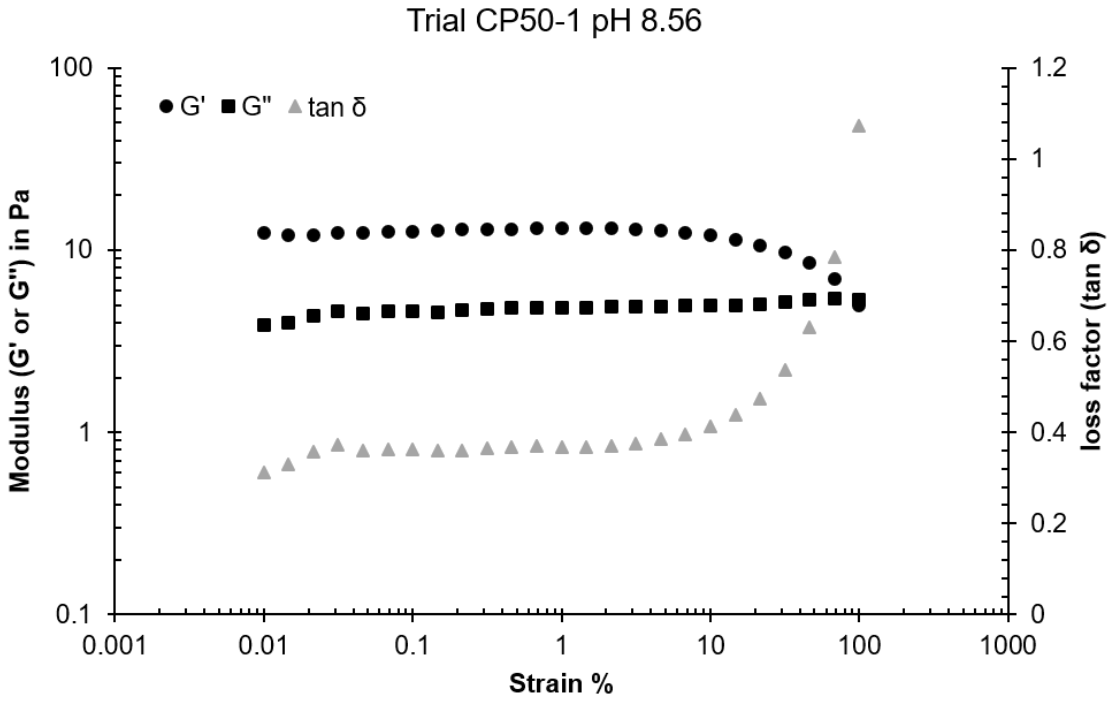

Figure 6.10: *Strain sweep at 10 rad/s (1.6 Hz) from 0.01 % to 100 % strain amplitude on CSM protein gel prepared at 10* wt% *and pH 8.56, and aged for 24 hours*

Rheometric strain sweep and frequency sweeps were used to investigate the effect of pH on the solid-like viscoelastic behaviour of the CSM protein suspensions and gels. Solid-like behaviour of the wet-gels may be linked to the mechanical behaviour of the dried aerogels, subsequently highlighting possible processing-structure-property relationships (see objective outlined in **Section 3.1.5**). Strain amplitude sweeps revealed stable LVRs could be identified in samples at pH 8.2 but not in samples at pH 9.3 (**Figure 6.11**). Suspensions of CSM protein prepared at pH 9.3 have visibly lower viscosities like those prepared at higher pH values in previous viscometry and rheometry experiments. A sample prepared at pH 6.2 was also analysed on the rheometer. This sample was difficult to prepare as the CSM protein extract did not readily dissolve or emulsify in the aqueous solution and lumpy precipitates remained in the final 'gel' sample. However, this sample was stable under rheometric analysis (**Figure 6.12**) and measured the highest G′ values (solid-like component) across the pH range tested.

The data collected from 3 replicates of each strain sweep and frequency sweep were averaged to permit a comparative analysis of the viscoelastic properties of the CSM protein gels. Initially, the strain amplitudes that correspond to the LVR of the strain sweeps, and a set of frequency values that represented a linear region of the frequency sweeps were determined. It was determined that strain amplitudes from 0.1 – 1.0 % (at a frequency of 1 Hz) were consistently in the LVR for each sample, providing 5 data points in this range for each experimental run that were averaged. These averages within a single strain sweep were then further averaged between the 3 repeats of each sample to provide comparative data.

Frequency sweeps may reveal tanδ values of 1 or greater if there is a crossover of the G′ and G′' values. As seen in viscometry measurements, the viscosity can also be frequency (strain rate)-dependent and must therefore be compared across samples where frequency and strain amplitude are kept constant. Frequency sweep data revealed most samples were dependent on frequency for the measurement of moduli, but a range of 0.1 – 1 Hz (at 0.1 % ε) was used to provide average values for each experimental run, which were also then averaged across 3 replicates. The standard deviations were calculated from the three replicates and used to indicate variability in the reported averages,

therefore these variations would not indicate the extent of frequency-dependence within one sample if all repeats behaved in a similar manner. Investigation of the frequency dependence was reported as the slope of the log-log plot of G′ and frequency. Slopes nearer to zero indicate more solid-like behaviour as the G′ is independent of frequency when there is no slope.

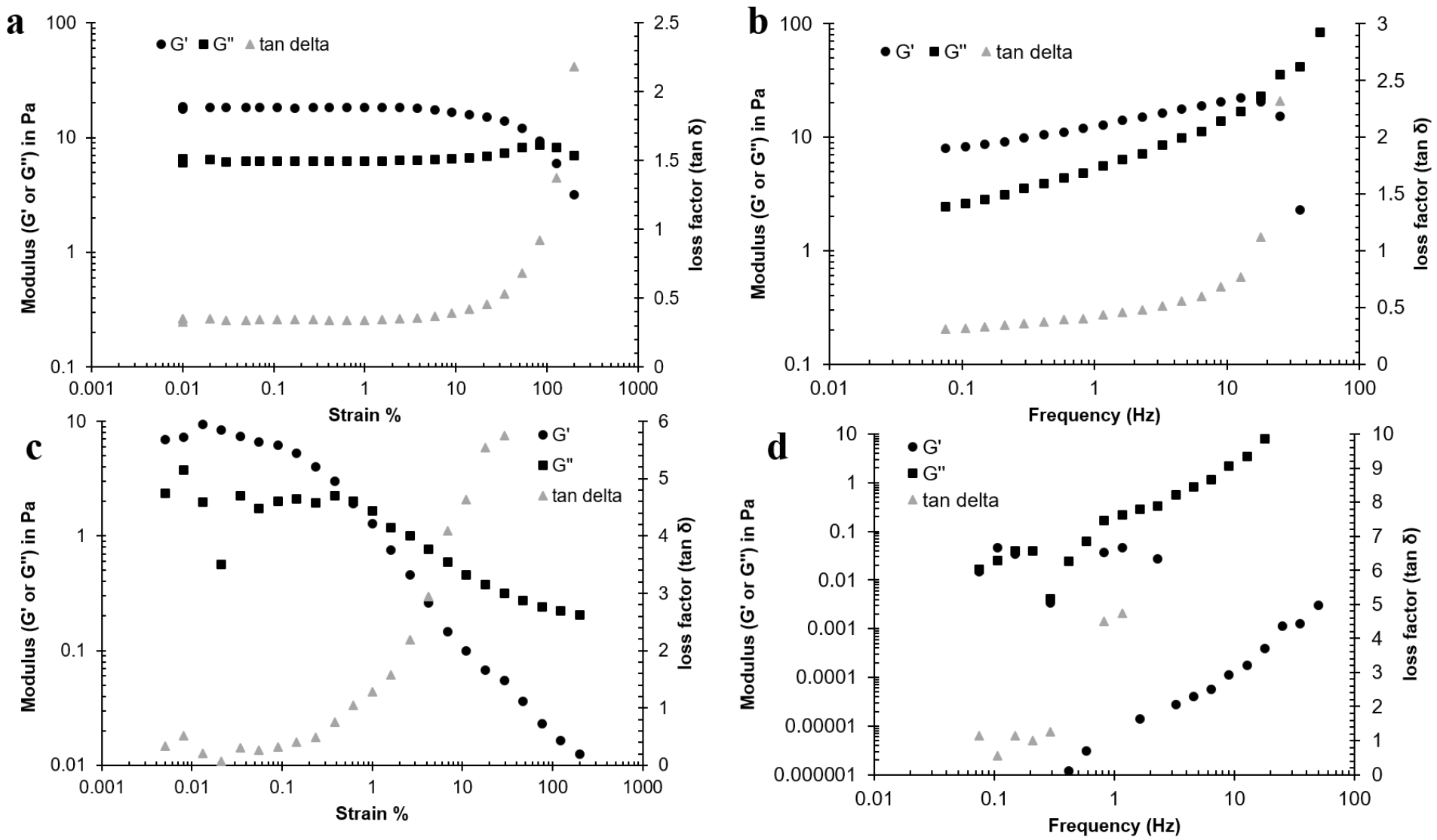

Figure 6.11: *Strain amplitude sweeps* ***(a & c)*** *and frequency sweeps* ***(b & d)*** *of CSM protein gels at pH 8.2* ***(a-b)*** *and pH 9.3* ***(c-d)***

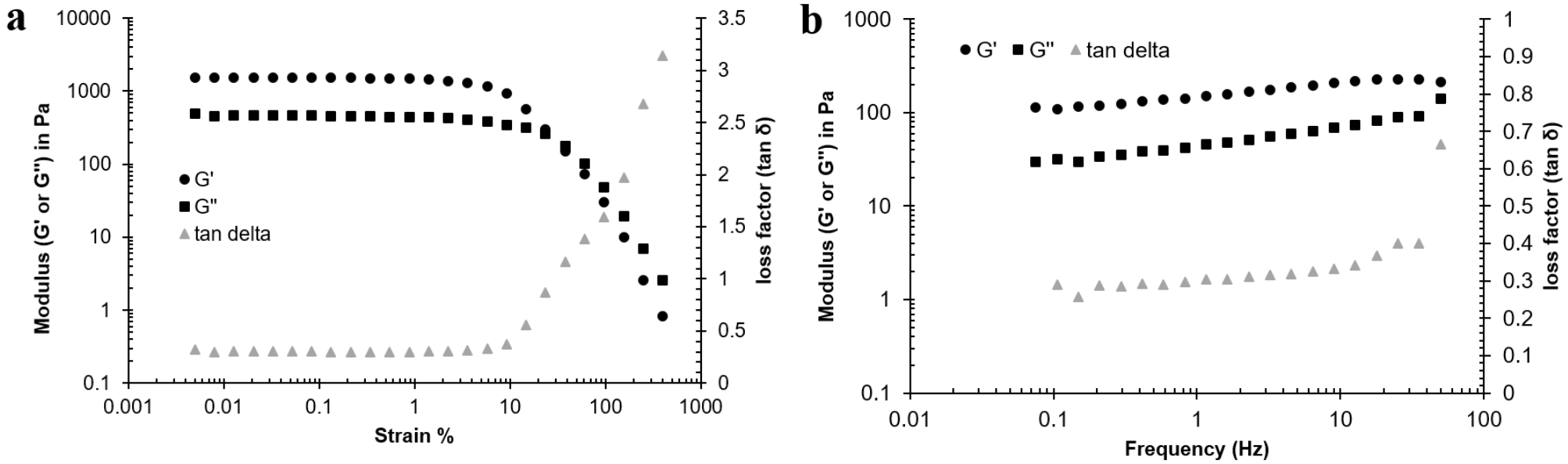

Figure 6.12: *Strain amplitude sweep (a) and frequency sweep (b) of CSM protein suspension at pH 6.2*

The objective of the rheometric analysis was to compare the viscoelastic properties of CSM protein gels across a range of pH values and across heat-treated and non-heat-treated samples at the same pH. Data from the strain amplitude sweep experiments was used to compare the gel viscosity, stiffness (G*), storage and loss components of the modulus, tanδ, and critical strain (% ε at tanδ = 1) of the samples.

The suspensions prepared above pH 9 revealed the lowest viscosities and gel stiffness as well as the greatest deviations across repeats due to reaching the lower limitations of measurement as discussed previously. Gels at pH 8 exhibited more stable measurements and an increase in viscosity and shear modulus of 7 times the measurements of the pH 9.3 samples. The pH 6.2 samples were 110-fold stiffer and more viscous than at pH but due to the inability for the CSM protein to solubilise or emulsify at this pH these samples are not described as gels. The high resistance to shear strain is likely a result of visible (therefore μm to mm scale in size) lumps of wet protein in the sample making them inappropriate candidates for aerogel production (**Figure 6.13**). Early canola protein gel research reports that high viscosity and high elasticity can be a result of protein insolubility (lumpy aggregates) rather than gel structural integrity (homogenous network structure), specifically in gel formulations at pH 6 as compared to those at pH ≥ 8 [203].

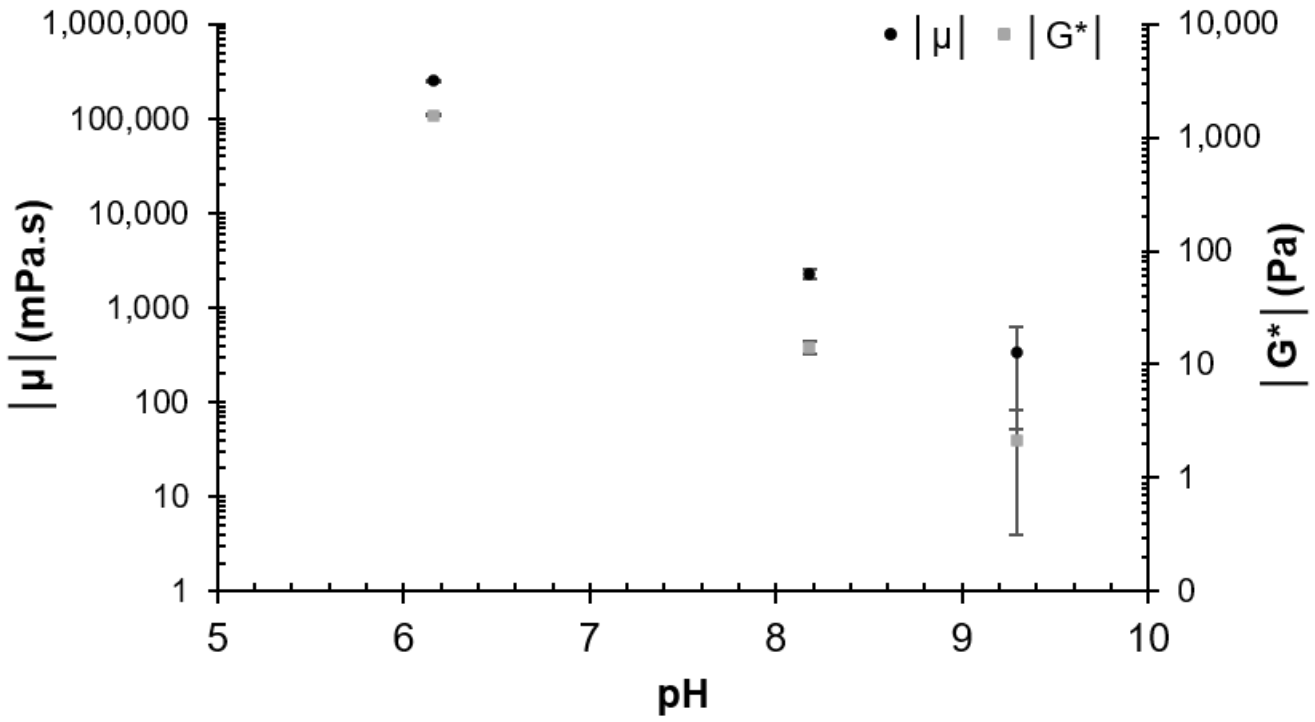

Figure 6.13: *Average complex viscosities (|μ|) and complex moduli (|G*|) calculated from the LVR of strain sweep experiments (0.1 – 1.0 % ε) in CSM protein gels. Error bars represent standard deviation where n = 3*

The pH influence on the shear modulus was further analysed by a comparison of the elastic and viscous components as reflected in G′ and G′’, respectively. The ratio of the loss to storage components (tanδ) showed that most of the pH 9.3 samples were more viscous than elastic (tanδ > 1) though a large variance in sample repeats meant it was difficult to accurately measure the absolute values of the storage and loss moduli. The samples at pH 8 and 6.2 were both clearly more elastic than viscous with loss factors consistently below 1 (0.3 – 0.4) in the LVR of the strain sweep (**Figure 6.14**).

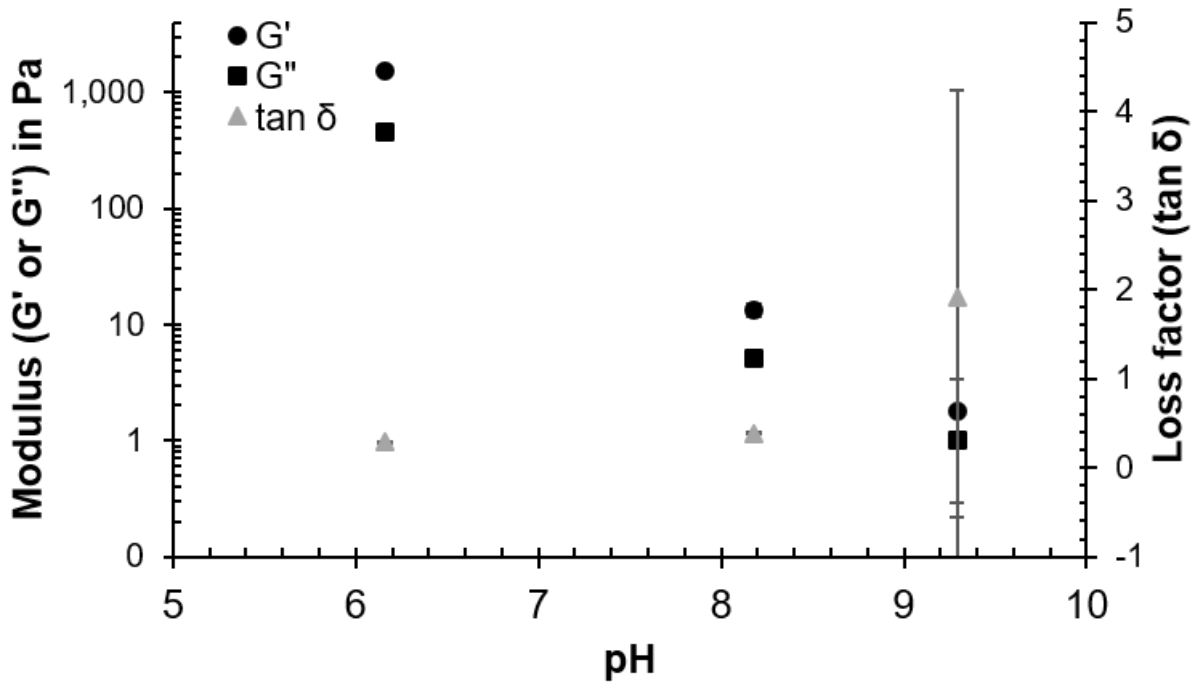

Figure 6.14: *Average storage moduli (G'), loss moduli (G"), and loss factors (tan δ) calculated from the LVR of strain sweep experiments (0.1 – 1.0 % ε) in CSM protein gels. Error bars represent standard deviation where n = 3*

The critical strain was determined in each repeat of the strain sweep as the strain at the point where tanδ = 1 (to within 1 decimal place). The rheometer collects the data from the strain sweep at the same strain values as it spans the amplitude range for the test, resulting in the exact same value for % ε at the crossover point. The tanδ at this point can vary, though it is the closest to a value of 1 in the data set. For example, the critical strain was measured as 97.3 % in all 3 repeats in the samples with a pH of 8.0, while this corresponded to a tanδ value of 1.06 (on average) (**Figure 6.15**). The individual repeats returned tanδ values of 1.051, 1.039, and 1.077 to give this average. The high consistency of these results meant that there was no deviation in the critical strain value measured across these 3 repeats and the pH 8 gels can be confidently said to have a critical strain of 97 %. At a pH value of 9.3 the critical strain was not conclusively determined (though represented in **Figure 6.15** as 4 %). This was due to the first two repeats returning critical strain values of 7.5 % and 0.6 % (a range of 6.9 % with an average of 4 %) while the critical strain was not detected in the third repeat as the tanδ was > 1 at all strain amplitudes measured. These results reveal the unstable nature of suspensions at pH 9.3

which are largely more viscous than elastic and therefore testing strain amplitudes are not small enough to detect the real critical strain.

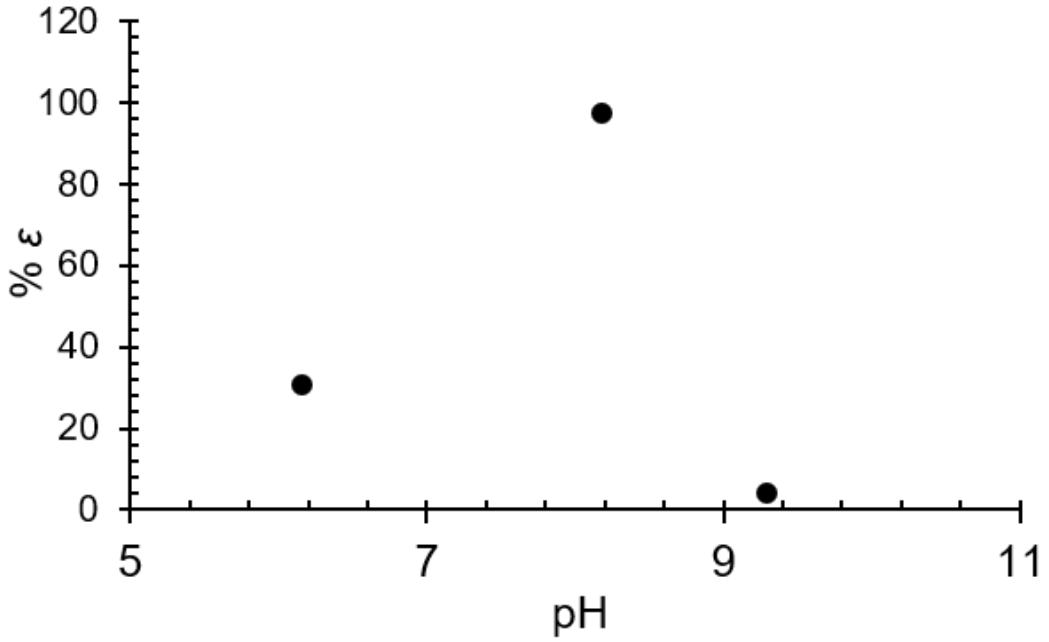

Figure 6.15: *Critical strain values recorded in CSM protein gels under a strain sweep at a frequency of 1 Hz*

The pH 6.2 sample was only tested once and delivered a critical strain of 31 % (**Figure 6.15**). This result supports the observation that pH 6.2 formulations were not gel-like as the pH 8.0 formulations are. A higher extent of elastic deformation in the pH 8.0 sample reflects a microstructure of an interconnected solid matrix. Such a matrix allows for greater recoverable deformation (higher critical strain) before flow behaviour occurs because molecules are bonded to surrounding molecules and this network of connectivity spans the entire sample. Large strains are required to break this network while isolated aggregates in non-gel like samples can flow past one another at lesser strain as molecule connectivity is confined to within the aggregate.

Following the identification of the LVR in strain sweep experiments, the strain was set to a value of 0.1 % and a frequency sweep experiment was carried out on the samples. These experiments revealed a slight tendency for CSM protein gels to destabilise or flow more easily (increasing tanδ) with increasing frequency (shear rate) (**Figure 6.11b,d** and **Figure 6.12b)**. This was known from earlier

viscometry measurements which demonstrated shear thinning behaviour in pH 8 gels. The variation in this response across the three pH values tested revealed that the true gels (pH 8) had a predictable shear thinning response with an identifiable *G′-G′′* cross-over frequency when tested at 0.1 % strain (approx. 25 Hz) (**Figure 6.11b**). At frequency values less than this value the slope of the log G′ – log f plot was 0.18 ± 0.01 (**Figure 6.16**). Comparison of this frequency dependence with the pH 6.2 formulation showed that the precipitated pH 6.2 sample had a lesser dependence on frequency with a slope of only 0.13 (no variance data available) (**Figure 6.16**). The likely explanation for the more frequency-independent pH 6.2 formulations is that the G′ is mostly a result of the individual precipitates that are solid in nature and therefore frequency-independent. In contrast, the pH 8.0 gels are more viscoelastic in nature (and consistently so) due to the even distribution of the aqueous medium in the gels. The pH 9.3 formulations presented with a tanδ > 1 for much of the frequency sweep and no discernible cross-over point. The average slope was – 0.8 with a deviation of 2.0, revealing the instability of these formulations (**Figure 6.16**). The lack of a gel-like structure in the pH 9.3 formulations meant no meaningful data could be extracted from the frequency sweep experiments.

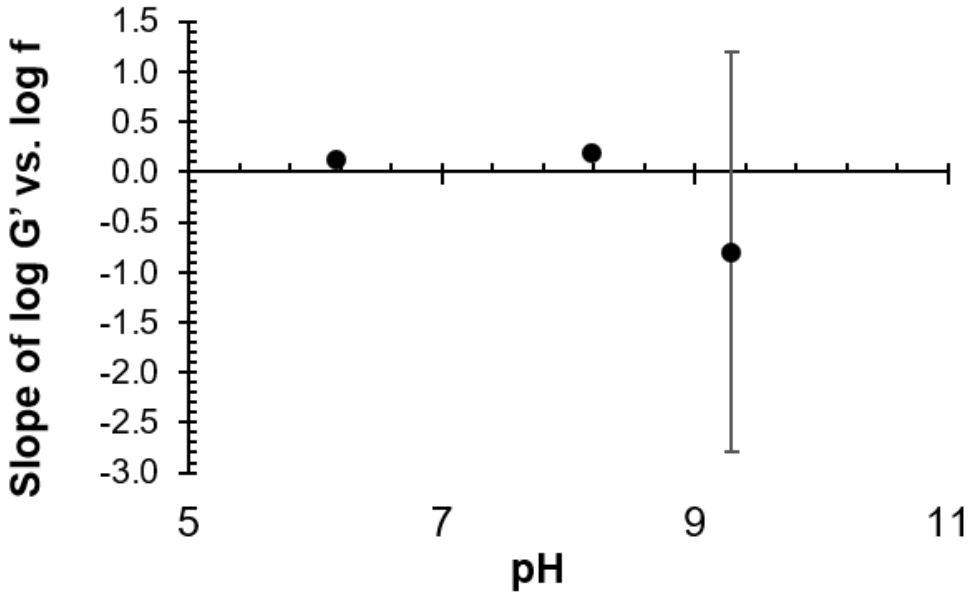

Figure 6.16: *The slopes of the log of G′ versus log of f plots taken from frequency sweep data on CSM protein gels at varying pH values. Error bars represent the standard deviation of 3 repeats*

Strain amplitude sweep experiments were also carried out on CSM protein gels and suspensions with differing heat treatments. The gels chosen for these experiments were prepared at either a pH of 8 ± 0.1 or 10 ± 0.1 and were either subject to a heating treatment (immersion in a 95 °C water bath for 30 minutes during formulation) or no heating. The gels were then allowed to cool to room temperature, and all were stored at 4 °C overnight before being subject to rheometric analysis at room temperature. This investigation was designed to probe the effect of heating on the strength and stiffness of the gel networks. Heat is a known method of gelation in CSM proteins (see Section **2.3.3**) which leads to increased stiffness and strength in gels.

The shear modulus of the gels revealed an overall increase in stiffness to the pH 8 gels when subject to the heating treatment, likely indicating the heat-induced presence of protein crosslinks in the gel network (**Figure 6.17**). Natural protein crosslinks are generally covalent bonds formed between sulphide-containing amino acids though lysinoalanine crosslinking can also be induced through UV, heat, or chemical treatments, and crosslinking can also result from salt bridging between charged residues when a salt is present (refer **Section 2.2.3.2**). Heat induced crosslinks tend to occur as denaturation of the protein exposes different amino acid residues on the surface of individual proteins which can then associate with and form new bonds to adjacent protein molecules, increasing the interconnectivity of the gel network in an irreversible manner.

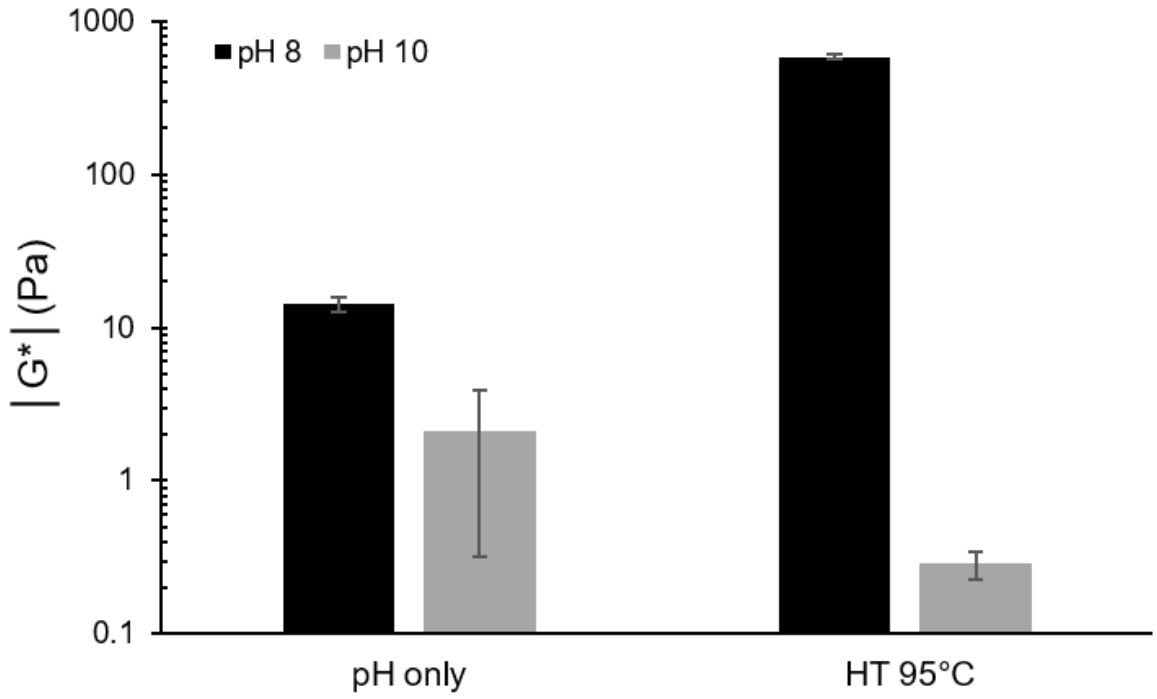

Figure 6.17: *Complex shear moduli of CSM protein gels with and without a heat treatment during formulation*

Interestingly, the pH 10 formulations experience a drop (from 2.12 Pa to 0.29 Pa) in the complex shear modulus after being subject to the heat treatment. While the result for the non-heat-treated pH 10 samples displays high variance across repeats, this variance reduces in the heat-treated samples' result suggesting that the change may be a genuine phenomenon of heating pH 10 samples. However, as previously discussed, these formulations display a more liquid-like behaviour under rheological analysis which limits the data that can be obtained from these tests and variance in data remains problematic. The drop of approximately 2 Pa (86 % decrease) in the complex shear modulus for the pH 10 formulations appears much less consequential when compared to the clear increase of 572 Pa (42-fold) seen in the pH 8 samples. An identical trend is observed in the storage moduli of the heat-treated samples (**Figure 6.18**), indicating that the solid component of the gels is significantly increased with the heat treatment in the pH 8 formulations.

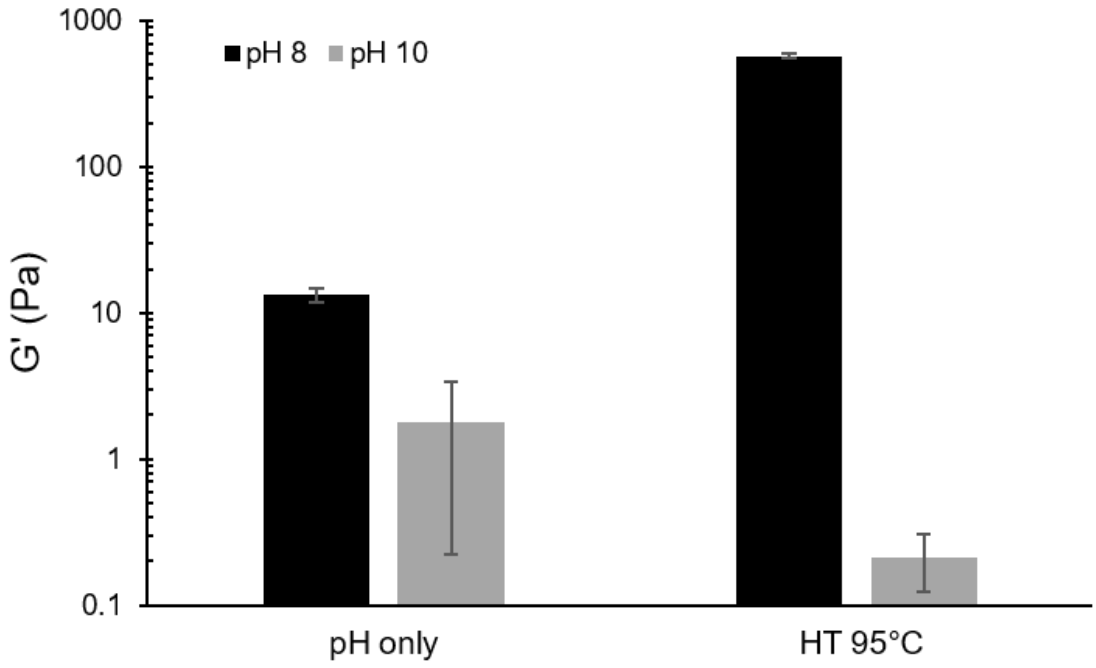

Figure 6.18: *Average storage moduli (G') calculated from the LVR of strain sweep experiments (0.1 – 1.0 % ε) in CSM protein gels at pH 8 and pH 10, with and without a heat treatment of 95°C for 30 mins. Error bars represent the standard deviation where n= 3*

Kim *et al.* conducted differential scanning calorimetry (DSC) analysis alongside heat sweep rheological testing of canola protein gels (25 °C to 95 °C at 0.1 Hz and 1 % strain amplitude). Their studies revealed that the denaturation temperatures (identified as endothermic peaks in DSC) occurred in a similar temperature range to the gelation temperatures (marked by sudden rise in G′ in the rheometer temperature sweep) [200]. Their studies show formulations (7 *% wt*. CSM protein) at pH values of 5, 7 and 9 experienced these simultaneous events at temperatures between 82 – 89 °C, although no pH-related trend was identified within this pH range [200]. A clear switch in G′ and G″ at T_{gel} indicated the conversion to a more elastic structure [200]. The study by Kim *et al.* sheds light on why CSM protein gels in the current work also experience a significant increase in G′ after heating at a temperature of 95 °C. Heat-induced protein denaturation is required before substantial gel networking can occur, acting synergistically with a specific gel-inducing pH of around 8. Other

measures of the heat-induced gel changes include viscosity (**Figure 6.19**), loss factor (**Figure 6.20**), and critical strain (**Figure 6.21**).

The complex viscosity of the pH 8 samples also increases after heat treatment (41-fold), while is reduced in the pH 10 samples after heat treatment (7-fold), once again reflecting a similar trend to the complex shear modulus and the storage modulus (**Figure 6.19**).

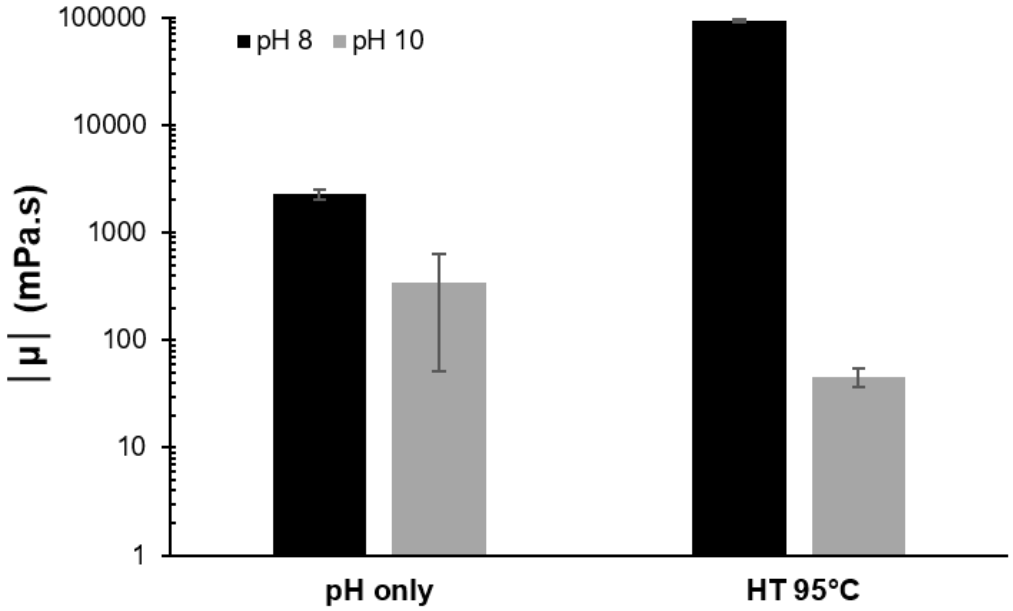

Figure 6.19: *Average viscosities (|μ|) calculated from the LVR of strain sweep experiments (0.1 – 1.0 % ε) in CSM protein gels at pH 8 and pH 10, with and without a heat treatment of 95°C for 30 mins. Error bars represent the standard deviation where n = 3*

A comparison of tanδ in the same experiments shows the halving of tanδ in pH 8 gels after heat-treatment (**Figure 6.20**), which reflects the increasing solid-like component likely caused by heat-induced crosslinking. Suspensions at pH 10 are not stable in experiments (large variance across multiple repeats), although heat-treated suspensions may be slightly more stable but remain liquids (tanδ > 1) rather than gels (**Figure 6.20**).

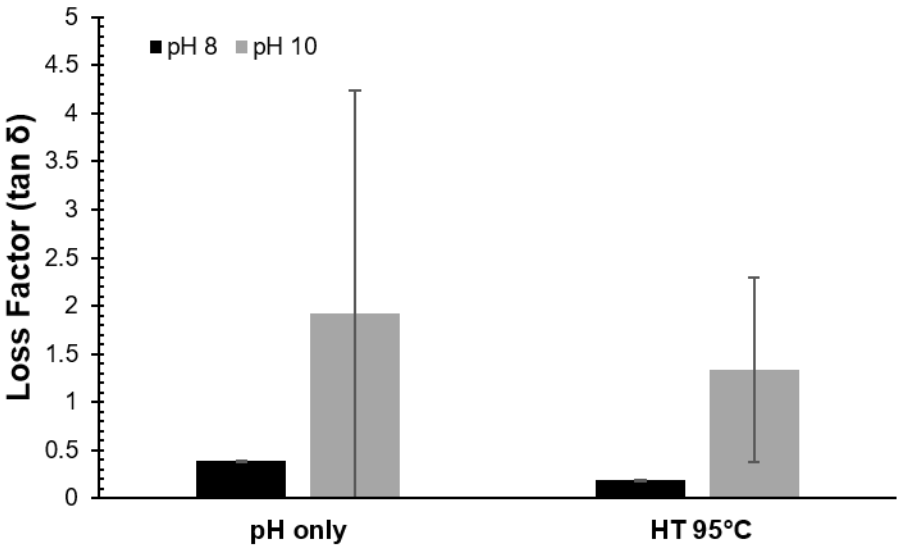

Figure 6.20: *Average loss factor (tan δ) calculated from the LVR of strain sweep experiments (0.1 – 1.0 % ε) in CSM protein gels at pH 8 and pH 10, with and without a heat treatment of 95°C for 30 mins. Error bars represent the standard deviation where n= 3*

Critical strain ($\varepsilon_{critical}$) is reduced in both heat-treated samples as compared to the corresponding non-heated sample (**Figure 6.21**). The drop from 97 % $\varepsilon_{critical}$ to 17 % (± 1 %) $\varepsilon_{critical}$ in the pH 8 formulations reveals the extent to which heat-treatment embrittles the gels. The 5-fold drop in $\varepsilon_{critical}$ indicates that the amount of recoverable deformation is much reduced in heat-treated samples. Although protein denaturation is a key change induced by heat-treatment, it is also likely that heat-treatment causes increased protein-protein interactions (*e.g.* secondary bonding). Chemical associations within the network strengthen and stiffen the network (increased G* and μ) ultimately restricting molecular movement of heat-treated gels. Loosely constrained molecules in networks with fewer chemical bonds (*e.g.* non-heat-treated) allow for greater molecular movement before giving way to flow behaviour. Non-heat-treated CSM protein gel networks may be comprised of weaker or fewer protein-protein chemical interactions. A discussion on the likely gelation mechanisms of the canola gels in this study can be found in **Section 8.4** where rheometric data is discussed alongside other evidence (*e.g.* biochemical studies).

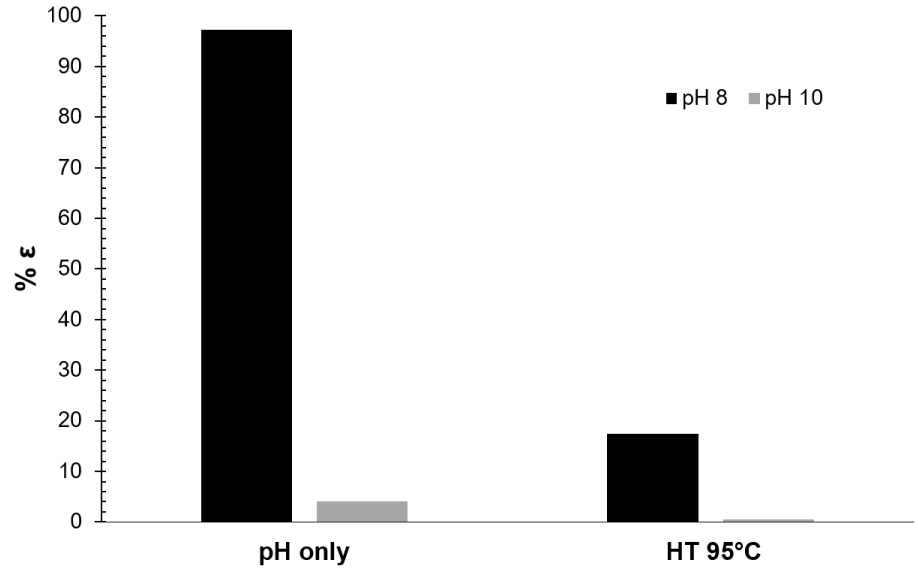

Figure 6.21: *Average critical strain (% ε at tan δ = 1) in CSM protein gels at pH 8 and pH 10, with and without a heat treatment of 95 °C for 30 mins*

Cross-linked gels have an increased quantity of intermolecular bonding within the gel network. These bonds impart stiffness in the gels (higher G*) but they strain over only a short distance before rupture and flow behaviour occurs (reduced $\varepsilon_{critical}$). The types of protein crosslinks induced by heating the gels remains to be investigated. A common protein crosslink is the disulphide bond formed between thiol groups on cysteine or methionine residues. However, this type of crosslinking is unlikely to be a major factor in CSM protein gels, since the cruciferin protein possesses such low quantities of sulphur-containing amino acids (refer **Section 2.3.2**). Literature evidence may suggest that free amino groups, such as the ε-amino in lysine, could be responsible for CSM protein gel crosslinking. Gill and Tung reveal that methylation of free amino groups in canola protein inhibits gelation, though they cannot identify exactly which amino acid residues are responsible for this phenomena [203].

Critical strain is also reduced in pH 10 samples after heat-treatment, however, standard deviation in the repeats of the non-heat-treated samples is greater than the measured critical strain (4 % ± 4.9 %). Therefore, it cannot be conclusively stated that heat-induced changes to the critical strain exist in CSM protein formulations at pH 10.

The final rheological analysis carried out on heat-treated CSM protein gels was a frequency sweep analysis to compare the degree of frequency dependence in the samples (slope of the log G′ vs. log f plot). As with earlier results on pH variable samples, the gels demonstrated slight shear thinning behaviour (positive slope) which was slightly reduced after the heat-treatment in samples at pH 8 (0.18 in non-heated gels to 0.11 post-heat-treatment), revealing a reduction in frequency-dependence of the rheological behaviour (**Figure 6.22**). Substances that are frequency-independent are more gel-like (elastic) in nature [200]. This result also supports the conclusion that heat-treated pH 8 gels are more highly associated and/or crosslinked and thus behave more solid-like than their non-crosslinked counterparts. The suspensions at pH 10 are too unstable in these tests to determine any relationship between G′ and frequency, and as with other rheological testing the tanδ for pH 10 samples remains above 1, even after heat treatment.

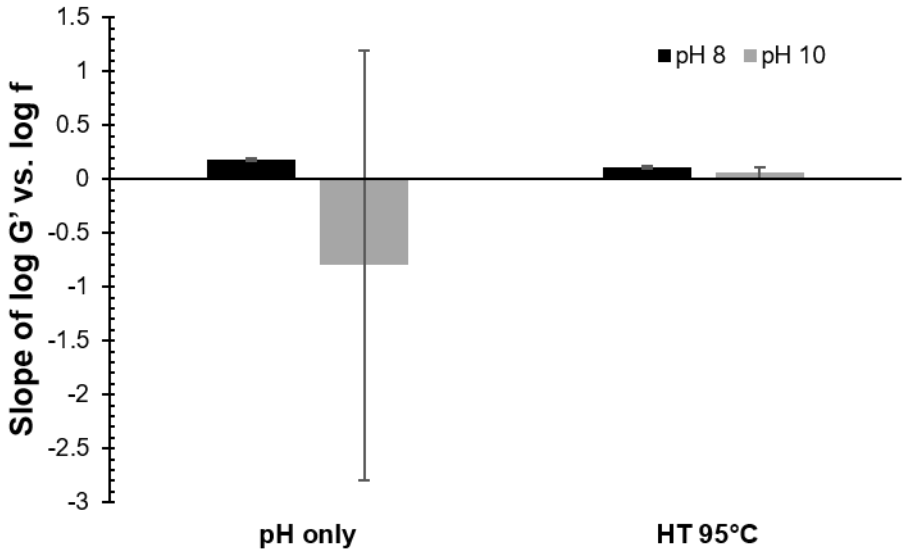

Figure 6.22: *The slopes of the log of G' versus log of f plots taken from frequency sweep data on CSM protein gels at pH 8 and pH 10, with and without a heat treatment of 95 °C for 30 mins. Error bars represent the standard deviation of 3 repeats*

The rheological studies in this thesis provide evidence of variable gelation capacities in CSM protein gels when prepared at varying pH values and with varying heat treatment. Gels are demonstrably more viscous and more solid-like at a pH around 8, while the gelation mechanism that occurs at pH 8

appears to be largely unavailable at pH ≥ 10. Insolubility of protein restricts network elasticity and eventually inhibits network formation at pH values ≤ 6.2, though aggregates of protein cause an increase in solution/gel viscosity. Gelation is also improved following heat treatments as seen in viscosities and storage moduli in heat treated pH 8 samples. Rheometry confirms that selected CSM protein gels are promising candidates for aerogel production, where those prepared at a pH of 8 and with heat treatments are hypothesised to subsequently produce the strongest aerogels (investigated in the following sections of this Chapter).

6.4. Morphology of canola protein aerogels

Aerogels are defined by morphology. Trademark aerogel properties such as thermal and electrical insulative properties, high specific surface areas, and high strength-to-weight ratios emerge from the uniquely micro- and nano-sized pore structures within aerogels which afford them uniquely low densities (refer **Sections 2.1.2** and **2.1.3**). In this Section the porosity, density, and macroscopic appearance of the aerogels are discussed. Generally, the porosity of an aerogel is classified according to pore size (or width) such that macro-pores, meso-pores and micro-pores are > 50 nm, 2-50 nm, and < 2 nm in width, respectively. The pore morphology is a critical factor that largely determines the suitability of an aerogel in a specific application. For example, the thermal insulation afforded by an aerogel is maximised when the pore size of the aerogel lies in the mesoporous range [27]. Typically, protein-based aerogels have low fractions of meso- or micro-pores, with a tendency for their structures to be dominated by macro-pores, often attributed to freeze drying [95]. Pore morphology of aerogels is governed by the polymer choice, gelation mechanisms, and drying technique used in manufacture (refer **Section 2.1.2**). Therefore, variations in the gelation parameters are also discussed in this Section.

6.4.1. Macroscopic appearance and density

The central aim of this thesis was to develop aerogels from CSM protein, where aerogels are defined by low density and porosity. An important first evidence to confirm this achievement was the measurement of bulk density of the resulting monolithic structures. CSM protein aerogels were successfully produced in this thesis using a simple pH manipulation of CSM protein aqueous suspensions (**Section 6.2.1**), followed by a freeze drying process (**Section 6.2.2**). The resulting dried monoliths can be described as lightweight, brittle, golden/tan-coloured, solid foams (**Figure 6.23**). The aerogel monoliths largely retained the cylindrical and conical shape of the Falcon™ tubes from within which they were formed (**Figure 6.23**, **Figure 6.27** – **Figure 6.32**), although accompanied by a wide range of shrinkage (2 – 30 %) depending on preparation factors. These factors include protein concentration (higher concentration results in reduced shrinkage) and mould choice (larger tubes have reduced shrinkage). Occasional power outages during freeze-dryer operation also affected aerogel

shrinkage by allowing defrosting to occur in partially dried samples. If defrosting of the protein gels occurs prior to complete drying then shrinkage is increased, monoliths appear glossy (**Figure 6.30**, near cone tips), and lose their porosity in those affected areas. Affected regions of these samples appear as if dried like xerogels (refer **Section 2.1.1**).

Initial efforts to create CSM protein aerogels involved experimentation with the concentration of the CSM protein. Various mass fractions (denoted as a wt%) ranging from 3 wt% to 15 wt% were used in the wet-gel preparation of initial samples (pH range 10 – 11) (**Figure 6.23**). All chosen mass fractions were amenable to aerogel production, though some of the 3 wt% samples were too fragile to be handled for density measurements due to ease of fracture (**Figure 6.23a**).

The most striking observation upon recovery of the aerogels was that CSM protein aerogels possess a unique golden-brown 'sparkle'. The structures that were produced *via* freeze drying reflect light in a way that makes the surface of the aerogels sparkle and shimmer. However, this was a bulk optical property of the aerogel structure as the sparkle effect was also observed in flakes or fragments removed from the main monolith. The sparkle of the aerogels is left unexplored for the remainder of this Chapter and appears to be a small, quirky, and almost inconsequential observation. However, the unique application potential of CSM protein aerogels because of this unique optical property is later discussed in **Section 8.6.2**.

The surface of the aerogel monoliths was arranged in patches of localised directionality with respect to the reflection of the light, indicating that the internal structure of the monoliths was also anisotropic. The anisotropic arrangement of the aerogel microstructure is further examined in **Section 6.4.2**. The resulting monoliths were brittle to touch and presented some difficulty when cutting. A very sharp scalpel and/or microscopy blade was required to cut and trim the monoliths into regular shapes (cylindrical or rectangular prisms) for density and mechanical strength measurements. The monoliths were trimmed and cut using a careful see-saw motion, to prevent crushing of the structures (particularly those of lowest densities) during specimen preparation for subsequent testing or microscope imaging. The mechanical properties of the monoliths are investigated in **Section 6.5.1**.

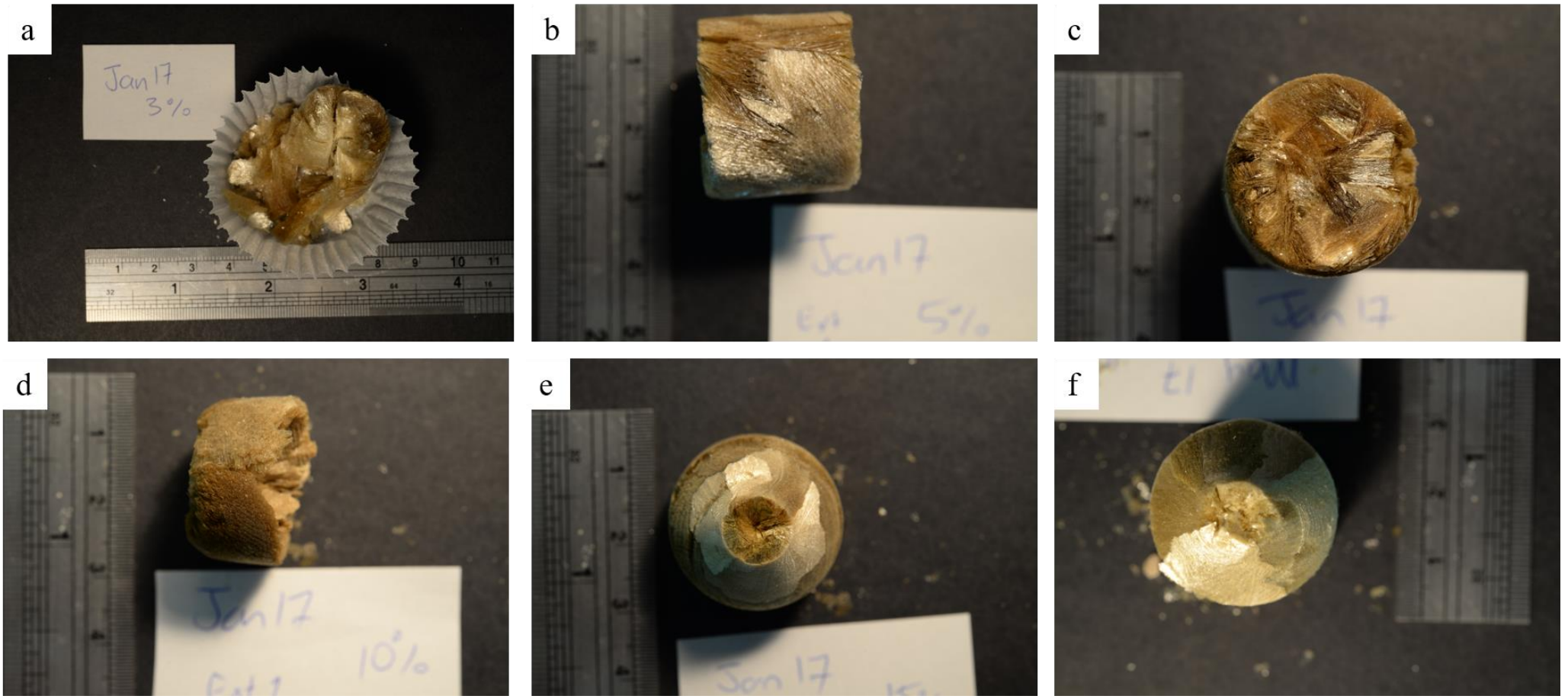

Figure 6.23: *Photographs of the first CSM protein aerogels produced by freeze drying at* ***(a)*** *3.0 wt% CSM powder (ρ = 37 g/L)* ***(b)*** *5.0 wt% (ρ = 59 g/L)* ***(c)*** *7.5 wt% (ρ = 88 g/L)* ***(d)*** *10 wt% (ρ = 111 g/L)* ***(e)*** *15 wt% (ρ = 160 g/L), and* ***(f)*** *10 wt% (ρ = 112 g/L). Samples were made using CSM protein powder from the alkali-acid extraction method* ***(a-e)*** *or PMM extraction method* ***(f)*** *formulated at a pH of 10.2 – 10.9*

Aerogel densities can vary from the ultra-low (< 0.01 g/cm^3) to denser structures (~0.5 g/cm^3) (see **Section 2.1**), with the density being strongly influenced by the concentration of the polymer in the wet-gel. The density of an aerogel is also influenced to a lesser degree by the production method. The successful production of CSM protein aerogels in this work was evidenced by attaining bulk densities as low as 0.037 g/cm^3 in the 3 wt% samples (19 % shrinkage) (**Figure 6.24**). The compressive properties of the aerogels are later investigated in more detail, but initial handling of the first samples found that aerogels with densities less than ~0.08 g/cm^3 were impractically weak for specimen preparation. Thus, a mass fraction of 10 wt% CSM protein was subsequently selected for aerogel production.

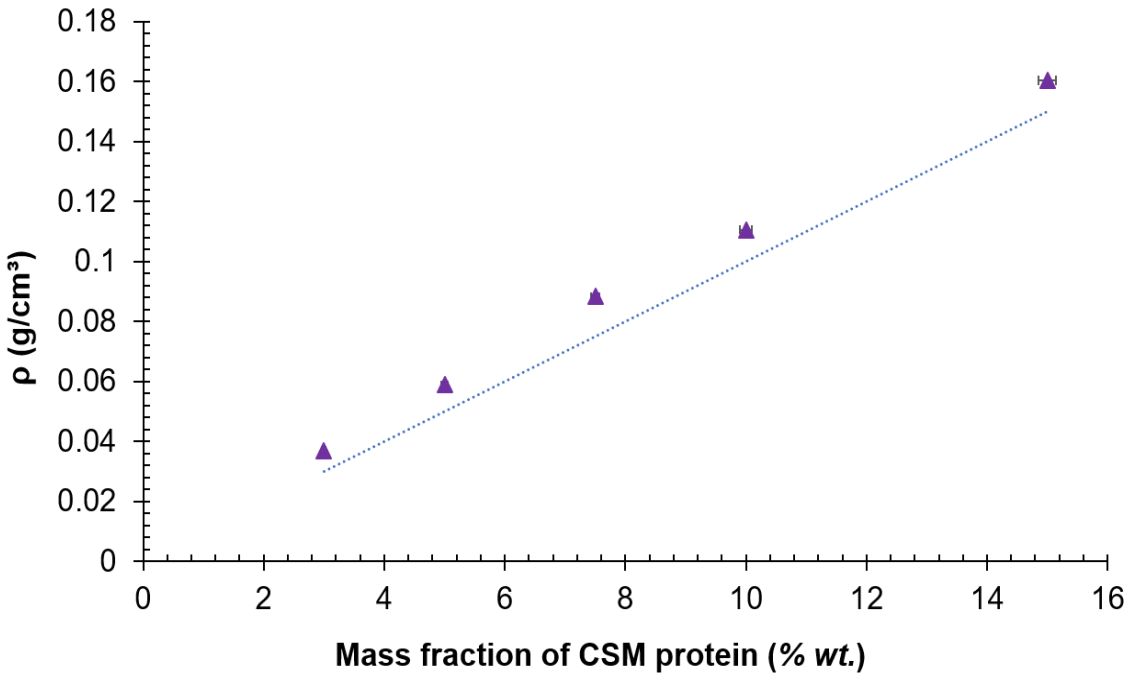

Figure 6.24: *Bulk densities (ρ) of CSM protein aerogels with varying mass fractions of CSM protein in the corresponding wet-gel. Trendline represents hypothetical densities for aerogels produced without change to the wet-gel volume (i.e. no shrinkage). Error bars represent absolute error calculated using balance accuracy*

The average amount of shrinkage in the first aerogel samples was 13 %, with later samples showing an average of 21 % shrinkage. This difference was attributed to the different sized Falcon™ tubes used to dry the aerogels, with the larger tubes resulting in less shrinkage (**Figure 6.25**). Larger tubes expose a greater surface area per volume of gel (707 mm^2 for the 30 mL tubes *cf.* 177 mm^2 for the 15

mL tubes) to the vacuum conditions during freeze drying, since only the ends of the Falcon™ tubes are open. Exposing a greater surface area per volume of gel achieves a uniform vacuum in the sample more quickly, reducing the likelihood of defrosting (and associated shrinkage). However, constraints on sample volumes due to protein supply did not always allow for the use of 30 mL Falcon™ tubes, therefore the 21 % shrinkage in the smaller samples was an acceptable compromise given densities achieved were < 0.13 g/cm^3 and protein-based aerogels in the literature average around 0.2 g/cm^3 in density (see **Section 2.2.3**).

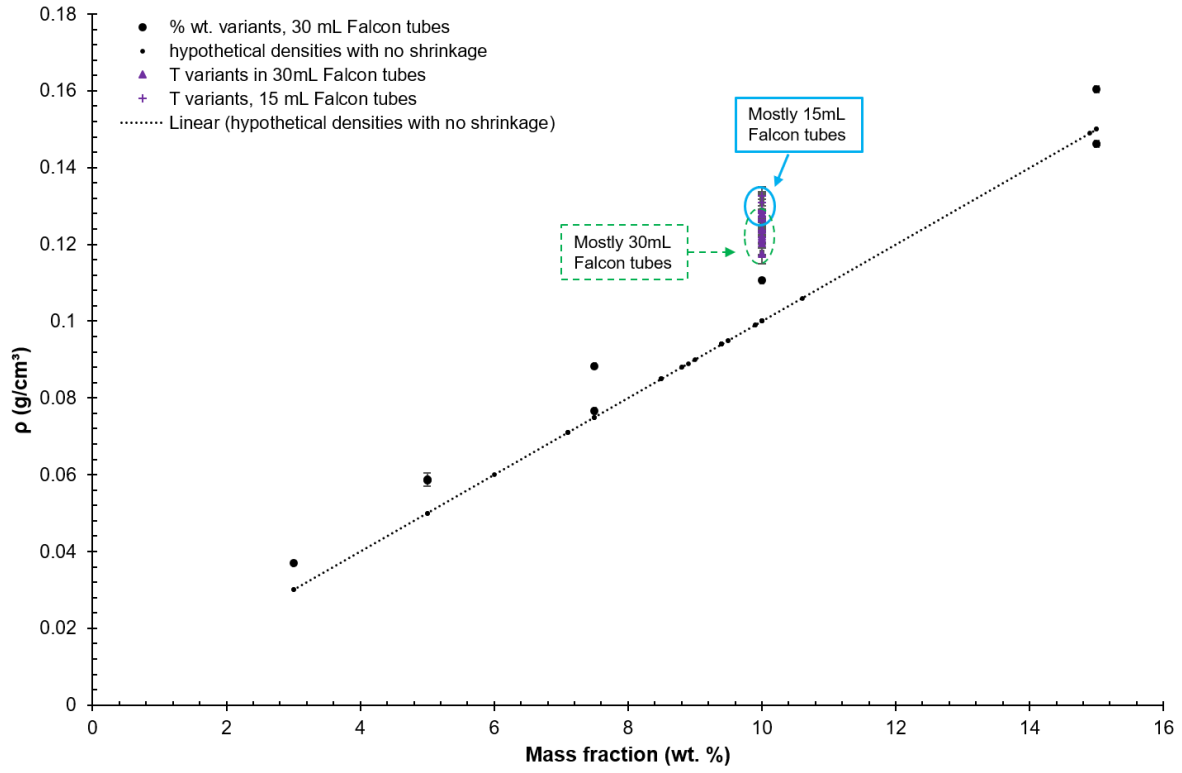

Figure 6.25: *Bulk densities (ρ) of CSM protein aerogels. Presented as batches (series) with varying wt%, varying gelation temperatures, and varying tube size. Trendline represents hypothetical densities for aerogels produced without change to the wet-gel volume (i.e. no shrinkage). Error bars represent the standard deviation in samples with identical preparation conditions*

During the development of the CSM protein aerogels, alternate moulds were trialled, including two purpose-built stainless-steel moulds (cylindrical and rectangular prism) and block moulds with 10 × 40 × 10 mm cavities made from polyethylene (HDPE). These mould trials failed to decrease

shrinkage of the aerogels, and in most cases the density and shrinkage of the resulting aerogels was increased (**Figure 6.26**). The increased shrinkage in some batches was attributed to the slow on-set of the vacuum during freeze drying because of the larger manifold vessels required to contain the block moulds. Prolonged exposure to room pressure and temperature during the establishment of the vacuum resulted in partial defrosting of the samples. Defrosted samples experience evaporation rather than sublimation due to crossing of the liquid-gas phase boundary (see **Figure 2.4**) and foaming is seen when this occurs. The freeze drying technique relies on the sublimation of the water in the pores of the gels, avoiding evaporation and associated structure collapse (refer **Figure 2.6**). The foaming that was observed in some samples revealed a failure of the freeze drying technique to achieve complete sublimation due to the prior defrosting of the samples. One success with respect to aerogel density was the use of the stainless-steel mould (rectangular prism shape) combined with a snap freezing technique using liquid nitrogen. This sample experienced only 1.2 % shrinkage; however, the mechanical properties were visibly impaired (extremely brittle sample, unable to be removed from mould without fracture) such that this mould and freezing technique was also abandoned. Consequently, Falcon™ tubes, mostly with a diameter of 15 mm, were the chosen vessel to produce freeze dried aerogel samples in the remainder of this thesis.

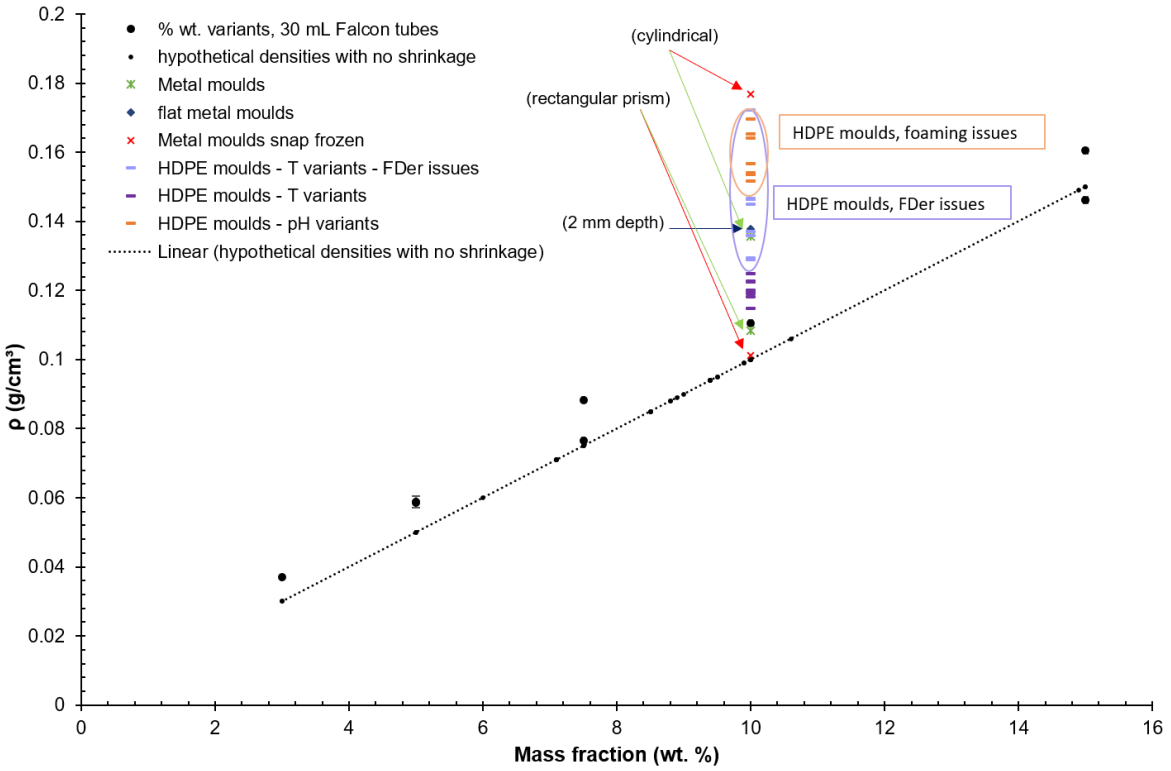

Figure 6.26: *Bulk densities (ρ) of CSM protein aerogels. Presented as batches with varying gelation conditions and mould types (refer to plot legend). Trendline represents hypothetical densities for aerogels produced without change to the wet-gel volume (i.e. no shrinkage)*

Processing variations to gelation conditions (temperature, gelation time, ageing time, and pH) were introduced to investigate their possible influence on the properties of the resulting aerogels. Effects of gelation conditions on the microstructure and mechanical properties are presented in later **Sections** (**6.4.2.** and **6.5.1**, respectively). Initially, visual observations and density measurements were used to determine if the basic aerogel densities were affected by changes to the gelation conditions. Macroscopic observations suggest that the most important gelation factor is the pH of the gel formulation (**Figure 6.27**). The pH of the formulation alone can be used to influence the viability of the aerogels. Viscosity variations in the wet-gels due to pH were known from rheology studies (refer **Section 6.3**) and could be expected to influence aerogel viability. Images (**Figure 6.27c-f**) reveal how alkaline pH values (≥ 7) formed viable aerogel structures once dried, but suspensions of CSM extract at acidic pH values (3 – 6), notably near the isoelectric point (3.5) of the extracts, did not form aerogel monoliths but rather crumbled to powders upon freeze drying (**Figure 6.27b**). Surprisingly, extremely

low pH values (*e.g.* pH = 1.85, **Figure 6.27a**) also form viable aerogel structures. Gel viscosities were not measured for pH 1.9, however observations prior to freeze drying suggest that the viscosity at pH 1.9 is similar to pH ≥ 10 gels (see **Section 8.4.1** for discussion on pH-induced gelation).

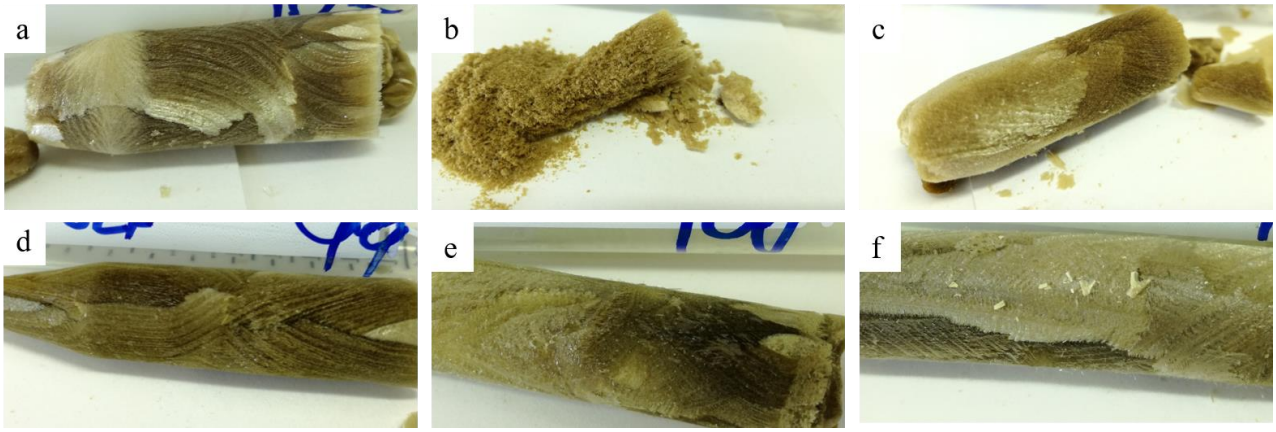

Figure 6.27: *CSM protein aerogels formulated at 10 wt% CSM protein and 25 °C at a pH of* ***(a)*** *1.9* ***(b)*** *6.0* ***(c)*** *8.0* ***(d)*** *10.2* ***(e)*** *12.1 and* ***(f)*** *13.1*

The densities of the viable aerogels are largely uninfluenced by the pH, except for the aerogel prepared at pH 1.85 (**Figure 6.28**). This sample was cut into three specimens for mechanical testing and these specimens had an average density of 0.116 ± 0.002 g/cm^3 while the specimens prepared at a pH ≥ 7.0 had an average density of 0.125 ± 0.001 g/cm^3.

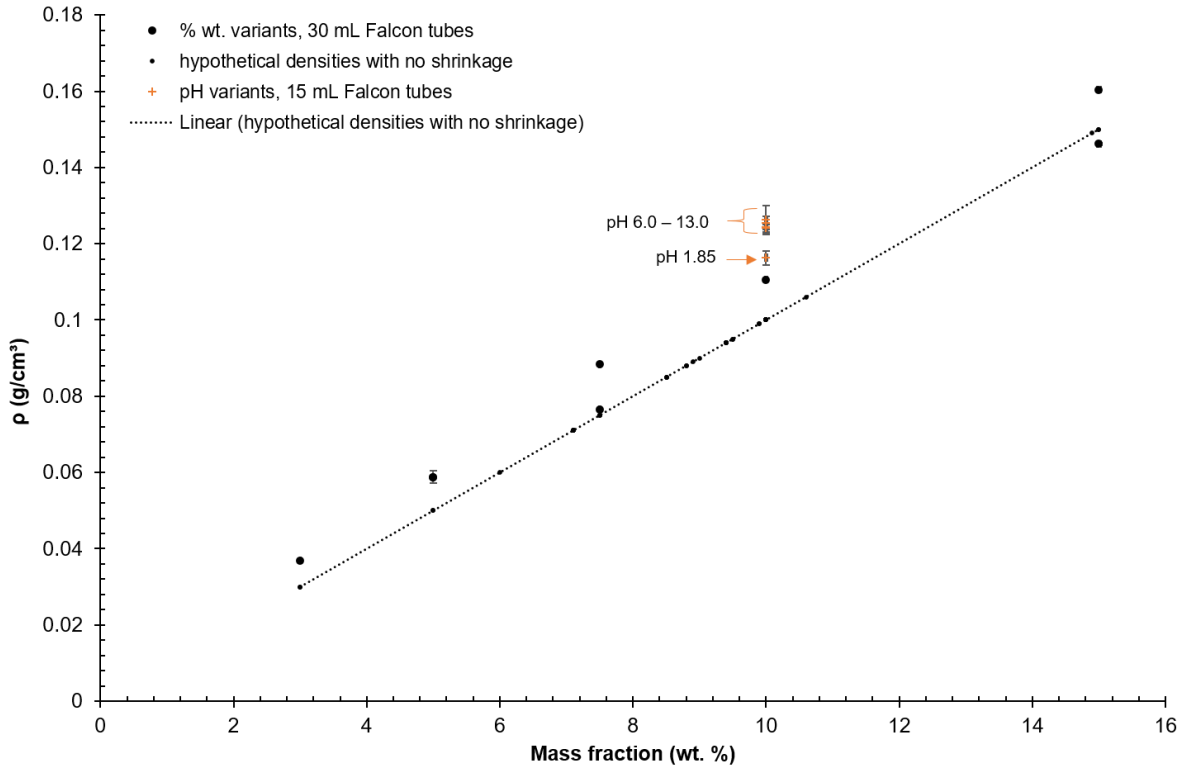

Figure 6.28: *Bulk densities (ρ) of CSM protein aerogels. Presented as batches (series) with varying wt% or varying gelation pH values. Trendline represents hypothetical densities for aerogels produced without change to the wet-gel volume (i.e. no shrinkage). Error bars represent the standard deviation in samples with identical preparation conditions*

Further experiments with gelation pH produced an additional 45 aerogels with pH values ranging from 7.1 to 12.0 and found that while variance in density was large, it was not associated to the pH changes (**Figure 6.29**). The large variance in the density (and shrinkage) of these sample sets was attributed to non-uniform drying in some samples, possibly caused by variable sample volumes. Sample volumes were controlled more carefully in subsequent aerogel manufacture (experiments discussed in **Chapter 7** of this thesis) and consequently the variances in the density measurements were reduced (refer **Sections 7.3.1** and **7.4.4**).

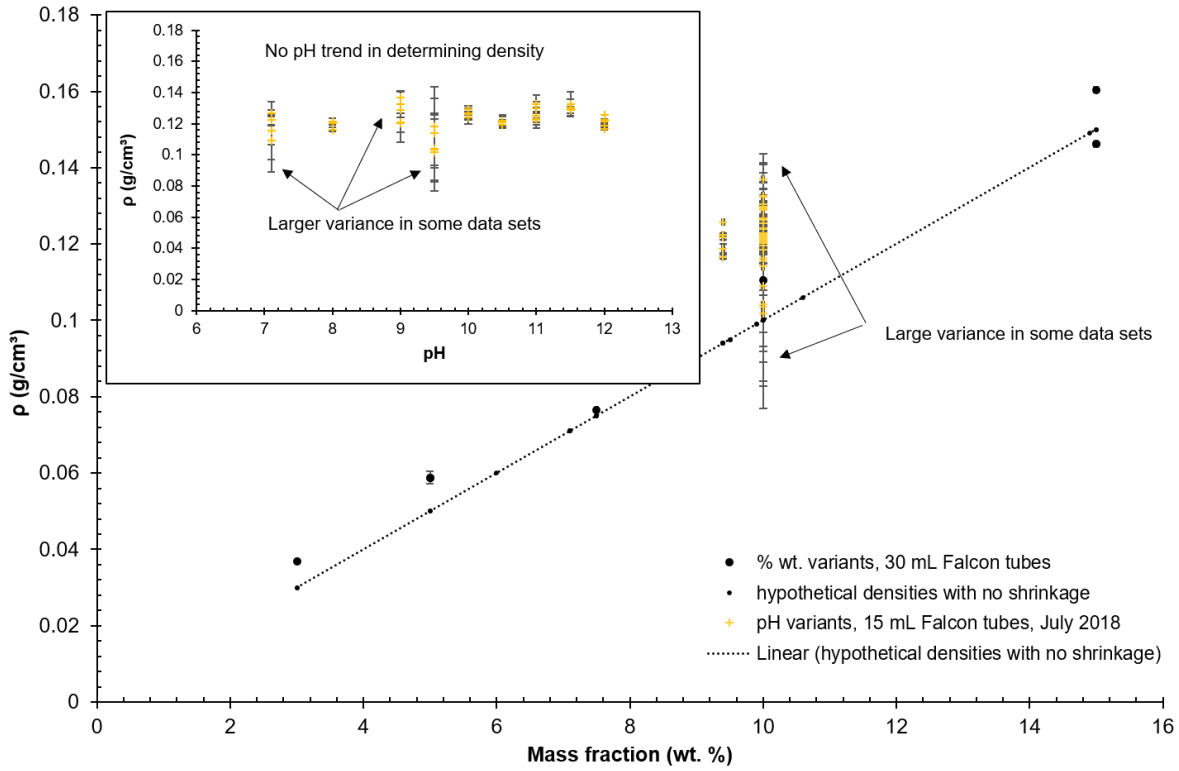

Figure 6.29: *Bulk densities (ρ) of CSM protein aerogels with respect to CSM protein mass fraction (main plot) or gelation pH (insert). Presented as batches (series) with varying wt% or varying gelation pH values (refer to plot legend). Trendline represents hypothetical densities for aerogels produced without change to the wet-gel volume (i.e. no shrinkage). Error bars represent the standard deviation in samples with identical preparation conditions*

Other variations such as gel temperature (**Figure 6.30**), gelation times (**Figure 6.31**), and gel ageing times (**Figure 6.32**) do not appear to influence the macroscopic appearance of the aerogels. The specimens from these experiments remain brittle, golden/tan-coloured, solid foams, and with anisotropic structures suggested by a patchwork appearance.

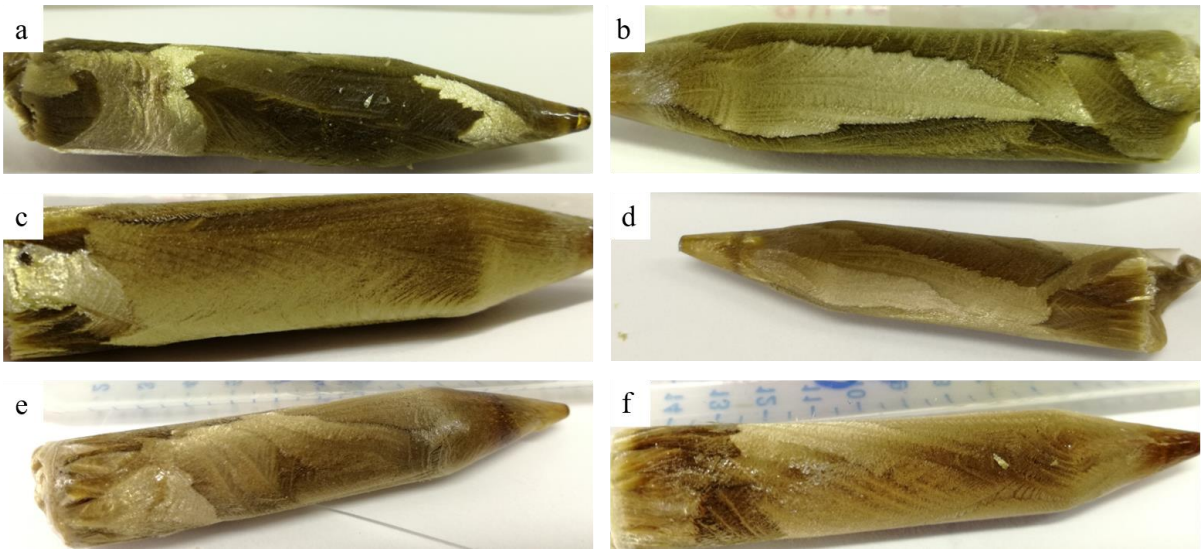

Figure 6.30: *CSM protein aerogels formulated at a pH of 11.2 and 10 wt% CSM protein, with heat-treatments for 30 minutes at* ***(a)*** *4 °C* ***(b)*** *25 °C* ***(c)*** *40 °C* ***(d)*** *60 °C* ***(e)*** *80 °C and* ***(f)*** *100 °C*

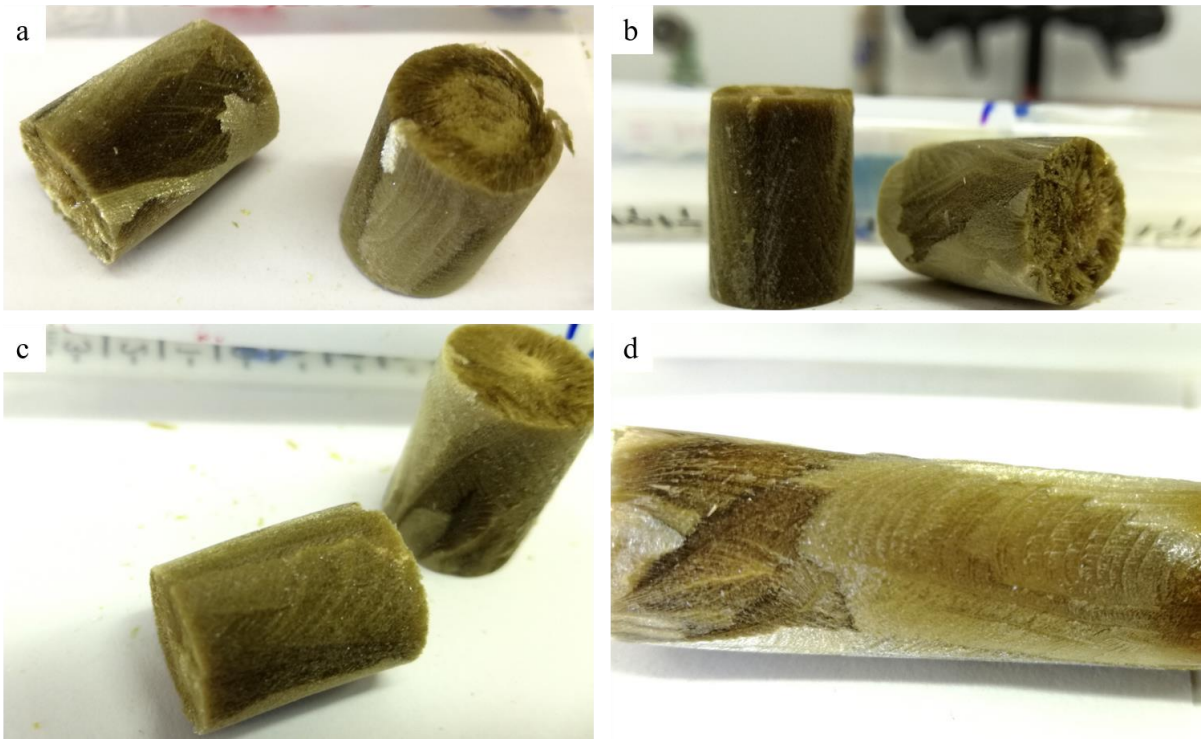

Figure 6.31: *CSM protein aerogels formulated at a pH of 12 and 10 wt% CSM protein, with gel ageing times prior to freezing of* ***(a)*** *0,* ***(b)*** *2,* ***(c)*** *6, and* ***(d)*** *12 h*

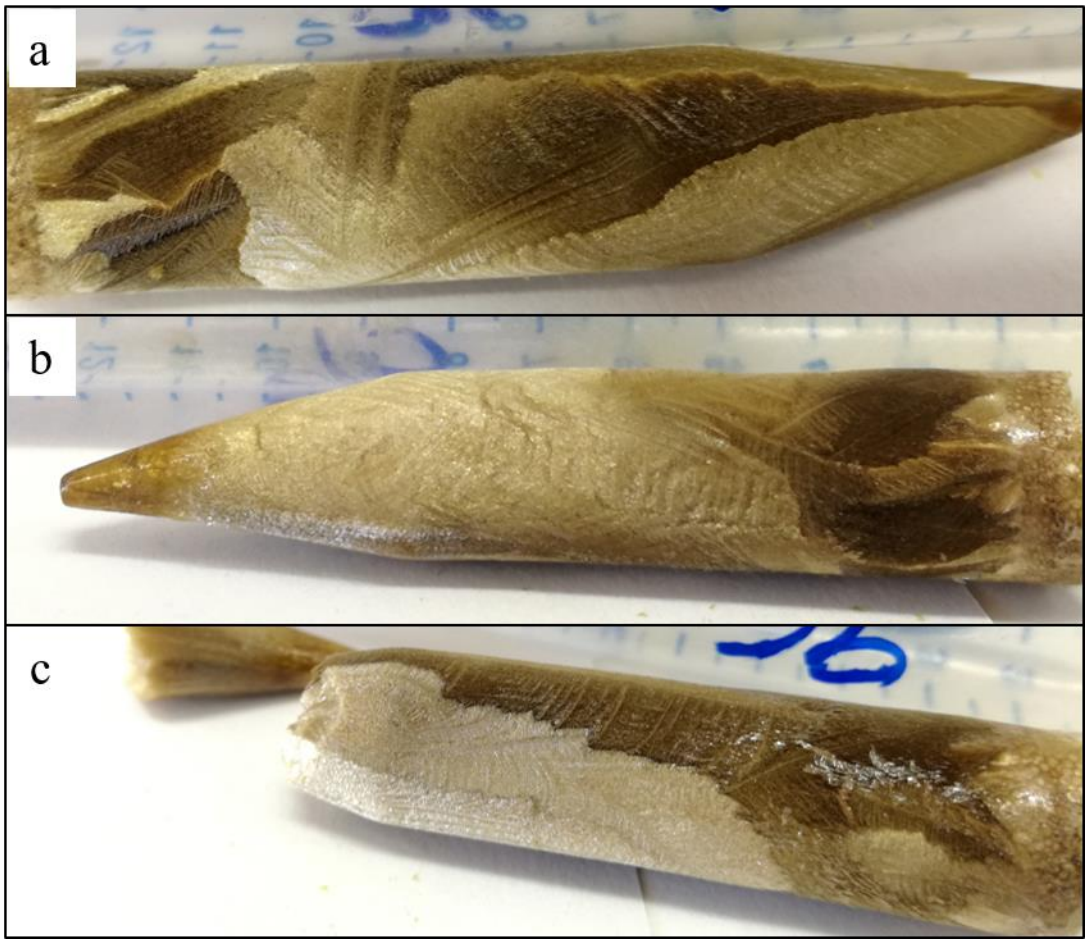

Figure 6.32: *CSM protein aerogels formulated at a pH of 12 and 10 wt% CSM protein, subjected to heat treatment at 80 °C for* ***(a)*** *10,* ***(b)*** *60, and* ***(c)*** *120 min*

There are no differences in the aerogels from the gelation temperature experiment that allow for identification of the gelation temperature based on the physical appearance or feel of the aerogels. Likewise, the density measurements of these samples reveal no dependence on gelation temperature (**Figure 6.33a**). Ageing time variants and gelation time variants also appear to be unaffected by these gelation variations, and no dependence of density on these factors was observed (**Figure 6.33b**). Shrinkage measured in the aerogels prepared with variant gelation and ageing times (23 % shrinkage) was consistent with aerogels dried in the 15 mm diameter Falcon™ tubes (**Figure 6.34**).

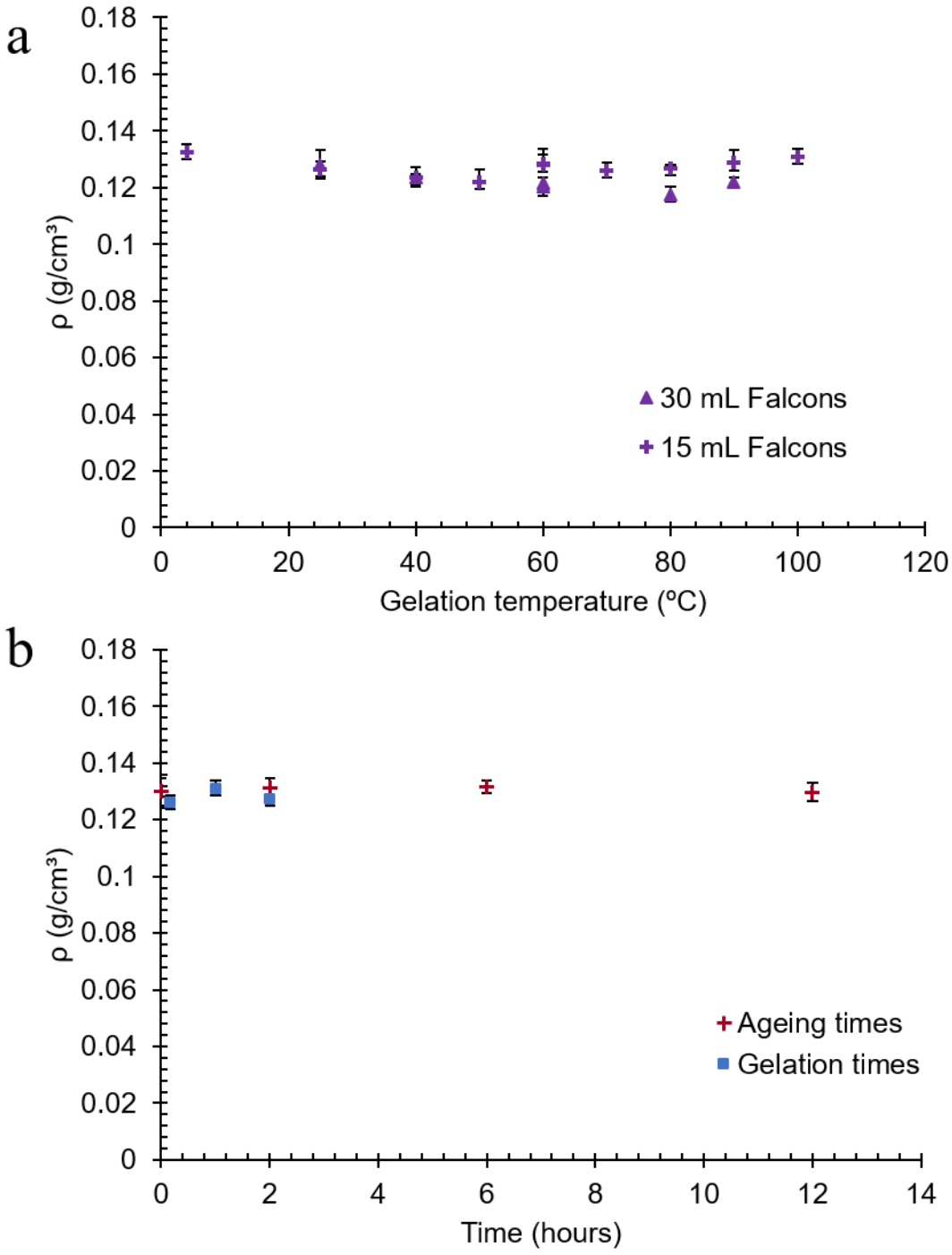

Figure 6.33: *Bulk densities (ρ) of CSM protein aerogels with respect to gelation temperature* ***(a)****, gel ageing times, or gel heating times* ***(b)****.* ***(a)*** *Gels were prepared at a pH of 11 – 12 and then gelled at a range of temperatures for 30 minutes ('15mL Falcons' temperature variants) or 60 minutes ('30mL Falcons' temperature variants).****(b)*** *Gels were prepared at 25ºC and a pH of 12 before being aged for a varying number of hours (ageing variants). Additional gel specimens were prepared at a pH of 12 at gelled at 80ºC for a varying number of minutes (gelation time variants)*

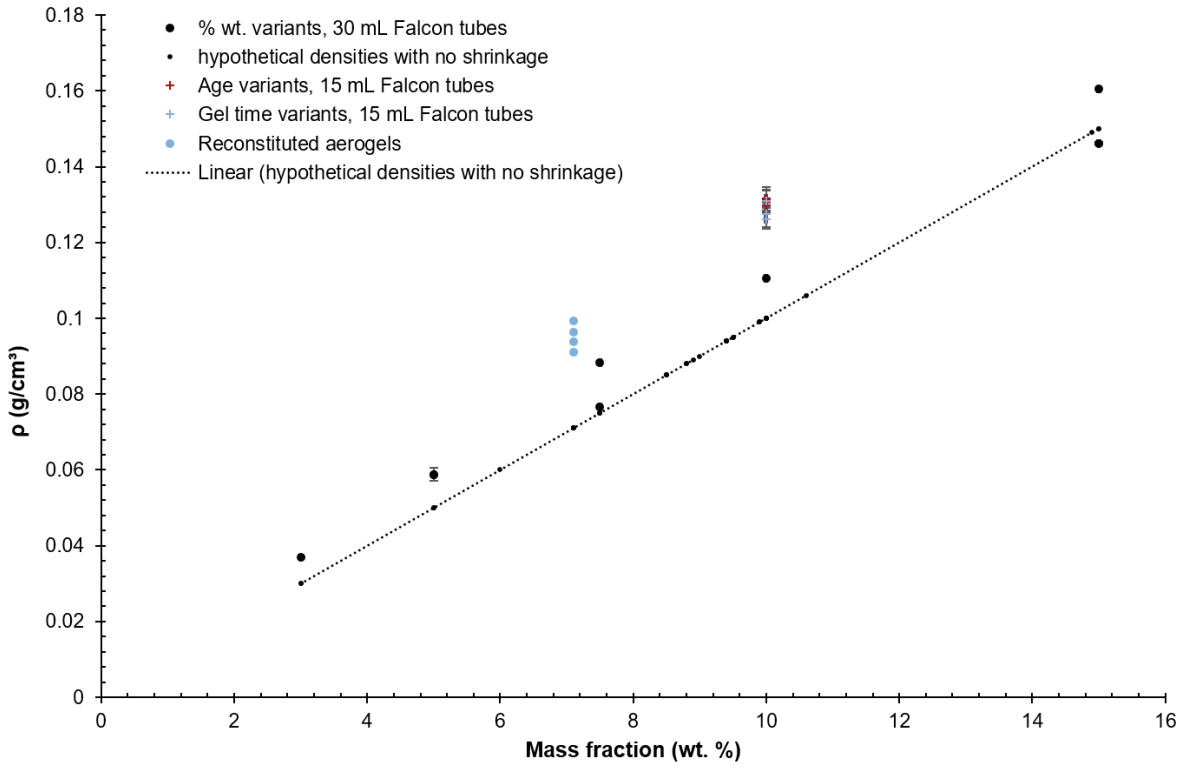

Figure 6.34: *Bulk densities (ρ) of CSM protein aerogels. Presented as batches (series) with varying wt%, varying gel ageing times, varying gelation times, or prepared from reconstituted aerogels (refer plot legend). Trendline represents hypothetical densities for aerogels produced without change to the wet-gel volume (i.e. no shrinkage). Error bars represent the standard deviation in samples with identical preparation conditions*

Two additional aerogels were prepared using the crushed remains of previously prepared CSM protein aerogels to investigate the possibility of recycling the aerogels into new formulations. Crushed pieces of CSM aerogel, obtained from a variety of pH and temperature variants, were mixed in water until no more could be dissolved, amounting to 7.1 wt% of solids. Complete dissolution required heating to 60 ºC for over 1 hour and pH adjustment to 10.5 using 2 M NaOH solution. New aerogels were produced from these gels using freeze drying. The density of aerogel specimens obtained from these samples averaged 0.095 g/cm^3 (25.3 % shrinkage) (**Figure 6.34**). Interestingly, the reconstituted aerogel samples did not possess the golden shimmer or sparkle, typical of all other CSM protein, freeze dried, aerogels (**Figure 6.35**). This is likely an indication that the reconstituted aerogel has a different microstructure, perhaps due to incomplete protein dissolution and retention of parts of prior aerogel networks.

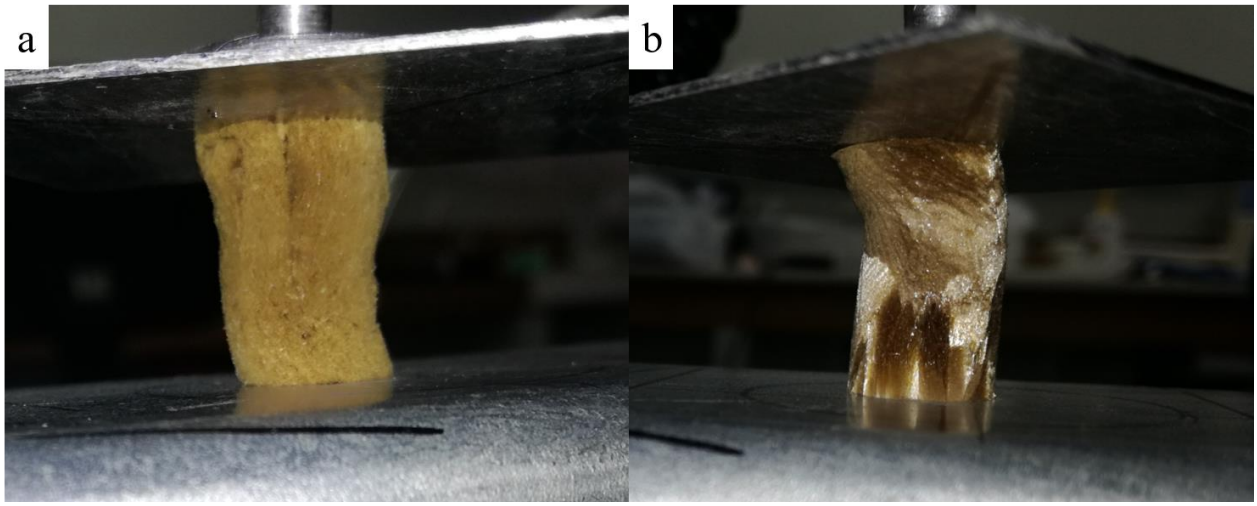

Figure 6.35: *CSM protein aerogel produced from* ***(a)*** *reconstituted, crushed CSM protein aerogels, and* ***(b)*** *fresh CSM protein powder*

A comparison of the various CSM protein aerogel variants discussed in this **Section** reveals that the critical factors in determining the density (and viability) of the aerogels are threefold: (i) mass fraction of CSM protein (wt%), (ii) geometry of mould or vessel used to dry the gels, and (iii) pH of the gels (viable pH values are 2 and ≥ 7). Most aerogels dried in the Falcon™ tubes were selected for further studies (results in **Sections 6.4.2** and **6.5**), while the samples dried in alternate moulds were not used (**Figure 6.36**) except for early thermal analyses (see **Section 6.5.2**). CSM aerogels (10 wt%) selected for further investigations had an average density of 0.122 g/cm^3 (standard deviation 0.006 g/cm^3).

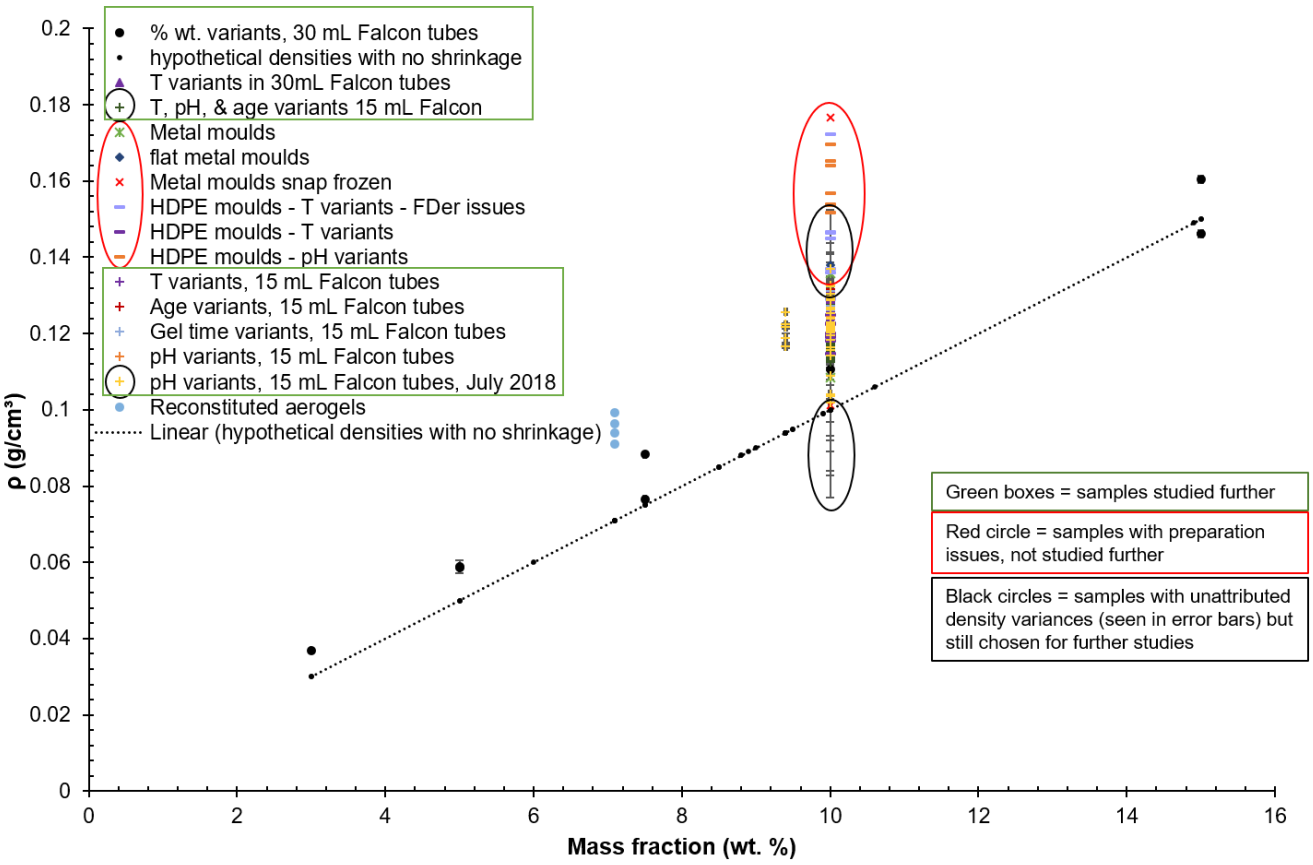

Figure 6.36: *Bulk densities (ρ) of CSM protein aerogels as a function of the mass fraction of CSM protein. Presented as batches (series) with varying preparatory conditions (refer plot legend). Trendline represents hypothetical densities for aerogels produced without change to the wet-gel volume (i.e. no shrinkage). Error bars represent the standard deviation in samples with identical preparation conditions. Red circles summarise samples with unacceptable shrinkage levels. Black circles highlight large density variance unattributed to gelation condition variations.*

6.4.2. Porosity and microstructure

Alongside density measurements, confirmation of an aerogel structure should also include evidence of porosity. Imaging the sample is a common and accessible way to verify and measure porosity. This can include non-invasive 3D imagery (X-ray microtomography) or more commonly, 2D imaging of sections cut from the sample (scanning electron microscopy). Analysis of the CSM protein aerogel microstructures was completed using both techniques, where scanning electron microscopy (SEM) was used to analyse a selection of samples and was complemented with µ-CT imaging of one sample. SEM imaging achieves higher resolution and provides detail about topological features of the aerogel pores. X-ray microtomography (µ-CT) was introduced as a non-invasive imaging technique to verify the accuracy of porosity descriptions obtained from SEM images after blade damage was identified as the cause of artefacts in some SEM images. 3D reconstruction from the µ-CT images also allows for a measurement of total porosity in the aerogel, complementing density measurements from **Section 6.4.1**.

X-ray microtomography (µ-CT)

A single freeze dried CSM protein aerogel, prepared at 10 wt% CSM protein, a pH of 11.7, and gelled at 60 ºC for 30 mins, was examined by X-ray microtomography (µ-CT). This aerogel was found to mainly exhibit macro-porosity, as expected in protein aerogels produced by freeze drying (**Figure**

6.37).

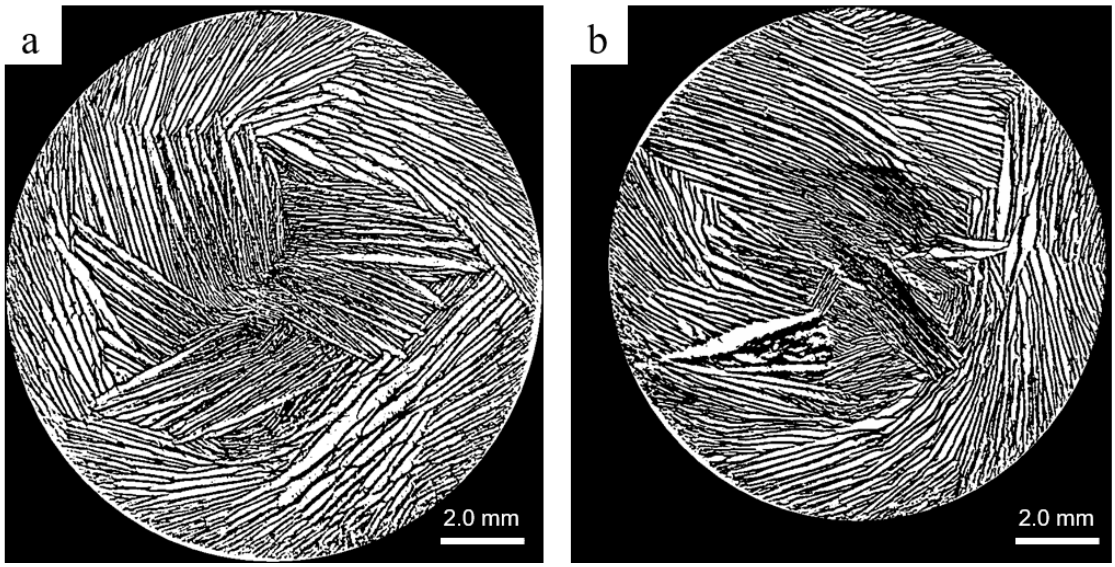

Figure 6.37: *X-Ray micro-tomograms of a CSM aerogel, prepared at 10 wt% and pH of 12, taken at z-axis positions of* ***(a)*** *0.030 mm and* ***(b)*** *15.182 mm, where z = 0 mm the end of specimen near opening of the Falcon™ tube and z = 36.18 mm is the end of the specimen at the conical point*

The porosity observed in the CSM protein aerogels was largely found to be organised in layers of elongated macro-pores that range in width from 30 to 200 µm and from 100 µm to over 3000 µm in length. The macro-pores exhibit localised regions of parallel pores, but with an overall anisotropic arrangement. The pattern of pore growth is very likely to be caused by ice crystal growth that has occurred in the wet-gel as it was frozen, and the resulting porosity is largely determined by that ice formation. Two-dimensional µ-CT images of the transverse cross-sections allow for the three-

dimensional reconstruction of the aerogel sample and visualisation from other axes (**Figure 6.38**).

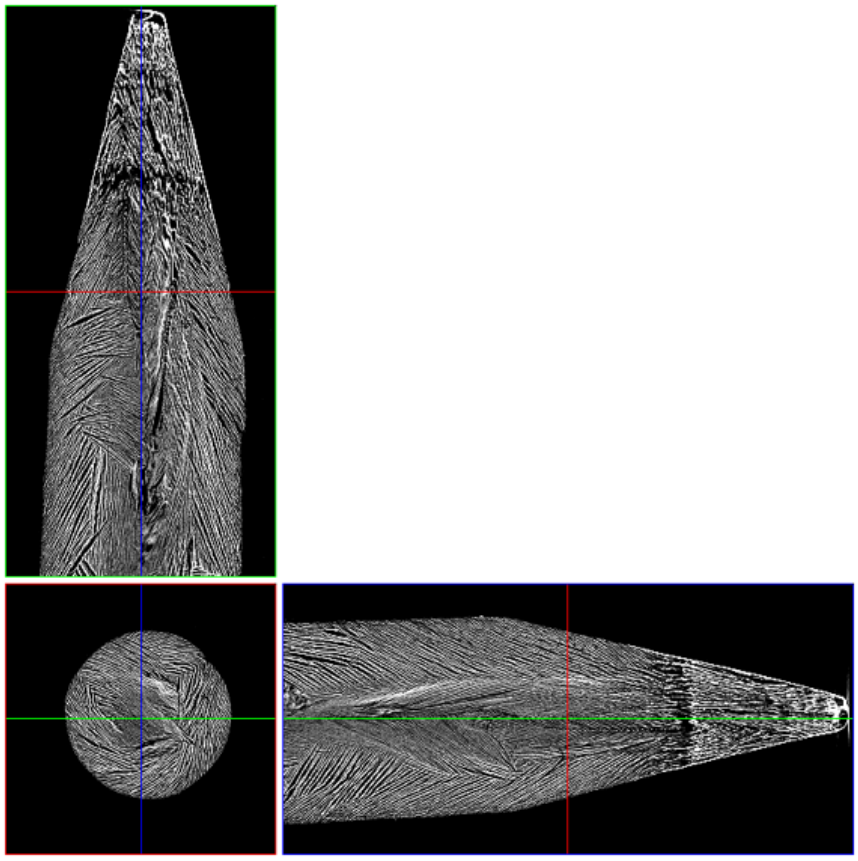

Figure 6.38: *Reconstruction of longitudinal cross-sections of CSM protein aerogel from 2D transverse micro-computed tomograms*

The 3D reconstruction reveals a value of 52.6 % porosity in the entire specimen as calculated from the binarized images at 15 µm resolution. Considering the density of the specimen was 0.125 g/cm^3 and the theoretical density of a perfectly dried, 10 wt% CSM protein aquagel with 0 % shrinkage is 0.100 g/cm^3 (90 % porous), the shrinkage in the sample was estimated at 20 %. Using the assumption that the solid protein has a density of 1 g/cm^3, the total porosity of the sample is therefore estimated at 87.5 %. The finding of approximately 53 % porosity in the µ-CT 3D-reconstruction indicates that approximately 35 % of the porosity can be found in pores of less than 15 µm in size. Higher resolution is required to visualise this porosity and can be achieved using electron microscopy. Subsequent Scanning electron microscopy (SEM) analysis aims to image this smaller-scale porosity

in the aerogel specimens. Additionally, gas adsorption experiments can be used to further study micro- and meso-porosity and quantify the porosity according to each category (see **Section 7.4.3**).

Scanning electron microscopy (SEM)

SEM analysis of the aerogels looked at three different areas of the freeze dried gels: surface, transverse cross-section, and longitudinal cross-section (**Figure 6.39**). Most images are of the transverse cross-section with the direction and proximity to the surface indicated.

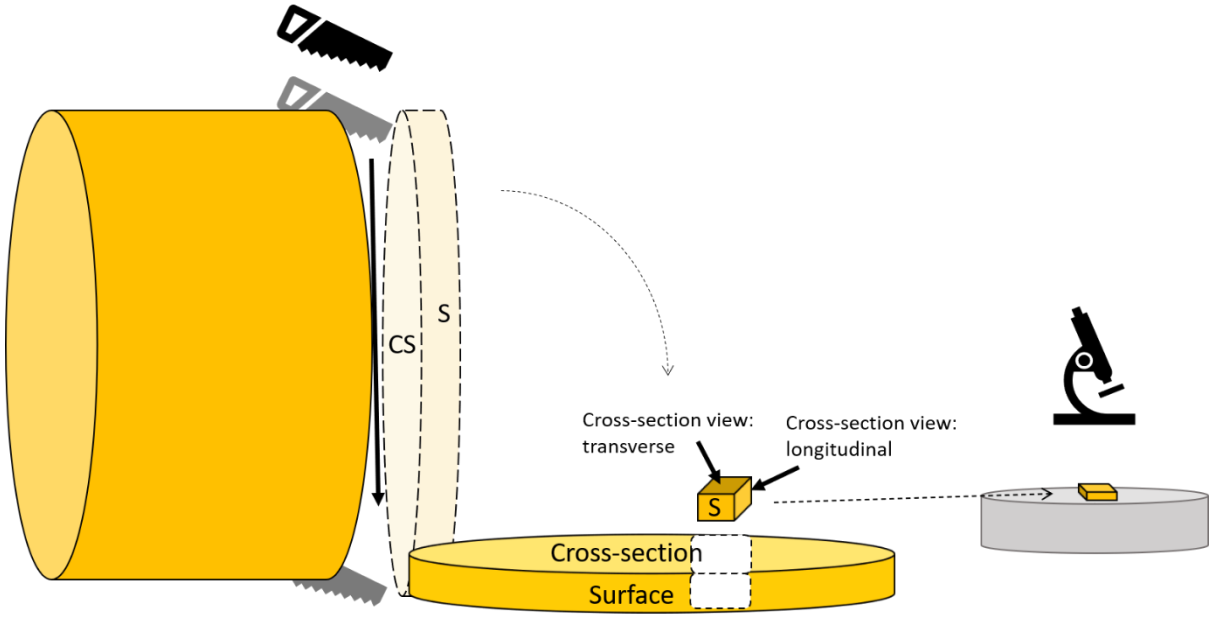

Figure 6.39: *Schematic of specimen preparation for SEM imaging, showing the cross-section (CS) and surface (S) regions of the cylindrical aerogels*

SEM imaging of the same aerogel sample that was imaged with µ-CT, revealed the macroporous structure in finer detail (**Figure 6.40**). The macro-pores change in shape and size in different locations within the aerogel, with the average sample containing macro-pores ranging from 50 µm near the core up to 125 µm in width near the surface (average 75 µm). The walls of the macro-pores range from 1–20 µm in thickness with an average of 6 µm. The transverse cross-section of the aerogel reveals a range of pore shapes, from almost circular to elongated oval pores (**Figure 6.40 a & b**) and pores appear to extend into the aerogel along the longitudinal axis (z-axis in **Figure 6.40**). Two interesting features identified in the SEM images at higher magnification include vein-like protrusions on the

surfaces of the pore walls (**Figure 6.40c**) and amorphous lumps or particles, possibly tiny gel pieces or large protein aggregates (**Figure 6.40d),** also found on, and inside, the pore walls**.** The protrusions may be remnants of partially formed pore walls as the distance between branches of the veins (30 – 100 µm) is similar to pore widths. The macro-pores also demonstrate localised regions of anisotropy attributed to unidirectional growth of ice-crystals during the freezing process. All CSM aerogel specimens imaged using SEM revealed these same major features; a porous landscape dominated by macropores on a scale of 50 – 2000 µm, with textured pore walls around 5 – 10 µm in thickness, some possessing surface protrusions and aggregates.

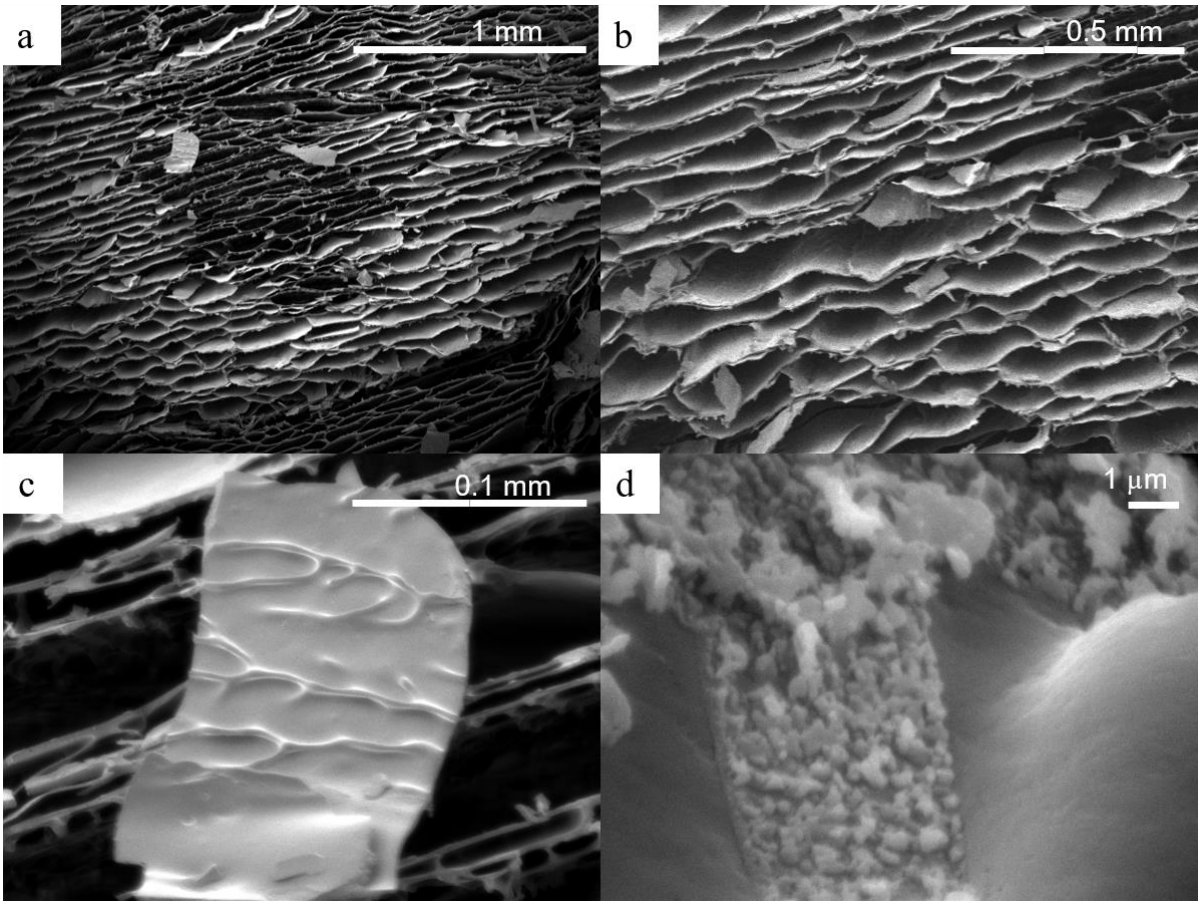

Figure 6.40: *SEM micrographs of the same CSM aerogel sample previously imaged by µ-CT, showing the transverse cross-section at 50 × magnification* ***(a)*** *and near the centre at 100 × magnification* ***(b).*** *Broken piece of pore wall with vein-like protrusions* ***(c)*** *and textured surface of pore walls at 11000 × magnification* ***(d)***

A comparison of aerogel morphology across specimens with varying gelation conditions was then carried out, with a focus on the CSM protein concentration (wt%*)* and gelation pH. Increasing aerogel density with increasing protein concentration was established in **Section 6.4.1.** Therefore, a change in the microstructure of the aerogels with changing wt% of CSM protein was expected. Changes to the layered morphology with changing wt% were found, with the average spacing between macro-pores decreasing from 150 to 40 µm with an increase in protein concentration from 3 to 15 wt% (**Figure 6.41 a – c**).

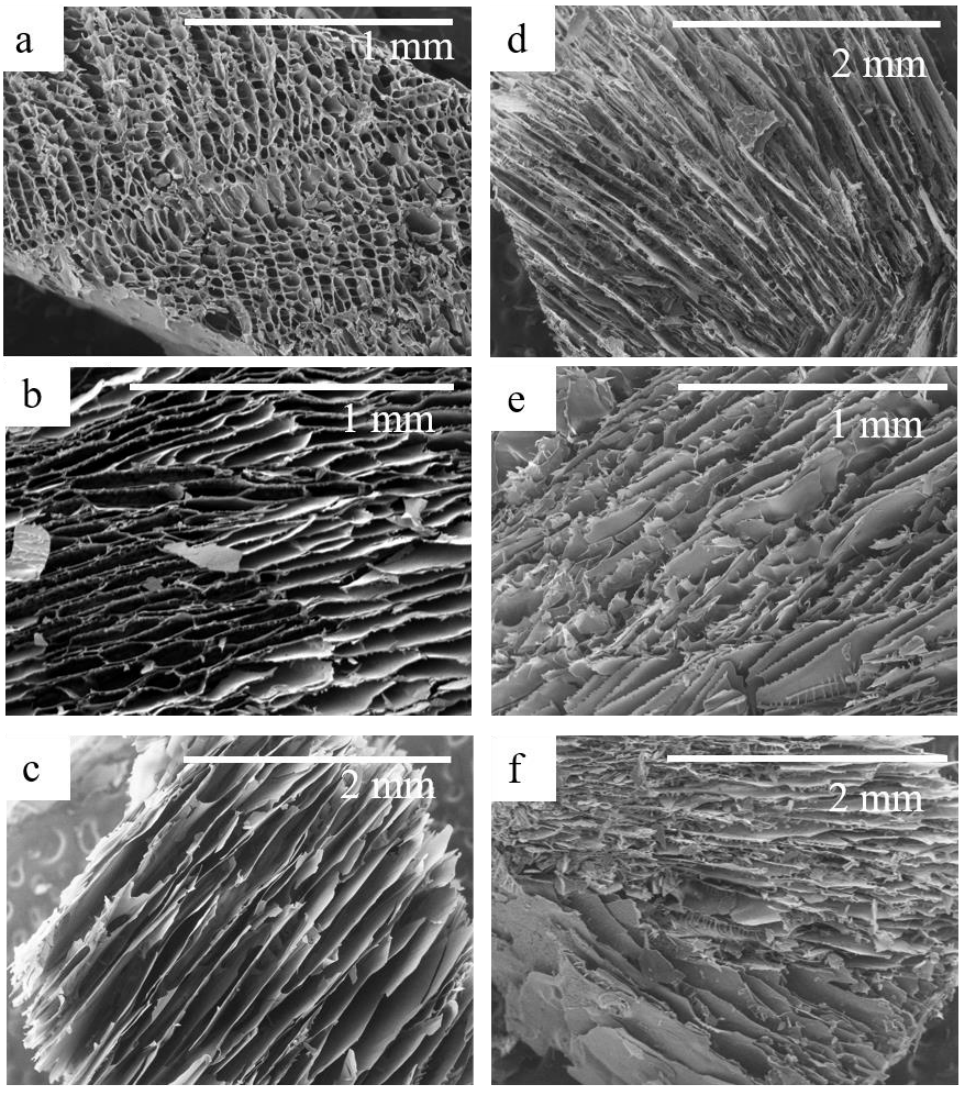

Figure 6.41: *SEM micrographs of CSM protein aerogel morphology as a function of protein concentration* ***(a – c)*** *and pH* ***(d – f)****. Protein concentrations were prepared at 15 wt%* ***(a),*** *10 wt%* ***(b)*** *and 3 wt%* ***(c)*** *at a pH of 11. Further pH variations with prepared at pH 8* ***(d),*** *pH 10* ***(e),*** *and pH 12* ***(f)*** *at protein concentrations of 10 wt%*

Remarkably, changes in the pH did not change the average spacing between the macro-pores (**Figure 6.41d – f**). The lack of influence of pH on the aerogel macro-porosity is consistent with the macro-porosity being largely determined by the freeze drying process and total amount of protein (wt%).

Next, the SEM analysis focused on imaging of pore surfaces and walls at the sub-micron scale (**Figure 6.42**).

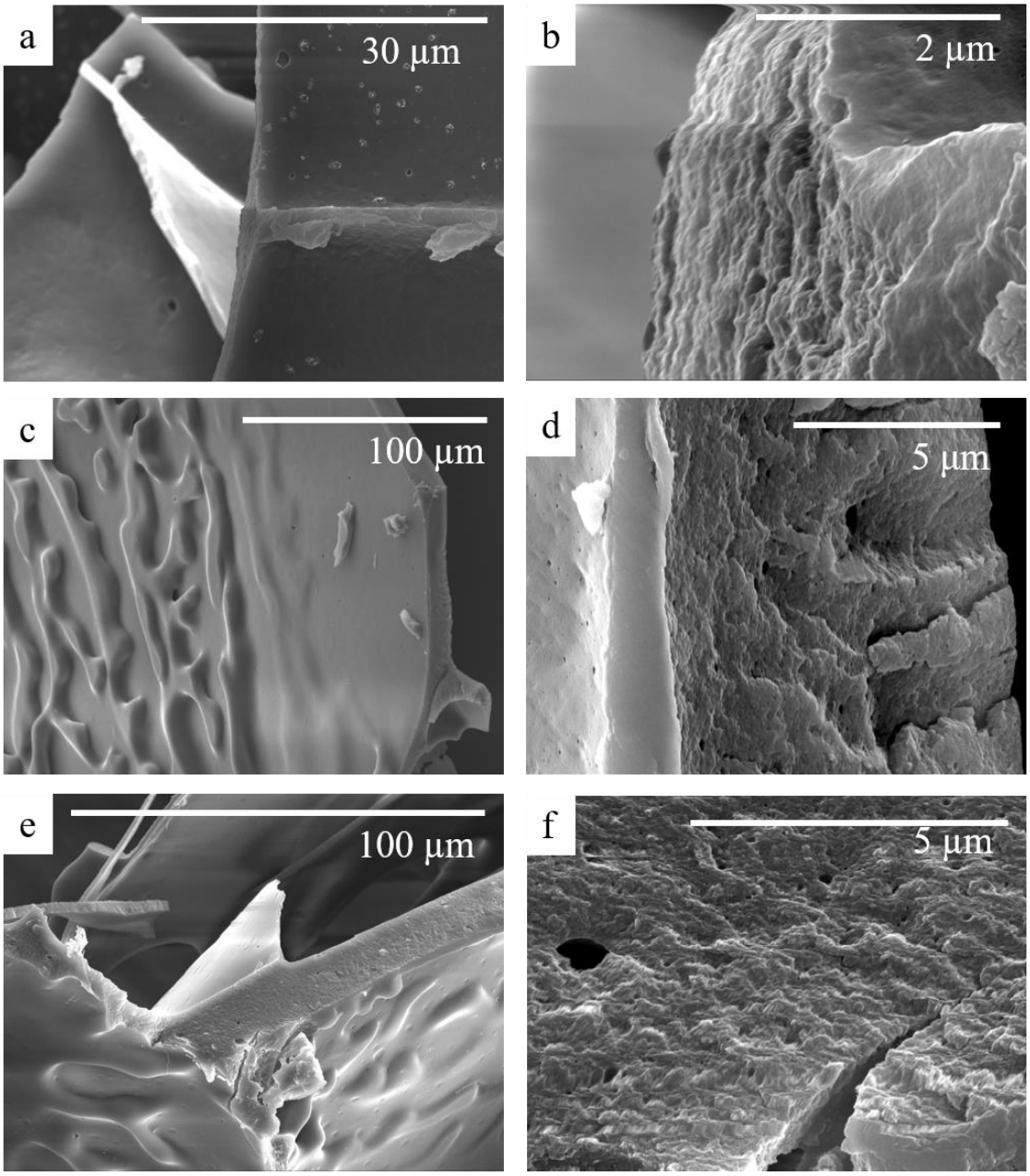

Figure 6.42: *SEM micrographs of CSM protein aerogels at high magnification. Cross-sections of aerogel samples prepared at: pH 8* ***(a & b)****, pH 9* ***(c & d)****, and pH 11* ***(e & f)***

The SEM micrographs demonstrate occasional holes and pockets of sub-micron scale at high magnification (**Figure 6.42 b, d, & f**), indicating the possibility of mesopores (< 50 nm in diameter) inside the protein matrix or in the pre-dried gel structure. The macroporous freeze dried aerogel structure may be the result of a mesoporous wet-gel network that has been compressed by ice crystal growth during the freezing which is required prior to freeze drying. The layered macro-pores are very distinct from the much smaller macro-pores (1-10 μm diameter) and possible meso-pores (< 50 nm) that occur sparsely within the matrix of the aerogel, further suggesting that the origin of these pores is likely different to that of the much larger, layered macropores. Furthermore, varying the pH of the CSM protein aerogels does not appear to alter the presence and size of smaller macro-pores (< 1 μm) or mesopores (< 50 nm) within the protein matrix across a pH range of 8 – 11 (**Figure 6.42**).

The intriguing presence of particles on the surface of the otherwise smooth matrix walls was further investigated with SEM imaging **(Figure 6.43).** Interestingly, these particles do appear to be influenced by the pH of the wet-gels. They range in diameter from 100 nm to >1 μm and notably increase in size from a pH of 7 to 8 (**Figure 6.43**). The average diameter of these particles at pH 7 is 170 nm while at pH 8 they increase to an average diameter of 1.2 μm then decrease to 600 nm at a pH of 12. Proteins will undergo a process of denaturation and aggregation during gelation, that results in a particle-based network (as observed in other globular proteins such as whey and egg proteins [146]). It is probable that the 100 – 1000 nm sized particles visible in micrographs may be manifestations of a similar particle-based gelation process in the formation of CSM protein gels. This idea is explored further alongside additional evidence in **Section 8.4**.

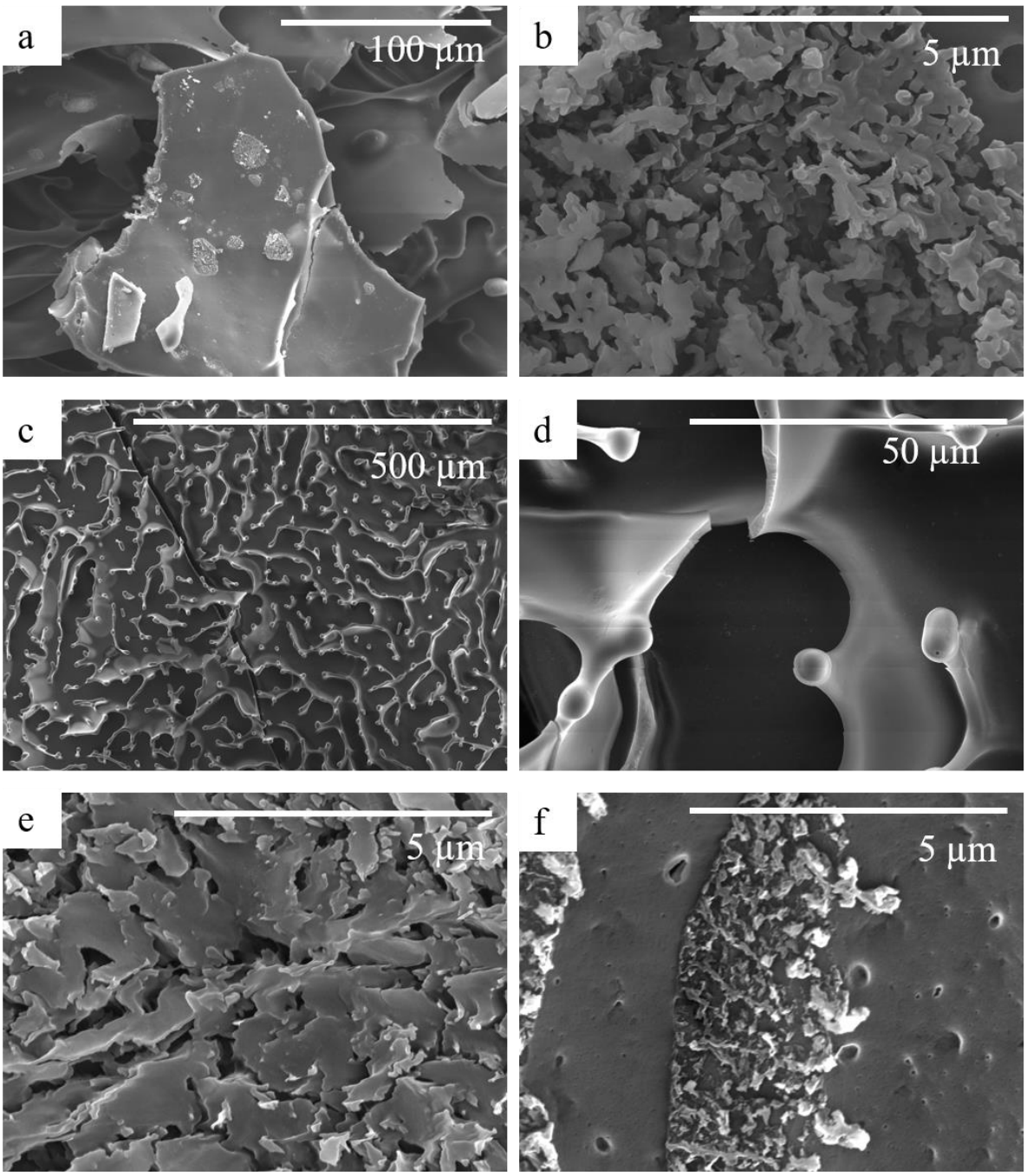

Figure 6.43: *SEM micrographs of morphological features appearing on the surface of CSM protein aerogel matrices. Surface of matrix from CSM protein aerogel prepared at pH 12* ***(a & b)****, pH 10* ***(c & d)****, pH 8 I and pH 7* ***(f)*** *at 10 wt% protein concentration*

The final gelation parameter that was investigated using SEM imaging was the effect of gelation temperature on the microstructure of the aerogels. The samples selected for SEM imaging were prepared at temperatures ranging from 25 to 100 °C. However, these samples were also among those that exhibited enhanced shrinkage (represented in black circle in **Figure 6.36** showing higher than average densities). Inspection of the aerogels post-drying revealed sections of the outer surfaces,

particularly those at the conical end of the aerogel, had a hard, glossy, shell or coating (**Figure 6.44**). This glossy coating and associated high shrinkage were attributed to partial defrosting of the samples prior to complete drying. Defrosting results in evaporation of the water, rather than sublimation of the ice, causing gel structure to collapse. The coating occurred in the segments of the aerogels furthest from the vacuum source (the conical end of the Falcon™ tubes) and hampered attempts to look for structural variances. Some evidence was found that higher gelation temperatures lead to smaller, more rounded pores with thinner pore walls (**Figure 6.44e-f).** However, the above differences cannot be conclusively attributed to the gelation temperature variances due to the poor quality of the specimens and probable effects of sample defrosting.

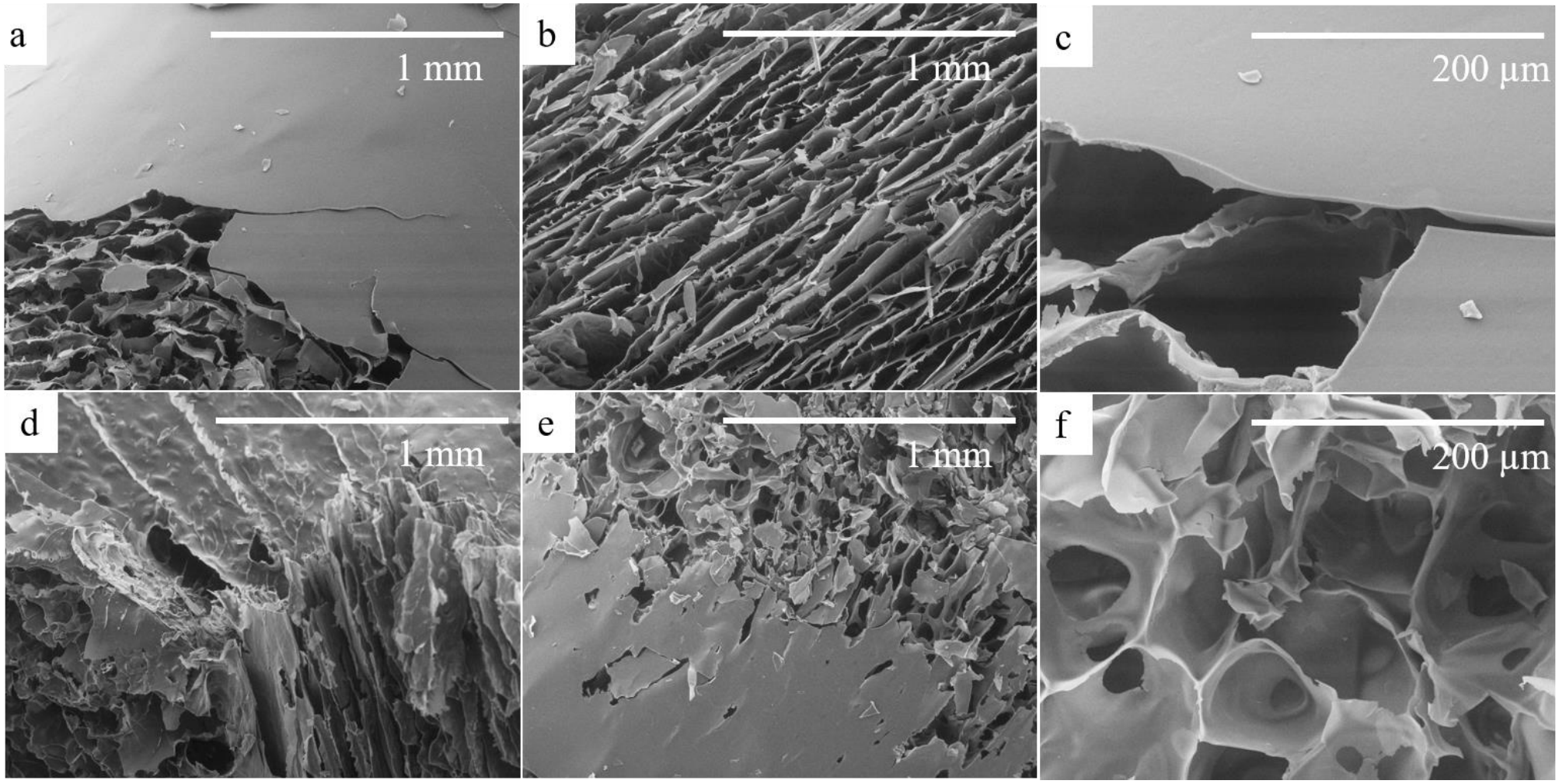

Figure 6.44: *SEM micrographs of CSM protein aerogels prepared at 25 °C* ***(a – c),*** *70 °C* ***(d),*** *and 100 °C* ***(e – f),*** *at a pH of 12 and 10 wt% protein concentration. Micrographs are taken at x 100 magnification* ***(a – b, d – e)*** *and x 500 magnification* ***(c & f),*** *and show the aerogel surfaces (****a, c, & e),*** *and cross-sections (transverse* ***(b & f)*** *and longitudinal* ***(d)).***

SEM and μ-CT images have revealed how CSM protein aerogels produced *via* a freeze drying route, are largely macroporous dried solids, with approximately 35 % porosity hidden in sub-15 μm-sized pores. CSM protein aerogels contain pore walls that are approximately 8 % thickness of the corresponding pore width. These pore walls are revealed at higher magnification to possess a range of vein-like and amorphous particle-shaped protein deposits and have an internal textured structure that likely contains some mesoporosity. The mass fraction (wt%) of the protein wet-gel determines the size of the macropore width (increasing mass fraction reduces pore sizes) and corresponding aerogel densities. Ice-crystal growth likely causes the anisotropic layered appearance of aerogel macro-pores observed in all freeze-dried specimens. Other gelation parameters, for example temperature and pH, were not determined to influence the porous structure of the aerogels, but possibly alter the finer structure of the gel network, such as the size of protein aggregates (see **Figure 6.43**).

6.5. Properties of canola protein aerogels

A fundamental tenant of materials science, explored in **Chapter 2**, is the dependence of material properties upon the material morphology. Many aerogel properties are directly dependant on the porosity and microstructure, though in some cases (*e.g.* the hydrophobicity of some silica aerogels) the chemistry of the polymer can also influence the aerogel properties. The current Section explores the basic mechanical properties of the CSM protein aerogels as a benchmark property with which to compare the CSM protein aerogels against other protein-based and bio-based aerogels (**Section 6.5.1**). Other properties that are briefly explored include the thermal properties (**Section 6.5.2**) and the solubility of CSM protein aerogels in aqueous solutions (**Section 6.5.3**). The combined knowledge of a range of aerogel properties allows the CSM protein aerogels to be placed in context with existing aerogel types and for assessment of their application potential.

6.5.1. Mechanical properties

Mechanical properties of aerogels are useful measurements for establishing an application of the final aerogel product. The structures must be capable of withstanding forces that might be applied during use of the aerogel and/or possess a certain level of machinability, depending on the application. The high strength-to-weight ratio of the aerogel is one of its defining features, and often the strength alone is not as useful as the specific strength (strength to density ratio) of the aerogel. Mechanical properties of interest include the strength, elastic modulus (a determining factor for stiffness), and strain to failure. Examples of aerogels in applications where mechanical properties are of high importance include: polyimide aerogels for aircraft panels; silica aerogel panels for building insulation and day-lighting; bioaerogels for tissue engineering; aerogels for packaging; and aerogels subject to pressurised liquids (such as in filtering applications). Aerogels too fragile to be subsequently handled and processed for application-specific purposes are not appropriate candidates for those applications, regardless of the complimentary properties, such as thermal insulation, they may possess. Additionally, it is the mechanical performance of protein-based materials that often fails to achieve

comparable standards to more popular biopolymers such as cellulose, therefore excluding proteins as a viable choice of precursor molecule for bio-based polymeric materials. An assessment of the mechanical performance of protein aerogels permits their evaluation as green alternatives for existing aerogel applications. The compressive properties of whey protein aerogels [120], whey protein hybrid (with alginate) aerogels [118], silk fibroin aerogels [42, 92, 102, 110, 123], casein hybrid (with clay) aerogels [121], and egg-white protein aerogels [103] are reported in the protein aerogel literature.

Measuring the mechanical properties of aerogels, particularly protein-based aerogels, can be a challenging task due to the brittle and sometimes delicate nature of the samples. Mechanical testing of aerogels can be easier with a compressive test as compared to a tensile test which is a popular standard for testing of polymeric materials. The compressive test does not require the use of grips that could damage the sample prior to measurement, and it can also be a more appropriate measure of application-related properties (*e.g.* compressive strength and stiffness for packaging or insulation). A typical aerogel stress-strain curve generated from a static compressive test exhibits linear elastic behaviour prior to a 'yield' stress. The yield stress of an aerogel is, perhaps more accurately, referred to as the collapse strength, and is used for comparison of compressive strength in aerogels [248]. A plateau in stress is observed at strains beyond the yield point that marks the onset of the compaction phase in aerogel deformation where the gradual collapse of the pore structure begins. Silica aerogels are well known for their brittle nature and have an onset of the plateau occurring at a compressive strain of ~ 5 %. Following the plateau, at much greater strain, aerogels undergo a densification phase where stress increases once more, and the structure is compacted until little to no porosity remains.

In this work, the CSM aerogel strength is determined from the measurement of the yield stress (collapse strength) in static compression tests where the monolith is compressed at a constant rate of displacement. Identifying the yield stress in the stress-strain plot can be difficult and relies on concurrent observation of the onset of the plateau region and of the collapse and/or fracture in the specimen. Determining the strain at the point of yield (or elastic limit) is also a useful property for comparison since the linear region generally represents recoverable deformation of the specimen. The yield strain of aerogels is useful measurement for applications such as tissue engineering where

flexibility and compressibility are important for compatibility with physiological systems [249]. Some exemplary aerogels demonstrate a linear elastic regime up to 60 % compression [250]. The elastic modulus is also determined from the static compressive tests using the slope of the stress-strain plot within the linear region. The elastic modulus is also a key property for comparative assessment of stiffness in aerogels. Resistance to deformation is useful for applications where aerogel monoliths are required to maintain shape under applied forces, for example, as insulating panels in construction or packaging.

6.5.1.1. General compressive testing of CSM protein aerogels

Static compression tests carried out on cylindrical monolithic specimens of the CSM protein aerogels produced typical aerogel stress-strain curves (**Figure 6.45**). Linear regimes were followed by a plateau (or slight decrease) in stress with the onset of aerogel collapse, eventually leading to a densification region at strains > 0.6 (**Figure 6.45a**). Yield (or collapse) strengths and yield strains were determined from stress-strain data by identifying the end of the linear regimes. Additionally, elastic moduli were calculated by the slope of applied linear trends to the linear regimes where the coefficient of determination (R^2) was > 0.99 (**Figure 6.45 c-d**). Stress-strain plots presented with an initial non-linear region ('toe region') at < 2 % strain that was initially attributed to samples bedding in the platens due to the imperfect specimen surfaces. The delicate nature of the samples meant perfectly parallel cuts were difficult to achieve and so it was assumed that imperfect specimens were the cause of the toe regions. However, later evidence (see cyclic testing below) suggests that the toe regions may be a phenomenon of the aerogels. Small gaps in the data from the origin to the first measurements can sometimes be noted, due to initiation of data recording occurring after preloading in some cases. Often these gaps encompass the toe regions (**Figure 6.45 b-d**).

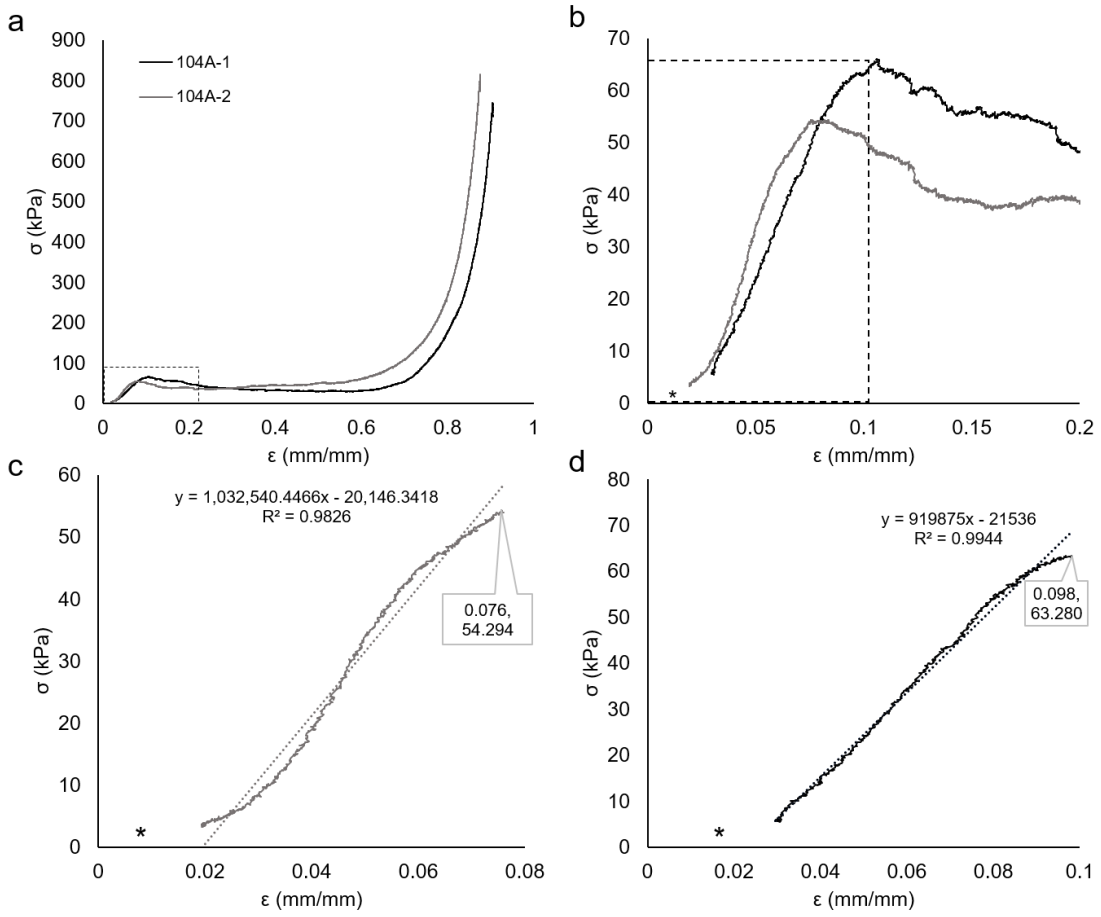

Figure 6.45: *Typical stress-strain curves generated from compression testing of CSM protein aerogel specimens* ***(a)*** *with the linear regimes enlarged* ***(b)*** *and with annotations to show identification of elastic modulus, yield strength, and elastic limit* ***(c – d). ****Delayed initiation of data recording (post preloading) sometimes caused a gap to the origin*

Cyclic testing was also carried out on selected aerogel samples to briefly assess the recoverability of the deformation in the aerogels. The observation of the toe region in repeated cycles of compression testing (**Figure 6.46**) may indicate that initial non-linear behaviour is not attributable to sample bedding in platens but is a phenomenon of the aerogels. The return of the toe region upon unloading is inconsistent with the assumption that protrusions on the sample surfaces are bedding in platens. Protrusions generated from poor cutting would be compressed to irrecoverable strains before the entire cross-sectional area of the sample embraces the load and the onset of the linear region occurs.

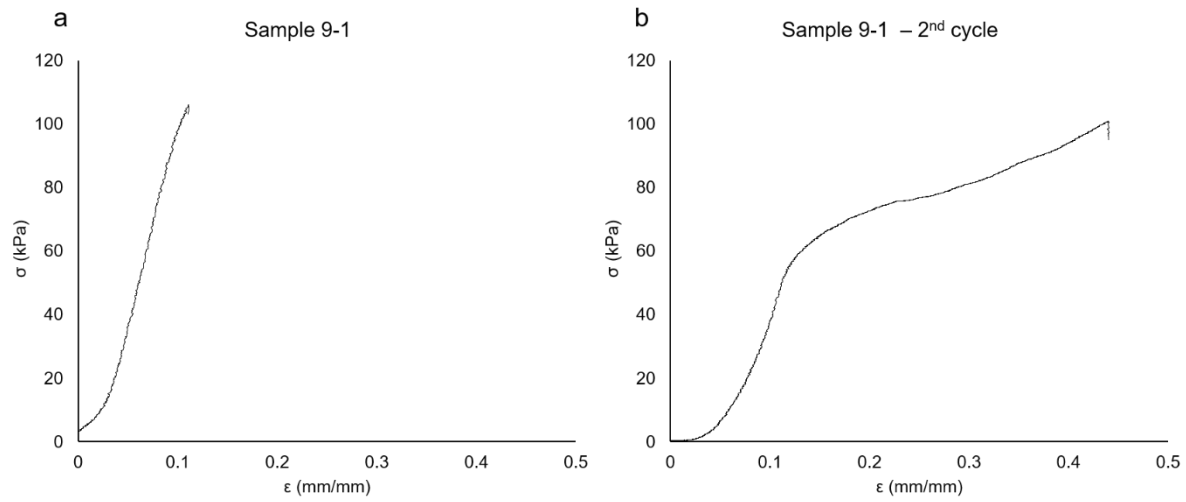

Figure 6.46: *Example of stress-strain curves generated from **(a)** an initial compression test and **(b)** a repeated compression test on the same CSM protein aerogel (prepared at 15 wt% CSM protein, pH 10.9). NB: data recording was commenced after preloading in test **(a)** consequently truncating initial toe region*

Interestingly the toe region can also be noted in compressive testing of bioaerogels from other studies [121, 125] (see **Figure 6.47**) though Finlay *et al.* (naming the region an 'induction period') also attribute it to non-parallel compression surfaces on the aerogels [125].

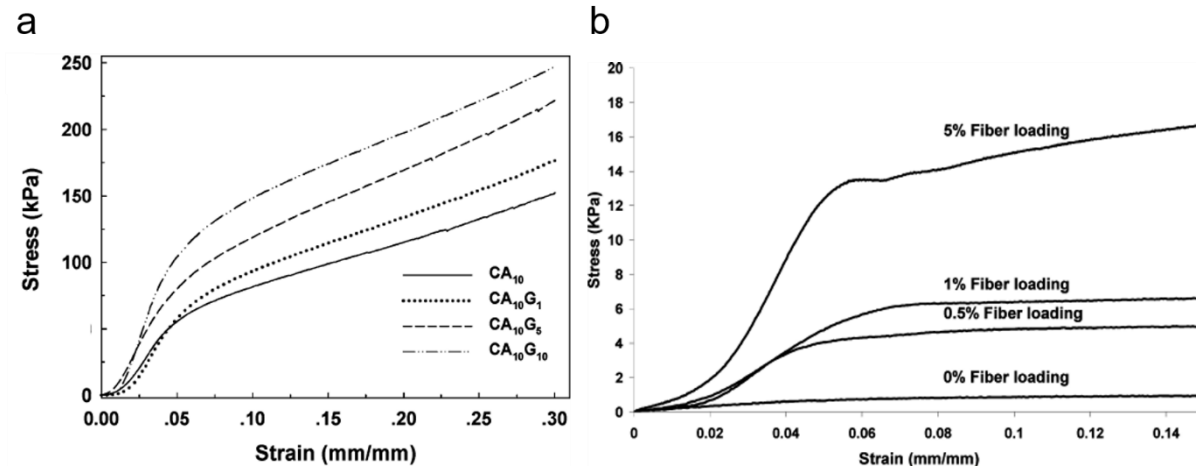

Figure 6.47*: Examples of **(a)** a casein-clay composite aerogel and **(b)** a clay-soy silk fibre composite aerogel that display an initial non-linear response to compressive testing. Figures are adapted and reprinted from **(a)** Pojanavaraphan, T., et al., (2010), Biomacromolecules, 11(10), 2640-2646 [121] and **(b)** Finlay, K., et al., (2008), Industrial and Engineering Chemistry Research, 47(3), 615-619 [125]*

One explanation for the consistent appearance of the toe region is that one part of the aerogel structure may demonstrate a low modulus which is then succeeded by stiffer structures once the toe region is exceeded. However, further investigations into the toe region were not conducted in the current work since compressive data was primarily collected for comparison of collapse strengths and elastic

moduli. The contribution of the toe region to the mechanical data is small over the complete strain range of testing and did not impact measurements for collapse strength or elastic modulus.

CSM protein aerogels (10 wt% protein concentration) have an average compressive modulus of 1.11 ± 0.32 MPa and average compressive strength of 56 ± 12 kPa, respectively, where error represents the standard deviation (n = 58). Average values for specific modulus and strength are 0.009 ± 0.002 MPa/(kg/m³) and 0.46 ± 0.10 kPa/(kg/m³), respectively. These averages are calculated from 58 aerogel samples prepared with a unique set of gelation pH and temperature conditions, though each sample was measured (and sometimes manufactured) as multiple specimens (*i.e.* replicate number ranging from n = 2 to 10). The variances seen within individual batches, where each batch is designed to investigate a specific gelation condition, are reported in **Sections 6.5.1.2** to **6.5.1.5**. The range of values seen for the compressive modulus is 0.14 – 2.66 MPa, while for the compressive strength values range from 11 – 134 kPa. The above ranges represent the effects that the gelation conditions have on the aerogel properties as discussed in subsequent Sections.

An average value for the yield strain of the aerogels was also found (7.9 ± 2.8 % compression (n = 58)), while ranging from 3.0 to 17.2 %. While some variance could be expected due to gelation parameters (see **Section**s **6.5.1.2** to **6.5.1.5**.) there is also a possibility that methodological issues arising from inclusion of the toe region limit the accurate detection of yield strain. Thus, inclusion of the toe region may contribute to the large variance seen. Calculation of the elastic modulus and yield strength can still be consistently carried out on plots with and without (*e.g.* where data acquisition was only commenced after application of a preload) the toe region. However, it is more difficult to establish a consistent method for removing the toe region when measuring the strain value at yield. The chosen methodology was to include this toe region in measurements of yield strain since it was not clear whether the toe region is a phenomenon of the aerogels or an artefact of poor sample geometry (see above). Therefore, the inclusion of the toe region in yield strain calculations could have resulted in over-estimates of the true yield strain if the toe region is caused by non-parallel compression surfaces. For this reason, comparisons of yield strain in CSM protein aerogels should be made with caution and the true value for the average yield strain could be less than the reported 7.9

%.The yield strain is referred to as the ‘elastic limit’ in following tests, indicating its connection to aerogel elasticity and application relevance.

Cyclic testing has also revealed the aerogels retain reasonable strength and stiffness following compression beyond the yield point (**Figure 6.48**). Though repeated compression tests after yield reveal an expected decrease in the elastic modulus in most aerogels (**Figure 6.48a**), this response was not always present with some aerogels maintaining the elastic modulus in repeated compression cycles following initial yield (**Figure 6.48b**). Variable cyclic responses may be dependent on gelation parameters such as pH or temperature. Interestingly, the cyclic testing of sample 85 (**Figure 6.48a**) revealed that the recoverable deformation (19.2 %) can also exceed the extent of the linear regime alone (up to 5.5 % compression) suggesting that some of the deformation represented in the plateau region is recoverable. The cyclic testing of sample 98 (**Figure 6.48b**) followed a more conventional pattern of recoverable deformation (5.7 %) which matched more closely to the extent of the linear regimes of successive cycles. However, the calculation of recoverable deformation is also complicated by the inclusion of toe regions in both the yield strain and the onset of the second compression cycle. Cyclic testing was not a focus of CSM protein aerogel analysis, but these interesting findings suggest the possibility of a viscoelastic response in some CSM protein aerogels which could be investigated further in future studies. Further work should aim to elucidate the exact role of the toe region in the mechanical response of CSM protein aerogels to establish a refined methodology for calculating yield strain and recoverable deformation.

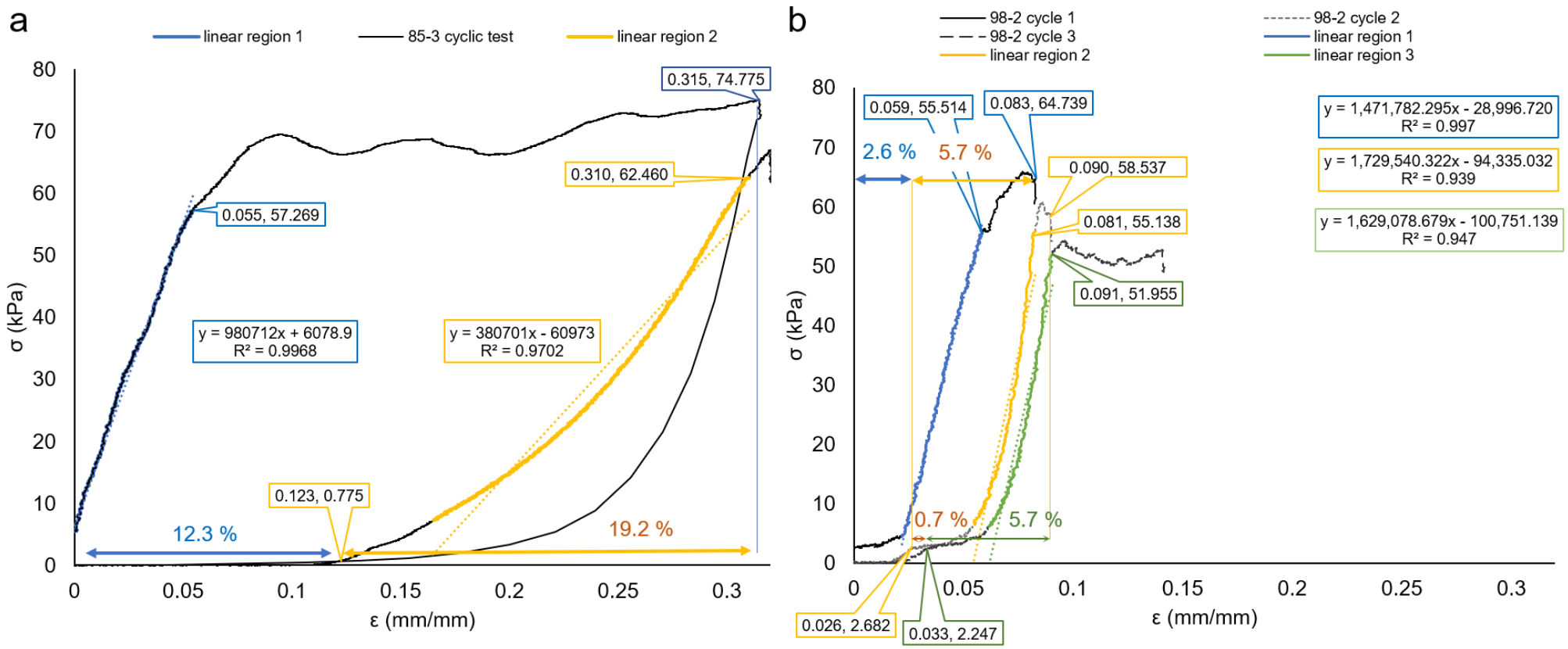

Figure 6.48 *Cyclic compression testing of CSM protein aerogels from sample 85, specimen 3 (pH 11.2, 60 °C)* ***(a)*** *and sample 98, specimen 2 (pH 8.0, 25 °C)* ***(b)****. Initial linear regions are highlighted in blue with subsequent cycles labelled in yellow and green.*

One further interesting note on mechanical behaviour comes from the use of reconstituted aerogels. These aerogels are produced from the crushed pieces of existing CSM aerogels rather than the use of fresh CSM protein powder (see **Figure 6.35**) in an effort to examine the recyclability of CSM protein aerogels. Mechanical analyses on these samples reveal a departure from the typical aerogel curve (**Figure 6.49**) with the plateau region disappearing and being replaced by a second, 'pseudo-linear' region, following the true linear regime. Consequently, identification of the yield stress was difficult and resulted in measurement of lower specific strengths (0.27 ± 0.08 kPa / (kg/m^3)) and elastic limits (3 – 6 %) than fresh CSM protein aerogels (0.46 ± 0.10 kPa / (kg/m^3) and 7.9 %, respectively). However, the inclusion of the second, 'pseudo-linear' region in calculations of elastic moduli and collapse strengths would indicate that these specimens are ultimately less stiff (40 - 60 % reduction) and stronger (at least 3.8-fold) than their 'freshly made' counterparts. Furthermore, cyclic testing reveals the 'recycled' aerogels also demonstrate discrepancies between the recoverable deformation and the true linear regime (*e.g.* 11.1 % recoverable deformation after an initial linear regime of up to 2.9 % deformation in **Figure 6.49c**). The 'pseudo-linear region' was not accompanied by obvious fracture in the specimen as was usual with other samples, perhaps indicating that the collapse of the pore network is a more gradual process and compressibility is much greater in reconstituted aerogels. The recycling of CSM protein aerogels was not a major study in this thesis, however, the above findings invite further tests in future studies to gauge the potential of increased compressibility and toughness in recycled CSM protein aerogels.

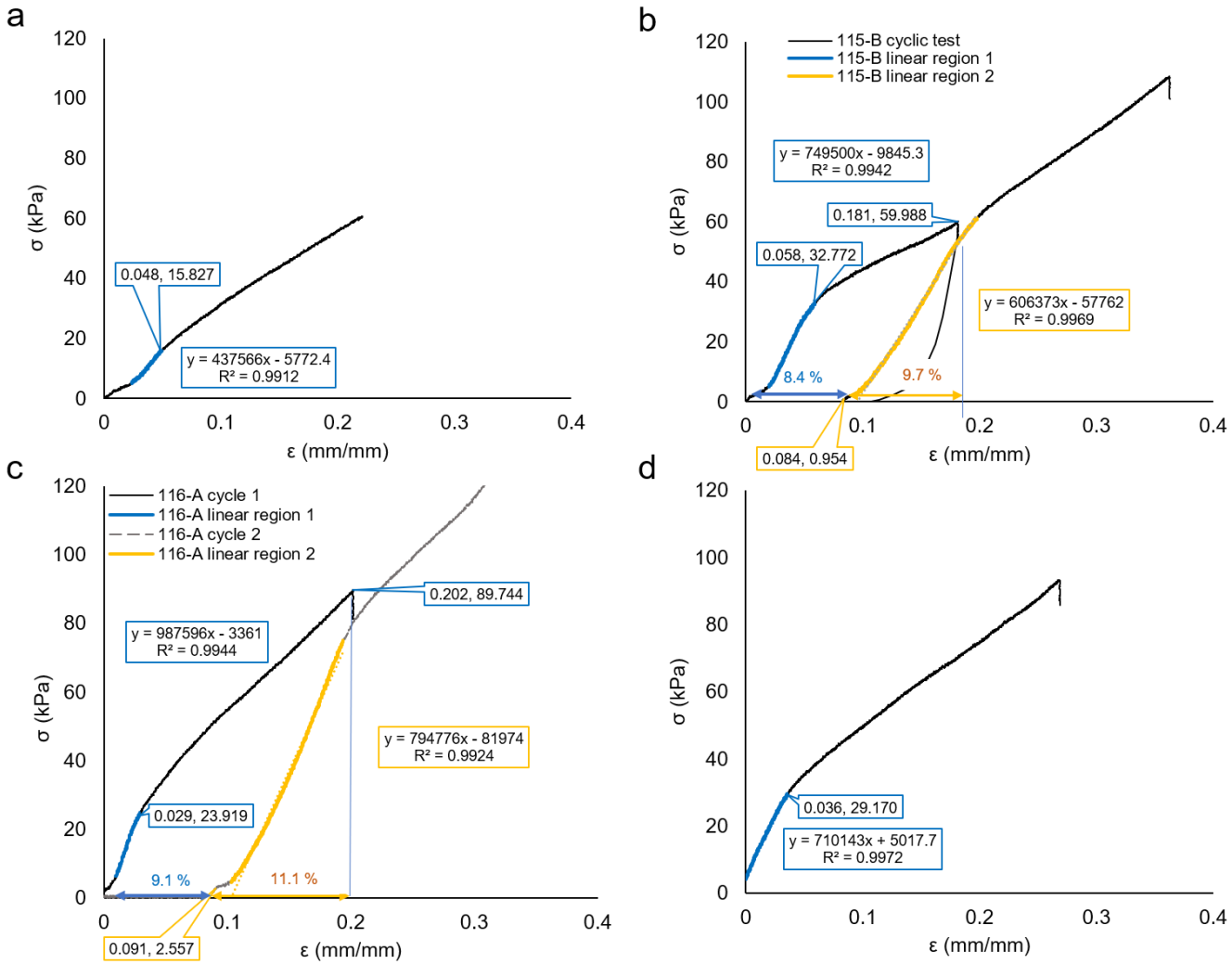

Figure 6.49**: Stress-strain curves generated from compressive testing of reconstituted CSM protein aerogels prepared with **(c-d)** and without **(a-b)** the use of sonication to assist dissolution of aerogel pieces into new formulation. Cyclic testing was carried out on two of the specimens **(b-c)

6.5.1.2. Effect of the CSM protein mass fraction (wt%)

Some of the first CSM protein aerogels produced and studied in this thesis were prepared with varying mass fractions (wt%) of CSM protein in the wet-gel, allowing for control of the corresponding aerogel densities (see **Section 6.4.1**). As for other porous media, the mechanical performance of the material is directly correlated to the porosity (or density) of the aerogel (**Figure 6.50**). Controlling the wt% of protein in the wet-gels directly affects the mechanical properties of the corresponding aerogels: increased protein concentration (wt%) results in increased strength and stiffness but reduced elasticity (**Figure 6.50d**). In these CSM protein aerogels (prepared at a pH of 10 – 10.8) the 15 wt% protein sample achieved the highest collapse strength of 101 kPa and elastic modulus of 1.24 MPa, while the 5 wt% sample achieved the greatest elasticity with an elastic limit of 23 % compression. Other studies have already suggested that preparation of aerogels at lower wt% concentrations may be one route for improving (increasing) elasticity and assessing potential for application in tissue engineering applications, as demonstrated in silk fibroin aerogels [92]. A compromise between bulk density of the sample, desired elasticity, and desired strength and stiffness must be struck when selecting a wt% in aerogels manufactured for a specific application. A protein concentration of 10 wt% was used for subsequent aerogel formulations to ensure that CSM formulation concentration remained comparable with other protein aerogels such as egg white protein [94], whey protein [127], and silk fibroin [251] aerogels.

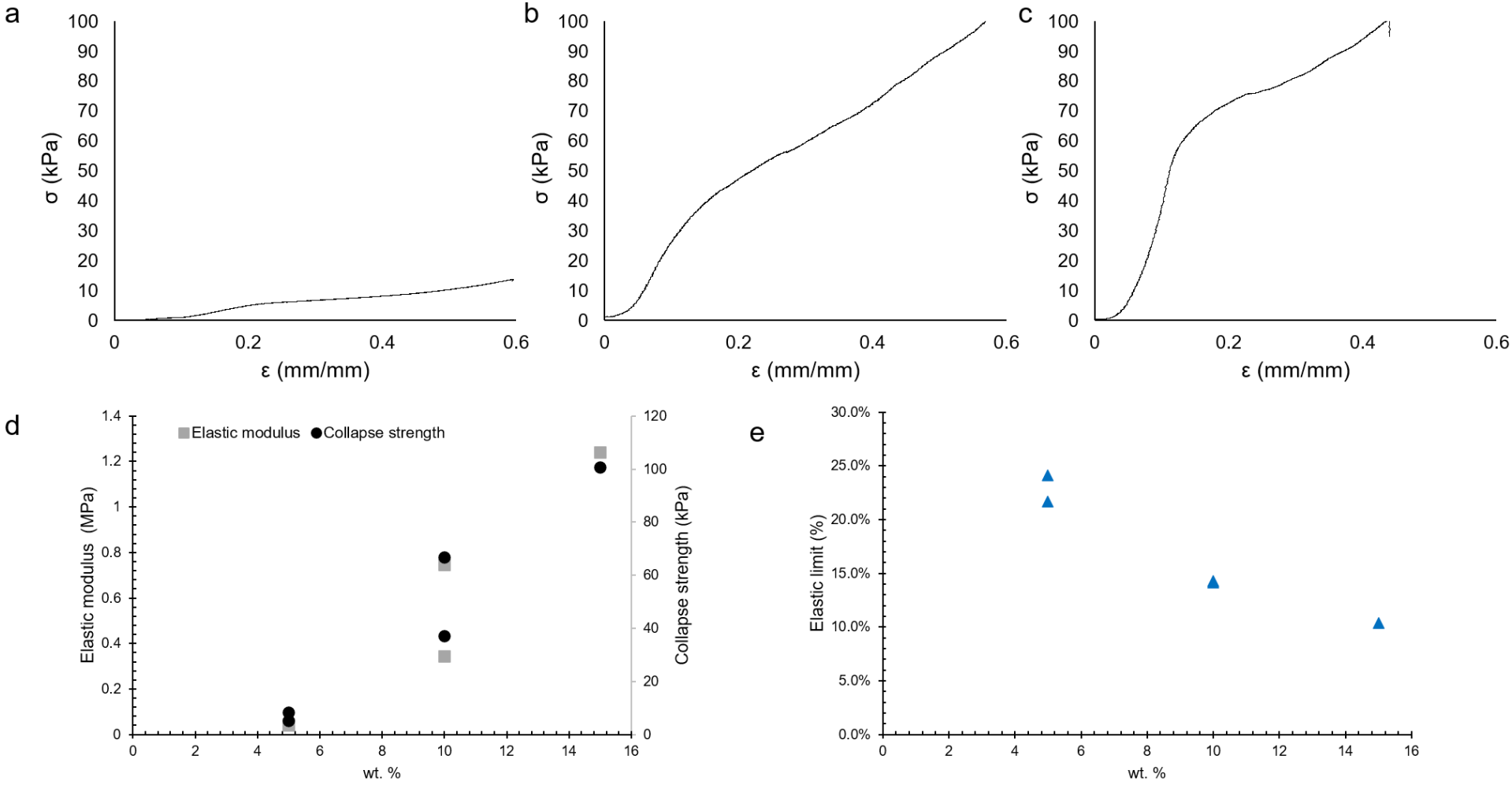

***Figure 6.50**: Stress-strain plots for CSM protein aerogels prepared at a pH of 10 – 10.8 and 25 °C with a CSM protein concentration of **(a)** 5 wt%, **(b)** 10 wt%, and **(c)** 15 wt%. Compressive strength **(d)**, moduli **(d)**, and elastic limit **(e)** values for aerogel specimens with varied CSM protein concentrations (wt%). Each data point in **(d)** and **(e)** is generated from one specimen (replicate samples for 5 & 10 wt% are plotted individually)*

The mechanical properties of CSM protein aerogels also increase with aerogel density (**Figure 6.51a**). A non-linear dependence on density is a characteristic of nearly all biopolymer aerogels as summarised in a recent review by Zhao *et al.* [11]. The authors summarised the compressive modulus dependency on density and found a strong correlation between $log_{10}E$ and $log_{10}\rho$. Subsequently, the authors identified the scaling component α in the simple scaling law $E \sim \rho^{\alpha}$, for a range of biopolymer aerogels and their composites [11]. However, protein-based aerogels were not included in the selected bioaerogels.

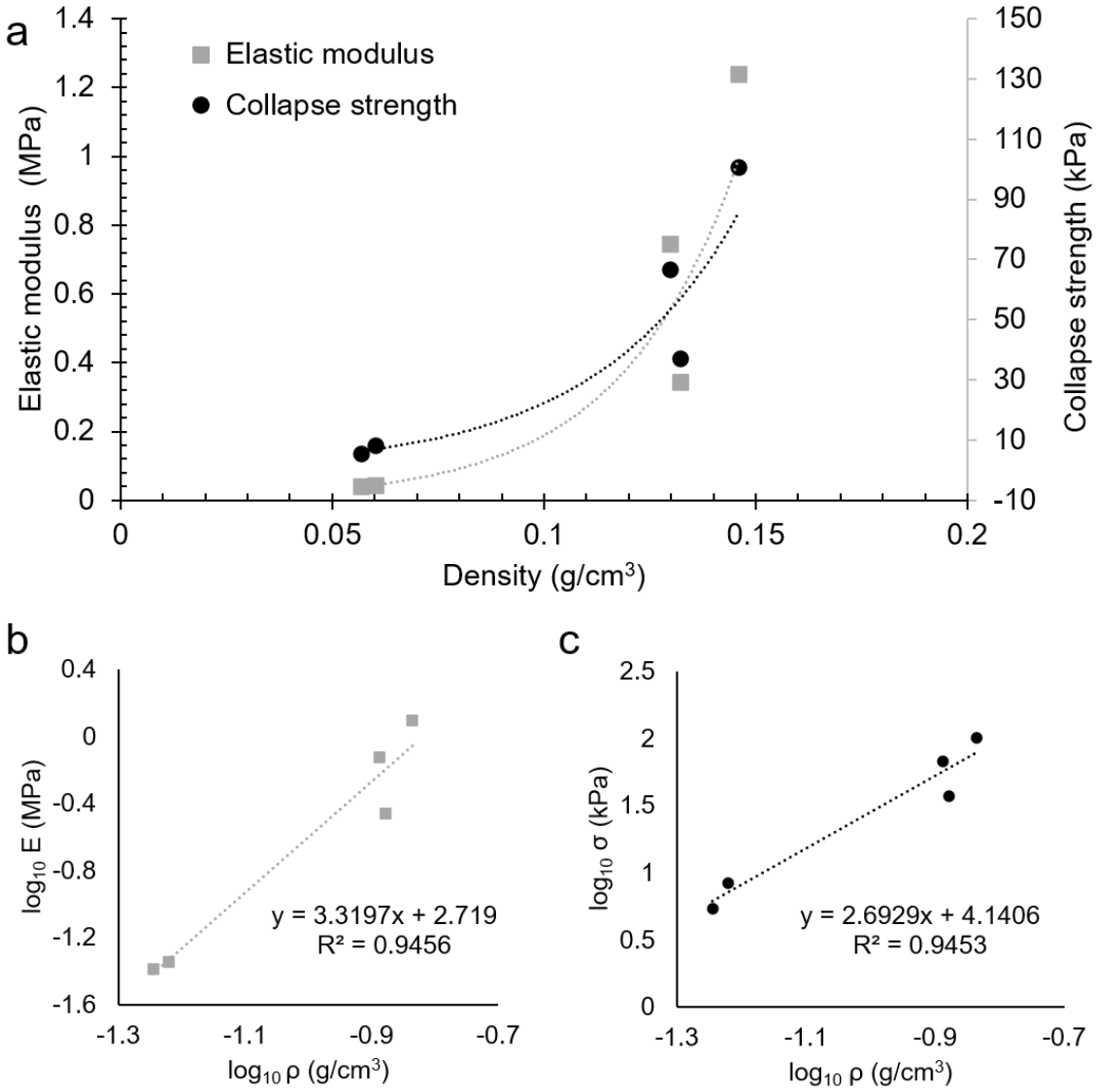

Figure 6.51: *Compressive elastic moduli and collapse strengths of CSM protein aerogels as a function of density* ***(a)*** *(each data point for modulus and strength is generated from one specimen) and the* $log_{10}E$ ***(b)*** *and* $log_{10}\sigma$ ***(c)*** *plotted as a function of* $log_{10}\rho$*. No variability data available as n = 1 for each data point.*

The findings in this thesis demonstrate that protein-based aerogels are likely to also have a non-linear dependence of E on ρ, where $E \sim \rho^{3.3}$ (**Figure 6.51b**) and $\sigma \sim \rho^{2.7}$(**Figure 6.51b**) for CSM protein aerogels. The CSM protein aerogels in the present study are macroporous with varied pore sizes and directionality (see **Figure 6.41**). The density-dependence of mechanical properties has been connected to morphology types in studies of organic aerogels, where the authors predict $\alpha > 3$ (for $E \sim \rho^{\alpha}$) in foams with irregular, fractal morphologies [252]. Therefore, CSM protein aerogels demonstrate a density dependence of compressive moduli that is consistent with predictions based on morphology.

One explanation for high variance in mechanical data is the observation of macroscopic anisotropy in the aerogels. The control of thermal gradients during the freezing process may allow for production of isotropic CSM protein aerogels and should be investigated as a possible method for reducing variance in CSM protein aerogel properties. Additionally, limited sample numbers may explain the variance observed in above results. The wt% variants (producing the above variation in densities) were early samples in this thesis that lacked more than two repeats for compressive testing, making it impossible to identify any outliers. They also lacked the method consistency developed over time with the production and testing of over 100 further aerogel specimens. Though the results **Figure 6.51** are consistent with the literature, they could be further consolidated with a repeated investigation into the effect of protein concentration on aerogel mechanical performance.

6.5.1.3. Effect of the gelation pH

CSM protein wet-gels are known to have pH- and temperature-dependent rheological properties, where alkaline pH and a temperature above 82 °C is optimal for gel network formation [178]. These pH- and temperature-dependent rheological features were also found in the CSM protein wet-gel precursors for the aerogels in this study (see **Section 6.3**). Thus, it is expected that the aerogels would follow a similar trend and have mechanical properties dependent on these same gelation parameters. CSM protein aerogels gelled at a range of pH values were subsequently investigated for mechanical properties post-drying, using static compression testing. These aerogels also generated typical aerogel

compressive stress-strain plots (example plots in **Figure 6.52**) and were analysed for collapse strength, elastic modulus, and the elastic limit

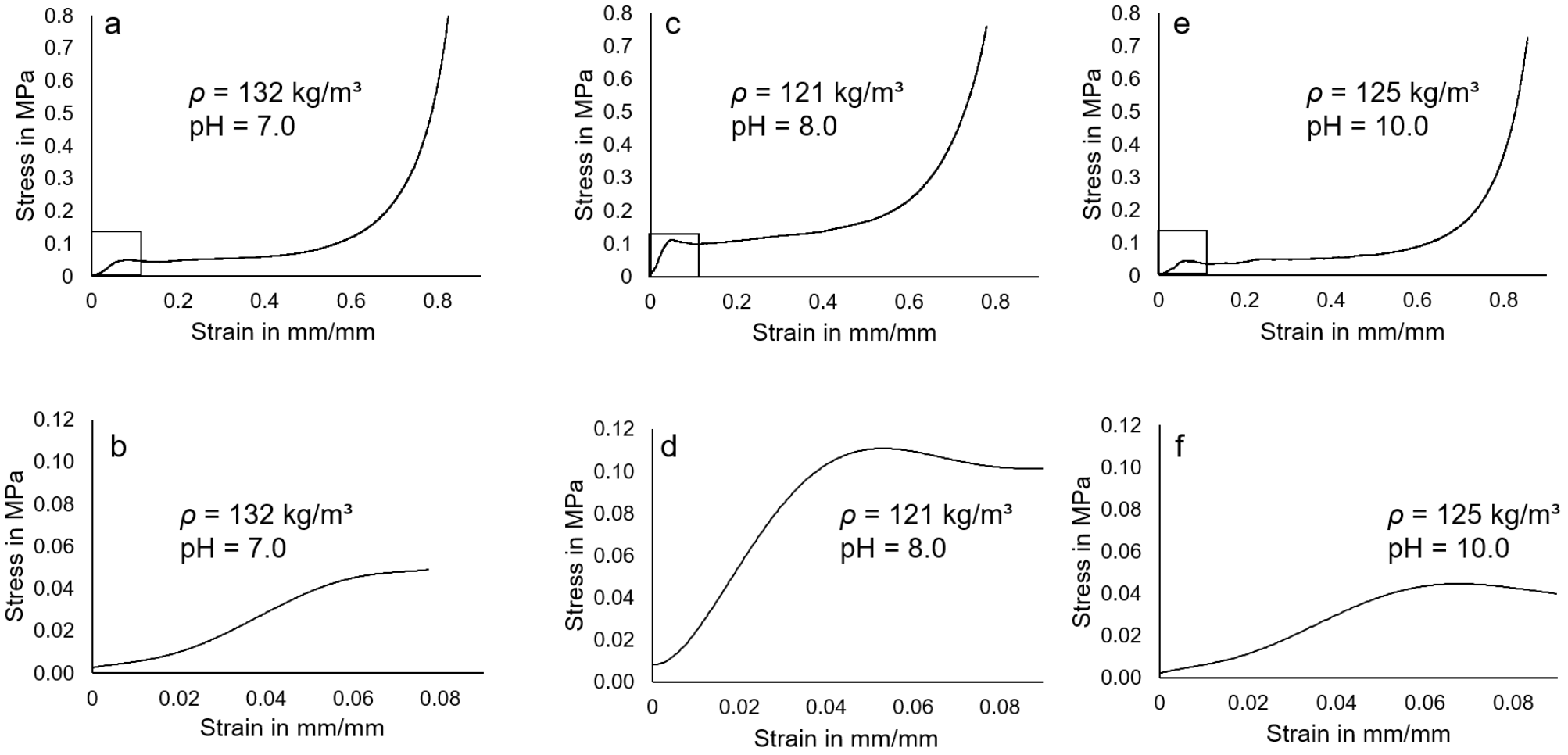

Figure 6.52: *Examples of stress-strain data from compressive tests of selected CSM protein aerogels prepared at varying pH values. Selected specimens are: pH 7* ***(a & b),*** *pH 8* ***(c & d),*** *and pH 10* ***(e & f),*** *at a 10 wt% protein concentration (aerogel densities of 132 kg/m3, 121 kg/m3, and 125 kg/m3 respectively). The linear elastic regions of plots* ***a, c, & e*** *are shown enlarged in plots* ***b, d, & f,*** *respectively*

One of the earliest investigations of CSM protein aerogels was of samples 25 to 49 which were prepared as five batches of 4 or 5 aerogel samples. Each batch of samples had a separate gelation pH (8, 10, or 12) and each sample within a batch was prepared at a unique temperature (ranging from 25 – 100 °C). Furthermore, the ageing times (time held at room temperature before freezing) of certain batches were also varied. Consequently, each sample in these batches was prepared with a unique set of gelation conditions and subsequent mechanical testing allowed for two specimens from each sample. These samples offered early analysis of the effect of gelation pH on the aerogel mechanical properties (**Figure 6.53**). The results displayed large variances within specimens of identical gelation conditions, which limited the information that could be extracted from these batches. Surprisingly, the only conclusive result regarding pH was the low specific strengths and moduli of samples prepared at a pH of 8 (**Figure 6.53a**). Gels prepared at pH 8 had been expected to measure the greatest aerogel strengths and elastic moduli, since higher gel viscosities and a greater solid-like behaviour had been measured in rheometric analysis of wet-gels prepared at pH 8 over other pH values (of viable aerogels) (see **Section 6.3**) One explanation for the lower compressive strength and stiffness of pH 8 gels in samples 25 – 49 could be an incorrect reading of pH due to poor calibration of the pH meter (*i.e.* true value pH < 8.0). Later experiments (see below and also **Section 7.4**) confirm the optimal pH of CSM protein gels is 8.0 ± 0.2 and that values below 8 (*e.g.* pH = 7.0) are detrimental to gel and aerogel strength

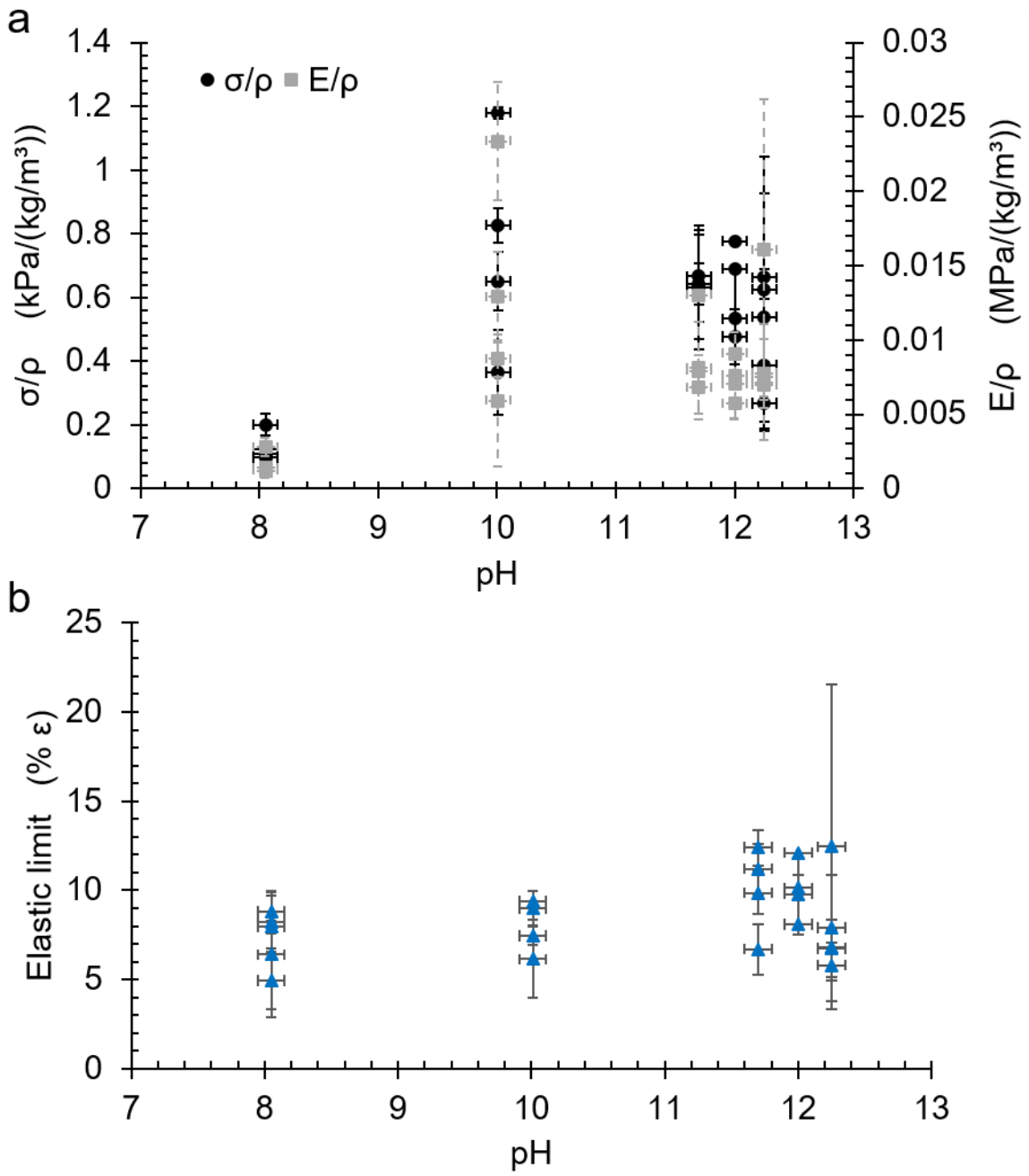

Figure 6.53: *Specific elastic moduli, specific collapse strengths* ***(a),*** *and elastic limits* ***(b)*** *of CSM protein aerogel samples 25 to 49, prepared at a range of pH values, temperatures, and gel ageing times. Error bars represent the standard deviation where n = 2*

The intra-sample variance in samples 25 to 49 was connected to the large density variances seen in the same samples (refer to data in black circles in **Figure 6.36**) and possibly attributed to non-uniform drying during the freeze drying process. Non-uniform freeze drying may occur because samples in

tubes can only be exposed to the vacuum from one end, could result in non-homogenous density distribution in a sample that is later cut into multiple specimens for mechanical analysis. The possible effect of temperature and ageing times on the mechanical performance of these samples is considered in **Section**s **6.5.1.4** and **6.5.1.5**.

Following the unexpected result from samples 25 – 49, further investigations into the effect of the gelation pH on mechanical properties of the aerogels were launched. Another batch of samples (samples 97 – 102) were prepared at varying pH values (at 25 °C). These samples allowed for two specimens for mechanical testing (**Figure 6.54**) to be cut from each sample, except for the sample prepared at pH 6.0 which did not produce a viable aerogel (see **Figure 6.27b**, **Section 6.4.1**). The failed pH 6.0 aerogel revealed the importance of gelation pH to aerogel stability, a finding that previous mechanical investigations had failed to reveal given the limited pH range trialled thus far. However, the remaining (viable) aerogels revealed no further effects of pH on the mechanical properties except for the possibility that at a pH of around 10 the elasticity is reduced (**Figure 6.54b**) and the strength and stiffness may be slightly increased (**Figure 6.54a**). Once more, high variance within some sample sets restricted the usefulness of this investigation (samples at pH 1.9, 12.1, and 13.1, in **Figure 6.54a**). This batch also does not show the reduced strength at pH 8 seen previously in samples 25 – 49. This latest study shows that, surprisingly, the influence of pH on the mechanical properties of viable aerogels appears inconsequential, although pH is clearly a critical factor for aerogel viability as evidenced by the pH 6.0 sample.

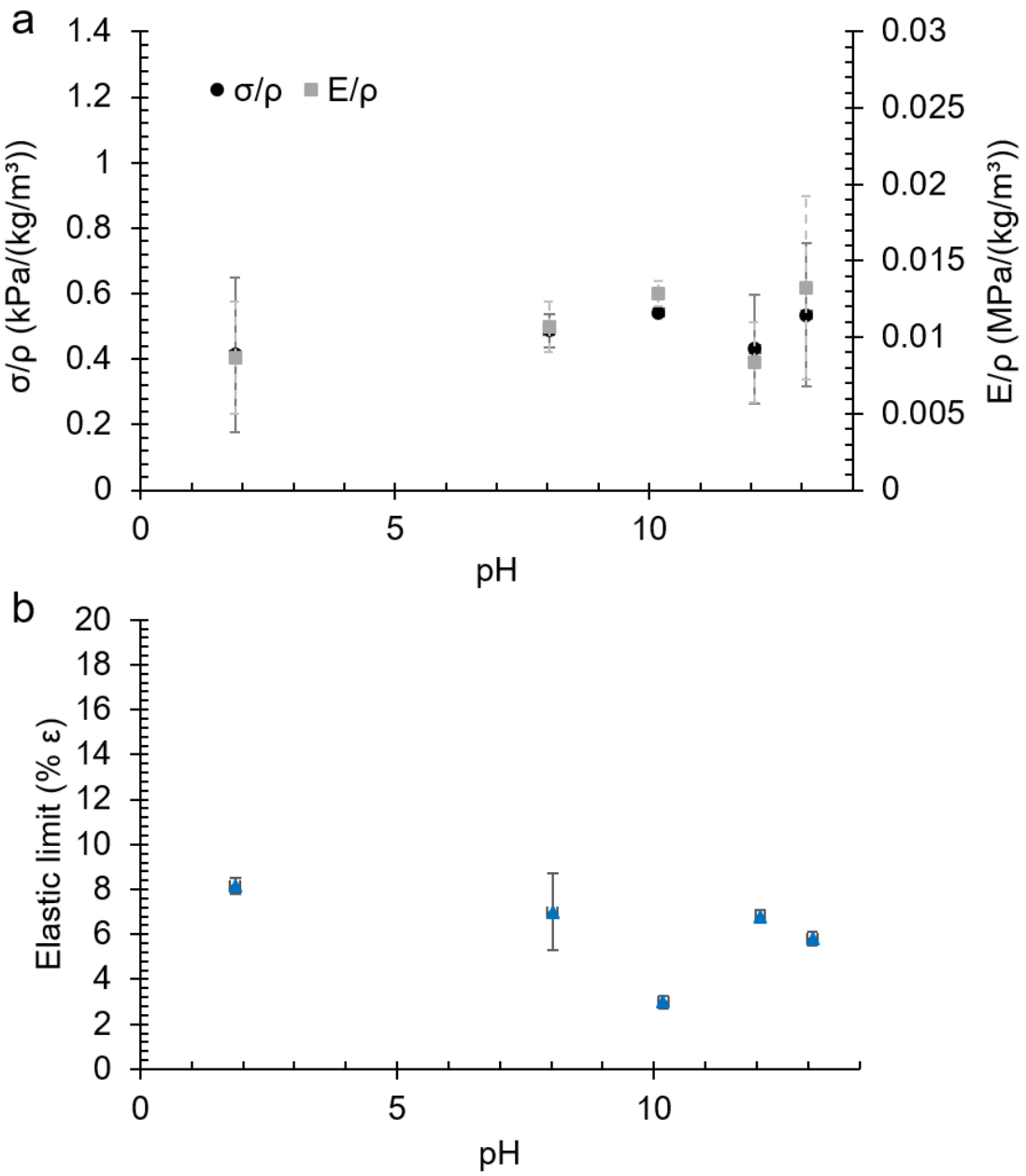

Figure 6.54: *Specific elastic moduli, specific collapse strengths* ***(a),*** *and elastic limits* ***(b)*** *of CSM protein aerogel samples 98 – 102, prepared at a range of pH values at 25 °C. Error bars represent the standard deviation where n = 2*

Hence, the two pH investigations carried out here suggest that gelation pH influences aerogel viability, and yet, contradictorily, does not appear to have a substantive influence on the mechanical properties of the viable aerogels. Accordingly, a final investigation into gelation pH influence was required. The production of only one aerogel specimen (of 15 mL Falcon™ tube size) for each pH

variant had resulted in only two specimens being prepared per pH value for compressive testing. Greater quantities of CSM protein were required to increase the number of specimens, improve the quality of the investigation, and increase the likelihood of finding a conclusive correlation between gelation pH and aerogel mechanical properties.

The most comprehensive pH investigation was carried out over aerogel samples 103 – 109, 113 – 114. These samples were prepared in repeats of 5 aerogel samples per pH condition (*e.g.* 103 A-E) and each aerogel was cut into 2 specimens for mechanical analysis, generating duplicate measurements for each repeat. Therefore, a total of 10 stress-strain plots each were generated for gelation pH values of: 7.1, 8.0, 9.1, 9.5, 10.0, 10.6, 11.0, 11.5, and 12.0. These plots were analysed for the aerogel collapse (or yield) strength (**Figure 6.55a**), compressive elastic modulus (**Figure 6.55b**), and elastic limit (**Figure 6.56**). During the compressive testing, some samples underwent premature buckling from poor sample shape or due to prior sample damage and were purged from the resulting data sets (**Figure 6.55c & d**). These refined data sets were used to generate averages (n = 5, 7, 8, 9, or 10) for further analysis of the effect of gelation pH on mechanical properties.

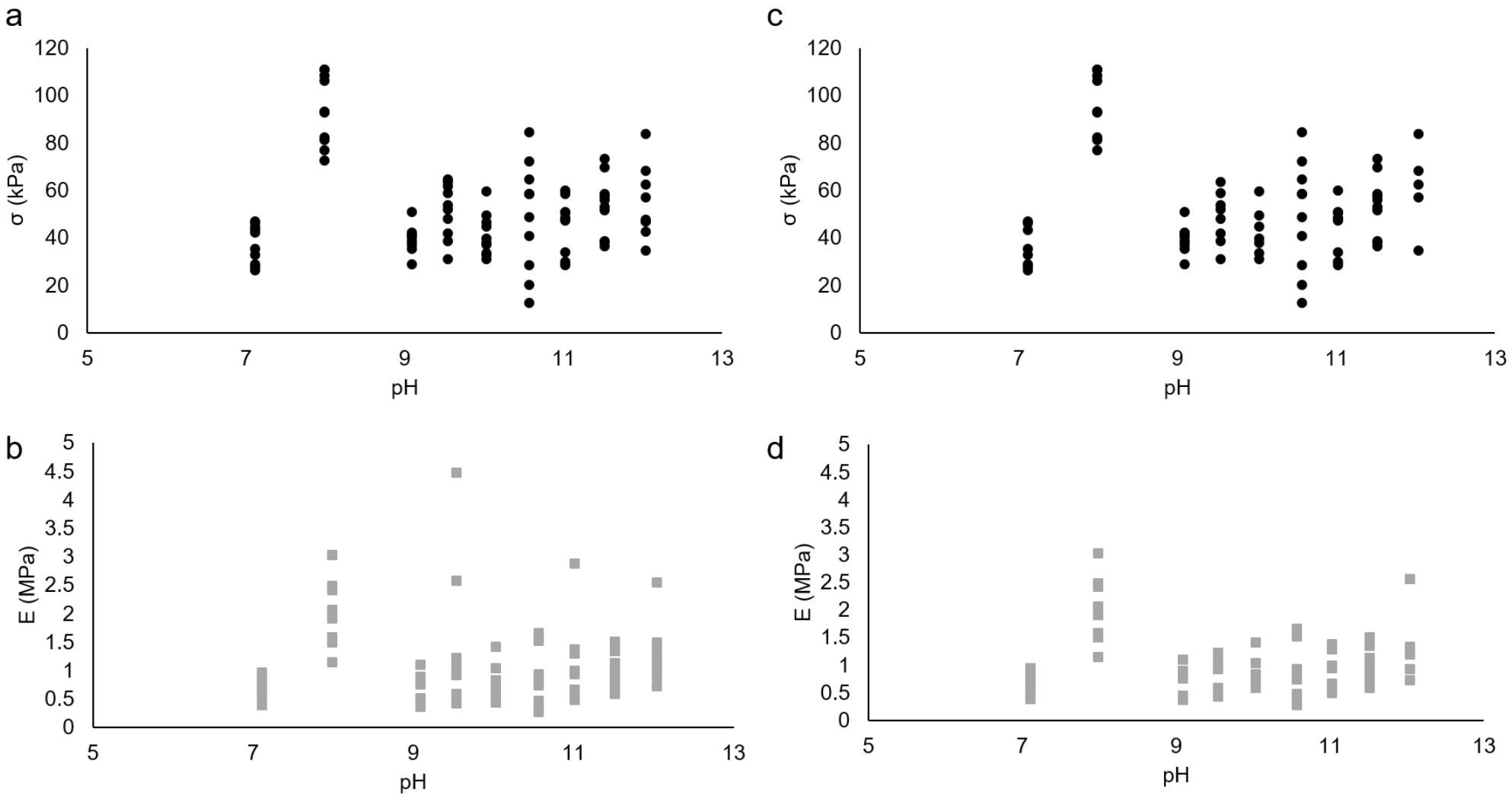

Figure 6.55: *Compressive strength **(a & c)** and elastic moduli **(b & d)** of CSM protein aerogels as a function of pH. Results are from samples 103-109, 113, 114 where n = 9 or 10 for each pH value **(a & b).** Refined results where buckled or damaged samples were removed are shown in adjacent plots **(c & d)** where n = 5 for pH 12, n = 7 for pH 10, n = 8 for pH 7, 9, & 9.5, n = 9 for pH 8 & 11, and n = 10 for all others*

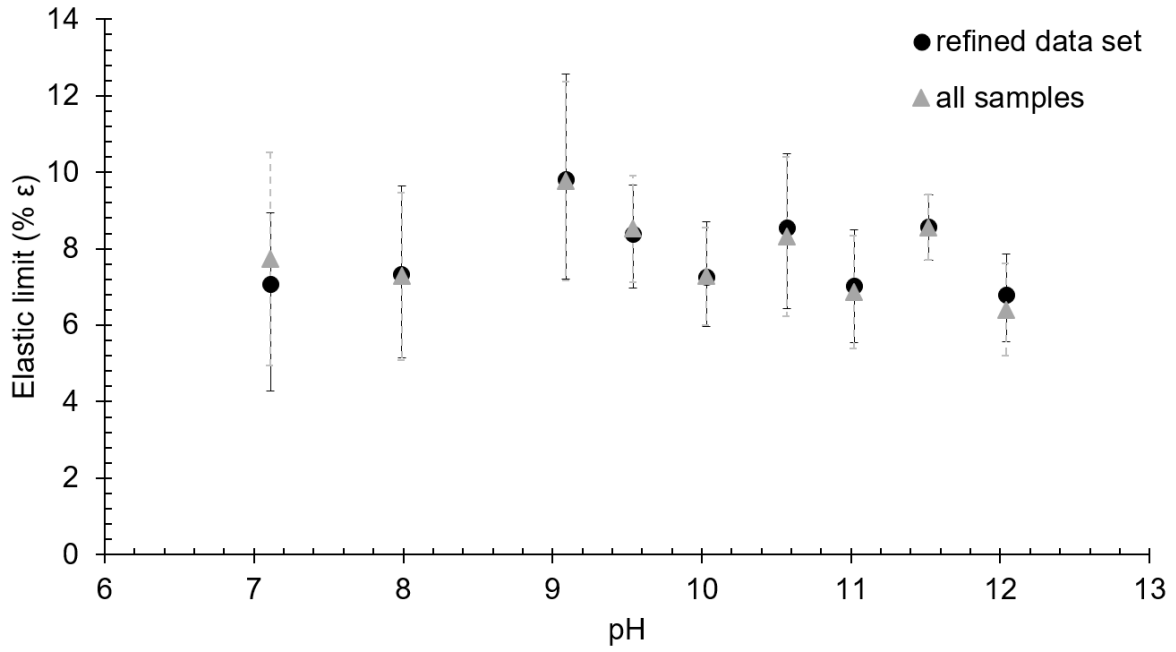

Figure 6.56: *Elastic limits for CSM protein aerogels as a function of pH. Averages are shown for complete samples sets (grey triangles) with error bars representing standard deviation (n = 9 or 10), and for refined sample sets where the buckled or damaged sample results are removed from the average (black circles). Error bars in the refined data set also represent the standard deviation but where n = 5 for pH 12, n = 7 for pH 10, n = 8 for pH 7, 9, & 9.5, n = 9 for pH 8 & 11, and n = 10 for all others*

The increase in specimen numbers per variable finally allowed for some pH-dependent trends to emerge from the aerogels. Variance remains high, with some data sets showing strength range from 25 – 173 % of the average (pH 10.5) and modulus range from 58 – 154 % of the average (pH 8.0), but nevertheless there was an interesting anomaly identified at pH 8.0. The average compressive strength for samples prepared at pH 7.0 and 9.0 remained very similar at 36 ± 8 kPa and 39 ± 6 kPa, respectively. However, there is a jump to a strength of 96 ± 14 kPa at pH 8.0. Likewise, the pH 8.0 result for the elastic modulus shows a jump to 2.0 ± 0.6 MPa while the neighbouring values at pH 7.0 and 9.0 do not exceed moduli of 0.7 MPa. The analysis of elastic limits in these samples proves less interesting with no clear pH-dependent changes to the elastic limit, hovering between 7 and 9 % (**Figure 6.56**) and close to the average for all CSM protein aerogels (7.9 %). Elastic limit measurements may be complicated by toe region inclusion and should be elucidated further in future testing (see **Section 6.5.1.1**). Another observation is a slight tendency for increased strength and

stiffness with increasing pH in the samples from pH 9 – 12. However, the high variance in these data sets obscures any clear link between pH and changing mechanical properties in this pH range.

The specific strengths and moduli of the above samples were also calculated to remove any influence from varying density. Correspondingly, the specific values exhibited the same trends as the absolute values (**Figure 6.57**). The specific modulus at pH 8.0 is the highest at 0.017 ± 0.005 MPa/(kg/m^3)) and the specific compressive strength is also the greatest at pH 8.0 with an average of 0.80 ± 0.13 kPa/(kg/m^3)). The clear finding from these comprehensive pH variant studies is that a pH at or near 8 plays a role in the gel strength and stiffness of CSM protein aerogels.

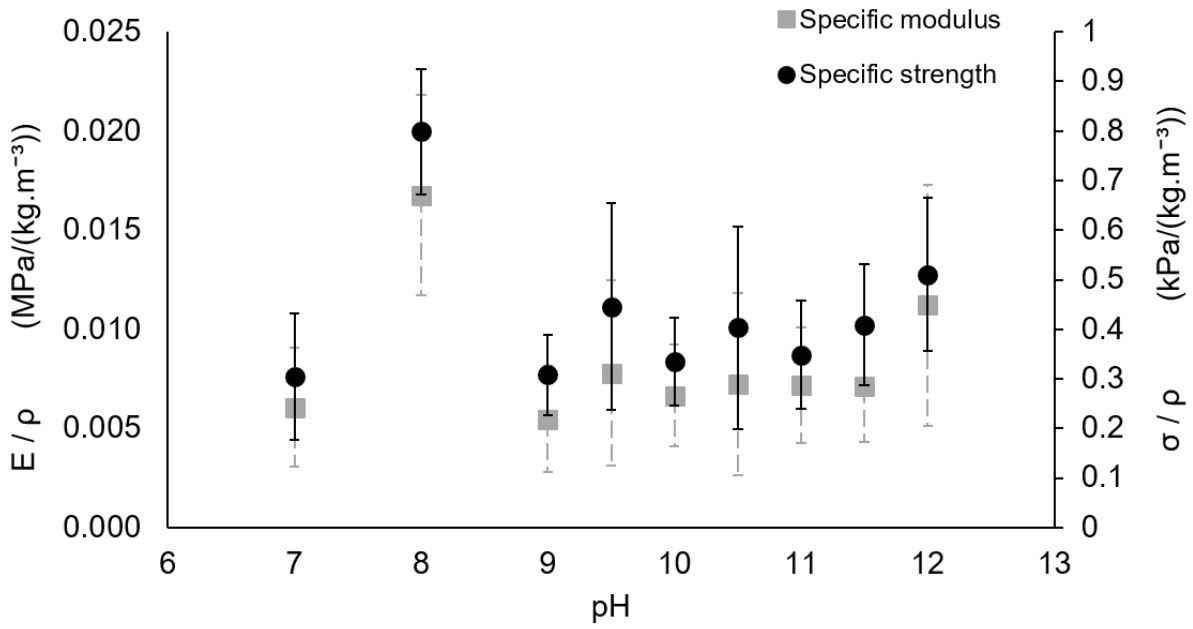

Figure 6.57: *Specific compressive strength and elastic moduli of CSM protein aerogels as a function of pH, prepared at 10* wt% *protein and 25 C. Error bars represent the standard deviation where n = 5 – 10*

Successive investigations into the effect of gelation pH have highlighted the pH as an important gel variable for the control of aerogel strength and stiffness, independent of aerogel density. This finding is discussed in **Section 8.4** alongside rheological and morphological evidence with the aim of uncovering the gelation mechanism of CSM protein that links the gel chemistry to aerogel strength.

6.5.1.4. Effect of the gelation temperature

The literature reveals that CSM protein has a greater propensity for gelation upon heating to temperatures above 82 °C (refer **Section 2.3.3**) and other protein aerogels are known to have demonstrable links between heating and final aerogel strength [127]. CSM protein aerogels were also investigated for possible effects of the gelation temperature on mechanical performance. Static compressive testing of these specimens showed the typical stress-strain curves generated by most CSM protein aerogels (**Figure 6.58**).

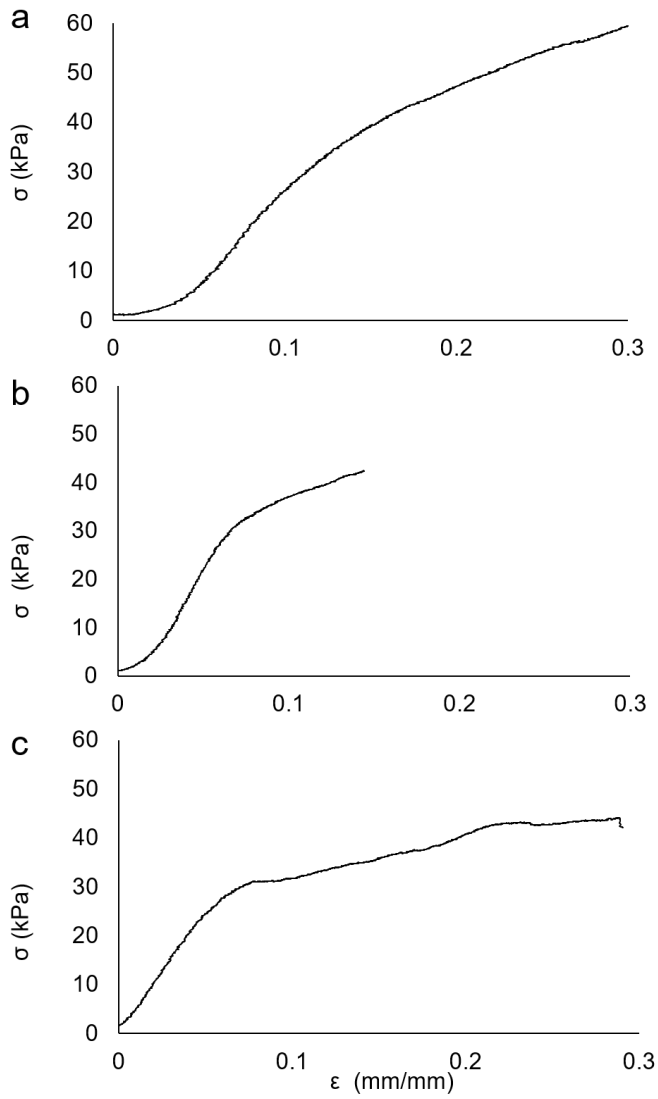

Figure 6.58: *Example stress-strain plots generated from CSM protein aerogels prepared at 10* wt% *protein, pH 10, and with varying gelation temperatures including 25 °C* ***(a),*** *60 °C* ***(b)*** *and 90 °C* ***(c)***

However, there were some specimens, particularly from earlier samples, that demonstrated a less distinctive transition from the linear regime to plateau (**Figure 6.58a**).

There were three separate batches of aerogel samples prepared with varied gelation temperatures. The first group (samples 16 – 21), some of the earliest aerogels prepared in this thesis, were prepared at a pH of 10.0 and in 30 mL Falcon™ tubes (differing from all subsequent aerogel samples) and produced just one sample (cut into two specimens) per temperature value for analysis (**Figure 6.59a-b**). The second temperature-dependant batches were samples 25 – 49 (discussed in **Section 6.5.1.3**) and were designed to concurrently investigate the effect of pH, temperature, and ageing times on the aerogels. These aerogels were also produced with only two specimens per sample condition and experienced issues with variable density (discussed in **Section 6.4.1**) and uncharacteristically low strengths for the batch produced at pH 8.0 (see **Section 6.5.1.3**). However, these samples are still assessed for possible effects of the gelation temperature on the mechanical performance within a given pH value (**Figure 6.60**). Lastly, a repeat of the temperature study was carried out at a pH of 11.2 and produced samples 80 – 89 which included a refrigerated sample in addition to the 25 – 90 °C range (**Figure 6.59c-d**).

The temperature investigations carried out at pH 10.0 did not reveal any temperature-dependent mechanical properties (**Figure 6.59a-b**), and further tests revealed that aerogel mechanical properties are most likely jointly dependent on gelation temperature and pH (**Figure 6.60**). The investigation carried out at pH 11.2 (**Figure 6.59c-d**) revealed that some CSM protein aerogels require a threshold gelation temperature of around 50 – 60 °C to experience an increase in specific strength. This increase was 1.7 – 2.0 times the ambient temperature measurements. However, no corresponding clear increase in the elastic modulus at 60 °C (large variance in the data is problematic) was found, nor any temperature-dependent change in elasticity that is greater than the normal sample variance. The sample refrigerated at 4 °C did not show any changes to strength, stiffness, or elasticity, as compared to the ambient temperature preparations.

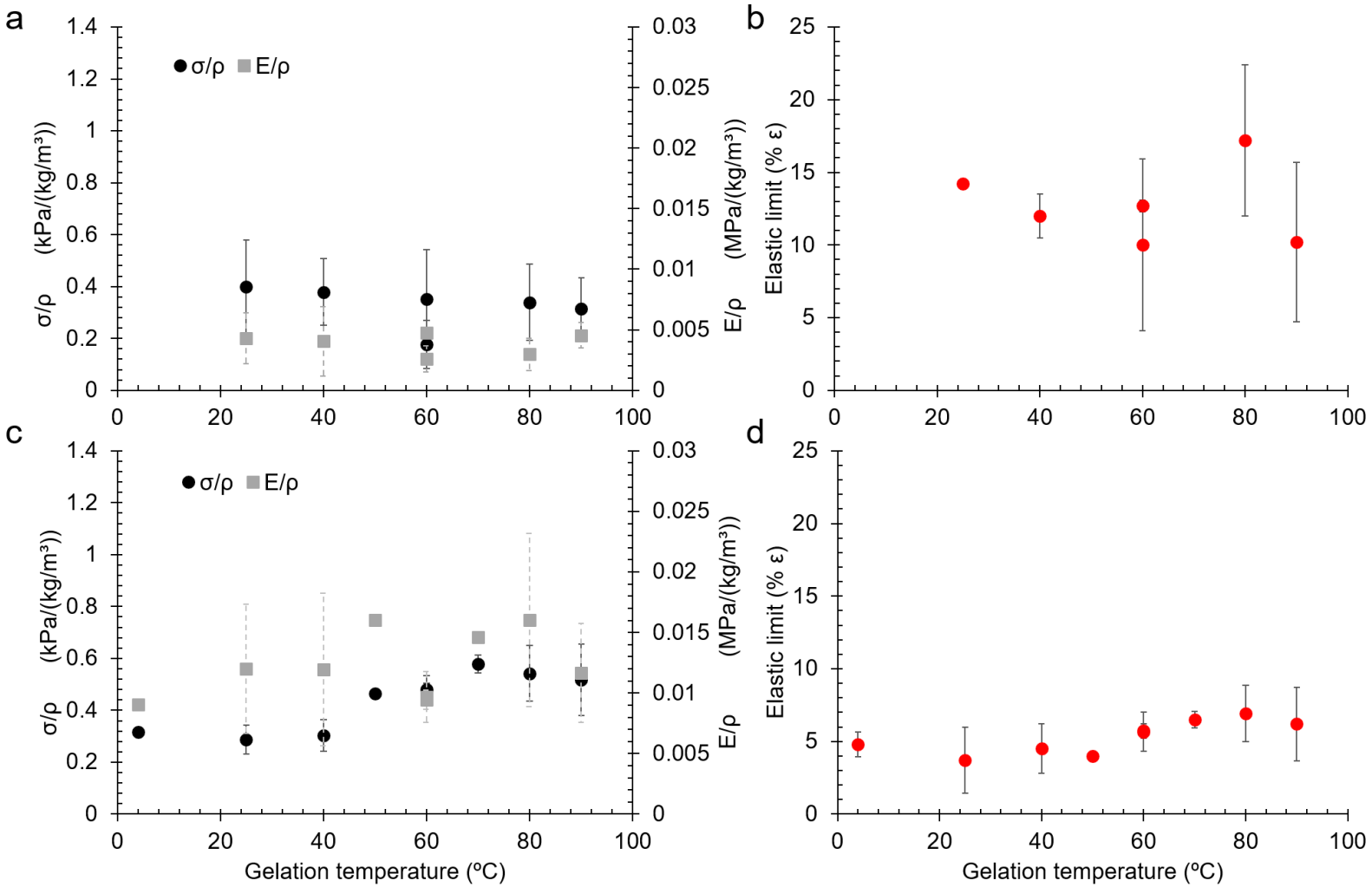

Figure 6.59: *Mechanical properties of CSM protein aerogels prepared at 10* wt% *protein and a pH of 10 (samples 16 – 21* ***(a – b)****) and a pH of 11.2 (samples 80 – 88* ***(c – d)).*** *The average values for specific compressive strength and elastic modulus* ***(a & c)*** *and the average elastic limit* ***(b & d)*** *are given where error bars represent the standard deviation (n = 2)*

The most revealing temperature-dependent mechanical results are seen in samples 36 – 39 (also prepared at pH 10) (**Figure 6.60b**) where a steady increase in strength and stiffness is seen with increasing temperatures from 60 °C to 90 °C. There is also a possible corresponding decrease in elasticity (**Figure 6.60d**), though sample variances make this result less conclusive. Previous elasticity decreases with increased strengths and stiffnesses have been noted (seen in **Section 6.5.1.2**) and indicate the increasingly brittle nature of stiffer aerogels. The result at pH 10 in **Figure 6.60b** differs from the first sample set (**Figure 6.59 a-b**) which was also prepared at pH 10. While both investigations were carried out with duplicate measurements per temperature value, samples 36 – 39 display a narrower variance and the measurements at 60 °C and 70 °C match more closely to the measurements from the later batch (samples 80 – 88, **Figure 6.59c**). It was also noted that some stress-strain curves generated in the early batch (samples 16 – 21) had indistinct linear regimes making analysis difficult and suggesting a less reliable result. Despite the trend identified in **Figure 6.60b** aligning with literature information, motivation for a repeated investigation remains. Sample variance is high and may be improved with refined data collated from multiple repeats as demonstrated in the pH investigations of **Section 6.5.1.3**.

Interestingly, formulations based on a pH of 8 or 12 do not appear to be influenced by changes in gelation temperature (25 – 90 °C) (**Figure 6.60a &c**), however, as previously noted, samples 30 – 34 demonstrate unexplained, uncharacteristically low mechanical properties and mechanical testing results for samples 40 & 41 could not be replicated. Additionally, the lack of observed increase to aerogel strengths in heated samples at pH 8 does not align with rheological studies. It was previously demonstrated that pH 8 formulations which are heated to 95 °C have improved gelation (see **Section 6.3**), and this was expected to correspond to observing improved strengths in their aerogel counterparts, a trend not seen in **Figure 6.60a**. The transfer of wet-gel rheometric properties to corresponding aerogel mechanical performance has been seen previously, both in literature and in the pH investigations of **Section 6.5.1.3**. Further discussion on the processing-property relationship of CSM protein aerogels is presented in **Section 8.6.1**., encompassing rheological and mechanical data of these temperature variants with additional evidence from **Chapter 7**.

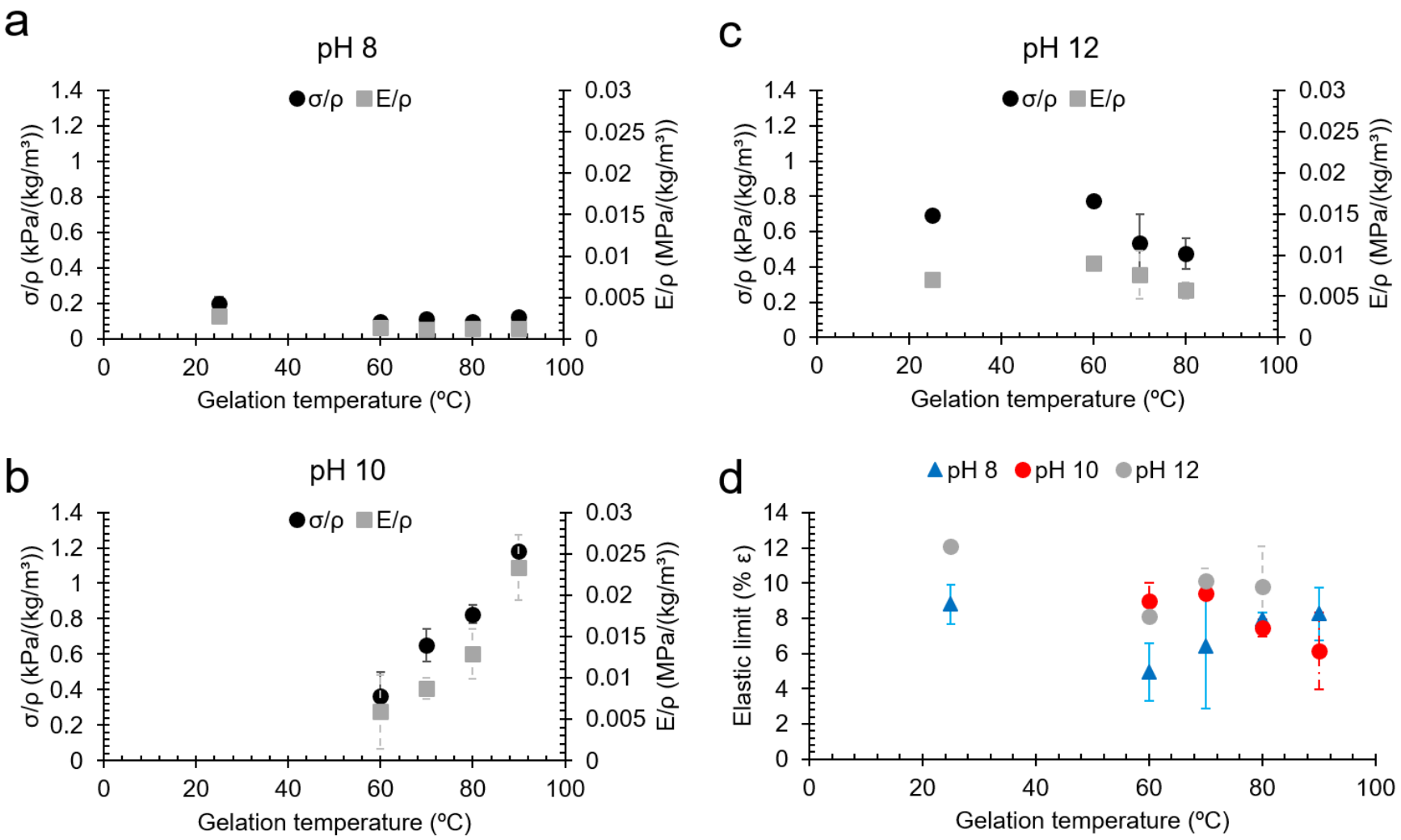

Figure 6.60: *Specific compressive mechanical properties of CSM protein aerogels as a function of temperature prepared at pH 8* ***(a),*** *pH 10* ***(b),*** *and pH 12* ***(c)*** *and the corresponding elastic limits as a function of temperature* ***(d).*** *Error bars represent the standard deviation of measurements where n = 2. The specimens prepared at pH 12 and temperatures of 25 °C & 60 °C allowed for only one measurement each, therefore no statistical information is available*

6.5.1.5. Effect of the gelation and ageing times

Literature indicates that ageing of CSM protein gels can influence rheometric properties [200, 203] and may be used to control corresponding aerogel properties. Gel ageing was therefore introduced as a variable to some of the aerogel batches in this project. Gel formulations that produced aerogel samples 25 – 49 (previously discussed for pH and temperature studies in **Sections 6.5.1.3** and **6.5.1.4**) included three formulations at pH 12 with varied ageing times (2, 4, and 20 hours) and a dedicated ageing study was later undertaken with samples 90 – 93, also at pH 12. This study was small, with only four ageing times selected and one sample generated (two specimens for mechanical testing) per ageing time. However, stress-strain curved generated from these samples were typical of CSM protein aerogels (**Figure 6.61**) and it was expected that any compelling effects would be identified in the longest aged sample (12 hours) which would motivate further investigations if proven an important gelation factor.

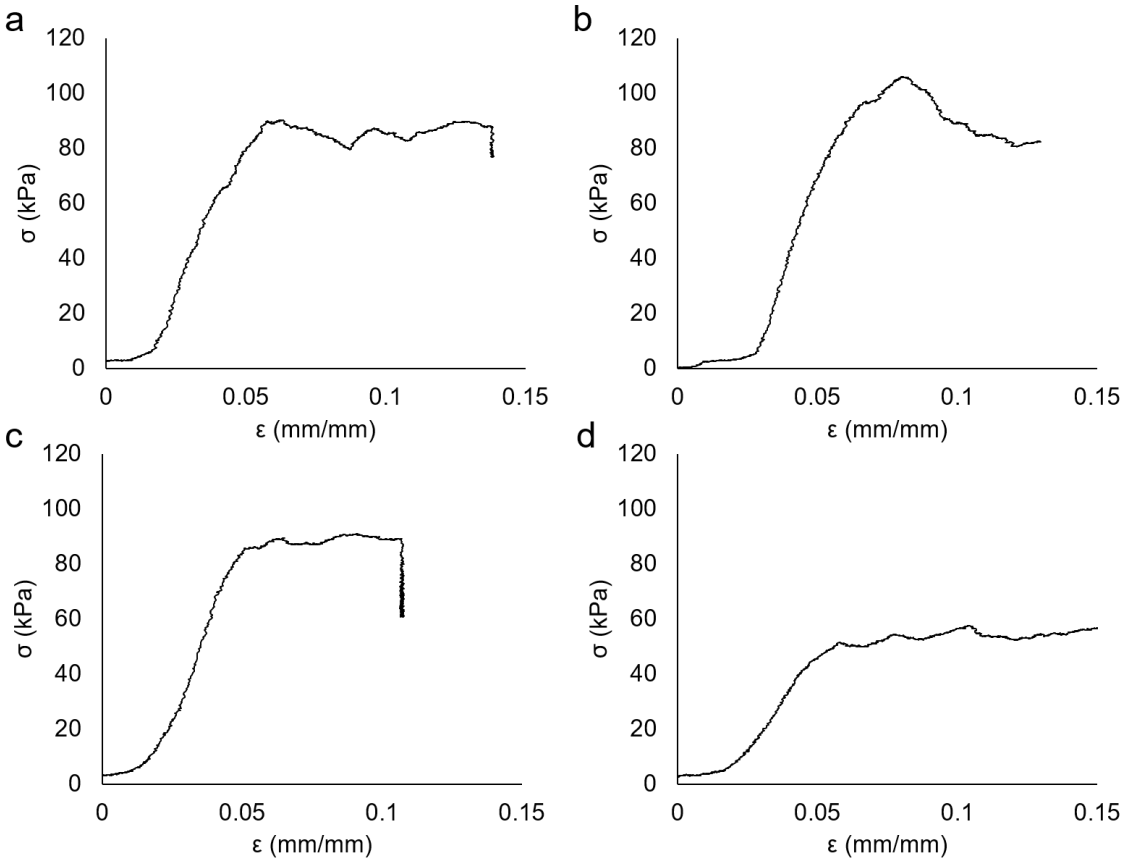

Figure 6.61: *Example stress-strain plots generated from CSM protein aerogels prepared at 10* wt% *protein, pH 11.9, and with varying gel ageing times including 0 hours* ***(a),*** *2 hours* ***(b),*** *6 hours* ***(c),*** *and 12 hours* ***(d)***

Interestingly there were no effects of ageing on the mechanical properties of the aerogels identified in these studies. Ageing to 21 hours in samples 25 – 29 did not improve aerogel strengths or stiffnesses (**Figure 6.62a**) nor did ageing to 12 hours in samples 90 – 93 (**Figure 6.62c**). Contradictorily, sample 93 which was aged to 12 hours demonstrates a possible drop in specific compressive strength and stiffness as compared to gels aged for a lesser time. One explanation for decreasing strength and stiffness with ageing is excessive aggregation leading to agglomeration of the protein and subsequent destabilisation of the gel network. However, the same drop in aerogel strength and stiffness with excessive ageing was not seen in samples 25 – 29 (aged to 21 hours) so excessive ageing was not considered detrimental to aerogel strength. Elasticity was also not affected (**Figure 6.62b & d**). The lowered strength and stiffness of sample 93 may represent a rouge result as samples 90 – 92 demonstrate a slight increase in elastic modulus with increasing age time (1.8 MPa to 2.4 MPa with 6 hours ageing) however, this increase is almost within the variance seen in sample 90 (1.8 ± 0.4 MPa) and was not sufficiently significant for ageing times to be considered a critical gelation parameter. The most likely explanation for the ageing time results not aligning with literature rheological evidence is the pH of the samples investigated here (pH 12) differing from other studies on CSM protein gels and ageing times. One gap in the current study is the lack of ageing time investigation using alternate pH values, such as pH 8 which has demonstrably improved gels and aerogels (see **Sections 6.3.2** and **6.5.1.3**), and may reveal an effect of gel ageing on the aerogel performance.

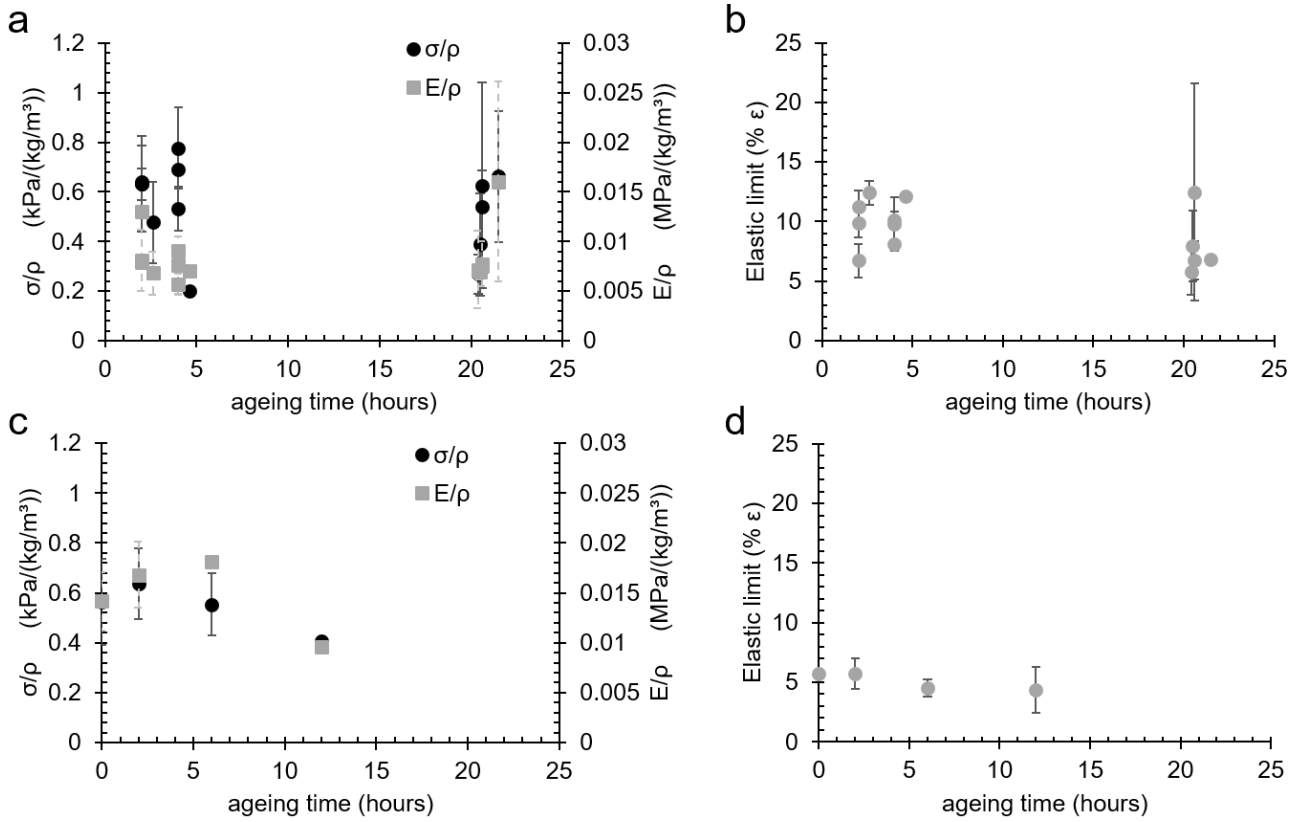

Figure 6.62: *Specific compressive strengths and moduli* ***(a & c)*** *and elastic limits* ***(c & d)*** *of CSM protein aerogels prepared at a pH of 12, as a function of gel ageing time from samples 25 – 49* ***(a – b)*** *and samples 90 – 93 (****c – d****). Error bars represent standard deviation where n = 2*

The possible influence of gel time at non-ambient temperatures was also investigated briefly with three samples being prepared at a gel temperature of 80 °C for 10, 60, and 120 minutes (**Figure 6.63**). A decrease in specific compressive strength with increasing gel time at 80 °C was observed, and a corresponding small drop in elasticity was noted. Variance was large and meant no clear trend could be identified in the elastic moduli of the gel time variants. The simultaneous drop in strength and elasticity was an unusual result with earlier trends demonstrating elasticity is usually reduced when strengths increase. Furthermore, extended heating times were not expected to reduce gel strength, though one explanation for this could be heat-induced protein degradation, suggesting that in heated samples, a balance must be struck between sufficient heating for protein gelation and excessive heating causing damage. This result required further elucidation by also including other gelation variables in the study, for example the gel pH, to confirm whether heat-induced gelation and heat-induced degradation are competing influencers of aerogel mechanical properties. A reoccurring issue

with the gelation time, ageing, and temperature studies in this thesis is the use of increasingly irrelevant pH values (such as pH ≥ 10) as pH studies reveal a pH value of around 8.0 to be the most agreeable for aerogel structural integrity and strengths.

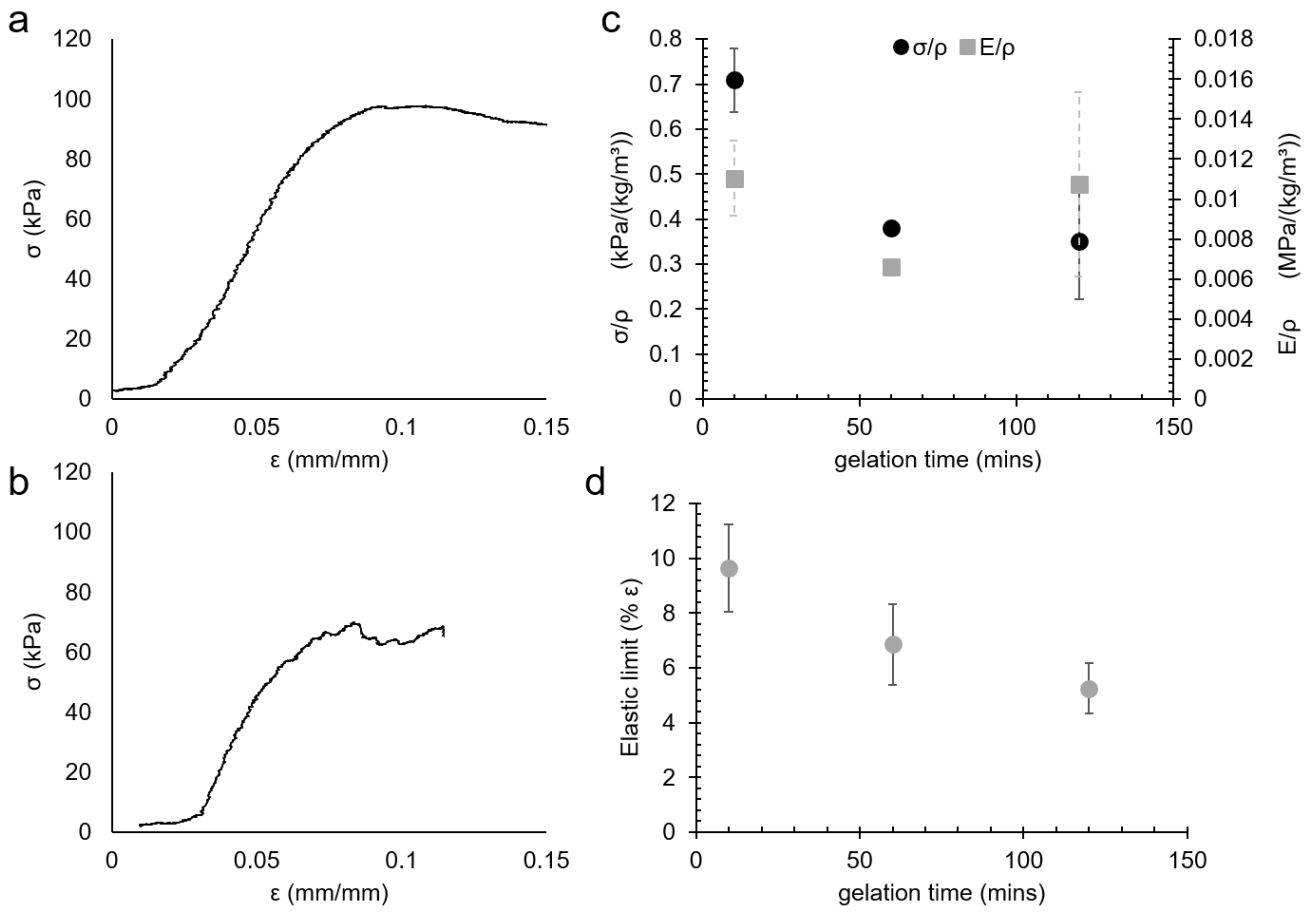

Figure 6.63: *Example stress-strain curves **(a-b)** from CSM protein aerogels prepared at pH 12 with variable gelation times at 80 °C, including 10 minutes **(a)** and 120 minutes **(b)**. Average specific compressive strengths and moduli (**c**) and average elastic limits (**d**) from CSM protein aerogels as a function of gelation time. Error bars represent standard deviation where n = 3 (10-minute samples) or n = 2 (others)*

Mechanical testing: summary

Static compressive tests on a range of CSM protein aerogel samples have revealed how these aerogels display a traditional aerogel stress-strain curve with a linear regime (< 8 % compression), followed by a substantial plateau region and a final compaction phase (> 60 % compression). Certain aerogel preparations also reveal evidence of viscoelasticity upon cyclic compression testing. CSM protein aerogels demonstrate yield strengths of 7 – 134 kPa, elastic moduli of 43 kPa – 2.7 MPa, and elastic limits of 3 – 23 %, dependent, in the first instance, on the protein concentration (wt% of CSM protein powder). Additionally, the compressive mechanical properties of the aerogels can be manipulated by altering the pH, and to a lesser extent the temperature, during gelation. The 10 wt% protein formulations which (consistently) had the highest elastic modulus and strength were prepared at a pH around 8.0, giving averages of 2.01 ± 0.57 MPa and 95.8 ± 13.6 kPa, respectively. Finally, ageing and gelation time do not appear to be important gelation parameters for the control of aerogel mechanical properties in CSM protein gels at pH ≥ 10 but remain to be investigated at more relevant pH values (*e.g.* pH ≈ 8).

6.5.2. Thermal properties of canola protein aerogels

Thermal techniques such as differential scanning calorimetry (DSC) and thermogravimetric analysis (TGA) are commonly used to analyse phase transitions and chemical stability in materials. These techniques apply heat energy to samples and can analyse physical and chemical processes occurring as a result of the absorption of this heat energy. DSC measures heat flow, capturing the absorbance and release of heat energy at specific temperatures associated with physical and chemical transitions in a substance. Commonly, DSC is used to identify glass transition, melting, and curing events in thermoplastic and thermoset materials, providing information about chemical bonding within the material. TGA measures the percentage weight change of a sample as it is heated beyond the temperature where it gasifies. The complete breakdown of a material into gaseous constituents (*e.g.* H_2O (g), CO_2 (g), N_2 (g)) destroys the principal molecule under investigation but provides information about covalent bonding in the material. Both techniques were used in the present work to briefly investigate chemical interactions in the CSM protein aerogels and extract. The thermal resistance of the CSM protein aerogels as determined by TGA can be directly compared with other aerogel types for an assessment of competitivity. Meanwhile heat flow measurements from DSC experiments provide information about possible thermal transitions in the canola protein. Tracking changes in these protein thermal transitions can elucidate chemical details about the process of gelation and ultimately aid in elucidation of a gelation mechanism.

6.5.2.1. Differential scanning calorimetry

DSC studies of the CSM protein aerogels aim to identify enthalpic changes in the protein, specifically protein denaturation (where the temperature at denaturation is denoted T_d) and protein aggregation, to determine their roles in gelation. Protein denaturation is somewhat analogous to melting (where melting temperature is denoted T_m) in thermoplastics, as both are endothermic events which can be identified in a temperature range of approximately 0 – 200 °C. However, the analogy has limitations. In their recent

review of thermal transitions in protein-based thermoplastics, *Bier et al.* [253] note that equating the denaturation of proteins to melting of crystals in polymers is not an accurate analogy, and care should be taken to distinguish protein melting from melting of semi-crystalline polymers. Protein denaturation (or 'melting') involves the disruption of some intramolecular (and mostly) secondary bonds, though some specific covalent bonds, such as disulphides, can be involved. The result is a significant conformational change in individual protein molecules, such as unfolding of globular structures into amorphous or sometimes fibrillar structures. However, it is not always a requirement that after denaturation the protein is completely devoid of all higher-order structure. In fact, the loss of the native conformation (an endothermic process) can occur with only partial changes leaving many denatured proteins with residual 'crystal-like' structure (*e.g.* β-sheets and α-helices). Additionally, denaturation is generally (protein type-dependent) irreversible due to the large change in conformation and formation of a 'stable' denatured structure, particularly in non-solvated protein (*e.g.* in protein-based extrusions and materials). Melting processes in thermoplastics are also attributed to the breaking of secondary bonds; however, this process is reversible (a corresponding exothermic peak can be seen) when the material is cooled below the crystallisation temperature.

Proteins can undergo a process of aggregation following denaturation – often a consequence of thermally-activated denaturation. DSC experiments can also identify protein aggregation as an exothermic event within a similar temperature range. Aggregation is the formation of larger, packed structures composed of many protein molecules that exclude the solvent and is a mostly irreversible process. Specific solvent conditions can be used to promote aggregated or non-aggregated samples. However, aggregation is generally inextricably tied to protein denaturation, where the latter is a prerequisite for the former. Aggregation is considered a competing process to the refolding of a denatured protein (the reverse reaction to denaturation). Fully unfolded proteins are not necessarily a prerequisite of aggregation if partial unfolding is sufficient for inter-molecular associations to occur. The term 'unfolding' can be used to describe a sub-set of denatured conformations which are more accurately analogous to melting.

Unfolded proteins can be thought of as having little or no residual structure and are open and extended, rather like an amorphous polymer melt. Protein aggregation events may be identified in a modulated DSC (MDSC) experiment since small exothermic events confined to the reversible component have been attributed to thermal aggregation in soy protein isolates [254].

Thus, it is important to consider three points in the thermal analysis of protein structures using DSC: (i) denaturation may not equate to melting in other polymers; (ii) denaturation is probably irreversible; and (iii) an exothermic aggregation event (also probably irreversible) may be associated with denaturation.

In this investigation, it was hypothesised that the non-gelled (native) CSM protein extract would reveal a thermal denaturation event at a temperature (T_d) of 78 – 87 °C, based on a study by Kim *et al.* where DSC experiments were used to identify exothermic events in canola protein gels that they attributed to denaturation. Furthermore, it was hypothesised that any detectable T_d in the protein extract would likely be irreversible given the desiccated nature of the samples. Denaturation events identified in the CSM protein powder were expected to be lessened (lower enthalpy changes associated with the transitions) or absent from the corresponding CSM protein aerogels. Less denaturation was expected in aerogel samples since they should comprise of pre-denatured and pre-aggregated protein gel networks, unable to undergo much (if any) further denaturation. The possible identification of protein aggregation was also hypothesised, again expected only in the (non-gelled) protein extract samples. A gel network, such as those expected in the aerogel samples, has extensive intermolecular interactions and can be considered analogous to a thermoset polymer. A truly covalent network would not melt at the temperatures used in the current DSC experiment (< 250 °C) but will undergo thermal decomposition at much higher temperatures (refer to thermogravimetric analysis in **Section 6.5.2.1**).

The CSM protein extract and aerogels were conditioned for 48 hours at standard atmospheric conditions (20 ± 2 °C and 65 ± 2 % relative humidity (RH)) and then analysed using DSC with a heating ramp of 10°C/min. The DSC plots obtained from conventional DSC subsequently revealed a total of four thermal

transitions in CSM protein aerogels (**Figure 6.64**) though only the major endothermic peak at around 100 °C was present in all samples ('Peak 3', **Table 6.3**).

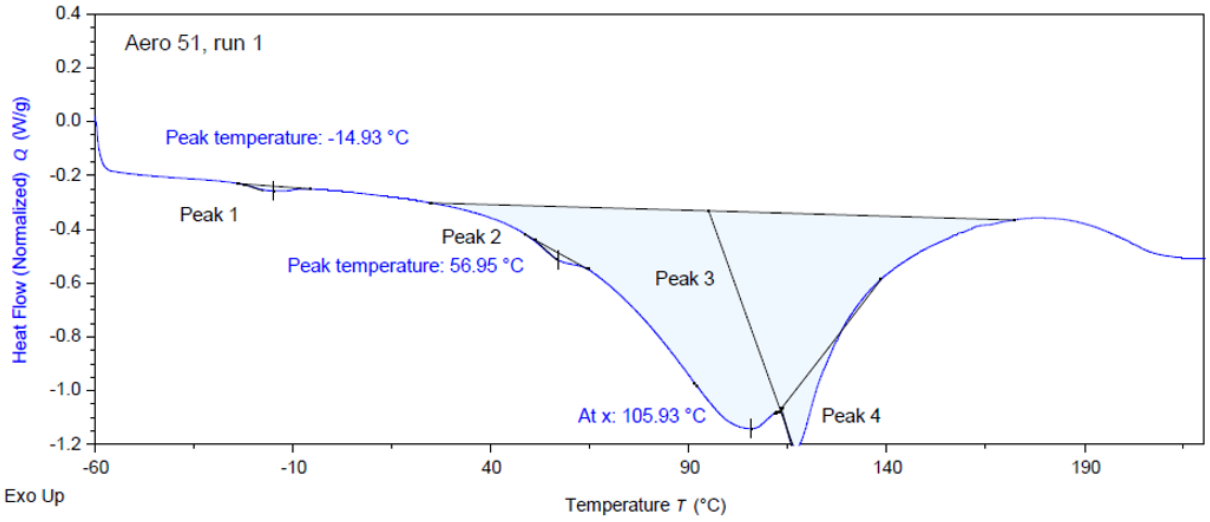

Figure 6.64: *Example DSC heat flow curve for a CSM protein aerogel with the four endothermic peaks found in CSM protein samples labelled Peak 1 – Peak 4*

It is highly likely that this major endothermic peak (Peak 3) is due to the release of absorbed water. The hygroscopic nature of the samples combined with a high RH of 65 % during conditioning is likely to result in substantial absorbance of atmospheric water in the freeze dried samples, particularly the aerogels. A brief analysis on a heated balance (conducted later) revealed the dried protein extract contained 5 – 8 wt% moisture after 'dry', frozen storage for multiple months and showed that the extract absorbs 2 – 3 wt% moisture in the immediate 2 minutes following complete drying (unknown, uncontrolled humidity and temperature). Upon heating, absorbed water will evaporate (endothermic process) from the sample at temperatures around 100 °C and will only be reversible in a closed system. Peak 3 demonstrates irreversibility in the heat-cool-heat cycles (highlighted in green and red in **Table 6.3**) since the aluminium pans used in this experiment were not hermetically sealed thus allowing water vapor to escape the system.

***Table 6.3**: Summary of thermal transitions identified in CSM protein extract and aerogel samples analysed with DSC*

Sample	Preparatory conditions	Endothermic peak 1 (−14 °C) (maybe reversible)	Endothermic peak 2 (50 °C) (irreversible)	Endothermic peak 3 (100 °C) (partially reversible in MDSC)	Endothermic peak 4 (> 110 °C) (probably irreversible ?)	Comment
Extract 1	Acid-alkali	D.N.A.[(1)]	×	✓	×	
Extract 4	Salt-PMM	✓	×	✓	×	
Extract 5[(3)]	Acid-Alkali	(first heating): ×	✓	✓	×	
		(cooling): ×	×	×	×	
		(second heating): ×	×	×	×	
Aerogel 4	3 wt%, pH 10.2, 25 °C	D.N.A.	✓	✓	×	Peak 2 only detected on one run
Aerogel 7	10 wt%, pH 10.2, 25 °C	D.N.A.	×	✓	×	
Aerogel 30	pH 8.1, 25 °C	×	✓	✓	×	Peak 2 only in 2 of 3 runs
Aerogel 35	pH 10.0, 25 °C	✓	✓	✓	×	
Aerogel 45[(2)]	pH 11.7, 25 °C	×	✓	✓	×	Peak 2 much reduced in 'glossy' samples [(2)]
Aerogel 51[(3)]	pH 11.0, 25 °C, metal mould	(first heating): ✓	✓	✓	✓	
		(cooling): ×	×	×	×	
		(second heating): ✓	×	×	×	
Aerogel 67[(3)]	pH 12.0, 4 °C, PE mould	(first heating): ×	✓	✓	✓	Peak 4 and its exothermic reversal only seen in 1 of 5 runs.
		(cooling): ×	×	×	✓	
		(second heating): ×	×	×	✓	
Aerogel 53[(4)]	pH 13.0, 25 °C, PE mould	×	✓	✓	×	
Aerogel 53 MDSC[(4)]	pH 13.0, 25 °C, PE mould	×	× (May be present as a slight shoulder on peak 3)	✓	×	Peak 3 is shown to be partially reversable with flat, broad, endotherm on reversing heat flow curve.

[(1)] D.N.A. = Data not available

[(2)] Aerogel 45 had a glossy edge after drying, attributed to partial defrosting of sample during poor freeze drying process. DSC analyses were carried out on both the glossy and non-glossy parts

[(3)] Aerogel samples 51 and 67, and extract 5 were analysed with an additional one (sample 51) or two (sample 67, extract 5) runs which were 'heat-cool-heat' cycles

[(4)] Aerogel 53 was analysed with both conventional and modulated DSC

Endothermic Peak 1 (around −14 °C) is quite small and only measurable in 3 samples with the greatest enthalpy from this transition measured in the salt-PMM extract (**Figure 6.65b**). Some DSC runs did not encompass a sufficiently wide temperature range for detection of Peak 1 (*e.g.* **Figure 6.65a**) and are denoted 'data not available' for this peak in **Table 6.3**. Peak 2, also endothermic, is located at variable temperatures (39 – 67 °C) around 50 °C, and also measures very small enthalpy changes (**Figure 6.65c**), sometimes appearing only as a slight 'shoulder' on the larger Peak 3 in which it is engulfed (**Figure 6.65b)**. Peaks 1 and 2 may both correspond to protein denaturation events which are the principal target of this investigation. Protein denaturation or unfolding events are associated with small enthalpy changes [254] making the small, and apparently irreversible peaks 1 and 2, probable candidates for denaturation or partial denaturation events. Another explanation is the possibility that one or both peaks are protein 'glass transition' events. A possible glass transition temperature (T_g) may apply particularly to Peak 2 which has an appearance and peak temperature similar to glass transitions in soy protein isolates [254]. Proteins are dynamic macromolecules where native protein may naturally shift between multiple, stable conformations all of which are biologically functional. This mobility is analogous to the mobility of amorphous segments in semi-crystalline polymers above their glass transition temperature (T_g). Furthermore, proteins can exhibit more than one such transition and so could be described as having multiple glass transition temperatures, that, unlike denaturation, are usually reversible. Peak 2 has not demonstrated reversibility in this study but may do so with further investigation using improved measuring conditions. Protein glass transitions are generally identified from the reversing heat flow curves in modulated DSC (MDSC) experiments where a subtle T_g at a similar temperature can be obscured by larger endotherms (*e.g.* water-loss) in conventional DSC curves.

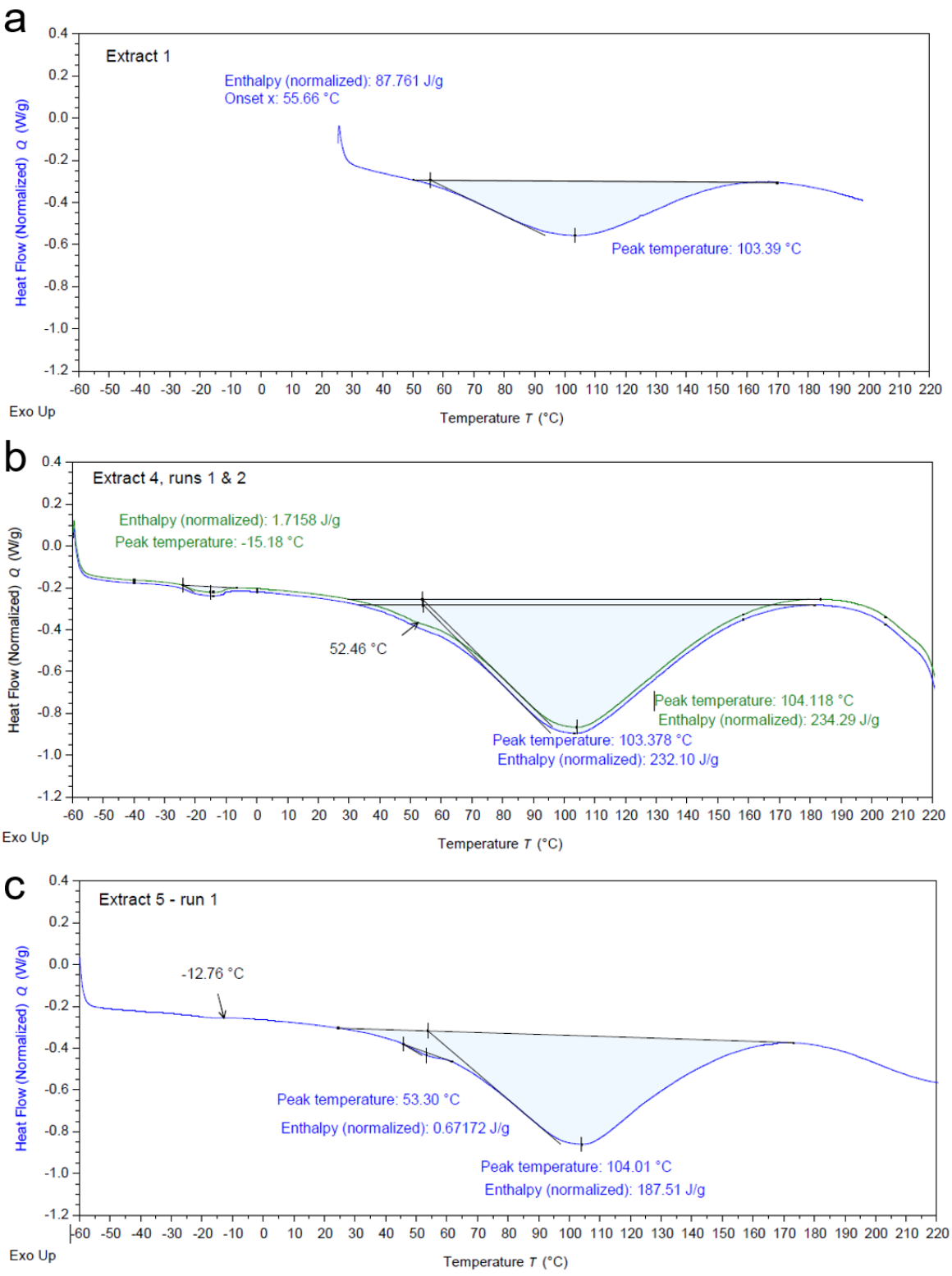

Figure 6.65*: DSC heat flow curves for CSM protein extract from acid-alkali extractions (batches 1* ***(a)*** *& 5* ***(c)****) and salt-PMM extraction (batch 4* ***(b)****). Curves are annotated to show the transition temperatures of the major endothermic peak (around 100 °C) and two smaller endothermic transitions (at approximately −14 °C and approximately 50 °C)*

MDSC studies should be conducted on CSM protein samples with clearly defined Peak 2 transitions to investigate the possibility that Peak 2 is a CSM protein glass transition. The lack of observed reversibility in the heat-cool-heat cycles of this study could be due to lost sensitivity from the high cooling rate (10 °C/min). Further DSC studies should also take into consideration that protein transitions (denaturation and aggregation) are themselves dependent on the presence of water which acts like a plasticising molecule in proteinaceous material. Water has the effect of lowering the T_d and T_g of proteins ([255, 256]) so careful control and measurement of the water content in the samples is required during both conditioning and measurement to understand levels of plasticisation and possible effects on the peaks observed.

An additional endothermic peak (Peak 4 in **Table 6.3**) was initially identified in two samples that were both analysed 3-4 times with standard runs and then 1-2 times with additional runs using a 'heat-cool-heat' cycle. During a 'heat-cool-heat' cycle, the sample is cooled again after the initial heating and then re-heated with heat flow measurements recorded during all stages. Peak 4 was subsequently determined to be two different thermal events in the two samples. In sample 67, Peak 4 demonstrated the only clear reversal upon a heat-cool-heat cycle (**Figure 6.66a**), a phenomenon not seen elsewhere in the entire DSC data set. Peak 4 was not reversible in the heat-cool-heat cycle of sample 51 (**Figure 6.66b**) and occurred at the lower temperature of 113 °C in sample 51, as compared to 132 °C in sample 67. Peak 4 was also clearly identifiable in all 5 repeat runs of sample 51 (**Figure 6.66c**) and therefore much more likely to be a true thermal transition of the CSM protein aerogel. Assigning of the elusive peak 4 to a protein transition is a challenging task given its rare detection, conflicting appearances, and its close association with the larger, neighbouring peak 3. Peak 4 in aerogel 67 could be attributed to possible contamination with some other substance since the peak was only seen in the last run of 5 repeats. Another explanation that could account for the clear reversibility of the transition in sample 67 and may even encompass the confusing appearance of this peak at variable temperatures is that Peak 4 is another possible denaturation event or glass transition.

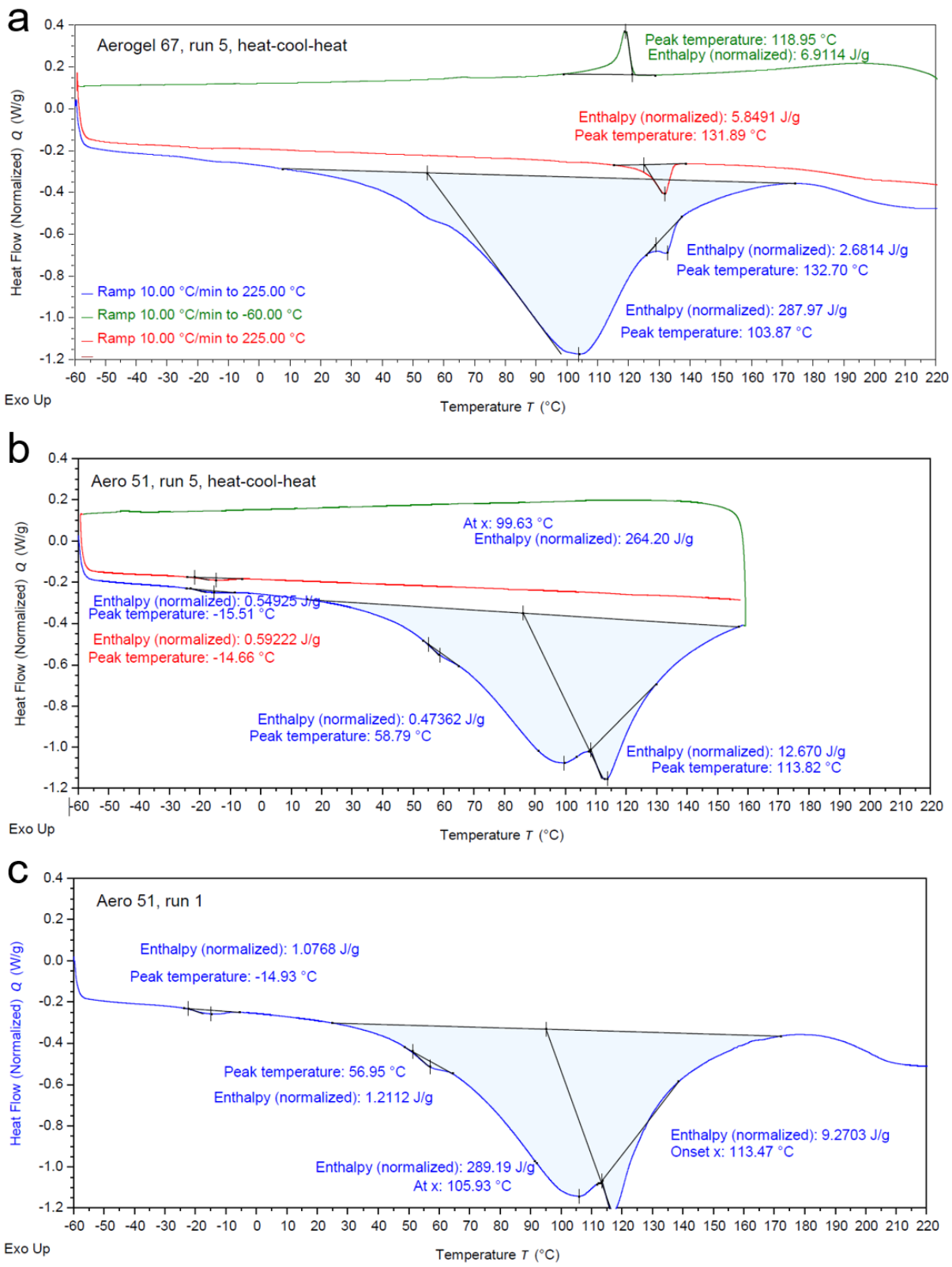

***Figure 6.66**: DSC heat flow curves for aerogel sample 67 (gelation pH: 12.0, temperature: 4°C) from a heat – cool – heat cycle **(a)** and for aerogel sample 51 (gelation pH: 11.0, temperature: 25°C) from a heat-cool-heat cycle **(b)** and from a single heating run **(c)**. Curves are annotated to show the transition temperatures and enthalpies associated with peaks*

The T_g of plasticized cruciferin protein can be estimated at around 180°C by considering calculations of the T_g of similar globular seed proteins (*e.g.* wheat, soy, corn and lupin proteins) which have T_g values grouped from 174 to 186°C [257]. Given that water can lower the T_g and T_d of proteins, it is plausible that a highly saturated (with water) CSM extract or aerogel could have a detectable T_g in the temperature range of peak 4 (113 – 132 °C). However, considering all the available information, it is much more likely the 132 °C peak in sample 67 (seen in run 5 only) is the result of contamination. The contamination is perhaps from an oil-based polymer such as the Parafilm® tape commonly used in the laboratory or the polyethylene mould used to produce sample 67 (which has a T_m around 130 °C). The sample 51 peak at 113 °C could then be attributed to a secondary or 'split peak' water-loss event, likely due to variable protein-water interactions. Indeed, Peak 4 at 113 °C and Peak 3 at 100-106 °C in sample 51 appear much more like the two split peaks of a single endotherm (**Figure 6.66 b-c**). This phenomenon, alongside the variable peak temperatures and broadness of the water loss endotherm across all samples, can be explained by the dependency of the water evaporation energy on variable protein-water interactions [254]. The unique identification of this split peak in only sample 51 could be explained by the extract type from which it was prepared. Sample 51 is the only aerogel in the DSC analysis that was prepared from a 'salt-PMM' CSM protein extract (see **Section 5.3.1**) which has been shown to contain a different array of protein molecules to the 'alkali-acid' extract (see **Section 5.3.3,** also **2.3.2**). Although cruciferin may still be the dominant protein (see **Section 5.3.4**), changing ratios of multimers, subunits, and smaller peptides in the 'salt-PMM' extract can change the quantities, locations, and types of molecular motions and bonds in the sample.

Another interesting finding from the DSC experiments of CSM protein aerogels is revealed in the MDSC curve generated from sample 53 (**Figure 6.67**). This was the only sample to be analysed with MDSC and revealed a broad endotherm in the reversing component with a peak temperature of around 64 °C.

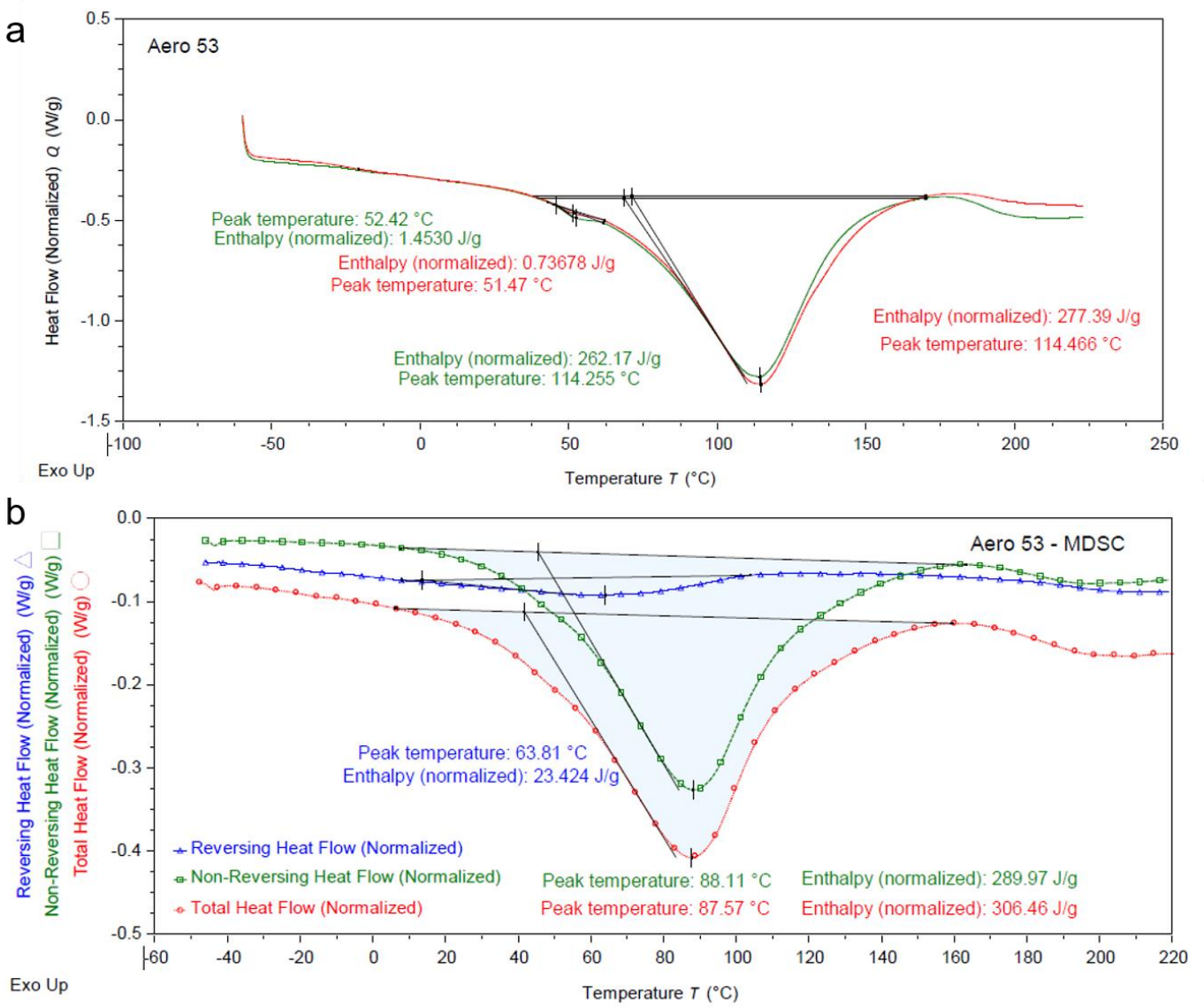

***Figure 6.67**: DSC heat flow curves from conventional **(a)** and modulated **(b)** DSC of aerogel sample 53 (gelation pH: 13.0, temperature: 25°C). Curves are annotated to show the transition temperatures and enthalpies associated with the transitions*

The reversing peak suggests that a component of the large Peak 3 is reversible and interestingly the peak temperature is shifted to more than 20 °C lower than the Peak 3 temperature (seen in the total and non-reversing heat flow curves). Indeed, the transition in the reversing heat flow curve is possible confirmation that Peak 2 is a glass transition event, as postulated earlier in this Section, though further MSDC experiments are still required to confirm this.

Finally, a brief comparison can be made of the peak temperatures and associated enthalpy changes between the different CSM protein extracts and aerogels (**Figure 6.68**). Given that Peak 1 was identified as the most likely denaturation event, it was used to examine the hypothesis of a reduced denaturation event in aerogels as compared to the non-gelled extract. Two of the three samples with clearly measurable enthalpies at Peak 1 were prepared from the salt-PMM extract, which, as previously discussed, may contain a different array of CSM proteins and peptides. The rarity of Peak 1 was therefore attributed to an endothermic event occurring in a salt-PMM-specific protein/peptide/subunit. A reduction in the enthalpy associated with this event is seen in the aerogel counterpart (square symbol) to the salt-PMM extract (circle symbol, Peak 1, **Figure 6.68**). The lack of this trend in Peak 2 could suggest that gelling of the samples does not restrict molecular movement which contributes to certain transitions (*e.g.* T_g) but can in others (such as the possible protein-specific T_d in Peak 1). However, further DSC studies are required to first confirm the presence of a Td confidently or T_g in multiple CSM protein samples before reductions or eliminations of certain thermal transitions can be attributed to gelation.

Interestingly, the associated change in enthalpy in Peak 3 is lower for the extracts as compared to the aerogels (**Figure 6.68**). Peak 3 is attributed to water-loss so increased enthalpy changes in the aerogels can be explained by their increased hygroscopic nature due to their porosity. The absorbance of greater volumes of water which are subsequently volatised explains a greater change in enthalpy associated with this endothermic peak.

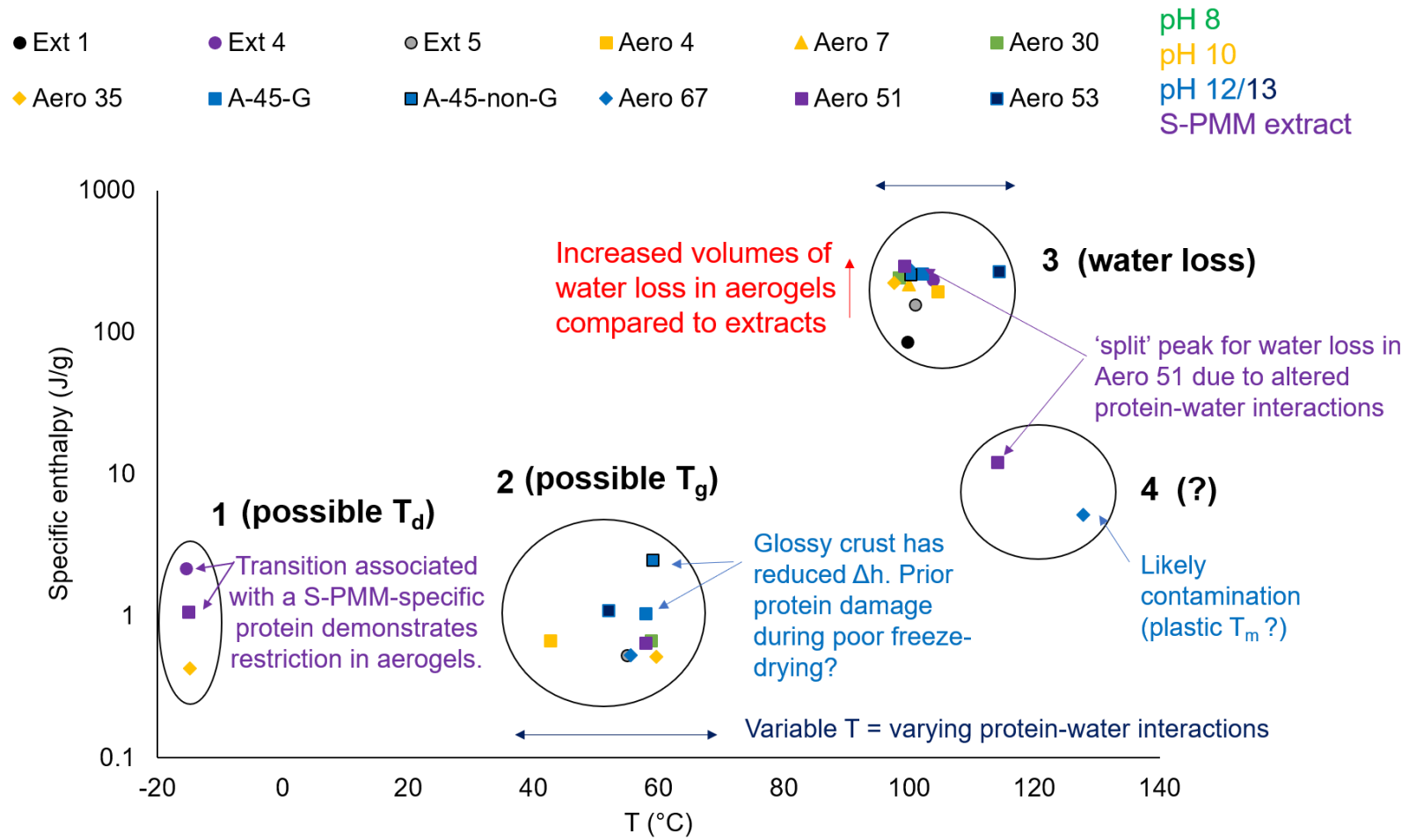

Figure 6.68: *Plot of enthalpy change as a function of peak temperatures for four endothermic transitions (identified with black rings and labelled 1 – 4) identified in DSC heat flow curves generated from CSM protein extracts (circles) and aerogels (squares, triangles, diamonds). Series represent different samples (refer to plot legend) where colour coding is used to identify samples prepared from varying gel pH values (refer to legend). Samples prepared from the 'salt-PMM' extract type are coloured purple while all others are prepared from the standard 'acid-alkali' extract type. Annotations adjacent to numbers and arrows summarise the discussions and significant findings from section 6.5.2.1*

A final observation (seen in aerogel sample 45, Peak 2, **Figure 6.68**) is the possible reduction of protein thermal transitions in poorly dried samples with glossy (labelled 'G') outer coats (refer to **Figure 6.44**, **Section 6.4.2**). Partial defrosting during incomplete freeze drying processes may lead to irreversibly aggregated and/or denatured protein which comprises these 'glossy' parts and subsequently restricts thermal transitions from occurring during DSC measurements. Prior protein 'damage' (irreversible denaturation and aggregation) due to excessive heating, desiccation, or other extreme treatments reduces the transitions which can be visualised in DSC experiments.

In summary, DSC analysis has not satisfactorily demonstrated that protein thermal transitions restricted in aerogels as compared to the non-gelled extract. However, these studies reveal the increased hygroscopic nature of CSM aerogels over their non-gelled extract counterparts due to their porous structures. Furthermore, two thermal transitions are tentatively identified as probable denaturation and protein glass transition events and an interesting anomaly to the water-loss endothermic peak is identified in a sample produced from the 'salt-PMM' extract. Improved accuracy may be achieved in future DSC studies on CSM protein aerogels through the control of absorbed water in the samples. Reducing the RH during sample conditioning and introducing a hermetically sealed sample pan for measurements will address the uncontrolled and unknown quantities of absorbed water. Investigation scope can also be widened to include other CSM protein extract and aerogel samples, such as those with prior heat-treatments. Finally, MDSC can be used to increase the tools available for accurate assigning of thermal events to specific molecular processes (denaturation, glass transition, aggregation *etc.*) particularly where heat flow peaks are partially or totally obscured by the endothermic loss of water from the samples.

6.5.2.2. Thermogravimetry

Thermogravimetric analysis (TGA) of CSM protein materials can determine their thermal stability and detect possible changes to thermal stability caused by gelation and aerogel production processes. The upper temperature limit for practical use of an aerogel is a relevant property in applications where aerogels may be subject to high temperatures. Additionally, TGA analysis can reveal distinct pyrolysis events in the samples and allow these events to be attributed to specific physical or chemical processes. Specific pyrolysis (or weight-loss) events may also vary between extract and aerogel samples, possibly providing information about chemical changes in the gelation process.

The thermogravimetric studies of Senoz *et al.* in keratin proteins elucidated the temperatures associated with specific volatiles emitted during pyrolysis [258]. Their analysis provides useful insight for the use of TGA in this thesis since keratin and CSM extract are both proteinaceous and therefore comprise of the same basic chemical formula. Coupling of TGA with mass spectrometry allowed Senoz *et al.* to identify H_2O^+ ions at temperatures around 200 °C, beyond the weight-loss plateau (around 150 °C) that typically follows initial water-loss events (at 100 °C). They attributed the release of these ions to non-disulphide crosslinking events (specifically the formation of isopeptide bonds between side-chain amines ($-NH_2$) and side-chain carboxyl groups (-COOH)) [258]. The weight-loss step associated with H_2O^+ ions (150 °C < T < 250 °C) occurred at higher temperatures and with smaller mass changes in samples pre-treated to induce crosslinking. Pre-crosslinked samples also demonstrated a smoothing of the TGA curve at T > 250 °C where rapid degradation of the protein occurs.

CSM protein aerogels are hypothesised to contain additional crosslinking compared to their non-gelled counterparts (the extracts). These crosslinks could include isopeptide crosslinks such as the formation of lysinoalanine. Identification of a weight-loss step in the 150 °C < T < 250 °C temperature range in CSM protein samples would allow for a comparison of 'cross-linking capacity' between aerogel and extract samples. Due to prior cross-linking events during gelation, the protein aerogels are expected to have a reduced weight-loss and an increased onset temperature for the 150 °C < T < 250 °C temperature range.

Additionally, the overall thermal stability, measured by the onset temperature of the largest weight-loss step, is expected to be greater in the aerogels (compared to the extracts).

Weight-loss curves obtained from TGA experiments on CSM protein extracts and aerogels revealed four common steps in the weight loss profile (**Figure 6.69**). Step 1 was attributed to the volatilisation of water from the samples and corresponded with endothermic transitions seen in DSC experiments (see **Section 6.5.2.1**). Analyses of Step 1 were bounded at 130 °C where a plateau in weight-loss was observed. Step 2 was observed mostly as a 'shoulder' to Peak 3 in the derivative curves but was nevertheless identified as the likely crosslinking event identified by Senoz *et al.*, with a temperature range of 130 °C < T < 230 °C.

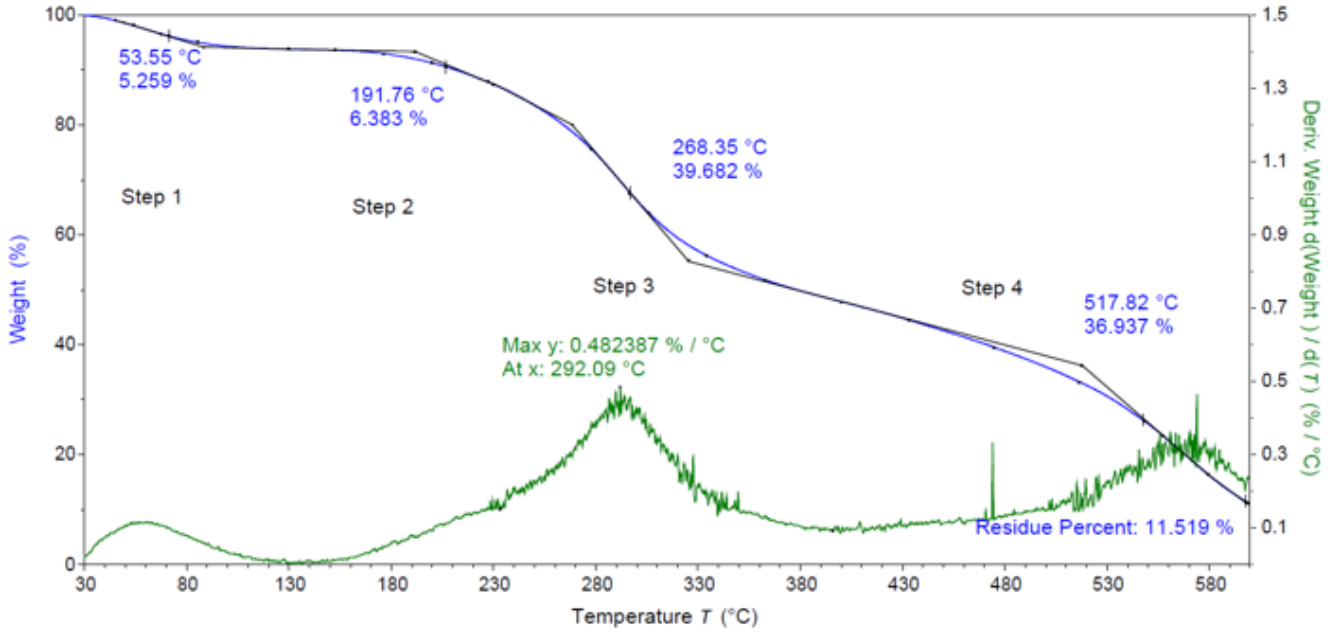

***Figure 6.69**: Example plot and analysis of TGA percentage weight loss curve (blue) and associated derivative (d(weight)/d(temperature) (green)). Weight-loss curves are analysed for the onset temperatures and percentage weight change over four steps in weight loss: a water-loss event from 30 – 130 °C (Step 1), a crosslinking and disulphide breaking event from 130 – 230 °C (Step 2), a rapid degradation region from 230 – 400 °C (Step 3) and a 'complete' degradation (Step 4). Weight-loss curves were also analysed for the residue percentage weight and the derivative curves were analysed for the maximum rate of weight loss in Step 3*

The thermal stability could be analysed using the onset temperature and the temperature at the maximum weight-loss rate of Step 3 (230 °C < T < 400 °C). Residual percentage weights and the weight loss at T >

400 °C (Step 4) were also examined in some samples, though large variability in these values limited the usefulness of Step 4 and the residual mass. Triplicate runs of individual samples had close agreeance (**Figure 6.70a**) with two representative curves each of the aerogel and extract results selected for quantitative analysis (**Figure 6.70b).**

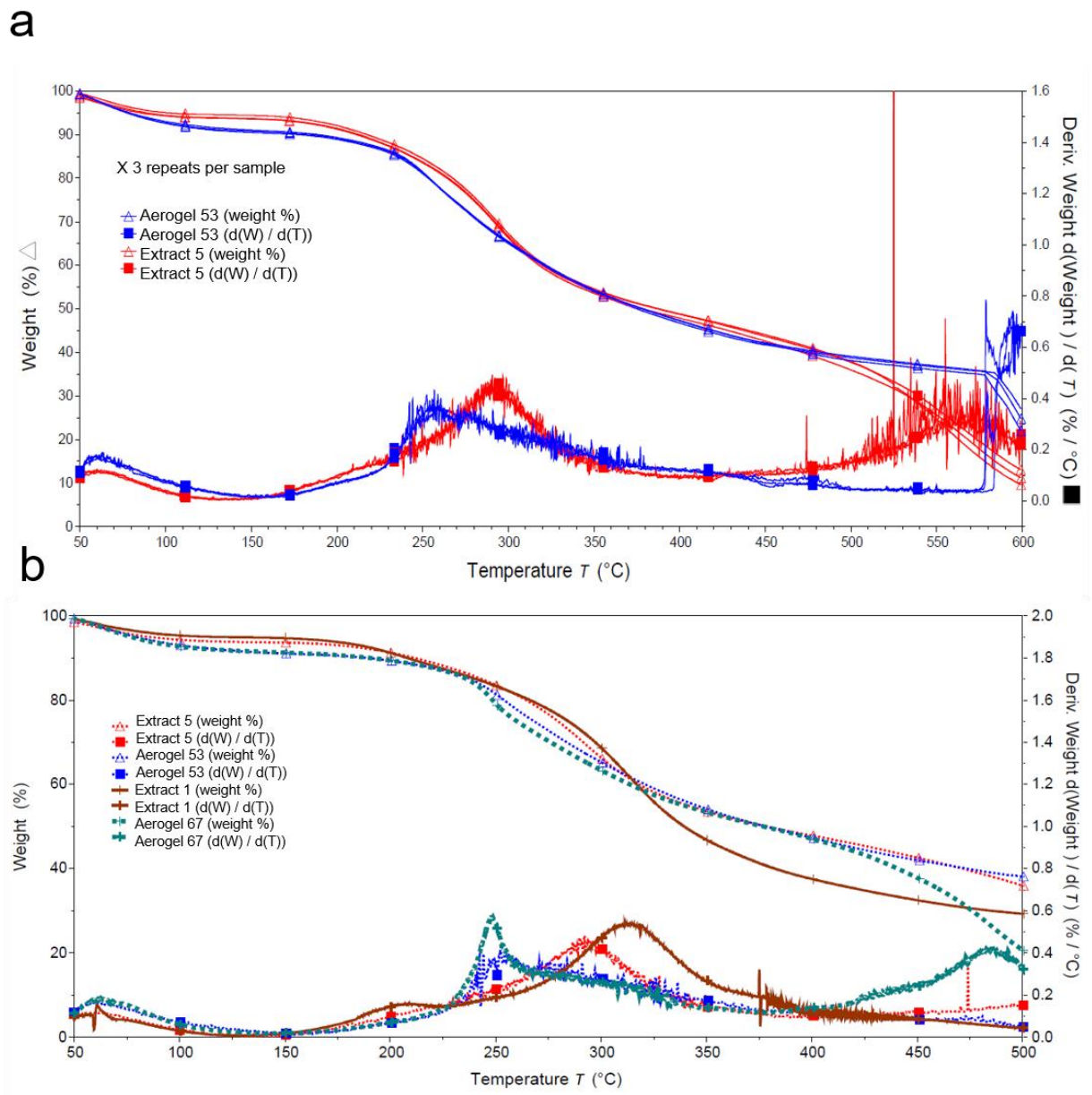

Figure 6.70: *Percentage weight loss curves and associated derivatives (d(weight)/d(temperature) for CSM protein aerogels and extracts from thermogravimetric analyses. Three repeats for aerogel sample 53 & extract batch 5 are shown* ***(a)*** *alongside additional examples of an aerogel (sample 67) and extract (batch 1), where the repeats are removed for clarity* ***(b)***

Aerogel sample 67 (teal curve, **Figure 6.70b**) and extract batch 1 (brown curve, **Figure 6.70b)** demonstrated the greatest differences between aerogels and extracts. The most interesting difference was a lower thermal stability in the aerogel samples. The greatest rates of weight loss in the aerogel samples occurred at a lower temperature (around 250 °C) compared to the extracts (around 300 °C) and corresponded to the onset of Step 3 in the aerogels samples (also around 250 °C) (**Figure 6.71**).

Conversely, the extract samples demonstrate an onset to Step 3 that is 20 – 30 °C higher than the aerogel samples. The total mass loss was expected to be the same irrespective of sample type, however inconsistent and wide-ranging residue weights at 600 °C (12 % to 27 %) may undermine weight loss comparisons at each step. High ash contents were not expected in either sample and probably indicate significant quantities of residual salts from the extraction and gelation processes. Furthermore, the residue weights showed no clear difference between ash levels in aerogels compared to extracts. Normalised (against residual ash content) weight loss percentages for steps 1-4 reveal clearer comparisons between the aerogels and extracts. A clear corroboration of findings from DSC analyses (**Section 6.5.2.1**) is seen in Step 1 with higher weight changes in the aerogel samples (approx.. 10 % of non-ash content) compared to the extracts (3 – 6 % of non-ash content). This is attributed to the greater hygroscopic nature of aerogels due to their porosity.

Step 2 reveals a possible link between the aerogels and the hypothesised reduction in 'cross-linking capacity'. Reduced weight losses are seen in the aerogels (approx. 6 % of non-ash content) as compared to the extracts (7 – 12 % of non-ash content). Crosslinking, including the condensation reaction of side-chain $-NH_2^+$ and -COOH groups, was expected during the gelation process. Consequently, the gelled samples demonstrate reduced weight loss in peak 2 since the number of side-chain $-NH_2^+$ and -COOH groups available for further cross-linking during the TGA experiment is lowered, liberating less H_2O^+. However, this demonstration of increased isopeptide bonds in CSM protein aerogels is a tentative finding that relies on the extrapolation of keratin protein data from other studies in assigning Step 2 to the isopeptide crosslink [258]. Further investigations using TGA-MS or TGA-IR analyses should be

conducted to identify the volatiles associated with each weight-loss step and conclusively connect pyrolysis events to chemical changes in the CSM proteins.

The combined weight losses occurring in Steps 3 and 4 (% weight loss at T > 230°C) do not reveal any further differences between the aerogels and extracts with all curves losing approximately 80 – 85 % of the non-ash content at T > 230°C. Most samples lose approximately 45 % in the main degradation event (Step 3) though specific samples demonstrate some variance in the Step 3 weight loss (*e.g.* 70 % non-ash content in extract 1 (**Figure 6.71b**)).

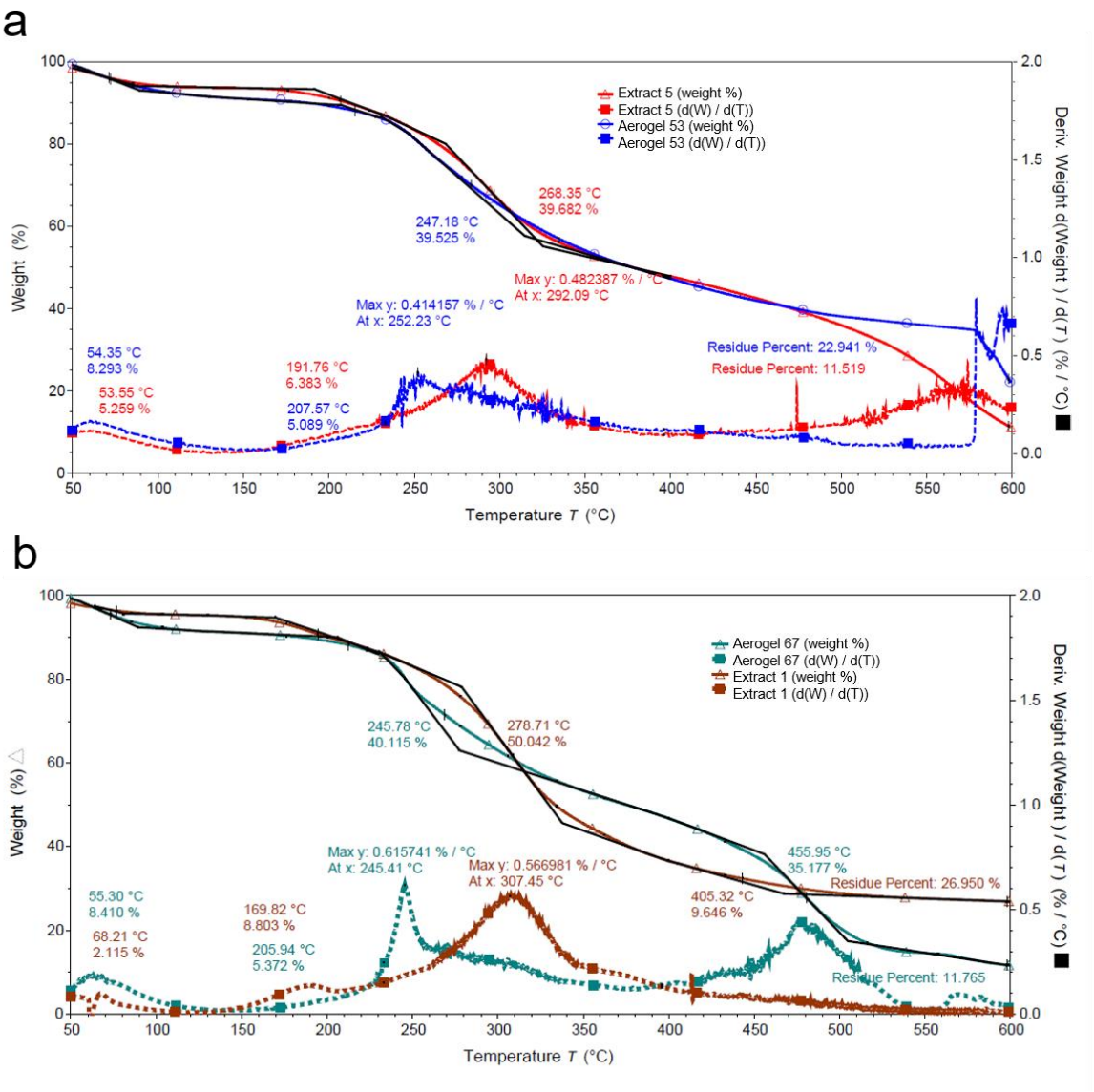

Figure 6.71: *Analyses of percentage weight loss curves and associated derivatives (d(weight)/d(temperature) comparing aerogel sample 53 & extract batch 5* ***(a)*** *and comparing aerogel sample 67 and extract batch 1* ***(b)****. Weight-loss curves are analysed for the onset temperatures and percentage weight change for steps 1 – 3* and for the residue percentage weights. Derivative curves were analysed for the maximum rate of weight loss in step 3. *Analysis of weight-loss step 4 was added for aerogel sample 67 and extract 1* ***(b)***

Individual anomalies such as the weight loss step at 455 °C in aerogel 67 (**Figure 6.71b**) remain unexplored and indicate a broader TGA investigation could provide a deeper understanding of pyrolysis in CSM proteins. Additionally, confidence in the findings can be improved if TGA is coupled with chemical analyses of the released volatiles, chemical assays of the residual ash content, and a wider selection of protein treatments for comparison. TGA analyses have revealed that CSM protein aerogels

are, at best, no more resistant to thermal degradation than the raw proteinaceous material from which they are produced.

6.5.3. Solubility of CSM protein aerogels

A common chemical attribute of bio-based materials is their lack of water-resistance due to the hydrophilic nature of most naturally derived polymers. Consequently, the absorption of water can be problematic, jeopardising the structural integrity of a material and exposing the material to premature biodegradation from microorganisms [259]. Many naturally derived polymeric materials demonstrate persistent performance issues due to post-production absorbance of water [260]. Meanwhile, waterproofing of biological materials remains challenging; successful waterproofing and toughening of biobased polymers generally results in a reduction of inherent biodegradability [261, 262]. Chemical modifications or blending with non-biodegradable polymers is often necessary to improve hydrophobicity [262]. Biodegradability studies of CSM protein materials are not included in the scope of this thesis. However, the CSM protein aerogels are hypothesised to retain the inherent biodegradability of the constituent proteins since they have not been exposed to chemical modifiers or crosslinking molecules (see **Section 8.6.2**). Furthermore, since water solubility often (but not always [263]) accompanies biodegradability, information pertaining to the solubilisation of CSM protein aerogels in aqueous solutions can be used to indicate biodegradability. CSM protein aerogels are expected to succumb to water damage since the proteins are water-soluble. Indeed, it is the water-soluble nature of the CSM extract which has been exploited in this work to facilitate the 'green' chemical approaches central to aerogel synthesis.

A brief investigation using a simple visual assessment was conducted which assessed the longevity of the aerogel structures in three aqueous solutions. A single aerogel sample prepared at 10 wt% concentration of CSM protein extract, pH 10.7, and 25 °C was cut into three equally sized pieces. These aerogel pieces were carefully placed on the surface of three different aqueous solutions and subsequently photographed over the course of 10 days. The aqueous solutions were: water at pH 7.0 (**Figure 6.72a-b**), water at pH 3.3 (**Figure 6.72c-d**), and a saline solution (1 M $NaCl_2$ (aq)) at a pH of 5.8 (**Figure 6.72e-f**) where pH adjustment was carried out with 0.5 M HCl and 0.5 M NaOH.

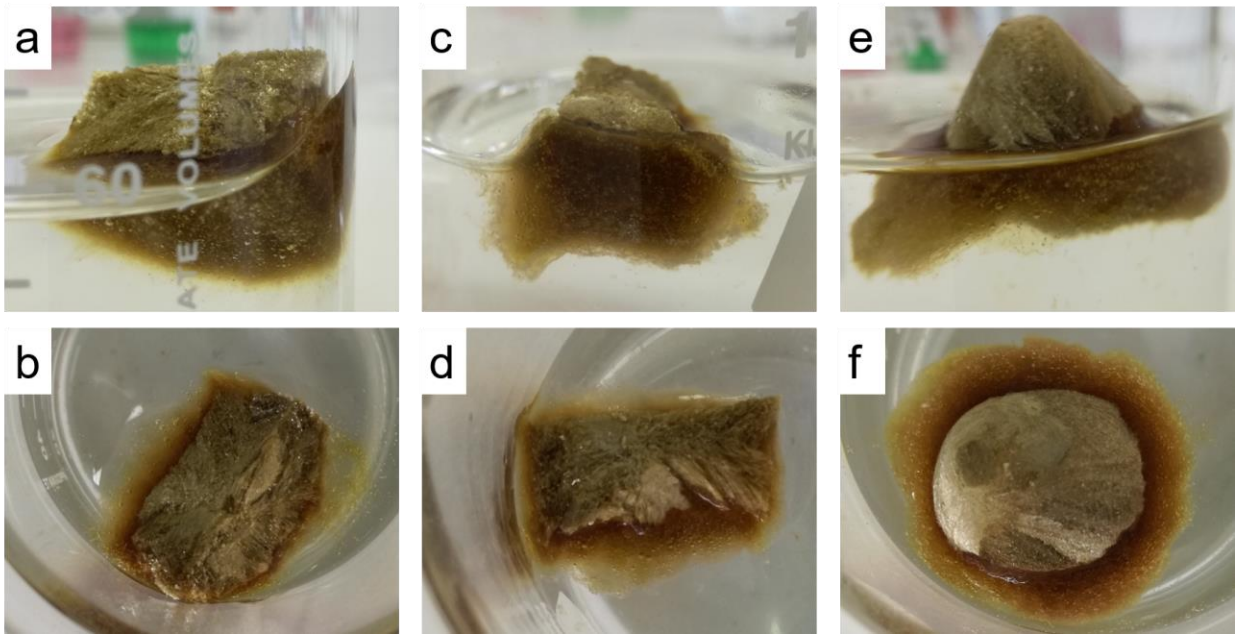

Figure 6.72: *Pieces of CSM protein aerogel (gelled at 10.0* wt% *extract concentration, pH 10.7, and 25°C) photographed at 5 minutes after being placed in water at pH 7.0* ***(a-b),*** *pH 3.3* ***(c-d),*** *and in a 1 M aqueous solution of* $NaCl_2$ *at pH 5.8* ***(e-f)***

During the first day of exposure to the aqueous solutions there were no visible differences across the three solution types with respect to the degree of structure loss in the aerogel pieces (**Figure 6.73**). However, a slightly slower response to re-solubilisation was seen in the pH 3.3 solution as a reduced amount of discolouration to the water as compared to the other solutions (**Figure 6.73c-d**). The dark colouration of CSM protein isolates is attributed to phenolic compounds such as tannins [264]. The reduced discolouration of the pH 3.3 solution (**Figure 6.73 c-d**) is probably due to a reduced re-solubilisation of these phenolic molecules at this pH value. Interestingly, this trend demonstrated a complete reversal after three days of exposure with the disappearance of the aerogel structure in the pH 3.3 solution (**Figure 6.74c-d**) but defined pieces still present in the other solutions (**Figure 6.73 a-b, e-f**). The saline solution was discoloured but appeared less opaque than the other two solutions, suggesting a lower protein content (**Figure 6.74e-f**). Opacity in the pH 7.0 solution suggests that it is also as effective at re-dissolving the proteins as the pH 3.3 solution after 3 days, and that the remaining aerogel piece likely survived dissolution as it stuck to the beaker above the water line during evaporation of the solution over the 3 day period (**Figure 6.74a**).

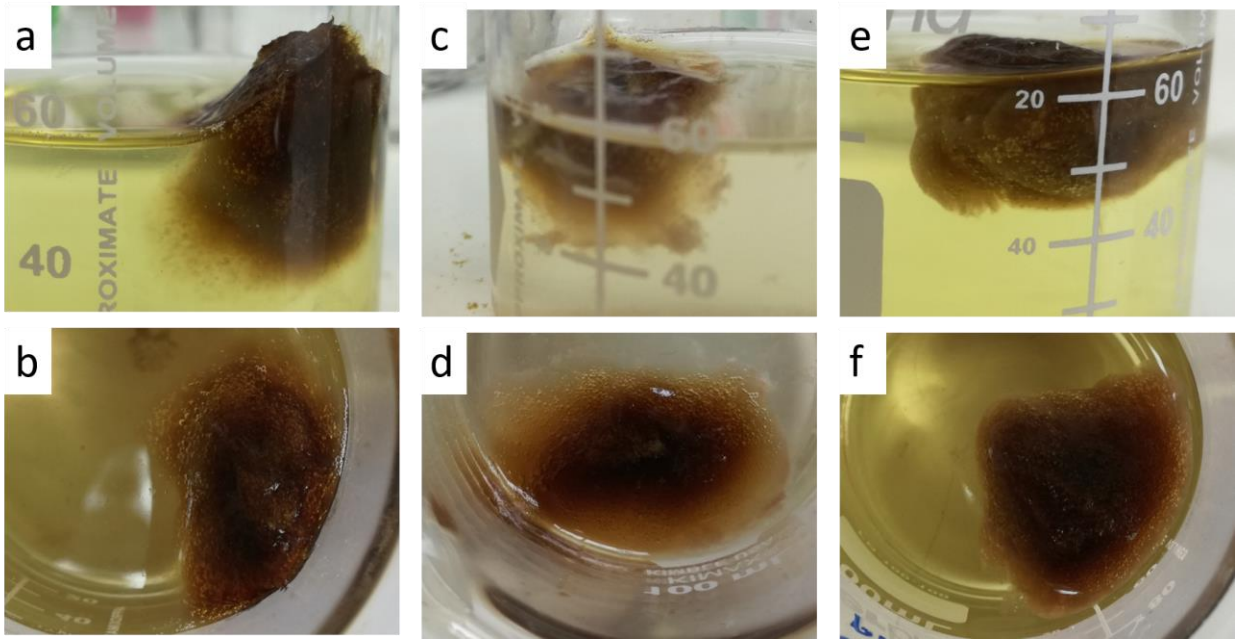

Figure 6.73: *Pieces of CSM protein aerogel (gelled at 10.0 wt% extract concentration, pH 10.7, and 25°C) photographed at 6 hours and 30 minutes after being placed in water at pH 7.0* ***(a-b),*** *pH 3.3* ***(c-d),*** *and in a 1 M aqueous solution of $NaCl_2$ at pH 5.8* ***(e-f)***

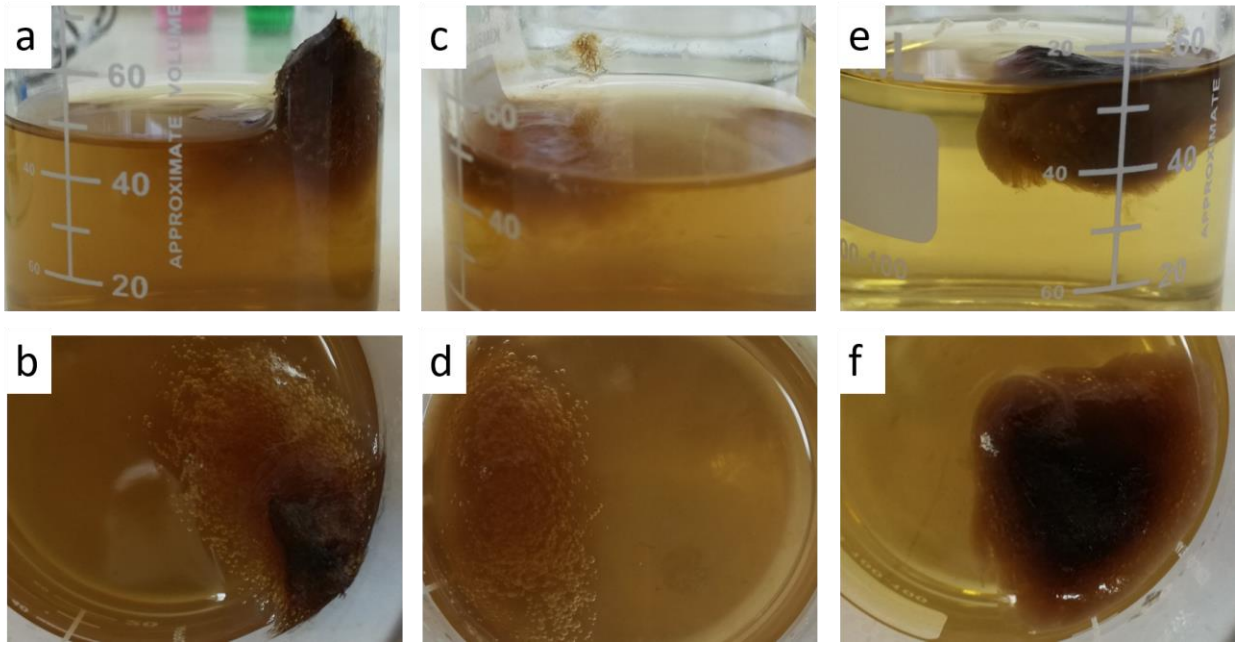

Figure 6.74: *Pieces of CSM protein aerogel (gelled at 10.0 wt% extract concentration, pH 10.7, and 25°C) photographed at 3 days after being placed in water at pH 7.0* ***(a-b),*** *pH 3.3* ***(c-d),*** *and in a 1 M aqueous solution of $NaCl_2$ at pH 5.8* ***(e-f)***

The differences outlined across the three solutions at day 3 were further exaggerated by day 10, with the saline solution demonstrating significantly greater preservation of the aerogel structure (**Figure 6.75e-f**) over the water at either pH value (**Figure 6.75a-d**).

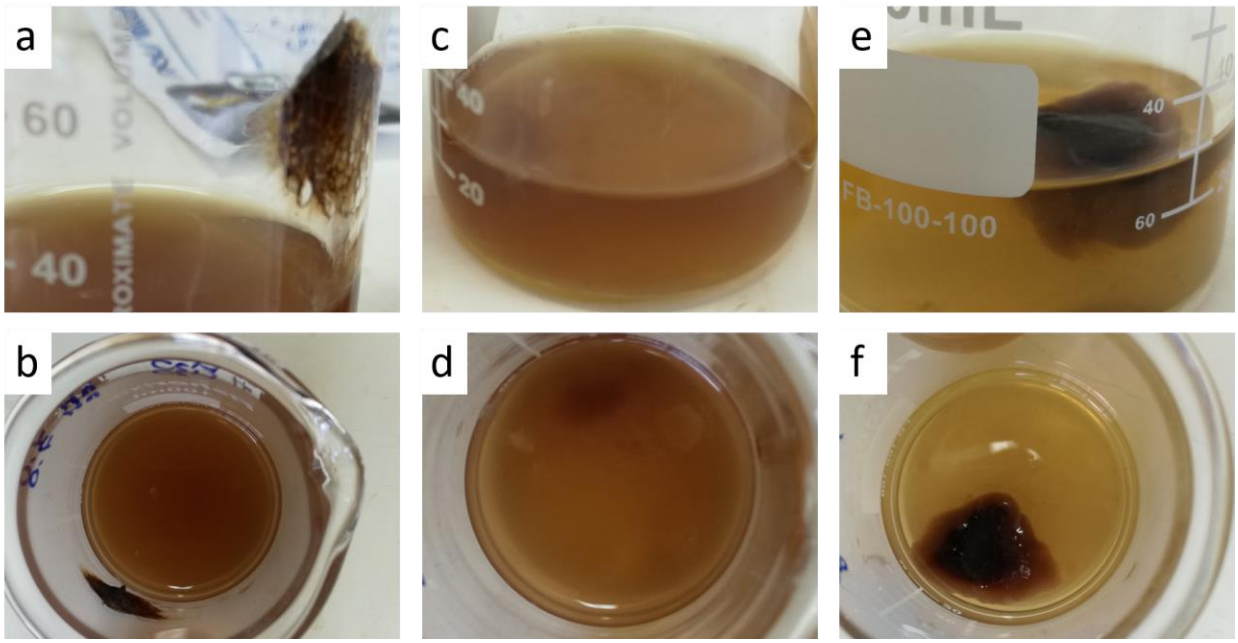

Figure 6.75: *Pieces of CSM protein aerogel (gelled at 10.0 wt% extract concentration, pH 10.7, and 25°C) photographed at 10 days after being placed in water at pH 7.0* ***(a-b),*** *pH 3.3* ***(c-d),*** *and in a 1 M aqueous solution of* $NaCl_2$ *at pH 5.8* ***(e-f)***

The single re-solubilisation test was conducted to establish a general indication of the times for degradation of CSM protein aerogels in water. The results from this test are intended as a guide for assessing the suitability of CSM protein aerogels in applications where exposure to water may be of concern. The substantial loss of structural integrity and corresponding solubilisation of protein in aqueous solutions indicates that CSM protein aerogels are not suitable (in their current form) for water-based applications where aerogel strength is needed. However, variable re-solubilisation rates across different solution types reveal the possibility of tailorable degradation in CSM protein aerogels. Additionally, there is some evidence that natural tannins are preferentially retained or released at early stages of exposure to solution depending on the solution salinity and pH.

6.6. Summary

Novel aerogels were successfully produced from canola seed meal (CSM) protein using pH-controlled gelation and a freeze drying process. CSM protein gels and aerogels were also successfully analysed for their rheological traits, morphologies, and selected properties. The golden-tan coloured aerogel monoliths are generally brittle and friable, water-soluble, hygroscopic, and possess a unique reflective property, best described as a sparkle.

General morphological features include porosities of approximately 88 %, a macroporous microstructure, and an average density of 0.12 g/cm^3 at 10 wt% protein concentration. Morphological analyses also revealed probable mesoporosity that is mostly lost during the freeze drying process. Vestiges of mesoporosity are strong motivation for an attempt to produce CSM protein aerogels using alternate drying methods which better preserve the wet-gel structure (explored in **Section 7.4**). The average compressive elastic moduli and strength of the aerogels were 1.11 ± 0.32 MPa and 56 ± 12 kPa, respectively. Aerogel densities and pore sizes were closely correlated to the protein concentration in the wet-gels. Meanwhile, mechanical properties demonstrated a non-linear dependence on density, and by extension, protein concentration. A comparison of morphological traits and mechanical properties from CSM protein aerogels and other aerogel types is provided in **Section 8.3**.

Tailorability of many gel and aerogel traits was achieved by manipulating the pH during CSM protein gelation, particularly the wet-gel strength, aerogel viability, and aerogel strength. Gelation pH appears to play an invaluable role in CSM protein gelation and can provide clues about the molecular mechanism of the gelation process. Gelation temperature was revealed as a secondary factor for influence of gel, and possibly aerogel, characteristics. A discussion in **Section 8.4** links findings regarding gelation parameters to protein molecular processes and the likely gelation mechanism of CSM protein extracts. Additionally, the potential for pH-control over the re-solubilisation of the protein matrix and/or release of small molecules was also seen during a brief degradation experiment. This was a small, but important finding, that is revisited in **Section 8.6.2**.

Thermal analyses reveal the apparently contradictory finding that CSM protein aerogels may be more vulnerable to thermal degradation but also more heavily crosslinked than the non-gelled protein extract from which they are derived. However, evidence of protein crosslinking in the aerogels from thermal analyses is tentative and the probable benefit of further investigations using these techniques alongside others is explored in **Section 9.2**. Additional gaps in the studies presented here include a lack of sufficient investigation into additional gelation parameters such as gel ageing times and freezing rates. The recycling of CSM protein aerogels into new 'reconstituted' formulations was demonstrated to alter subsequent mechanical behaviour in the aerogels. An outline of additional variables and aerogel samples (including reconstituted CSM protein aerogels) that could be added to these studies is presented in **Section 9.2**.

Chapter 7

7. Improved canola protein aerogels: techniques for tailoring canola aerogels

7.1. Introduction

Recent aerogel research is being conducted with an end goal of creating manufacturable aerogels for applications. Aerogel products are targeted at a wide range of industries including construction, aviation, medicine, laboratory sciences, energy, cosmetics, and electronics. Maximisation of the application potential of an archetypical aerogel can be achieved when aerogel properties are shown to be tailorable. For example, the use of surface modifications or coatings is a well-established method for tailoring the hydrophobicity and permeability of aerogels [265]. One archetypical aerogel, such as silica, can then be modified for use in radically different fields such as construction and medicine. Two key characteristics of aerogels that can be tailored are the mechanical properties and porosity, which are explored further for canola seed meal (CSM) protein aerogels in this Chapter.

The extraordinary insulative properties of silica aerogels are overshadowed by the brittleness and friability of the aerogel monoliths (refer **Section 2.1.3**). However, silica aerogels can be strengthened and toughened by the addition of biopolymers [11]. Biopolymeric aerogels with exemplary mechanical properties include those made from chitosan (compressible to 95 % strain without fracture [266]), pectin (elastic limits up to 60 % compression [161]), and cellulose (flexural strength and modulus of 7 MPa and 280 MPa, respectively [267]). It is of note that these biopolymers are all types of polysaccharides. The mechanical performance of most protein aerogels is generally not as impressive, with typical compressive strengths and moduli less than 1 MPa (refer to **Section 2.2.3**). CSM protein aerogels exhibit brittleness, not unlike silica aerogels (see **Section 6.5.1**), with compressive moduli (1 MPa) and strengths (0.1 MPa) that are comparable to other (non-reinforced) protein aerogels (refer to **Section 8.3.2**). Consequently, CSM protein aerogels require strengthening

and/or toughening for applications where machinability or moderate levels of mechanical durability are required. Investigations into the reinforcement of CSM protein aerogels are presented in **Section 7.3** and **Section 7.4.4**.

The pore size distribution of aerogels is directly linked to many properties such as low thermal conductivities and high absorbance capacities. Record-breaking specific surface areas and insulative properties are permitted by the microporous and mesoporous fractions of the aerogel's porosity (see **Section 2.1.3**). CSM protein aerogels have shown a macroporous morphology, attributed to the use of freeze drying (see **Section 6.4**). Due to macroporosity, the CSM protein aerogels produced by freeze drying (also referred to as cryogels) are unlikely to achieve competitive specific surface areas. Mesoporosity (and the associated high specific surface areas) is a prerequisite for possible application in absorbency (*e.g.* filtration and environmental clean-up) or controlled release of actives (*e.g.* drug delivery) (see **Section 2.1.3**). Therefore, the CSM protein aerogels are unfit for such applications until samples with significant quantities of mesoporosity can be developed. A processing procedure that should permit mesoporosity in the CSM protein aerogels is supercritical drying. Microporous and mesoporous structures are generally only attainable using supercritical drying which is accepted as the best method for preservation of the wet-gel structure (see **Section 2.1.1**).

Furthermore, motivation is strong for the development of truly mesoporous CSM protein aerogels. Few proteinaceous aerogels with mesoporous structures have been reported in the literature, as freeze drying of proteins is a readily adaptable technique for aerogel production making it a popular choice of drying method for proteins (refer **Table 2.1**). However, recent years (since 2017) have seen the establishment of supercritical carbon dioxide (SC-CO_2) drying as a routinely successful method in protein-based aerogel research, producing truly mesoporous aerogels from silk, egg, and milk proteins (see **Table 2.2**). These protein aerogels boast mesoporous morphologies with BET surface area measurements from 48 m^2/g to 420 m^2/g and are touted as potential encapsulation vessels [75, 138, 139], energy storage tools [137], oil separation filters [126], and fire retardants [126]. Moreover, the presence of some mesoporosity in CSM protein cryogels (see **Section 6.4.2**) suggests that a homogenous, mesoporous structure may be obtainable in CSM protein gels using supercritical fluid

extraction with appropriate solvents. Additionally, preparation of CSM protein aerogels by SC-CO_2 drying may aid the elucidation of the canola protein gelation mechanism. The SC-CO_2 drying method may sufficiently preserve the wet-gels to allow for improved scrutiny of the finer gel structure. Suspected pH-induced morphological differences were difficult to observe in CSM protein cryogels (see **Section 6.4.2**). However, it is hypothesised that SC-CO_2-dried aerogels will offer improved imaging opportunities of the protein aggregates and particles hypothesised to make up the gel network. The development of CSM protein aerogels using SC-CO_2 drying is presented in **Section 7.4** alongside the concurrent discovery of Ca^{2+}-induced gelation in CSM protein gels.

7.2. Experimental methods

The experimental materials and procedures for the techniques in this Chapter can be found in **Sections 4.1** & **4.4** and are summarised in **Table 7.1**.

Table 7.1: *Summary of experimental techniques from Chapter 7 and the corresponding sections of Chapter 4 describing the experimental procedures*

Section (Chapter 7)	Technique	Section of Chapter 4 pertaining to this technique
7.3.1	Preparation of canola protein hybrid gels	4.4.1
7.3.1 & 7.4.4	Preparation of aerogels using freeze drying	4.1.4
7.3.1 & 7.4.4	Bulk density measurements	4.1.5
7.3.1 & 7.4.3	Scanning electron microscopy (SEM)	4.1.6
7.3.2 & 7.4.4	Static compression testing	4.1.7
7.3.2	Dynamic mechanical analysis (DMA)	4.4.2
7.3.3	Sodium dodecyl sulphate – polyacrylamide gel electrophoresis	4.1.1
7.4.1	Preparation of canola protein gels using $CaCl_2$	4.4.3
7.4.1	Viscometry of gels	4.1.2
7.4.1	Rheometry of gels	4.1.3
7.4.2	Preparation of aerogels using the SamDri 795 Critical Point dryer	4.4.4
7.4.3	Nitrogen gas sorption porosimetry	4.4.5

The adaptation of the solvent exchange, supercritical drying and gas porosimetry techniques to the CSM protein gels and aerogels revealed the need for novel methodological approaches. Consequently, some of the methods are useful advancements for protein aerogel research. While all methods are presented in full in **Chapter 4**, highlights from the following processes are presented in the relevant Chapter Section: (i) preparation of Ca^{2+}-treated CSM protein gels (**Section 7.4.1**), (ii) the preparation of CSM protein alcogels for SC-CO_2 drying (**Section 7.4.2**), (iii) the use of the SamDri 795 Critical Point dryer (Tousimis®) for producing bioaerogels (**Section 7.4.2**), and (iv) the preparation of CSM protein aerogels for N_2 gas physisorption experiments (**Section 7.4.3**).

7.3. Enhancing the mechanical performance of CSM protein aerogels

The use of polysaccharides to mechanically reinforce silica and other protein aerogels inspired a similar approach to strengthening CSM protein aerogels. The simple aqueous chemistry required for gelation of CSM protein extract allowed for facile addition of three other biopolymers with the primary goal of mechanically reinforcing the aerogel structures. Casein, (a protein derived from milk), collagen and its derivative gelatine (a protein derived from animal skins, bones, and cartilage), and chitin (a polysaccharide derived from marine animal exoskeletons) were chosen as candidates for CSM protein aerogel hybrids. The term 'hybrid' is used broadly for these new aerogels, since aerogels with different constituents that remain macroscopically distinct may also be referred to as 'composite' aerogels (*e.g.* chopped chitin fibres suspended in a canola protein matrix [268]). The biopolymers selected for hybridisation (casein, chitin, collagen, and gelatine) were readily available in-house and knowledge of their material and biochemical properties was easily extracted from literature. Additionally, the overarching bio-based nature of the aerogels is maintained with these choices as they are all derived from animal sources.

Casein was used for the production of a single hybrid specimen for initial investigation into the plausibility of hybridising the canola protein gels. Casein may offer biochemical advantages due to extensive studies on the bioactive potential of this protein [269], with a future goal of synergistic effects with potential bioactivity from canola proteins (**Section 5.4**). Casein was not chosen for notable mechanical properties. In contrast, collagen and chitin are both fibrous biopolymers [270-272] with structural functions in cells and were both selected for possible mechanical reinforcement capability. Collagen, gelatine, and chitin were expected to strengthen and stiffen the CSM protein aerogels. Chitin and collagen can both be used for the preparation of bio-based materials including films, beads, fibres, cell scaffolds, and monolithic hydrogels [273, 274]. Collagen aerogels present exciting opportunities in medical applications such as cell scaffolding and wound care [48, 275] while chitin is used to make aerogels with competitive mechanical properties that have application potential in thermal insulation and medicine [276, 277]. All three biopolymers are readily obtained co-products

from existing food industries [278-280] thus, when combined with canola proteins are promising candidates for the design of low-cost, sustainable, and biodegradable materials.

7.3.1. Gelation and morphologies

The creation of CSM protein hybrid aerogels was limited to a few trial examples for casein and chitin, with a heavier focus on the hybrids produced from collagen and gelatine (**Table 7.2**). The facile addition of casein to CSM protein gels was achieved by simply mixing the casein powder with water at the same point in preparation as the CSM powder (see **Section 4.4.1**). The processing of the gel and aerogel were no different to the typical CSM protein aerogels and the only visible difference was a paler colouration (**Figure 7.1**). The casein-CSM hybrid had an aerogel density typical of preparations at 10 wt% total solids (0.114 g/cm^3) showing that the addition of casein had no noteworthy effect on shrinkage (**Figure 7.2**, **red square**).

CSM protein-chitin hybrid aerogels are more accurately described as composite aerogels. Chitin, a non-soluble fibre, was first ground to a powder using a cryo-mill (liquid N_2 temperature) to facilitate suspension in the CSM protein gel. The preparation of chitin composites was limited to the preparation of three samples, where the chitin fibres used in each were milled to a varying degree of refinement (see **Section 4.4.1**).

Table 7.2: *Summary of CSM protein hybrids and the subsequent analyses undertaken for each aerogel sample*

Samples	Biopolymer types	Ratio of CSM protein to added biopolymer	Total wt%	Density measurements	SEM	Compressive mechanical testing		SDS-PAGE
						Static	Dynamic	
2	CSM protein : Casein	1:1	10	✓		✓		
22 – 24	CSM protein : Gelatine	2:1, 5:1, 4:1	7.5, 6, 8.4	✓	✓	✓		
110 – 112	CSM protein : Chitin (experiment with grind type)	4:1, 4.3:1, 1.8:1	9, 10.6, 14.9	✓		✓		
117	CSM protein : Collagen : Gelatine	16:3:1	9.5	✓		✓		
118 – 119	CSM protein : Collagen/Gelatine	3.9:1, 4:1	8.8, 10	✓✓		✓✓		
120	CSM protein (control)	-	9.9	✓		✓		
136	CSM protein : Gelatine (moulds trial)	4:1	10	✓	✓	✓	✓	
137	CSM protein : Gelatine (UV trial)	4:1	10					
138	CSM protein (control)	-	10	✓	✓	✓	✓	✓
139	CSM protein : Collagen	4:1	10	✓	✓	✓	✓	✓
140	CSM protein : Gelatine (UVB 30 mins)	4:1	10	✓	✓	✓	✓	✓
141	CSM protein : Gelatine	4:1	10	✓	✓	✓	✓	✓

Figure 7.1: *Casein-CSM protein aerogel (left) and a CSM protein aerogel (right) at 10 wt% total solids (casein-CSM hybrid with 5 wt% casein and 5 wt% CSM protein)*

During preparation of the chitin-CSM composite gels, only the chitin with the finest level of refinement produced a homogenous suspension upon mixing with the CSM protein gel. This sample (#112) was analysed for its mechanical properties and density, while the other two samples (#110, #111) were discarded due to the accumulation of the heavier chitin fibres at the bottom of the gels. Mechanical tests (see **Section 7.3.2**) of sample 112 were sufficient to establish a basic effect of the chitin addition so further investigations with chitin were not carried out in this project. The chitin composite was prepared at 15 wt% total solids and therefore had a higher density of 0.173 g/cm³, however the associated shrinkage was acceptable for aerogels prepared at this concentration (**Figure 7.2**, **green triangle**).

.

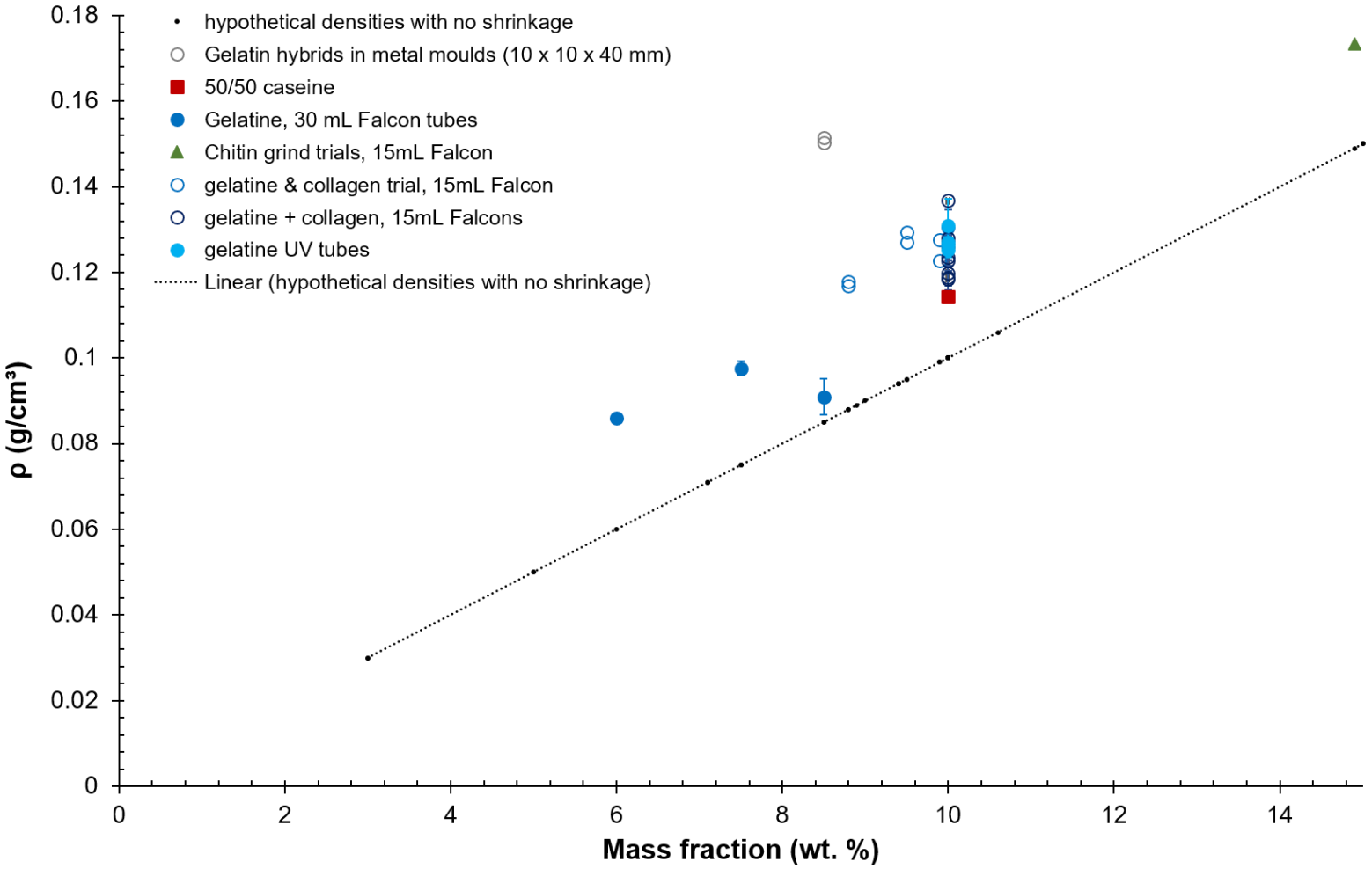

Figure 7.2: *Density of CSM protein-hybrid aerogels as a function of mass fraction. Hybrid aerogels constitute CSM protein mixed with an additional biopolymer. Mass fraction is calculated as the total weight percentage of biopolymers in the gel. Added biopolymers include collagen and its derivative gelatine (blue circles) in various moulds (refer to plot legend), also casein (red square) and chitin (green triangle)*

Hybrid aerogels were also prepared using collagen and gelatine. The collagen used was Type I, derived from bovine Achilles tendon, and was cryo-milled (liquid N_2 temperature) to a fine powder (see **Section 4.4.1**) for mixing into the CSM protein gel. Type I collagen is fibrillar and is the most common type, usually extracted from skin, bones, tendons, and ligaments [281]. Owing to the insoluble nature of the fibrous Type I collagen, CSM-collagen aerogels may be called composites like the CSM-chitin aerogels.

Gelatine (sometimes 'gelatin') is partially hydrolysed collagen obtained from animal by-products using chemical solubilisation (acidic or alkaline) and heat treatment of collagen-rich tissues [282]. Gelatine produced from an acidic hydrolysation of collagen is known as Type A gelatine (isoelectric point ~ 8-9), while gelatine from the corresponding alkaline process is Type B (isoelectric point ~ 4-5) [282]. The thermal and rheological properties of gelatines are determined by the collagen source (variability in amino acid composition) and by the processing conditions (variability in molecular weight) [282]. Gelatine used to produce CSM protein hybrid aerogels was Type B gelatine from bovine skin collagen, therefore also likely to comprise of Type I collagen and its hydrolysed polypeptides and oligopeptides [281]. The gelatine, being soluble, allowed for complete dissolution in the CSM protein gel when gentle heating ($T < 65$ °C) was applied. It was anticipated that soluble gelatine would intersperse among canola proteins more easily than insoluble collagen fibres, creating a single gel network of molecular-scale mixing.

Various CSM-gelatine and CSM-collagen hybrid aerogels were produced along with one sample containing all three constituents (CSM protein, ground collagen, and gelatine). Initial trials using gelatine in various ratios with CSM protein produced aerogels that were stiffer and stronger to the touch (**Figure 7.3**) and were subsequently analysed for compressive mechanical properties (see **Section 7.3.2**). Further preparations of hybrid aerogels aimed to compare the effects of collagen and gelatine (samples 117 – 120) and the possible use of UVB radiation to induce protein crosslinking in gelatine gels (samples 137, 140) (**Table 7.2**).

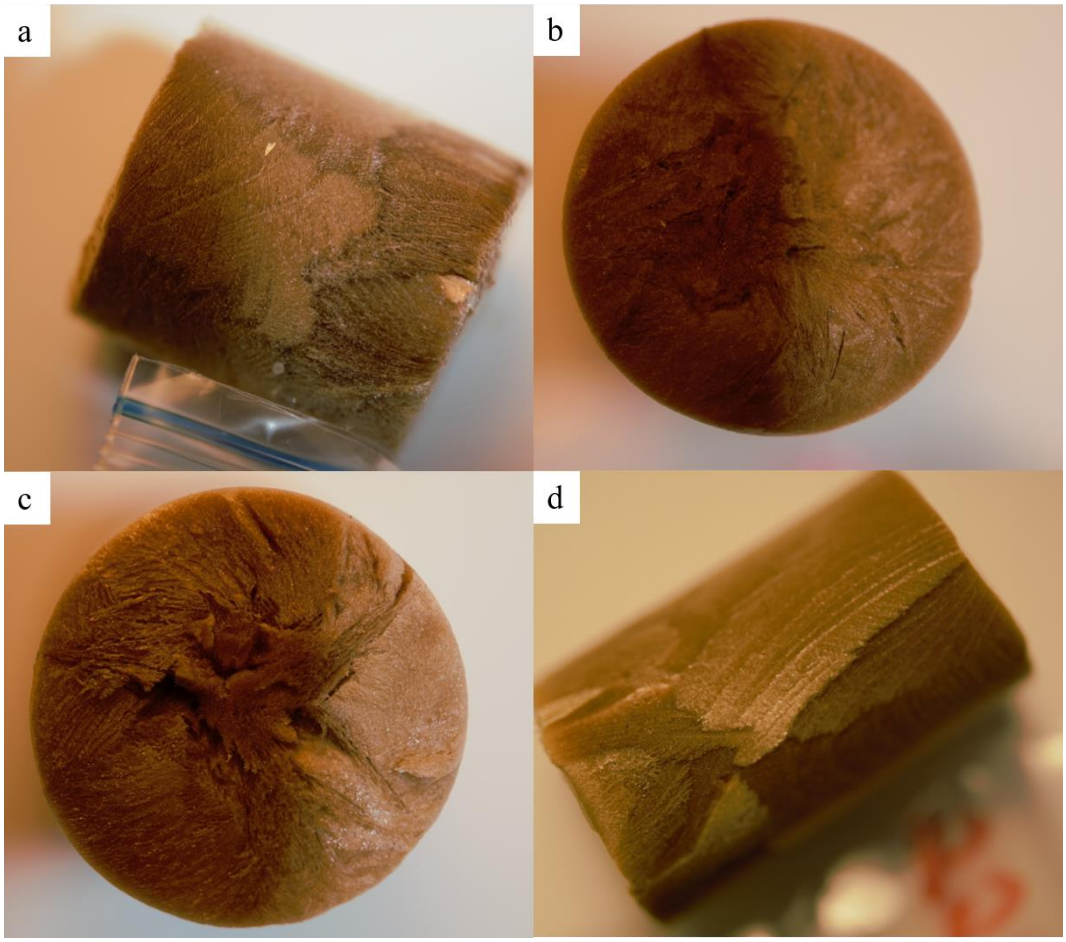

Figure 7.3: *CSM protein-gelatine hybrid aerogels prepared with* ***(a)*** *a 5:1 ratio (total solids 6 wt%),* ***(b)*** *a 4:1 ratio (total solids 8.4 wt%), and* ***(c)*** *a 2:1 ratio (total solids 7.5 wt%) of CSM protein to gelatine*

CSM protein hybrid aerogels made with gelatine and collagen demonstrated densities dependent on the total concentration of solids in the gel (**Figure 7.2**) with shrinkage typical of freeze dried aerogels. However, samples prepared in alternate moulds (**Figure 7.2, grey rings**) were an exception, showing unusually high densities (> 0.14 g/cm^3). Earlier studies have shown that freeze dried aerogel density is influenced both by the mass fraction of total solids and by the type of mould used to freeze the wet-gels (see **Section 6.4.1**). Therefore, the use of gelatine and collagen to create hybrid CSM protein aerogels did not change the expected aerogel densities.

Morphological analysis of CSM protein hybrid aerogels were also carried out using scanning electron microscopy (SEM) imaging. Initial SEM micrographs were collected from sample 22 (CSM protein-gelatine (2:1) hybrid) to determine how incorporation of fibrous biopolymers may influence the

aerogel morphology (**Figure 7.4**). The CSM protein-gelatine hybrid had a regular arrangement of 'cell' shaped pores 50 – 300 µm in width (**Figure 7.4a**) with circular openings (20 – 50 µm) on the surface of the gel (**Figure 7.4b-c).** The microstructure of CSM protein aerogels with no added biopolymers (see **Section 6.4.2**) was dominated by larger, elongated pores in a layered arrangement. Deposits of protein aggregates or particles found in CSM protein aerogels (see **Figure 6.43**) were also found in the gelatine hybrid (**Figure 7.4e-f**). Interestingly, in some areas these deposits were interspersed with areas of randomly arranged fibres of approximately 100 nm in diameter and 1 µm in length (**Figure 7.4f**). These visible fibres are attributed to partially hydrolysed collagen fibrils from the gelatine powder since collagen fibril diameters are also approximately 100 nm [271]). The micrograph evidence suggests that the gelatine is well homogenised across the visible area, although no images were obtained of collagen fibrils in the cross-section of the pore walls. Improved imaging with increased magnification of areas such as in **Figure 7.4d** would confirm the homogeneity of collagen fibrils throughout the entire CSM protein gel matrix. The random arrangement of the collagen fibrils on the gel surface and the more 'cell-like' macropores suggest that gelatine hybrid aerogels will be more isotropic in nature than their pure CSM protein counterparts which have an anisotropic layering of macropores (see **Section 6.4.2**).

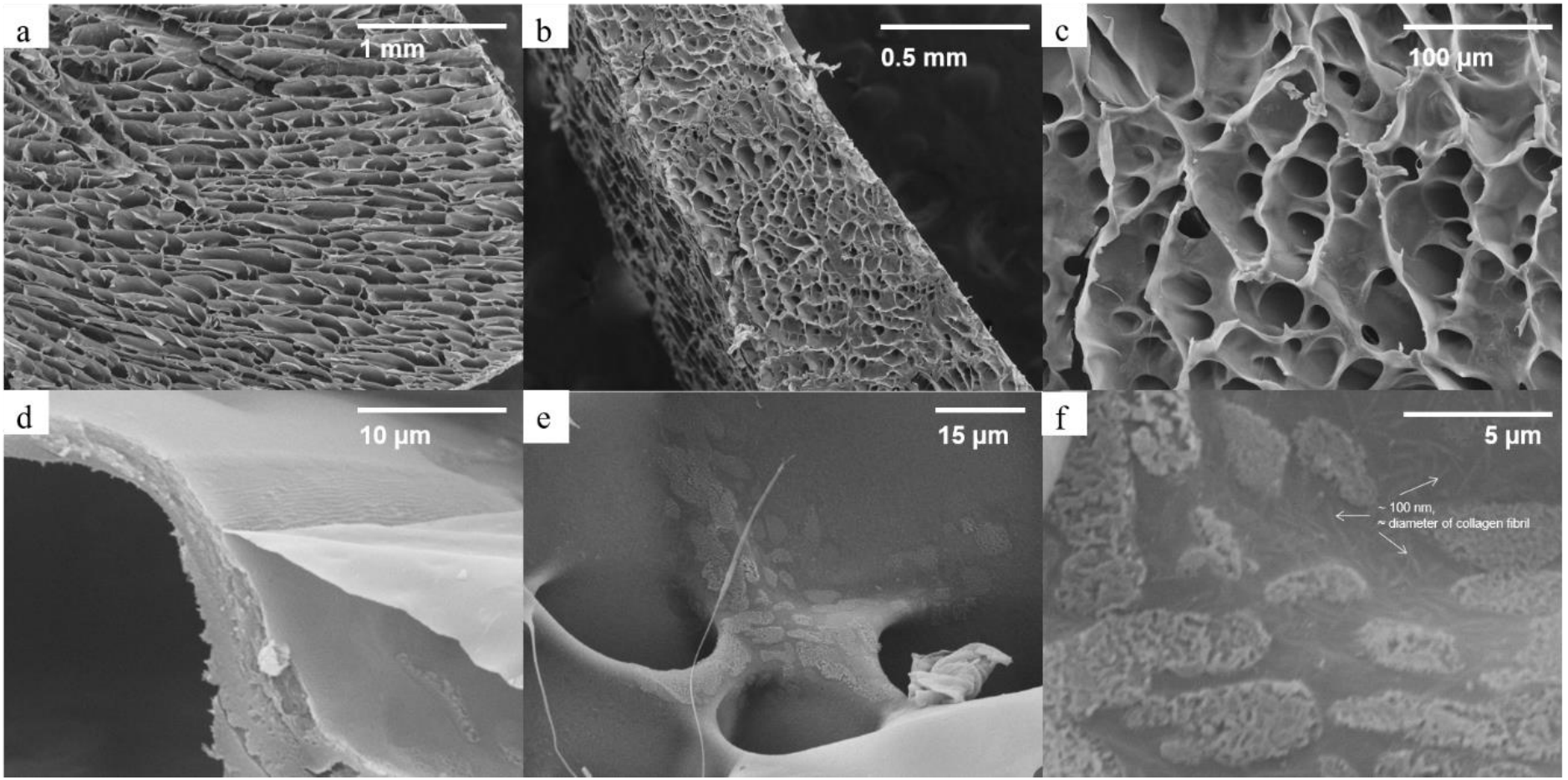

Figure 7.4: *SEM micrographs of CSM protein-gelatine hybrid aerogel prepared at 7.5 wt% (total solids) with a 2:1 ratio of CSM protein to gelatine. Transverse cross-section through entire specimen at x 50 magnification* ***(a)*** *and near the surface at x 8,000 magnification* ***(d).*** *Surface (along Falcon™ tube wall) at x 100 magnification* ***(b)****, x500 magnification* ***(c)****, x 2,000 magnification © and x 10,000 magnification* ***(f)***

Subsequent SEM imaging of a CSM protein-gelatine aerogel was carried out with the specimen prepared using either a scalpel cut at -195 °C (**Figure 7.5**) or cryofracture at -195 °C (**Figure 7.6**). Cut samples revealed smooth cross-sections of the pore walls with no identifiable collagen fibrils (**Figure 7.5b, d**) though possible collagen fibrils were identified on pore surfaces in low magnification images (**Figure 7.5c**).

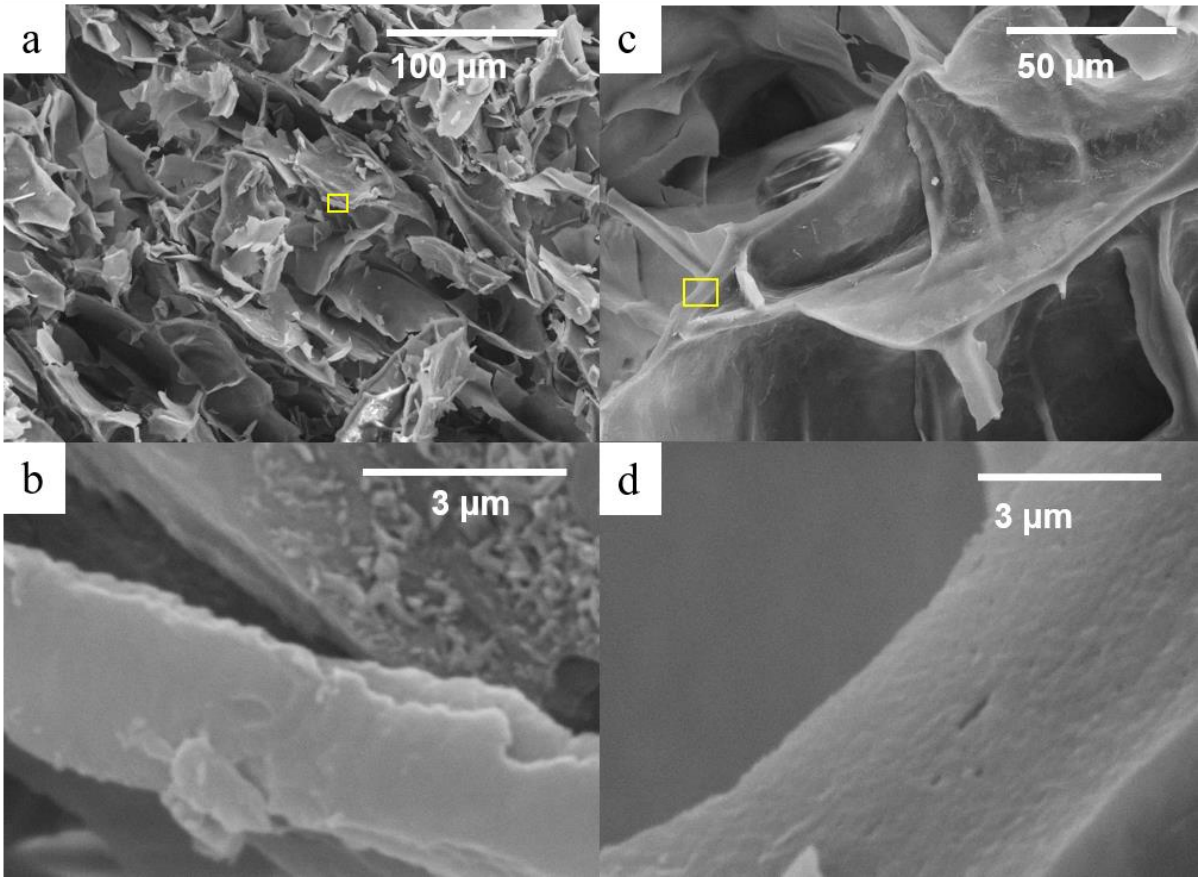

Figure 7.5: *SEM micrographs of CSM protein-gelatine hybrid aerogel prepared at 10 wt% (total solids) with a 4:1 ratio of CSM protein to gelatine. Specimen was prepared for imaging by cutting with a scalpel blade at -195 °C (liquid nitrogen temperature) followed either by drying at room temperature and pressure* ***(a-b)*** *or freeze drying at -100 mT and room temperature* ***(c-d)****. Images are cross-sections at x 500* ***(a)****, x 1000* ***(c)****, x 18,000* ***(d)****, or x 20,000* ***(b)*** *magnification. Micrographs* ***(b)*** *&* ***(d)*** *correspond to the areas in the yellow rectangles overlain on micrographs* ***(a)*** *&* ***(c)***

Cryofracture can assist in determining the strength of interaction between collagen fibrils and CSM protein in the gel matrix. A cryo-fractured cross-section of pore wall material is expected to fracture along the edge of collagen fibrils when interaction with canola proteins is poor. A cleaner fracture without evidence of collagen fibrils might indicate a strong interaction between canola and collagen protein molecules reducing the likelihood of separating the two during fracture. The cryo-fractured

surfaces showed an increased roughness as expected, but no clear evidence of collagen fibrils was found (**Figure 7.6**). Sections of the pore walls appeared to tear the gel matrix and reveal protein particles of a few hundred nm in size (**Figure 7.6b, d**).

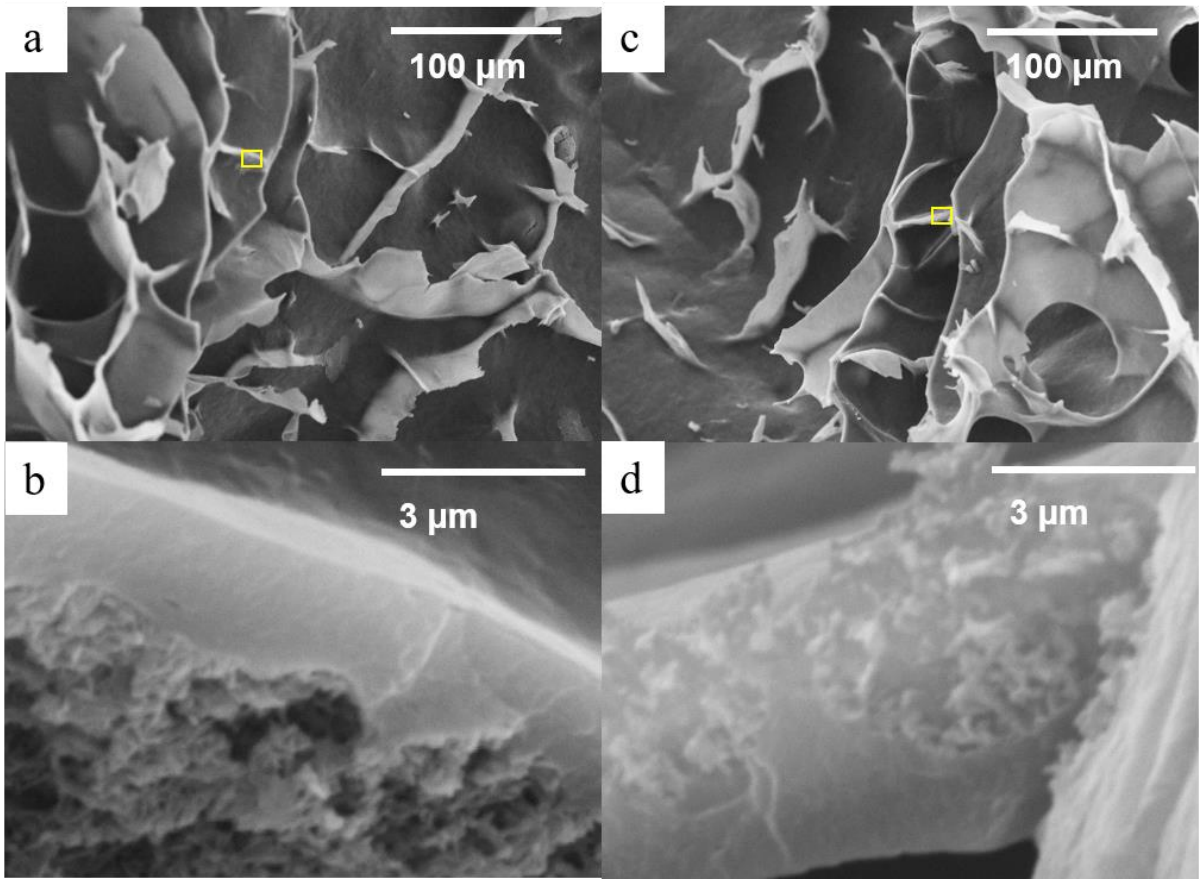

Figure 7.6*: SEM micrographs of CSM protein-gelatine hybrid aerogel prepared at 10 wt% (total solids) with a 4:1 ratio of CSM protein to gelatine. Specimen was prepared for imaging by cryo-fracture (snapping at -195 °C (liquid nitrogen temperature)) followed either by drying at room temperature and pressure* ***(a-b)*** *or freeze drying at -100 mT and room temperature* ***(c-d)****. Images are cross-sections at x 500* ***(a, c)****, or x 20,000* ***(b, d)*** *magnification. Micrographs* ***(b)*** *&* ***(d)*** *correspond to the areas in the yellow rectangles overlain on micrographs* ***(a)*** *&* ***(c)***

The lack of evidence of collagen fibrils in these images invites discussion. Firstly, the total amount of collagen peptides identifiable at x 20,000 magnification may be too low to easily detect in this specimen. The CSM protein-gelatine hybrid here was prepared with only a 4:1 ratio of CSM protein to gelatine. The lack of detection of collagen fibrils even on the pore surfaces corroborates with this explanation. However, earlier imaging of collagen fibrils in a CSM protein-gelatine aerogel with a 2:1 ratio showed an abundance of fibrils at the pore surface (**Figure 7.4f**), suggesting that some should be seen even when the concentration of gelatine is halved (as in **Figure 7.6**). Another explanation is that

collagen fibrils and smaller polypeptides present in the gelatine powder may undergo crosslinking with the canola proteins and become closely associated in the gel matrix. Upon cryo-fracture, collagen fibrils with such a close association to the canola protein may be harder to visualise as distinct macromolecules. Difficulty in visualising strongly associated collagen molecules could be accentuated in images produced from secondary electrons (as in **Figure 7.6**) as this imaging mode best captures topological differences and provides no information about sub-surface structures or chemical differences. Furthermore, the identification of collagen fibrils may also be difficult if fibrils run perpendicular to the fractured surface and/or are obscured by the larger gel particles or aggregates.

However, the scale of the particles seen in **Figure 7.6b & d** is similar to that of collagen fibrils and there is also clear imaging of collagen fibrils on the pore surfaces in **Figure 7.4f.** These features suggest that if fibrils were present in the cross-sections of **Figure 7.6,** they should be identifiable in the micrograph. Considering all the above, it is likely that collagen fibrils are not present in the cross-sections imaged here and therefore not homogenously mixed throughout the gel matrix. **Figure 7.4f** and **Figure 7.6b** suggest that collagen fibrils possibly concentrate on the matrix surface and are therefore not cross-linked or closely associated with the canola proteins. The long-distance mobility within the gel that is required for collagen fibrils to migrate to the surface during gelation would not be possible with extensive crosslinking between the two protein types.

Finally, a series of SEM micrographs were obtained from samples 138 – 141, where both collagen and gelatine were used to make hybrid aerogels alongside a control CSM protein aerogel (**Figure 7.7**). The layered macroporous morphology typical of a CSM protein aerogel was seen in the control sample (**Figure 7.7a**, layering parallel with image) and the collagen sample (**Figure 7.7b**), while the cell-like pores previously associated with a gelatine hybrid were seen in samples 140 & 141 (**Figure 7.7c-d**). However, pore sizes were typically > 100 µm in the gelatine hybrid which had received UVB light exposure during gelation (**Figure 7.7c**) while the non-UVB exposed gelatine sample had macropores 10 – 50 µm in diameter (**Figure 7.7d**). Exposure to UVB light during gelation was hypothesised to induce protein crosslinking between collagen and canola polypeptides in the gel since

UV radiation is a known method for crosslinking collagens [283]. Extensive crosslinking was expected to alter the wet-gel structure and subsequently influence aerogel morphology.

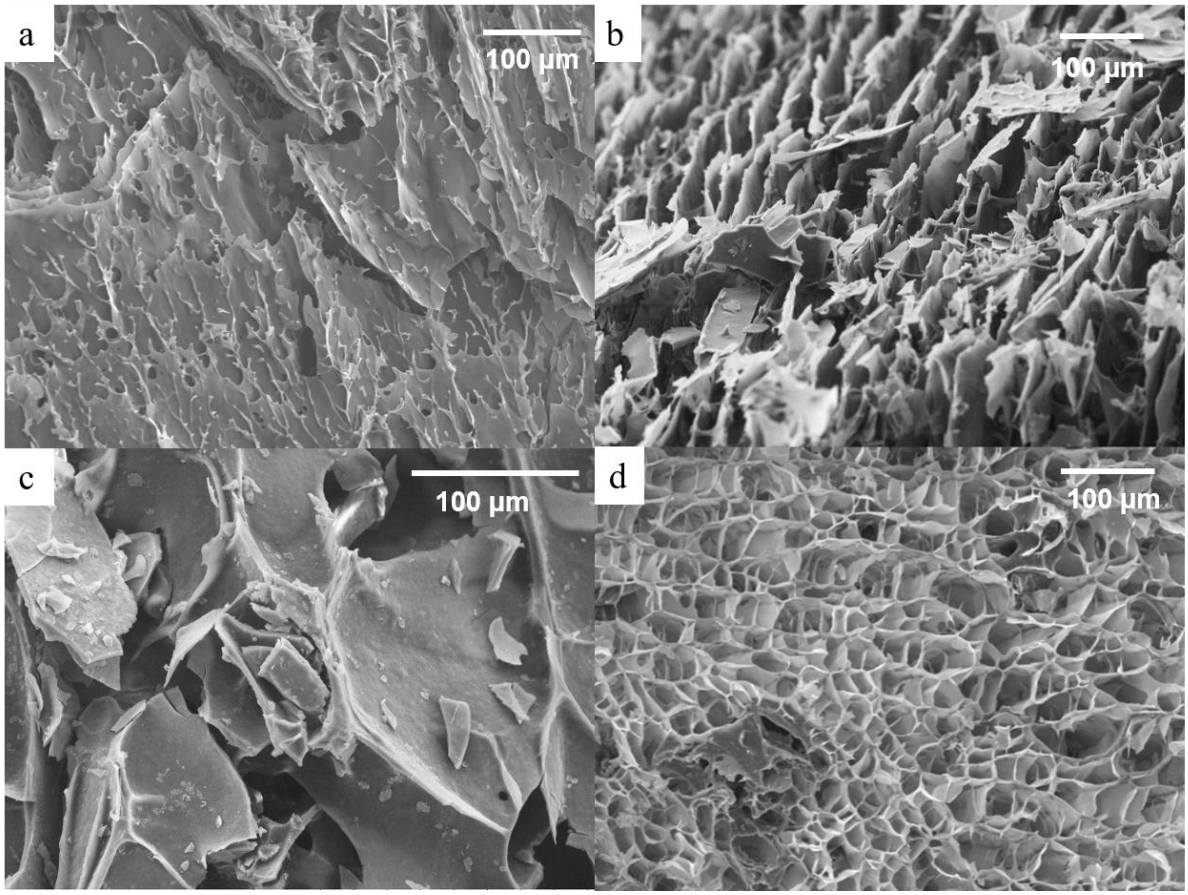

Figure 7.7: *SEM micrographs of:* ***(a)*** *CSM protein aerogel prepared at 10* wt%, ***(b)*** *CSM protein-collagen hybrid aerogel prepared at 10 wt% total solids with a 4:1 ratio of CSM protein to collagen,* ***(c)*** *CSM protein-gelatine hybrid aerogel prepared at 10 wt% total solids with a 4:1 ratio of CSM protein to gelatine and exposed to UBV radiation for 30 minutes during gelation, and* ***(d)*** *CSM protein-gelatine hybrid aerogel prepared at 10 wt% total solids with a 4:1 ratio of CSM protein to gelatine (no UVB-exposure). Micrographs are taken of the transverse cross-sections at x 190* ***(d)*** *x 200* ***(a)*** *x 250* ***(b)*** *and x 500 (****c****) magnification*

However, the larger pore sizes suggest that the morphology of the UVB-exposed gelatine hybrid is entirely determined by ice crystal growth during the freezing process. Extensive crosslinking could be expected to reduce gel elasticity making UVB-treated gels less resistant to ice crystal growth resulting in the larger pore sizes and thicker pore walls seen in **Figure 7.7c.**

High magnification images collected of these hybrid aerogels also failed to identify any collagen fibrils either on the surface or in the cross-section of the gel matrices (**Figure 7.8**). Given that the CSM protein-collagen hybrid comprised of insoluble collagen fibres suspended in the CSM protein gel, this specimen was expected to show identifiable fibres in the micrographs. The lack of fibre or fibril

formations seen along a natural fracture in the gel (**Figure 7.8a-b**) again suggests either an insufficient quantity of collagen or a lack of homogeneity in the gel. Development of further CSM protein-collagen specimens should investigate the concentration at which collagen fibrils can reliably be visualised in SEM imaging.

The gelatine hybrid aerogels are expected to be homogenous due to the soluble nature of the hydrolysed collagen polypeptides in gelatine powders. Thus, the lack of observable collagen fibrils in these gel matrices is more puzzling. Collagen fibrils and particles may be hard to identify due to successful canola-collagen association rendering the collagen fibrils an inseparable part of the protein gel matrix. Furthermore, successful co-gelation of canola and gelatine in these specimens suggests that earlier observations of collagen fibrils on the surface of a gelatine hybrid (**Figure 7.4f**) could be due to an excess of collagen fibrils because of a higher concentration of gelatine (2:1 ratio of CSM protein to gelatine).

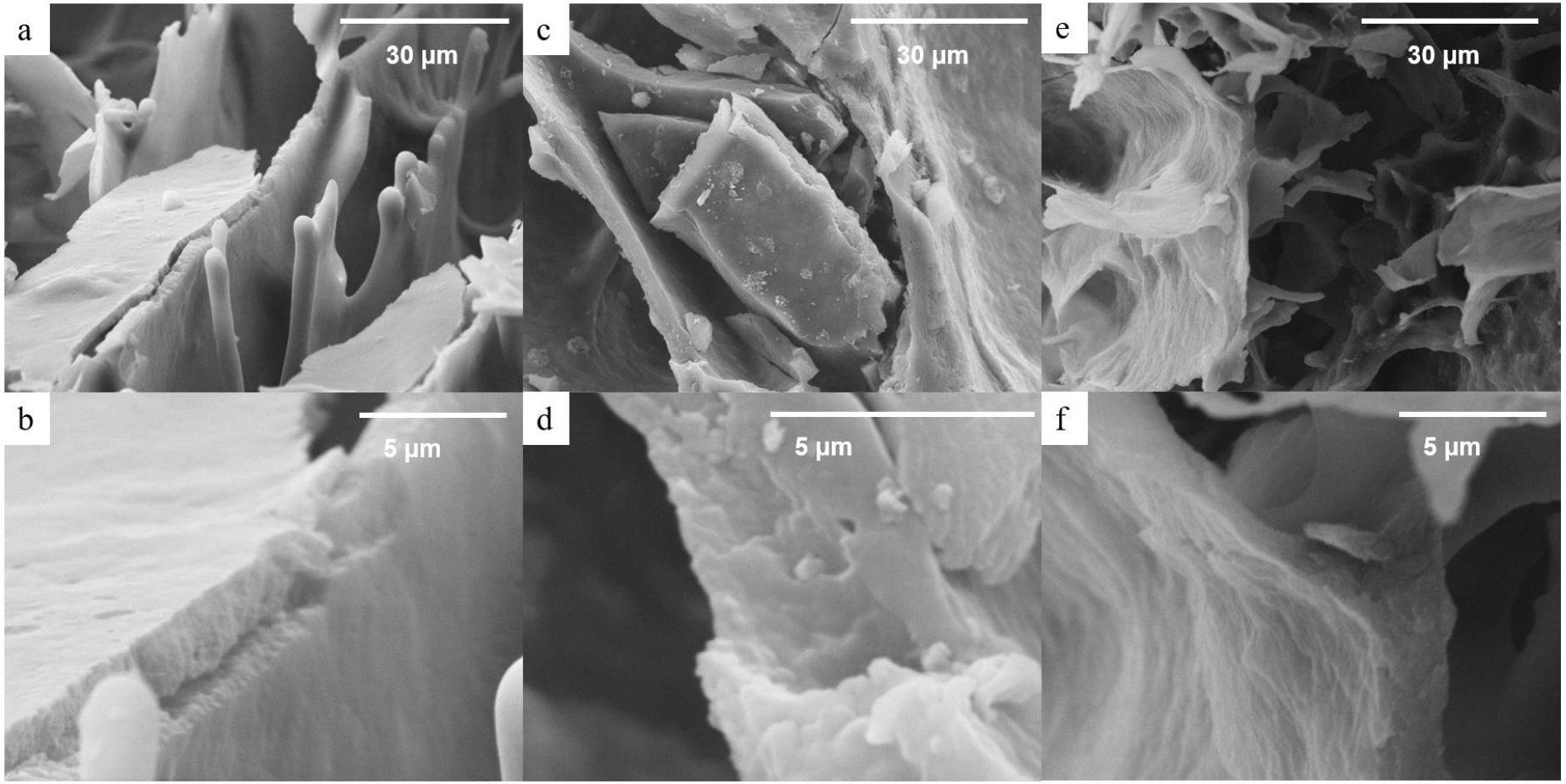

Figure 7.8: *SEM micrographs of:* ***(a-b)*** *CSM protein-collagen hybrid aerogel prepared at 10 wt% total solids with a 4:1 ratio of CSM protein to collagen,* ***(c-d)*** *CSM protein-gelatine hybrid aerogel prepared at 10 wt% total solids with a 4:1 ratio of CSM protein to gelatine and exposed to UVB radiation for 30 minutes during gelation, and* ***(e-f)*** *CSM protein-gelatine hybrid aerogel prepared at 10 wt% total solids with a 4:1 ratio of CSM protein to gelatine (no UVB-exposure). Micrographs are taken of the transverse cross-sections at x 2,000* ***(a, c, e)****, x 10,000 (****b, f****), and x 18,000* ***(d)*** *magnification*

7.3.2. Mechanical properties

Following the successful gelation of CSM protein hybrid aerogels, compressive mechanical testing using an Instron universal electro-mechanical testing system was conducted to confirm the reinforcing function of casein, chitin, collagen, and gelatine. Static tests of hybrid aerogels produced stress-strain curves (**Figure 7.9** & **Figure 7.10**) similar to prior testing of CSM protein aerogels (see **Section 6.5.1**). Some tests approached the load limit of the 10 N load cell with no evidence of specimen yield (**Figure 7.9c-d**), necessitating the use of the 100 N load cell for further testing of CSM protein-gelatine aerogels.

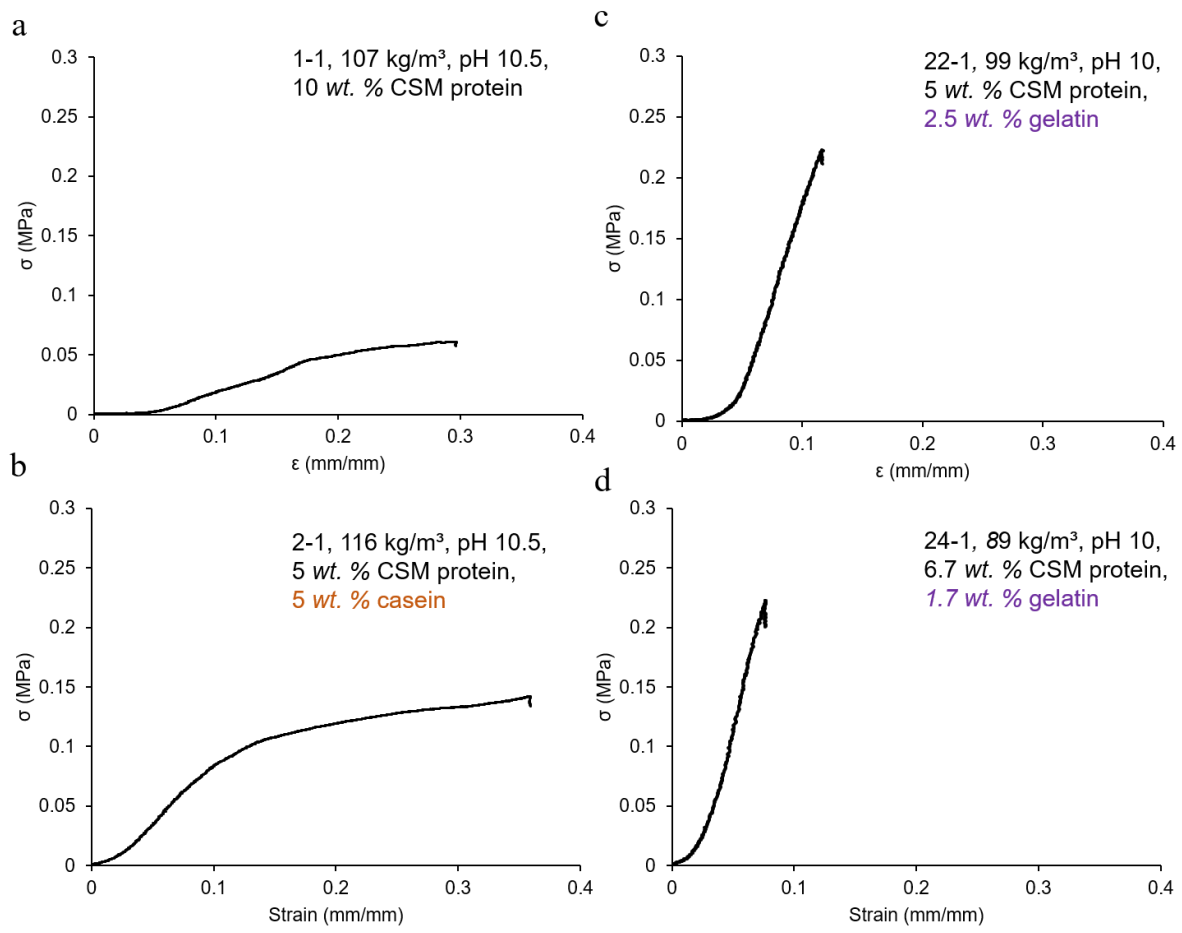

Figure 7.9: *Example stress-strain curves generated from static compressive testing of early hybrid aerogels at pH 10 – 10.5 (samples 1, 2, 22, & 24). Specifically, these samples are: a CSM protein aerogel* ***(a)****, a CSM protein-casein aerogel* ***(b)****, and a CSM protein-gelatine aerogel at a 2:1 ratio* ***(c)*** *and a 4:1 ratio* ***(d)*** *of CSM to gelatine.*

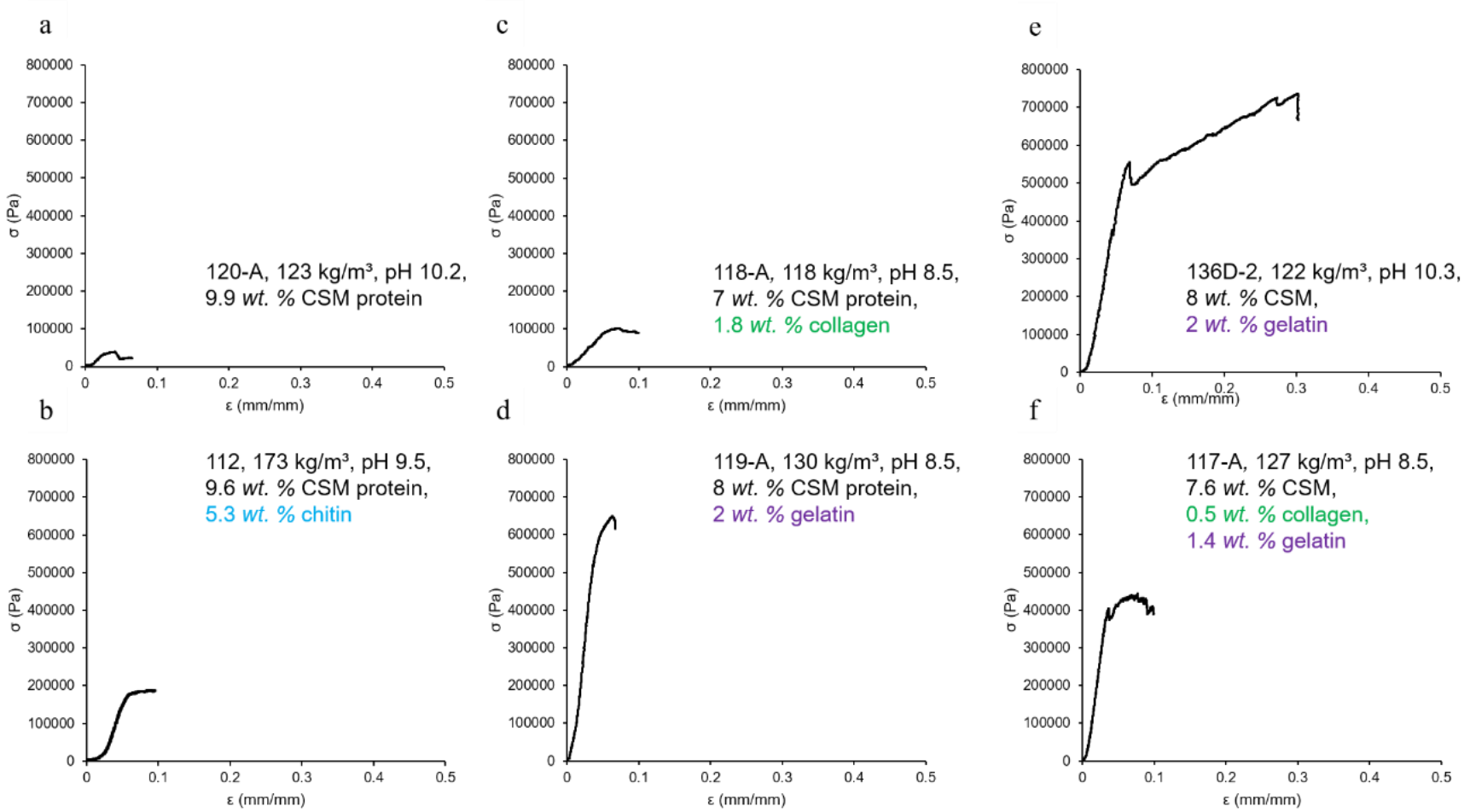

Figure 7.10: *Example stress-strain curves generated from static compressive testing of CSM protein hybrid aerogels (samples 112, 117 – 120, 136). Specifically: a CSM protein aerogel at pH 10.2* ***(a)****, a CSM protein-chitin aerogel (pH 9.5)* ***(b)****, a CSM protein-collagen aerogel (pH 8.5)* ***(c)****, a CSM protein gelatine aerogel at pH 8.5* ***(d)*** *and pH 10.3 © and a hybrid aerogel comprising of CSM protein, collagen, and gelatine (pH 8.5)* ***(f)***

Compressive testing of hybrids included only one specimen each for the CSM protein-casein (**Figure 7.9b**) and chitin (**Figure 7.10**) aerogels, however further focus was given to CSM protein-collagen and gelatine hybrids.

A comparison of the specific compressive moduli and strengths revealed that the hybridisation of CSM protein aerogels increases both the stiffness and strength of the monoliths independently of density (**Figure 7.11**). Casein hybridisation had not been expected to significantly improve the mechanical properties of the CSM protein aerogel and had been incorporated as a proof-of-concept hybrid. Surprisingly, casein hybridisation caused a 2-fold increase in compressive modulus and a 1.6-fold increase in strength as compared to a control sample (CSM protein only). However, the specific compressive modulus measured in the casein hybrid (0.009 MPa / (kg / m^3)) was comparable with the average values achieved in pure CSM protein aerogels, while the specific compressive strength (0.77 kPa / (kg / m^3)) was comparable to values achieved in CSM protein aerogels through pH manipulation (see **Figure 6.57**). Casein was discounted for further studies as a reinforcement of CSM protein aerogels but remains a plausible candidate for hybridisation research focussing on other properties (*e.g.* biochemical attributes). Gelatine hybrid aerogels displayed a clear increase in specific compressive moduli (**Figure 7.11**) and strengths. The specific moduli (0.027 – 0.043 MPa / (kg / m^3)) were 6- to 9-fold higher than the control sample (0.004 MPa / (kg / m^3) and 3- to 5-fold greater than for the average CSM protein aerogel (0.009 MPa / (kg / m^3), see **Section 6.5.1.1**). Despite incomplete measurements (yield strength exceeded the force limit on the 10 N load cell), the specific compressive strengths in initial gelatine hybrids (samples 22 and 24) were also greater (at least 2.1 kPa / (kg / m^3) than the CSM protein control sample by at least 4-fold.

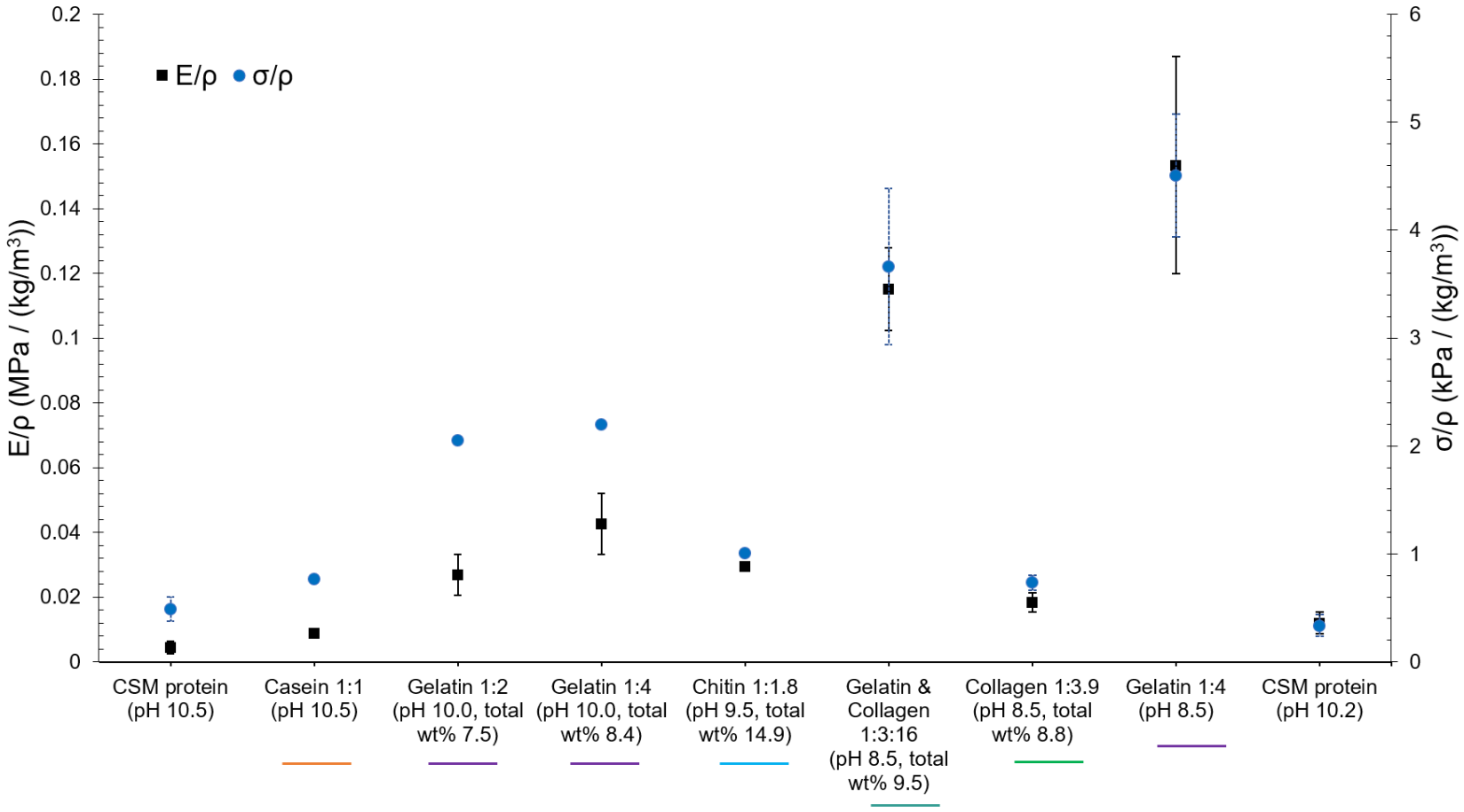

Figure 7.11: *Specific compressive moduli (black squares) and strengths (blue circles) of CSM protein hybrid aerogels measured from samples 1, 2, 22, 24, 112, 117 – 120. Ratio of specified biopolymer to CSM protein provided under axis label (e.g. "Gelatine 1:4" implies a Gelatine-CSM protein aerogel with a 1:4 ratio of gelatine to CSM protein). Samples were prepared at a total solids concentration of 10 wt% unless otherwise stipulated in axis label. Error bars represent the standard deviation where n = 2*

Fascinatingly, a reduction in the gelatine concentration led to an increase in the compressive modulus, however the extent of variation in such measurements remains unclear. Variable densities due to a 0.9 wt% discrepancy in total solids concentration between the two samples is a probable explanation for reduced stiffness in the 1:2 ratio gelatine hybrid. Gelation pH may also be an influencing factor on aerogel strengths and moduli in the gelatine hybrids. A second batch of gelatine and collagen samples prepared at a pH of 8.5 (samples 117 – 120) produced a gelatine hybrid with a 3.6-fold increase in modulus over a pH 10 counterpart (**Figure 7.11)**. The increase in strength was not determined but was at least 3.5-fold. Hybridisation with gelatine led to pH buffering around pH 8.5 and hybrid gels of pH < 8.5 (*e.g.* 8.0) were impractical to prepare using 1 M HCl due to excessive dilution from the required volume of acid. Further pH variants of CSM protein-gelatine hybrids are required for investigation into the combined effects of hybridisation and pH. Collagen as an insoluble powder was also used to produce hybrid CSM protein aerogels which were twice as strong and slightly stiffer (1.5-fold increase in modulus) than pure CSM protein aerogels. However, collagen is far less effective at reinforcing the CSM protein than its hydrolysed counterpart gelatine. Furthermore, a combination of the two collagenous substances proved less effective at reinforcing than the use of gelatine alone. The superior reinforcing abilities of gelatine over the non-soluble fibres (collagen and chitin) are discussed further in **Section 8.4.3**.

Analyses of the linear region associated with each stress-strain curve allowed for a measurement of the elastic limit of each hybrid aerogel (**Figure 7.12**). However, no discernible trends were revealed due to the highly variable measurements in elastic limits obtained from the control samples (3.1 – 16.5 %). Previous discussions have established that inclusion of the toe region in yield strain measurements is a possible reason for this variation (see **Section 6.5.1.1**). Nevertheless, a comparison of hybrid measurements with the average elastic limit of CSM protein aerogels (7.9 ± 2.8 %) suggests that hybridisation may reduce the elasticity of the aerogels (**Figure 7.12**) and should be investigated further with appropriate methodological improvement (*i.e.* exclusion of toe region in yield strain measurements).

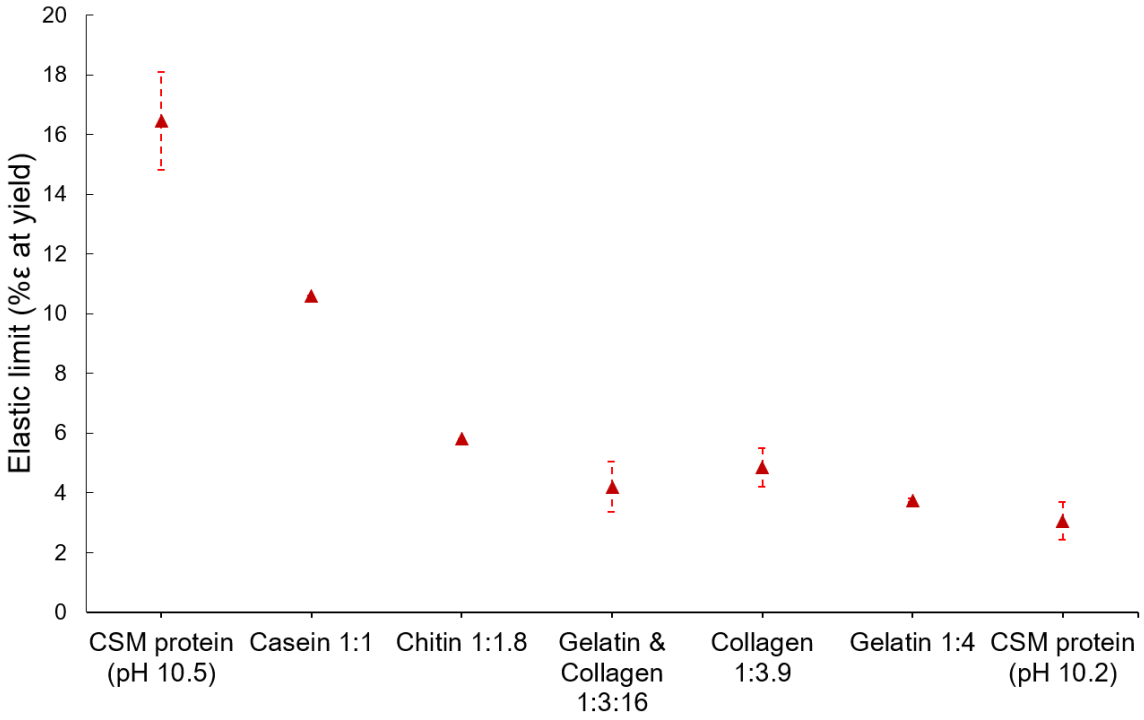

Figure 7.12: *Elastic limit (determined as the % ε at the yield stress) of CSM protein hybrid aerogels measured from samples 1, 2, 112, 117 – 120. Error bars represent the standard deviation where n = 2*

Further specimens of collagen and gelatine hybrid aerogels investigate the use of UVB light as a possible method for inducing protein crosslinking. The stress-strain curves produced from these hybrids also demonstrated typical aerogel behaviour with a linear region until the collapse strength that is followed by a plateau in stress (**Figure 7.13**).

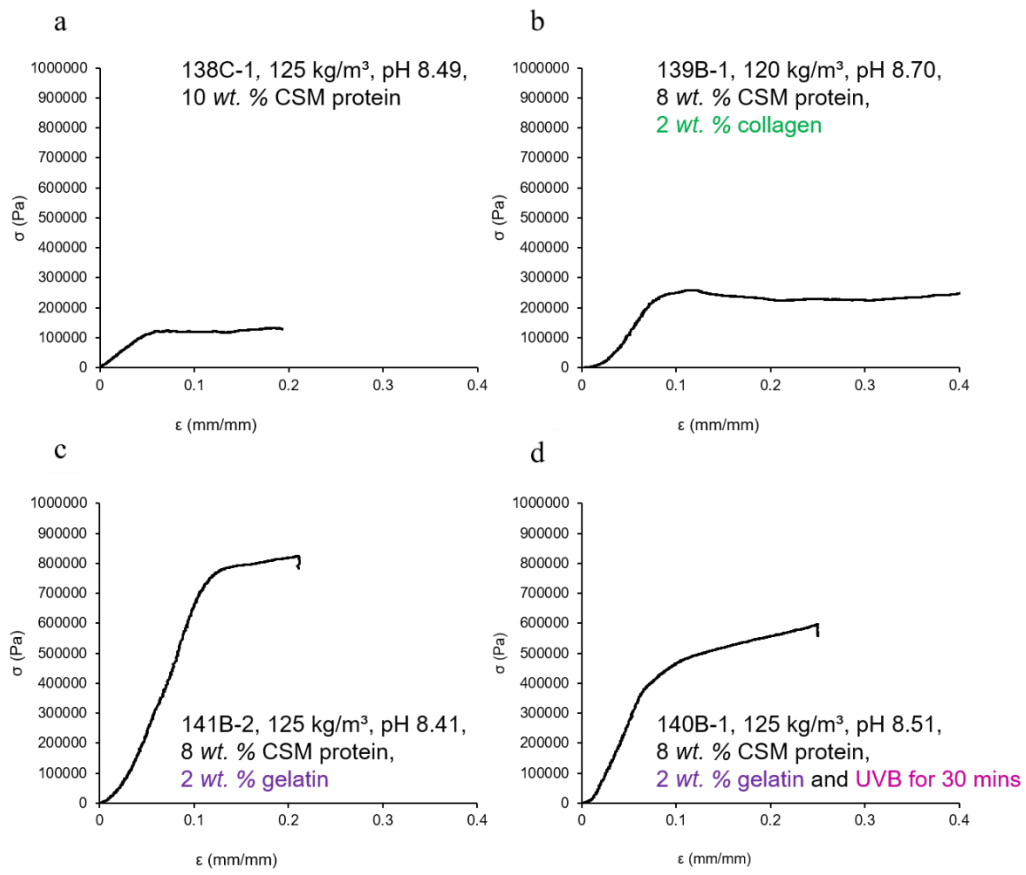

Figure 7.13: *Example stress-strain curves generated from static compressive testing of CSM protein hybrid aerogels at pH 8.5 – 8.7 (samples 138 – 141). Specifically, these samples are a CSM protein aerogel* ***(a)****, a CSM protein-collagen aerogel* ***(b)****, a CSM protein-gelatine aerogel* ***(c)****, and a CSM protein gelatine aerogel exposed to UVB light during gelation* ***(d)***

Analyses of compressive testing of samples 138 – 141 confirm previous findings that gelatine hybrids demonstrate the greatest aerogel strengths and stiffnesses (**Figure 7.14a**). Irrespective of the UVB treatment, the CSM protein-gelatine aerogels have specific compressive strengths and moduli 3- to 5-times greater than the control. Collagen hybridisation only increases the strength and modulus of the control sample by 1.8-fold and 1.4-fold, respectively. Interestingly, the use of UVB light during the gelation of the gelatine hybrids does not significantly change the elastic modulus and appears to reduce the strength of the hybrid aerogels as compared to those not exposed to UVB light (**Figure 7.14a**). A possible corresponding reduction in elasticity (**Figure 7.14b)** is identified more cautiously since earlier measurements of the elastic limit presented huge variance in control samples (**Figure 7.12**). Specimens subject to UVB light were expected to display an increase in strength and modulus

since UV-crosslinking in collagen fibres increases tensile strengths and moduli [283]. The observed lack of increase suggests that covalent crosslinking was insufficient, that aerogel mechanical properties are largely independent of gel molecular structure, or that maximum crosslinking is achieved even without UVB light exposure. The slight reduction in specific strength of the UVB-treated hybrids as compared to other gelatine hybrids (**Figure 7.14**) may even suggest that UV-induced photodegradation of protein molecules has occurred and consequently weakened these aerogels. The UVB light experiment presents an intriguing result that elicits further discussion alongside morphological and literature evidences (see **Section 8.4.3**).

One effect of gelatine hybridisation that requires further elucidation is the exact extent of the mechanical reinforcement effect. The investigations summarised in **Figure 7.11** & **Figure 7.14** clearly demonstrate the increased stiffness and strength of CSM protein-gelatine aerogels but the amount by which gelatine provides mechanical enhancement varies considerably (such as a 3- to 13-fold increase in aerogel strength). Additional gelation factors such as aerogel pH (mentioned briefly in **Figure 7.11**) should be incorporated into more extensive measurements of a range of CSM protein-gelatine hybrids.

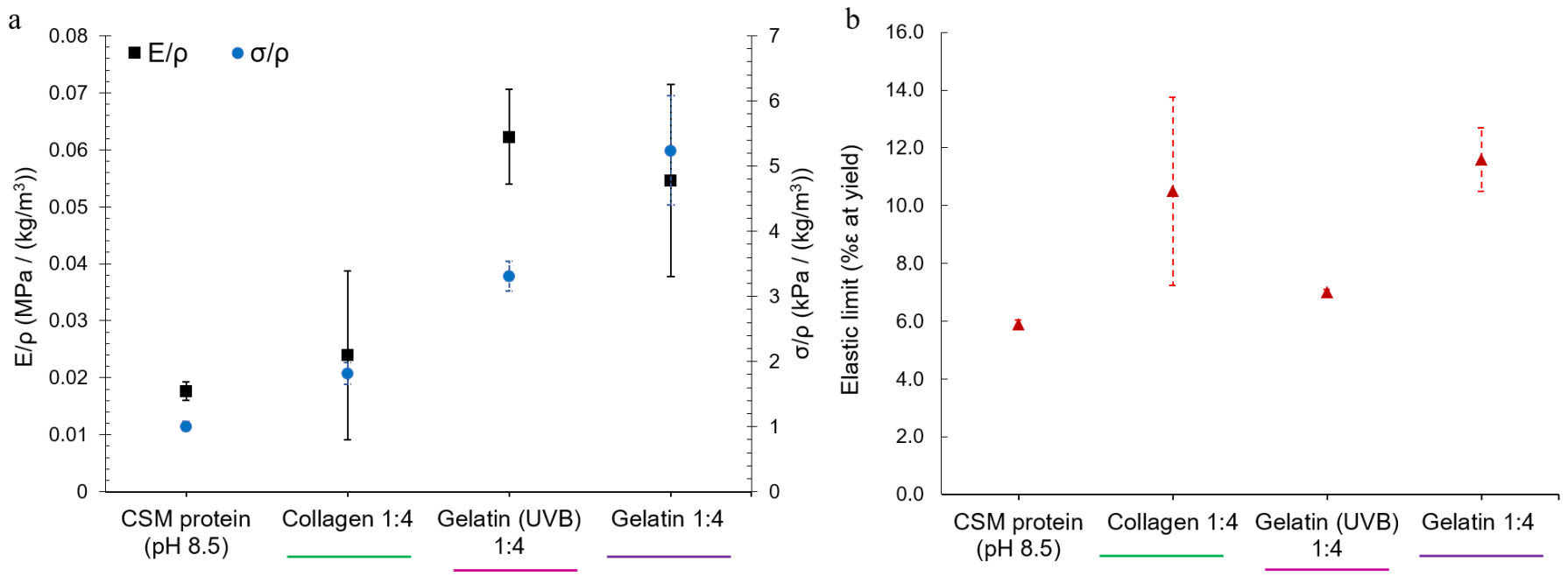

Figure 7.14: *Specific compressive moduli (black squares,* ***(a)****), strengths (blue circles,* ***(a)),*** *and elastic limits* ***(b)*** *of CSM protein hybrid aerogels measured from samples 138-141 (pH 8.5 – 8.7). Error bars represent the standard deviation where n = 2 (control and collagen samples) or n = 3 (gelatine samples)*

Static compressive testing also included cyclic testing of selected specimens where a second compression was conducted following initial compression to 20 – 30 % strain (**Figure 7.15**) and allowing for recovery of the specimen. The objective of cyclic testing was to establish the amount of recoverable deformation after initial compression and compare with the extent of the linear region. Aerogels for use in applications such as packaging may be subject to further application of force after an initial collapse event and therefore knowledge of recoverable deformation and post-collapse mechanical behaviour is useful.

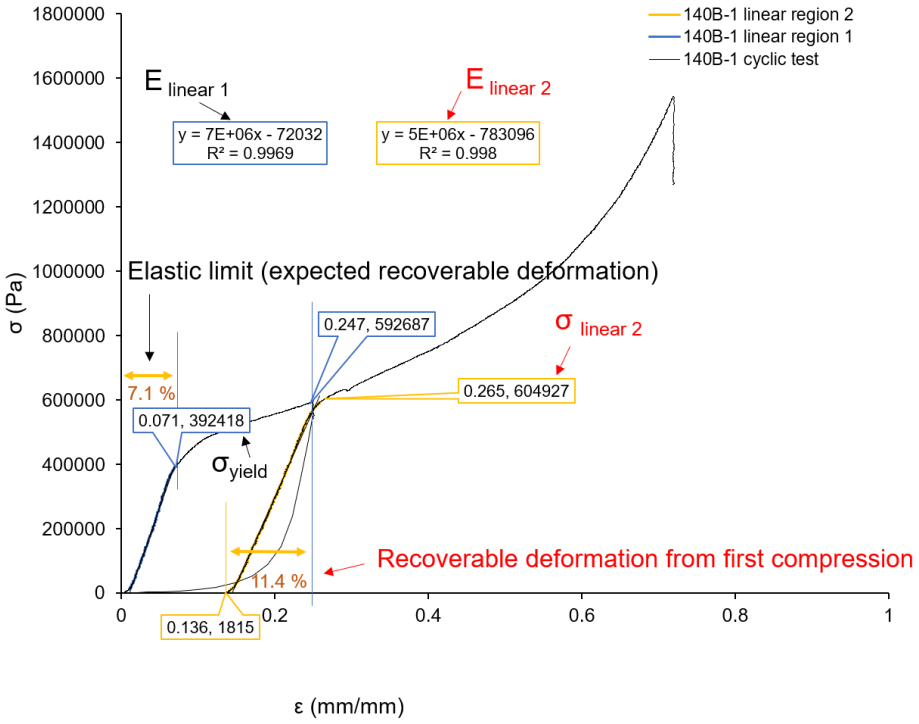

Figure 7.15: *Example stress-strain curve with analysis of cyclic compressive testing in CSM protein hybrid aerogels (sample 140, CSM protein-gelatine with UVB exposure)*

Cyclic tests revealed that most hybrid aerogels have a reduction in compressive modulus and compressive strength after initial compression beyond the yield strength (**Figure 7.16a &b**). The exception was the gelatine hybrids that demonstrated increases in both properties in subsequent compressive cycles (**Figure 7.16a &b**).

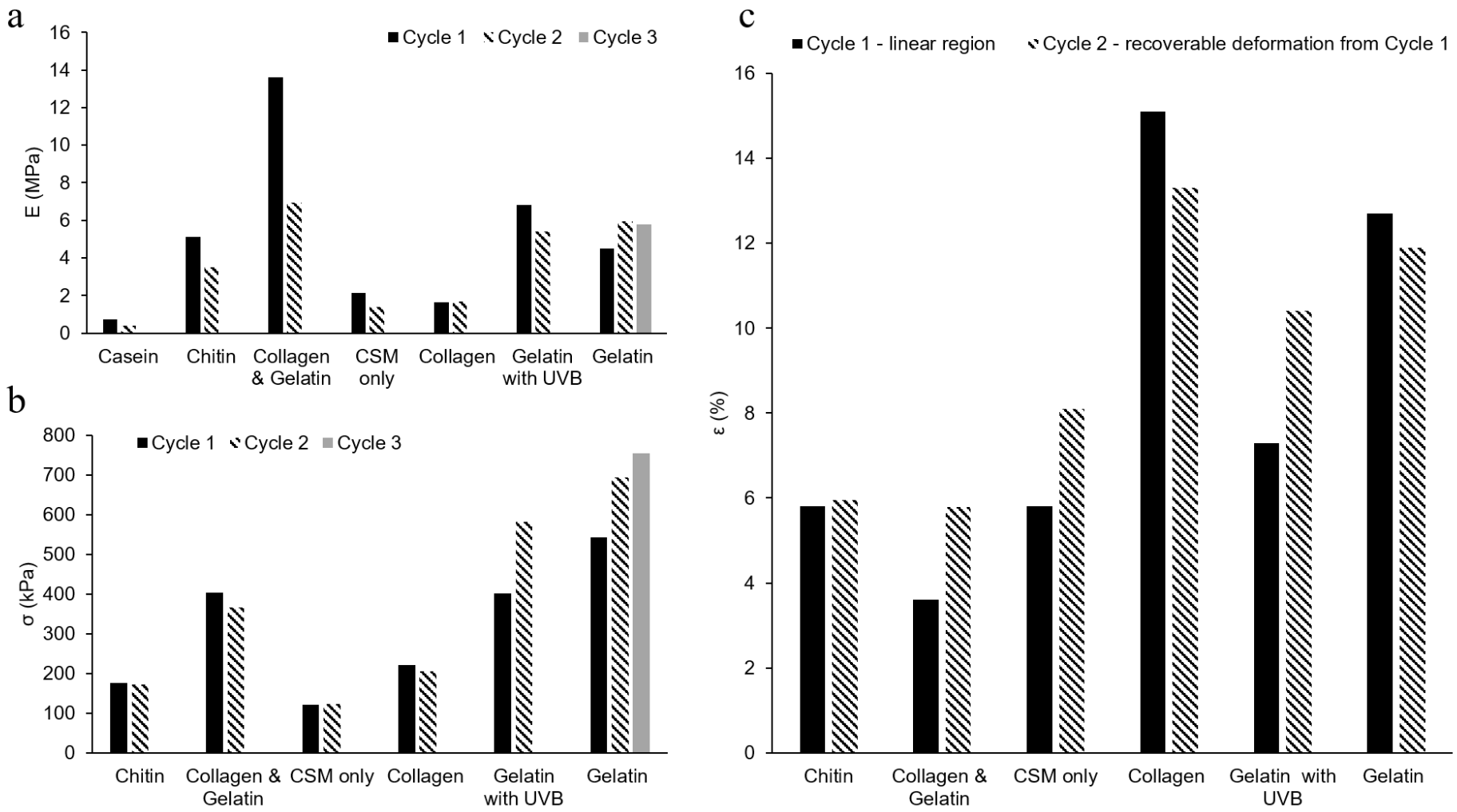

Figure 7.16: *Compressive moduli **(a)**, strengths **(b)**, and recoverable deformation **(c)** of CSM protein hybrid aerogels from cyclic compressive testing of samples 2, 112, 117, 138 – 141. Recoverable deformation (as determined from a second compressive cycle (refer **Figure 7.15**)) is compared with the expected recoverable deformation (strain associated with linear region of initial compression) to assess recoverability of the deformation in the plateau region of the stress-strain curve*

The gelatine hybrids were also distinguished by a lack of plateau region in the stress-strain curves, instead displaying a more subtle shift from the linear region to a 'pseudo-linear' region and a reduction in the tangential modulus (**Figure 7.15**). The post-yield, 'pseudo-linear' region demonstrates that pore collapse may occur more gradually and concurrently with some elastic deformation. Furthermore, the amount of recoverable deformation was shown to be greater than the initial linear region in specimens where yield occurred before approximately 8 *% ε* (*i.e.* 'elastic limit' < 8 *% ε* ≠ recoverable deformation) (**Figure 7.16c**). Complicating interpretation of the elastic limit data are previously outlined concerns around the prevalent toe regions in stress-strain data and possible influence on elasticity measurements. However, the large discrepancies in recoverable deformation and elastic limit measurements may be understood as the concurrent occurrence of elastic and permanent deformation mechanisms at the onset of the plateau region. Delayed mechanical responses due to viscoelastic behaviour may also explain the recoverable deformation discrepancies seen in cyclic testing. Evidence of similar behaviour was also found in pure CSM protein aerogels (refer to **Section 6.5.1.1**) and could likewise be attributed to possible viscoelastic effects.

Hybrid samples 138 – 141 were subject to further static and dynamic compressive testing using a Dynamic Mechanical Analyser (DMA) to investigate thermomechanical behaviour (**Figure 7.17** – **Figure 7.22**). Static testing was used to establish a stress limit for dynamic measurements to follow and also allowed for brief analysis of the effect of stress rate on compressive mechanical properties (**Figure 7.17**). A limited supply of specimens for DMA experiments allowed for only one set of stress-rate measurements to be conducted on samples 138 – 141. Consequently, no statistical information is available to establish the variance in the mechanical properties of these specimens. Earlier static compressive testing conducted using the Instron testing system (**Figure 7.14**) suggests that the variance in mechanical data can be significant and should be factored into overall trends. Therefore, the effect of stress-rate on mechanical properties from **Figure 7.17** and **Figure 7.18** is discussed with caution.

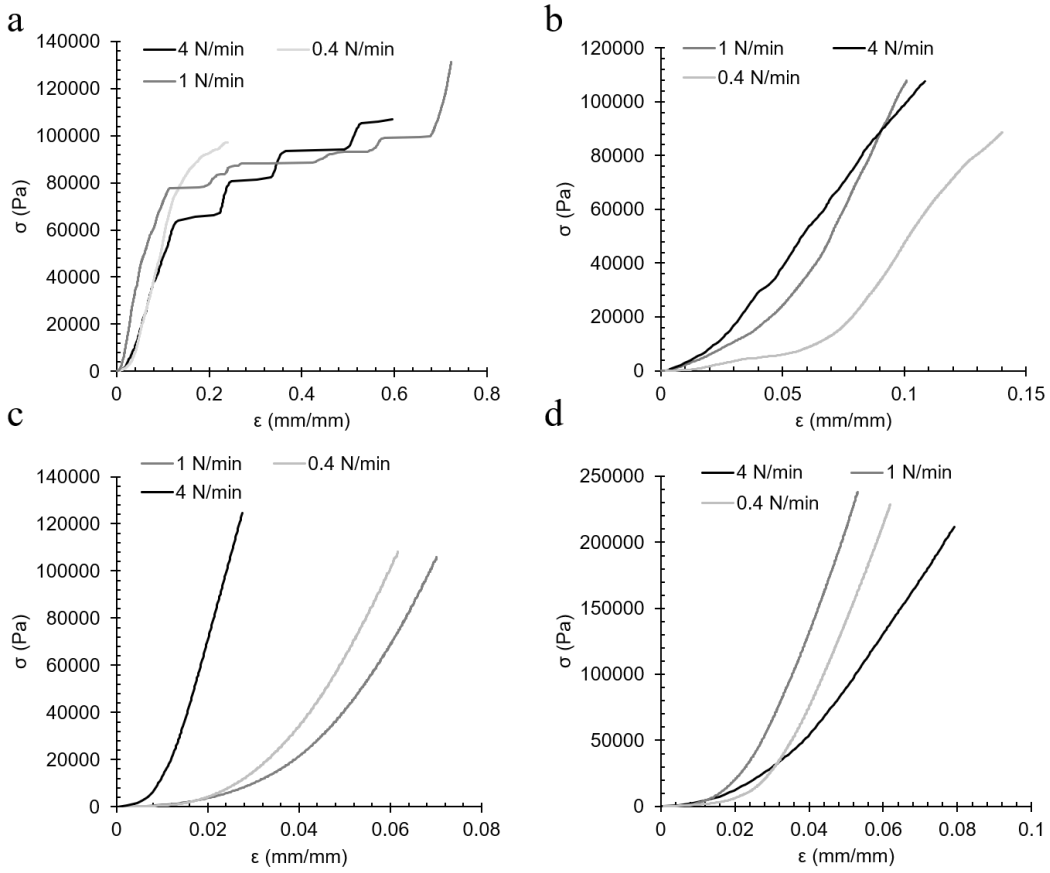

Figure 7.17*: Stress-strain curves generated from static compressive tests of CSM protein hybrid aerogels on a Dynamic Mechanical Analyser using varying compression rates (0.4, 1.0, 4.0 N/min). Samples tested were a CSM protein aerogel (pH 8.5)* ***(a)****, CSM protein-collagen (4:1) aerogel (pH 8.7)* ***(b)****, CSM protein-gelatine (4:1) aerogel (pH 8.4)* ***(c)****, and CSM protein-gelatine (4:1) aerogel (pH 8.5) with exposure to UVB light during gelation* ***(d)****.*

The compressive moduli of the CSM protein hybrid aerogels demonstrated changes associated with the rate of applied stress although a clear trend for increasing modulus with increasing strain rate could not be established (**Figure 7.18**). It is possible that an increasing stress-rate elicits an increase in compressive modulus as seen in most comparisons of the 0.4 and 1.0 N/min stress rates. However, data collected from tests conducted at 4.0 N/min appears to contrast this trend. Only the gelatine hybrid sample experienced an increase of the modulus (more than double) at the highest compression rate of 4.0 N/min (**Figure 7.18**).

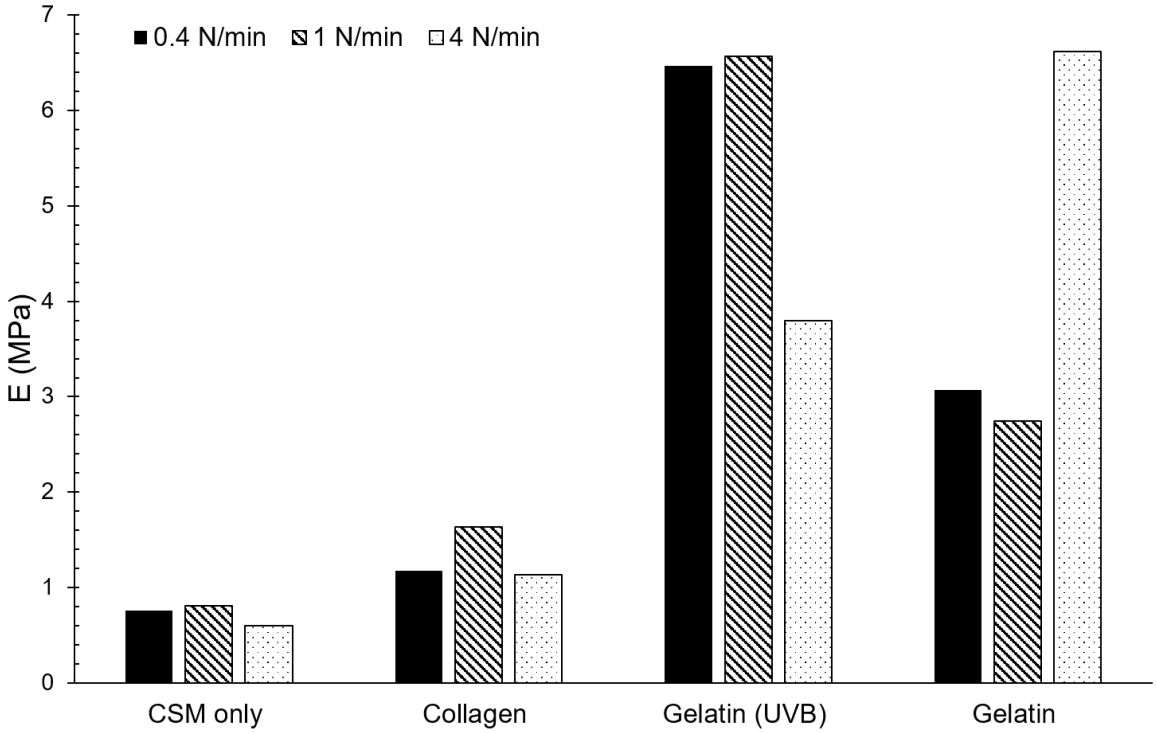

Figure 7.18: *Compressive elastic moduli of CSM protein hybrid aerogels measured from compressive testing on a Dynamic Mechanical Analyser using varying compression rates (0.4, 1.0, 4.0 N/min). Samples tested were CSM protein only (pH 8.5), CSM protein-collagen (4:1) (pH 8.7), CSM protein-gelatine (4:1) (pH 8.4), and CSM protein-gelatine (4:1) (pH 8.5) with exposure to UVB light during gelation*

An increase in stiffness with increasing stress rates would align with data recorded in other polymer-based materials. Thermoplastic polymers demonstrate viscoelastic mechanical behaviour attributed to a semi-crystalline microstructure with time-dependant mechanical responses [284]. Low strain- or stress-rates reduce elastic moduli and yield strengths as time-dependent deformation mechanisms in amorphous regions can progress to completion. High strain- or stress-rates lead to greater resistance to deformation (higher yield strengths and elastic moduli) attributed to crystalline regions of the material with less time-dependent deformation mechanisms. Proteinaceous materials display related viscoelastic properties (*e.g.* glass transitions, see **Section 6.5.2**) due to analogous highly structured ('α-helix' and 'β-sheet' secondary structure) and amorphous ('random coil') regions [253] so evidence of viscoelastic mechanical behaviours can also be expected. However, hypothesised viscoelastic behaviour in protein-based plastics may prove inapplicable to protein aerogels where mechanical properties are largely determined by porosity rather than polypeptide chains. The

suggestion of rate-dependant properties found in the current investigation (**Figure 7.18**) and earlier evidence of discrepancies in elasticity measurements (**Figure 7.15** & **Figure 7.16**) is an invitation for future focussed study on viscoelastic mechanical behaviour in protein aerogels (*e.g.* frequency-sweep analyses using dynamic mechanical testing).

DMA tests conducted on CSM protein hybrid aerogels were ultimately devised to investigate the possibility of thermal transitions and provide information regarding molecular structures. Dynamic testing was conducted on specimens from samples 138 – 141 using a temperature sweep to examine the thermomechanical response of the aerogels. The storage and loss moduli were tracked alongside the loss factor to indicate changes in how energy is stored and dissipated within the sample. The elastic structure of viscoelastic materials (or 'solid-like' structure) is responsible for stored energy which is represented in the storage modulus (G′) while liquid-like or flowable structure dissipates energy from applied stress or strain and is represented in the loss modulus (G″). The loss factor (tanδ) represents the ratio of these two moduli, indicating how the balance of viscous and elastic structures may change during an experiment. During thermally induced molecular transitions (*e.g.* glass transitions) changes in molecular motion or structure lead to changes in tanδ measurements allowing clear identification of such transitions from a DMA experiment.

CSM protein aerogels subject to dynamic compressive testing revealed an intriguing increase in G′ accompanied by variable changes in damping (tanδ) with increasing temperature up to 80 °C (**Figure 7.19a & Figure 7.20a**). Owing to the lack of observed glass transition in these specimens (no characteristic peak of tanδ at a specific temperature) no conclusions regarding the effects of co-gelation with collagen protein can be drawn. Thermoplastic polymers normally display a characteristic softening (drop in G′) with increasing temperature at and beyond the glass transition temperature. However, thermoset plastics undergoing curing can display a hardening (increase in G′) with temperature as heat-induced covalent bonding occurs within the material. Similarly, it is possible that some thermally-induced change in molecular bonding (*e.g.* formation of new hydrogen bonds) may be causing the increase in G′ seen in the CSM protein aerogel as thermal energy disrupts existing bonds (*e.g.* causes evaporation of water from the sample). Water is a very efficient plasticising

molecule in proteinaceous materials and its desorption can alter mechanical properties (*e.g.* increased brittleness) [253]. Moreover, the volatilization of plasticiser (*i.e.* water) is a common problem identified in testing of protein-based thermoplastics [253] and is arguably more pertinent in protein aerogels where porosity facilitates water gain and loss.

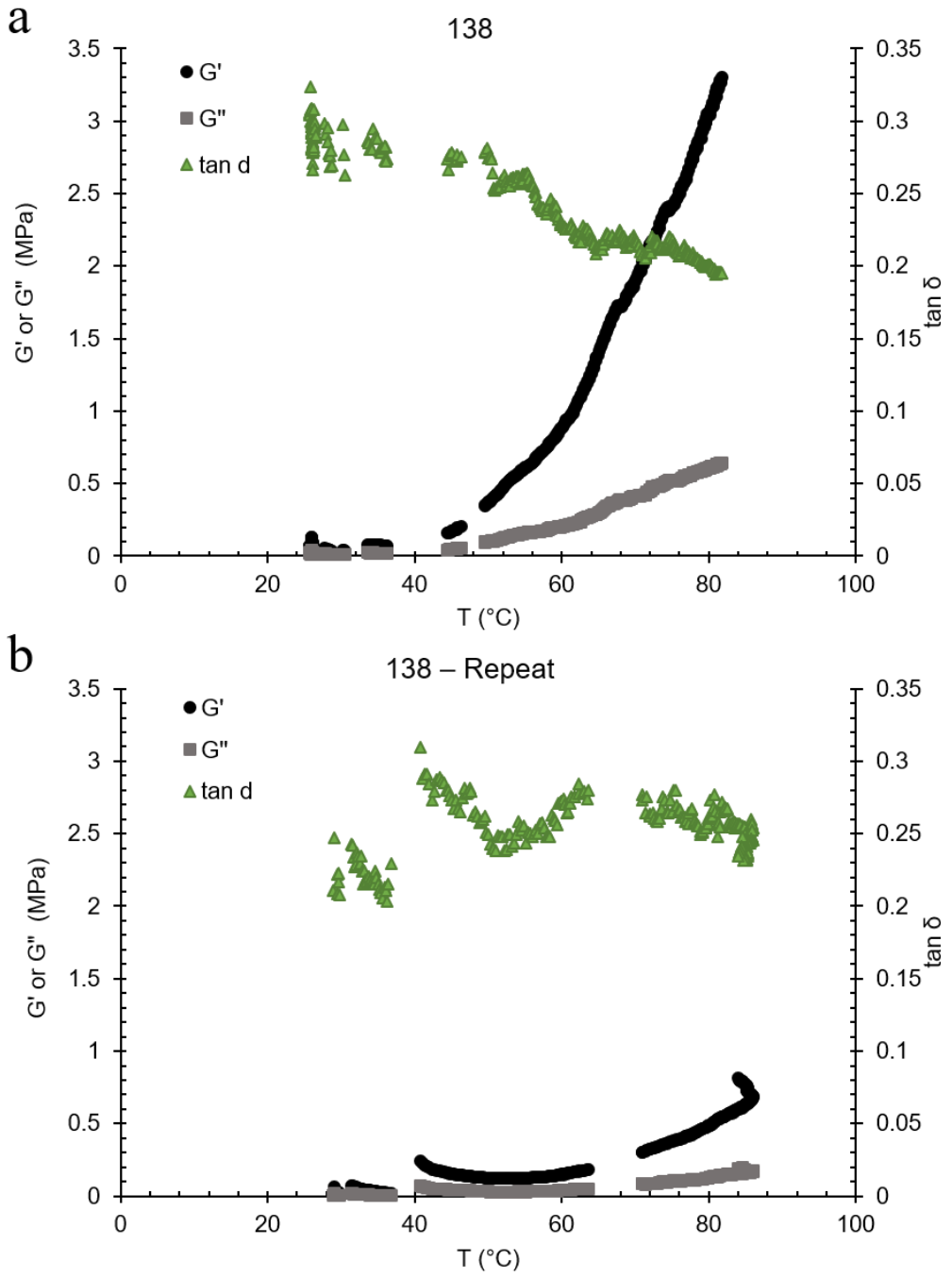

Figure 7.19: *Storage moduli, loss moduli, and loss factors of a CSM protein aerogel (10* wt%, *pH 8.5) as a function of temperature. Measurements were generated from dynamic compressive testing of a first run at 3 °C/min* ***(a)*** *and a repeat run at 5 °C/min* ***(b)*** *of a single aerogel specimen tested with a strain amplitude of 0.2 % and frequency of 1 Hz*

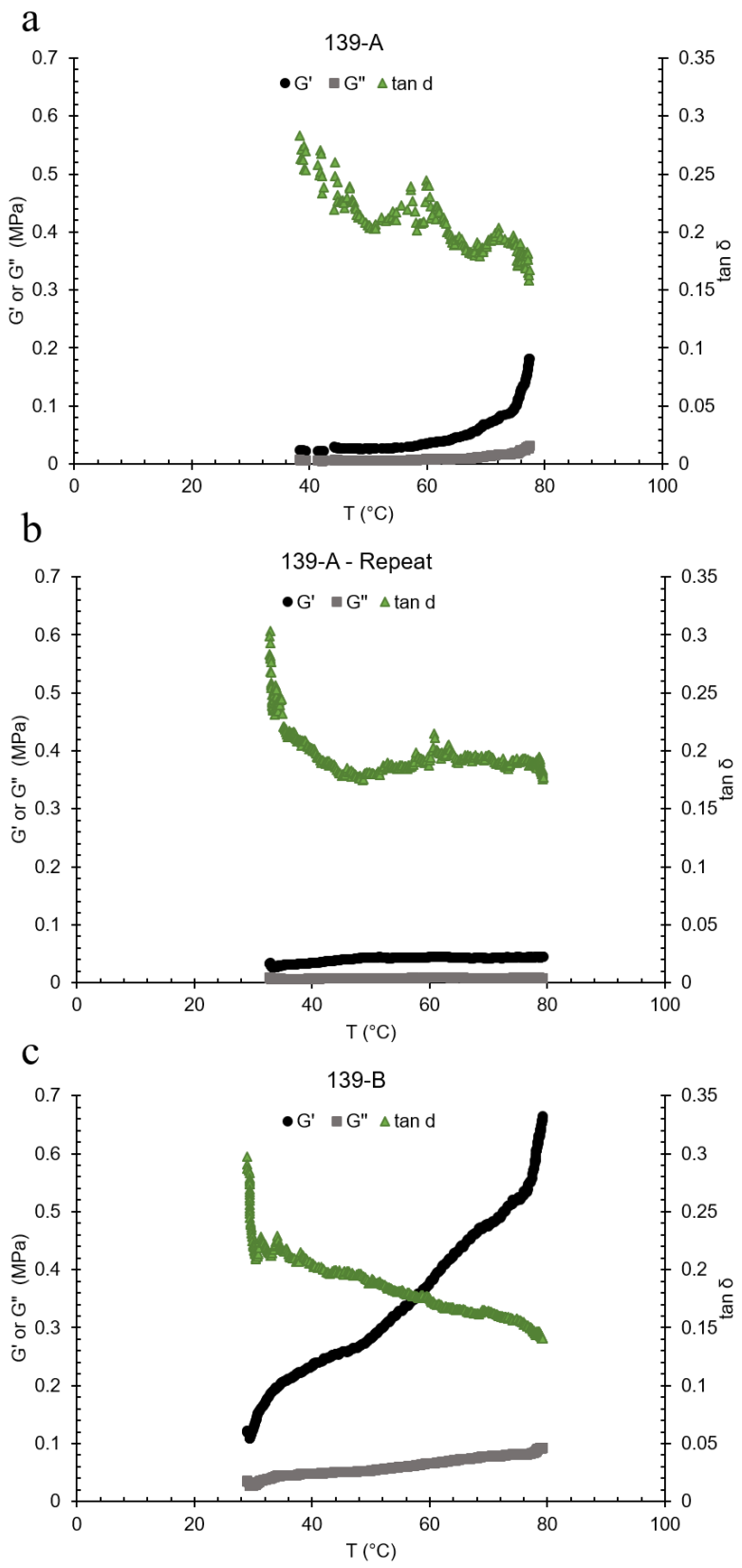

Figure 7.20: *Storage moduli, loss moduli, and loss factors of a CSM protein-collagen aerogel (4:1 ratio, pH 8.7) as a function of temperature. Measurements were generated from dynamic compressive testing of two specimens* ***(a, c)*** *and a repeat run of the first specimen* ***(b)*** *at a strain of 0.2 %, a frequency of 1 Hz, and a heating rate of 4 °C/min*

The hygroscopic nature of the CSM protein aerogels has been noted previously alongside the measurement of significant water loss events in calorimetry experiments (see **Section 6.5.2**). The increased G′ seen with temperature sweeps in DMA testing correspond with the onset of water loss from other experiments (40 – 50 °C, **Section 6.5.2**). Furthermore, repeated temperature sweeps of the same specimens show a reduction (**Figure 7.19b)** or elimination (**Figure 7.20b**) of this behaviour where, after the evaporative water loss, specimens display stable G′ behaviour at increased G′ measurements. The formation of new protein-protein interactions in replacement of protein-water interactions may explain the higher G′ values in retested (dehydrated) specimens. The extent of this increase in G′ could correspond to the amount of water loss and/or new protein-protein interactions. Variability in this effect could be explained by variable levels of initial water content (**Figure 7.20a** *cf.* **Figure 7.20c**) or variable water loss due to differing chemistries (control *cf.* hybrids) and porosities (**Figure 7.19a** *cf.* **Figure 7.21a**). Repeated temperature sweeps of the CSM protein aerogels and hybrids fail to reveal any further thermal transitions indicating that once dehydrated, CSM protein aerogels and hybrids are thermally stable up to 80 °C, analogous to thermoset materials. However, the hygroscopic nature of the CSM protein cryogels indicates that reabsorption of atmospheric water (and consequently reversibility of stiffening) is possible upon re-exposure to humid environments. Further dynamic testing of CSM protein aerogels is required to properly elucidate the thermally-induced mechanical responses highlighted in this brief investigation. Such tests should include comparisons with non-porous CSM protein materials (*e.g.* films) and employ careful atmospheric (*e.g.* testing under N_2 (g)) and humidity controls (conditioning in a range of relative humidity values).

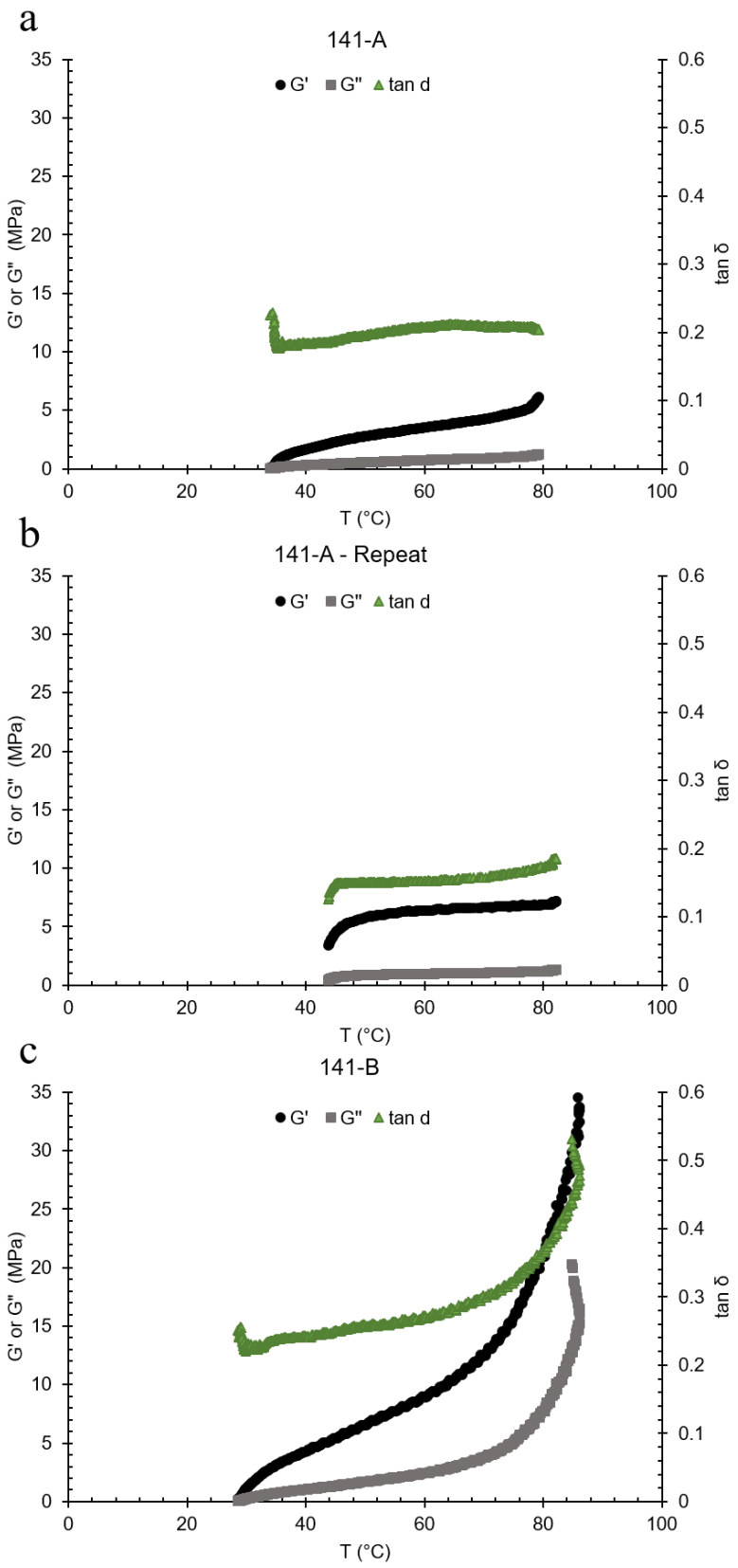

Figure 7.21: *Storage moduli, loss moduli, and loss factors of a CSM protein-gelatine aerogel (4:1 ratio, pH 8.4) as a function of temperature. Measurements were generated from dynamic compressive testing of two specimens at 4 °C/min* ***(a, c)*** *and a repeat run of the first specimen at 6 °C/min* ***(b)*** *at a strain of 0.2 % and a frequency of 1 Hz*

Despite possible water loss events complicating analyses, it is possible to make some basic comparisons between the CSM protein hybrid aerogels testing in the current investigation by comparing only the repeat runs (*i.e.* dehydrated samples). G′ measurements for CSM protein hybrids after initial water-loss events reveal that gelatine hybrids (**Figure 7.21 & Figure 7.22**) once more display improved mechanical properties over CSM protein-collagen (**Figure 7.20**) and control samples (**Figure 7.19**). Furthermore, the stable G′ measurements for CSM protein-gelatine specimens reveal the first clear evidence that UVB-treatment of gelatine hybrids alters mechanical properties. Earlier studies using static testing failed to identify any benefit of UVB treatment, however a clear increase in storage modulus is seen in dynamic testing of UVB-treated gelatine hybrids (14-15 MPa, **Figure 7.22b & 22c**) over non-UVB exposed gelatine hybrids (5-7 MPa, **Figure 7.21b**). Furthermore, reduced damping is observed in the UVB-treated samples (0.1) as compared to the non-UVB treated gelatine hybrids (0.2), further confirming that UVB treatment has successfully increases the aerogel stiffness. Stiffness differences are also seen in the difference between initial G′ of UVB-treated (4.5 MPa (**Figure 7.22a**)) and non-UVB-treated (< 1 MPa (**Figure 7.21a**)) samples prior to the water-loss event. The use of UVB radiation was hypothesised to induce chemical crosslinking between collagen (principal component of gelatine powder in the form of hydrolysed polypeptides and oligopeptides) and canola proteins. Such crosslinking is also analogous to a curing reaction in thermoset polymers and would also result in increased storage moduli and decreased tanδ. The tanδ of UVB-treated hybrids stabilise consistently at 0.09 – 0.1 (**Figure 7.22b**) while in non UVB treated hybrids tanδ stabilises at 0.18 (**Figure 7.21b**). The possible use of UVB light to induce crosslinking in CSM protein-gelatine aerogels is discussed further alongside morphological evidences in **Section 8.4.3**).

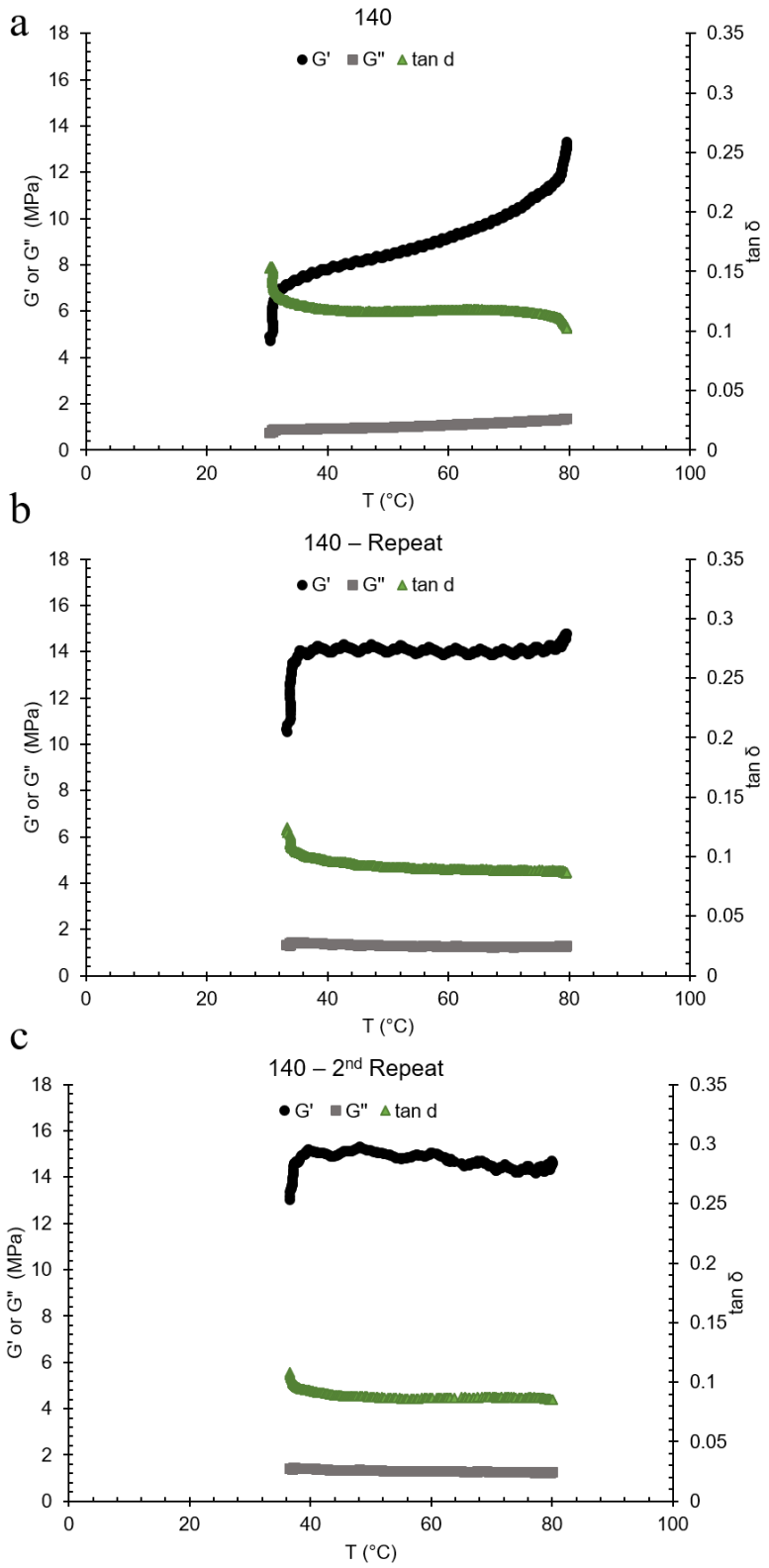

Figure 7.22: *Storage moduli, loss moduli, and loss factors of a CSM protein-gelatine aerogel (4:1 ratio, pH 8.5) with exposure to UVB light during gelation, as a function of temperature. Measurements were generated from dynamic compressive testing of a first run at 4 °C/min* ***(a)*** *with two repeat runs at 4 °C/min* ***(b)*** *and 8 °C/min* ***(c)*** *using one aerogel specimen at a strain of 0.2 % and a frequency of 1 Hz*

7.3.3. SDS-PAGE analysis of hybrid aerogels

The identification of protein-protein crosslinks, particularly between collagen and canola polypeptides, represents an important step towards describing the gelation mechanism in CSM protein and hybrid aerogels. Earlier experiments used sodium dodecyl sulphate polyacrylamide gel electrophoresis (SDS-PAGE) to analyse the molecular weights of the major proteins found in CSM protein extract (see **Section 5.3.3**). CSM protein aerogels and hybrid aerogels are also analysed using SDS-PAGE to examine possible changes in the molecular weight profile following gelation. Proteins that are bound in the gel by secondary interactions (*e.g.* hydrogen bonding, hydrophobic interactions) will be disrupted and denatured during solubilisation with electrophoresis buffer and heating. The resulting denatured protein molecules are detected in SDS-PAGE analysis at their original molecular weights. This solubilisation process is analogous to the denaturation of proteins from their native (biologically active) conformations where similar chemical disruption occurs. Crosslinks formed during gelation (except between thiol residues which are reduced by dithiothreitol (DTT)) are not susceptible to reduction by the electrophoresis buffer and heating protocol. These crosslinks result in increased molecular weights of the constituent gel proteins due to the new covalent connections between previously separate protein molecules. Increases in molecular weight are seen in SDS-PAGE as bands which travel less distance through the gel. Complete crosslinking of a gel (*e.g.* an extensive crosslinked network analogous to a thermoset polymer) results in an insoluble sample where little or no polypeptides are transferred to the SDS-PAGE gel during sample preparation. CSM protein hybrids are expected to have an intermediate level of crosslinking resulting in a general shift of the molecular weight profile to larger molecules.

CSM protein extract and aerogel were analysed alongside gelatine powder and CSM protein- hybrid aerogels. Resulting molecular weight profiles appeared highly similar to previous SDS-PAGE analyses of CSM protein extracts (see **Section 5.3.3**) with major protein bands found at 10, 16 -18, 20, 25, & 28, kDa (**Figure 7.23**).

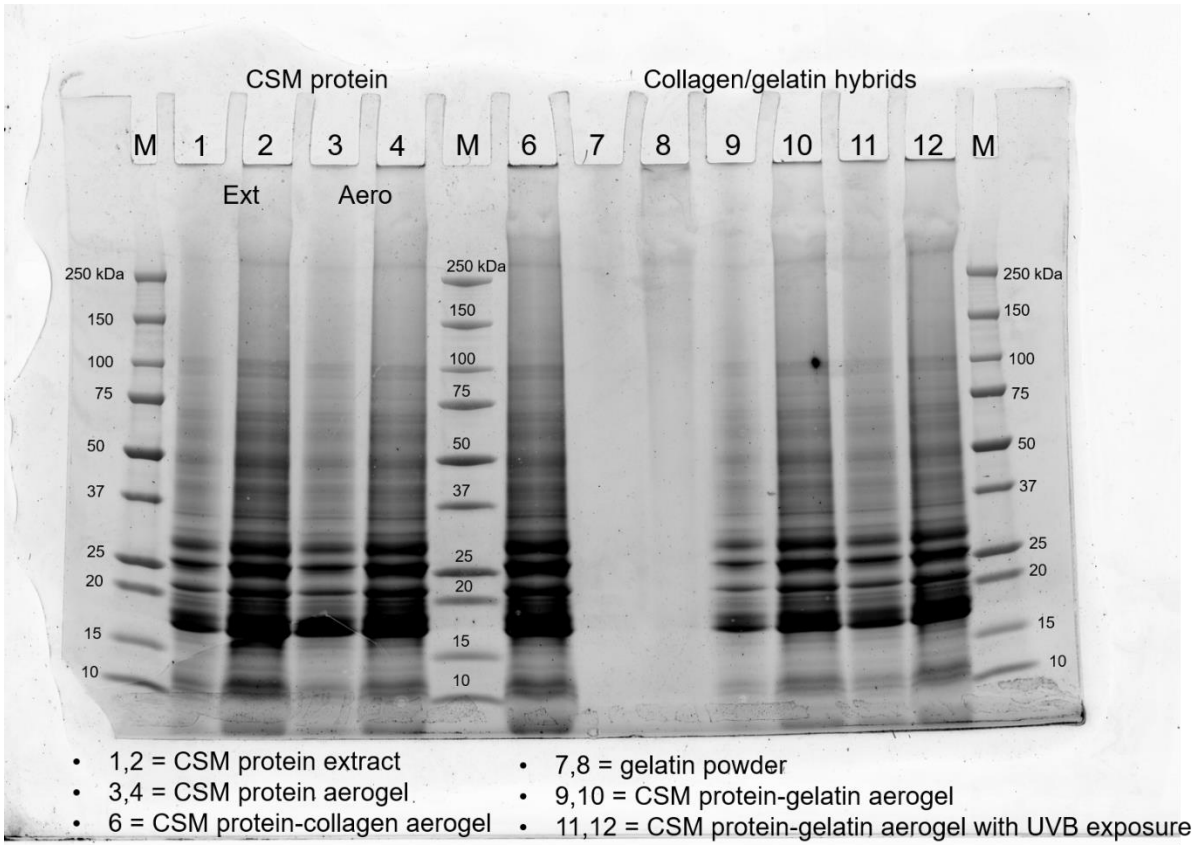

Figure 7.23: *SDS-PAGE gel showing molecular weight profiles of CSM protein extract, CSM protein aerogel, CSM protein hybrid aerogels (collagen and gelatine), and gelatine powder*

The SDS-PAGE results display remarkable similarity between all profiles containing CSM proteins, suggesting that there is probably no non-disulphide crosslinking occurring in the gels. However, small differences between the profiles and between the overall quantity of protein transferred to the gel may yet reveal effects of hybridisation on gel crosslinking. Careful quantitative analysis of band intensities using fluorescence imaging tools reveal a mild drop in total fluorescence following gelation of CSM protein (**Figure 7.24**). The total measurable protein in SDS-PAGE analysis is indicative of the total solubilised protein in the samples. Protein aggregates and macrostructures such as fibrils that cannot be broken down by the buffer are too large and bulky to be drawn into the PA gel and are therefore not measured. A 13% reduction in the total fluorescence of the aerogel sample as compared to the non-gelled extract therefore suggests that some protein was restricted from entering the PA gel due to crosslinking or insolubility. However, the difference is minimal and repeat analysis have not been carried out to determine variability in this result. Considering that extensive crosslinking would render a gel completely impervious to SDS-PAGE analysis, gelation in CSM protein is probably

predominantly driven by non-covalent interactions and disulphide bonding with only a small, if any, contribution from permanently crosslinked residues.

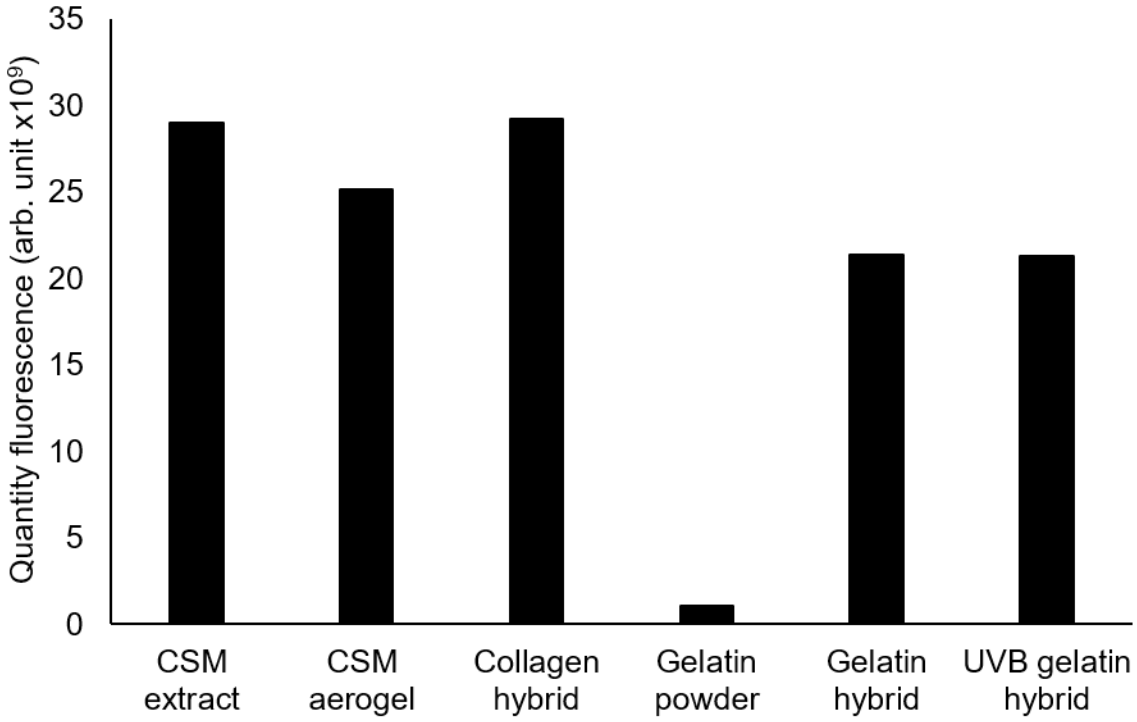

Figure 7.24: *Total volume of fluorescence detected from protein bands in SDS-PAGE analysis of hybrid aerogels. Aerogels and powders were solubilised in buffer at 6.67 mg/ mL with 10 µL loaded onto the PA gel*

A reduction of total fluorescence was also detected in the gelatine hybrid aerogels while gelatine powder was barely measurable (**Figure 7.24**). Gelatine powder proteins are ≤ 310 kDa [285] and therefore should be amenable to SDS-PAGE analysis. The transfer of gelatine to the PA gel is very poor (4 % of the fluorescence from CSM extract proteins) and is likely indicative of gelation. The 26 % reduction in fluorescence from CSM extract to the gelatine hybrid aerogels suggests that some CSM proteins are incorporated into crosslinked gelatine proteins. CSM protein-collagen aerogels demonstrate no reduction in fluorescence, suggesting that no cross-linking has restricted the solubility of these proteins. Collagen molecules in the 'CSM protein-collagen' hybrid are present in their natural, fibrillar form which is insoluble. No change in total amount of soluble canola proteins is consistent with collagen fibrils suspended in the CSM protein gels which are themselves bound only by non-covalent interactions.

Quantitative analysis of individual protein bands in the SDS-PAGE gel can reveal changes to the molecular weight (MW) profile of each sample. A general shift to larger MWs might be expected in gelled samples where proteins become crosslinked but are not so extensively crosslinked as to limit amenability to SDS-PAGE analysis. Inspection of MW profiles reveals similar MW values across all samples containing CSM proteins (**Figure 7.25**) with no clear trend towards increased MWs seen in the gelled samples. One weight range of interest includes the largest detected proteins at around 300 kDa which provides a small piece of evidence that UVB gelled hybrids have a slightly increased MW value for some proteins. However, this change is a tiny reflection of the hypothesised changes which were to shift the entire profile of gelled samples to significantly greater MW values. Analysis of individual protein bands simply reflects the trends seen in **Figure 7.24** showing slightly reduced quantities of protein in gelatine-hybrid and CSM protein aerogels. Therefore, any crosslinking in these aerogels only renders crosslinked proteins too large to be detected by SDS-PAGE analysis rather than affecting a visible change in the MW profile. Overall assessment of the role of crosslinking in CSM protein aerogels and hybrids is presented in **Section 7.4**.

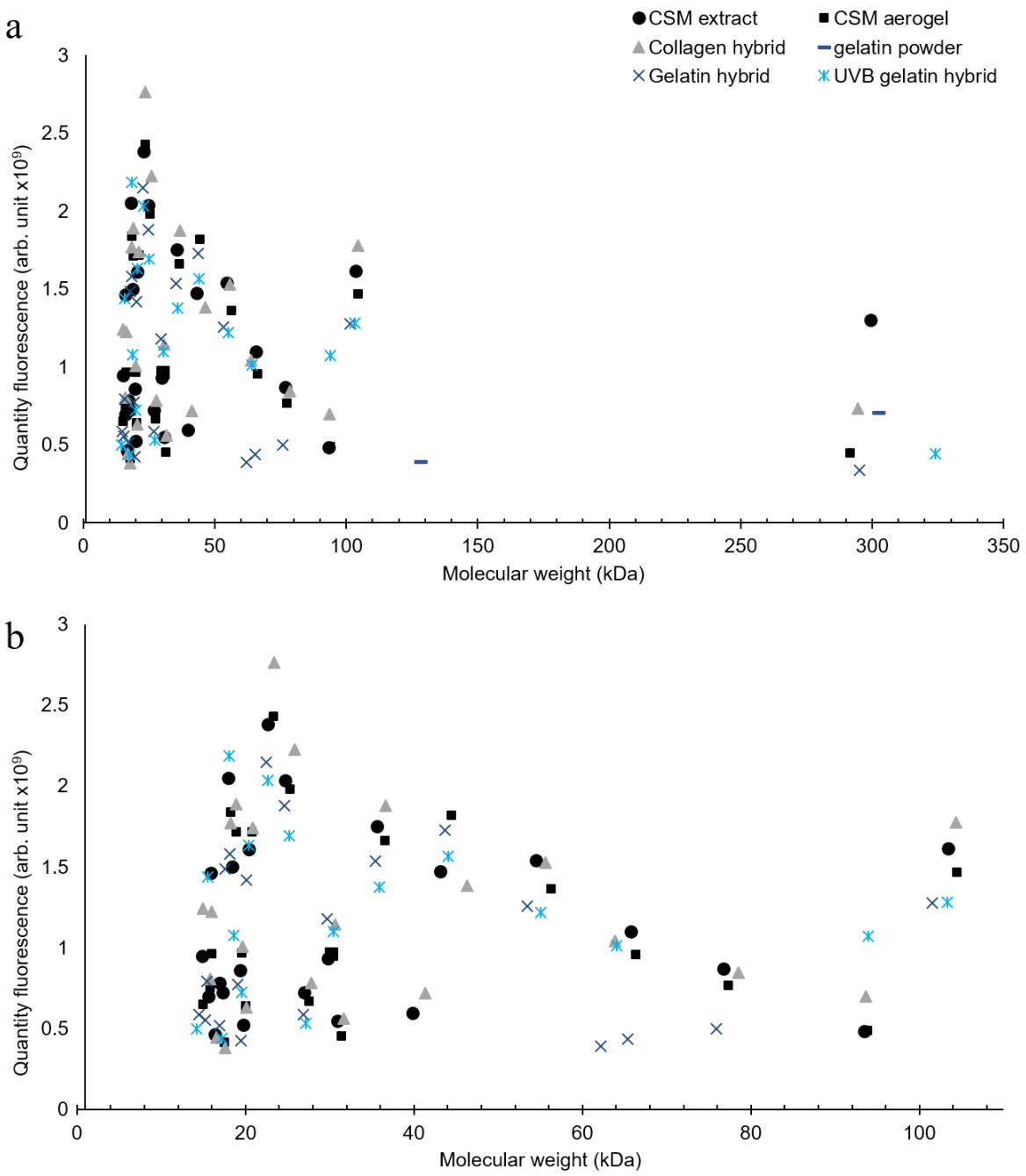

Figure 7.25: ***(a)*** *Volume of fluorescence detected from protein bands as a function of molecular weight in SDS-PAGE analysis of hybrid aerogels. Aerogels and powders were solubilised in buffer at 6.67 mg/ mL with 10 µL loaded onto the PA gel.* ***(b)*** *Data from plot (a) up to 110 kDa only.*

7.4. Mechanically and morphologically improved canola protein gels *via* Ca^{2+}-controlled gelation

Supercritical carbon dioxide (SC-CO_2) drying, the most commonly used drying method for aerogel production, promises to produce truly mesoporous CSM protein aerogels (see **Section 7.1**). The development of supercritically dried CSM protein aerogels using conventional solvent exchange protocols and SC-CO_2 technology presented two key challenges.

The first is the requirement for a free-standing gel that can be cut and transferred between solvents without damage. Many of the canola protein formulations used thus far in this thesis have a low viscosity ($|\mu| < 1000$ mPa.s, (see **Section 6.3.2**), are unable to support their own weight, and require a vessel for the entire formulation process. Only certain formulations using heat and a pH of 8, produced gels approaching free-standing structures ($|\mu| \approx 3000$ mPa.s) though gels were still susceptible to damage with handling. In strict IUPAC terminology, these formulations do not constitute 'gels' since they behave like liquids and have measurable viscosities. The gel point of a liquid generally occurs when viscosity tends towards infinity and the material becomes one network, or chemically cross-linked polymer, across the entire system [286]. The reduced viscosity presented no issues when producing cryogels since a freezing step solidifies the water and allows the structures to be dried into monoliths. However, such gels are not amenable to the supercritical fluid drying process since they cannot be transferred as self-supporting structures into an appropriate solvent (*e.g.* ethanol). CSM protein gels with low viscosities experienced significant mass and/or structure loss upon transferral to solvents due to partial dissolution. The early failures of transferral to ethanol indicate that the CSM protein gels are not extensively crosslinked and are largely bound by secondary interactions which are easily disrupted with ethanol. Free-standing, stiffer gels are routinely transferred from aqueous solutions to ethanol (*e.g.* polysaccharide gels [287]) as they can be cut or handled like solid materials. Therefore bio-based hydrogels can be amenable to solvent exchange with ethanol and the SC-CO_2 drying process given sufficient viscosity. The challenge of mass-loss during

attempted solvent exchange appears unique to the CSM protein gels due to the non-covalent nature of network formation.

Severe gel shrinkage is the second challenge predicted and is a common problem for bioaerogel researchers. Shrinkage occurs frequently with aquagels which are transferred to ethanol or other solvents [287]. However, gel shrinkage (with corresponding increase in density) is generally accepted as an unavoidable cost with researchers employing appropriate mitigation strategies. Shrinkage is typically managed using gentle solvent exchange methods entailing exchange from water to absolute ethanol using intermediate solutions that reduce concentration gradients [288]. Shrinkage can also be minimised when gels are extensively cross-linked and therefore strong enough to resist excessive structure collapse during solvent exchange [289].

Increasing the viscosity and stiffness of the CSM protein gels with crosslinking offers a simultaneous solution to both challenges. Canola protein gels prepared with 0.5 M and 0.1 M NaCl demonstrate high viscosities with NaCl facilitating gelation by improving physical entanglement of protein molecules [203]. Other protein gels and aerogels demonstrate improved stiffnesses with the addition of NaCl [118], KCl [290], and $CaCl_2$ [290, 291]. Additionally, Ca^{2+} is known to form ionic crosslinks in other bioaerogels making it a common choice for gelation agent in polysaccharide gels [292-294]. The use of salts to enhance bio-based gels offers an environmentally friendly approach, preferable to the use of oil-based and harmful organic chemicals (*e.g.* aldehydes) commonly used to crosslink biomolecules. Therefore, the incorporation of Ca^{2+} ions in CSM protein gels was investigated as a possible method for increasing gel stiffnesses and amenability to solvent exchange processes.

7.4.1. Gelation and rheometry

Preparations of CSM protein gels (10 wt% protein) containing varying concentrations of calcium chloride ($CaCl_2$) were prepared and visually assessed for effectiveness of Ca^{2+}-assisted gelation. The preservation of the structures after immersion in ethanol was considered a key requirement for later development of supercritically dried aerogels. Initial samples revealed a ‘goldilocks effect’ of the

calcium ion concentration ([Ca^{2+}]). Low [Ca^{2+}] made gels susceptible to crumbling in ethanol solutions (**Figure 7.26c**) while high [Ca^{2+}] led to lumpy precipitates (**Figure 7.26a**) and non-viable freeze dried aerogels (not shown). A [Ca^{2+}] of 20 mmol/L was selected for further gel preparations given the smooth consistency (**Figure 7.26b**) and stability in ethanol (see **Section 7.4.2**) of the corresponding CSM protein-Ca^{2+} gel.

Figure 7.26: *CSM protein gels prepared at 10* wt% *protein and* ***(a)*** *200 mM $CaCl_2$,* ***(b)*** *20 mM $CaCl_2$, or* ***(c)*** *2 mM $CaCl_2$ (shown in 100 % ethanol)*

Prior investigations had revealed that CSM protein gels prepared at pH 8 and with heat-treatments at 95 °C had the highest viscosities ($|\mu| \approx 80000$ mPa.s) and gel stiffness ($G' \approx 600$ Pa, see **Section 6.3**) of CSM protein gels. Therefore, pH and heat-treatment variations were incorporated into the Ca^{2+} gel trials. Gelation using 20 mmol/L $CaCl_2$ was investigated in both pre-heated (30-minute immersion in a water bath at 95 °C) and non-heated (prepared at 25 °C) gels at a pH value of 8 (**Figure 7.27**). An identical set of gels were prepared at a pH of 10 (**Figure 7.28)** and a control sample for each pH value was also prepared (non-heated and without $CaCl_2$). Gel viscosities were measured during formulation before being dried *via* freeze drying (**Section 7.4.4**) or SC-CO_2 drying (**Section 7.4.2**). Further analyses of gel stiffnesses and viscosity were conducted on fresh samples using the more powerful technique of rheometry (see below).

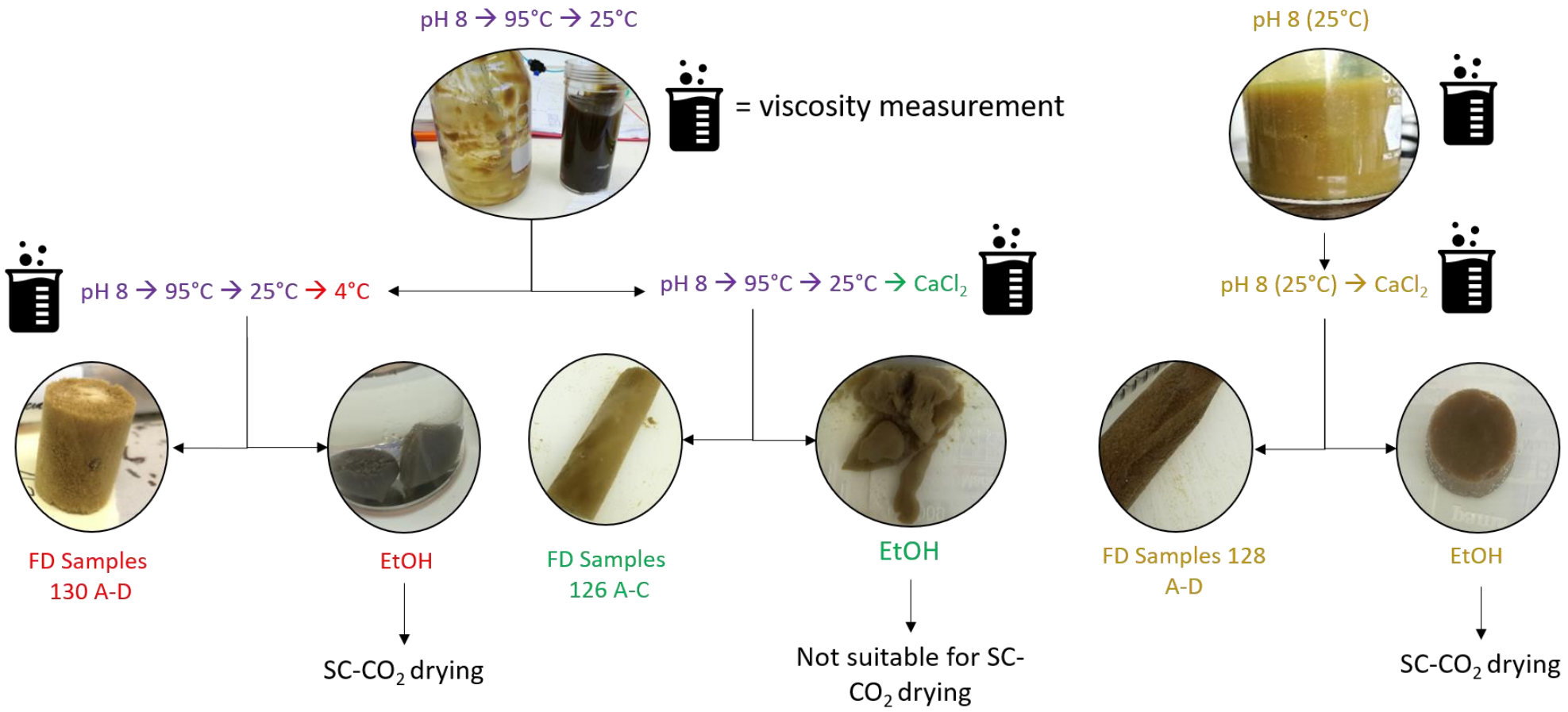

Figure 7.27: *Summary of CSM protein gels prepared at pH 8.0 – 8.2 for Ca^{2+}- & heat-treatment trials. Heat-treatments at 95 °C were for 30 minutes. $CaCl_2$ was added to a final concentration of 20 mmol/L. Samples were subject to viscometry measurements (indicated with a beaker symbol), freeze dried aerogel production (indicated with 'FD' and sample numbers), and immersion in 96 % ethanol (indicated with 'EtOH'). Suitable samples were then subject to supercritical carbon dioxide drying (indicated with 'SC-CO_2 drying'). Samples unstable in ethanol are annotated to show that they were not suitable for SC-CO_2 drying*

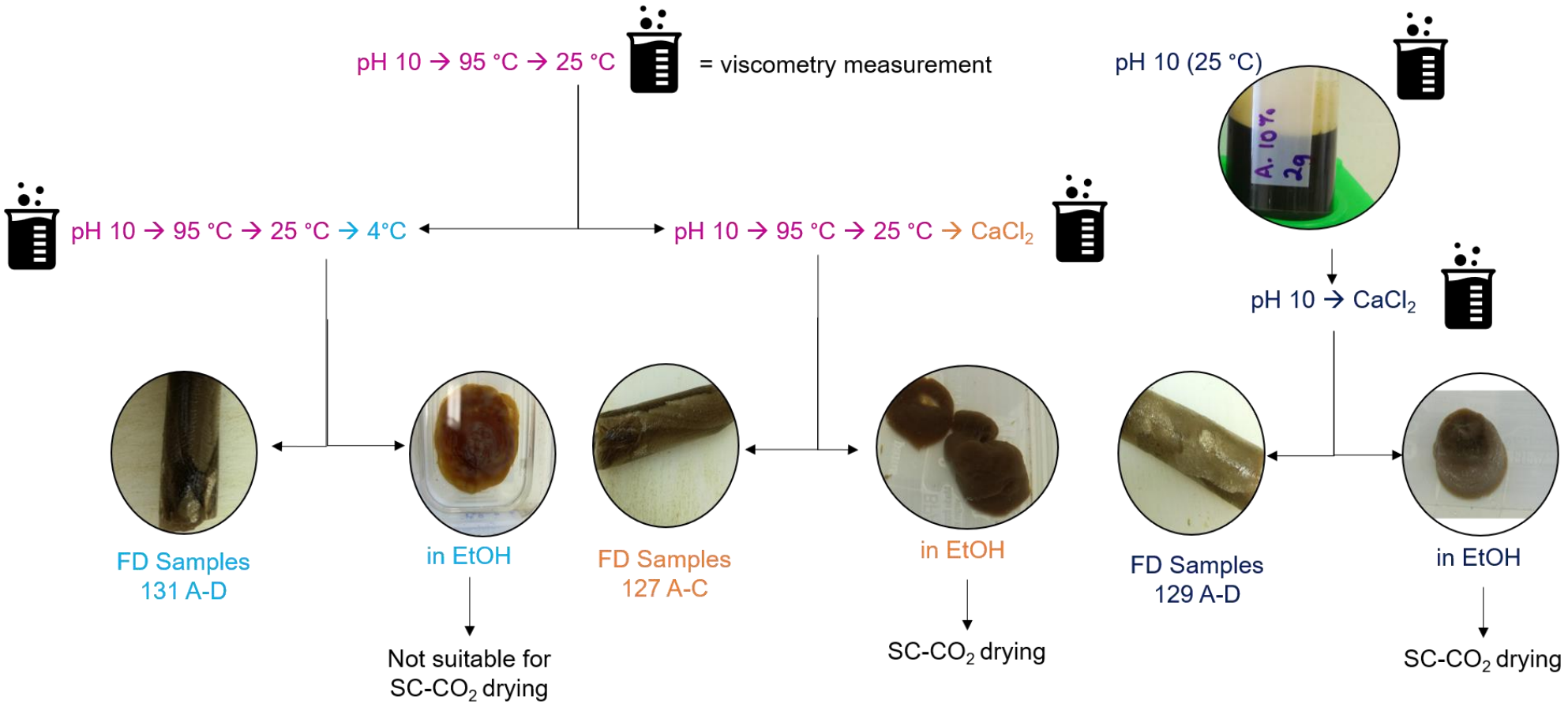

***Figure 7.28**: Summary of CSM protein gels prepared at pH 10.0 – 10.2 for Ca^{2+}- & heat-treatment trials. Heat-treatments at 95 °C were for 30 minutes. $CaCl_2$ was added to a final concentration of 20 mmol/L. Samples were subject to viscometry measurements (indicated with a beaker symbol), freeze dried aerogel production (indicated with 'FD' and sample numbers), and immersion in 96 % ethanol (indicated with 'EtOH'). Suitable samples were then subject to supercritical carbon dioxide drying (indicated with 'SC-CO_2 drying'). Samples unstable in ethanol are annotated to show that they were not suitable for SC-CO_2 drying*

Viscometry measurements taken during the formulation of the gels (refer to beaker symbols in **Figure 7.27** & **Error! Reference source not found.**) confirmed earlier findings (see **Section 6.3.1**). Heated CSM-protein gels are more viscous than non-heated gels (**Figure 7.29**) and pH 8 gels (**Figure 7.29a**) have a 10- to 100-fold increase in viscosity over those prepared at pH 10 (**Figure 7.29b**). The addition of $CaCl_2$ predictably increased gel viscosities in all samples except for heat-treated pH 8 gels. Viscosities were increased by up to 6-fold in non-heat-treated gels at pH 8 (**Figure 7.29a,** grey to green circles), up to 20-fold in non-heated pH 10 formulations (**Figure 7.29b,** black to green squares), and up to 7-fold in heat-treated pH 10 formulations (**Figure 7.29b,** red to purple triangles). However, viscosities were reduced to only 50 – 75 % of pre-Ca^{2+} values in the heat-treated pH 8 gels (**Figure 7.29a,** orange to purple triangles), suggesting a disruption of the existing gel network under these conditions. Additionally, changes to gel viscosities with $CaCl_2$ addition were shear-rate dependant with greater differences at lower shear-rates. Shear thinning behaviour was therefore slightly more pronounced in gels containing $CaCl_2$.

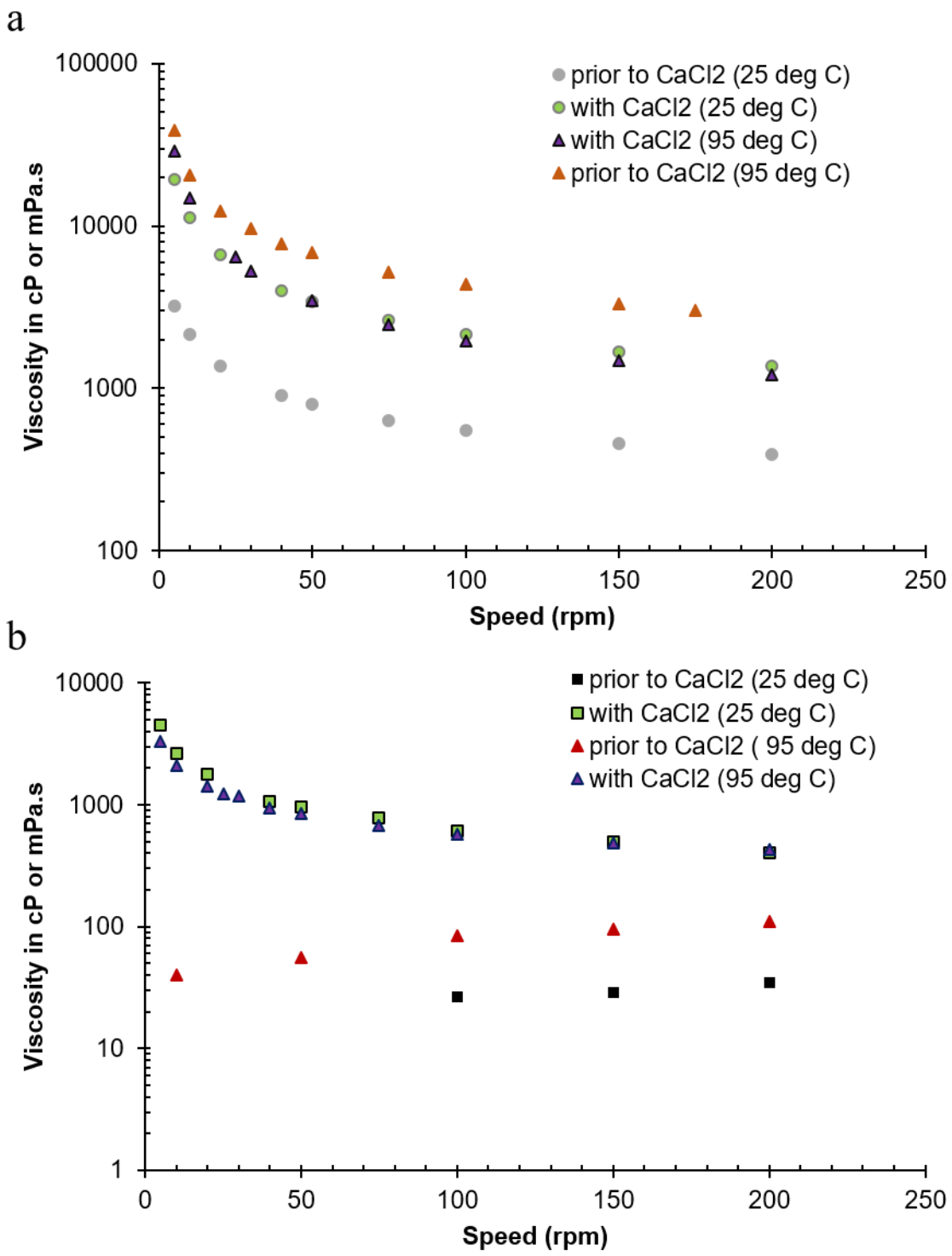

***Figure 7.29**: Viscosity measurements of CSM protein gels prior to, and after, the addition of $CaCl_2$ (final concentration 20 mM). $CaCl_2$ was added to pre-heated (95°C, 30 mins) (triangles) and non-heated (25 °C) (circles **(a)** or squares **(b)**) samples at pH values of 8 **(a)** or 10 **(b)**. Pre-heated gels were cooled to room temperature before the addition of $CaCl_2$ and viscosity measurements. Data for samples without $CaCl_2$ previously presented in Section 6.3*

Rheometric analysis using an oscillating rheometer allowed for measurements of gel viscosities (**Figure 7.30**), storage moduli (**Figure 7.31**), loss factors (**Figure 7.32**), and critical strains (**Figure 7.33**) from the LVR of strain-sweep experiments. Rheometric data confirms that $CaCl_2$ increases gel viscosities in all but heat-treated pH 8 gels. Interestingly the use of $CaCl_2$ shows all gels (of comparable pH values) had comparable viscosities after the addition of $CaCl_2$, irrespective of prior heat-treatments. The use of $CaCl_2$ possibly indicates a new gelation mechanism (*e.g.* ionic crosslinking) is overriding a previous heat-induced mechanism (*e.g.* hydrophobic associations), even where heat-induced gels demonstrate higher viscosities (pH 8 samples, **Figure 7.30**).

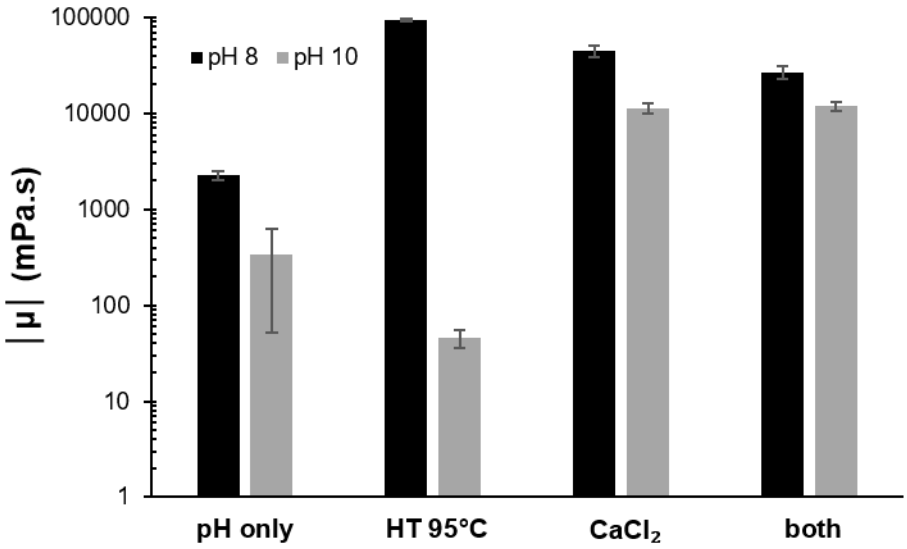

Figure 7.30: *Complex viscosity measurements averaged from the LVR (0.1 – 1.0 % ε) of strain sweep rheometry experiments in CSM protein gels prepared at pH 8 and 10. Gels were pH adjusted and either heated to 95 °C for 30 mins ('HT 95°C') or subject to $CaCl_2$ addition to a final concentration of 200 mM ('$CaCl_2$'). Additional samples were subject to the heat-treatment followed by $CaCl_2$ addition ('both') or no additional treatment after pH adjustment ('pH only'). Error bars represent the standard deviation where n= 3. Data for samples without $CaCl_2$ previously presented in Section 6.3*

Storage moduli show $CaCl_2$ also increases gel stiffness in all gels except heat-treated pH 8 gels (**Figure 7.31**). Heat-treated pH 8 gels have a storage modulus of 576 Pa (only 13.3 Pa with no heat-treatment) while $CaCl_2$ addition increases the storage modulus from 13.3 to 270 Pa. Combined use achieves a storage modulus of 164 Pa, greater than pH 8 gels alone but fails to realise the full potential of either treatment.

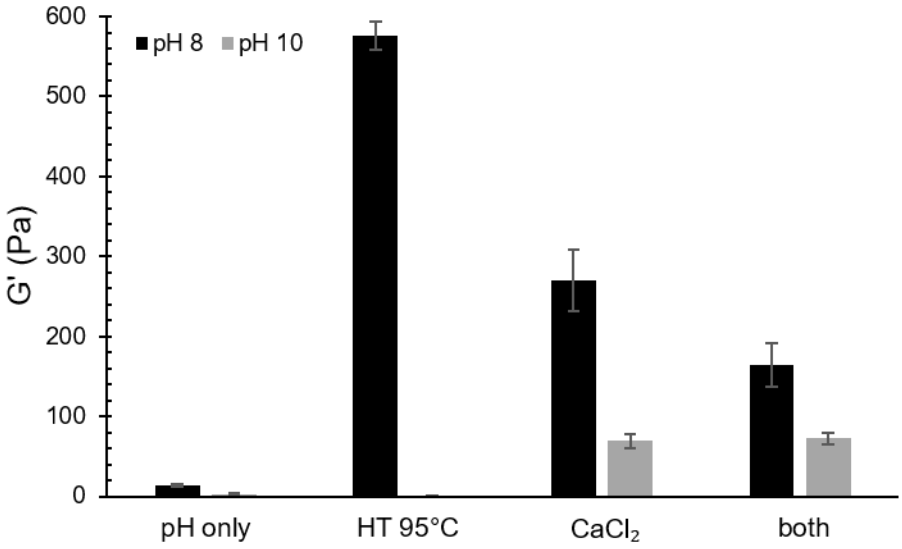

Figure 7.31*: Storage moduli measurements averaged from the LVR (0.1 – 1.0 % ε) of strain sweep rheometry experiments in CSM protein gels prepared at pH 8 and 10. Gels were pH adjusted and either heated to 95 °C for 30 mins ('HT 95°C') or subject to $CaCl_2$ addition to a final concentration of 200 mM ('$CaCl_2$'). Additional samples were subject to the heat-treatment followed by $CaCl_2$ addition ('both') or no additional treatment after pH adjustment ('pH only'). Error bars represent the standard deviation where n= 3. Data for samples without $CaCl_2$ previously presented in Section 6.3*

Gels prepared at pH 10 have increased moduli upon $CaCl_2$ addition (from 1.8 Pa to 69 – 73 Pa), irrespective of prior heat-treatment (**Figure 7.31**) and both heated and non-heated pH 10 formulations have storage moduli < 2 Pa. Loss factor measurements, representing the ratio of the loss to storage moduli, reveal the overall liquid-like or solid-like nature of the gels. Loss factor measurements demonstrate that Ca^{2+}-addition makes gels more solid-like but so also does heat-treatment in gels at pH 8 (**Figure 7.32**).

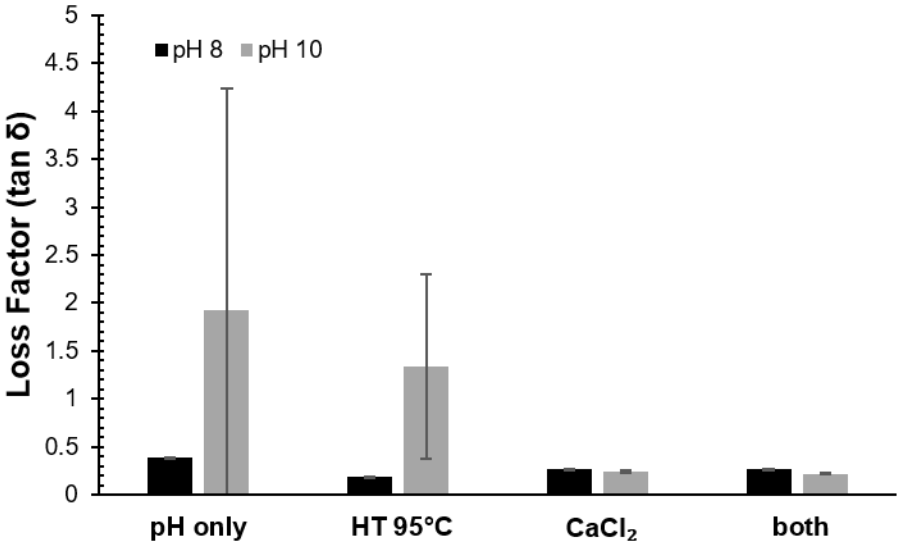

Figure 7.32: *Loss factor measurements averaged from the LVR (0.1 – 1.0 % ε) of strain sweep rheometry experiments in CSM protein gels prepared at pH 8 and 10. Gels were pH adjusted and either heated to 95 °C for 30 mins ('HT 95°C') or subject to $CaCl_2$ addition to a final concentration of 200 mM ('$CaCl_2$'). Additional samples were subject to the heat-treatment followed by $CaCl_2$ addition ('both') or no additional treatment after pH adjustment ('pH only'). Error bars represent the standard deviation where n= 3. Data for samples without $CaCl_2$ previously presented in Section 6.3*

Strain sweep experiments were also used to determine the critical strain (strain at which flow is initiated) in CSM protein gels, thus providing a measure of gel elasticity. Critical strains were extremely low or immeasurable in pH 10 samples except where $CaCl_2$ was introduced, increasing gel stiffness and allowing for detection of critical strains (**Figure 7.33**). Interestingly the combination of heat-treatment and $CaCl_2$ treatment increased elasticity in pH 10 gels over $CaCl_2$ treatment alone, while storage moduli and viscosity remained similar for these two samples (see above). CSM protein gels at pH 8 demonstrated a reduction in critical strain with either heat-treatment or $CaCl_2$ addition, clearly demonstrating that increased stiffness corresponds with a reduction in gel elasticity in the stiffest gels. An extensive gel network is expected to have reduced elasticity, particularly where strong bonding such as covalent or ionic crosslinking is present. The reduced elasticity (**Figure 7.33**) and increased stiffness (**Figure 7.31**) of pH 8 gels with heat- or Ca^{2+}-treatments suggests the increase in protein intermolecular bonding is long-ranging within the gels. However, slight variations in rheological behaviour between heat- and Ca^{2+}-treated gels suggest that gelation is likely due to

competing mechanisms and different bond types in the two different treatments (see **Section 8.4** for further discussion).

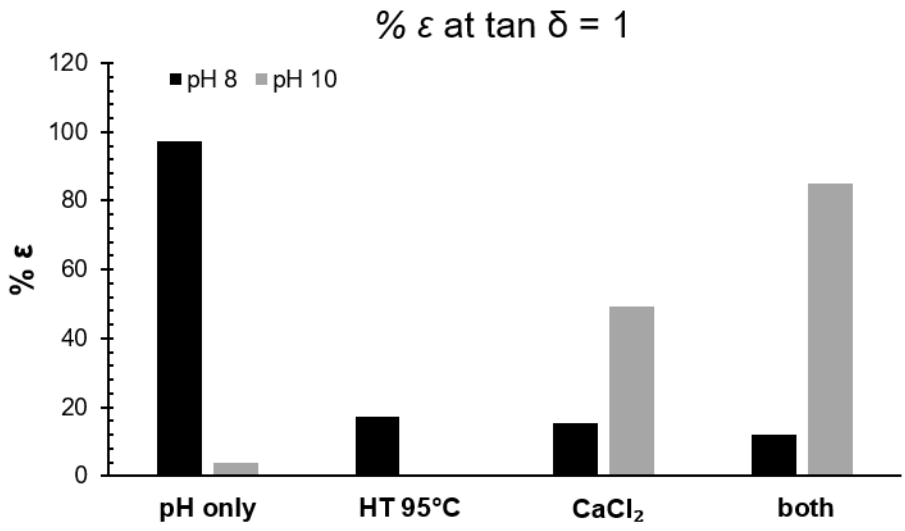

Figure 7.33: *Critical strain (% ε at tan δ = 1) measurements averaged from strain sweep rheometry experiments in CSM protein gels prepared at pH 8 and 10 with various gelation treatments. Gels were pH adjusted and either heated to 95 °C for 30 mins ('HT 95°C') or subject to $CaCl_2$ addition to a final concentration of 200 mM ('$CaCl_2$'). Additional samples were subject to the heat-treatment followed by $CaCl_2$ addition ('both') or no additional treatment after pH adjustment ('pH only'). Data for samples without $CaCl_2$ previously presented in Section 6.3*

Rheometry experiments were also conducted using a frequency sweep to assess the frequency-dependant nature of gel rheometric properties. The resulting storage moduli can be analysed for frequency-independence by assessing the slope of a log G′ versus log frequency plot. Positive slope values indicate increasing gel stiffness with increasing frequency (shear rate) while slope values near zero represents high frequency independence. CSM protein gels prepared at pH 8 demonstrate a small, shear thickening response (slight increase in G′ with increasing frequencies between 0.1 and 1 Hz) (**Figure 7.34**). Gels prepared at pH 10 were more difficult to analyse as measurements were complicated by tanδ measurements > 1 and a corresponding instability in G′ measurements (reflected in large variance seen in **Figure 7.34**). Furthermore, pH 10 gels with $CaCl_2$ experienced shear thinning behaviour (reduction of G′ with increasing frequency) while heat-treated pH 10 gels underwent shear thickening, even when $CaCl_2$ was also added. Once more the use of heat-treatments and Ca^{2+}-treatments appears to produce contrasting rheological behaviours and may implicate different gelation mechanisms.

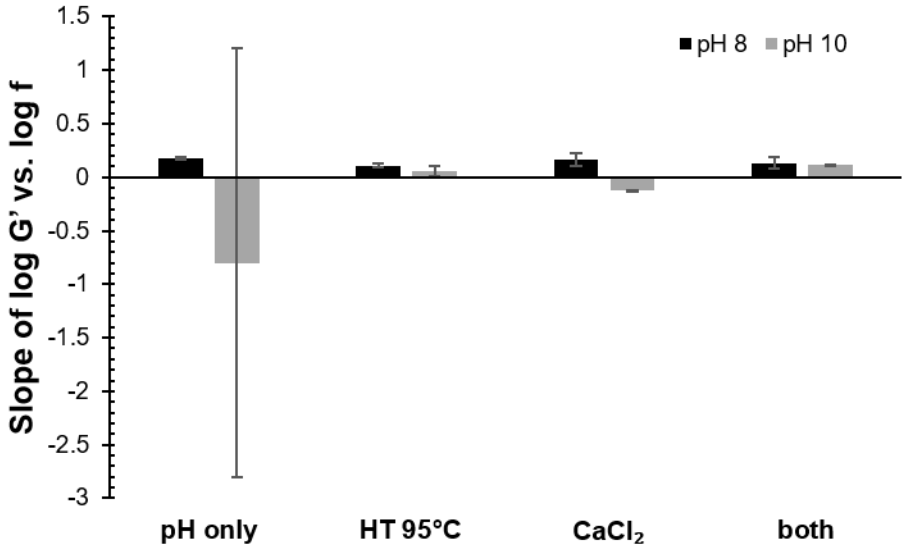

Figure 7.34: *The slopes of the log of G' versus log of f plots taken from frequency sweep data (0.1 – 1 Hz) from rheometry experiments at 0.1 % strain in CSM protein gels prepared at pH 8 and 10 with various gelation treatments. Gels were pH adjusted and either heated to 95 °C for 30 mins ('HT 95°C') or subject to $CaCl_2$ addition to a final concentration of 200 mM ('$CaCl_2$'). Additional samples were subject to the heat-treatment followed by $CaCl_2$ addition ('both') or no additional treatment after pH adjustment ('pH only'). Error bars represent the standard deviation of 3 repeats. Data for samples without $CaCl_2$ previously presented in Section 6.3*

The overall enhancement of gel viscosities and stiffnesses with the addition of $CaCl_2$ represented a successful first step towards eventual production of mesoporous CSM protein aerogels. Rheological information suggests that CSM protein gels with Ca^{2+} treatments, alongside pH 8 heat-treated gels, have a higher likelihood of enduring the solvent exchange processing necessary for SC-CO_2 drying.

7.4.2. Development of supercritically dried CSM protein-Ca^{2+} aerogels

The various CSM protein gels (refer **Figure 7.27** & **Figure 7.28**) were subject to immersion in ethanol to attempt SC-CO_2 drying. Initially, Ca^{2+}-CSM protein gels and pH 8 heat-treated gels were transferred to low concentration (10 – 50 %) solutions of ethanol as per common literature protocols for bioaerogel manufacture. Additionally, these immersed gels were subject to gentle agitation to facilitate solvent penetration of gel pores. Regrettably, high solubility in the (mostly) aqueous solutions led to partial destruction of the samples, further accelerated by the gentle agitation. Loss of gel structure in ethanol solutions was previously noted in initial attempts to immerse pure CSM protein gels in ethanol solutions (see **Section 7.4.1**). The gradual solvent exchange process was eventually rendered implausible in CSM protein gels (both fortified by Ca^{2+} addition and without) due to the significant loss of material which occurred at low ethanol concentrations. Consequently, direct immersion in 96 % ethanol was trialled (**Figure 7.35**).

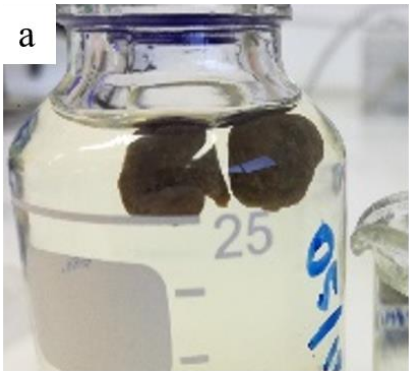

Figure 7.35: *CSM protein-Ca^{2+} gels prepared at 10* wt% *protein, pH 10.9, and 20 mM $CaCl_2$ immersed in 96 % ethanol*

Amazingly the Ca^{2+}-CSM protein gels demonstrated a remarkable retention of gel shape, mass, and volume in 96 % ethanol (**Figure 7.35**). The retention of volume was particularly important, suggesting ethanol-induced shrinkage is negligible in CSM protein gels and unlike other biopolymeric gels. Indeed, gelatine gels underwent severe (> 80 %) shrinkage in ethanol, even in graduated solvent exchange processes (see below). Heat-treated, Ca^{2+}-treated, or mixed-treatment gels prepared at pH 8 or pH 10 (see **Section 7.4.1**) were first transferred to syringes that had the needle ends cut to make a flat base, which was then sealed with Parafilm™. The gels were stored at 4 °C for 24 hours standing

upright on the cut end of the syringe. Subsequent transferral to 96 % ethanol was achieved by using the syringe plunger to gently force the gel monoliths from the syringe into a bath of 96 % ethanol. Direct immersion in 96 % ethanol allowed for successful solvent exchange processing in four of the six CSM protein gels trialled: the pH 8 heat-treated gel, the pH 8 Ca^{2+}-treated gel, the pH 10 Ca^{2+}-treated gel, and the pH 10 gel with both heat- and Ca^{2+}-treatment (**Figure 7.36 a-b, e-f**). The sample prepared at pH 10 with no added $CaCl_2$ remained too liquid-like for successful transferal, irrespective of heat treatment (**Figure 7.36d**). Interestingly, the pH 8 sample subject to both heat- and Ca^{2+}-treatment was also too fragile for solvent exchange and underwent significant damage to the structure upon transferral to ethanol (**Figure 7.36c**). The gel with the best shape retention after transferral into ethanol was the Ca^{2+}-CSM protein gel prepared at pH 8 (**Figure 7.36b**).

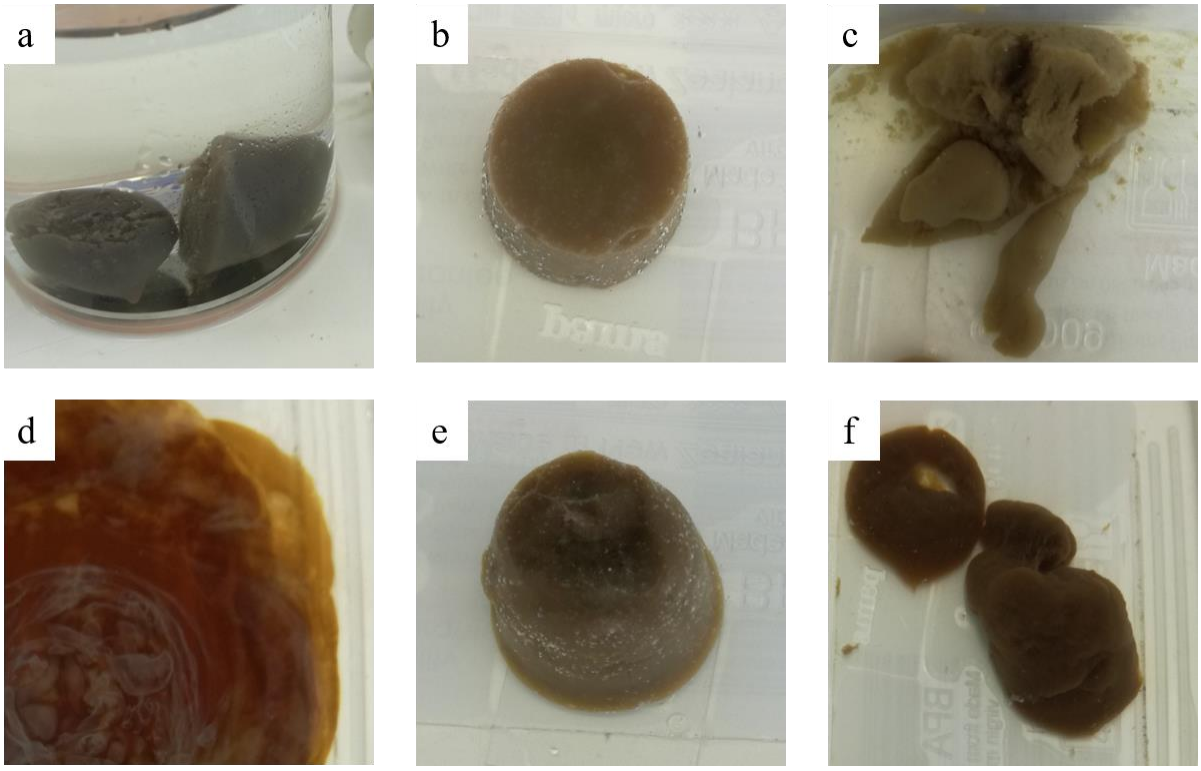

Figure 7.36: *CSM protein gels after direct immersion in 96 % ethanol:* ***(a)*** *pH 8 heat-treated sample,* ***(b)*** *pH 8 Ca^{2+}-treated sample,* ***(c)*** *pH 8 heat- and Ca^{2+}-treated sample,* ***(d)*** *pH 10 heat-treated sample,* ***(e)*** *pH 10 Ca^{2+}-treated sample,* ***(f)*** *pH 10 heat- and Ca^{2+}-treated sample*

The four successful gels were left immersed in the 96 % ethanol for 48 hours with a refreshment of the ethanol after 24 hours. During this time the ethanol became discoloured as alcohol-soluble

molecules were removed from the gel (possibly tannins and other polyphenols) demonstrating the persistence of such molecules from the original canola seed in the CSM extract and gels (**Figure 7.37**).

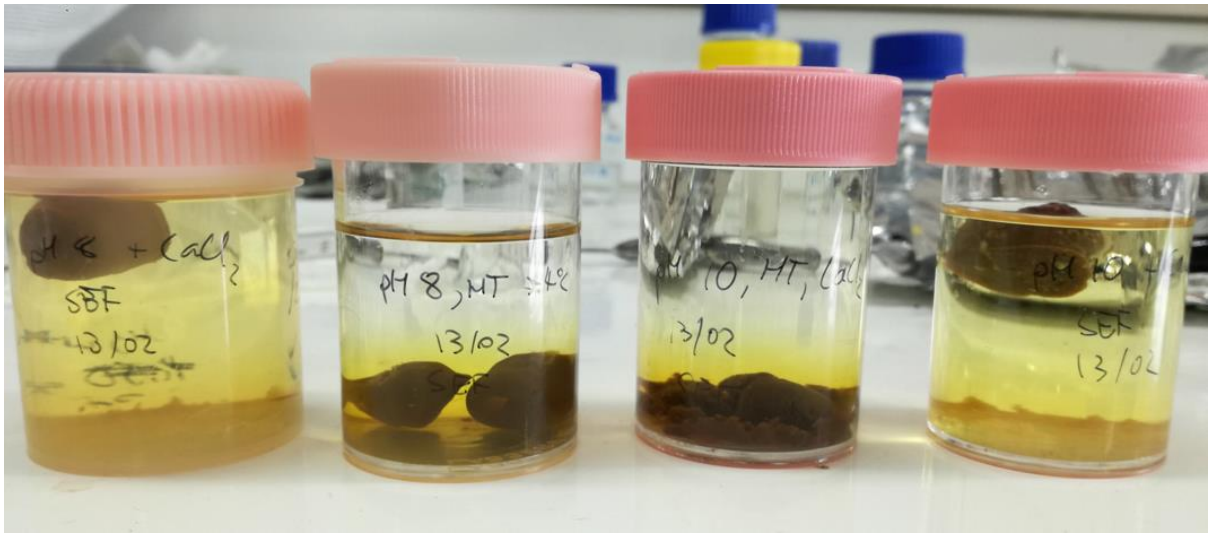

Figure 7.37: *CSM protein gels after 24 hours of immersion in 96 % ethanol. From left to right samples are pH 8 Ca^{2+}-treated sample, pH 8 heat-treated sample, pH 10 heat- and Ca^{2+}-treated sample & pH 10 Ca^{2+}-treated sample*

Following the initial 48 hours in 96 % ethanol the gels were subsequently transferred to 100 % ethanol for a further 4 days with daily replacement of the ethanol. Discolouration of ethanol solutions did not persist beyond the first 48 hours in 96 % ethanol (**Figure 7.38**).

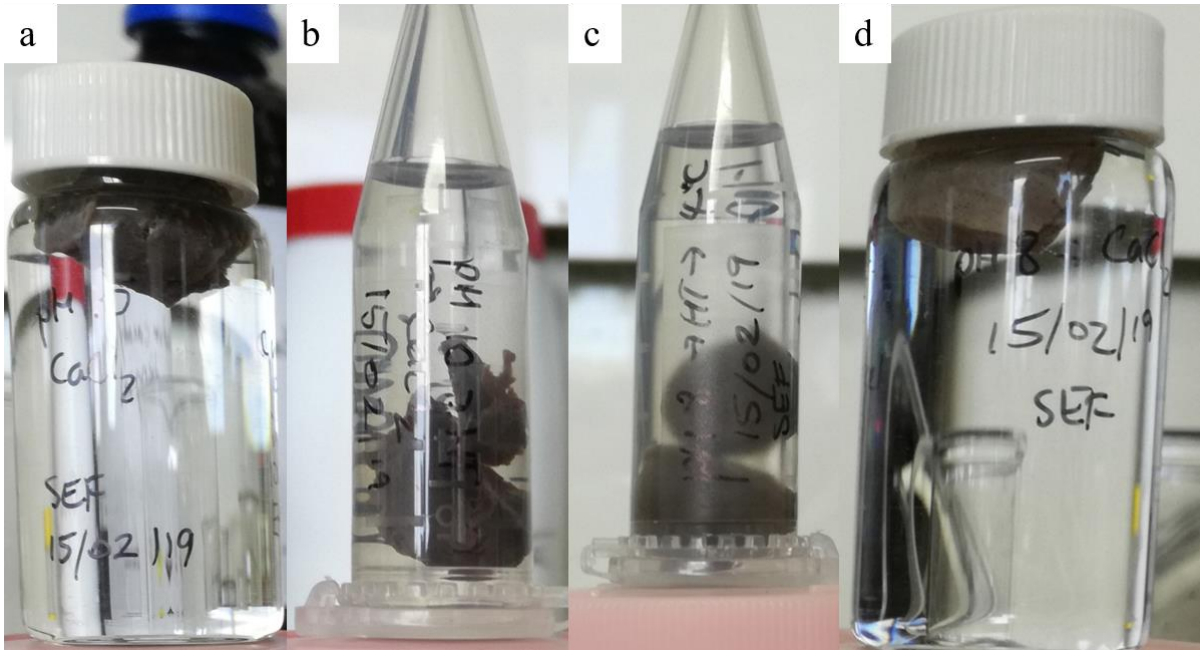

Figure 7.38: *CSM protein gels after 2 days immersion in 96 % ethanol and a further 4 days immersion in absolute ethanol:* ***(a)*** *pH 10 Ca^{2+}-treated sample,* ***(b)*** *pH 10 heat- and Ca^{2+}-treated sample,* ***(c)*** *pH 8 heat-treated sample, and* ***(d)*** *pH 8 Ca^{2+}-treated sample*

SC-CO_2 drying was first attempted with gelatine gels for the purposes of trialling the SamDri – 795 Critical Point (CP) Dryer (Tousimis®) for the preparation of aerogels. The SamDri -795 CP dryer is purpose-built for the preparation of microscopy samples using critical point drying and so chamber volume is smaller than typical SC-CO_2 systems for aerogel production. However, conceptually, the drying process is identical and aerogel manufacture can be achieved with some modifications to standard operating procedures (see below). Additionally, refer to **Section 8.7.2** for discussion of usual supercritical fluid extractor systems employed in aerogel research.

Experiments using gelatine show the typical processing results of a bio-based gel undergoing the various methods of drying (**Figure 7.39**). Gradual solvent exchange of the aquagel with ethanol resulted in significant shrinkage in the alcogel structure (**Figure 7.39a-b**). Subsequent drying using SC-CO_2 drying successfully maintained the volume of the alcogel (minimal further shrinkage) though the dried 'aerogels' were opaque and possessed a hard, shiny 'crust' (**Figure 7.39c-d).** Attempts to use Ca^{2+} salt to strengthen the gelatine gel structure and reduce shrinkage during solvent exchange were unsuccessful, resulting in similar opaque and shrunken gels upon SC-CO_2 drying (**Figure 7.39e**). Air

dried gelatine also undergoes structure-damaging shrinkage producing a typical xerogel (**Figure 7.39f**) while freeze drying remained the only successful method for producing a low-density specimen, minimising shrinkage (**Figure 7.39g**).

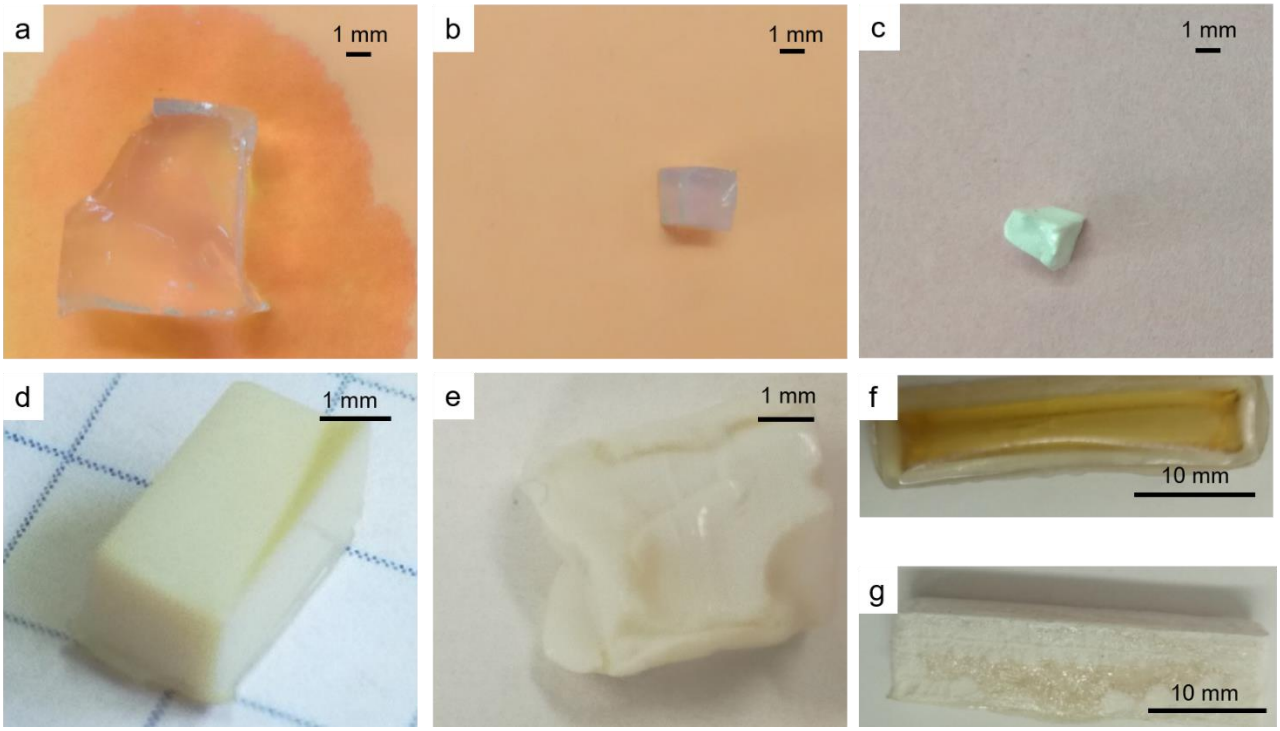

Figure 7.39: *Gelatine gel prepared at 10* wt% *in water* ***(a)****, after solvent exchange to absolute ethanol using a series of gradual EtOH concentration changes from 0 – 100 %* ***(b)****, and after subsequent drying in supercritical CO2 using the SamDri 795 CP dryer* ***(c & d)****. Gelatine gel prepared in water with 2 mol/L* $CaCl_2$*, solvent exchanged to EtOH and supercritically dried* ***(e)****. Gelatine gels prepared at 10* wt% *in water and air dried* ***(f)*** *or freeze dried* ***(g)***

The surprising success of directly immersing the CSM protein gels in absolute ethanol promised a better result for aerogel production than had been observed in gelatine gels. However, initial experiments with protein gels revealed the need for some modification to recommended operating procedures when using 'off-the-shelf' (*e.g.* the SamDri – 795 Critical Point Dryer (Tousimis®)) critical point dryers to produce aerogels. Several technical problems were encountered before CSM protein aerogels could finally be produced using the SamDri CP drying system. The principal problem was the incomplete solvent exchange of ethanol (EtOH) with carbon dioxide (CO_2) during the 'purge' stage of the CP dryer operation (**Figure 7.40**). The semi-automated nature of the CP dryer requires a purge time (up to 45 minutes) to be set by the operator before the chamber is filled with liquid CO_2.

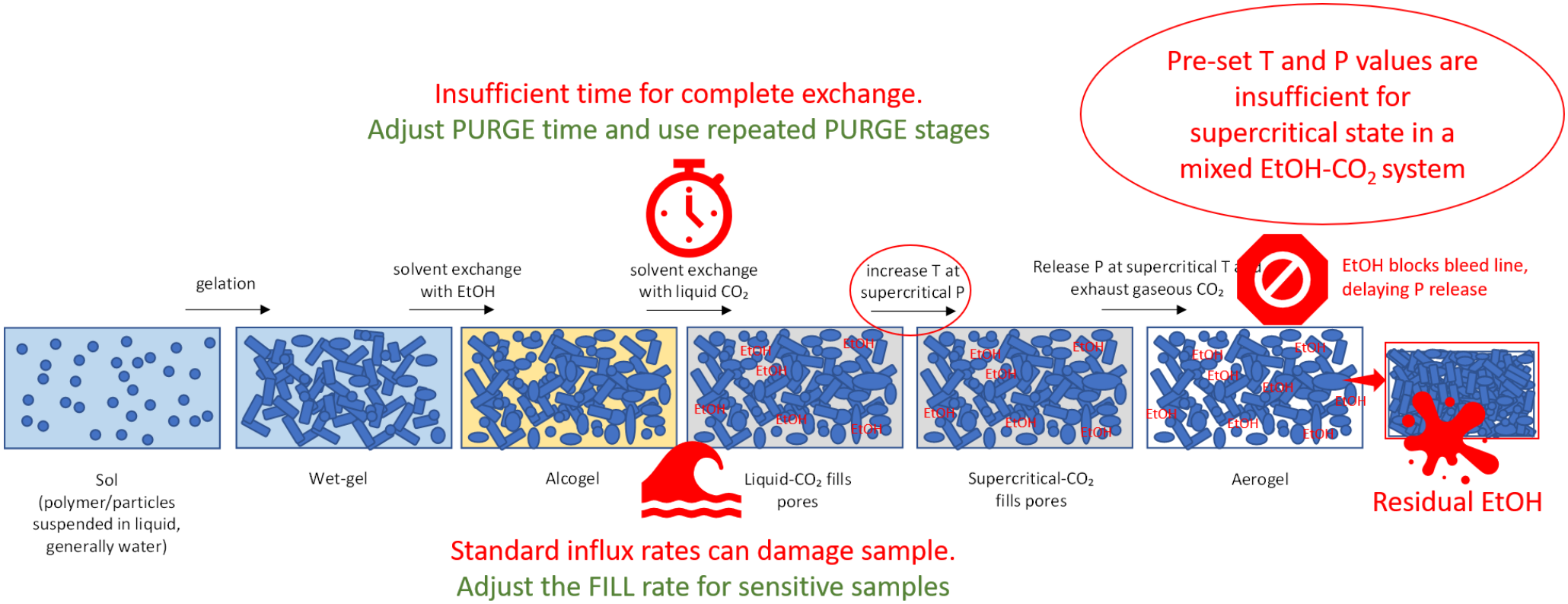

Figure 7.40: *Diagrammatic representation of common problems encountered during supercritical drying of CSM protein gels using the SamDri - 795 (Tousimis®) Critical Point dryer*

Purge time required for complete ethanol removal is dependent on gel type and gel size and can also be further delayed in monolithic samples as compared to gel particles [295]. Investigations using conventional supercritical drying systems reveal monolithic samples (3.0 cm (*l*) x 1.2 cm (ø)) of starch gels take in excess of 100 minutes to approach 100 % removal of ethanol from the system (sample and chamber) [295]. Initial attempts to dry CSM protein gels (10 – 12 mm (ø)) on the SamDri – 795 revealed evidences of incomplete ethanol purging (shrunken samples, residual solvent in chamber, fluid (ethanol) in CO_2 bleed line). Attempted drying of the pH 10 heat- and Ca^{2+}-treated sample resulted in high levels of shrinkage and evidences of incomplete solvent exchange with CO_2 (residual ethanol in chamber and 'wet' sample) after a 20-minute purge time. Purge time was increased from 20 to 30 minutes for the pH 8 heat-treated gel but also resulted in incomplete drying due to residual ethanol. Purge time was further increased to 40 minutes for the subsequent drying of the pH 10 Ca^{2+}-treated and consequently no residual ethanol was found in the chamber. However, the sample experienced shrinkage (approximately 50 %), structure collapse, and deforming of the monolithic shape during drying (**Figure 7.41**).

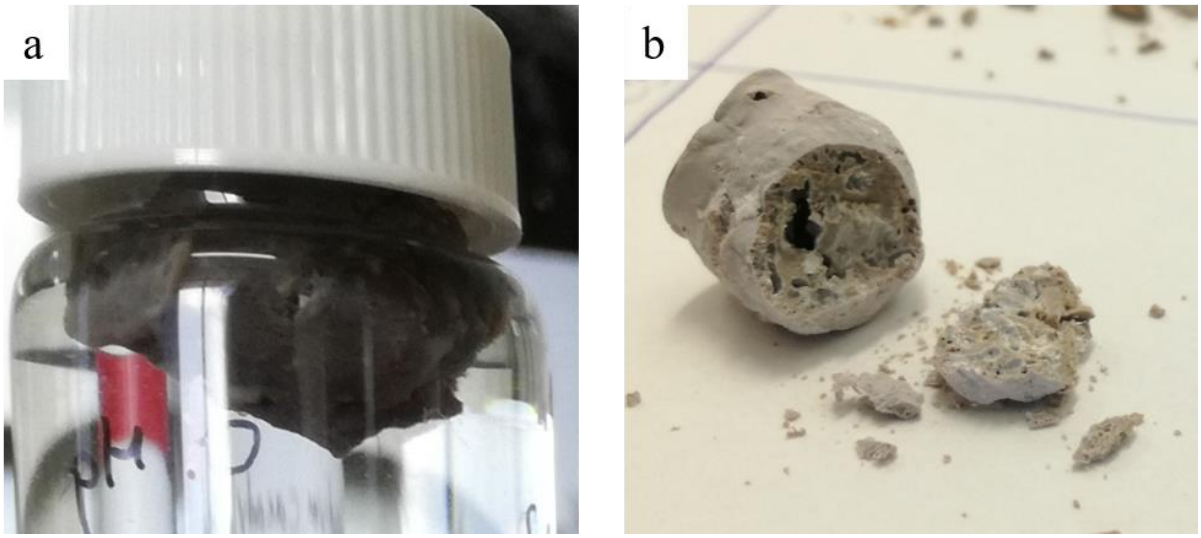

Figure 7.41: (a) *CSM-protein gel prepared at pH 10 and with 20 mM $CaCl_2$ immersed in 100 % ethanol and* ***(b)*** *close up photograph of corresponding supercritically dried aerogel*

Resolution to this problem required the operator to manually override automated stage transitions to increase purge times beyond 45 minutes (see **Section 8.7.2** for modifications to standard operating

procedures of the SamDri 795 CP dryer). Additionally, the size of the gel samples was reduced (< 7 mm diameter) and the fill rate for the initial influx of liquid CO_2 into the chamber was reduced to minimise structure damage by the influx of fluid.

The first successful CSM protein aerogel produced using the SamDri – 795 was the Ca^{2+}-treated gel at pH 10.9 which was dried with minimal volume change from alcogel to aerogel (**Figure 7.42**) using a 30 minute purge time but smaller sample size (ø ≈ 6 mm). The aerogel was lightweight (could be suspended on sides of plastic Eppendorf® tube by static electricity) and had an approximate bulk density of 0.2 g/cm^3, where density measurement was calculated by approximating as a sphere and using an average diameter measurement. The supercritically dried aerogel was now an opaque cream colour, having lost the golden-brown colouration typical of the CSM protein gels during the SC-CO_2 drying (yellow colouration was observed in the purged ethanol). A likely explanation for the loss of colour during ethanol purging is the ability of pressurised ethanol to further solubilise and remove coloured molecules (*e.g.* tannins) (see **Figure 7.37**).

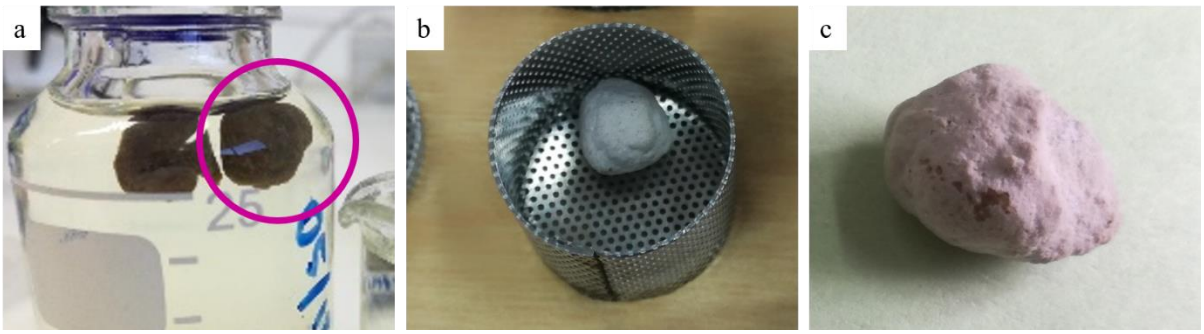

Figure 7.42: (a) *CSM-protein gel prepared at pH 10.9 and with 20 mM $CaCl_2$ immersed in 97 % ethanol,* ***(b)*** *in 12 mm sample basket following supercritical drying, and* ***(c)*** *close-up image of corresponding dried aerogel*

One additional CSM protein aerogel was produced by successful SC-CO_2 drying in the SamDri – 795 CP dryer. This aerogel was produced using the pH 8 Ca^{2+}-treated gel which had been held in 100 % ethanol for 14 weeks (intermittent refreshing of ethanol) and was subsequently dried with a 75-minute purge time, experiencing minimal shrinkage (**Figure 7.43**). The bulk density was also calculated at ≈ 0.2 g/cm^3 using a spherical approximation of shape.

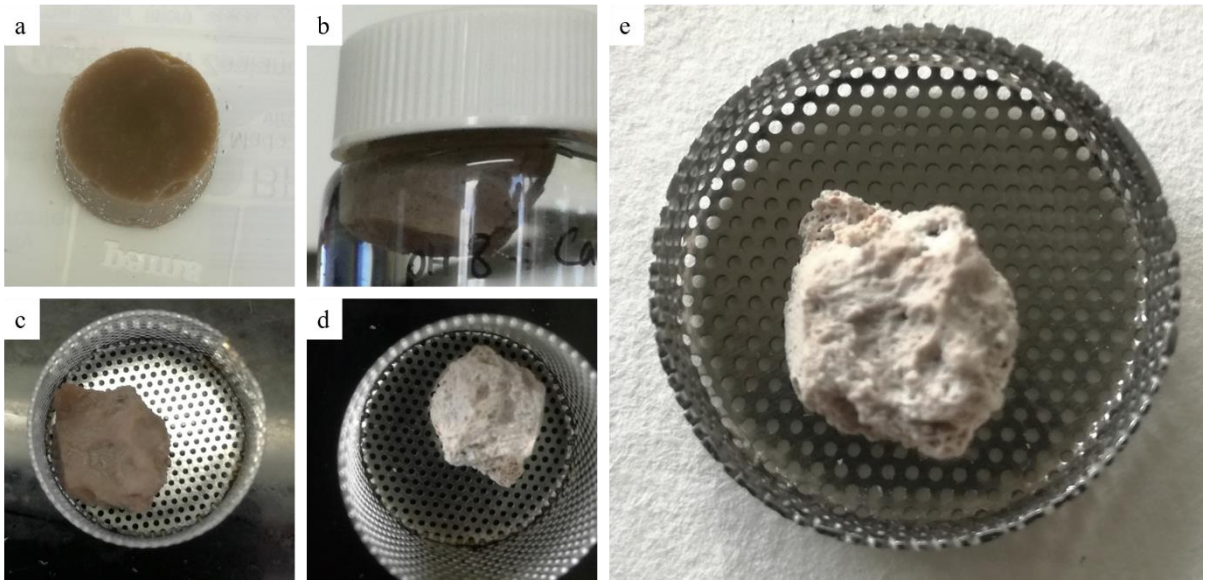

Figure 7.43: *CSM-protein gel prepared at pH 8 and with 20 mM $CaCl_2$ immersed in* ***(a)*** *97 % ethanol and* ***(b)*** *100 % ethanol following 6 days of solvent exchange.* ***(c)*** *Piece of the same gel photographed in 12 mm sample basket after 14 weeks in 100 % ethanol and* ***(d-e)*** *corresponding dried aerogel directly after supercritical drying*

7.4.3. Characterisation of supercritically dried CSM protein-Ca^{2+} aerogels

The aerogel microstructure was analysed using Scanning electron microscopy (SEM), revealing a significant change of microstructure in the supercritically dried aerogels (**Figure 7.44**) as compared to the cryogels from earlier studies (**Figure 6.40**). The bulk of the aerogel sample appears quite solid with minimal porosity when viewed at low magnification (**Figure 7.44 a, d**). However, higher magnification reveals images of a mesh-like gel network featuring sub-micron 'strands' of protein (**Figure 7.44, b-c, e-f**). The mesh-like aerogel structure is reminiscent of nanofibrillar networks in polysaccharide aerogels (see **Figure 2.8**), although denser and having an appearance more like cotton candy rather than a web. The strands are likely composed of protein particles in a 'string of pearl' arrangement as the strands appear 'lumpy' and multi-branched (**Figure 7.44 c, e, f**). Micrographs at x 10, 000 magnification suggesting a width of a few hundred nanometres for the strands (**Figure 7.44 f**) although more powerful microscopy is required to provide clear measurements and better visualise mesoporosity (< 50 nm pore width). Substantial areas of the sample still lack the new microstructure. Parts of the structure appear less porous (**Figure 7.44 b, c, e**) and large 'craters' are also visible, likely from gas bubbles, possibly water, forming in the gels during supercritical heating (**Figure 7.44 a, d**). Improved solvent exchange with both ethanol and CO_2 can ensure no solvents are left trapped in internal parts of the gel, thereby reducing damage to the microstructure upon supercritical heating. Nevertheless, in revealing a mesoporous microstructure, these first examples of supercritically dried samples promise new potential for the CSM proteins aerogels (see **Section** 7.X.X).

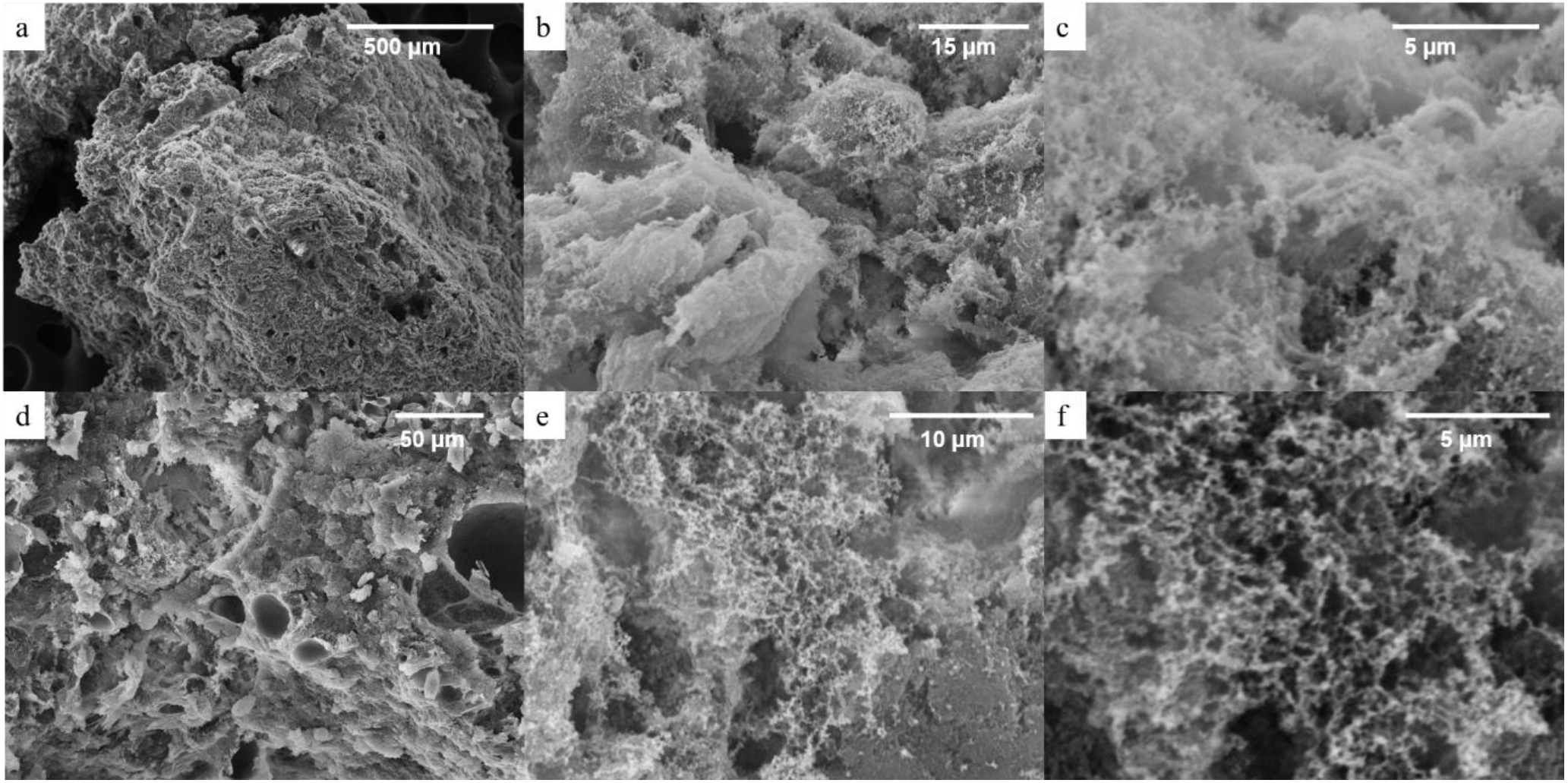

Figure 7.44: *SEM images of the surface* ***(a-c)*** *and cross-section* ***(d-f)*** *of the CSM protein-Ca^{2+} aerogel prepared at pH 10.9 and successfully dried by SC-CO_2 drying using a SamDri - 795 CP dryer. Micrographs were taken at x 100 (a), x 600 (d), x 2500 (b), x 5000 (e), and x 10,000 (c, f) magnification*

Evidence of the same microstructure is also visible in isolated areas of the pH 10 heat- and Ca^{2+}-treated gel (**Figure 7.45b-c**), which underwent incomplete supercritical drying due to residual ethanol in the sample. However, most of the specimen appeared non-porous and reflects an evaporative drying process (**Figure 7.45a**).

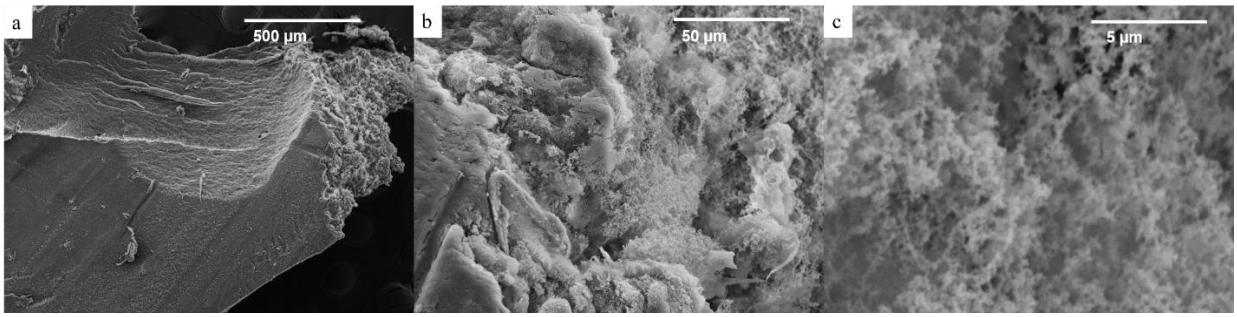

Figure 7.45: *SEM images of the surface* ***(a)*** *and torn cross-section* ***(b-c)*** *of the heat- and Ca^{2+}-treated aerogel prepared at pH 10 and subject to incomplete drying using a SamDri - 795 CP dryer due to residual ethanol. Micrographs were taken at x 100 (a), x 1000 (b), and x 10,000 (c) magnification*

Furthermore, the pH 10 Ca^{2+}-treated sample which underwent supercritical drying but experienced significant shrinkage (refer to **Figure 7.41**), revealed a microstructure comprising of larger particles (≈ 500 – 1000 nm) in a clear 'string of pearl' arrangement (**Figure 7.46c**), reminiscent of resorcinol-formaldehyde aerogels (see **Figure 2.7**). The shrunken sample also exhibited the more refined mesh-like microstructure in other areas (**Figure 7.46d-e**).

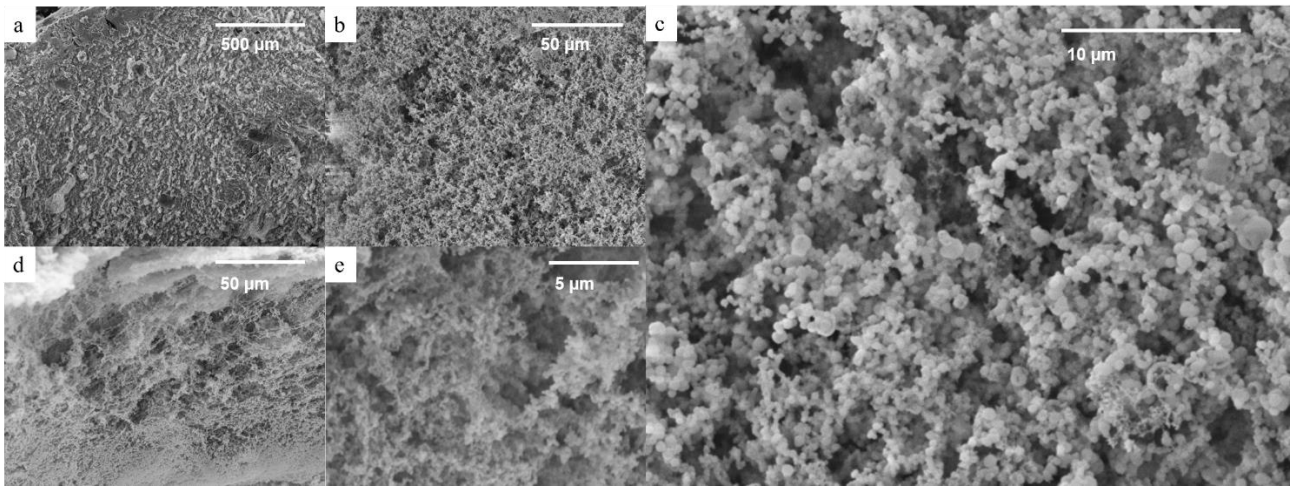

Figure 7.46: *SEM images of the surface* ***(a)*** *and cross-section* ***(b-e)*** *of the pH 10 Ca^{2+}-treated gel after drying using a SamDri - 795 CP dryer and experiencing 50 % shrinkage. Micrographs were taken at x 100 (a), x 1000 (b & d), x 5000 (c) and x 10,000 (e) magnification*

Particle size differences may be due to gelation factors such as pH or may be due to effects of the drying process. Regrettably, possible pH-induced gel structure differences are not sufficiently investigated due to the limited number of successful supercritically dried aerogels. However, the variations in particle sizes observed between the two CSM protein-Ca^{2+} aerogels imaged here (pH 10.9 (**Figure 7.44**) and pH 10.0 (**Figure 7.46**)) suggest pH-induced structure differences warrant further investigation. The dependence of gel microstructures on gelation pH (or other parameters) can clearly be assessed now that preservation of gel structure is possible using the SC-CO_2 drying technique.

The mesh-like, nanoscale gel structure bodes extremely well for improved mesoporosity in supercritically dried CSM protein aerogels. Measurements used to assess mesoporosity include the Brunauer-Emmett-Teller (BET) specific surface area and the Barrett-Joyner-Hallett (BJH) pore volume. BET specific surface area and BJH pore volume measurements are calculated using data from gas sorption porosimetry. Adsorption-desorption isotherms are generated, and mathematical models are applied for calculating surface areas and other values of interest from the measured quantities of adsorbed gas (usually nitrogen) (see **Section 4.4.5** for detailed description of gas sorption porosimetry). The models most widely applied to isotherms generated from aerogels are those of Brunauer, Emmet & Teller (BET theory) and of Barrett, Joyner and Halenda (BJH theory) which seek to account for specific shapes of isotherms from pores of very specific sizes (2 – 50 nm in the case of BET theory, and < 2 nm in the case of BJH micropore volumes). Macropores (> 50 nm) produce adsorption isotherms characteristic of non-porous materials as these pore sizes are effectively too large to facilitate pore condensation. Consequently, nitrogen is adsorbed according to a theory of multi-layer adsorption that occurs without any pore-facilitated condensation mechanisms, described in the Langmuir model.

Nitrogen gas adsorption-desorption experiments were used to establish values for the specific (mesoporous) surface areas, (mesoporous) pore volumes, and average (meso)pore size each in a CSM protein aerogel and cryogel. Early attempts to analyse a CSM protein cryogel revealed the need for method modifications before adsorption-desorption experiments could successfully generate a 'closed-loop' isotherm. Standard operating procedures in N_2 (g) sorption experiments require the

degassing of samples at high temperatures (≈ 200 °C) and low pressure (≈ 5 mT) for 24 hours prior to analysis. Proper degassing is required to ensure sample surfaces are void of any competing adsorbates (*e.g.* water). Biological molecules such as protein undergo thermal degradation from approximately 120 °C (see **Section 6.5.2.2**), therefore CSM protein aerogels would thermally decompose at the standard degassing temperature. However, bioaerogels are also hygroscopic (see **Section 6.5.2**) and therefore require thorough degassing to remove adsorbed water molecules and other contaminant adsorbates. Consequently, degassing protocols for biological aerogels must be modified to much lower temperatures (25 – 60 °C) for extended time periods (*e.g.* up to 10 days) (see **Section 8.7.2** for further discussion of the adaptation of gas sorption porosimetry methods for protein aerogel analysis).

The first successful gas sorption isotherm (**Figure 7.47**) was generated for the CSM protein aerogel prepared at pH 10.9 with 20 mmol/L $CaCl_2$ that had been dried by SC-CO_2 drying (aerogel photographed in **Figure 7.42**). A corresponding cryogel (pH 10.2, 20 mmol/L $CaCl_2$, freeze dried) was also subject to gas sorption porosimetry and generated a small isotherm with a maximum adsorbed gas quantity of 0.0186 mmol/g (**Figure 7.48**). Maximum adsorbed gas for the supercritically dried aerogel was 14.29 mmol/g (**Figure 7.47**), immediately indicating the superior adsorptive capacity of the supercritically dried aerogel.

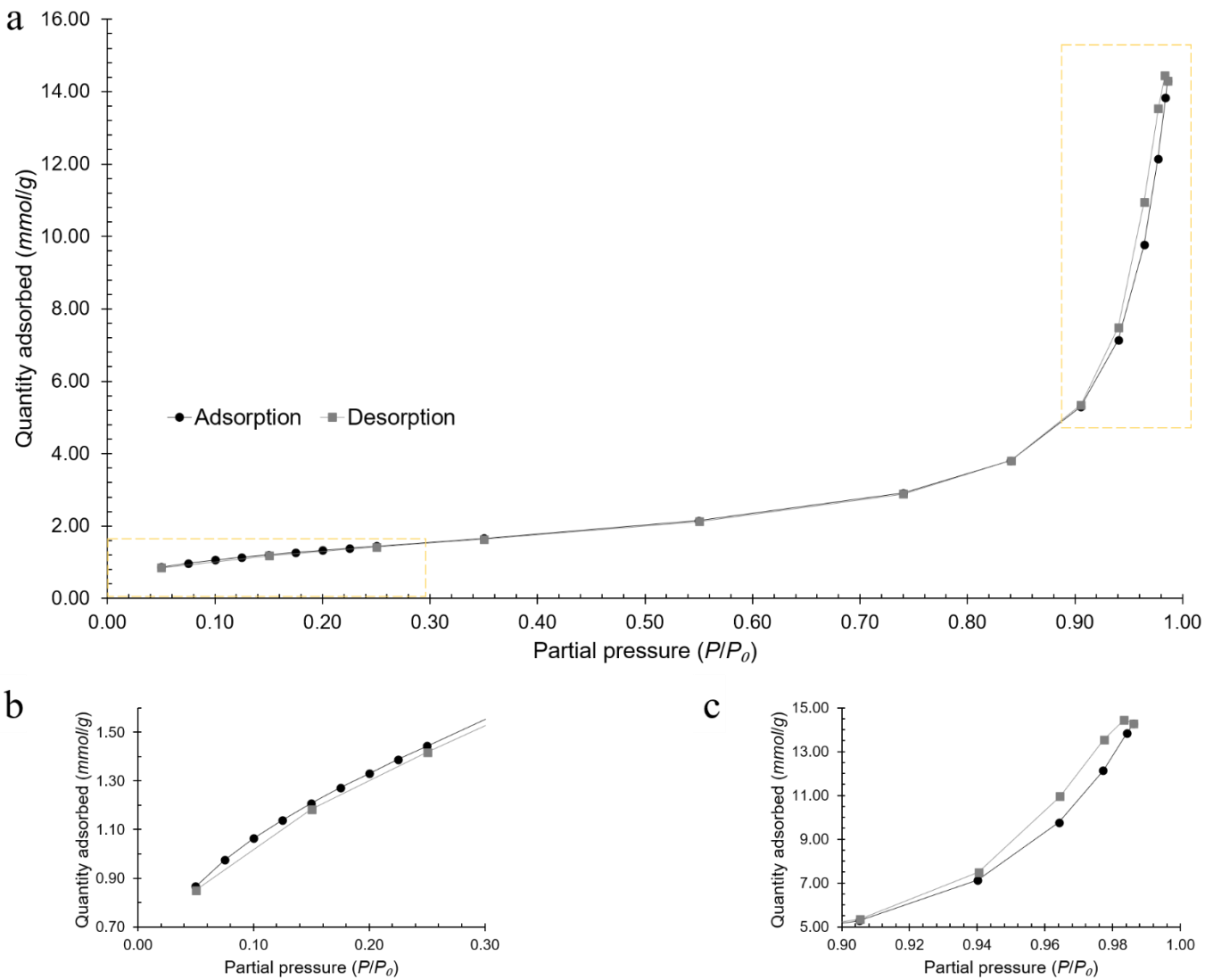

Figure 7.47: *Adsorption-desorption isotherm* ***(a)*** *from nitrogen gas sorption porosimetry on a CSM protein aerogel prepared at pH 10.9 and 20 mmol/L $CaCl_2$ and dried by SC-CO_2 drying. Measurements from 0 – 0.3 P/P_0* ***(b)*** *and 0.9 – 1.0 P/P_0* ***(c)*** *(corresponding to yellow dashed boxes in (a)) are shown enlarged for detail*

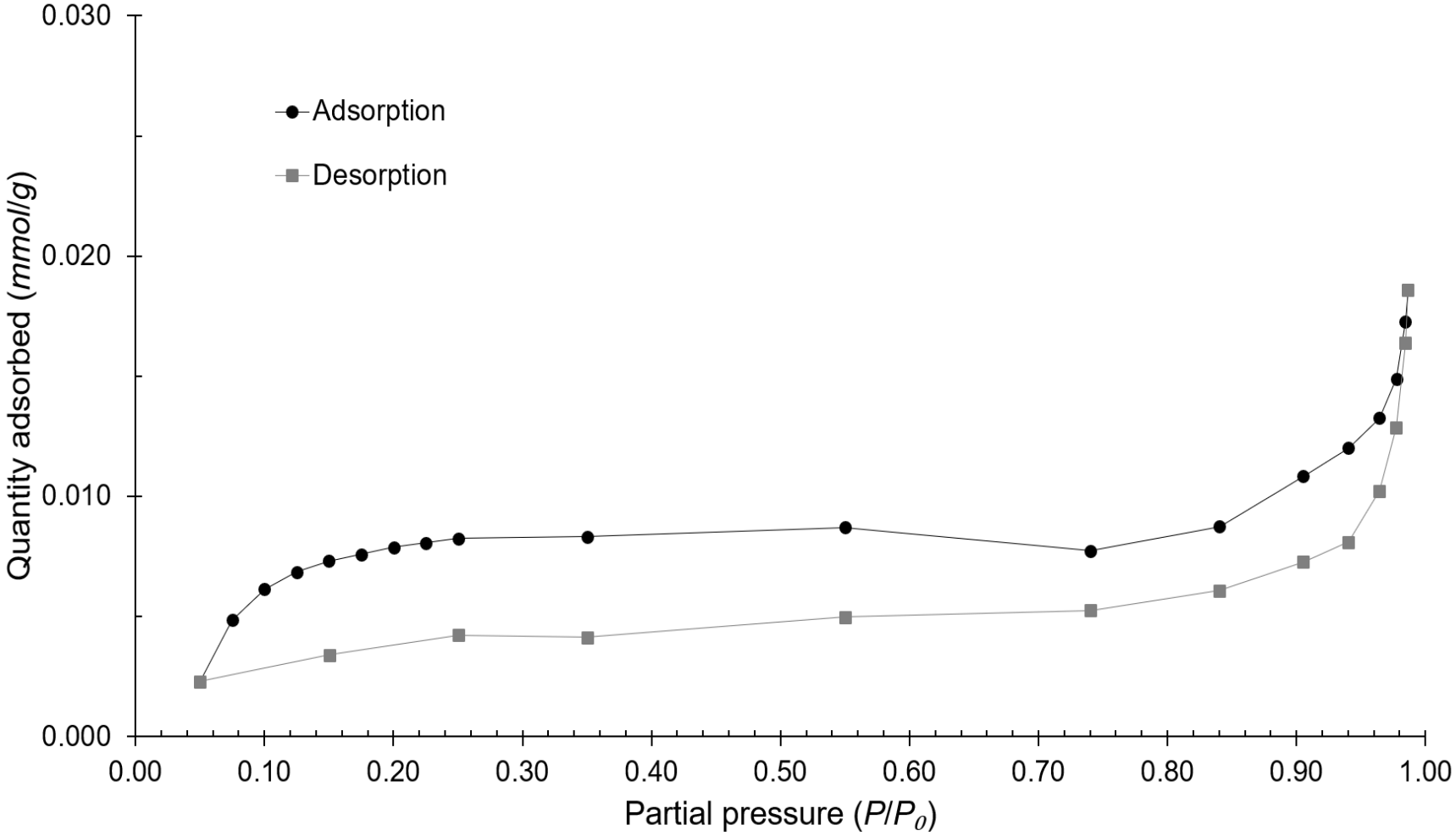

Figure 7.48: *Adsorption-desorption isotherm from nitrogen gas sorption porosimetry on a CSM protein cryogel prepared at pH 10.2 with 20 mmol/L $CaCl_2$ and dried by freeze drying. Maximum adsorption measurement << adsorption measurements for corresponding supercritically dried aerogel in* ***Error! Reference source not found.***

The isotherm data collected for the supercritically dried aerogel showed close agreement between measurements taken during adsorption and during desorption, at the lowest partial pressure and at the highest. A simple visual assessment of this agreement provides a quick assessment of data quality and involves checking that hysteresis loops appear closed. Previous attempts to analyse CSM protein cryogels using the nitrogen sorption technique had revealed a non-closed loop at low partial pressures, indicating incomplete degassing of the sample prior to analysis.

Using BET analysis of the isotherm data the supercritically dried aerogel was revealed to have substantial mesoporous surface area of 113 m^2/g (**Table 7.3**). The freeze dried cryogel measured a BET surface area (SA) of only 0.051 m^2/g, despite a lower density (**Table 7.3**). BET SA measurements confirm that cryogel porosity is restricted to mostly macropores while the supercritically dried CSM protein aerogels can boast a truly mesoporous aerogel structure.

The use of two other models shows how SA measurements can change as larger pore sizes and flat surfaces are incorporated into the models (**Table 7.3**). There is a 2200-fold increase in SA from the cryogel to the aerogel with BET analysis (includes pore sizes 2 - 50 nm), a 1670-fold increase with BJH (1.7 – 300 nm pore sizes), and a 122-fold increase with the use of the Langmuir model (non-porous/macroporous structures). While the clear increase in mesoporosity from cryogel to aerogel is seen using all three models, the lessening disparity as the models incorporate larger pore sizes can be explained by the different pore size distributions of the two samples. Correlation coefficients demonstrate that the supercritically dried aerogel is best analysed using the BET model (over Langmuir) while the cryogel data is better suited to the Langmuir model (though is still a poor fit to both) (**Table 7.3**).

Table 7.3: *Summary of porosity information calculated from adsorption-desorption isotherms from nitrogen gas sorption porosimetry on CSM protein aerogels*

Sample	**Density** (g/cm^3)	**BET analysis** (pores 2 – 50 nm)		**BJH analysis** (pores 1.7 – 300 nm)			**Langmuir analysis** (non-porous/macroporous materials)	
		Surface area (m^2/g):	**Correlation coefficient**:	**Surface area** (m^2/g):	**Pore volume** (cm^3/g):	**Average pore width** (nm):	**Surface area** (m^2/g):	**Correlation coefficient**:
SC-CO_2-dried aerogel (pH 10.9, 20 mM $CaCl_2$)	≈ 0.2	113	0.9999638	130	0.499	15.3	171	0.996204
Freeze dried (cryogel) (pH 10.2, 20 mM $CaCl_2$)	0.117	0.0513	0.7881285	0.078	< 0.001	19.5	1.40	0.898481

Other measurements of interest are the BJH (1.7 – 300 nm sized pores) pore volume and average pore width. Predictably the more mesoporous aerogels have a greater pore volume (0.499 cm^3/g) and smaller average pore width (15.3 nm) than the cryogels (< 0.001 cm^3/g and 19.5 nm, respectively). The BJH model is restricted to analysing pores < 300 nm and therefore does not provide any information about macroporosity. The average pore widths provided by the model are unlikely to represent the true average in the specimens (particularly the cryogel) since macropore sizes are not included.

The use of nitrogen sorption porosimetry has revealed that not only are mesoporous surface areas and pore volumes measurable in CSM protein aerogels but that they are significantly increased in a sample that was supercritically dried successfully. Further gas sorption porosimetry experiments can be used to establish the full range of mesoporous surface area measurements in CSM protein aerogels.

7.4.4. Mechanical properties of freeze dried CSM protein-Ca^{2+} aerogels

Following the success of Ca^{2+}-assisted gelation in CSM protein gels, the amenability of the CSM protein-Ca^{2+} gels to freeze drying was assessed. Cryogels were produced using earlier freeze drying methods (see **Section 6.2.2**) from the various pH 8 and pH 10 gels prepared with heat- and Ca^{2+}-treatments (preparation methods summarised in **Figure 7.27** & **Figure 7.28**). Control samples were also prepared at pH 8 and pH 10 without heat- or Ca^{2+}-treatment. The freeze drying process produced viable cryogels from all preparations (**Figure 7.49**) though interestingly the pH 8 samples prepared with both a heat- and Ca^{2+}-treatment had visibly reduced structural integrity (**Figure 7.49h**). Bulk density measurements confirmed acceptable levels of shrinkage in these cryogels since the densities (**Figure 7.50a**) were within the normal range (0.116 – 0.128 g/cm^3, average shrinkage of 18 – 21 %) of freeze dried CSM protein aerogels from earlier work (see **Section 6.4.1**), with the exception of one specimen which measured no shrinkage. Furthermore, bulk density was not affected by pH or by heat- and Ca^{2+}-treatments during gelation (**Figure 7.50b**).

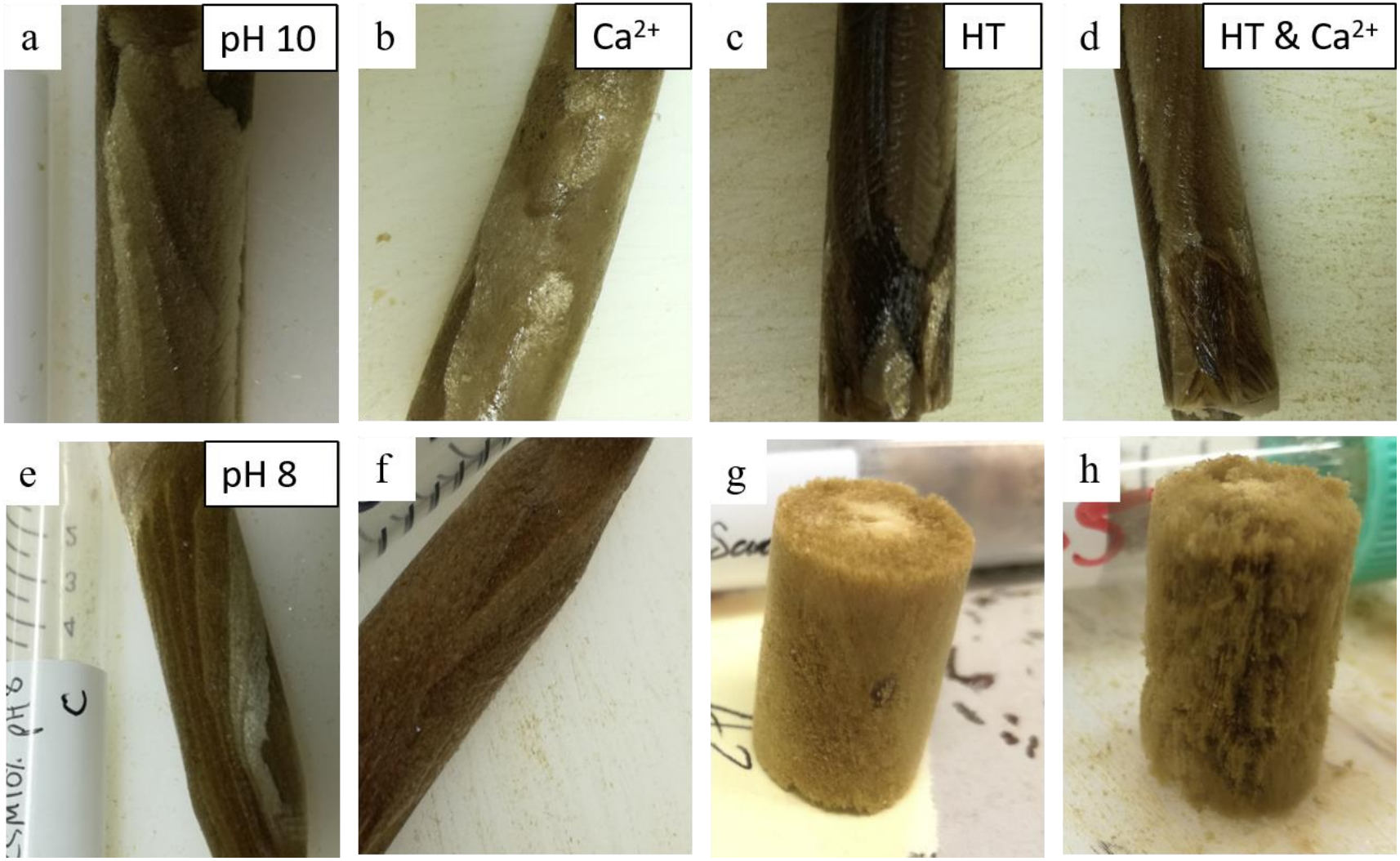

Figure 7.49**: Photographs of CSM protein cryogels (freeze dried) prepared at pH 10 **(a-d)** or pH 8 **(e-h)** with varying gelation parameters. Gelation variables include some gels with 20 mM $CaCl_2$ addition **(b, f)**, a 30 minute heat treatment at 95 °C **(c, g)**, some gels with received both the heat-treatment and the $CaCl_2$ addition **(d, h)** and control samples which received neither treatment **(a, e)

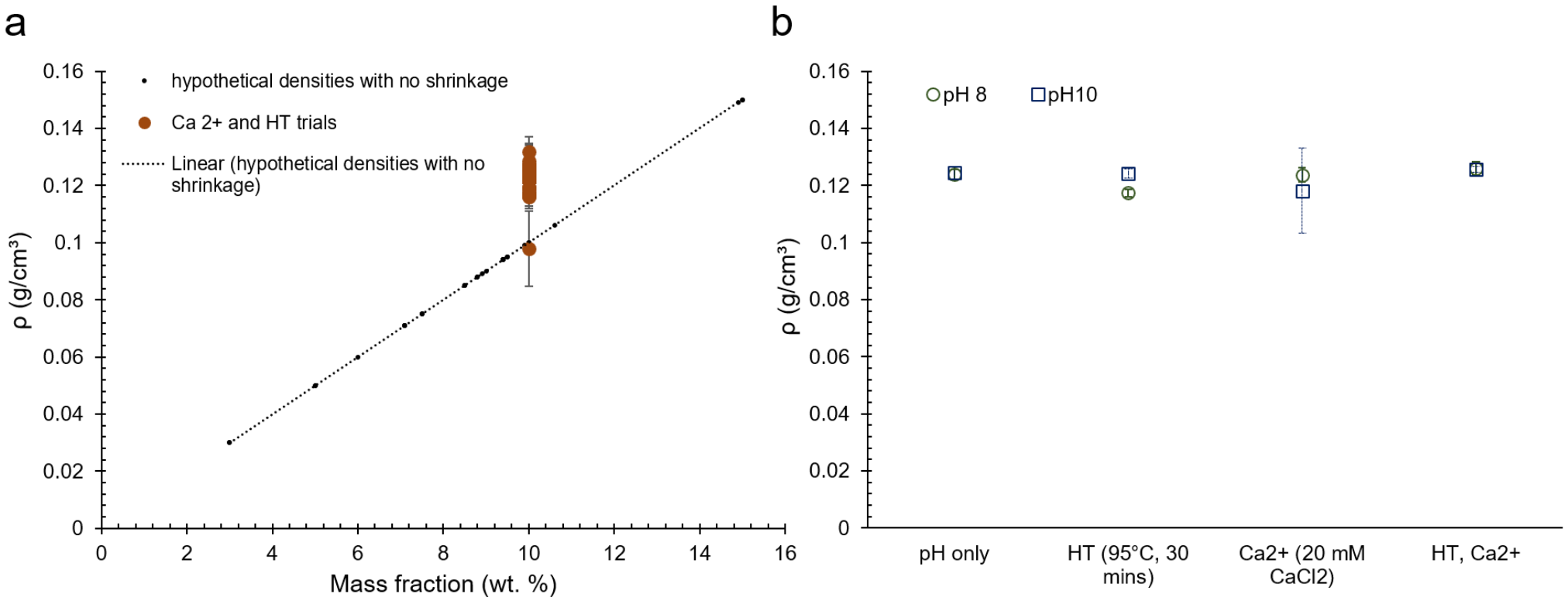

Figure 7.50: *Density of CSM protein-Ca^{2+} freeze dried aerogels as a function of mass fraction* ***(a)*** *and as categorised by gelation conditions* ***(b)***

The specific mechanical properties of the Ca^{2+}- and heat-treated cryogels were assessed using static mechanical testing as in prior studies of pure CSM protein (**Section 6.5.1**) and CSM protein-hybrid cryogels (**Section 7.3.2**). Stress-strain data generated from both the pH 8 (**Figure 7.51**) and pH 10 (**Figure 7.52**) specimens demonstrated the typical curves associated with CSM protein aerogels. Curves featured an initial linear region (sometimes with a 'toe region' (**Figure 7.51a**)) followed by plateau (**Figure 7.51b**) and densification (**Figure 7.52a**) regions.

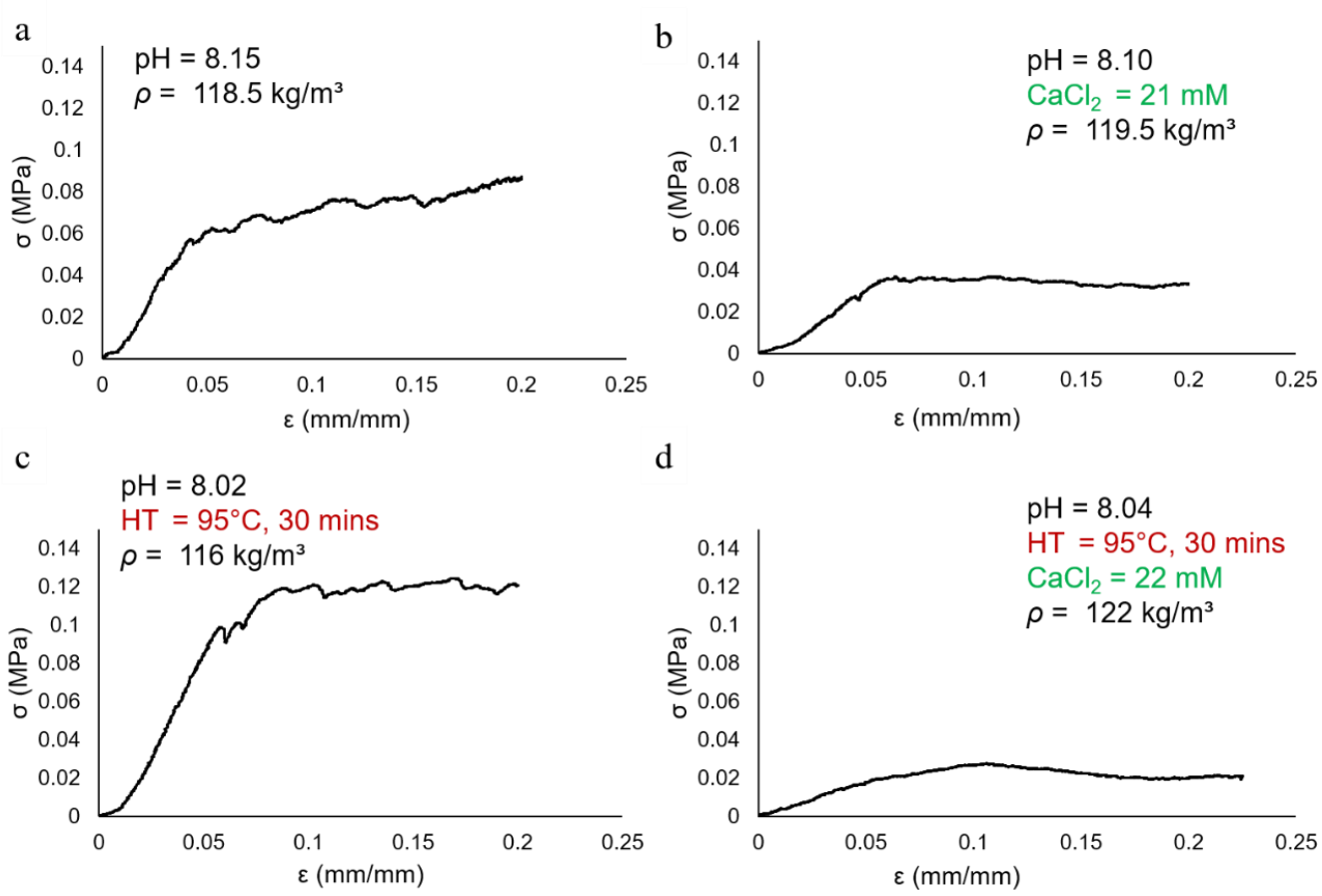

Figure 7.51: *Example stress-strain curves generated from static compressive testing of CSM protein aerogels prepared at pH 8. Specifically: a control sample of a CSM protein aerogel at pH 8.15* ***(a)****, a CSM protein aerogel prepared with a Ca^{2+}-treatment (21 mmol/L $CaCl_2$) (pH 8.10)* ***(b)****, a CSM protein aerogel prepared with a heat-treatment at 95 °C for 30 minutes (pH 8.02)* ***(c)****, and a CSM protein aerogel prepared with both the heat- and the Ca^{2+}-treatment (22 mmol/L $CaCl_2$, pH 8.04)* ***(d)***

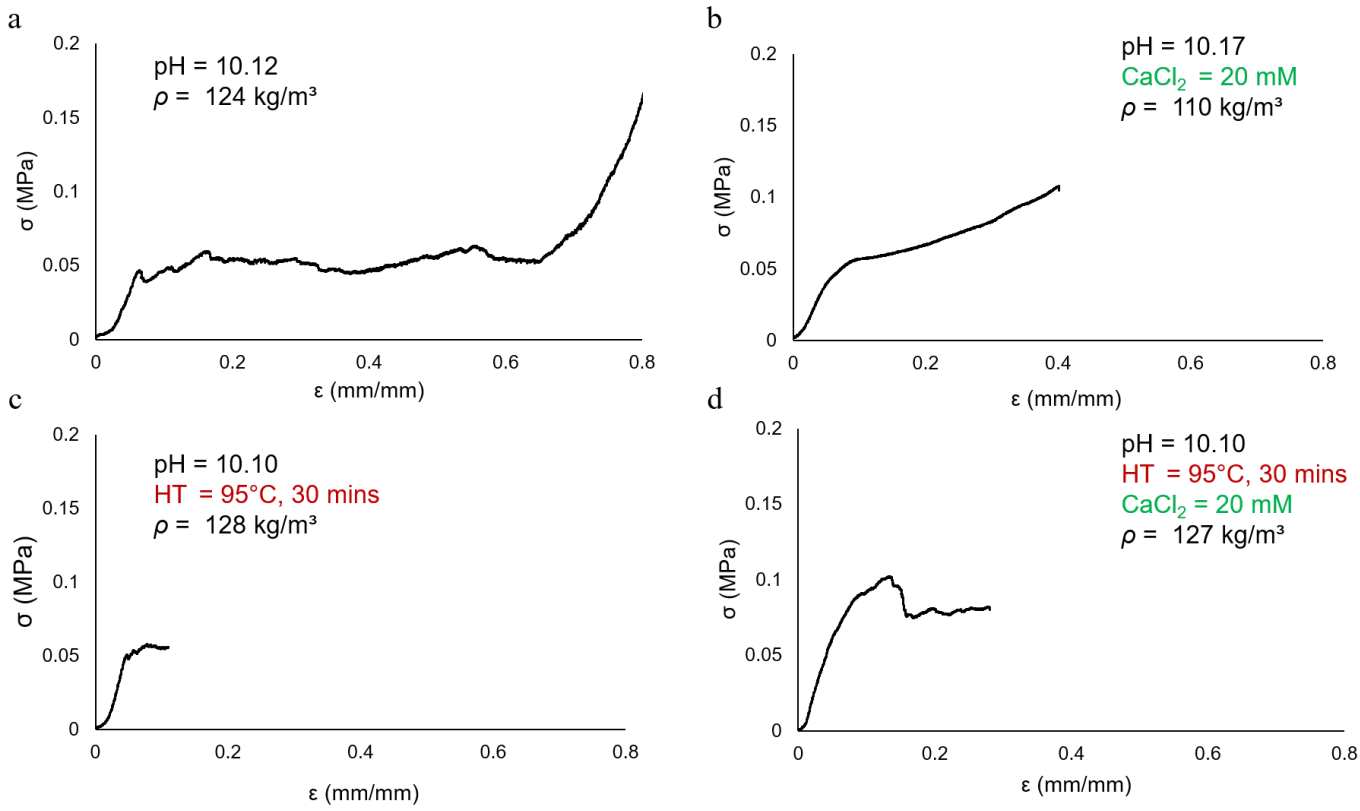

Figure 7.52: *Example stress-strain curves generated from static compressive testing of CSM protein aerogels prepared at pH 10. Specifically: a control sample of a CSM protein aerogel at pH 10.12* ***(a)****, a CSM protein aerogel prepared with a Ca^{2+}-treatment (20 mmol/L $CaCl_2$) (pH 10.17)* ***(b)****, a CSM protein aerogel prepared with a heat-treatment at 95 °C for 30 minutes (pH 10.10)* ***(c)****, and a CSM protein aerogel prepared with both the heat- and the Ca^{2+}-treatment (20 mmol/L $CaCl_2$, pH 10.10)* ***(d)***

An analysis of specific compressive moduli and strengths in cryogels prepared at pH 10 reveal a similar trend to that observed in rheological data (see **Section 7.4.1**): the use of $CaCl_2$ increases cryogel strength and stiffness (**Figure 7.53a**). However, the effect of Ca^{2+}-treatment on cryogel mechanical properties is less pronounced than the analogous effects on wet-gel rheological properties with large variances to average measurements leading to significant overlap in data sets (**Figure 7.53**). Earlier work demonstrates the significant influence of the freeze drying process on cryogel morphologies (compare **Sections 6.4.2** and **7.4.3**) and morphological differences may directly impact aerogel properties. Thus, parameters which influence wet-gel properties (*e.g.* Ca^{2+}-treatment or pH) may have reduced effects on aerogels after drying, particularly in gels dried by freeze drying (cryogels).

Additionally, the effect of Ca^{2+} on the mechanical properties of cryogels prepared at pH 8 is less clear. Initial measurements in pH 8 samples revealed that, while both heat- and Ca^{2+}-treatment increased specific compressive moduli and strengths, a combination of the two treatments resulted in lowered measurements (**Figure 7.53b**, black & blue symbols). A repeated investigation into this effect confirmed the low moduli and strengths in heat- & Ca^{2+}-treated pH 8 cryogels, but also measured reduced values in the samples treated with Ca^{2+} alone (**Figure 7.53b**, grey symbols). A possible destabilising effect of $CaCl_2$ on existing (*e.g.* heat- or pH-induced) gel networks could explain the reduced mechanical properties in certain Ca^{2+}-treated cryogels. The possibility of competing gelation mechanisms in Ca^{2+}-treated CSM protein gels is further discussed in **Section 8.4.2** alongside rheological data and other observations. Cryogel elasticity appears unaffected by Ca^{2+}-treatment with no changes observed in the average elastic limits of Ca^{2+}-treated cryogels prepared at pH 8 or 10 (**Figure 7.53c-d**).

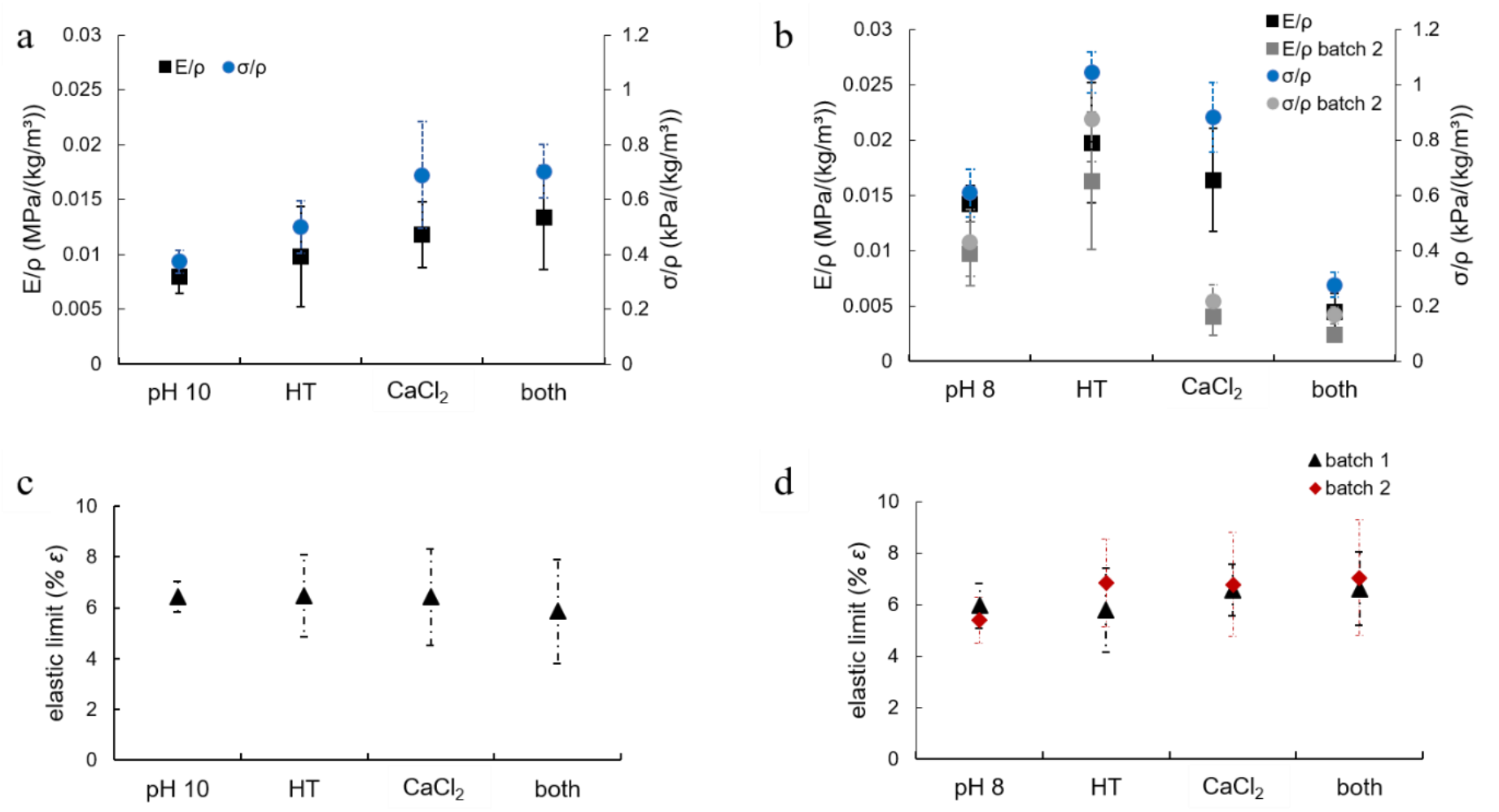

Figure 7.53: (a-b) *Specific compressive moduli (E/ρ, (squares)), specific compressive strengths (σ/ρ, (circles)), and* ***(c-d)*** *elastic limits (% ε) of CSM protein Ca^{2+}- and heat-treated cryogels prepared at pH 10* ***(a, c)*** *or pH 8* ***(b, d)****. A repeat batch of samples at pH 8 was also measured (****(b)*** *grey symbols and* ***(d)*** *red diamonds). Error bars represent standard deviation where n = 4*

7.5. Summary

Chapter 7 has explored how CSM protein aerogels can be tailored through hybridisation with additional biopolymers, by using Ca^{2+}-induced gelation, and through supercritical carbon dioxide ($SC\text{-}CO_2$) drying. Aerogels produced *via* freeze drying (cryogels) are up to 13 times stronger and up to 9 times stiffer when they are hybridised with gelatine (hydrolysed collagen protein). CSM protein cryogels also have increased compressive moduli and strengths when hybridised with collagen fibres (from bovine tendon), chitin (marine animal polysaccharide), and casein (milk protein) and there may be a reduction in elasticity with hybridisation that requires further elucidation. The use of $CaCl_2$ as a gelation agent also appears to improve CSM protein cryogel strengths and stiffnesses though some interplay with competing pH- and heat-induced gelation mechanisms occurs with Ca^{2+}-treatment (see **Section 8.4** for discussion). Additionally, evidence of viscoelastic behaviour and a stiffening upon heating to 80 °C (likely due to change in gel structure analogous to a curing reaction) were identified in CSM protein cryogels, providing further processing information for application of the aerogels in industry (see **Section 8.6.2**).

Chapter 7 also documented the use of $CaCl_2$ as a gelation agent which allowed for the successful production of supercritically dried CSM protein aerogels. The aerogels produced by $SC\text{-}CO_2$ drying possessed a radically different microstructure to analogous cryogels with clear evidence of mesoporosity and a marked increase in specific surface area (0.05 m^2/g in a cryogel to 113 m^2/g in a supercritically dried aerogel). The development of supercritically dried CSM protein aerogels represents a significant milestone towards applicability of the aerogels for a variety of applications. Although specimens were limited, their development allows for continued research that may culminate in the routine production of mesoporous CSM protein aerogels by $SC\text{-}CO_2$ drying. The demonstrable increase in BET surface area makes CSM protein aerogels truly viable candidates for applications that require high specific surface areas (see **Section 8.6.2**) and progress the use of 'off-the-shelf' critical point dryers as tools in bioaerogel research (see **Section 8.7.2**).

The improvements described in Chapter 7 further the potential of CSM protein aerogels in applications as diverse as drug/active molecule delivery, soft tissue or bone biomatrix for regenerative

healing and packaging while broadening the scope for continued research on CSM protein gels and protein-based aerogels. Hybridisation studies can be progressed further by introducing crosslinking catalysts (*e.g.* the transglutaminase enzyme) or molecules (*e.g.* glutaraldehyde) and by introducing additional analyses (*e.g.* Transmission Electron Microscopy, Fourier-transform Infrared Spectroscopy, NanoIR-AFM and Differential Scanning Calorimetry) to conclusively confirm the presence of covalently-crosslinked, gel networks. The current investigation does not include application-specific studies (*e.g.* drug tethering and release studies) that would assess application potential based on measurements such as specific surface areas. Such studies are the logical continuation (refer to **Section 9.2**) of the current project which has focussed on the development and tailorability of novel bioaerogels from canola seed meal protein.

Chapter 8

8. Discussion

8.1. Introduction

The development of novel protein aerogels from canola seed meal (CSM) protein has seen the investigation of five central hypotheses (outlined in **Section 3.1**). Principally, this project aimed to develop bioaerogels using canola protein, thereby creating materials which have not previously been seen in aerogel research (**Section 8.2**). The aerogels were expected to be comparable, and possibly competitive, with similar bioaerogels (**Section 8.3**) and reveal unique biochemical properties (**Section 4.1**). During the development it was also expected that a gelation mechanism would be elucidated (**Section 8.4**) and that certain processing-structure-property relationships would be described (**Section 8.6**).

Numerous experimental techniques were employed to address these objectives. Results from these techniques have been divided into three Chapters focussing on (i) the starting material (**Chapter 5**), (ii) the archetypical CSM protein aerogel (**Chapter 6**), and (iii) improving the properties of the CSM protein aerogel (**Chapter 7**). Information from Chapters 5 and 6 address the main goals: developing the aerogels, assessing their competitivity, and understanding the gelation mechanism & tailorability. Biochemical analyses from Chapter 5 provide information about unique biochemical potential while Chapter 7 contributes additional information to questions of competitivity, tailorability, and application potential. Discussions below highlight the key findings from this work and collate information from the various Chapters to address the project hypotheses.

8.2. Aerogels from canola seed meal protein

Canola seed meal (CSM) protein was reliably extracted from raw canola seed meal, manipulated into a variety of gels using aqueous chemistry, and successfully dried into low-density, porous structures known as aerogels. Over two hundred individual samples of CSM protein aerogels were produced by freeze drying (cryogels) while two aerogels (with others of lesser success) were produced using supercritical carbon dioxide (SC-CO_2) drying.

8.2.1. Wet-gels

Successful extraction of protein from CSM was achieved at the outset of the project using two well referenced aqueous extraction methods. The revelation that the simpler and faster 'alkali-acid' extraction method produced greater yields boded well for continued production and future manufacturing possibilities. Polypeptides in the extract, separated by molecular weight, were attributed to three dominant and well-researched proteins from the *Brassica* genus: cruciferin, napin, and oleosin. Interestingly, most of these polypeptides (as categorised by molecular weight) were identified as the protein cruciferin or one of its multimers or subunits. A heavy cruciferin presence is reflective of some literature evidence where up to 60 % of the total protein content is cruciferin (see **Section 2.3.2**). However, minimal detection of napin raises queries around extraction efficiency and the possibility of acid-soluble proteins being discarded during extraction. Further effort to optimise the protein extraction process is warranted if manufacture is to be upscaled. Additionally, future researchers or manufacturers may wish to explore whether preferential extraction of the cruciferin protein has occurred in this work. Happily, the cruciferin content was considered beneficial for aerogel research since cruciferin is known to form gels more readily than other CSM proteins (refer **Section 2.3.3**). The extracts were therefore deemed fit for purpose in this project and molecular components were not examined further.

The production of CSM protein wet-gels was predictably successful using the cruciferin-rich extracts. Aqueous chemical methods such as pH manipulation and heat-treatments proved to be fundamental

tools for gelation. Indeed, gelation success was so profoundly dependent on the pH of the solution that pH values were optimised to 8.0 ± 0.2 where free-standing gels were required (*e.g.* for solvent exchange in ethanol). CSM protein gels were best optimised where a heat-treatment or Ca^{2+}-addition was combined with a pH of 8 (resulting viscosities > 10,000 mPa.s). Ca^{2+}-addition also proved effective at broadening the useful pH range (pH = 8 - 11) by increasing viscosities 20- to 100-fold. Generally, the gelation of CSM protein in this work was a success but was more difficult than expected. Literature descriptions of facile gelation in CSM protein extracts (see **Section 2.3.3**), especially cruciferin-rich extracts, suggest that a broader pH range than described here is usually amenable to gelation, particularly where heat-treatments are used. Contrastingly, heat-set CSM protein gels in this project were limited to the highly optimised pH range (8.0 ± 0.2) with heat-treatments ineffective at increasing viscosity in gels prepared at pH 7, or 9 – 12. Changes in optimal pH ranges for gelation may be attributed to varying protein profiles and/or purity in extracts. CSM protein extracts may contain a range of protein types alongside impurities such as salts and minerals, phytates, phenolics, glucosinolates, tannins, residual carbohydrates, and residual oil (see **Section 2.3.2**). The extracts used in this work are not highly purified like isolates nor subject to nitrogen content analyses. Consequently, the role of non-proteinaceous components in gelation remains to be investigated. Other studies suggest some pH-dependent interference from phenolic contaminants is detrimental for gelation [296]. Additionally, later solvent exchange experiments with CSM protein gels reveal that small, colour-bearing molecules such as tannins probably persist in the extract and gels (see **Figure 7.37**). Furthermore, the effect of the protein profile on gelation has also not been examined other than to note that gels in this work appear to contain a high cruciferin content.

Considering the successful gelation observed with CSM protein, despite pH restrictions, this work indicates to future manufacturers that a careful understanding of protein profiles and/or extract impurities is not required for basic gel production using aqueous chemistry. Additionally, rheological information generated from these gels can be directly applied in future research or manufacture. The use of $CaCl_2$ as a gelation agent in CSM protein is a novel gelation approach for canola protein. Thus, documentation of CSM protein-Ca^{2+} gel viscosities, shear thinning behaviour, critical strains, and

storage moduli, may assist in experimental or manufacture design of future canola gel studies and products. Use of exclusively aqueous methods to produced canola gels may also benefit researchers outside of the aerogel field where focus is on the environmentally friendly production of bio-based gels (*e.g.* food, biodegradable adhesives/films, medical hydrogels).

8.2.2. Aerogels

Following the revelation that pH values must be highly controlled to induce free-standing gels, it was expected that aerogel production from CSM protein gels might be similarly restricted to a narrow pH range. However, the compensatory discovery that even non-gelled suspensions (viscosity < 100 mPa.s) can retain monolithic shapes and volumes after freeze drying in a vessel, broadened the useful pH range for cryogel production. Indeed, so few technical challenges were encountered during cryogel production that 244 specimens were produced for this thesis. Eventual up-scaling of cryogel production seems highly viable given the amenability of the gels to freeze drying.

The production of the low density (< 0.13 g/cm^3), highly porous cryogels signalled an important progress in the merging of aerogel technology with canola protein science. The addition of CSM protein to the scant collection of proteins used in aerogel manufacture furthers the market potential of this canola oil industry co-product. Bioaerogel researchers may be emboldened to experiment further with sustainable, affordable, plant proteins in aerogel production. Meanwhile canola researchers may now add aerogels to the repertoire of non-food uses for canola seed meal. This thesis also demonstrates the use of a naturally sourced biopolymer to produce aerogels using only aqueous chemical methods. Thus, any future aerogel products to arise from this work, may provide an environmental advantage over many competing aerogels.

Probably the greatest highlight of the project was the development of supercritically dried CSM protein aerogels, and the subsequent morphological improvements endowed on the aerogels. Many more challenges were met during the development of the supercritically dried aerogels than for freeze dried samples. A key achievement was the surmounting of low viscosities using $CaCl_2$ as a gelation

agent. Subsequent free-standing gels were both amenable to a modified solvent exchange process and impervious to the ethanol-induced shrinkage commonly seen in bioaerogels. The successive supercritical drying of two alcogels demonstrated that CSM protein aerogels with truly mesoporous microstructures are viable. Aerogel production by supercritical carbon dioxide (SC-CO_2) drying remains restricted to gels with pH values at or near 8 or with $CaCl_2$ addition but is nevertheless achievable with canola protein. The work provided a clear directive for future optimisation of the SC-CO_2 drying process in the production of CSM protein aerogels, but importantly, the initial innovation was achieved.

Morphological characterisation of the CSM protein cryogels and aerogels established an understanding of their densities, porosities, pore size distributions, BET specific surface areas, specific (meso)pore volumes, and gel network microstructures. Morphological information of CSM protein aerogels can be directly compared with other aerogels to establish the relevance of canola protein in the aerogel field (see **Section 8.3.1**). Furthermore, a clear connection between microstructure and processing parameters, principally the drying process was observed. The dependence of pore size distributions on drying methods is commonly noted in aerogel research and was expected in CSM protein gels. However, the possible influence of aqueous gelation parameters on morphology (**Section 8.6.1**) suggests that 'green' chemical methods may bring additional tailorability to protein aerogels.

Mechanical properties, gas adsorptivities, and thermal behaviour in the aerogels were also chosen for analysis. Arguably of more relevance than morphological data, information about aerogel properties is also used to place the CSM protein aerogels in context with other aerogel types (**Section 8.3.2**). A key tenant of materials science that underpins the characterisation of these aerogels is the concept of processing-structure-property relationships. Alongside gel rheological properties and aerogel morphological information, characterisation of aerogel properties can be used to assess the effects of processing methods on the gel-aerogel system. Processing-structure-property relationships become useful tools for manufacturers looking to tailor aerogels for specific purposes (explored in **Section** 8.6).

8.3. CSM protein aerogels in context

Chapter 2 has revealed how protein-based aerogels are a comparatively small segment of aerogel research with only a recent interest in their development. However, the combined characteristics of being sustainably sourced, biodegradable, (sometimes) edible, and chemical specificity make proteins interesting candidates for the development of aerogels that expectantly share these characteristics. The challenge within protein-based aerogel research is to achieve porosities and properties that are comparable to other aerogels. The following summaries compare the morphologies and properties of CSM protein aerogels with those described for other protein aerogels, bioaerogels, and more broadly with representative non-bioaerogels.

8.3.1. Morphology

A comparison of all aerogels should begin with density. Low-density is a defining characteristic of all aerogels. Density-specific properties such as specific surface areas and strength-to-weight ratios provide aerogels with their pioneering advantages in many applications. Bulk density measurements from CSM protein aerogels (0.037 – 0.2 g/cm^3) fall well within the usual range of aerogel densities (from 0.003 g/cm^3 to 0.6 g/cm^3) and are on average (0.13 g/cm^3) quite low compared to most aerogels (**Table 8.1**). Like in other aerogel types, the use of freeze drying generates lower density structures than those prepared from supercritical drying but at the cost of the high specific surface areas (**Table 8.1**). The change in BET surface area associated with changing the drying technique is due to the well documented shift in pore size distributions towards larger macropores. Despite higher overall porosities in freeze dried aerogels, large pore sizes due to ice crystal growth do not contribute to BJH pore volume analyses, resulting in lower measurable pore volumes [119]. The shift to mesoporosity with the change from freeze drying to supercritical drying was observed in CSM protein aerogels. Consequently, it is important to note the drying technique for each specimen when comparing aerogels due to the vastly different morphologies and subsequent advantages of using SC-CO_2 or freeze drying.

Table 8.1: *Summary of processing information, physical data, and morphological data from CSM protein aerogels (rows 1 - 11), protein and protein hybrids aerogels (rows 12 – 53), polysaccharide aerogels (rows 54 – 71), and non-biobased aerogels and related porous materials (rows 72 – 83)*

Ref.	Aerogel description	wt% total solids	Ratio (multiple polymers)	Drying method	Porosity (%)	Density		Gel network type	Pore size distribution			BET surface area (m^2/g)	BJH pore volume (cm^3/g)	BJH average mesopore width (nm)
						[g/cm^3]	[kg/m^3]		Micro < 2 nm	< Meso <	50 nm < Macro			
this work	CSM protein pH 10	10	-	FD	87.8*	0.122	122	particles	macropores ~ 75 µm			-	-	-
this work	CSM protein, pH 10	3	-	FD	96.3*	0.037	37	-	macropores ~ 150 µm			-	-	-
this work	CSM protein, pH 10	5	-	FD	94.1*	0.059	59	-	-			-	-	-
this work	CSM protein, pH 8	10	-	FD	88*	0.12	120	particles	macroporous			-	-	-
this work	CSM protein, pH 8, HT	10	-	FD	88.3*	0.117	117	-	macroporous			-	-	-
this work	CSM protein, Ca^{2+}, pH 8	10	-	FD	87.7*	0.123	123	-	-			-	-	-
this work	CSM protein-Ca^{2+}, pH 10	10	-	FD	88.2*	0.118	118	-	-			0.0513	< 0.001	19.5
this work	CSM protein-Ca^{2+}, pH 10-11	10	-	SC-CO_2	80*	0.2	200	string-of-pearl particles	mostly mesoporous		macropores < 1 µm	113	0.499	15.3
this work	CSM protein-gelatine	10	4:1	FD	87.1*	0.129	129	particular & fibrillar	macropores ~ 50 µm			-	-	-
this work	CSM protein-chitin	15	1.8:1	FD	82.7*	0.173	173	probably particular and fibres but no clear evidence				-	-	-
this work	CSM protein-collagen	10	4:1	FD	88.1*	0.119	119	probably particular and fibres but no clear evidence	macropores ~ 75 µm			-	-	-
[95]	Whey protein isolate (WPI)	20	-	SC-CO_2	-	0.30-0.43	300- 430	'spherical agglomerates' (particles)	mesoporous and macroporous			14 - 447	1.34-1.72	12 - 27
[95]	WPI	20	-	FD	-	0.23-0.30	230-300	particles	mostly macroporous			< 5	n.d.	n.d.
[127]	WPI	10-25	-	FD	-	0.11-0.26	110 -260	-	mostly macroporous			-	-	-
[127]	WPI-alginate-clay / WPI-alginate	15	4:1:1 and 2:1	FD	-	0.047 - 0.129	47 - 129	-	mostly macroporous			-	-	-
[120]	WPI	8	-	FD	-	0.13	130	-	some micro and mesoporous volumes measured		mostly macroporous	2.08	0.0061	-
[120]	WPI-cellulose	9	8:1	FD	-	0.11 - 0.16	110 - 160	-	some micro and mesoporous volumes measured		mostly macroporous	1.72-3.04	0.0025-0.0078	-
[91]	β-lactoglobulin amyloid (WP)	1-3	-	SC-CO_2	98-99.9	0.003-0.03	3-30	fibrillar	-	10 % meso	mostly macroporous	325	2.7	-
[75]	WPI	20	-	SC-CO_2	-	0.285	285	particles	-	-	-	420	-	-

[75]	Casein (with transglutaminase)	10	-	$SC\text{-}CO_2$	-	-	-	-	-	-	-	140	-	-
[138]	WPI	20	-	$SC\text{-}CO_2$	-	0.241	241	-	-	-	-	354	1.55	14
[138]	Casein (with transglutaminase)	10	-	$SC\text{-}CO_2$	-	0.443	443	-	-	-	-	48	0.28	13.4
[42]	Silk fibroin (SF)	5.8 - 17	Salt-leaching/Xerogel/FD		87-99	0.03 - 0.12	30 - 120	silk aggregates	macroporous - 15 - 155µm			-	-	-
[102]	SF	4-10	Salt-leaching/Xerogel		85-96	-	-	fibrous	Large macropores (400 - 900 µm)			-	-	-
[110]	SF	5	Salt-leaching		-	-	-	particles	macroporous (380 - 390 µm)			-	-	-
[128]	SF	4	-	$SC\text{-}CO_2$	-	0.058	58	-	mostly mesopores up to 130 nm			424	-	20
[129]	SF	4 - 13	-	$SC\text{-}CO_2$	-	-	-	fibrillar	mesoporous and macroporous			-	-	-
[92]	SF	2-6	-	$SC\text{-}CO_2$	-	bead-and-string′ (2 wt %) 'leaf-like' (6 wt %) but nano-scale fibrils			mostly mesoporous		With some macropores	266	1.6	11
[92]	SF	2-6	-	FD	-	-	-	leaf-like	macroporous			49	0.05	3
[96]	SF	10 - 15	-	$SC\text{-}CO_2$	88-93	-	-	fibrillar	mesoporous and macroporous			-	-	-
[130]	SF-graphene	0.2	1:1.5, 1:4, 1.5:1, 4:1	FD	-	-	GO sheets with SF block association		1-160 nm mesopores within large macroporous sheets			180.7	-	11
[137]	SF-PD/Pt/Au	4	-	$SC\text{-}CO_2$	-	-	-	nanofibrils with nano particles	mesoporous and macroporous			268	-	-
[126]	SF	3	-	$SC\text{-}CO_2$	99	0.02	20	fibrous	mesoporous and macroporous			412	49.7	482.7
[126]	SF-PMSQ (silicon)	8.4	1:6.7	$SC\text{-}CO_2$	97	0.08	80	string-of-pearl particles	mesoporous and macroporous			900	10.9	53.6
[125]	Clay-SF	12.5	2.2:1	FD	-	0.121	121	-	macroporous			-	-	-
[98]	Soy protein isolate (SPI)-tannin - formaldehyde	14	6.45 : 3.2 : 1	$SC\text{-}CO_2$	84-88	0.19-0.25	190 - 230	filamentous structure	3-4%	40-50%	40-60%	384-478	3.31-4.67	30-40
[114]	SPI	-	-	FD	-	-	-	-	macroporous			0.12 - 4.49	0.001-0.009	8-40
[125]	Clay : Soy protein 'silk' : PVOH	12.5	2:2:1	FD	-	0.093	93	-	macroporous			-	-	-
[131]	SPI-cellulose	8	range from 0:1 to 1:0	FD	92.7	0.111-0.115	111-115	fibrous and 'leaf-like' structures	macroporous			1.9	-	-
[113]	SPI-graphene	-	6:01	FD	-	-	brick and mortar' (graphene = brick, soy protein = mortar)		14%	85%	1%	30 - 119	0.714	10
[104]	Glucose - Ovalbumin	11.5	20:3	Carbonisation	95 -97 %	0.07	70	coral-like' nano,	8 - 24 %	85 - 92 %	low	247-476	0.38-0.7	-

				→ SC-CO_2				branched network						
[94]	Ovalbumin (egg protein)	10 - 15	-	SC-CO_2	-	0.2 - 0.5	200 - 500	particles	mesoporous and macroporous			16-380	0.2-2.4	12-30
[138]	Egg white protein	10	-	SC-CO_2	-	0.179	179	-	-			232	2.28	41.7
[133]	Ovalbumin-cellulose	14	1:2	Carbonisation →FD	-	-	-	branched fibrous network	some microporous volume detected	mostly mesoporous		38	0.18	-
[75]	Egg white protein	10	-	SC-CO_2	-	0.285	285	particles	-			380	-	-
[139]	Egg white protein	15	-	SC-CO_2	-	1.33	1330	particles	mesoporous			252	1.5	24.67
[111]	Gluten (and gluten-cellulose)	11-17	11:1 or 14:1	FD	49 - 93	0.076 - 0.200	76 - 200	-	mostly macro (30 - 73 μm)			-	-	-
[134]	Zein-agar	3-4.5	1:1 - 2:1	FD	-	0.033 - 0.041	33-41	-	mesoporous and macroporous			451	-	43
[48]	Collagen-cellulose	2.3 - 7.3 **	1:1	FD	90 - 95	0.021 - 0.032	21 - 32	fibrillar	mesoporous and macroporous			-	-	-
[136]	Collagen-alginate	3	1:1	SC-CO_2	-	0.043	43	-	mesoporous and macroporous			208	3.24	-
[140]	PLA-collagen-gelatine	-	-	FD	-	-	-	fibrous	macroporous			-	-	-
[121]	Casein	10	-	FD	-	0.11	110	-	macroporous			-	-	-
[121]	Casein-glyceraldehyde-clay	20	2:1:1	FD	-	0.109	109	-	macroporous			-	-	-
[297]	Starch	8	-	SC-CO_2	-	0.14	140	fibrous	mesoporous and macroporous			254	-	-
[298]	Alginate	4	-	FD	66	0.616	616	-	macroporous			16.76	-	-
[299]	Pectin	-	-	SC-CO_2	-	0.2	200	-	mesoporous and macroporous			485	3.62	-
[299]	Alginate	-	-	SC-CO_2	94	0.13	130	-	mesoporous and macroporous			680	4.05	14
[299]	Carrageenan	-	-	SC-CO_2	52	1.48	1480	-	mesoporous and macroporous			230	1.2	10
[299]	Agar	-	-	SC-CO_2	89	-	-	-	mesoporous and macroporous			320	0.3	18
[300]	Cellulose	0.5 - 13	-	SC-CO_2	-	0.069	69	fibrous	mesoporous and macroporous			209	-	-
[301]	Cellulose	3	-	SC-CO_2	92	0.125	125	fibrous	mesoporous and macroporous			290	-	-
[301]	Cellulose-silica	4.7	1.8 : 1	SC-CO_2	87	0.225	225	string-of-pearl	mesoporous			810	-	-
[299]	Cellulose	-	-	SC-CO_2	95	0.008	8	-	mesoporous and macroporous			200	0.5	5
[299]	Chitosan	-	-	SC-CO_2	-	0.38	380	-	mesoporous and macroporous			845	3.5	5
[299]	Chitin	-	-	SC-CO_2	84-92	0.12	120	-	mesoporous and macroporous			560	1.2	10
[161]	Pectin	6	-	SC-CO_2	-	0.09	90	fibrous	mesoporous and macroporous			-	1.14	11
[302]	Agar	-	-	SC-CO_2	-	-	-	-	mesoporous and macroporous			320	0.23	36

[302]	Alginate	-	-	SC-CO_2	-	-	-	fibrous	mesoporous and macroporous			570	1.16	37
[302]	Carrageenan	-	-	SC-CO_2	-	-	-	fibrous	mesoporous and macroporous			200	0.96	18
[302]	Chitosan	-	-	SC-CO_2	-	-	-	-	mesoporous and macroporous			330	0.57	12
[302]	Chitin	-	-	SC-CO_2	-	-	-	-	mesoporous and macroporous			560	1.24	20
[2]	Silica aerogel	0.13 - 15	-	SC-CO_2	-	0.003 - 0.35	3 - 350	particles (2 - 5 nm)	few	mostly mesoporous	small macropores	600 - 1200	-	20
[10]	Silica	-	-	SC-CO_2	-	0.241 - 0.564	241-564	-	mostly mesoporous			140 - 541	-	-
[303]	Resorcinol-formaldehyde (RF)	8-20	-	SC-CO_2	84 - 97	0.10-0.26	100 - 260	string-of-pearl	microporous and mesoporous			-	-	-
[304]	RF - carbonised	50	-	subcritical drying with acetone	-	0.6	600	-	significant micropore volume	mostly mesoporous		654	-	-
[58]	RF	3	-	SC-CO_2	-	-	-	string-of-pearl	25%	mostly mesoporous	small macropores	270	0.36	1.3***
[58]	RF	3	-	Xerogel	-	-	-	string-of-pearl	31%	mesoporous		110	0.13	1.29***
[58]	RF	3	-	FD	-	-	-	fibrous	29%	mesoporous and macroporous		570	0.76	1.33***
[58]	RF - carbonised	3	-	SC-CO_2	-	-	-	-	57%	mesoporous and macroporous		1010	0.79	0.75***
[58]	RF - carbonised	3	-	Xerogel	-	-	-	-	77%	mesoporous		891	0.44	0.54***
[58]	RF - carbonised	3	-	FD	-	-	-	-	51%	mesoporous and macroporous		2650	2.05	0.7***
[305]	Graphene	0.4	-	FD	-	0.006 - 0.016	6-16	GO sheets	-	-	-	-	-	-
[306]	Metal-organic framework		-	-	-	-	-	-	-	-	-	6143	-	-

* assumes protein has skeletal density of 1 g/cm^3

** of collagen only

*** average micropore width

Aerogels can comprise of particulate-based or filamentous/fibrillar gel networks (**Figure 8.1**). Silica aerogels are typically particulate with a mesoporous microstructure (**Figure 8.1a**), while bioaerogels are typically filamentous and have a mix of meso- and macro- pore sizes (**Figure 8.1b-c**). However, many protein-based aerogels are developed from globular proteins which tend to produce aerogels with particulate-based microstructures (**Figure 8.1f**). Certain proteins with a fibrillar quaternity structure (*e.g.* silk fibroin (**Figure 8.1e**)) produce the filamentous gel networks commonly seen in polysaccharide aerogels. Meanwhile, the more macroporous cryogels are can appear web-like where fibrous precursors are used (*e.g.* cellulose (**Figure 8.1c)**) or comprise of unidirectional 'cells' where non-fibrous precursors are used (*e.g.* whey protein isolate (**Figure 8.1d**)).

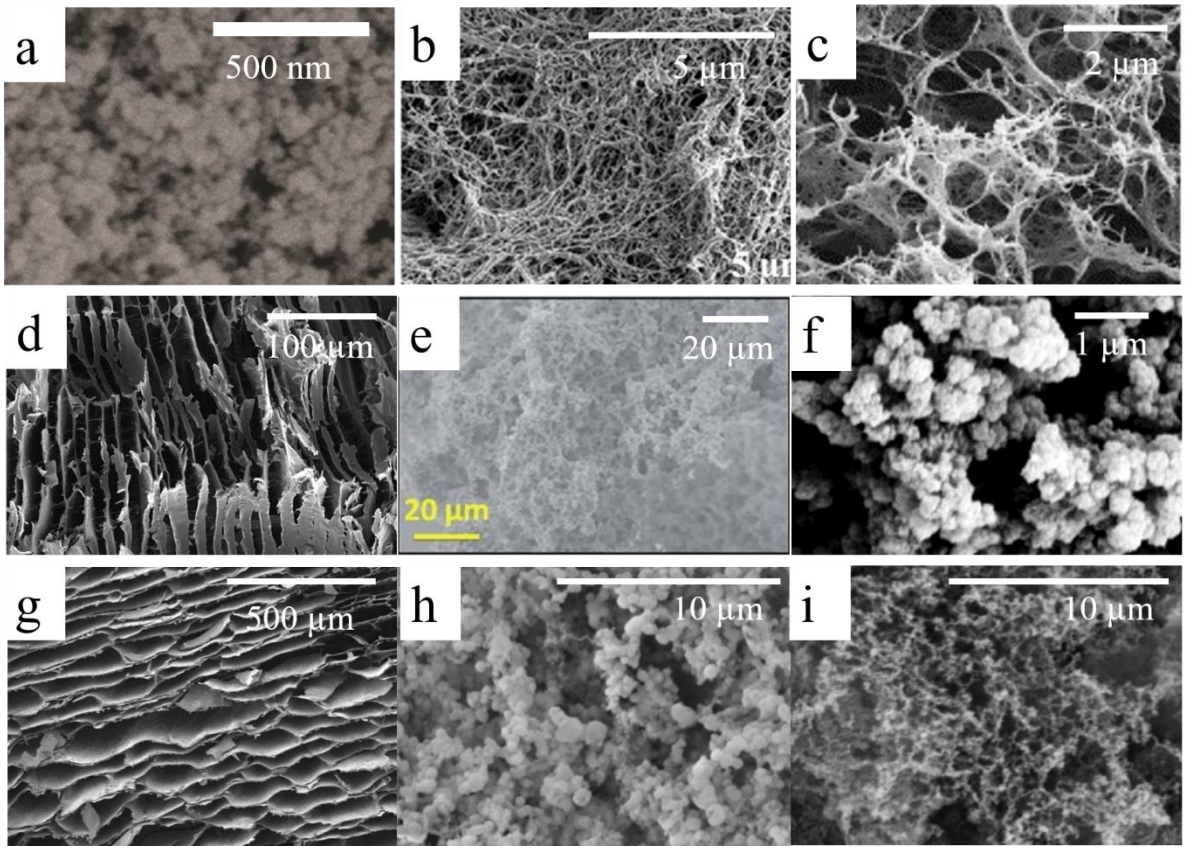

Figure 8.1: *Scanning Electron micrographs from* ***(a)*** *silica aerogel,* ***(b)*** *cellulose aerogel,* ***(c)*** *cellulose cryogel, (d) whey protein isolate (WPI) cryogel, (e) silk fibroin (SF) aerogel, (f) egg white protein (EWP) aerogel, (g) canola seed meal (CSM) protein cryogel, (h-i) CSM protein aerogels. Adapted and reprinted from:* ***(a)*** *[307] Huber, L., et al., Fast and Minimal-Solvent Production of Superinsulating Silica Aerogel Granulate. Angewandte Chemie International Edition, 2017.* ***56(17):*** *p. 4753-4756.* ***(b)*** *[308] Ciftci, D., et al., Lupin hull cellulose nanofiber aerogel preparation by supercritical CO2 and freeze drying. The Journal of Supercritical Fluids, 2017.* ***127****: p. 137-145.* ***(c)*** *[309] Jin, H., et al., Nanofibrillar cellulose aerogels. Colloids and Surfaces A: Physicochemical and Engineering Aspects, 2004.* ***240(1):*** *p. 63-67.* ***(d)*** *[127] Chen, H.-B., Y.-Z. Wang, and D.A. Schiraldi, Foam-like materials based on whey protein isolate. European Polymer Journal, 2013.* ***49****(10): p. 3387-3391.* ***(e)*** *[126] Maleki, H., L. Whitmore, and N. Hüsing, Novel multifunctional polymethylsilsesquioxane–*

silk fibroin aerogel hybrids for environmental and thermal insulation applications. Journal of Materials Chemistry A, 2018. 6(26): p. 12598-12612. ***(f)*** *[94] Selmer, I., et al., Development of egg white protein aerogels as new matrix material for microencapsulation in food. Journal of Supercritical Fluids, 2015.* ***106****(Aerogels: Synthesis and Applications): p. 42-49.* ***(g – i)*** *This work.*

CSM protein cryogels and aerogels present microstructures typical of non-fibrous biopolymers according to drying technique trends. Cryogels have unidirectional cell-like macropores (**Figure 8.1g**) while aerogels have particulate-based *meso*- and *macro*-porous networks. The particles in CSM protein gel networks appear as aggregates in the pore walls of freeze dried cryogels (see **Section 6.4.2**) and as clear spherical building-blocks in supercritically dried aerogels (**Figure 8.1h**). Some particulate-based networks can appear slightly filamentous as the particles associate in a 'string-of-pearl' arrangement. This 'string-of-pearl' microstructure can also be seen in a CSM protein aerogel produced using supercritical drying (**Figure 8.1i**).

Trends associated with the different drying techniques are prevalent throughout the morphological and porosimetry data collected on the CSM protein aerogels. The BET specific surface areas measured in CSM protein aerogels are predictably determined by the drying technique (cryogel < 1 m^2/g, aerogel > 100 m^2/g, (**Table 8.1**)), although limited measurements were made and the need for further porosimetry analyses is evident (see **Sections 7.4.2** and **7.4.3**). The measured BET surface areas of the two CSM protein samples (one cryogel, one aerogel) are slightly lower than expected considering expectations based on other aerogels (black circles, **Figure 8.2b**). Lower measurements of BET surface areas in this work suggest that optimisation of the CSM protein aerogels is needed before competitive specific surface areas can be attained.

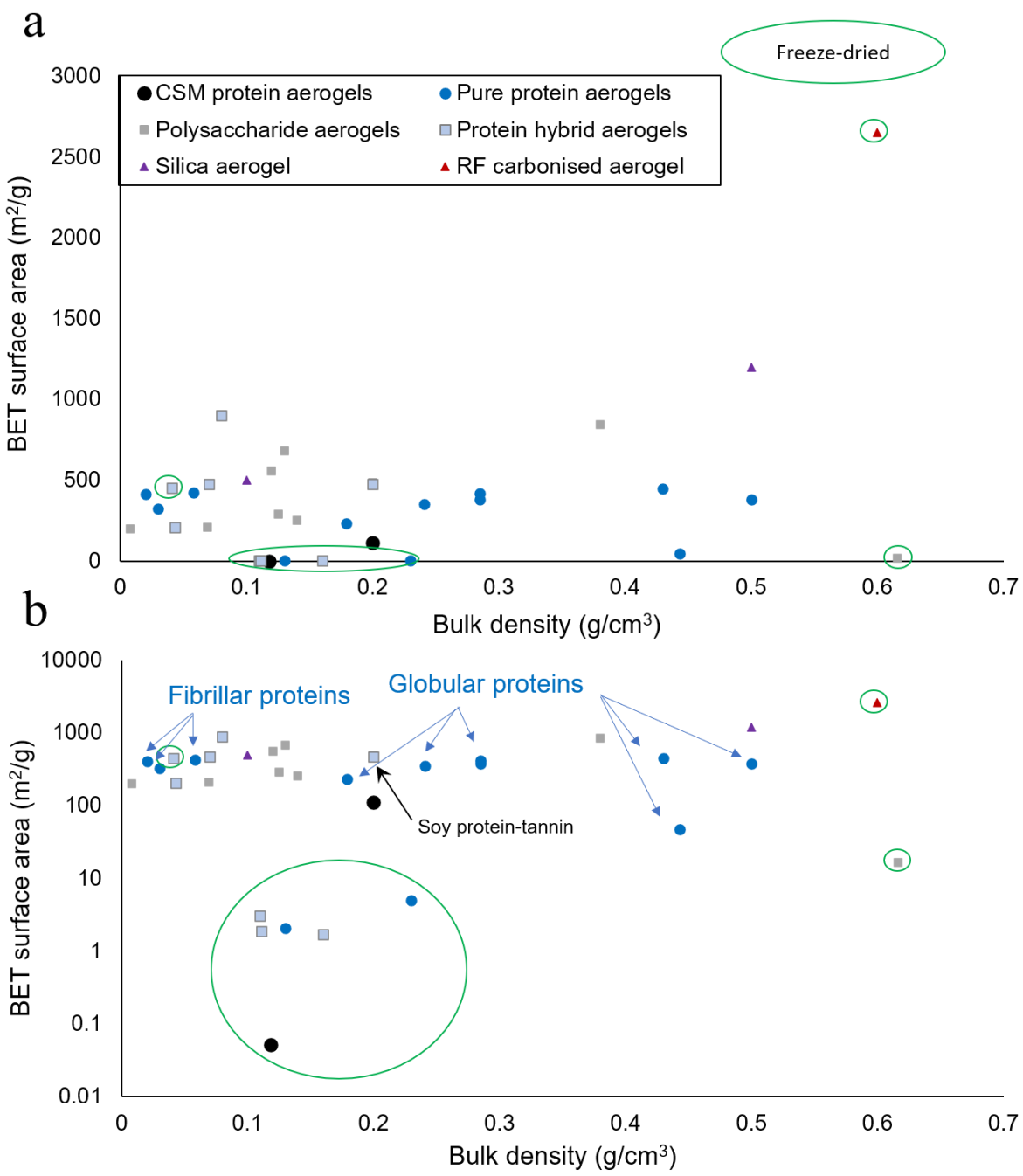

Figure 8.2: (a) *Specific surface areas determined by BET-N_2 sorption analyses as a function of density (ρ) for CSM protein aerogels (black circles), other protein aerogels, and selected non-proteinaceous aerogels (refer to legend) as referenced in* ***Table 8.1****. Aerogels are prepared by supercritical drying except where indicated as freeze dried by green rings.* ***(b)*** *Data from (a) presented on a logarithmic scale for BET surface area and protein aerogels are identified as comprising either fibrillar or globular proteins*

Interestingly the protein quaternary structure may also play a role (**Figure 8.2**). Particle-based networks seen in other protein aerogels made from globular proteins include those from milk (whey, casein), soy, and egg (ovalbumin/egg white isolate) (**Table 8.1**, **Figure 8.1f**). The protein aerogel

literature also features aerogels made from fibrillar proteins (β-lactoglobulin amyloid fibrils, silk fibroin, collagen) or those hybridised with fibrous polysaccharides (cellulose, agar). Resulting aerogels have fibrillar gel networks (**Figure 8.1e**) and generally measure much lower densities while maintaining high BET specific surface areas (where drying methodology is a controlled variable) (**Figure 8.2b**). A single example of a crosslinked soy protein aerogel from the work of Amaral-Labat *et al.* demonstrates how BET surface areas and mesopore volumes in aerogels from globular proteins may be increased at no cost to density [98] (indicated by arrow, **Figure 8.2b**). The soy protein undergoes a controlled crosslinking reaction with tannin to reduce pore sizes and consequently achieve a BET specific surface area (478 m^2/g, ρ = 0.2 g/cm^3) greater than other globular proteins (232 – 354 m^2/g) of similar densities (0.18 – 0.24 g/cm^3). Tannins are present in canola seed meal and may offer a route for further optimisation of CSM protein aerogels using the methods described by Amaral-Labat *et al.* and existing impurities (*i.e.* tannins) in the extract.

Further work on producing and characterising supercritically dried examples of CSM protein aerogels may yet demonstrate competitive BET specific surface areas. Considering the current work is the first report of CSM protein aerogels and their analysis by gas physisorption, a BET surface area of 113 m^2/g is an encouraging start to this research. Additionally, the use of enzymatic crosslinking techniques (*e.g.* transglutaminase) to improve the gel networks may also prove an effective tool for inducing mesoporous microstructures and increasing specific surface areas in the CSM protein aerogels and cryogels.

8.3.2. Properties

The characterisation of CSM protein cryogels focussed on mechanical properties: the compressive moduli, strengths, and elastic limits alongside assessments of cyclic compressibility and viscoelastic behaviour. Comparisons of CSM protein aerogels and other aerogels are made using only density specific compressive moduli and strengths to accurately describe strength-to-weight and stiffness-to-weight ratios (**Table 8.2**). Specific compressive moduli of CSM protein cryogels are generally 0.01 – 0.02 MPa/(kg/m^3) increasing up to 10-fold after hybridisation with other biopolymers (included at 25 – 50 % of the dry weight of the CSM protein). Specific compressive strengths are generally 0.5 – 0.8 kPa/(kg/m^3) with hybrid varieties achieving up to 4.5 (kPa/(kg/m^3). The linear elastic regimes of the CSM protein cryogels (under compression) are generally limited to strains of 6 – 8 % but are reduced to around 4 % when the gels are stiffened and strengthened using gelatine.

Table 8.2: *Summary of processing information, physical data, and mechanical data from CSM protein aerogels (rows 1 - 9), protein and protein hybrids aerogels (rows 10 – 24), polysaccharide aerogels (rows 25 – 37), non-biobased aerogels (rows 38 – 42), and related polymeric materials (rows 43 - 44)*

Ref.	Aerogel description	wt% total solids	Ratio (multiple polymers)	Drying method	Porosity (%)	Density		Modulus [MPa]	Strength [kPa]	Elastic limit (%)	Specific Modulus [MPa/(kg/m³)]	Specific Strength [kPa/(kg/m³)]
						[g/cm³]	[kg/m³]					
this work	CSM protein pH 10	10	-	FD	87.8*	0.122	122	1.10 ± 0.30	56 ± 12	7.9 ± 1.7	0.009 ± 0.002	0.46 ± 0.10
this work	CSM protein, pH 10	5	-	FD	94.1*	0.059	59	0.043	6.9	-	0.00073	0.11695
this work	CSM protein, pH 8	10	-	FD	88*	0.12	120	2.00 ± 0.57	95.8 ± 13.6	7.3 ± 2.3	0.017 ± 0.005	0.80 ± 0.11
this work	CSM protein, pH 8, HT	10	-	FD	88.3*	0.117	117	2.32 ± 0.66	122 ± 9	5.8 ± 1.6	0.012 ± 0.005	1.04 ± 0.07
this work	CSM protein, Ca^{2+}, pH 8	10	-	FD	87.7*	0.123	123	2.10 ± 0.52	113 ± 11	6.6 ± 1.0	0.016 ± 0.005	0.88 ± 0.13
this work	CSM protein-Ca^{2+}, pH 10	10	-	FD	88.2*	0.118	118	1.39 ± 0.39	83.5 ± 31	6.4 ± 1.9	0.012 ± 0.003	0.69 ± 0.19
this work	CSM protein-gelatine	10	4:1	FD	87.1*	0.129	129	19.75 ± 4.3	580 ± 74	3.8 ± 0.07	0.153 ± 0.034	4.50 ± 0.57
this work	CSM protein-chitin	15	1.8:1	FD	82.7*	0.173	173	5.1	175	5.8	0.029	1.01
this work	CSM protein-collagen	10	4:1	FD	88.1*	0.119	119	2.85	216	10.5	0.024	1.82
[127]	WPI	10-25	-	FD	-	0.11-0.26	110 -260	0.18 - 18.2	10 - 100	~ 5	0.002 - 0.071	0.877
[127]	WPI-alginate-clay / WPI-alginate	15	4:1:1 and 2:1	FD	-	0.047 - 0.129	47 - 129	0.48 - 12.9	200 -300	~ 5	0.1	3.66
[120]	WPI	8	-	FD	-	0.13	130	0.38	20 - 30	7	0.0029	0.154
[120]	WPI-cellulose	9	8:1	FD	-	0.11 - 0.16	110 - 160	0.35 - 0.54	45 - 55	7-15	0.0034	0.344
[42]	Silk fibroin (SF)	5.8 - 17	Salt-leaching/Xerogel/FD		87-99	0.03 -0.12	30 - 120	0.01 – 1	5 - 280	-	0.025	2.8
[102]	SF	4-10	Salt-leaching/Xerogel		85-96	-	-	0.07-3.33	11-320	-	-	-
[110]	SF	5	Salt-leaching		-	-	-	0.03 - 0.24	150	9	-	-
[126]	SF	3	-	$SC\text{-}CO_2$	99	0.02	20	0.2	330	-	0.01	16.5
[126]	SF-PMSQ (silicon)	8.4	1:6.7	$SC\text{-}CO_2$	97	0.08	80	5.2	1200	-	0.065	15
[125]	Clay-SF	12.5	2.2:1	FD	-	0.121	121	8.86	108	-	0.0732	0.893
[125]	Clay : Soy protein 'silk' : PVOH	12.5	2:2:1	FD	-	0.093	93	8.5	42	4	0.0914	0.452
[131]	SPI-cellulose	8	range from 0:1 to 1:0	FD	92.7	0.111-0.115	111-115	4.4	50 - 500	10 - 20 %	0.0400	0.450
[140]	PLA-collagen-gelatine	-	-	FD	-	-	-	2.2	-	-	-	-
[121]	Casein	10	-	FD	-	0.11	110	1.6	50	5	0.0145	0.455

[121]	Casein-glyceraldehyde-clay	20	2:1:1	FD	-	0.109	109	5.6	200	6	0.0514	1.835
[301]	Cellulose	3	-	SC-CO_2	92	0.125	125	2.8	9200	80	0.0224	73.6
[301]	Cellulose-silica	4.7	1.8 : 1	SC-CO_2	87	0.225	225	11.5	6300	60	0.0511	28
[161]	Pectin	6	-	SC-CO_2	-	0.09	90	4	-	-	0.0444	-
[10]	Silica	-	-	SC-CO_2	-	0.241 - 0.564	241-564		10 - 4000	-	-	-
[310]	Silica	-	-	SC-CO_2	-	0.24	240	16.4	1010	10	0.0683	4.208
[310]	Silica (reinforced with silica, alumina, or aluminaborosilicate fibres)		20:1	SC-CO_2	-	0.32	320	36	1450	5.3	0.1125	4.531
[303]	Resorcinol-formaldehyde (RF)	8-20	-	SC-CO_2	84 - 97	0.10-0.26	100 - 260	0.1 - 1.3	30 - 350	-	-	-
[305]	Graphene Aerogel	0.4	-	FD	-	0.006 - 0.016	6-16	-	-	75	-	-
[311]	Expanded polystyrene (EPS)	-	-	-	-	0.013	13	2.7	89	< 4	0.207692308	6.846153846
[312]	LDPE (non aerogel)	-	-	-	-	0.925	925	200	-	-	0.216216216	-

P_{air} = 0.001225 g/cm^3 or 1.225 kg/m^3 (International Organization for Standardization, Standard Atmosphere, ISO 2533:1975, 1975)

* assumes polymer has skeletal density of 1 g/mL

The CSM protein cryogels are comparable to other protein-based aerogels and cryogels with respect to compressive mechanical properties, showing close similarity to the mechanical properties of casein-based cryogels (**Figure 8.3** and **Figure 8.4**) [121]. Like morphological features, the specific mechanical properties of the CSM protein cryogels can be grouped alongside others that also comprise of globular proteins. Here, it must be noted that only five other examples of pure protein aerogels providing both density and compressive mechanical data can be found in literature. These examples include cryogels from whey protein isolate [120, 127], casein [121], and silk fibroin [42], and one supercritically dried aerogel from silk fibroin [126]. Whey protein and casein have globular quaternary structures while silk fibroin is fibrillar. Silk fibroin aerogels demonstrate high mechanical performance (σ/ρ = 2.5 – 16.5 kPa/(kg/m^3)) while maintaining ultra-light densities (0.02 – 0.04 g/cm^3). Therefore, it may be possible that CSM protein gels, like other globular protein gels, have limited potential in aerogel structures due to inherent globular protein conformation and the subsequent particulate-based network. The development of fibrillar structures (*e.g.* amyloid fibrils) from globular proteins (as demonstrated by Nyström *et al.* [313]) may present a route for improving porosity and mechanical properties in globular protein-based aerogels, such as CSM protein, without a compromise in aerogel density. Additionally, different drying techniques are likely to impact mechanical properties due to changes in microstructure but comparative mechanical data of aerogels and cryogels from the same source are scarce.

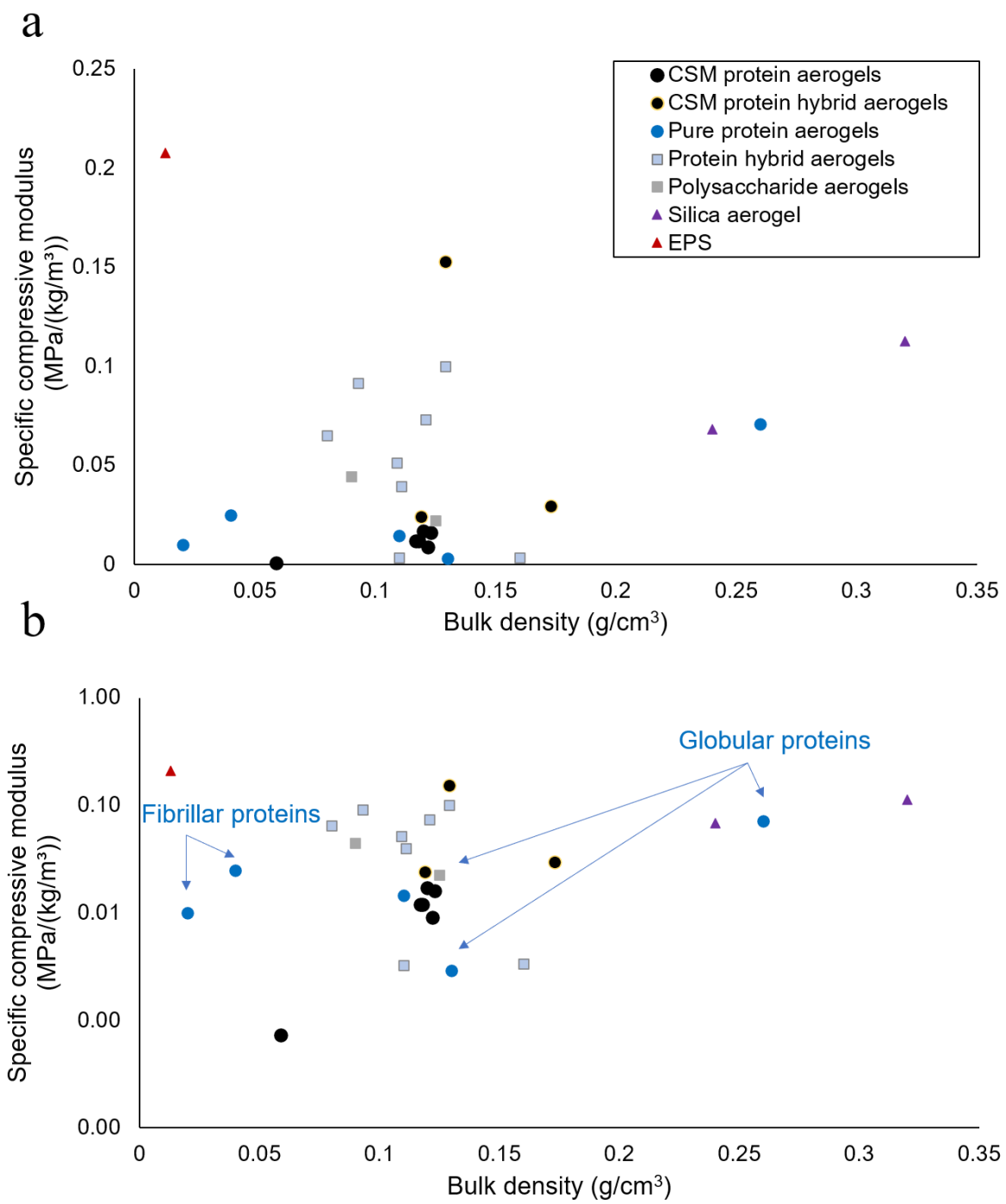

Figure 8.3: (a) *Specific compressive moduli (E/ρ) as a function of density (ρ) measured in CSM protein aerogels (black circles), other protein aerogels, and selected non-proteinaceous aerogels and porous materials (refer to legend) as referenced in* ***Table 8.2****.* ***(b)*** *Data from (a) presented on a logarithmic scale for E/ρ and protein aerogels are identified as comprising either fibrillar or globular proteins*

Further comparative data can be found from protein hybrid aerogels, including whey protein with added alginate and clay [127], whey protein with added cellulose [120], silk fibroin with added silica [126], silk fibroin with added clay [125], soy protein with added clay [125], soy protein with added

cellulose [131], and casein with added clay and crosslinked with glyceraldehyde [121]. **Section 7.3** discusses how the hybridisation of CSM protein with other biopolymers was most effective in the gelatine hybrids. Comparisons with protein hybrids from literature show how CSM protein-gelatine cryogels have competitive specific moduli (0.15 MPa/(kg/m^3) which are greater than most protein aerogels and hybrid aerogels (E/ρ < 0.1 MPa/(kg/m^3) (**Figure 8.3**). Specific strengths in CSM protein-gelatine hybrids (4.50 kPa/(kg/m^3)) also reach respectable values as compared to other hybrid aerogels which are generally stronger than their pure protein or polysaccharide counterparts (**Figure 8.4**). The mechanical success of the CSM protein-gelatine hybrids is likely due to the inherent network-forming properties of gelatine, allowing it to generate extended intermolecular interactions following dissolution and re-cooling [314] (see **Section 8.4.3**).

Elasticity in CSM protein aerogels is disappointingly low (elastic limit = 4 – 10 *% ε*) compared to exemplary bioaerogels from cellulose (elastic limit = 60 - 80 *% ε*) (see **Table 8.2**). This brittle nature of CSM protein aerogels could exclude them from certain applications (*e.g.* tissue engineering) but may be favourable for others (see **Section 8.6.2**).

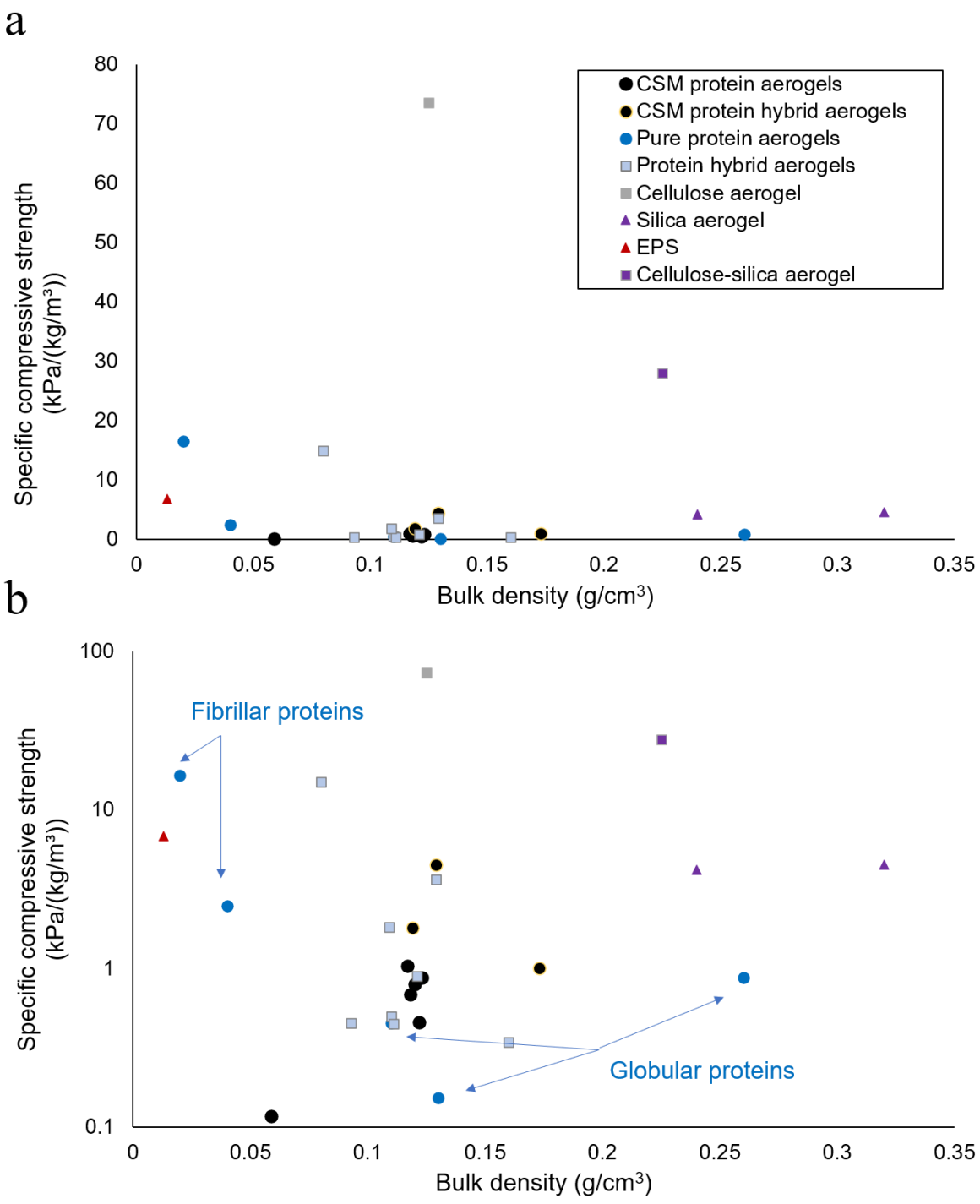

Figure 8.4: (a) *Specific compressive strengths (σ/ρ) as a function of density (ρ) measured in CSM protein aerogels (black circles), other protein aerogels, and selected non-proteinaceous aerogels and porous materials (refer to legend) as referenced in* ***Table 8.2****. **(b)** Data from (a) presented on a logarithmic scale for σ/ρ and protein aerogels are identified as comprising either fibrillar or globular proteins*

One important finding to emerge from these comparisons is the scarcity of comparative data. The lack of combined reporting on protein aerogel densities, porosity information, and mechanical properties highlights the importance of the current research in presenting a complete description of CSM protein aerogels using physical, morphological, and mechanical data. Additionally, it must be noted that CSM protein aerogels were prepared without the use of chemical crosslinking factors (such as aldehydes) due to research aims incorporating an environmentally friendly approach. The comparative data obtained from other studies of protein-based aerogels contains examples of protein hybrids that use synthetic organic molecules such as polyvinyl alcohol (PVOH) ([125]), polymethylsilsesquioxane (PMSQ) ([126]) and glyceraldehyde [121]. These molecules play a role in crosslinking the gel networks and consequently strengthening the aerogels but are oil-based and not likely to be biodegradable. Therefore, CSM protein cryogels, particularly the CSM protein-gelatine hybrid cryogel, are a promising addition to the small group of protein aerogels as they broaden the available data on mechanical testing and demonstrate comparable or improved mechanical properties without the use of oil-based ingredients. Finally, no mechanical data was collected on CSM protein aerogels produced by SC-CO_2 drying due to impracticality and the limited production of these samples. Supercritically dried CSM protein aerogels should be assessed for their mechanical properties in future studies (see **Section 9.2.2**).

Other properties assessed in CSM protein aerogels included resistance to thermal degradation (using thermogravimetric analyses) and the longevity of the structures in aqueous solutions. Upon heating, canola seed meal protein undergoes water loss at temperatures up to 130 °C followed by protein degradation into fragments (from 130 °C) and eventually the complete breakdown of the peptide backbone (from 680 °C) [315]. CSM protein cryogels in this work demonstrated a lowered resistance to thermal degradation (peak degradation rate at ~ 250 °C) compared to corresponding CSM protein extract (peak degradation rate at ~ 300 °C) (see **Section 6.5.2.2**) and to canola protein from other studies (peak degradation rate ~ 300 °C [315]). This was a surprising discovery given aerogels are well known for extremely low thermal conductivity and have been touted as flame retardants. Consequently, aerogels commonly present with higher onset and peak temperatures for thermal

degradation than their non-aerogel counterparts in other thermogravimetric studies [316, 317]. One explanation for this discrepancy in thermal resistance between CSM protein cryogels and literature is the large pore sizes found in cryogels. Low thermal conductivity in aerogels is associated with mesoporous and microporous gel networks (see **Section 2.1.3**) therefore macroporous structures such as CSM protein cryogels do not necessarily restrict heat flow and consequently resist thermal degradation. Furthermore, little evidence of crosslinking has been found from other analyses (see **Section 8.4**) therefore the expectation that CSM protein aerogels might be more heat resistant due to additional covalent linkages is unsupported by any evidence of additional covalent crosslinking. Further investigations on CSM protein aerogels should investigate whether chemical changes associated with gelation possibly aid thermal degradation thus explaining the 50 °C reduction in thermal resistance.

CSM protein aerogel structures were also briefly assessed for degradation rates in water. Overall re-solubilisation of the protein from the aerogels was quick (matter of days) and complete (little remnants of gel networks after 10 days) indicating that CSM protein aerogels are highly susceptible to aqueous degradation. This property is markedly different to aerogels made from insoluble materials (including other bioaerogels such as cellulose aerogels) which can be used like absorbent sponges in water-treatment applications [10]. Interestingly, the possibility of controlled degradation of the CSM protein aerogels may have unique application potential (this idea is explored in **Section 8.6.2**) as slightly delayed degradation is seen when the aerogels are exposed to saline solutions (see **Section 6.5.3**).

8.4. Gelation mechanism of CSM protein extract

Chapter 2 describes how most aerogel precursors have well-understood gelation mechanisms that researchers employ to produce aerogels with predictable morphologies. Recognized gelation chemistry in silica aerogels allows researchers to control morphologies: 12 nm diameter 'string-of-pearl' silica aerogels are produced by base catalysis while 2 nm diameter filamentous silica aerogels by acid catalysis [318]. Bioaerogels each have unique gelation mechanisms as determined by the biopolymer chemistry and additional compounds such as salts which can be added (see **Section 2.2.2**). Many polysaccharide aerogels have gelation mechanisms involving the use of divalent cations. For example, added Ca^{2+} salts melt and then crosslink insoluble cellulose chains by coordination with carboxyl and hydroxyl groups.

Protein gelation is a more complex situation. Various functional groups (*-OH, -SH, -NH_2, -COOH, -CH_3,* aromatic groups) can take part in a variety of chemical interactions (hydrogen bonding, hydrophobic interactions, salt bridging, covalent bonding) which contribute to the overall effect of gelation (see **Section 2.2.3**). Furthermore, a complex interplay of intrinsic and extrinsic variables determines the specific functional groups that are available under certain conditions which ultimately influence gelation propensity, gel network structure, and gelation kinetics (refer to **Figure 2.12**). However, a general summary of gelation mechanisms in protein gels describes a two-step process where protein gels are produced from native solubilised protein. First, partial denaturation (or unfolding) occurs and then aggregation is driven by hydrophobic residues exposed during the unfolding of the native protein structure. Subsequent network formation occurs with the development of new molecular interactions, both covalent and secondary, which span multiple protein molecules.

Additionally, some specific knowledge of canola protein gelation has been elucidated in other studies (see **Section 2.3.3**) and can provide a foundation for descriptions of CSM protein gelation in this thesis. CSM protein, specifically cruciferin, experiences gelation following heat treatments at alkaline pH values. Heat-induced exposure of hydrophobic residues is therefore considered an important factor in the gelation method. Interestingly, hydrogen bonding and disulphide linkages are supposed to play a minimal role in the gelation process [203], though more recent studies suggest some level of

hydrogen bonding is essential for gelation [198]. Free amino groups (*e.g.* the ε-amino group in lysine) are also suspected of involvement, possibly in crosslinking after the initial association of hydrophobic residues. The role of alkalinity has not been linked to a specific chemical mechanism but probably plays a general role in protein unfolding or molecular repulsion/attraction.

8.4.1. Alkaline gelation

The gelation mechanism for the (10 wt%) CSM protein gels developed using only pH-control has a single trigger: the manipulation of the pH to around 8.0. This pH adjustment may begin a denaturation process or change in protein charge, which necessarily has a 'knock-on' effect of inducing aggregation and network formation. Additionally, CSM protein concentration is high (> 10 wt%) and may explain why gels in this work can be produced at ambient temperature while other studies report the additional use of heating at alkaline pH as necessary for gelation. Polymeric solutions require a critical concentration for gelation as molecules must be present in sufficient numbers for cross-over and entanglement. Higher concentrations therefore provide an additional driving force for gelation even when other gelation driving forces (*e.g.* heat-induced denaturation) are absent.

During heat-induced denaturation, hydrophobic groups are driven from the inside of the protein conformation to being exposed on the outside. Consequently, this unfolded protein undergoes association with neighbouring molecules as the exposed hydrophobic residues are buried at the interface of multiple molecules (**Figure 8.5**). The result is aggregation of the protein. When aggregation kinetics fall within a specific range, gel network formation can result. Alternatively, precipitation may occur under rapid aggregation conditions while neither precipitation nor gelation may occur with slow aggregation of the protein. Heat-induced gels are observed at pH values around 8.0 but not at 10.0 or 6.0. The failure of heating to induce gels outside a specific pH range means electrostatic forces arguably play an even greater role than heat-exposed hydrophobic groups. Hydrophobic interactions may play an important secondary role given the high viscosities and storage moduli of heat-treated gels at pH ≈ 8.

Furthermore, native PAGE analysis shows heating probably causes conformational changes that lead to aggregation, which is a pre-requisite for gelation in many proteins. However, hydrophobic interactions are not required for initial gelation (ambient gelation does occur at pH ≈ 8, 10 wt% CSM protein) and can be overcome by competing electrostatic influences (heat-treated, pH 10 solutions of 10 wt% CSM protein do not gel). The reduction in gel and aerogel strength beyond pH 8 is explained by the increasing influence of repulsive negative charges to protein aggregates that reduces the association of protein molecules during gel formation (**Figure 8.5**). Interestingly this can be counteracted by cations added to the gels (see **Section 8.4.2**).

Altering the pH can also denature protein molecules. This is achieved by changing the protonation state of certain chemical moieties. Consequently, newly charged, or neutralised residues are driven to new conformations according to the change in electrostatic forces. Similarly (to hydrophobic interactions), new electrostatic interactions can lead to aggregation and network formation. Electrostatic attractions and repulsions endowed by overall molecular charge also control the rate of aggregation in denatured protein molecules, allowing for association and entanglement in precisely the right manner and rate for gelation. There is little evidence from CD spectroscopy studies that pH plays a strong role in protein conformational changes (see **Section 5.5.1**) and therefore it is unlikely to be the primary reason for CSM protein denaturation. Indeed, the CSM protein extracts used in this study display different proportions of secondary structure (*e.g.* α-helices, β-sheets, unordered structures) as compared to native protein from other studies, even when pH is similar. One explanation for these differences is that some prior denaturation or unfolding may have occurred during protein extraction processes. However, these changes are small when compared with the secondary structural changes normally associated with denatured CSM protein (*e.g.* heat-denatured protein). It is noteworthy that stronger wet-gels at a pH (9.0) distant to the pI (5.6) have previously been attributed to the role of an alkaline environment in the denaturation of the canola protein [200]. Such associations from literature and the limited scope and quality of CD spectroscopy studies in this project may suggest that pH could yet be implicated in conformational changes and subsequent protein denaturation.

However, assuming pH is unlikely to be a prominent factor in denaturation, it is nevertheless the key trigger for gelation (refer to gel production in **Section 6.2**). A pH value around 8 is correlated with the strongest and stiffest CSM protein gels (see **Section 6.3.2**) and increases protein aggregate size (noted on protein aggregate deposits from the pore walls of cryogels (see **Section**s **6.4.2**)). The use of pH to manipulate particle size in SC-CO_2 dried aerogels may also be possible (see **Section 7.4.3**) and pH-induced changes in aggregate sizes are seen in other studies of protein gels [94]. Variations in pH provide variations to the degree and type of overall electrostatic charge on protein molecules. Native PAGE analyses suggest that a pH ≈ 8 may play an important balancing role in aggregation kinetics. CSM proteins have increased solubility at pH values above 6 but begin to accumulate an overall negative charge beyond a pH around 8 (see **Section 5.5.2**). The negative charge on protein molecules at higher pH values (*e.g.* pH ≈ 10) explains the corresponding loss in gelation ability since like negative charges cause protein molecules to repel one another (**Figure 8.5**). Consequently, pH will influence the gelation success and particle size in CSM protein suspensions and gels and could ultimately influence the pore sizes of aerogels when supercritically dried. The observation that extremely low pH (pH = 1.9, **Figure 6.27a**) allows for viable cryogel production may also be explained by changes in electrostatic charge. Acidic values generally promote protein insolubility since the pI (pH where protein has overall neutral charge) of the CSM protein extract is at pH ≈ 3.5. Protein molecules resolubilise at pH values sufficiently distant from the pI (as seen at pH ≥ 7) allowing gelation to occur. Owing to the broad applicability of the freeze-drying method, the protein in the pH 1.9 sample is sufficiently protonated (electrostatically charged) to allow for re-solubilisation and cryogel production. However, the low viscosity at pH 1.9 suggest that full gelation is likely impeded by repulsive charge in a similar manner to highly (pH ≥ 10) alkaline formulations.

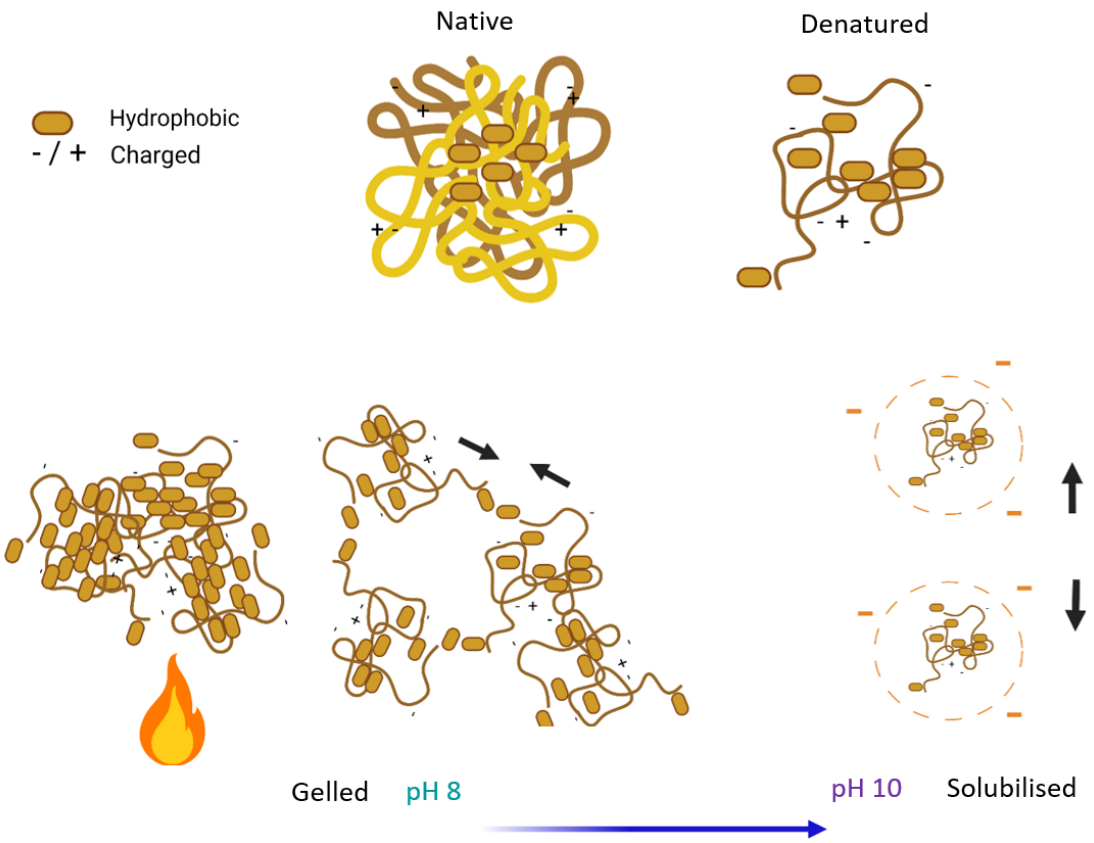

***Figure 8.5**: Schematic representation of the intrinsic (protein chemical groups and conformations) and extrinsic (solution pH and temperature) driving forces implicated in the gelation mechanism of CSM protein extracts. Schematic created using BioRender.com*

Another consideration is the possible influence of covalent crosslinking (*e.g.* disulphide bridging or lysinoalanine cross-linking) in later stages of gel formation. No convincing evidence for covalent crosslinking was found using thermal analyses, electron microscopy, or SDS-PAGE. Little or no implication of covalent crosslinks during gel formation is largely consistent with other studies of canola protein gels. However, disulphide bonding is suggested to play a role in stabilising and strengthening heat-treated gels after initial gel formation [319]. Thus, further investigation to directly examine the role of disulphide bonding in gelation may be necessary. Furthermore, amino acid analysis indicates that cysteine is present in the CSM protein extract at 1.74 mg / 100 mg dry meal, corresponding to 2.33 % of the total detected amino acid content. Disulphide bonding is considered a major component in the chemical interactions of other protein gels (*e.g.* ovalbumin gels) at concentrations around 5 % [320]. Targeted chemical disruption of disulphides (*e.g.* using reducing agents such as dithiothreitol) may be one method for examining the role of disulphide bonding in

CSM protein aerogels in future investigations. Despite the requirement for future work on the possible role of disulphide bonding, most of the chemical interactions in pH- and heat-controlled CSM protein gels are likely secondary interactions (electrostatic and hydrophobic). These secondary interactions may be partially or fully destroyed by re-solubilisation in aqueous solutions (see **Section 6.5.3** and the 'recycling' of aerogels in **Section 6.4.1**).

In summary, the gelation mechanism for CSM protein in this study seems primarily driven by electrostatic forces due to the highly important role of pH in the gelation success. Partially denatured protein (possibly denatured in extraction processing) is solubilised sufficiently at alkaline pH (> 7) for molecular association and aggregation to occur. Further denaturation and association occur upon heating. However, pH values around 9 or higher are detrimental to gelation due to repulsive electrostatic charge, irrespective of attractive hydrophobic forces from denaturation. Therefore, gel networks comprise only of secondary interactions, primarily electrostatic but with substantial strengthening by hydrophobic interactions.

8.4.2. Gelation in the presence of Ca^{2+}

The use of $CaCl_2$ in CSM protein gels was intended to imitate similar use of divalent cations in polysaccharide gels. $CaCl_2$ provides free Ca^{2+} to the protein suspensions which can be coordinated by negatively charged groups (*e.g.* COO^- and OH^-) on the protein molecules. Prior investigations (see **Section 8.4.1**) have revealed how gelation in CSM protein extract is driven by electrostatic and hydrophobic groups balanced by overall molecular charge and solubility. The conditions for gelation are determined by prior protein denaturation, a specific pH range, and further, heat-induced, denaturation of protein molecules. Given that electrostatic interactions and overall charge play a role in gelation, calcium ions are likely to interact with CSM protein and influence this gelation mechanism.

The addition of Ca^{2+} was trialled both at the optimised pH range (pH = 8.0 ± 0.2) and at a non-gelling pH where the protein remained soluble (pH ≈ 10). Earlier investigations using native PAGE analyses indicated that CSM protein interacts well with Ca^{2+} (see **Section 5.5.2**) and was effective at neutralising negative charges on the protein at high pH. Rheological analyses on CSM protein-Ca^{2+} gels revealed Ca^{2+} had an overall positive influence on gelation in pH 8 and pH 10 samples except those at pH 8 which had been previously heat-treated (see **Section 7.4.1**). However, the $CaCl_2$ concentration was an important factor with excessive ionic strength leading to precipitation of the CSM protein and non-viable gels.

Ca^{2+} likely induces gelation by creating salt bridges (*e.g.* ~$RCOO^-$ Ca^{2+} ^-OOCR~) between negatively charged amino acid residues, *i.e.* glutamate and aspartate (**Figure 8.6**). The use of alkaline pH in combination with $CaCl_2$ led to the success of these gels by first promoting negatively charged residues on the protein molecules. Some evidence from CD spectroscopy suggests $CaCl_2$ may also promote a more unordered secondary structure in CSM proteins (see **Section 5.5.1**). Thus, Ca^{2+} binding to CSM protein could induce secondary structural changes that support aggregation and gelation, even where Ca^{2+} salt bridging does not necessarily occur. The binding of Ca^{2+} to CSM protein may allow for more filamentous microstructures in the gels, as seen in some supercritically dried aerogels (see **Section 7.4.3**). However, microstructural changes are yet to be specifically attributed to the use of Ca^{2+} since

no non-Ca^{2+} aerogels were produced by SC-CO_2 drying for comparison. **Section 9.2.2** explores the need for further samples of supercritically dried CSM protein aerogels.

Interestingly, the Ca^{2+}-induced gelation mechanism appears to compete with heat-induced gelation, seen in the destabilisation of heat-treated gels (pH 8) by $CaCl_2$ addition (see **Section 7.4.1**). The formation of ionic bonds (*e.g.* ~$RCOO^-$ Ca^{2+} ^-OOCR~) is more enthalpically favourable than hydrophobic bond formation, therefore Ca^{2+} can disrupt the existing hydrophobic gel network. However, the overall quantity of ionic bonding is small compared to the capacity for hydrophobic interactions since the greatest gel viscosities are achieved in the heat-treated gels without $CaCl_2$ (pH 8). The pH 8 gels subject to a combined heat-treatment and Ca^{2+}-treatment fail to achieve the gel properties seen with either individual treatment, suggesting that these two gelation mechanisms compete rather than complement. Owing to their influences on very different chemical moieties (hydrophobic *cf.* charged), heat-treatment and Ca^{2+}-treatment may induce mutually exclusive conformational changes in the canola proteins where only like-conformations can form a gel. Thus, a mixed treatment leads to a mixed system of two gelation mechanisms that are incompatible.

Another key action of Ca^{2+} ions is the shielding of overall repulsive charges on protein molecules at high pH, allowing for gelation in previously non-gelling samples prepared at pH ≈ 10. At greater alkalinity (pH ≈ 10) heat-treatment alone is an ineffective gelation tool. It is not clear whether the subsequent gelation in the presence of Ca^{2+} is due to the formation of protein-Ca^{2+}-protein salt bridges or due to charge shielding. Ca^{2+} binding to charged residues may simply cause gelation by removing repulsive electrostatic forces, allowing molecules to interact *via* hydrophobic regions. However, there is likely some involvement of both bond types since pH 10 gels with a combined heat- and Ca^{2+}-treatment have increased gel elasticity over those exposed to Ca^{2+} alone but are non-viable without the Ca^{2+}-treatment. The change in elasticity suggests that some flexible bond types (*e.g.* hydrophobic interactions) are present but Ca^{2+}-protein interactions remain essential for gelation.

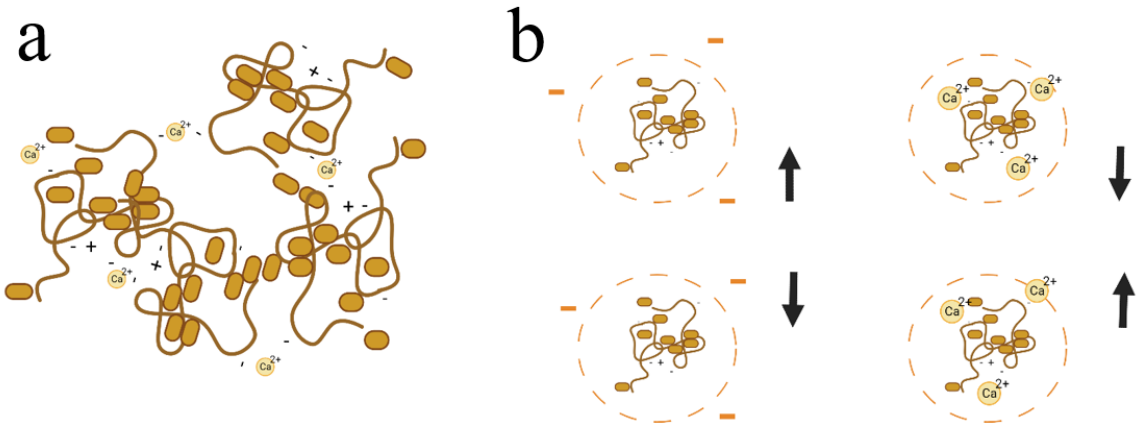

Figure 8.6: *Schematic representation of* ***a)*** *ionic bonding between calcium ions and negatively charged residues on CSM protein and* ***b)*** *the influence of calcium ions on molecular attraction and subsequent gelation of protein at high pH. Schematic created using BioRender.com*

Finally, the precipitation of the CSM protein in excessive concentrations of Ca^{2+} (200 mmol/L $CaCl_2$) suggests that protein solubility is negatively affected at high ionic strengths. High salt concentrations act to dehydrate the solvated protein, accelerating aggregation beyond the gelation point to cause precipitation.

In summary, Ca^{2+}-induced gelation in CSM protein is triggered by the formation of ionic bonds between Ca^{2+} and negatively charged protein residues. These ionic bonds may form salt bridges (*e.g.* ~$RCOO^-$ Ca^{2+} ^-OOCR~) and cause 'knock-on' conformational changes favourable for gelation. Ca^{2+} binding also alters the overall electrostatic charge on CSM protein molecules, permitting the molecule-to-molecule interaction necessary for aggregation and gelation, especially at pH values previously obstructive to gelation.

8.4.3. Gelation with collagen

The influence of additional biopolymers on the CSM protein gelation mechanism was not investigated specifically in this work. However, in the case of hybridisation with collagen (both as soluble gelatine and as insoluble, ground fibre) some investigations were dedicated to detecting possible crosslinking of the two protein types. Evidence of canola-collagen crosslinking was not found in image analysis of the aerogel structures. The detection of collagen fibrils in micrographs was scarce. Furthermore, where they were identified in a gelatine hybrid, collagen fibrils were found only at the surface of pore walls and not in cross-sections. Crosslinking between the canola proteins and the added collagen proteins (either as gelatine or insoluble fibres) had been expected to improve hybrid gel homogeneity. Successful co-gelation involving crosslinking was also expected to reduce pore sizes by imparting added resistance to ice crystal growth during freeze drying. Changes in macropore shape and size were identified upon hybridisation with gelatine alongside very clear improvements in mechanical properties providing early evidence that co-gelation was successful.

However, SDS-PAGE analysis of CSM protein hybrid aerogels revealed little likelihood of extensive crosslinking in the CSM protein-gelatine/collagen hybrids (see **Section 7.3.3**). Some reduction in measurable protein (*i.e.* molecular weight < 400 kDa) may be attributable to the formation of large crosslinked molecules in the gelatine hybrids (*e.g.* canola-collagen complexes). However, the impact is minimal, suggesting that canola proteins are largely free to resolubilise at original molecular weights (MWs). Furthermore, no new MW bands were seen, which were expected upon formation of new (crosslinked) canola-collagen complexes. Interestingly, this was also true of CSM protein-gelatine hybrids which had been exposed to UVB light and consequently expected to undergo UV-catalysed crosslinking. Some mechanical data (see compressive strengths in **Figure 7.14**) suggests that the UVB-treatment employed in this experiment may have caused photodegradation of the canola and/or collagen molecules and consequently jeopardised the gel integrity. However, other mechanical data (see elastic modulus in **Figure 7.14** and storage moduli in **Figure 7.22**) indicate that the UVB treatment has effectively stiffened the gelatine hybrids. One explanation for loss of strength with a

corresponding increase in stiffness is that successful co-gelation has increased aerogel brittleness and lead to early mechanical failure in static compressive tests.

Despite the minimal evidence of covalent crosslinking, co-gelation of CSM proteins with collagen (in both insoluble and gelatine forms) occurs successfully. The co-gelation is likely a result of physical entanglement of collagen polypeptides with other collagen molecules and/or with canola proteins. Physical entanglement is the described method of gelation for pure gelatine gels [314]. Following dissolution, the hydrolysed collagen molecules (*i.e.* polypeptides) in the gelatine have a propensity to re-associate and partially revert to ordered helical molecules (like native collagen chains). This 'renaturation' of the gelatine polypeptides to a quasi-collagen structure results in the formation of extensive 'junction zones' with neighbouring molecules, creating a gel network of pseudo-helical collagen connected *via* physical entanglements and secondary bonding [314]. Hybrid gelatine networks are found in gelatine-polysaccharide gels where the two biomolecules interact through van der Waals forces and hydrogen bonds [321]. Therefore, it may be plausible that CSM protein-gelatine hybrids also possess a single, hybrid network connected through secondary interactions and physical entanglement. Aerogel strength and stiffness may be further enhanced by intrinsic mechanical properties of collagen fibrils, even in the CSM protein-collagen hybrids where collagen fibres are suspended less homogenously in a network that is predominantly CSM protein.

8.5. The biochemical potential of CSM protein aerogels

Certain biological functions of proteins can be retained during aerogel processing (*e.g.* enzymatic function, see **Section 2.2.3.5**) leading to highly specific bio-applications for the resulting aerogels. One of the thesis aims postulated that canola protein might be a uniquely useful polymer for aerogel production due to inherent biochemical attributes. **Chapter 2** summarises how canola seed meal protein has been identified as containing physiologically useful bioactive peptides and amino acid ratios agreeable for human consumption (see **Section 2.3.4**). Amino acid profiling of the CSM protein extract in this thesis has revealed similar amino acid ratios to studies that have found canola protein nutritionally valuable. Furthermore, potential bioactive peptides (in the form of cryptides) have been identified in both the CSM protein extract and the subsequent cryogels developed in this thesis. It is of note that the detection of cryptides was possible in cryogel samples since this finding demonstrates the retention of potentially bioactive molecules even after aerogel processing.

The presence of physiologically relevant bioactives could make the canola protein aerogels candidates for related applications in therapeutics or nutraceutical products (see **Section 8.6.2**). However, a major restriction on the applicability of these findings is that cryptides are only potential sources of bioactivity (see **Section 5.4.1**). The presence of cryptides does not guarantee that a proteinaceous substance will possess corresponding bioactivities. Cryptides indicate a likelihood of bioactivity based on the possibility that chemical cleavage will release specific, smaller molecules. Therefore, it cannot be concluded that CSM protein aerogels are necessarily bioactive. However, the findings of this investigation indicate that subsequent targeted research into bioactive properties of CSM protein aerogel products is a viable project. The identification of cryptides also provides some framework for how such future research may be conducted, including the prerequisite for further chemical degradation before bioactivities will be measurable *in vitro* or *in vivo*.

8.6. Aerogel tailorability and application potential

The development of novel bioaerogels from canola protein has necessarily focussed on an archetypal description of the CSM protein aerogel. However, some interesting leads have been developed in areas focussed on aerogel improvements, processing variations, and the overall industrial relevance of these novel bioaerogels. Ultimately, this project aimed to introduce new application prospects for both canola protein and bioaerogels. The following Section will collate these leads and summarise the overall relevance of the current research for future researchers, manufacturers, and marketers.

Although application-ready bioaerogels from CSM protein is an on-going goal of the current research, it is sensible to pause and assess the likelihood of developing marketable CSM protein aerogels at the conclusion of the current project. **Section 8.6.2** summarises the application potential of CSM protein aerogels to guide future research in commercially beneficial directions. However, prior to conducting application-specific experiments, future researchers of CSM protein aerogels must first utilise manufacturing and processing information to proficiently produce CSM protein aerogels for their purposes. Achieving an optimised processing route to enhance specific aerogel properties requires knowledge of processing parameters and their influence on resulting gels and aerogels. The final thesis goal was to elucidate these effects and the processing-structure-property relationships that underpin them, producing practicable information for CSM protein aerogel manufacture. **Section 8.6.1** highlights key processing parameters and the resulting tailorability that can be achieved in CSM protein aerogels.

8.6.1. Processing parameters affecting aerogels

CSM protein gelation is heavily dependent on many aqueous chemical parameters. The basic preparation of CSM protein gels requires selection of an appropriate extract type, extract concentration, and suspension pH. These parameters alone account for changes in gel protein components, bioactive potential, gel viscosity (μ), gel stiffness (G') and gel elasticity ($\%\ \varepsilon_{critical}$). This gel variability translates to effects on aerogel bioactive potential, pore size distribution, stiffness (E/ρ),

strength (σ/ρ), elasticity (*% ε* at yield), and optical properties ('sparkle') (**Table 8.3**). Additional changes to gel viscosity, aerogel morphology, aerogel mechanical properties, and aerogel porosity features can occur with the subsequent use of heating, calcium salt (*i.e.* $CaCl_2$), or additional biopolymers during gel formulation (**Table 8.3**). This extensive list of processing parameters provides clear evidence that CSM protein aerogels can be tailored using many, environmentally friendly manufacture approaches (*i.e.* without the use of toxic, oil-based, or energy-intensive chemicals and processing). Furthermore, the subsequent drying of the wet-gels requires the selection of either freeze drying the aqueous gels or choosing to use supercritical carbon dioxide drying of alcogels. The selection of an appropriate drying technique for desired aerogel properties is arguably more important than earlier gelation parameters. Drying techniques have a fundamental influence on resulting aerogel morphologies and properties due to inherent differences in the mechanisms of gel preservation. Additionally, gelation parameters selected at earlier stages play a critical role in the amenability of samples to supercritical drying. Difficulties with sample preparation limited the scope of supercritically dried aerogels, consequently only a small number of these CSM protein aerogels were produced. Despite this limitation, these aerogels have demonstrated the potential for profound improvements to morphologies, surface areas, and pore volumes using the supercritical drying technique (see **Section 7.4.3**).

Table 8.3: *Summary of processing parameters that influence gel and aerogel properties in CSM protein aerogel production*

Processing parameter	**Influence on wet-gel**	**⟶**	**Influence on aerogel morphology**	**Influence on aerogel property**
Extraction method	• Protein components differ • Bioactive potential differs	(Freeze drying)	• None identified	• Bioactive potential differs
[CSM protein]	• *Positive correlation with gel viscosity (μ) **	(Freeze drying)	• Negatively correlated with macropore size • Positively correlated with bulk density (*ρ*)	• Positively correlated with specific mechanical properties (*E/ρ* & *σ/ρ*) • Negatively correlated with elasticity (*% ε* at yield) • Negatively correlated with aerogel 'sparkle'
pH	• Optimal pH for gel *μ*, stiffness (*G′*), and elasticity (*% $\varepsilon_{critical}$*) is ≈ 8 • *Gel aggregate size linked to pH.*	(Freeze drying)	• Aggregate deposits on pore surfaces linked to pH • No influence on macropore size or structure	• Optimal pH for *E/ρ* & *σ/ρ* also ≈ 8
		($SC\text{-}CO_2$ drying)	• Gel particulate size (and subsequent pore sizes) *probably*** linked to pH	• ***Possible influence on specific surface area (SA) and pore volume (PV) if linked to pore size changes*
Heat-treatment	• pH-dependent, positive correlation with *μ*, and *G′*, but embrittles gels with a drop in *% $\varepsilon_{critical}$* and is overridden by Ca^{2+} effects.	(Freeze drying) *(SC-CO_2 drying is probably possible**)*	• None identified	• Positive correlation with *E/ρ* & *σ/ρ* but pH and Ca^{2+} influences override heating effects.
Freeze drying vessel	N/A ***	(Freeze drying)	• Important factor for minimising shrinkage	N/A
[$CaCl_2$]	• 'goldilocks' concentration around 20 mmol/L for positive correlation with *μ*, and *G′*, but embrittles gels with a drop in *% $\varepsilon_{critical}$* • Weakens heat-treated gels at pH = 8.	(Freeze drying)	• No influence on *ρ*	• Positive correlation with *E/ρ* & *σ/ρ* except in heat-treated pH 8 gels.
		($SC\text{-}CO_2$ drying)	• Profound increase in mesoporosity • Increase in *ρ*	• Profound increase in SA and PV • *Probable influence on mechanical properties due to influence on ρ.*
Hybridisation with additional biopolymers	• *Positive correlation with μ*	(Freeze drying)	• No influence on *ρ* • Can alter macropore shape and size	• Profound increases in *E/ρ* & *σ/ρ* • Can reduce *% ε* at yield
Reconstituted aerogels as source for CSM protein ('recycling′ CSM protein aerogels into new ones)	• Difficulty homogenising gels	(Freeze drying)	• *Probable change in macropore shape, size, and arrangement.* **	• Eliminates 'sparkle' • Accentuates viscoelastic behaviour in mechanical testing ** • *Possible increase in elasticity* **

**italics indicates observation or assumption based on other consequences but not specifically tested*

*** further experimentation required *** N/A = not applicable*

Due to the important role of supercritical drying in gel preservation, it is compelling that many freeze dried aerogels (cryogels) demonstrate processing-property relationships that are dependent on gelation parameters (*e.g.* pH dependence of cryogel strength). The drastic morphological changes induced in the gel structure by the freeze drying technique would suggest an overriding of prior gel characteristics. A clear example of this is the viability of low viscosity pH 10 formulations in cryogel production. However, there are identifiable links between certain processing parameters (gel pH, heat-treatment, hybridisation) and cryogel mechanical properties but which have no currently identifiable links to morphological changes. There are also some gelation parameters that may influence gel rheological properties (*e.g.* heating duration) but do not appear to affect cryogel properties. Since supercritically dried aerogels better preserve gel structures, further investigations using SC-CO_2 drying may provide a more complete picture of the connections between gelation parameters, gel properties, aerogel morphologies, and aerogel properties. One example of such an investigation would be confirmation of pH-dependence in protein aggregate sizes and consequently the pH-dependence of aerogel pore sizes, BET specific surface areas, and BJH specific pore volumes. The opportunity to tailor for application specific properties (*e.g.* high surface areas for drug absorption) could then be clearly linked to simple, aqueous chemical techniques (*e.g.* pH changes). Although the scope and specific aims of the current research may exclude the use of other methodologies (*e.g.* chemical crosslinkers such as glutaraldehyde or the use of a transglutaminase enzyme), these are also plausible methods for further tailoring of CSM protein aerogels and could be explored in the future.

Other information relevant to future researchers and manufacturers includes details on processing parameters which were not so critical for subsequent gel or aerogel production. The gelation time (ageing up to 21 hours) does not appear to have a strong influence on gel rheological properties or cryogel appearance and mechanical properties, though some rheological evidence suggests extended ageing (up to 18 days) could improve the gels. These preliminary findings can assist future production and research of CSM protein aerogels by indicating viable manufacturing times and possible time-saving shortcuts as compared to other gels which require ageing for gelation. Another possible cost-saving discovery is a minimal temperature requirement for heat-treated gels. Brief investigations in

this work suggest that heat-treated gels may only require temperatures of 50 - 60 °C to achieve improved mechanical performance in corresponding cryogels. Therefore, the temperatures of 95 °C and heating times up to 30 minutes used in most of the current work may prove superfluous to the requirements of future manufacturers.

8.6.2. Application potential

Throughout this project there have been many suggestions of possible commercial uses for CSM protein aerogels. Many of these suggestions are based on existing applications for bioaerogels, dependent therefore on the comparative performance of CSM protein aerogels against these existing types. Owing to prominence in bioaerogel literature, the CSM protein aerogels are assessed for commercial viability in the following applications: (i) active molecule (*e.g.* drug/nutrient) delivery, (ii) tissue engineering, (iii) packaging, (iv) filtration/water or air treatment, (v) absorbent materials (*e.g.* wound care), (vi) cosmetics and personal-care products, (vii) biosciences and forensics (*e.g.* biosensors/biocatalysts) (**Table 8.4**). Application potential of both CSM protein aerogels and cryogels is firstly dependent on the protein itself. Extraction processes used to obtain CSM protein are based on aqueous chemistry, using simple, and safe chemical techniques. These extraction techniques are likely to keep the resulting protein affordable, non-toxic, and potentially bioactive, essential requirements for application of the resulting canola protein products to industries such as food, medicine, and cosmetics. In applications involving single-use products (*e.g.* packaging) affordability and amenability to mass production (*e.g.* simplicity of processing) are also important.

The commercial potential of CSM protein cryogels is limited by their macroporosity and the consequentially low specific surface areas. Application in active molecule delivery and filtration applications can be almost completely dismissed due to the low surface areas alone. Lacking the high specific surface areas required to carry, protect, and release useful quantities of active ingredients, the cryogels are unlikely to be competitive in controlled-release studies of absorbed actives. An additional

complication for both the controlled-release of actives and filtration applications is the solubility of CSM protein cryogels in aqueous solutions.

However, if delayed/controlled degradation in saline solutions is possible (see **Section 6.5.3**) this may allow for niche potential in active molecule release where the ultimate solubilisation of the aerogel matrix is desired. Nevertheless, the usefulness of controlled degradation in aqueous solutions is best combined with the high surface areas of supercritically dried CSM protein aerogels rather than freeze dried cryogels. Other commercially useful materials that may not be possible from CSM protein cryogels due to low surface areas include catalytic, biosensor, and absorbent materials. High surface areas are generally required for ultra-absorbency and ultra-sensitive detection devices. Nevertheless, CSM protein cryogels have demonstrable hygroscopicity and may yet prove to be useful materials for absorbency applications. Humidity-dependent mechanical properties or humidity-dependent release of actives may offer a unique avenue of application for CSM protein cryogels. Humidity-dependent mechanical properties could allow for biosensor capability in wound-care or other physiological applications since CSM protein aerogels are also likely to be biocompatible. Humidity-dependent release of actives might also allow for unique application in veterinary science or cosmetics where skin humidity can trigger the release of pharmaceuticals or nutraceuticals. However, as with controlled solubility, this property is best combined with the high specific surface areas of supercritically dried CSM protein aerogels. Furthermore, the exact impacts of CSM protein cryogel hygroscopicity on mechanical (and other) properties are yet to be explicitly investigated.

Table 8.4: *Comparison of CSM protein aerogel properties to commercially relevant applications of bioaerogels, based on properties determined in this thesis ("?" indicates property not investigated)*

	CSM protein aerogels	**CSM protein cryogels**	**Active molecule (*e.g.* drug, nutrient) delivery**	**Tissue engineering**	**Packaging**	**Filtration/water or air treatment**	**Absorbent materials (*e.g.* wound care)**	**Cosmetics & personal-care products**	**Biosensors/biocatalysts (*e.g.* in forensic science)**
Density	Low	Very low	Light-weight	Low	Very low	Low	Very low	Low	Light-weight
Surface area & Pore volume	Medium	Very Low	Very high	Medium	N/A	Very high	High	Application-specific (*e.g.* actives delivery vs. exfoliant)	High
Porosity	Meso	Macro	Micro/meso	Macro	N/A	Micro/meso	Meso/macro	Application-specific	Application-specific (*e.g.* molecular vs. cell entrapment)
Strength-to-weight ratio	?	High	Medium	High	Very high	High	High	Application specific (*e.g.* exfoliant vs. make-up)	High
Elasticity / stiffness	?	Stiff	Some stiffness (*e.g.* for machinability)	Tailorable Elasticity	Stiff (*e.g.* EPS)	Stiff	Elastic	Some stiffness (*e.g.* resist shear forces during application)	Application-specific (*e.g.* wearable items vs. pressure-resistant chips)
Hydrophilicity	?	Soluble in water, hygroscopic	Controlled solubility in water	Insoluble but functional in water	Water resistant	Insoluble but functional in water	Hydrophilic / hygroscopic	Controlled solubility in water	Insoluble but functional in water
Thermal resistance/ insulation	?	Low	N/A	N/A	Medium-High	Medium-High	Heat-dissipating	N/A	Medium (*e.g.* can be stored frozen)
Unique chemical properties	• Potential for bioactivity and nutritive value • Sparkle (cryogels only)		Bioactivity and/or reversible binding of active molecule	Bioactivity (*e.g.* growth stimulant)	U/V light protection	Reversible binding of contaminants (*e.g.* oil, heavy metals)	Bioactivity (*e.g.* healing properties)	Bioactivity (*e.g.* anti-microbial), UV protection, cosmetic effect (*e.g.* colouration)	Biochemical specificity (*e.g.* enzymatic action)
Degradability and toxicity	Likely* biocompatible and biodegradable		biocompatible, biodegradable, edible	biocompatible, biodegradable	Biodegradable	No leaching of toxic compounds	Biocompatible	Biocompatible, biodegradable	Biocompatible

**not specifically studied*

The key advantage of the CSM protein cryogels is their density-specific stiffnesses and strengths (particularly of CSM protein hybrid cryogels) that allow the low-density structures to retain monolithic shape under reasonable compressive forces. High strength-to-weight ratios are useful across several applications (refer to **Table 8.4**). However, a corresponding lack of elasticity may restrict their use in medical applications such as wound-dressing or tissue engineering (despite relevant pore sizes and likely biocompatibility). Specific stiffnesses and strengths of the CSM protein cryogels, combined with appropriate research into water-resistance, could translate to serious potential in the packaging market as light-weight biodegradable foams. Ultimately, the CSM protein cryogels are probably best suited to niche applications in cosmetic or personal-care products. Dry cosmetics may offer a unique commercial opportunity by avoiding problematic exposure to aqueous solutions that destroy the aerogel. Optical properties (sparkle and colour) and friability (allowing dispersion of a monolith) hint at potential use in dry beauty products. Probable biodegradability and possible bioactivity, specifically anti-oxidative and anti-microbial properties, provide further validation for future research of CSM protein cryogels as potential cosmetic ingredients.

The application potential of supercritically dried CSM protein aerogels follows a more traditional path. Like other supercritically dried aerogels, these structures demonstrate impressive specific surface areas due to a mesoporous microstructure. Although the surface area measurements obtained in CSM protein aerogels are mediocre in comparison to polysaccharide and inorganic aerogels (see **Section 8.3**), there is potential to achieve comparable values with further research. Large specific surface areas should allow for substantial absorbance of other molecules from liquid or gaseous mediums into practicably small samples of aerogel. Thus, CSM protein aerogels may be candidates for applications in active molecule delivery (drugs, nutrients, pesticides), filtration (*e.g.* water or air treatment), forensic sciences (*e.g.* capture/detection of biomolecules/cells), and absorbent materials. Food-based applications have been suggested for protein-based aerogels made from other proteins (specifically as delivery vehicles for micronutrients [103]) and is an obvious application for CSM protein aerogels owing to existing research on human consumption of canola protein (see **Section 2.3**). There may be scope for a novel application where health benefits are achieved by the aerogel

matrix itself releasing essential amino acids or bioactive molecules. Alternatively, the nutritive value of the CSM matrix could be considered a secondary function to the primary role of the CSM aerogel, for example if it were a drug-delivery vehicle where an active substance or micronutrient is impregnated in the matrix.

An obvious caveat on considering these aerogels for commercial potential is the need for further research (refer to "?" symbol in **Table 8.4**). Some characteristics of the cryogels are likely to be shared by the supercritically dried aerogels (*e.g.* water solubility) but are yet to be investigated specifically. Operating under the assumption that mechanical and chemical properties of the cryogels are probably translatable to the aerogels, they are best touted as possible active molecule delivery vehicles in food or cosmetics. Properties shared with the cryogels such as tailorable water solubility and inherent biochemical attributes, would enhance this potential. Finally, it is noteworthy that the use of SC-CO_2 drying is generally considered less environmentally friendly than freeze drying methods, is more expensive, and more difficult to scale-up for commercial production. Technical and environmental costs associated with the supercritically dried aerogels may demand application in more lucrative products (*e.g.* pharmaceuticals) while simultaneously preferencing the cryogels for low-end and environmentally conscious markets (*e.g.* packaging, cosmetics).

8.7. Other contributions of this thesis

During the development and characterisation of CSM protein aerogels, unexpected challenges arose which led to the modification of some common aerogel production and characterisation techniques. Some of these modifications and findings have been discussed in the relevant thesis Sections (*e.g.* **Section 7.4**) but are summarised specifically in the following Section to highlight methodological importance. Certain methodological contributions of this thesis that were not explicit aims of the original project may provide directives for other research in protein science or aerogel testing.

8.7.1. Canola protein science

The use of $CaCl_2$ in canola protein gelation (see **Section 7.4**) has led to exciting progress in this project and may have a wider impact of on canola protein research in other fields (*e.g.* other canola-based or protein-based materials). Although the use of divalent salts in bio-based gels is not unique, to the best of our knowledge, the calcium-induced gelation of canola proteins is a novel approach to forming canola protein-based materials. There may be scope for the use of calcium salts as co-gelation agents in the formation of other canola-based products such as extrusions and films. Indeed, the formation of canola-based materials from raw canola meal may be possible (*i.e.* no requirement for prior extraction of the protein) and the effects of the aqueous chemical treatments in this project (*i.e.* heat, pH, calcium chloride) could be investigated for these types of canola-based materials.

Another area of canola protein science explored (briefly) in this thesis is the application of differential scanning calorimetry (DSC) to protein-based materials. One key outcome of DSC studies on CSM protein cryogels was the clear directive for methodological improvement in future work. The use of hermetically sealed pans and modulated DSC should provide methodological certainty for queries about water-loss and protein conformational changes in the current investigations. Thermal studies of dried, proteinaceous materials, particularly where testing regimes are designed to mimic similar studies in thermoplastics, are scarce. Protein thermal transitions are more commonly studied in aqueous solutions such as in experiments using Nano DSC equipment. Therefore, even the possible

detection of denaturation or glass transition events (see **Section 6.5.2**) in the CSM protein cryogels/extract may be useful data for other thermal studies on solid, proteinaceous materials.

8.7.2. Adaptation of aerogel methods for proteins

The successful development of the supercritically dried CSM protein aerogels relied on the concurrent development of both Ca^{2+}-gelled samples and the single-step immersion of the gels in high-concentration ethanol. One surprising consequence of this development was the revelation that the CSM protein gels were less affected by ethanol-induced shrinkage. Shrinkage appeared minimal even without the gradual solvent exchange processing that is normally employed to manage this problem. The current development of CSM protein aerogels demonstrates that extensive crosslinking is not always a requirement for shrinkage-resistant bioaerogels. Therefore, time-consuming solvent exchange processes may not always be mandated by the bio-based nature of an aerogel. Future protein aerogel researchers may consider solvent exchange trials where higher ethanol concentrations are used for initial immersion of the gels, particularly when similar issues with solubility are encountered in low-concentration ethanol (see **Section 7.4**).

Another key advancement relating to development of supercritically dried CSM protein aerogels is the successful use of an off-the-shelf critical point dryer in the production of bioaerogel samples. Many aerogel-focussed research facilities have purpose-built systems that use in-house designs for supercritical fluid extractors. These can be ‘dynamic/continuous’ supercritical extractors or ‘static/batch’ supercritical extractors. Continuous extraction is preferred as it allows the wet gel specimen to be in contact with a continuous flow of supercritical CO_2. A continuous flow ensures complete replacement of the initial solvent (usually ethanol) with CO_2 at faster rates than batch processing allows, but at the cost of using more CO_2 per run. A similar system can be adapted for static processing, by holding the gel in the supercritical CO_2 for a set time, then introducing fresh supercritical CO_2 for a second hold time, repeating this for several cycles (operator-determined) before finally releasing the CO_2 gas after the final purge [295]. The SamDri – 795 Critical Point (CP)

Dryer (Tousimis®) used in this research is a semi-automated bench-top CP dryer principally designed for use in microscopy. The Samdri – 795 is similar to static processing in purpose-built SC-CO_2 driers, but has limitations relating to CO_2 flow and purge times (see **Section 7.4.2**). Operator control over aerogel purge times is important for tailoring supercritical processing to specific aerogel samples (*e.g.* size and type variations) therefore the in-built time limits on off-the-shelf CP dryers can impede aerogel production. Importantly in this work, the time limit was overridden by forcing the purge stage to be 'held' for an indefinite time frame. This was achieved by powering off the Samdri – 795 once in purge mode. Furthermore, fresh CO_2 can be introduced to the chamber (and sample) by either restarting the instrument at the purge stage after a hold time, or simply manually initiating a new purge phase at the automatic completion of the prior purge. Consequently, the sample experiences repeated purging (each time for a maximum of 45 minutes in the case of the Samdri- 795 CP dryer) improving the likelihood of complete solvent exchange with CO_2. Through a combination of 'held' and repeated CO_2 purge stages the operator can mimic the extended total purge times of custom-made SC-CO_2 batch processors. Ultimately, continuous flushing with CO_2 is more desirable and is preferable for manufacturing purposes. However, the adaptation of an off-the-shelf CP dryer for bioaerogel production increases the accessibility of this technique for some researchers, particularly where these instruments are part of existing laboratory resources.

A final contribution of the current work to aerogel science is the adaptation of nitrogen gas porosimetry methods to CSM protein aerogels. Specifically, the modification of degassing protocols to allow for successful preparation of heat-sensitive, low-density, biological samples for gas physisorption analyses (see **Section 7.4.3**). Although reduced temperature degassing protocols must be commonly used in bioaerogel analyses, the specific timeframes required for low-temperature degassing of CSM protein aerogels are documented here to aid future research. Initial nitrogen physisorption measurements of a CSM protein cryogel were carried out after 24 hours of degassing at 25 °C. A wide hysteresis loop and insufficient desorption measurements (lowest desorption measurement at 0.15 P/P_0) meant it was not possible to determine whether the hysteresis loop would remain open (indicating failed degassing) or closed (indicating good-quality measurements on a clean

sample). The effectiveness of the degassing protocol after 24 hours was therefore left unassessed. Experimentation with silica aerogels demonstrated that successful degassing can be achieved at low temperatures (25 °C) using extended degassing times (3 days). Successful measurements of the CSM protein aerogels were subsequently achieved with low temperature (25 - 50 °C) degassing at 5 mT with a minimum degassing time of 6 days (at 25 °C) for the supercritically dried CSM protein aerogel and 7 days (25 °C, with final 24 hours at 50 °C) for the CSM protein cryogel.

Chapter 9

9. Conclusions and Future Work

9.1. Concluding remarks

Novel bioaerogels produced *via* the gelation of protein extracts from canola seed meal (CSM) are described for the first time, adding to the scant collection of aerogels that are derived from plant proteins. The canola-based aerogels were synthesised by manipulating aqueous chemical parameters of the protein solution to form gels, and subsequently drying the gels using freeze drying or supercritical carbon dioxide drying. The processing-structure-property relationships in CSM protein aerogels were also investigated, alongside the competitivity and application potential of these novel bioaerogels.

Gelation success and gel properties were dependent in the first instance on protein concentration and solution pH. Additional variation was possible using heat-treatment and calcium chloride ($CaCl_2$). $CaCl_2$ and pH limits proved essential tools for the development of supercritically dried aerogels, while freeze dried gels were possible from a broader range of CSM protein solutions. Gelation of canola protein extracts using pH, $CaCl_2$, and heating has shown how these bioaerogels were developed using environmentally friendly chemical techniques. The absence of toxic or oil-based chemicals from this production process likely ensures the final aerogel products are environmentally safe, biocompatible, and potentially bioactive. Furthermore, tailorability of gel and aerogel characteristics are possible using these same aqueous chemical techniques. Tailorable pore sizes and gel morphologies were identified after variations to protein concentration, solution pH, and drying methods. Variations to morphological features consequently influenced aerogel properties such as strength-to-weight ratios and specific surface areas. Owing to fundamental structural differences, supercritically dried and freeze dried gels (‘aerogels’ and ‘cryogels’, respectively) demonstrated distinct property differences, therefore possessing different application potentials.

CSM protein gels had a particulate-based network like other gels based on globular proteins, with substantial gel viscosities (up to 80,000 mPa.s) despite a lack of covalent bonding. Sub-micron particles visible in micrographs are attributed to protein aggregates. Denatured canola proteins are driven to aggregation and gelation by hydrophobic bonding and electrostatic interactions, heavily dependent on overall molecular charge. High pH values (≥ 9) introduce strong negative charge to protein molecules and consequently impede gelation while low pH values (< 7) accelerate aggregation to cause protein precipitation rather than gelation. Hydrophobic bonding that binds heat-treated gels is disrupted by the competing formation of ionic bonds when $CaCl_2$ is added. Although heat-treated gels have superior gel viscosities and stiffnesses, the shielding of molecular charges and the formation of salt bridges permit Ca^{2+}-induced gelation at a wider range of pH values. During freeze drying, the aggregate-based gel networks are distorted from mesoporous string-of-pearl microstructures to macroporous layered cells by ice crystal growth. A key difference between CSM protein cryogels and supercritically dried aerogels was the measured Brunauer-Emmett-Teller (BET) specific surface area: 0.051 m^2/g versus 113 m^2/g, respectively. Supercritically dried CSM protein aerogels also demonstrated a mesoporous (Barrett-Joyner-Hallett) pore volume of 0.5 cm^3/g and an average mesopore width of 15.3 nm, while cryogels remained predominantly macroporous.

The CSM protein aerogels demonstrated competitively low densities: 0.13 g/cm^3 in the cryogels (average) and approximately 0.2 g/cm^3 in the supercritically dried aerogels. CSM protein cryogels were able to resist reasonable compressive forces given their low densities, and consequently demonstrated competitive strength-to-weight and stiffness-to-weight ratios. Hybridisation of CSM protein with fibrous biopolymers further enhanced this mechanical potential, with CSM protein-gelatine cryogels possessing specific compressive strengths (4.5 $kPa/(kg/m^3)$) and specific compressive moduli (0.15 $MPa/(kg/m^3)$) that surpass many other bioaerogels. However, CSM protein cryogels were also brittle. Elastic limits were mostly below 8 % compressive strain, consequently limiting the applicability of CSM protein cryogels in applications that require substantial elasticity (*e.g.* tissue engineering).

CSM protein aerogels are hygroscopic and can be resolubilised in water making them unfit for applications requiring water resistance or insolubility, such as filtration applications. However, controlled degradation of the aerogels in specific aqueous conditions may permit unique application potential in active molecule release. This application potential is enhanced by the detection of a range of cryptides in the CSM protein extracts themselves, present even after processing into aerogels. This degradation potential, alongside high specific surface areas, make the supercritically dried CSM protein aerogels candidates for applications in pharmaceutics, cosmetics, and food science. CSM protein cryogels are more suited to possible application in biodegradable cosmetics due to friability and unique optical properties.

9.2. Future work

The current research project has generated many directives for future research involving both canola seed meal protein and bioaerogels. These can be categorised into three areas based on the overarching direction of a set of investigations. These directives are further elucidation of gelation chemistry (**Section 9.2.1**), additional aerogel specimens for further processing-structure-property information (**Section 9.2.2**), and application-specific testing (**Section 9.2.3**).

9.2.1. Biochemical analyses for detailed gelation chemistry

There are a set of biochemical investigations that can further elucidate the components and purity of the protein extracts, eventually assisting with queries relating to the gelation mechanism. Such studies do not directly impact the applicability of CSM protein aerogel products, however information relating to gelation can generate novel ideas for improvements to gelation and subsequent aerogels. Biochemical analyses should first establish the purity of the protein extract in more detail than explored in **Section 5.3.2**, by complementing amino acid analyses with total nitrogen (*e.g.* Kjeldahl method) and ash content measurements. Targeted chemical assays can also be used to determine and quantify other non-proteinaceous molecules which may be implicated in gelation of the extract. These include polysaccharides (measured with phenol-sulphuric acid hydrolysis [322] or gas-liquid chromatography [323]), phytates (assessed by measuring iron binding capacity [324]), and phenolics (measured colourmetrically with Folin-Denis reagent [325]). Understanding the possible role of these non-proteinaceous molecules in gelation, may require gelation experiments with prior removal or addition of these non-proteinaceous components.

Some biochemical analyses conducted in this project can be revisited in future work, with an aim to improve experiment quality and scope. These include investigations using circular dichroism (CD) spectroscopy and native-PAGE analyses where both are conducted using a broader selection of solution conditions. Additionally, data from native-PAGE analyses can be complemented with a zeta potential assay to establish the exact isoelectric point (pI) of the CSM protein extracts and the

subsequent effects of salts (*e.g.* $CaCl_2$) on the isoelectric point. Chemical information can also be garnered using Fourier-transform infrared (FTIR) spectroscopy, allowing for direct confirmation of hypothesised chemical changes in gelled protein. Through improvements to current analyses and using additional techniques, the precise relationship between protein secondary structure, solution conditions, chemical bonds, and gelation success can be confirmed.

Finally, the quantification of specific proteins in the extracts can also assist with confirmation of the gelation mechanism outlined in this thesis. Understanding the exact proportions of cruciferin, napin, and other proteins, alongside their amino acid sequences, could eventually lead to a stoichiometric description of CSM protein gelation. One clear example of this is establishing a cruciferin-to-napin ratio for the extracts. The comparative amounts of cruciferin and napin (alongside minor proteins) can indicate the likelihood of specific associations (*e.g.* disulphide bridges, hydrophobic interactions, *etc.*) in the final gels using sequence information. Napin protein, for example, contains 4 disulphide bonds in a 12 kDa monomer, while cruciferin contains just 2 disulphide bonds in a 60 kDa monomer. Disulphide linkages are therefore unlikely to play a crucial role in gelation of a cruciferin dominated extract, such as in this work. However, the exact ratio of cruciferin to other proteins is yet to be quantified, therefore the quantity of thiol groups available for covalent bonding in the canola protein gels is unknown. The collection of eluted fractions from gel filtration chromatography (GFC) can allow for the concurrent identification and quantification of proteins. Unlike SDS-PAGE analyses which are only semi-quantitative, GFC fractions can be analysed for protein concentration using classic spectrophotometric techniques. The concentration of each fraction can be matched to a specific protein as identified by tandem mass spectrometry on the same GFC fraction.

9.2.2. Additional aerogel samples and characterisation

There was a broad selection of processing parameters that were left either unexplored or under-explored. Production and characterisation of additional variants can provide further information for the current thesis aims, specifically processing-property relationships and the development of more

competitive aerogels. Additional gel variants should include a greater selection of pH values that aim to determine optimal gel pH with more accuracy (*e.g.* pH = 7.50, 7.75, 8.25, 8.50, 9.00). Parameters such as gelation temperature, gelation time, and ageing time can also be revisited in future research, given the brevity of these investigations in the current work. Additionally, gelation techniques used in the current thesis were restricted to manipulation of aqueous chemical parameters, but future work may incorporate other gelation methods. As suggested in **Section 8.6.1**, these can include the use of a transglutaminase enzyme or chemical crosslinker (*e.g.* glutaraldehyde) with an aim to increase covalent bonding in the gel networks. Consequently, crosslinked gels and aerogels will have modified rheological, chemical, and mechanical properties. Indeed, the introduction of covalent bonding to the CSM protein gels may alter gel chemistry so fundamentally that resulting aerogels possess an entirely different set of properties and application potential.

There is also a need to develop many more supercritically dried CSM protein aerogels. Variations to pH, Ca^{2+} concentration, protein concentration, temperature, and hybridisation with fibrous biopolymers, should all be explored for supercritically dried gels. Supercritically dried aerogels are likely to reveal more accurate descriptions of processing-structure-property relationships given the high quality of gel network preservation achieved with this technique. Relationships that are suggested from the current work (*e.g.* pH may control particulate size in gels and consequently aerogel pore sizes) can be specifically probed with additional experiments in SC-CO_2 drying. Characterisation of these new variants should also include properties which were left unexplored in the supercritically dried aerogels, namely mechanical and chemical properties. Meanwhile, further measurements in gas porosimetry and density will better place these supercritical variants in context with other aerogel types. Accuracy in density measurements can be improved by the combined use of a geopycnometer (for bulk density) and a gaspycnometer (for skeletal density), particularly where monoliths have irregular shape as in the supercritically dried samples.

9.2.3. Applied testing for application potential

Thirdly, applied investigations that directly assess application potential can continue the current project towards commercialisation of CSM protein aerogels. A key area of interest in proteinaceous aerogels is the possibility of unique bioactive potential from specific proteins. The detection of cryptides in extract and aerogel samples from this thesis represents promising bioactive potential from a one-off investigation using a minimal sample set. Further *in silico* assessments of bioactive potential in CSM protein aerogels should include a broader sample set (*i.e.* supercritically processed and hybridised aerogels) and aim to quantify the bioactive potential. Subsequent *in vitro* and *in vivo* investigations can be developed, aiming to release, detect, and measure the real-life bioactive effects of canola proteins, both in extracts and as aerogel structures.

Biodegradability and biocompatibility (*e.g.* digestibility, non-toxicity) of CSM protein aerogels are assumed qualities essential for application potential. However, neither property is specifically investigated in this thesis, requiring targeted future research before commercialisation can be realised. Upon establishing the biodegradability, biocompatibility, and bioactive potential, specific application trials such as inclusion in dry cosmetics (cryogels) or active molecule release (aerogels) can be designed for these novel, protein-based aerogels.

References

1. Sun, H., Z. Xu, and C. Gao, *Multifunctional, ultra-flyweight, synergistically assembled carbon aerogels.* Advanced Materials, 2013. **25**(18): p. 2554-2560.
2. Dorcheh, A.S. and M. Abbasi, *Silica aerogel; synthesis, properties and characterization.* Journal of materials processing technology, 2008. **199**(1): p. 10-26.
3. Hrubesh, L.W. and R.W. Pekala, *Thermal properties of organic and inorganic aerogels.* Journal of Materials Research, 1994. **9**(03): p. 731-738.
4. Fricke, J. and T. Tillotson, *Aerogels: production, characterization, and applications.* Thin Solid Films, 1997. **297**(1–2): p. 212-223.
5. Tabata, M., et al., *Development of transparent silica aerogel over a wide range of densities.* Nuclear Instruments and Methods in Physics Research Section A: Accelerators, Spectrometers, Detectors and Associated Equipment, 2010. **623**(1): p. 339-341.
6. Jones, S.M. and J. Sakamoto, *Applications of aerogels in space exploration*, in *Aerogels Handbook*. 2011, Springer. p. 721-746.
7. Akimov, Y.K., *Fields of application of aerogels (review).* Instruments and Experimental Techniques, 2003. **46**(3): p. 287-299.
8. Hrubesh, L., *Aerogels for electronics*. 1994, Lawrence Livermore National Lab., CA (United States).
9. Maleki, H., et al., *Synthesis and biomedical applications of aerogels: Possibilities and challenges.* Advances in Colloid and Interface Science, 2016. **236**: p. 1-27.
10. Maleki, H., *Recent advances in aerogels for environmental remediation applications: A review.* Chemical Engineering Journal, 2016. **300**: p. 98-118.
11. Zhao, S., et al., *Biopolymer Aerogels and Foams: Chemistry, Properties, and Applications.* Angewandte Chemie International Edition, 2018. **57**(26): p. 7580-7608.
12. Hrubesh, L.W., *Aerogel applications.* Journal of Non-Crystalline Solids, 1998. **225**: p. 335-342.
13. Gesser, H. and P. Goswami, *Aerogels and related porous materials.* Chemical Reviews, 1989. **89**(4): p. 765-788.
14. Yokogawa, H., *Transparent silica aerogel blocks for high-energy physics research*, in *Aerogels Handbook*. 2011, Springer. p. 651-663.
15. Gash, A.E., R.L. Simpson, and J.H. Satcher, *Aerogels and sol–gel composites as nanostructured energetic materials*, in *Aerogels Handbook*. 2011, Springer. p. 585-606.
16. Carroll, M.K. and A.M. Anderson, *Aerogels as platforms for chemical sensors*, in *Aerogels Handbook*. 2011, Springer. p. 637-650.
17. Stergar, J. and U. Maver, *Review of aerogel-based materials in biomedical applications.* Journal of Sol-Gel Science and Technology, 2016. **77**(3): p. 738-752.
18. Woignier, T., J. Reynes, and J. Phalippou, *Sintering of Silica Aerogels for Glass Synthesis: Application to Nuclear Waste Containment*, in *Aerogels Handbook*, M.A. Aegerter, N. Leventis, and M.M. Koebel, Editors. 2011, Springer New York: New York, NY. p. 665-680.
19. Ratke, L. and B. Milow, *Aerogels for Foundry Applications*, in *Aerogels Handbook*, M.A. Aegerter, N. Leventis, and M.M. Koebel, Editors. 2011, Springer New York: New York, NY. p. 763-788.
20. Yin, W. and D.A. Rubenstein, *Biomedical applications of aerogels*, in *Aerogels Handbook*. 2011, Springer. p. 683-694.
21. Smirnova, I., *Pharmaceutical applications of aerogels*, in *Aerogels Handbook*. 2011, Springer. p. 695-717.
22. Cassin, G. and S.P. Fristot, *Cosmetic composition comprising silica aerogel particles and silicone oils*. 2018, Google Patents.
23. Mikkonen, K.S., et al., *Prospects of polysaccharide aerogels as modern advanced food materials.* Trends in Food Science & Technology, 2013. **34**(2): p. 124-136.

24. McCormick, B., *Insights and Analysis of Manufacturing and Marketing Consumer Products with Aerogel Materials*, in *Aerogels Handbook*, M.A. Aegerter, N. Leventis, and M.M. Koebel, Editors. 2011, Springer New York: New York, NY. p. 835-845.
25. Alemán, J.V., et al., *Definitions of terms relating to the structure and processing of sols, gels, networks, and inorganic-organic hybrid materials (IUPAC Recommendations 2007)*, in *Pure and Applied Chemistry*. 2007. p. 1801.
26. Everett, D.H., *Manual of Symbols and Terminology for Physicochemical Quantities and Units, Appendix II: Definitions, Terminology and Symbols in Colloid and Surface Chemistry*, in *Pure and Applied Chemistry*. 1972. p. 577.
27. Aegerter, M.A., N. Leventis, and M.M. Koebel, *Aerogels handbook*. 2011: Springer Science & Business Media. 932 p.
28. Hench, L.L. and J.K. West, *The sol-gel process.* Chemical Reviews, 1990. **90**(1): p. 33-72.
29. Kistler, S.S., *Coherent Expanded Aerogels and Jellies.* Nature, 1931. **127**: p. 741.
30. C. Pierre, A., *History of Aerogels*. 2011. p. 3-18.
31. Hüsing, N. and U. Schubert, *Aerogels—Airy Materials: Chemistry, Structure, and Properties.* Angewandte Chemie International Edition, 1998. **37**(1-2): p. 22-45.
32. Kistler, S., *Coherent expanded-aerogels.* The Journal of Physical Chemistry, 1932. **36**(1): p. 52-64.
33. Gash, A.E., et al., *New sol–gel synthetic route to transition and main-group metal oxide aerogels using inorganic salt precursors.* Journal of Non-Crystalline Solids, 2001. **285**(1): p. 22-28.
34. Clapsaddle, B.J., et al., *A sol–gel methodology for the preparation of lanthanide-oxide aerogels: preparation and characterization.* Journal of Sol-Gel Science and Technology, 2012. **64**(2): p. 381-389.
35. Tappan, B.C., S.A. Steiner, and E.P. Luther, *Nanoporous Metal Foams.* Angewandte Chemie International Edition, 2010. **49**(27): p. 4544-4565.
36. Hair, L.M., et al., *Low-density resorcinol–formaldehyde aerogels for direct-drive laser inertial confinement fusion targets.* Journal of Vacuum Science & Technology A, 1988. **6**(**4**): p. 2559-2563.
37. Wu, D., et al., *Low-density organic and carbon aerogels from the sol–gel polymerization of phenol with formaldehyde.* Journal of Non-Crystalline Solids, 2005. **351**(10): p. 915-921.
38. Westfahl Jr, H., *Smectic ordering in polymer liquid crystal-silica aerogel nanocomposites: Studies of DSC and SAXS.* Journal of thermal analysis and calorimetry, 2005. **79**(3): p. 579-585.
39. Aegerter, M., N. Leventis, and M.M. Koebel, *Aerogels handbook*. 2011: Springer Science & Business Media.
40. Zhang, X., et al., *Mechanically strong and highly conductive graphene aerogel and its use as electrodes for electrochemical power sources.* journal of materials chemistry, 2011. **21**(18): p. 6494-6497.
41. Glenn, G.M. and D.W. Irving, *Starch-based microcellular foams.* Cereal chemistry, 1995. **72**(2): p. 155-161.
42. Nazarov, R., H.-J. Jin, and D.L. Kaplan, *Porous 3-D Scaffolds from Regenerated Silk Fibroin.* Biomacromolecules, 2004. **5**(3): p. 718-726.
43. Woignier, T., et al., *Mechanical Properties and Brittle Behavior of Silica Aerogels.* Gels, 2015. **1**(2): p. 256-275.
44. Pekala, R. and F.M. Kong, *Resorcinol-formaldehyde aerogels and their carbonized derivatives*. 1988, Lawrence Livermore National Lab., CA (USA).
45. Pekala, R.W., et al., *Carbon aerogels for electrochemical applications.* Journal of Non-Crystalline Solids, 1998. **225**: p. 74-80.
46. Tan, C., et al., *Organic aerogels with very high impact strength.* Advanced Materials, 2001. **13**(9): p. 644-646.
47. Draper, E.R. and D.J. Adams, *Photoresponsive gelators.* Chemical Communications, 2016. **52**(53): p. 8196-8206.

48. Lu, T., et al., *Composite aerogels based on dialdehyde nanocellulose and collagen for potential applications as wound dressing and tissue engineering scaffold.* Composites Science and Technology, 2014. **94**: p. 132-138.
49. H. Zhang, C.H.a.Y.Q., *Synthesis, Structural and Thermal Properties of Nano-porous SiO2-based Aerogels N2* in *Advances in Nanocomposites - Synthesis, Characterization and Industrial Applications*, B. Reddy, Editor. 2011, InTech. p. 39 - 60.
50. Poco, J.F., et al., *Synthesis of high porosity, monolithic alumina aerogels.* Journal of Non-Crystalline Solids, 2001. **285**(1): p. 57-63.
51. Mack, C., *Fundamental principles of optical lithography: the science of microfabrication*. 2008: John Wiley & Sons.
52. Du, A., et al., *A Special Material or a New State of Matter: A Review and Reconsideration of the Aerogel.* Materials, 2013. **6**(3): p. 941.
53. Smith, D.M., et al., *Preparation of low-density xerogels at ambient pressure.* Journal of Non-Crystalline Solids, 1995. **186**: p. 104-112.
54. Steiner, S., *SUPERLIGHT AND NOW SUPERSIZED—WORLD'S LARGEST AEROGEL PAVES WAY FOR 10X LIGHTER PLASTICS*. 2018 http://www.aerogeltechnologies.com/.
55. Gurav, J.L., et al., *Silica Aerogel: Synthesis and Applications.* Journal of Nanomaterials, 2010. **2010**: p. 1-11.
56. Tamon, H., et al., *Preparation of mesoporous carbon by freeze drying.* Carbon, 1999. **37**(12): p. 2049-2055.
57. Borisova, A., et al., *A Sustainable Freeze-Drying Route to Porous Polysaccharides with Tailored Hierarchical Meso- and Macroporosity*. Macromolecular Rapid Communications, 2015. **36**(8): p. 774-779.
58. Czakkel, O., et al., *Influence of drying on the morphology of resorcinol–formaldehyde-based carbon gels.* Microporous and Mesoporous Materials, 2005. **86**(1): p. 124-133.
59. Pierre, A.C. and A. Rigacci, *SiO 2 aerogels*, in *Aerogels handbook*. 2011, Springer. p. 21-45.
60. Mulik, S. and C. Sotiriou-Leventis, *Resorcinol–formaldehyde aerogels*, in *Aerogels handbook*. 2011, Springer. p. 215-234.
61. Mirzaeian, M. and P.J. Hall, *The control of porosity at nano scale in resorcinol formaldehyde carbon aerogels.* Journal of Materials Science, 2009. **44**(10): p. 2705-2713.
62. Zhang, H., et al., *Controlling the microstructure of resorcinol-furfural aerogels and derived carbon aerogels: Via the salt templating approach.* RSC Advances, 2019. **9**: p. 5967-5977.
63. Baumann, T.F., A.E. Gash, and J.H. Satcher, *A robust approach to inorganic aerogels: the use of epoxides in sol–gel synthesis*, in *Aerogels Handbook*. 2011, Springer. p. 155-170.
64. Leventis, N. and H. Lu, *Polymer-Crosslinked Aerogels*, in *Aerogels Handbook*, M.A. Aegerter, N. Leventis, and M.M. Koebel, Editors. 2011, Springer New York: New York, NY. p. 251-285.
65. Koebel, M.M., A. Rigacci, and P. Achard, *Aerogels for superinsulation: a synoptic view*, in *Aerogels Handbook*. 2011, Springer. p. 607-633.
66. Sattayatam, P., J. Del Pinto, and D. Long, *Polyimide aerogel insulated panel assembly*. 2018, Google Patents.
67. Wang, D., et al., *Adsorption of oils from pure liquid and oil–water emulsion on hydrophobic silica aerogels.* Separation and Purification Technology, 2012. **99**: p. 28-35.
68. Rao, A.V., et al., *Superhydrophobic and flexible Aerogels*, in *Aerogels Handbook*. 2011, Springer. p. 79-101.
69. Sabu Thomas, L.A.P., Rubie Mavelil-Sam, *Biobased Aerogels : polysaccharide and protein-based materials*. Biobased Aerogels : polysaccharide and protein-based materials, ed. L.A.P. Sabu Thomas, Rubie Mavelil-Sam. 2018, Cambridge: Royal Soc of Chemistry. 330.
70. Iwata, T., *Biodegradable and Bio-Based Polymers: Future Prospects of Eco-Friendly Plastics.* Angewandte Chemie International Edition, 2015. **54**(11): p. 3210-3215.
71. Mohanty, A.K., M. Misra, and G. Hinrichsen, *Biofibres, biodegradable polymers and biocomposites: An overview.* Macromolecular Materials and Engineering, 2000. **276-277**(1): p. 1-24.

72. Huber, T., et al., *A critical review of all-cellulose composites.* Journal of Materials Science, 2012. **47**(3): p. 1171-1186.
73. Chen, H.-B., et al., *Biodegradable Pectin/Clay Aerogels.* ACS Applied Materials & Interfaces, 2013. **5**(5): p. 1715-1721.
74. Ulker, Z. and C. Erkey, *An emerging platform for drug delivery: Aerogel based systems.* Journal of Controlled Release, 2014. **177**: p. 51-63.
75. Kleemann, C., et al., *Tailor made protein based aerogel particles from egg white protein, whey protein isolate and sodium caseinate: Influence of the preceding hydrogel characteristics.* Food Hydrocolloids, 2018. **83**: p. 365-374.
76. Yang, W.-J., et al., *Recent progress in bio-based aerogel absorbents for oil/water separation.* Cellulose, 2019. **26**(11): p. 6449-6476.
77. Ratke, L., *Monoliths and fibrous cellulose aerogels*, in *Aerogels handbook*. 2011, Springer. p. 173-190.
78. Quignard, F., R. Valentin, and F. Di Renzo, *Aerogel materials from marine polysaccharides.* New Journal of Chemistry, 2008. **32**(8): p. 1300-1310.
79. Wei, S., Y.C. Ching, and C.H. Chuah, *Synthesis of chitosan aerogels as promising carriers for drug delivery: A review.* Carbohydrate Polymers, 2019: p. 115744.
80. Soorbaghi, F.P., et al., *Bioaerogels: Synthesis approaches, cellular uptake, and the biomedical applications.* Biomedicine & Pharmacotherapy, 2019. **111**: p. 964-975.
81. Ubeyitogullari, A., et al., *Enhancing the Bioaccessibility of Phytosterols Using Nanoporous Corn and Wheat Starch Bioaerogels.* European Journal of Lipid Science and Technology, 2019. **121**(1): p. 1700229.
82. Buisson, P., et al., *Encapsulation of lipases in aerogels.* Journal of Non-Crystalline Solids, 2001. **285**(1): p. 295-302.
83. Harper-Leatherman, A.S., E.R. Pacer, and N.D. Kosciuszek, *Encapsulating Cytochrome c in Silica Aerogel Nanoarchitectures without Metal Nanoparticles while Retaining Gas-phase Bioactivity.* Journal of visualized experiments: JoVE, 2016(109).
84. Veres, P., et al., *Mechanism of drug release from silica-gelatin aerogel—Relationship between matrix structure and release kinetics.* Colloids and Surfaces B: Biointerfaces, 2017. **152**: p. 229-237.
85. Wallace, J.M., et al., *Silica nanoarchitectures incorporating self-organized protein superstructures with gas-phase bioactivity.* Nano Letters, 2003. **3**(10): p. 1463-1467.
86. Totosaus, A., et al., *A review of physical and chemical protein-gel induction.* International Journal of Food Science & Technology, 2002. **37**(6): p. 589-601.
87. Fitzpatrick, S.E., et al., *Chapter 6 Protein-based Aerogels: Processing and Morphology*, in *Biobased Aerogels: Polysaccharide and Protein-based Materials*. 2018, The Royal Society of Chemistry. p. 67-102.
88. Shi, W. and M.-J. Dumont, *Review: bio-based films from zein, keratin, pea, and rapeseed protein feedstocks.* Journal of Materials Science, 2014. **49**(5): p. 1915-1930.
89. Ricci, A., et al., *Chitosan aerogel: a recyclable, heterogeneous organocatalyst for the asymmetric direct aldol reaction in water.* Chemical Communications, 2010. **46**(34): p. 6288-6290.
90. Li, Y.K., et al., *A novel method for preparing a protein-encapsulated bioaerogel: Using a red fluorescent protein as a model.* Acta Biomaterialia, 2008. **4**(3): p. 725-732.
91. Nyström, G., et al., *Amyloid Templated Gold Aerogels.* Advanced Materials, 2016. **28**(3): p. 472-478.
92. Mallepally, R.R., et al., *Silk fibroin aerogels: potential scaffolds for tissue engineering applications.* Biomedical Materials, 2015. **10**(3): p. 035002.
93. Doi, E., *Gels and gelling of globular proteins.* Trends in Food Science & Technology, 1993. **4**(1): p. 1-5.
94. Selmer, I., et al., *Development of egg white protein aerogels as new matrix material for microencapsulation in food.* Journal of Supercritical Fluids, 2015. **106**(Aerogels: Synthesis and Applications): p. 42-49.
95. Betz, M., et al., *Preparation of novel whey protein-based aerogels as drug carriers for life science applications.* Journal of Supercritical Fluids, 2012. **72**: p. 111-119.

96. Baldino, L., S. Cardea, and E. Reverchon, *Loaded silk fibroin aerogel production by supercritical gel drying process for nanomedicine applications*, in *Chemical Engineering Transactions*, E. Bardone, T. Keshavarz, and M. Bravi, Editors. 2016, Italian Association of Chemical Engineering - AIDIC. p. 343-348.
97. Jiang, J., et al., *A multifunctional gelatin-based aerogel with superior pollutants adsorption, oil/water separation and photocatalytic properties.* Chemical Engineering Journal, 2019. **358**: p. 1539-1551.
98. Amaral-Labat, G., et al., *Highly mesoporous organic aerogels derived from soy and tannin.* Green Chemistry, 2012. **14**(11): p. 3099-3106.
99. Arboleda, J.C., et al., *Soy protein–nanocellulose composite aerogels.* Cellulose, 2013. **20**(5): p. 2417-2426.
100. Hair, L.M., et al., *Low-density resorcinol–formaldehyde aerogels for direct-drive laser inertial confinement fusion targets.* Journal of Vacuum Science & Technology A, 1988. **6**(4): p. 2559-2563.
101. S.S. Kistler, *Coherent Expanded Aerogels and Jellies. Nature*, 1931. **127**: p. 741.
102. Kim, U.-J., et al., *Three-dimensional aqueous-derived biomaterial scaffolds from silk fibroin.* Biomaterials, 2005. **26**(15): p. 2775-2785.
103. Selmer, I., et al., *Development of egg white protein aerogels as new matrix material for microencapsulation in food.* The Journal of Supercritical Fluids, 2015. **106**: p. 42-49.
104. White, R.J., et al., *A sustainable synthesis of nitrogen-doped carbon aerogels.* Green Chemistry, 2011. **13**(9): p. 2428-2434.
105. Alatalo, S.-M., et al., *Versatile Cellulose-Based Carbon Aerogel for the Removal of Both Cationic and Anionic Metal Contaminants from Water.* ACS Applied Materials & Interfaces, 2015. **7**(46): p. 25875-25883.
106. Mallepally, R.R., M.A. Marin, and M.A. McHugh, *CO 2-assisted synthesis of silk fibroin hydrogels and aerogels.* Acta Biomaterialia, 2014. **10**(10): p. 4419-4424.
107. Marin, M.A., R.R. Mallepally, and M.A. McHugh, *Silk fibroin aerogels for drug delivery applications.* The Journal of Supercritical Fluids, 2014. **91**: p. 84-89.
108. Yun, Y.S., S.Y. Cho, and H.-J. Jin, *Carbon aerogels based on regenerated silk proteins and graphene oxide for supercapacitors.* Macromolecular Research, 2014. **22**(5): p. 509-514.
109. Baldino, L., S. Cardea, and E. Reverchona, *Loaded Silk Fibroin Aerogel Production by Supercritical Gel Drying Process for Nanomedicine Applications.* CHEMICAL ENGINEERING, 2016. **49**.
110. Yao, D., et al., *Salt-leached silk scaffolds with tunable mechanical properties.* Biomacromolecules, 2012. **13**(11): p. 3723-3729.
111. Blomfeldt, T.O.J., et al., *Novel Foams Based on Freeze-Dried Renewable Vital Wheat Gluten.* Macromolecular Materials and Engineering, 2010. **295**(9): p. 796-801.
112. Zhuang, Y., et al., *Adsorption of ciprofloxacin onto graphene–soy protein biocomposites.* New Journal of Chemistry, 2015. **39**(5): p. 3333-3336.
113. Zhuang, Y., et al., *Graphene as a template and structural scaffold for the synthesis of a 3D porous bio-adsorbent to remove antibiotics from water.* RSC Advances, 2015. **5**(35): p. 27964-27969.
114. Bi, B., et al., *Effect of freezing treatment on structure and adsorption characteristic of soy protein porous materials crosslinked by aldehydes.* Transactions of the Chinese Society of Agricultural Engineering, 2016. **32**(7): p. 309-314.
115. Zhuang, Y., et al., *Facile synthesis of three-dimensional graphene–soy protein aerogel composites for tetracycline adsorption.* Desalination and Water Treatment, 2016. **57**(20): p. 9510-9519.
116. Shamsuri, A.A., D.K. Abdullah, and R. Daik, *Fabrication of agar/biopolymer blend aerogels in ionic liquid and co-solvent mixture.* Cell. Chem. Technol, 2012. **46**(1-2): p. 45-52.
117. Verdolotti, L., et al., *Bio-hybrid foams by silsesquioxanes cross-linked thermoplastic zein films.* Journal of Cellular Plastics, 2014: p. 0021955X14529138.
118. Chen, H.-B., Y.-Z. Wang, and D.A. Schiraldi, *Foam-like materials based on whey protein isolate.* European Polymer Journal, 2013. **49**(10): p. 3387-3391.

119. Betz, M., et al., *Preparation of novel whey protein-based aerogels as drug carriers for life science applications.* The Journal of Supercritical Fluids, 2012. **72**: p. 111-119.
120. Ahmadi, M., A. Madadlou, and A.A. Saboury, *Whey protein aerogel as blended with cellulose crystalline particles or loaded with fish oil.* Food chemistry, 2016. **196**: p. 1016-1022.
121. Pojanavaraphan, T., et al., *Development of Biodegradable Foamlike Materials Based on Casein and Sodium Montmorillonite Clay.* Biomacromolecules, 2010. **11**(10): p. 2640-2646.
122. Altman, G.H., et al., *Silk-based biomaterials.* Biomaterials, 2003. **24**(3): p. 401-416.
123. Lv, Q. and Q. Feng, *Preparation of 3-D regenerated fibroin scaffolds with freeze drying method and freeze drying/foaming technique.* Journal of Materials Science: Materials in Medicine, 2006. **17**(12): p. 1349-1356.
124. Bardajee, G.R., A. Pourjavadi, and R. Soleyman, *Novel highly swelling nanoporous hydrogel based on polysaccharide/protein hybrid backbone.* Journal of Polymer Research, 2011. **18**(3): p. 337-346.
125. Finlay, K., M.D. Gawryla, and D.A. Schiraldi, *Biologically based fiber-reinforced/clay aerogel composites.* Industrial and Engineering Chemistry Research, 2008. **47**(3): p. 615-619.
126. Maleki, H., L. Whitmore, and N. Hüsing, *Novel multifunctional polymethylsilsesquioxane–silk fibroin aerogel hybrids for environmental and thermal insulation applications.* Journal of Materials Chemistry A, 2018. **6**(26): p. 12598-12612.
127. Chen, H.B., Y.Z. Wang, and D.A. Schiraldi, *Foam-like materials based on whey protein isolate.* European Polymer Journal, 2013. **49**(10): p. 3387-3391.
128. Marin, M.A., R.R. Mallepally, and M.A. McHugh, *Silk fibroin aerogels for drug delivery applications.* Journal of Supercritical Fluids, 2014. **91**: p. 84-89.
129. Mallepally, R.R., M.A. Marin, and M.A. McHugh, *CO2-assisted synthesis of silk fibroin hydrogels and aerogels.* Acta Biomaterialia, 2014. **10**(10): p. 4419-24.
130. Yun, Y.S., S.Y. Cho, and H.J. Jin, *Carbon aerogels based on regenerated silk proteins and graphene oxide for supercapacitors.* Macromolecular Research, 2014. **22**(5): p. 509-514.
131. Arboleda, J.C., et al., *Soy protein-nanocellulose composite aerogels.* Cellulose, 2013. **20**(5): p. 2417-2426.
132. Zhuang, Y., et al., *Adsorption of ciprofloxacin onto graphene-soy protein biocomposites.* New Journal of Chemistry, 2015. **39**(5): p. 3333-3336.
133. Alatalo, S.M., et al., *Versatile Cellulose-Based Carbon Aerogel for the Removal of Both Cationic and Anionic Metal Contaminants from Water.* ACS Applied Materials and Interfaces, 2015. **7**(46): p. 25875-25883.
134. Shamsuri, A.A., D.K. Abdullah, and D. Rusli, *Fabrication of agar/biopolymer blend aerogels in ionic liquid and co-solvent mixture.* Cellulose Chemistry and Technology, 2012. **46**(1-2): p. 45-52.
135. Verdolotti, L., et al., *Bio-hybrid foams by silsesquioxanes cross-linked thermoplastic zein films.* Journal of Cellular Plastics, 2015. **51**(1): p. 75-87.
136. Raman, S.P., P. Gurikov, and I. Smirnova, *Hybrid alginate based aerogels by carbon dioxide induced gelation: Novel technique for multiple applications.* Journal of Supercritical Fluids, 2015.
137. Mitropoulos, A.N., et al., *Noble Metal Composite Porous Silk Fibroin Aerogel Fibers.* Materials (Basel, Switzerland), 2019. **12**(6): p. 894.
138. Selmer, I., et al., *Encapsulation of fish oil in protein aerogel micro-particles.* Journal of Food Engineering, 2019. **260**: p. 1-11.
139. Menshutina, N.V., et al., *THE PROCESS OF EGG PROTEIN AEROGELS PRODUCTION.* International Multidisciplinary Scientific GeoConference : SGEM, 2019. **19**(6.1): p. 459-465.
140. Weng, L., et al., *Novel 3D Hybrid Nanofiber Aerogels Coupled with BMP-2 Peptides for Cranial Bone Regeneration.* Advanced Healthcare Materials, 2018. **7**(10): p. 1701415.
141. Finlay, K., M.D. Gawryla, and D.A. Schiraldi, *Biologically Based Fiber-Reinforced/Clay Aerogel Composites.* Industrial & Engineering Chemistry Research, 2008. **47**(3): p. 615-619.
142. Totosaus, A., et al., *A review of physical and chemical protein-gel induction.* International journal of food science & technology, 2002. **37**(6): p. 589-601.

143. Van Kleef, F., J. Boskamp, and M. Van den Tempel, *Determination of the number of cross-links in a protein gel from its mechanical and swelling properties.* Biopolymers, 1978. **17**(1): p. 225-235.
144. Matsumoto, A., et al., *Mechanisms of Silk Fibroin Sol−Gel Transitions.* The Journal of Physical Chemistry B, 2006. **110**(43): p. 21630-21638.
145. Ahmadi, M., A. Madadlou, and A.A. Sabouri, *Isolation of micro-and nano-crystalline cellulose particles and fabrication of crystalline particles-loaded whey protein cold-set gel.* Food chemistry, 2015. **174**: p. 97-103.
146. Alting, A.C., et al., *Cold-set globular protein gels: interactions, structure and rheology as a function of protein concentration.* Journal of Agricultural and Food Chemistry, 2003. **51**(10): p. 3150-3156.
147. Brunauer, S., P.H. Emmett, and E. Teller, *Adsorption of Gases in Multimolecular Layers.* Journal of the American Chemical Society, 1938. **60**(2): p. 309-319.
148. Dubinin, M., *Fundamentals of the theory of adsorption in micropores of carbon adsorbents: characteristics of their adsorption properties and microporous structures.* Carbon, 1989. **27**(3): p. 457-467.
149. Barrett, E.P., L.G. Joyner, and P.P. Halenda, *The determination of pore volume and area distributions in porous substances. I. Computations from nitrogen isotherms.* Journal of the American Chemical Society, 1951. **73**(1): p. 373-380.
150. Sing, K., *The use of nitrogen adsorption for the characterisation of porous materials.* Colloids and Surfaces A: Physicochemical and Engineering Aspects, 2001. **187**: p. 3-9.
151. Brunauer, S., P.H. Emmett, and E. Teller, *Adsorption of gases in multimolecular layers.* J. Am. Chem. Soc, 1938. **60**(2): p. 309-319.
152. Westermarck, S., *Use of mercury porosimetry and nitrogen adsorption in characterisation of the pore structure of mannitol and microcrystalline cellulose powders, granules and tablets*. 2000: S. Westermarck.
153. Chang, X., D. Chen, and X. Jiao, *Chitosan-Based Aerogels with High Adsorption Performance.* The Journal of Physical Chemistry B, 2008. **112**(26): p. 7721-7725.
154. Al-Muhtaseb, S.A. and J.A. Ritter, *Preparation and Properties of Resorcinol–Formaldehyde Organic and Carbon Gels.* Advanced Materials, 2003. **15**(2): p. 101-114.
155. Kirkbir, F., et al., *Drying of aerogels in different solvents between atmospheric and supercritical pressures.* Journal of Non-Crystalline Solids, 1998. **225**: p. 14-18.
156. Pekala, R.W. and D.W. Schaefer, *Structure of organic aerogels. 1. Morphology and scaling.* Macromolecules, 1993. **26**(20): p. 5487-5493.
157. Sun, H., Z. Xu, and C. Gao, *Multifunctional, Ultra-Flyweight, Synergistically Assembled Carbon Aerogels.* Advanced Materials, 2013. **25**(18): p. 2554-2560.
158. Maldonado-Hódar, F.J., et al., *Synthesis and textural characteristics of organic aerogels, transition-metal-containing organic aerogels and their carbonized derivatives.* Carbon, 1999. **37**(8): p. 1199-1205.
159. Tillotson, T.M. and L.W. Hrubesh, *Transparent ultralow-density silica aerogels prepared by a two-step sol-gel process.* Journal of Non-Crystalline Solids, 1992. **145**: p. 44-50.
160. Pekala, R., et al., *Aerogels derived from multifunctional organic monomers.* Journal of Non-Crystalline Solids, 1992. **145**: p. 90-98.
161. Rudaz, C., et al., *Aeropectin: Fully Biomass-Based Mechanically Strong and Thermal Superinsulating Aerogel.* Biomacromolecules, 2014. **15**(6): p. 2188-2195.
162. Ahmadi, M., A. Madadlou, and A.A. Sabouri, *Isolation of micro- and nano-crystalline cellulose particles and fabrication of crystalline particles-loaded whey protein cold-set gel.* Food Chemistry, 2015. **174**: p. 97-103.
163. García-González, C.A., M. Alnaief, and I. Smirnova, *Polysaccharide-based aerogels—Promising biodegradable carriers for drug delivery systems.* Carbohydrate polymers, 2011. **86**(4): p. 1425-1438.
164. Gesser, H.D. and P.C. Goswami, *Aerogels and related porous materials.* Chemical Reviews, 1989. **89**(4): p. 765-788.
165. Baia, L., et al., *Type I collagen-TiO2 aerogel based biocomposites.* Journal of Optoelectronics and Advanced Materials, 2008. **10**(4): p. 933-936.

166. Sachithanadam, M. and S.C. Joshi, *A new phenomenon of compressive strain recovery in gelatin-silica aerogel composites with SDS.* Procedia Engineering, 2014. **75**: p. 51-55.
167. Raman, S.P., P. Gurikov, and I. Smirnova, *Hybrid alginate based aerogels by carbon dioxide induced gelation: Novel technique for multiple applications.* The Journal of Supercritical Fluids, 2015. **106**: p. 23-33.
168. Pierre, A.C. and G.M. Pajonk, *Chemistry of aerogels and their applications.* Chemical Reviews, 2002. **102**(11): p. 4243-4266.
169. Power, M., et al., *Aerogels as biosensors: viral particle detection by bacteria immobilized on large pore aerogel.* Journal of Non-Crystalline Solids, 2001. **285**(1–3): p. 303-308.
170. Braun, S., et al., *Biochemically active sol-gel glasses: the trapping of enzymes.* Materials Letters, 1990. **10**(1): p. 1-5.
171. Orçaire, O., P. Buisson, and A.C. Pierre, *Application of silica aerogel encapsulated lipases in the synthesis of biodiesel by transesterification reactions.* Journal of Molecular Catalysis B: Enzymatic, 2006. **42**(3–4): p. 106-113.
172. Harper-Leatherman, A.S., et al., *Simplified procedure for encapsulating cytochrome c in silica aerogel nanoarchitectures while retaining gas-phase bioactivity*. Langmuir, 2012. **28**(41): p. 14756-14765.
173. Wallace, J.M., et al., *The effect of particle size and protein content on nanoparticle-gold-nucleated cytochrome c superstructures encapsulated in silica nanoarchitectures.* Journal of Non-Crystalline Solids, 2004. **350**: p. 31-38.
174. Maury, S., et al., *Compared esterification kinetics of the lipase from Burkholderia cepacia either free or encapsulated in a silica aerogel.* Journal of Molecular Catalysis B: Enzymatic, 2005. **32**(5–6): p. 193-203.
175. Bell, J., *Factors affecting the nutritional value of canola meal: a review.* Canadian Journal of Animal Science, 1993. **73**(4): p. 689-697.
176. Vles, R., G. Bijster, and W. Timmer, *Nutritional evaluation of low-erucic-acid rapeseed oils*, in *Toxicological Aspects of Food Safety*. 1978, Springer. p. 23-32.
177. Tan, S.H., et al., *Canola proteins for human consumption: extraction, profile, and functional properties.* Journal of Food Science, 2011. **76**(1): p. R16-R28.
178. Wanasundara, J.P., et al., *Canola/rapeseed protein-functionality and nutrition.* OCL, 2016. **23**(4): p. D407.
179. Akbari, A. and J. Wu, *Cruciferin nanoparticles: Preparation, characterization and their potential application in delivery of bioactive compounds.* Food Hydrocolloids, 2016. **54**(Part A): p. 107-118.
180. Arntfield, S., *Canola and other oilseed proteins.* Handbook of food proteins, 2011: p. 289.
181. Commission, E.; Available from: https://ec.europa.eu/agriculture/sites/agriculture/files/cereals/presentations/cereals-oilseeds/market-situation-oilseeds_en.pdf.
182. Uppström, B., *Seed chemistry.* Brassica Oilseeds: Utilization, 1995: p. 291-300.
183. Consultation, R., *Dietary protein quality evaluation in human nutrition.* FAO food and nutrition paper, 2011. **92**.
184. Yoshie-Stark, Y., Y. Wada, and A. Wäsche, *Chemical composition, functional properties, and bioactivities of rapeseed protein isolates.* Food Chemistry, 2008. **107**(1): p. 32-39.
185. Klockeman, D.M., R. Toledo, and K.A. Sims, *Isolation and Characterization of Defatted Canola Meal Protein.* Journal of Agricultural and Food Chemistry, 1997. **45**(10): p. 3867-3870.
186. Schwenke, K.D., K.J. Linow, and D. Zirwer, *Modification of the oligomeric structure of 11 S globulin from sunflower (Helianthus annuus L.) and rape (Brassica napus L.) seeds by succinylation.* Food / Nahrung, 1986. **30**(3-4): p. 263-270.
187. Schwenke, K.D., *Rapeseed proteins*, in *New and Developing Sources of Food Proteins*, B.J.F. Hudson, Editor. 1994, Springer US: Boston, MA. p. 281-306.
188. Malabat, C., et al. *Genetic variability of rapeseed protein composition*. in *11th International Rapeseed Congress. Royal Veterinary and Agricultural University*. 2003.

189. Tandang-Silvas, M.R.G., et al., *Conservation and divergence on plant seed 11S globulins based on crystal structures.* Biochimica et Biophysica Acta (BBA) - Proteins and Proteomics, 2010. **1804**(7): p. 1432-1442.
190. Rico, M., et al., *1H NMR Assignment and Global Fold of Napin BnIb, a Representative 2S Albumin Seed Protein.* Biochemistry, 1996. **35**(49): p. 15672-15682.
191. Aider, M. and C. Barbana, *Canola proteins: composition, extraction, functional properties, bioactivity, applications as a food ingredient and allergenicity – A practical and critical review.* Trends in Food Science & Technology, 2011. **22**(1): p. 21-39.
192. Wu, J. and A. Muir, *Comparative structural, emulsifying, and biological properties of 2 major canola proteins, cruciferin and napin.* Journal of food science, 2008. **73**(3).
193. Cameron, J.J. and C.D. Myers, *Rapeseed protein isolate*. 1983, Google Patents.
194. Campbell, L., C.B. Rempel, and J.P.D. Wanasundara, *Canola/Rapeseed Protein: Future Opportunities and Directions—Workshop Proceedings of IRC 2015.* Plants, 2016. **5**(2): p. 17.
195. Murray, E.D., *Oil seed protein extraction*. 1999, Google Patents.
196. Milanova, R., E. Murray, and P. Westdal, *Protein extraction from canola oil seed meal*. 2004, Google Patents.
197. Guthrie, N. and R.A. Guthrie, *Canola extracts containing high levels of sinapic acid*. 2007, Google Patents.
198. Kim, J.H., et al., *Nature of protein-protein interactions during the gelation of canola protein isolate networks.* Food Research International, 2016. **89**: p. 408-414.
199. Tan, S.H., et al., *Gelling properties of protein fractions and protein isolate extracted from australian canola meal.* Food Research International, 2014. **62**: p. 819-828.
200. Kim, J.H.J., N.V. Varankovich, and M.T. Nickerson, *The effect of pH on the gelling behaviour of canola and soy protein isolates.* Food Research International, 2016. **81**: p. 31-38.
201. Doi, E. and N. Kitabatake, *Structure of glycinin and ovalbumin gels.* Food Hydrocolloids, 1989. **3**(4): p. 327-337.
202. Léger, L.W. and S.D. Arntfield, *Thermal gelation of the 12S canola globulin.* Journal of the American Oil Chemists' Society, 1993. **70**(9): p. 853-861.
203. Gill, T. and M. Tung, *Thermally induced gelation of the 12S rapeseed glycoprotein.* Journal of Food Science, 1978. **43**(5): p. 1481-1485.
204. Schwenke, K.D., A. Dahme, and T. Wolter, *Heat-induced gelation of rapeseed proteins: Effect of protein interaction and acetylation.* Journal of the American Oil Chemists' Society, 1998. **75**(1): p. 83-87.
205. Paulson, A.T. and M.A. Tung, *Thermally induced gelation of succinylated canola protein isolate.* Journal of Agricultural and Food Chemistry, 1989. **37**(2): p. 319-326.
206. Chang, C. and M.T. Nickerson, *Effect of plasticizer-type and genipin on the mechanical, optical, and water vapor barrier properties of canola protein isolate-based edible films.* European Food Research and Technology, 2014. **238**(1): p. 35-46.
207. Shi, W. and M.-J. Dumont, *Processing and physical properties of canola protein isolate-based films.* Industrial Crops and Products, 2014. **52**(Supplement C): p. 269-277.
208. Shi, W., M.-J. Dumont, and E.B. Ly, *Synthesis and properties of canola protein-based superabsorbent hydrogels.* European Polymer Journal, 2014. **54**(Supplement C): p. 172-180.
209. Sánchez-Vioque, R., et al., *Foaming Properties of Acylated Rapeseed (Brassica napus L.) Hydrolysates.* Journal of Colloid and Interface Science, 2001. **244**(2): p. 386-393.
210. Gerbanowski, A., et al., *Grafting of Aliphatic and Aromatic Probes on Rapeseed 2S and 12S Proteins: Influence on Their Structural and Physicochemical Properties.* Journal of Agricultural and Food Chemistry, 1999. **47**(12): p. 5218-5226.
211. Wang, C., J. Wu, and G.M. Bernard, *Preparation and characterization of canola protein isolate–poly(glycidyl methacrylate) conjugates: A bio-based adhesive.* Industrial Crops and Products, 2014. **57**(Supplement C): p. 124-131.
212. Manamperi, W.A.R., et al., *Plastics from an Improved Canola Protein Isolate: Preparation and Properties.* Journal of the American Oil Chemists' Society, 2010. **87**(8): p. 909-915.

213. Manamperi, W.A.R. and S.W. Pryor, *Properties of Canola Protein-based Plastics and Protein Isolates Modified Using SDS and SDBS.* Journal of the American Oil Chemists' Society, 2012. **89**(3): p. 541-549.
214. Schindelin, J., et al., *Fiji: an open-source platform for biological-image analysis.* Nature methods, 2012. **9**(7): p. 676-682.
215. Cohen, S.A., *Amino acid analysis using pre-column derivatization with 6-aminoquinolyl-N-hydroxysuccinimidyl carbamate. Analysis of hydrolyzed proteins and electroblotted samples*. Methods in molecular biology (Clifton, NJ), 2003. **211**: p. 143-154.
216. Koehn, H., et al., *Combination of acid labile detergent and C18 Empore™ disks for improved identification and sequence coverage of in-gel digested proteins.* Analytical and Bioanalytical Chemistry, 2011. **400**(2): p. 415-421.
217. Rodgers, D.S., S.C. Wilhite, and D.S. Rodgers, *Circular Dichroism: Theory and Spectroscopy*. 2011, Hauppauge, UNITED STATES: Nova Science Publishers, Incorporated.
218. Whitmore, L. and B.A. Wallace, *Protein secondary structure analyses from circular dichroism spectroscopy: methods and reference databases.* Biopolymers: Original Research on Biomolecules, 2008. **89**(5): p. 392-400.
219. Whitmore, L. and B. Wallace, *DICHROWEB, an online server for protein secondary structure analyses from circular dichroism spectroscopic data.* Nucleic acids research, 2004. **32**(suppl_2): p. W668-W673.
220. Lobley, A., L. Whitmore, and B. Wallace, *DICHROWEB: an interactive website for the analysis of protein secondary structure from circular dichroism spectra.* Bioinformatics, 2002. **18**(1): p. 211-212.
221. Compton, L.A. and W.C. Johnson Jr, *Analysis of protein circular dichroism spectra for secondary structure using a simple matrix multiplication.* Analytical biochemistry, 1986. **155**(1): p. 155-167.
222. Manavalan, P. and W.C. Johnson Jr, *Variable selection method improves the prediction of protein secondary structure from circular dichroism spectra.* Analytical biochemistry, 1987. **167**(1): p. 76-85.
223. Sreerama, N. and R.W. Woody, *Estimation of protein secondary structure from circular dichroism spectra: comparison of CONTIN, SELCON, and CDSSTR methods with an expanded reference set.* Analytical biochemistry, 2000. **287**(2): p. 252-260.
224. Sreerama, N., S.Y. Venyaminov, and R.W. Woody, *Estimation of protein secondary structure from circular dichroism spectra: inclusion of denatured proteins with native proteins in the analysis.* Analytical biochemistry, 2000. **287**(2): p. 243-251.
225. ALOthman, Z.A., *A review: fundamental aspects of silicate mesoporous materials.* Materials, 2012. **5**(12): p. 2874-2902.
226. Reichenauer, G., *Structural Characterization of Aerogels*, in *Aerogels Handbook*, M.A. Aegerter, N. Leventis, and M.M. Koebel, Editors. 2011, Springer New York: New York, NY. p. 449-498.
227. Raymer, P.L., *Canola: an emerging oilseed crop.* Trends in new crops and new uses, 2002. **1**: p. 122-126.
228. Tzeng, Y., L. Diosady, and L. Rubin, *Preparation of rapeseed protein isolates using ultrafiltration, precipitation and diafiltration.* Canadian Institute of Food Science and Technology Journal, 1988. **21**(4): p. 419-424.
229. Alashi, A.M., et al., *Antioxidant properties of Australian canola meal protein hydrolysates.* Food Chemistry, 2014. **146**: p. 500-506.
230. Ohlson, R. and K. Anjou, *Rapeseed protein products.* Journal of the American Oil Chemists' Society, 1979. **56**(3): p. 431-437.
231. Schwenke, K. and K.J. Linow, *A reversible dissociation of the 12 S globulin from rapeseed (Brassica napus L.) depending on ionic strength.* Food/Nahrung, 1982. **26**(1): p. K5-K6.
232. Monsalve, R.I., et al., *Structural analysis of the small chain of the 2S albumin, napin nIII, from rapeseed. Chemical and spectroscopic evidence of an intramolecular bond formation.* Biochimica et Biophysica Acta (BBA)-Protein Structure and Molecular Enzymology, 1991. **1078**(2): p. 265-272.

233. Frandsen, G.I., J. Mundy, and J.T.C. Tzen, *Oil bodies and their associated proteins, oleosin and caleosin.* Physiologia Plantarum, 2001. **112**(3): p. 301-307.
234. Riis, B., et al., *Eukaryotic protein elongation factors.* Trends in Biochemical Sciences, 1990. **15**(11): p. 420-424.
235. de Oliveira Carvalho, A. and V. Moreira Gomes, *Plant Defensins and Defensin-Like Peptides - Biological Activities and Biotechnological Applications.* Current Pharmaceutical Design, 2011. **17**(38): p. 4270-4293.
236. Wu, J., R.E. Aluko, and A.D. Muir, *Purification of angiotensin I-converting enzyme-inhibitory peptides from the enzymatic hydrolysate of defatted canola meal.* Food chemistry, 2008. **111**(4): p. 942-950.
237. Alashi, A.M., et al., *Blood pressure lowering effects of Australian canola protein hydrolysates in spontaneously hypertensive rats.* Food Research International, 2014. **55**: p. 281-287.
238. Zhang, S.B., Z. Wang, and S.Y. Xu, *Antioxidant and antithrombotic activities of rapeseed peptides.* Journal of the American Oil Chemists' Society, 2008. **85**(6): p. 521-527.
239. Alashi, A.M., et al., *Technological and bioactive functionalities of canola meal proteins and hydrolysates.* Food Reviews International, 2013. **29**(3): p. 231-260.
240. Lahrichi, S.L., et al., *Food Peptidomics: Large scale analysis of small bioactive peptides — A pilot study.* Journal of Proteomics, 2013. **88**: p. 83-91.
241. Corrêa, D.H. and C.H. Ramos, *The use of circular dichroism spectroscopy to study protein folding, form and function.* African Journal of Biochemistry Research, 2009. **3**(5): p. 164-173.
242. Wei, Y., A. Thyparambil, and R. Latour, *Protein Helical Structure Determination Using CD Spectroscopy for Solutions with Strong Background Absorbance from 190-230 nm.* Biochimica et biophysica acta, 2014. **1844**.
243. He, R., et al., *Effects of High Pressure and Heat Treatments on Physicochemical and Gelation Properties of Rapeseed Protein Isolate.* Food and Bioprocess Technology, 2014. **7**(5): p. 1344-1353.
244. Kleemann, C., et al., *In-vitro-digestion and swelling kinetics of whey protein, egg white protein and sodium caseinate aerogels.* Food Hydrocolloids, 2020. **101**: p. 105534.
245. Fitzpatrick, S.E., et al., *Novel protein-based bio-aerogels derived from canola seed meal.* Journal of Materials Science, 2020. **55**(11): p. 4848-4863.
246. Tunick, M.H., *Small-Strain Dynamic Rheology of Food Protein Networks.* Journal of Agricultural and Food Chemistry, 2011. **59**(5): p. 1481-1486.
247. Instruments, T. *Understanding Rheology of Structured Fluids* Available from: http://www.tainstruments.com/pdf/literature/AAN016_V1_U_StructFluids.pdf.
248. Lu, H., H. Luo, and N. Leventis, *Mechanical Characterization of Aerogels,* in *Aerogels Handbook*, M.A. Aegerter, N. Leventis, and M.M. Koebel, Editors. 2011, Springer New York: New York, NY. p. 499-535.
249. Wang, L., et al., *Ultralight Conductive and Elastic Aerogel for Skeletal Muscle Atrophy Regeneration.* Advanced functional materials, 2019. **29**(1): p. 1806200-n/a.
250. Si, Y., et al., *Ultralight nanofibre-assembled cellular aerogels with superelasticity and multifunctionality.* Nature Communications, 2014. **5**(1): p. 5802.
251. Kim, U.-J., et al., *Structure and Properties of Silk Hydrogels.* Biomacromolecules, 2004. **5**(3): p. 786-792.
252. Pekala, R.W., C.T. Alviso, and J.D. LeMay, *Organic aerogels: microstructural dependence of mechanical properties in compression.* Journal of Non-Crystalline Solids, 1990. **125**(1): p. 67-75.
253. Bier, J.M., C.J.R. Verbeek, and M.C. Lay, *Thermal Transitions and Structural Relaxations in Protein-Based Thermoplastics.* Macromolecular Materials and Engineering, 2014. **299**(5): p. 524-539.
254. Tang, C.-H., S.-M. Choi, and C.-Y. Ma, *Study of thermal properties and heat-induced denaturation and aggregation of soy proteins by modulated differential scanning calorimetry.* International Journal of Biological Macromolecules, 2007. **40**(2): p. 96-104.
255. Kitabatake, N., M. Tahara, and E. Doi, *Denaturation Temperature of Soy Protein under Low Moisture Conditions.* Agricultural and Biological Chemistry, 1989. **53**(4): p. 1201-1202.

256. Rouilly, A., et al., *DSC study on the thermal properties of sunflower proteins according to their water content.* Polymer, 2001. **42**(26): p. 10111-10117.
257. Matveev, Y.I., et al., *Glass transition temperature of proteins. Calculation based on the additive contribution method and experimental data.* Food Hydrocolloids, 1997. **11**(2): p. 125-133.
258. Senoz, E., et al., *Physical and chemical changes in feather keratin during pyrolysis.* Polymer Degradation and Stability, 2012. **97**(3): p. 297-307.
259. Kalka, S., et al., *Biodegradability of all-cellulose composite laminates.* Composites Part A: Applied Science and Manufacturing, 2014. **59**: p. 37-44.
260. Célino, A., et al., *The hygroscopic behavior of plant fibers: a review.* Frontiers in chemistry, 2014. **1**: p. 43.
261. Meereboer, K.W., M. Misra, and A.K. Mohanty, *Review of recent advances in the biodegradability of polyhydroxyalkanoate (PHA) bioplastics and their composites.* Green Chemistry, 2020. **22**(17): p. 5519-5558.
262. Bátori, V., et al., *Anaerobic degradation of bioplastics: A review.* Waste Management, 2018. **80**: p. 406-413.
263. Swift, G., *Requirements for biodegradable water-soluble polymers.* Polymer Degradation and Stability, 1998. **59**(1): p. 19-24.
264. Xu, L. and L.L. Diosady, *Removal of phenolic compounds in the production of high-quality canola protein isolates.* Food Research International, 2002. **35**(1): p. 23-30.
265. Smirnova, I. and P. Gurikov, *Aerogels in Chemical Engineering: Strategies Toward Tailor-Made Aerogels.* Annual review of chemical and biomolecular engineering, 2017. **8**(1): p. 307-334.
266. Takeshita, S. and S. Yoda, *Chitosan Aerogels: Transparent, Flexible Thermal Insulators.* Chemistry of Materials, 2015. **27**(22): p. 7569-7572.
267. Duchemin, B.J.C., et al., *Aerocellulose based on all-cellulose composites.* Journal of Applied Polymer Science, 2010. **115**(1): p. 216-221.
268. Alemán, J.V., et al., *Definitions of terms relating to the structure and processing of sols, gels, networks, and inorganic-organic hybrid materials (IUPAC Recommendations 2007).* Pure and Applied Chemistry, 2007. **79**(10): p. 1801-1829.
269. Phelan, M., et al., *Casein-derived bioactive peptides: Biological effects, industrial uses, safety aspects and regulatory status.* International Dairy Journal, 2009. **19**(11): p. 643-654.
270. Buehler, M.J., *Nature designs tough collagen: Explaining the nanostructure of collagen fibrils.* Proceedings of the National Academy of Sciences, 2006. **103**(33): p. 12285-12290.
271. Sherman, V.R., W. Yang, and M.A. Meyers, *The materials science of collagen.* Journal of the Mechanical Behavior of Biomedical Materials, 2015. **52**: p. 22-50.
272. Kumar, M.R., *Chitin and chitosan fibres: a review.* Bulletin of Materials Science, 1999. **22**(5): p. 905.
273. Shamshina, J.L., P. Berton, and R.D. Rogers, *Advances in Functional Chitin Materials: A Review.* ACS Sustainable Chemistry & Engineering, 2019. **7**(7): p. 6444-6457.
274. Liu, D., et al., *Collagen and Gelatin.* Annual Review of Food Science and Technology, 2015. **6**(1): p. 527-557.
275. Govindarajan, D., et al., *Fabrication of hybrid collagen aerogels reinforced with wheat grass bioactives as instructive scaffolds for collagen turnover and angiogenesis for wound healing applications.* ACS applied materials & interfaces, 2017. **9**(20): p. 16939-16950.
276. Heath, L., L. Zhu, and W. Thielemans, *Chitin nanowhisker aerogels.* ChemSusChem, 2013. **6**(3): p. 537-544.
277. Ding, B., et al., *Facile preparation of robust and biocompatible chitin aerogels.* Journal of Materials Chemistry, 2012. **22**(12): p. 5801-5809.
278. Mulvihill, D.M. and M.P. Ennis, *Functional Milk Proteins: Production and Utilization*, in *Advanced Dairy Chemistry—1 Proteins: Part A / Part B*, P.F. Fox and P.L.H. McSweeney, Editors. 2003, Springer US: Boston, MA. p. 1175-1228.
279. Schmidt, M.M., et al., *Collagen extraction process.* International food research journal, 2016. **23**(3): p. 913.

280. Hamed, I., F. Özogul, and J.M. Regenstein, *Industrial applications of crustacean by-products (chitin, chitosan, and chitooligosaccharides): A review.* Trends in Food Science & Technology, 2016. **48**: p. 40-50.
281. Burgeson, R.E. and M.E. Nimni, *Collagen Types. Molecular Structure and Tissue Distribution.* Clinical Orthopaedics and Related Research®, 1992. **282**: p. 250-272.
282. Gómez-Guillén, M.C., et al., *Functional and bioactive properties of collagen and gelatin from alternative sources: A review.* Food Hydrocolloids, 2011. **25**(8): p. 1813-1827.
283. Weadock, K.S., et al., *Physical crosslinking of collagen fibers: Comparison of ultraviolet irradiation and dehydrothermal treatment.* Journal of Biomedical Materials Research, 1995. **29**(11): p. 1373-1379.
284. Young, R.J. and P.A. Lovell, *Introduction to polymers*. 2011: CRC press.
285. Rice, R.V., et al., *On the length and molecular weight of tropocollagen from calf skin.* Archives of Biochemistry and Biophysics, 1964. **105**(2): p. 409-423.
286. Alemán, J., et al., *Definitions of terms relating to the structure and processing of sols, gels, networks, and inorganic-organic hybrid materials (IUPAC Recommendations 2007).* Pure and Applied Chemistry, 2007. **79**(10): p. 1801-1829.
287. Gurikov, P., et al., *110th Anniversary: Solvent Exchange in the Processing of Biopolymer Aerogels: Current Status and Open Questions.* Industrial & Engineering Chemistry Research, 2019. **58**(40): p. 18590-18600.
288. Ganesan, K., et al., *Review on the Production of Polysaccharide Aerogel Particles.* Materials, 2018. **11**(11): p. 2144.
289. Subrahmanyam, R., et al., *On the Road to Biopolymer Aerogels-Dealing with the Solvent.* Gels, 2015. **1**(2): p. 291-313.
290. Vilela, J.A.P., Â.L.F. Cavallieri, and R.L. Da Cunha, *The influence of gelation rate on the physical properties/structure of salt-induced gels of soy protein isolate–gellan gum.* Food Hydrocolloids, 2011. **25**(7): p. 1710-1718.
291. Marangoni, A., et al., *On the structure of particulate gels—the case of salt-induced cold gelation of heat-denatured whey protein isolate.* Food hydrocolloids, 2000. **14**(1): p. 61-74.
292. Au - Subrahmanyam, R., et al., *Preparation of Biopolymer Aerogels Using Green Solvents.* JoVE, 2016(113): p. e54116.
293. Yahya, E.B., et al., *A Review on Revolutionary Natural Biopolymer-Based Aerogels for Antibacterial Delivery.* Antibiotics, 2020. **9**(10): p. 648.
294. Torre, M., A.R. Rodriguez, and F. Saura-Calixto, *Study of the interactions of calcium ions with lignin, cellulose, and pectin.* Journal of Agricultural and Food Chemistry, 1992. **40**(10): p. 1762-1766.
295. García-González, C.A., et al., *Supercritical drying of aerogels using CO2: Effect of extraction time on the end material textural properties.* The Journal of Supercritical Fluids, 2012. **66**: p. 297-306.
296. Rubino, M.I., et al., *Phenolic protein interactions in relation to the gelation properties of canola protein.* Food Research International, 1996. **29**(7): p. 653-659.
297. Druel, L., et al., *Starch Aerogels: A Member of the Family of Thermal Superinsulating Materials.* Biomacromolecules, 2017. **18**(12): p. 4232-4239.
298. Chen, K. and H. Zhang, *Alginate/pectin aerogel microspheres for controlled release of proanthocyanidins.* International Journal of Biological Macromolecules, 2019. **136**: p. 936-943.
299. Garcia-Gonzalez, C.A., M. Alnaief, and I. Smirnova, *Polysaccharide-based aerogels-Promising biodegradable carriers for drug delivery systems.* Carbohydrate Polymers, 2011. **86**(4): p. 1425-1438.
300. Innerlohinger, J., H.K. Weber, and G. Kraft, *Aerocellulose: Aerogels and Aerogel-like Materials made from Cellulose.* Macromolecular Symposia, 2006. **244**(1): p. 126-135.
301. Demilecamps, A., et al., *Cellulose–silica aerogels.* Carbohydrate polymers, 2015. **122**: p. 293-300.
302. Robitzer, M., et al., *Nitrogen sorption as a tool for the characterisation of polysaccharide aerogels.* Carbohydrate Polymers, 2011. **85**(1): p. 44-53.

303. Alshrah, M., et al., *Development of high-porosity resorcinol formaldehyde aerogels with enhanced mechanical properties through improved particle necking under CO2 supercritical conditions.* Journal of Colloid and Interface Science, 2017. **485**: p. 65-74.
304. Saliger, R., et al., *High surface area carbon aerogels for supercapacitors.* Journal of Non-Crystalline Solids, 1998. **225**: p. 81-85.
305. Wang, Z., et al., *Ultralight, highly compressible and fire-retardant graphene aerogel with self-adjustable electromagnetic wave absorption.* Carbon, 2018. **139**: p. 1126-1135.
306. Farha, O.K., et al., *De novo synthesis of a metal-organic framework material featuring ultrahigh surface area and gas storage capacities.* Nature chemistry, 2010. **2**(11): p. 944-948.
307. Huber, L., et al., *Fast and Minimal-Solvent Production of Superinsulating Silica Aerogel Granulate.* Angewandte Chemie International Edition, 2017. **56**(17): p. 4753-4756.
308. Ciftci, D., et al., *Lupin hull cellulose nanofiber aerogel preparation by supercritical CO2 and freeze drying.* The Journal of Supercritical Fluids, 2017. **127**: p. 137-145.
309. Jin, H., et al., *Nanofibrillar cellulose aerogels.* Colloids and Surfaces A: Physicochemical and Engineering Aspects, 2004. **240**(1): p. 63-67.
310. Parmenter, K.E. and F. Milstein, *Mechanical properties of silica aerogels.* Journal of Non-Crystalline Solids, 1998. **223**(3): p. 179-189.
311. Chen, W., et al., *Static and dynamic mechanical properties of expanded polystyrene.* Materials & Design, 2015. **69**: p. 170-180.
312. Jordan, J.L., et al., *Mechanical Properties of Low Density Polyethylene.* Journal of Dynamic Behavior of Materials, 2016. **2**(4): p. 411-420.
313. Nystrom, G., et al., *Amyloid Templated Gold Aerogels.* Advanced Materials, 2016. **28**(3): p. 472-8.
314. Ross-Murphy, S.B., *Structure and rheology of gelatin gels: recent progress.* Polymer, 1992. **33**(12): p. 2622-2627.
315. Shi, W., M.-J. Dumont, and E.B. Ly, *Synthesis and properties of canola protein-based superabsorbent hydrogels.* European Polymer Journal, 2014. **54**: p. 172-180.
316. Ubeyitogullari, A. and O.N. Ciftci, *Fabrication of bioaerogels from camelina seed mucilage for food applications.* Food Hydrocolloids, 2020. **102**: p. 105597.
317. Liu, S., et al., *High CO 2 adsorption by amino-modified bio-spherical cellulose nanofibres aerogels.* Environmental Chemistry Letters, 2018. **16**(2): p. 605-614.
318. Pajonk, G.M., *Transparent silica aerogels.* Journal of Non-Crystalline Solids, 1998. **225**: p. 307-314.
319. Leger, L.W. and S.D. Arntfield, *Thermal gelation of the 12S canola globulin.* Journal of the American Oil Chemists' Society, 1993. **70**(9): p. 853-861.
320. Zhao, Y., et al., *Formation mechanism of ovalbumin gel induced by alkali.* Food Hydrocolloids, 2016. **61**: p. 390-398.
321. Derkach, S.R., et al., *Molecular structure and properties of κ-carrageenan-gelatin gels.* Carbohydrate Polymers, 2018. **197**: p. 66-74.
322. Nowotny, A., *Carbohydrate determination by phenol-sulfuric acid*, in *Basic exercises in immunochemistry*. 1979, Springer. p. 171-173.
323. Adewole, D.I., et al., *Chemical and nutritive characteristics of canola meal from Canadian processing facilities.* Animal Feed Science and Technology, 2016. **222**: p. 17-30.
324. Latta, M. and M. Eskin, *A simple and rapid colorimetric method for phytate determination.* Journal of Agricultural and Food Chemistry, 1980. **28**(6): p. 1313-1315.
325. Xu, L. and L.L. Diosady, *Rapid method for total phenolic acid determination in rapeseed/canola meals.* Food Research International, 1997. **30**(8): p. 571-574.

Appendix

a) Identification of peptide sequences from canola proteins

Proteins isolated from the SDS-PAGE gel were identified by conducting a database search on amino acid sequences identified by LC-MS/MS (see **Section 5.3.4**). The identified proteins are listed in **Table 5.6:** Proteins identified in CSM protein extracts identified by LC-MS/MS analysis The full list of peptide sequences identified is provided in **Table A.1** alongside the corresponding sample number, molecular weight (as identified by SDS-PAGE) analysis), and the code for the parent protein (where CRU-X refers to cruciferin, EF1A1 refers to elongation factor, OLES2 refers to oleosin, 2SS3 refers to napin, and DEF4 refers to defensin).

Table A.1: *Peptides identified in LC-MS/MS analysis of CSM protein bands excised from an SDS-PAGE gel.*

Sample	M_W (kDa)	Identified sequences	Parent protein code
1	350	K.TNANAQINTLAGR.T	**CRUA**
		R.LPLQDVYK.I K.IGGIGTVPVGR.V R.QTVAVGVIK.S	EF1A1
		R.GTSDTVPEQLDYAK.R R.MADAVGYAGQK.G R.MADAVGYAGQK.G R.MADAVGYAGQKG.K K.EMGQYVQDK.A	OLES2
		K.ISVETAQK.L N.AALYVTK.G R.VFDQEISK.G K.SNDNAQINTLAGR.T K.FSTLETTLTQSSGPMG.Y	**CRU4**
2	300	K.LQNQQVNR.G N.AALYVTK.G R.VFDQEISK.G K.SNDNAQINTLAGR.T K.FSTLETTLTQSSGPMG.Y	**CRU4**

		R.GTSDTVPEQLDYAK.R R.MADAVGYAGQK.G R.MADAVGYAGQKG.K	OLES2
		K.EVSSYLK.K R.LPLQDVYK.I K.IGGIGTVPVGR.V R.QTVAVGVIK.S	EF1A1
3	90 – 100	K.LQNQQVNR.G K.SNDNAQINTLAGR.T	**CRU4**
4	65 - 70	(no peptides identified)	
5	60 - 65	K.ISVETAQK.L K.LQNQQVNR.G N.AALYVTK.G R.VFDQEISK.G K.SNDNAQINTLAGR.T	**CRU4**
		R.YIIESK.G K.TNANAQINTLAGR.T	**CRUA**
6	40 - 45	R.YIIESK.G R.ATSEQFR.W K.TNANAQINTLAGR.T	**CRUA**
		K.ISYVVQGMGISGR.V R.LAQELQNQQDSR.G R.GILQGNAMVLPK.Y R.IQVVNDNGQNVLDQQVQK.G K.GQLVVIPQGF.A K.GQLVVIPQGFAY.V K.TNANAMVSTLAGR.T K.FNTLETTLTR.A	**CRU3**
		K.ISVETAQK.L K.LQNQQVNR.G N.AALYVTK.G R.VFDQEISK.G K.SNDNAQINTLAGR.T K.FSTLETTLTQSSGPMG.Y	**CRU4**
7	32	R.QSLGVPPQLGNACNLDNLDVLQPTETIK.S N.ACNLDNLDVLQPTETIK.S	**CRU3**

		C.NLDNLDVLQPTETIK.S D.VLQPTETIK.S R.VEYWDHNNPQIR.C R.CAGVSVSR.V K.ISYVVQGMGISGR.V C.LLDIANYQNQLDR.N D.IANYQNQLDR.N N.MLSGFDPQVLAQALK.I D.PQVLAQALK.I R.LAQELQNQQDSR.G R.QPYESEQWR.H K.TNANAMVSTLAGR.T K.FNTLETTLTR.A	
		R.CSGVSFVR.Y R.YIIESK.G R.TAQQLQNQQDNR.G K.TNANAQINTLAGR.T	**CRUA**
		K.LQNQQVNR.G R.VFDQEISK.G K.FSTLETTLTQSSGPMG.Y	**CRU4**
8	30	R.QSLGVPPQLGNACNLDNLDVLQPTETIK.S N.ACNLDNLDVLQPTETIK.S C.NLDNLDVLQPTETIK.S D.VLQPTETIK.S R.VEYWDHNNPQIR.C R.CAGVSVSR.V K.ISYVVQGMGISGR.V C.LLDIANYQNQLDR.N D.IANYQNQLDR.N N.MLSGFDPQVLAQALK.I D.PQVLAQALK.I R.LAQELQNQQDSR.G R.QPYESEQWR.H K.TNANAMVSTLAGR.T K.FNTLETTLTR.A	**CRU3**
		R.CSGVSFVR.Y R.YIIESK.G	**CRU1**

		K.GLYLPSFFSTAK.L K.GEGLMGR.V F.YLAGNNPQGQVWIEGR.E K.NILNGFTPEVLAK.A R.TAQQLQNQQDNR.G R.VQGPF.S R.VQGPFSVIRPPL.R	
		Q.NECNLDNLDVLQATETIK.S A.LLDIANYQNQLDR.N D.IANYQNQLDR.N K.FNTLETTLTR.A	**CRU3**
		R.CSGVSFVR.Y K.GQQGQSQGQQGQGQGFR.D R.TAQQLQNQQDNR.G R.VQGPF.G R.VQGPFGVIRPPL.K	**CRU2**
		K.ISVETAQK.L R.VFDQEISK.G R.ATSQQFQWIEFK.S K.SNDNAQINTLAGR.T	**CRU4**
9	26 -28	L.NALEPSQIIK.S N.ALEPSQIIK.S R.IEVWDHHAPQLR.C R.CSGFAFER.F C.SGFAFER.F R.FVIEPQGLYLPT.F R.FVIEPQGLYLPTFLNAGK.L Q.GLYLPTFLNAGK.L L.YLPTFLNAGK.L K.LTFVVH.G K.LTFVVHG.H D.SPVFGQGQGQEQGQGQGQGQGQGFR.D L.ILVAAADIANNLNQLDR.N L.VAAADIANNLNQLDR.N A.AADIANNLNQLDR.N A.ADIANNLNQLDR.N A.DIANNLNQLDR.N	**CRU4**

		D.IANNLNQLDR.N N.NLNQLDR.N R.NLRPFLLA.G F.LLAGNNPQGQQWLQGR.Q A.GNNPQGQQWLQGR.Q Q.QWLQGR.Q K.QNNIFNGFAPQIL.A K.QNNIFNGFAPQILAQ.A Q.ILAQAFK.I K.ISVETAQK.L K.LQNQQVNR.G K.VQGQFGVIRPP.L K.VQGQFGVIRPPL.R K.VQGQFGVIRPPLR.Q R.VFDQEISK.G R.ATSQQFQWIEFK.S K.SNDNAQINTLAGR.T	
		R.VEYWDHNNPQIR.C R.CAGVSVSR.V K.ISYVVQGMGISGR.V C.LLDIANYQNQLDR.N R.LAQELQNQQDSR.G R.VTSVNSYTLPILQYIR.L R.GILQGNAMVLPK.Y R.IQVVNDNGQNVLDQQVQK.G K.TNANAMVSTLAGR.T K.FNTLETTLTR.A	**CRU3**
		L.NALEPSQIIK.S N.ALEPSQIIK.S R.IEVWDHHAPQLR.C R.CSGFAFER.F C.SGFAFER.F K.LTFVVH.G K.LTFVVHG.R R.NLRPFLIA.G K.QNNIFNGFAPEILAQ.A K.QNNIFNGFAPEILAQAF.K	**CRU2**

		K.QNNIFNGFAPEILAQAFK.I E.ILAQAFK.I E.TAQQLQNQQDNR.G	
		R.ENQLDQVPR.M R.MFQLAGSR.T N.NAFSGFDPNIIAEAFK.I F.SGFDPNIIAEAFK.I	**CRU4**
		R.IEVWDHHAPQLR.C R.CSGVSFVR.Y R.YIIESK.G K.GLYLPSFFSTAK.L S.VLDLASHQNQLDR.N R.TAQQLQNQQDNR.G	**CRU1**
9	26-28	R.IEVWDHHAPQLR.C R.CSGVSFVR.Y K.NPQGQSWLHGR.G R.TAQQLQNQQDNR.G	**CRU2**
10	22 -23	N.GLEETICSMR.T R.THENIDDPAR.A R.ADVYKPNLGR.V R.VTSVNSYTLPILQY.I R.VTSVNSYTLPILQYIR.L N.SYTLPILQYIR.L Y.TLPILQYIR.L R.GILQGNAMVLPK.Y K.YNMNANEILYCTQGQAR.I R.IQVVNDNGQNVLDQQVQK.G R.IQVVNDNGQNVLDQQVQKG.Q K.GQLVVIPQGF.A K.GQLVVIPQGFAY.V K.TNANAMVSTLAGR.T K.TNANAMVSTLAGR.T R.ALPLEVITNAFQISLEEAR.R N.AFQISLEEAR.R K.FNTLETTLTR.A	**CRU3 (BRANA)**
		N.GLEETICSMR.S R.IQVVNDNGQNVLDQQVQK.G	**CRU3 (ARATH)**

		R.IQVVNDNGQNVLDQQVQKG.Q K.GQLVVIPQGF.A K.GQLVVIPQGFAY.V K.FNTLETTLTR.A	
		R.CSGFAFER.F R.FVIEPQGLYLPTFLNAGK.L A.AADIANNLNQLDR.N F.LLAGNNPQGQQWLQGR.Q K.LQNQQVNR.G K.VQGQFGVIRPPLR.Q R.ATSQQFQWIEFK.S K.SNDNAQINTLAGR.T	**CRU4**
		N.GLEETICSAR.C K.TNANAQINTLAGR.T	**CRUA**
11	18 -20	R.CSGFAFER.F N.GLEETLCTMR.C Y.ISTLNSYNLPILR.F N.SYNLPILR.F Y.NLPILR.F N.VNANAALYVTK.G N.AALYVTK.G R.VFDQEISK.G K.GQLLVVPQGFAVVK.R R.ATSQQFQWIEFK.S K.SNDNAQINTLAGR.T N.AQINTLAGR.T Q.INTLAGR.T R.GLPLEVISNGYQISPQEAR.S K.FSTLETTLTQSSGPMG.Y	**CRU4**
		N.GLEETICSAR.C Y.ISTLNSYDLPILR.F N.SYDLPILR.F R.VFDGQVSQGQLLSIPQGF.S R.VFDGQVSQGQLLSIPQGFSVVK.R R.ATSEQFR.W K.TNANAQINTLAGR.T N.AQINTLAGR.T	**CRUA**

		Q.INTLAGR.T R.GLPLEVISNGYQISLEEAR.R K.FNTIETTLTH.S K.FNTIETTLTHSSGPAS.Y K.FNTIETTLTHSSGPASYGGPR.K	
		R.LAQELQNQQDSR.G R.ADVYKPNLGR.V R.VTSVNSYTLPILQYIR.L Y.TLPILQYIR.L R.GILQGNAMVLPK.Y R.IQVVNDNGQNVLDQQVQK.G K.GQLVVIPQGF.A K.TNANAMVSTLAGR.T N.AMVSTLAGR.T M.VSTLAGR.T K.FNTLETTLTR.A	**CRU3**
		N.GLEETICSAR.C N.SYDLPILR.V R.VFDGQVSQGQLLSIPQGF.S R.VFDGQVSQGQLLSIPQGFSVVK.R K.TNANAQINTLAGR.T N.AQINTLAGR.T Q.INTLAGR.T K.FNTIETTLTH.S K.FNTIETTLTHSSGPAS.Y	**CRU2**
12	17-18	N.GLEETLCTMR.C Y.ISTLNSYNLPILR.F L.NSYNLPILR.F N.SYNLPILR.F Y.NLPILR.F R.GSIHNNAMVLPQWNVNAN.A N.VNANAALYVTK.G N.AALYVTK.G R.VFDQEISK.G K.GQLLVVPQGF.A K.GQLLVVPQGFAVVK.R R.ATSQQFQWIEFK.S	**CRU4 (BRANA)**

		K.SNDNAQINTLAGR.T D.NAQINTLAGR.T N.AQINTLAGR.T Q.INTLAGR.T R.GLPLEVISNGYQISPQEAR.S K.FSTLETTLTQSSGPMG.Y	
		N.GLEETICSAR.C R.VFDGQVSQGQLLSIPQGF.S R.ATSEQFR.W K.TNANAQINTLAGR.T A.NAQINTLAGR.T N.AQINTLAGR.T Q.INTLAGR.T K.FNTIETTLTH.S K.FNTIETTLTHSSGPAS.Y	**CRUA**
		R.LAQELQNQQDSR.G R.ADVYKPNLGR.V R.GILQGNAMVLPK.Y K.TNANAMVSTLAGR.T K.FNTLETTLTR.A	**CRU3**
		N.GLEETLCTMR.C Y.ISTLNSYNLPILR.L L.NSYNLPILR.L N.SYNLPILR.L Y.NLPILR.L K.AHIQMVNDNGER.V K.AHIQMVNDNGER.V	**CRU2**
		K.IHENIDD.P K.IHENIDDPER.S R.ISTLNSLNLPVLR.L N.SLNLPVLR.L	**CRU4 (ARATH)**
13	16-17	N.NLNQLDR.N Q.ILAQAFK.I K.ISVETAQK.L K.LQNQQVNR.G N.GLEETLCTMR.C N.SYNLPILR.F	**CRU4**

		Y.NLPILR.F N.VNANAALYVTK.G N.ANAALYVTK.G N.AALYVTK.G R.VFDQEISK.G K.GQLLVVPQGF.A K.GQLLVVPQGFAVVK.R R.ATSQQFQWIEFK.S K.SNDNAQINTLAGR.T Q.INTLAGR.T K.FSTLETTLTQSSGPMG.Y	
		K.TNANAQINTLAGR.T Q.INTLAGR.T K.FNTIETTLTHSSGPAS.Y	**CRUA**
		Q.GQQQQGFR.D R.LAQELQNQQDSR.G K.TNANAMVSTLAGR.T	**CRU3**
14	11-12	R.CSGFAFER.F Q.GLYLPTFLNAGK.L L.YLPTFLNAGK.L K.ISVETAQK.L K.GQLLVVPQGFAVVK.R R.ATSQQFQWIEFK.S K.SNDNAQINTLAGR.T	**CRU4**
		R.VEYWDHNNPQIR.C R.CAGVSVSR.V K.ISYVVQGMGISGR.V K.ISYVVQGMGISGR.V K.FNTLETTLTR.A	**CRU3**
		R.CSGVSFVR.Y R.YIIESK.G K.GLYLPSFFSTAK.L K.TNANAQINTLAGR.T	**CRU1**
		R.QQQGQQGQQLQQVISR.I K.VCNIPQVSVCPFQK.T	2SS3
		K.EYGGDVGFGFCAPR.I R.IYPSFCVQR.C	DEF4